science • industry • society

IMAGINENANO

Bringing together Nanoscience and Nanotechnology

2011

graphene 2011

NanoSpain Conf 2011

NanoSudoe Conference

nano bio&med

nanoscience HPC2011

TNA 2011 Trends in NanoApplications Energy

Photonics Plasmonics Magneto-Optics PPM 2011

www.imaginenano.com

On behalf of the International, Scientific and Technical Committees we take great pleasure in welcoming you to Bilbao for the first edition of ImagineNano.

ImagineNano 2011 is a step further, is the consolidation of years of work, an event that Phantoms Foundation has been thinking for years, totally dedicated to Nanoscience & Nanotechnology (N&N). ImagineNano plans to be a reference in Europe in the next upcoming years and the expertise, know-how in N&N enables us to create such an event.

Under the same roof will be held 5 International Conferences (Graphene, NanoSpain, nanoBio&Med, PPM and TNA Energy), 1 Symposium (HPC), a huge Exhibition showcasing cutting-edge advances in nanotechnology research and development, an Industrial Forum and a Nano Art Exhibition ("A walk through the Nanoworld") where everyone can meet and greet nanotechnology side by side.

Internationally renowned speakers will be presenting the latest trends and discoveries in nanoscience and nanotechnology.

We truly hope that ImagineNano serves as an international platform for communication between science and business.

We are indebted to the following Scientific Institutions, Companies and Government Agencies for their help and/or financial support:

Phantoms Foundation, Donostia International Physics Centre, CIC nanoGUNE, Universidad del País Vasco/Euskampus, Bilbao Exhibition Centre, Instituto Español de Comercio Exterior & "españa-technology for life" program, FEDER Funds, EU/NMP nanomagma project, Ministerio de Ciencia e Innovación, CIC biomaGUNE, NanoSciences Grand Sud-Ouest, Universidad Autónoma de Madrid, GDRi Graphene Nanotubes, COST Bio-Inspired Technologies, Sandia National Laboratories, Nanosciences Rhône Alpes, Centro de Física de Materiales/CSIC, Fundação para a Ciência e a Tecnologia, Instituto de Bioingeniería de Catalunya, Centro Español de Metrología, Observatoire des Micro et NanoTechnologies, ICT/FET nanoICT Coordination Action, SUDOE Interreg IV B, European Commission, TRAIN² - SUDOE, Euskaltel/Fundación Euskaltel, FEI, NanoMed Spain, Tecnan/Centro Tecnológico Lurederra, CIBER-BBN, EU Hinamox project, Enterprise Europe Network, Nanoscale Journal, Graphenea S.L., Sociedad para la Promoción y Reconversión Industrial, nanobasque and Viajes El Corte Inglés.

We also would like to thank all the exhibitors that joined us this year.

One thing we have for granted: very few industries, one way or another, will escape from the influence of nanotechnology and the impact on businesses is here to stay.

There´s no doubt that ImagineNano 2011 is the right place to see and be seen.

Hope to see you again in the next edition of ImagineNano (2013).

ImagineNano Organising Committee

PHANTOMS foundation

EUSKAMPUS
Nazioarteko Bikaintasun Campusa
Campus de Excelencia Internacional

Donostia International Physics Center

CIC nanoGUNE
nanoscience cooperative research center

eman ta zabal zazu
universidad del país vasco
euskal herriko unibertsitatea

BILBAO EXHIBITION CENTRE
EXPOSSIBLE!

IMAGINENANO MAIN ORGANISERS

Phantoms Foundation, based in Madrid is a non-profit organization which focus its activities on Nanoscience, Nanotechnology and Emerging Nanoelectronics, bringing together and coordinating the efforts of Spanish and European universities groups, research institutes and enterprises through scientific and technological events, networks and participation in important international events like ImagineNano. Today is a key player in structuring and promoting European excellence and improving collaborations in these fields. It is also essential as a platform for spreading excellence on funded projects and for establishing new networks of collaboration.

The **CIC nanoGUNE Consolider** is a newly established center created with the mission of addressing basic and applied world-class research in nanoscience and nanotechnology, fostering high-standard training and education of researchers in this field, and promoting the cooperation among the different agents in the Basque Science, Technology, and Innovation Network (Universities and Technological Centers) and between these agents and the industrial sector.

CIC nanoGUNE has been awarded as the first Consolider Center by the Spanish Education and Science Council. Consolider Centers are created under the Consolider-Ingenio 2010 Program which funds the highest ranked Spanish research consortiums with world-class research lines at the forefront of Science and Technology.

CIC NanoGUNE Consolider represents a necessary step for the promotion of a solid knowledge community with the vocation of transfering the results of reasearch to an industrial sector. A world-class research team, state-of-the-art facilities, close collaboration with other research laboratories and with industry, and a commitment to the society define CIC nanoGune way of understanding scientific research.

The **Donostia International Physics Center Foundation (DIPC)** was created in 1999, the fruit of institutional collaboration between the Departments of Education and Industry of the Basque government, the University of the Basque Country, the Diputación Foral de Guipúzcoa, the San Sebastián City Hall, the Kutxa of Guipúzcoa and San Sebastián. Iberdrola S.A. also participated in the project from 2000-2003. In 2004, Naturcorp Multiservicios S.A, joined, followed by Telefónica S.A in 2005.The DIPC was created as an intellectual centre whose main aim is to promote and catalyse the development of basic research and basic research oriented towards material science to reach the highest level. Since its creation, the DIPC has been an open institution, linked to the University of the Basque Country, serving as a platform for the internationalizing of basic science in the Basque Country in the field of materials.

The **UPV/EHU** is the academic institution that leads the way in higher education and scientific production in the Basque Country, and the proof of this lies in the wide range of its own qualifications and university Master's degrees that it offers.

The University of the Basque Country has three campuses (one in each territory), 31 centres and faculties, and offers a wide range of courses. The centres on its three campuses are spread out among different towns and cities in the Basque Country, namely in the three provincial capitals (Bilbao, San Sebastián and Vitoria-Gasteiz) and in towns such as Leioa, Portugalete, Barakaldo and Eibar.

The University of the Basque Country provides teaching in Spanish, Basque and English within its own educational model, known as IKD. This is a model based on a practical view of teaching and on student participation.

The UPV/EHU covers a large university community comprising over 50,000 people among students (45,000), teaching and research staff (5,200) and admin and service staff (1,800).

The university offers services geared to dealing with all student needs, ranging from university guidance to a cultural advisory service, sports and international relations, etc. It also provides services aimed at assisting people with disability and applied psychology, and has student halls of residence on its three campuses.

The University of the Basque Country boasts 350 research groups and over 600 partnership projects with companies. Around 300 PhD theses are read every year at the university and it has mobility programmes that have internationalized the make-up of its student body.

B! BILBAO EXHIBITION CENTRE
E!
C!
EXPOSSIBLE!

Bilbao Exhibition Centre, BEC, is a unique project aimed at bringing people, ideas, economic forces and enterprise together under the same roof. It is a meeting place where technology and innovation work hand in hand in the generation of new business opportunities. As a major promoter of economic, social and cultural development, the BEC has its sights set on becoming one of the world´s leading business centres.

The BEC is also a new concept in its sector, where exhibitors and visitors will benefit from more and improved means of communication. At the BEC, participants will have their own "Personal Trade Consultant" to assist them in any particular needs or formalities. In short, a continuously growing meeting place, always open, where everything is thought for your benefit and where virtually anything is possible.

SPONSORS

DIAMOND SPONSORS

PLATINUM SPONSORS

GOLD SPONSORS

SILVER SPONSORS

TRAIN² - SUDOE Transpyrenees Action on Advanced Infrastructures for Nanosciences and Nanotechnologies

BRONZE SPONSORS

WIFI SPONSORS

LANYARDS SPONSOR

OTHER SPONSORS

GENERAL INDEX

science • industry • society

IMAGINENANO

Bringing together
Nanoscience and Nanotechnology

www.imaginenano.com

PLENARY SESSION

INDEX: PLENARY SESSION CONTRIBUTIONS

FET FLAGSHIPS- A NOVEL APPROACH TO PARTNERSHIPS IN SCIENTIFIC RESEARCH

Wolfgang Boch

T. J. European Commission
Head of Unit, INFSO/FET - Proactive, Information Technologies and Media Directorate General
Belgium

Large-scale, science-driven Partnership as a new collaborative mechanism

FET Flagship Initiatives are science-driven, large-scale, multidisciplinary research initiatives oriented towards a unifying goal and nucleated from ICT future and emerging technologies. The goals of such initiatives should be visionary and highly ambitious, requiring cooperation among a range of scientific disciplines, building on European excellence. The overarching nature and magnitude implies that they can only be realised through a federated effort of key stakeholders (see examples below).

FET Flagships are envisioned to run for at least 10 years, with a budget of up to 100 M€ per year and per initiative. This scale can only be achieved through cooperation between the EU Framework Programme and national research programmes (and, where appropriate, global partners and industry). In comparison, the Human Genome project is reported to have cost about 3 B$ over a 13-year period.

FET Flagships will also extend to other FP Themes and programmes (such as Health, NMP, Capacities…) and scientific disciplines and have cascading effects into more application-oriented research leading towards innovation.

As Flagships will present a programme-level approach to a long-term scientific challenge, the activities funded in Flagships should extend beyond research, addressing aspects such as coordination, strategy development, mobility programmes, international cooperation, road-mapping activity, training and education, outreach / communication / PR activities.

ImagineNano April 11-14, 2011

ELECTRON DYNAMICS AT SURFACES AND NANOSTRUCTURES

P.M. Echenique

Dpto. de Física de Materiales UPV-EHU, Donostia International Physics Center (DIPC) and Material Physics Center (CFM)
P. Manuel de Lardizabal 4, 20018 San Sebastián, Basque Country, Spain

Femtosecond and subfemtosecond time scales typically rule electron dynamics at metal surfaces. Recent advances in experimental techniques allow the experimental study of such dynamics. In this talk we shall analyze electron dynamics at surfaces and nanostructures with emphasis on screening times, spin dependence of charge transfer of adsorbates and smaller system sizes. Condensed matter effects on attophysics will also be discussed.

GRAPHENE 2011

INDEX: INVITED CONTRIBUTIONS

INDEX: KEYNOTE CONTRIBUTIONS

INDEX: ORAL CONTRIBUTIONS

ALPHABETICAL ORDER

I: Invited / K: Keynote / O: Oral

I: Invited / K: Keynote / O: Oral

I: Invited / K: Keynote / O: Oral

GRAPHENE 2011

ABSTRACTS
ALPHABETICAL ORDER

GRAPHENE-BASED ELECTRONICS AND OPTOELECTRONICS

Phaedon Avouris

T. J. Watson Research Center, Yorktown Heights, NY 10598, USA
avouris@us.ibm.com

Graphene a two-dimensional, single atomic layer material with linear electron dispersion has rather unique electrical and properties [1]. There is currently strong interest in taking advantage of these properties for technological applications [2]. In my talk I will review the key properties of graphene, how these are affected by environmental interactions and how they can be utilized in electronics and optoelectronics.

Specifically, I will discuss high frequency (>100 GHz) graphene transistors [3], their fabrication and operation, as well as related device physics aspects, such as transport mechanisms, contacts, temperature effects, dissipation, etc. Simple integrated graphene circuits will also be presented. I will then discuss key optical properties of graphene and how they can be combined with its excellent electrical properties and used in optoelectronics applications. Specific examples involving ultrafast graphene photodetectors [4] and their applications in optical data detection[5] will be presented.

References:

[1] Geim, A.K. Science 3, 1530 (2009).
[2] Avouris, Ph., Nano Lett. 10, 4285 (2010).
[3] Lin, Y.-M.; Dimitrakopoulos, C.; Jenkins, K.A.; Farmer, D.B., Chiu, H.-Y. ; Grill, A.; Avouris, Ph. Science 327, 662 (2010); Wu , Y. et al., to be published.
[4] Xia, F.; Mueller, T.; Lin, Y.-M.; Valdes-Garcia, A.; Avouris, Ph. Nature Nano 4, 839 (2009).
[5] Mueller, T.; Xia, F.; Avouris, Ph. Nature Photon. 4, 297 (2010).

NANOELECTROMECHANICAL RESONATORS BASED ON GRAPHENE

Adrian Bachtold

ICN, CIN2, Campus UABarcelona, Bellaterra, Spain
adrian.bachtold@cin2.es

The theory of damping finds its roots in Newton's Principia and has been exhaustively tested in objects as disparate as the Foucault pendulum, mirrors used in gravitational-wave detectors, and submicron mechanical resonators. Owing to recent advances in nanotechnology it is now possible to explore damping in systems with transverse dimensions on the atomic scale. Here, we study the damping of mechanical resonators based on a graphene sheet, the ultimate two-dimensional nanoelectromechanical systems (NEMS). The damping is found to strongly depend on the amplitude of the motion; it is well described by a nonlinear force $\eta x^2 \dot{x}$ (with x the deflection and $\dot{x}$ its time derivative). This is in stark contrast to the linear damping paradigm valid for larger mechanical resonators. Besides, we exploit the nonlinear nature of the damping to improve the figure of merit of graphene resonators.

TWO-DIMENSIONAL THERMAL TRANSPORT IN GRAPHENE: INTRINSIC VS. EXTRINSIC EFFECTS

Alexander A. Balandin

Nano-Device Laboratory, Department of Electrical Engineering and Materials Science and Engineering Program, Bourns College of Engineering, Univ. of California, Riverside, CA 92521 USA
balandin@ee.ucr.edu

Recent years witnessed a rapid growth of interest of the scientific and engineering communities to thermal properties of materials. The increasing importance of thermal properties is explained both by practical needs and fundamental science. Heat removal has become a crucial issue for continuing progress in electronic industry [1]. The knowledge of how well and how fast the material conducts heat becomes essential for design of the next generation of integrated circuits. From another side, efficient thermoelectric energy conversion requires finding materials, which simultaneously have high electrical conductivity but strongly suppressed thermal conductivity *K*. Material's ability to conduct heat is deeply rooted in its atomic structure, and knowledge of thermal properties can shed light on many other materials' characteristics. Thermal conductivity of materials changes when they are structured on a nanometer scale. The latter can happen because of the intrinsic effects, e.g. phonon dispersion and velocities of the low-dimensional crystal differ from those in bulk [2], or extrinsic effects such as increased phonon - rough boundary scattering when the feature size of nanostructure becomes comparable to that of the phonon mean free path (MFP) in a given material [3]. Other extrinsic effects on thermal conductivity include strain in the lattice and phonon scattering on lattice defects or impurities.

The discovery of graphene [4-5] further stimulated the interest to thermal properties because, for the first time, it became possible to study experimentally heat conduction in strictly 2D crystals. The heat conduction in 2D crystals is particularly intriguing because of the theoretically predicted logarithmic divergence of thermal conductivity *K* with the size of 2D crystal [6-7]. The *K* divergence in 2D crystals means that unlike in 3D bulk, the crystal lattice anharmonicity along is not sufficient for restoring thermal equilibrium, and one needs to either limit the system size or introduce disorder to have the physically meaningful finite value of *K*. To elucidate the physics of heat conduction in graphene, it is important to determine whether thermal transport is mostly limited by the *intrinsic* properties, e.g. by the dimensionality of the lattice and its dynamics, or by the *extrinsic* effects, e.g. phonon scattering from rough interfaces, edges, defects and impurities or graphene – substrate interactions. Heat conduction in the suspended graphene will be closer to the intrinsic phonon transport regime while that in the encased graphene will be closer to the extrinsic transport regime. The first experimental study of the evolution of heat conduction in few-layer graphene (FLG), found that *K* of suspended uncapped FLG, which is the highest in the single-layer graphene (SLG), decreases with increasing number of the atomic planes *n*, and approaches the bulk graphite limit (see Figure 1a) [8]. For comparison, the thickness dependence of thermal conductivity of the encased disordered carbon films is also shown [9].

Recent years witnessed a rapid growth of interest of the scientific and engineering communities to thermal properties of materials. The increasing importance of thermal properties is explained both by practical needs and fundamental science. Heat removal has become a crucial issue for continuing progress in electronic industry [1]. The knowledge of how well and how fast the material conducts heat becomes essential for design of the next generation of integrated circuits. From another side, efficient thermoelectric energy conversion requires finding materials, which simultaneously have high electrical conductivity but strongly suppressed thermal conductivity *K*. Material's ability to conduct heat is deeply rooted in its atomic structure, and knowledge of thermal properties can shed light on many other materials' characteristics. Thermal conductivity of materials changes when they are structured on a nanometer scale. The latter can happen because of the intrinsic effects, e.g. phonon dispersion and velocities of the low-dimensional crystal differ from those in bulk [2], or extrinsic effects such as increased phonon - rough boundary scattering when the feature size of nanostructure becomes comparable to that of the phonon mean free path (MFP) in a given material [3]. Other extrinsic effects on thermal conductivity include strain in the lattice and phonon scattering on lattice defects or impurities.

The discovery of graphene [4-5] further stimulated the interest to thermal properties because, for the first time, it became possible to study experimentally heat conduction in strictly 2D crystals. The heat conduction in 2D crystals is particularly intriguing because of the theoretically predicted logarithmic divergence of thermal conductivity *K* with the size of 2D crystal [6-7]. The *K* divergence in 2D crystals means that unlike in 3D bulk, the crystal lattice anharmonicity along is not sufficient for restoring thermal equilibrium, and one needs to either limit the system size or introduce disorder to have the physically meaningful finite value of *K*. To elucidate the physics of heat conduction in graphene, it is important to determine whether thermal transport is mostly limited by the *intrinsic* properties, e.g. by the dimensionality of the lattice and its dynamics, or by the *extrinsic* effects, e.g. phonon scattering from rough interfaces, edges, defects and impurities or graphene – substrate interactions. Heat conduction in the suspended graphene will be closer to the intrinsic phonon transport regime while that in the encased graphene will be closer to the extrinsic transport regime. The first experimental study of the evolution of heat conduction in few-layer graphene (FLG), found that *K* of suspended uncapped FLG, which is the highest in the single-layer graphene (SLG), decreases with increasing number of the atomic planes *n*, and approaches the bulk graphite limit (see Figure 1a) [8]. For comparison, the thickness dependence of thermal conductivity of the encased disordered carbon films is also shown [9].

Acknowledgements:

This work was supported, in part, by U.S. ONR award N00014-10-1-0224, SRC-DARPA FCRP Center on Functional Engineered Nano Architectonics (FENA) and DARPA Defense Microelectronics Activity (DMEA) award H94003-10-2-1003. The author thanks S. Roche, A. Geim and K. Novoselov for useful discussions.

References:

[1] C. Lin and K. Banerjee, IEEE Trans. Electron Dev., 55, 245 (2008).
[2] A. Balandin and K.L. Wang, Phys. Rev. B, 58, 1544 (1998).
[3] T. Borca-Tasciuc, *et al*., Microscale Thermophys. Eng., 5, 225 (2001).
[4] K.S. Novoselov, A.K. Geim, *et al*., Science, 306, 666 (2004).
[5] A.K. Geim and K.S. Novoselov, Nature Mater., 6, 183 (2007).
[6] For a review, see S. Lepri, *et al*., Phys. Rep. 377, 1 (2003) and references therein.
[7] K. Saito and A. Dhar, Phys. Rev. Lett., 104, 040601 (2010).
[8] S. Ghosh, *et al*., Nature Materials, 9, 555 (2010).
[9] A.A. Balandin, *et al*., Appl. Phys. Lett., 93, 043115 (2008).
[10] W. Jang, *et al*., Nano Lett., 10, 3909 (2010).

Figures:

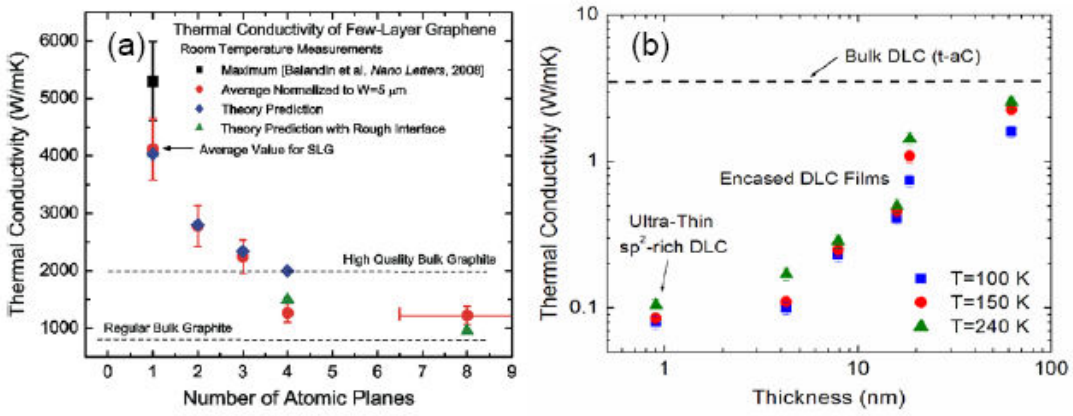

Figure 1: *Thermal conductivity of the suspended FLG (a) and in the encased ultra-thin diamond-like carbon films (b) as function of thickness. The figure (a) is adapted from Ref. [8] while the figure (b) is based on the data reported in Ref. [9].*

THE INTERACTION OF GRAPHENE WITH METALS STUDIED BY IN-SITU ELECTRON MICROSCOPY

F. Banhart[1], J. A. Rodríguez-Manzo[1], O. Cretu[1], A. Krasheninnikov[2,3]

[1] Institut de Physique et Chimie des Matériaux, UMR 7504, Université de Strasbourg, 23 rue du Loess, 67034 Strasbourg, France
[2] Materials Physics Division, University of Helsinki, P.O. Box 43, FI-00014 Helsinki, Finland
[3] Department of Applied Physics, Aalto University, P.O. Box 1100, FI-00076 Aalto, Finland
Banhart@ipcms.u-strasbg.fr

The interaction between graphene and metals is of high importance in the understanding of the growth of graphene from catalytically active metals but also from the viewpoint of doping graphene with foreign atoms. *In-situ* electron microscopy allows the atomic-scale observation of this interaction in a wide temperature range. Dissolution or precipitation phenomena, where carbon atoms are taken up by or extruded from metallic crystals, can be observed as well as the interaction between the graphenic lattice and individual metal atoms [1]. Of particular importance in this context are structural defects in graphene [2] due to the possibility of trapping dopant atoms and thus changing the electronic properties of graphene locally. Since the formation energy of single or multiple vacancies in graphene is above 7 eV, the replacement of carbon by other atoms needs an energetic process such as the ballistic atom displacement by electron beams [3]. Therefore, both defect formation and interaction of defective graphene with metal atoms can be observed in the same experiment in an electron microscope.

The mechanism of trapping metal atoms in graphene was studied by creating defects in the graphene lattice under electron irradiation while metal atoms were migrating on the surface of graphene [4, 5]. In a certain temperature range, tungsten atoms were seen to be trapped in localized defects but can also escape from the defects at sufficiently high temperature. A detailed analysis in a combination of experiments and computation shows that reconstructed divacancies (figure 1) such as the 555-777 type (3 pentagons and 3 heptagons) act as traps, binding the metal atom with an energy of 2 eV [4]. A direct replacement of carbon by metal atoms was excluded, showing the instability of single vacancies in graphene at elevated temperatures. The diffusive migration of trapped Au and Pt atoms was also studied by *in-situ* observation of the metal atoms. Activation energies of the order 2.5 eV were obtained [6].

Trapping of metal atoms at defects in graphene can also be induced selectively with atomic precision. In an electron microscope with aberration-corrected condenser, the electron beam spot with a diameter of 1 Å was focused on pre-selected positions of the graphene lattice, leading to subsequent trapping of metal atoms in these locations [5]. This was used to create a pattern of dots, decorated with foreign atoms, on a graphene sheet.

The interaction between graphene and catalytically active bulk crystals was studied by heating a bilayer system, consisting of an amorphous carbon film covered with a polycrystalline layer of Fe, Ni, or Co. Above approximately 600°C, the dissolution of carbon in the metal layer was observed, followed by the segregation of single- or multi-layer graphene on the metal surface (figure 2) [6]. Ostwald ripening of the metal crystals at increasing temperature allowed us to liberate the graphene areas and thus to observe the growth of graphene in-situ. This is a solid-state growth process (no gases are involved) which is induced by the lowering of the energy of the carbon system from the energetically higher amorphous phase to graphene by using a catalytically active metal. At the same time, the metal crystals act as a diffusion channel for carbon atoms.

References:

[1] F. Banhart, Nanoscale 1 (2009), 201
[2] F. Banhart, J. Kotakoski, A. Krasheninnikov, ACS Nano, DOI 10.1021/nn102598m.
[3] A. Krasheninnikov, F. Banhart, Nature Materials 6 (2007), 723.
[4] O. Cretu, A. V. Krasheninnikov, J. A. Rodríguez-Manzo, R. Nieminen, F. Banhart, Phys. Rev. Lett. 105 (2010) 196102.
[5] J. A. Rodríguez-Manzo, O. Cretu, F. Banhart, ACS Nano 4 (2010) 3422.
[6] Y. Gan, L. Sun, F. Banhart, Small, 4 (2008), 587.
[7] J. A. Rodríguez-Manzo, C. Pham-Huu, F. Banhart, ACS Nano, in the press.

Figures:

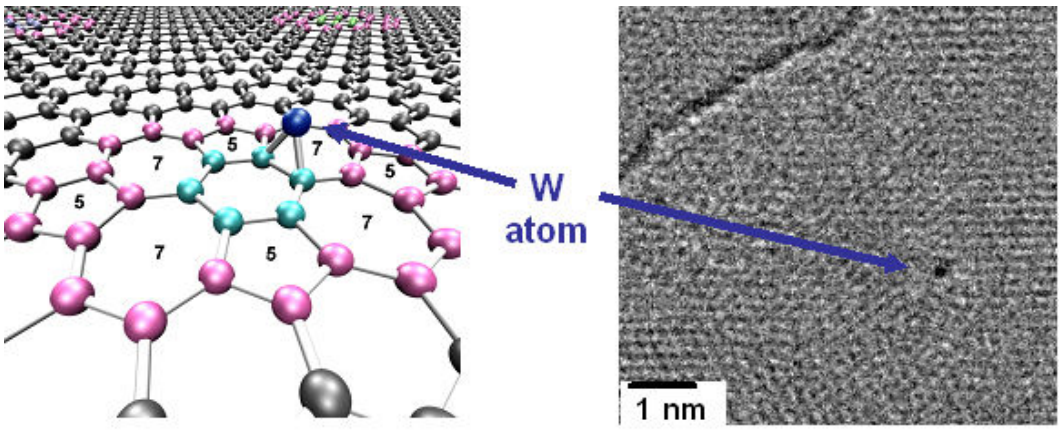

Figure 1: *Trapping of a W atom on a reconstructed divacancy such as the (5555-6-7777)-defect as shown in the model on the left hand side. The Electron microscopy image shows a W atom trapped on such a defect in the uppermost layer of a multi-layer graphene sheet [4].*

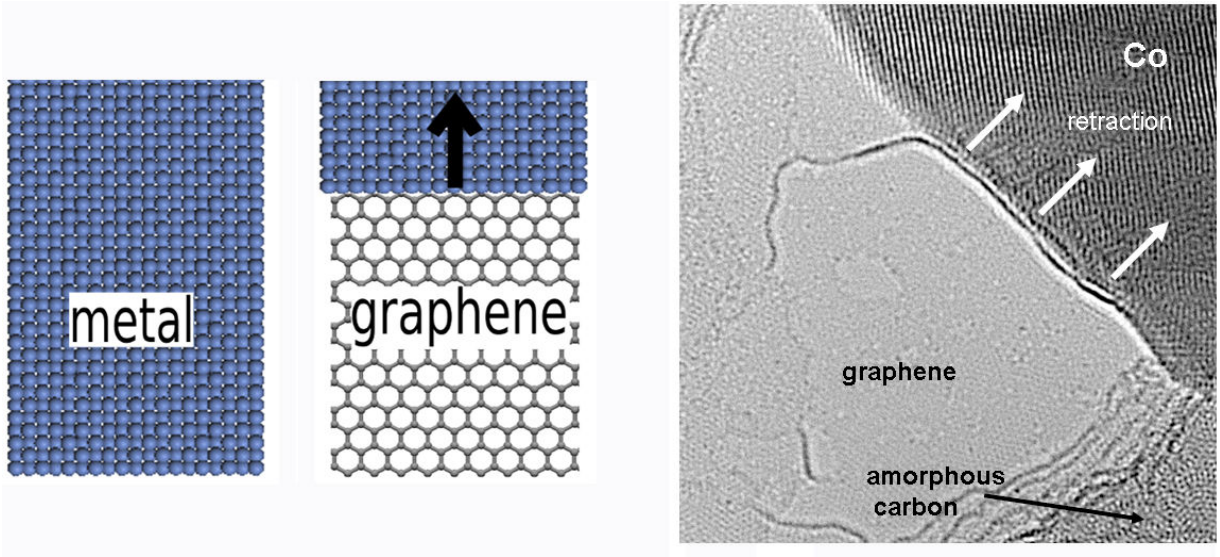

Figure 2: *Solid-state transformation of amorphous carbon to graphene in the presence of a catalytically active transition metal. The metal initially covers the amorphous carbon film. After heating, the amorphous carbon is taken up by the metal. Subsequently, graphene nucleates on the metal surface which can be seen as the metal retracts by a ripening effect (model image on the left hand side). The TEM image shows a retracting Co crystal, leaving a graphene layer in its trace [7].*

GRAPHENE-BASED NATURAL DYE-SENSITIZED SOLAR CELLS

Francesco Bonaccorso[a], Giuseppe Calogero[b], Giulia Privitera[a], Onofrio M. Maragò[b], Pietro G. Gucciardi[b], Gaetano Di Marco[b] and Andrea C. Ferrari[a]

[a] Engineering Department, Cambridge University, 9 JJ Thomson Avenue, Cambridge, UK
[b] Istituto per i Processi Chimico-Fisici, via Ferdinando Stagno-D'Alcontres 37, 98158 Faro Superiore, Messina, Italy
fb296@cam.ac.uk

Dye-sensitized solar cells (DSSCs) [1] have attracted much attention due to their good light-to-electricity conversion efficiency and simple fabrication. The counter electrode (CE) employed for the regeneration of electrolyte is commonly constituted of a catalytic Platinum (Pt) film deposited on TCOs. TCOs, usually Indium Tin-oxide (ITO) and Fluorine-doped Tin-oxide (FTO), require high temperature processing, hindering the deposition on some substrates (e.g., polymeric substrates). Moreover, they are brittle, limiting their use in applications where flexibility is required. On the other hand, Pt tends to degrade over time when in contact with the (I^-/I_3^-) liquid electrolyte, reducing the overall efficiency of DSSCs [2]. Thus, the replacement of such elements with low-cost and/or more versatile materials is at the centre of an ongoing research effort. In this context carbonaceous materials feature good catalytic properties, electronic conductivity, corrosion resistance towards iodine, high reactivity, abundance, and low cost [3,4]. Another fundamental part of a DSSC is the dye. Generally, transition metal coordination compound complexes [5] and synthetic organic dyes [6] are used as effective sensitizers in DSSCs. However, the preparation routes for these dyes are based on tedious and expensive chromatographic purification procedures. Natural dyes and their organic derivatives are non toxic, biodegradable, low in cost, renewable and abundant, so they are the ideal candidate for environmentally friendly solar cells [7].

Here we show that the combination of graphene and natural sensitizers opens up new scenarios for totally green, natural, environmentally friendly and low cost DSSCs, Figure 1. In particular, its unique electronic [8] and optical properties [9] make graphene an attractive material for CEs in DSSCs. Indeed, graphene matches all the key requirements needed for CE materials such as high specific surface area, high exchange current density and low charge-transfer resistance.

Graphene thin films were produced by liquid phase exfoliation of graphite [10], and spin-casted on stainless steel, FTO and glass. We show that graphene CEs have promising activity, similar to the Pt one. Indeed, DSSCs assembled with CE made of graphene deposited onto FTO (1.42%) outperform the total conversion efficiency of those based on Pt (1.21%). Moreover, we show that graphene, contrary to Pt, can both catalyses the reduction of tri-Iodide and back transfers the electrons arriving from the external circuit to the redox system. DSSCs assembled with graphene deposited onto glass as CE show efficiency ~0.8%. This demonstrates the potential of graphene to simultaneously replace both the Pt catalyst and the conductive glass. We also demonstrate an environmentally friendly DSSC assembled using natural dyes, which show high Internal Photocurrent Efficiency (Figure 2), and graphene as CE with efficiency of ~ 0.40%.

References:

[1] B. O'Regan, M. Gratzel, Nature, 353, (1991), 737.
[2] B.K. Koo, et al. Journal of Electroceramics, 17, (2006), 79.
[3] G. Calogero, et al. Dalton Transaction, 39, (2010), 2903.
[4] A.Kay and M. Gratzel, Solar.Ener. Mater. Solar Cells, 44, (1996), 99.
[5] M. K. Nazeeruddin, et. al. J. Am. Chem. Soc., 115, (1993), 6382.
[6] J. H. Yum, et. al. J. Am. Chem. Soc., 129, (2007), 10320.
[7] G. Calogero, G. Di Marco, Solar Energy Material & Solar Cells, 92, (2008), 1341.
[8] A. K. Geim and K. S. Novoselov, Nat. Mater., 6, (2007), 183.
[9] F. Bonaccorso et al. Nat. Photon., 4, (2010), 611.
[10] Y. Hernandez et al. Nat. Nano., 3, (2008), 563.

Figures:

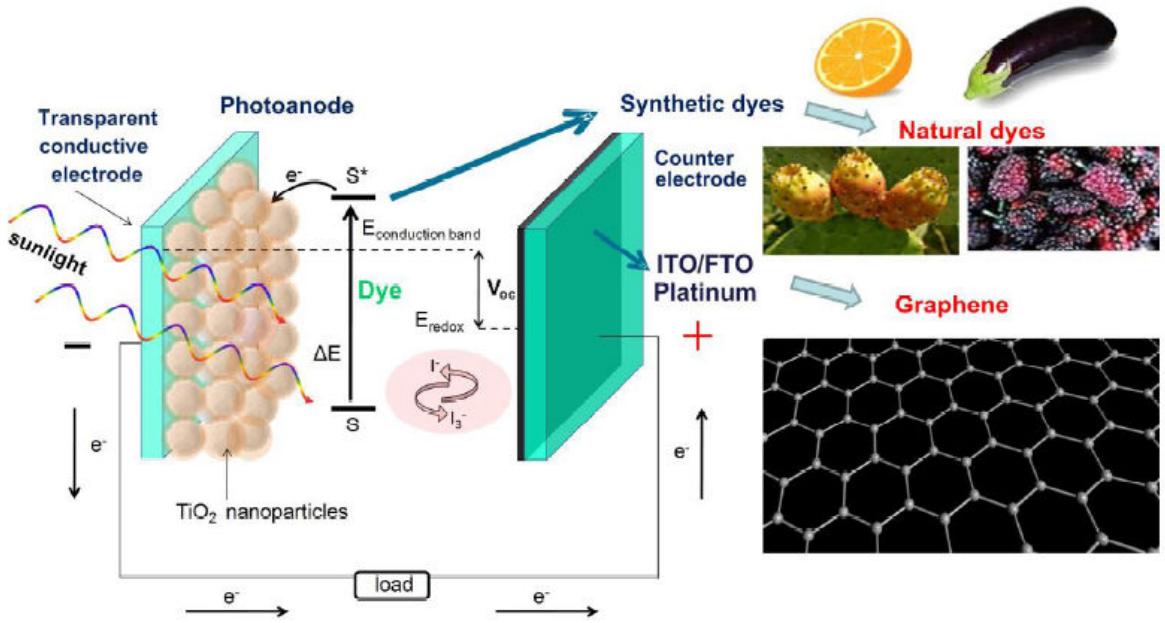

Figure 1: *Schematic representation of the where the synthetic dyes are replaced by the natural dyes and graphene is used at the CE to simultaneously replace TCO films and Pt.*

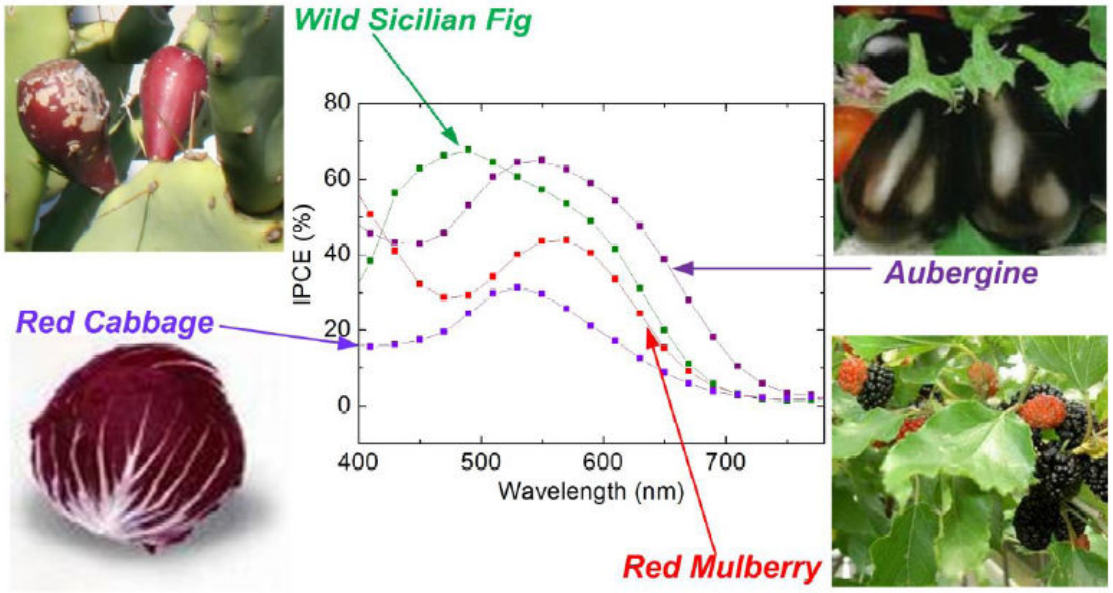

Figure 2: *Internal Photocurrent Efficiency spectra of: Wild Sicilian Fig (green line), Aubergine (purple line), Red Mulberry (red line) and Red Cabbage (violet line).*

HYSTERESIS LOOPS OF THE MAGNETOCONDUCTANCE IN GRAPHENE DEVICES

Andrea Candini[a], Christian Alvino[a,b], Wolfgang Wernsdorfer[c] and Marco Affronte[a,b]

[a] Istituto Nanoscienze – CNR Centro S3, Modena. Via Campi 213/a 41125 Modena. Italy
[b] Dipartimento di Fisica, Università di Modena e Reggio Emilia, Via Campi 213/a 41125 Modena. Italy
[c] Institut Néel, CNRS, BP166, 25 Av des Martyrs, 38042 Grenoble, France
andrea.candini@unimore.it

We report a systematic study of the low temperature magnetoconductance of various graphene devices with the field applied in the plane of graphene. At temperatures below 1K, the magnetoconductance signal depends on the gate and its sign is related to universal conductance fluctuations. When the field is swept at high enough rates (dB/dt > 10mT/s) a hysteresis is observed in the signal. We have systematically measured different devices of various sizes, form unpatterned large flakes down to narrow ribbons (50nm large) and constrictions (30nm in width), finding that the magnetic signal does not depend on the size nor on the transport regime of the device. We attribute the origin of the signal to the magnetization reversal of paramagnetic centers in graphene, which might originate from structural defects in the graphene layer, most probably vacancies [1]. Based on the field and temperature dependencies of the hysteresis, we conclude that the spin of the localized moments is higher than S = 1/2, in agreement with recent works[2,3].

References:

[1] A. Candini et al. accepted for publication in Phys Rev. B (2011) and selected as an Edotor's Suggestion. Available online at: arXiv:1101.3030v1
[2] M. Sepioni et al., Phys. Rev. Lett. 105, (2010) 207205
[3] D.W. Boukhvalov et al., arXiv:1012.3828v1 (2010)

Figures:

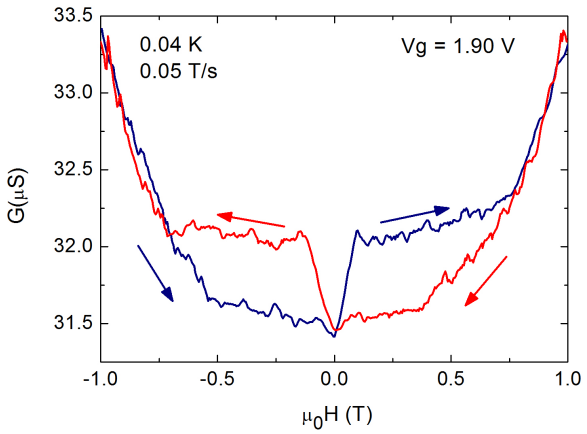

Figure 1: *Parallel magnetoconductance of a graphene device for a fixed gate voltage, taken at 0.04 K and at a field sweep rate of 0.05 T/s. The hysteresis is clearly visible. Figure taken from reference [1].*

MOBILITY OF SUSPENDED BILAYER GRAPHENE AT FINITE TEMPERATURE

Eduardo V. Castro[1], Héctor Ochoa[1], M. I. Katsnelson[2], F. Guinea[1]

[1]Instituto de Ciencia de Materiales de Madrid, CSIC, Cantoblanco, E-28049 Madrid, Spain
[2]Radboud Univ Nijmegen, Inst for Molecules and Materials, NL-6525 AJ Nijmegen, The Netherlands
evcastro @icmm.csic.es

Recent realization of suspended monolayer [1, 2] and bilayer [3] graphene samples made possible a direct probe of the intrinsic, unusual properties of these systems. In particular, intrinsic scattering mechanisms limiting mobility may now be unveiled [4]. In a recent publication we have shown [5] that in suspended, non-strained monolayer graphene room temperature mobility is limited to values observed for samples on substrate due to scattering by out of plane – flexural – acoustic phonons. This limitation can, however, be avoided by applying tension. Bilayer graphene has a different low energy electronic behavior as well as different electron-phonon coupling. It is then natural to wonder what is the situation in the bilayer regarding electron scattering by acoustic phonons, and in particular by flexural phonons.

In the present contribution, after reviewing the single layer graphene case, we will present our recent results for scattering by both acoustic in-plane phonons and flexural phonons in doped, suspended bilayer graphene. We have found the bilayer membrane to follow the qualitative behavior of the monolayer cousin [5]. Different electronic structure combine with different electron-phonon coupling to give the same parametric dependence in resistivity, and in particular the same temperature behavior. In parallel with the single layer, flexural phonons dominate the phonon contribution to resistivity in the absence of strain, where a density independent mobility is obtained. This contribution is strongly suppressed by tension, similarly to monolayer graphene [5]. However, an interesting quantitative difference with respect to suspended monolayer has been found. In the latter, as shown in [5], flexural phonons limit room temperature mobility to values obtained for samples on substrate,.~1 $m^2/(Vs)$, when tension is absent. In bilayer, quantitative differences in electron-phonon coupling and elastic constants lead to a room temperature mobility enhanced by one order of magnitude, ~10–20 $m^2/(Vs)$, even in nonstrained samples. This finding has obvious advantages for electronic applications.

References:

[1] K. I. Bolotin, K. J. Sikes, Z. Jiang, G. Fudenberg, J. Hone, P. Kim, and H. L. Stormer, Solid State Commun., 146 (2008) 351.
[2] X. Du, I. Skachko, A. Barker, and E. Y. Andrei, Nature Nanotech., 3 (2008) 491.
[3] B. E. Feldman, J. Martin, and A. Yacoby, Nature Phys., 5 (2009) 889.
[4] S. V. Morozov, K. S. Novoselov, M. I. Katsnelson, F. Schedin, D. Elias, J. A. Jaszczak, and A. K. Geim, Phys. Rev. Lett. 100 (2008) 016602.
[5] Eduardo V. Castro, H. Ochoa, M. I. Katsnelson, R. V. Gorbachev, D. C. Elias, K. S. Novoselov, A. K. Geim, and F. Guinea, Phys. Rev. Lett. 105 (2010) 266601.

STRAIN ENGINEERING IN GRAPHENE

Antonio Castro Neto

Department of Physics, Boston University, USA
Graphene Research Centre, National University of Singapore

Graphene is a unique example of a one atom thick metallic membrane. Hence, graphene brings together properties of soft and hard condensed matter systems. The elementary electronic excitations in graphene, the Dirac quasiparticles, couple in a singular way to structural distortions in the form of scalar and vector potentials. Therefore, graphene has an effective electrodynamics where structural deformations couple to the Dirac particles at equal footing to electric and magnetic fields. This so-called strain engineering of the electronic properties of graphene opens doors for a new paradigm in terms of electronic devices, where electronic properties can be manipulated at will using its membrane-like properties.

GRAPHENE: PROPERTIES, PREPARATION AND APPLICATION PERSPECTIVE

Yongsheng Chen

State Key Laboratory for Functional Polymer Materials and Center for Nanoscale Science & Technology, Institute of Polymer Chemistry, College of Chemistry, Nankai University, Tianjin 300071, China

The large scale preparation and characterization of graphene materials and their hybrid and composite materials, together with their various device applications will be presented. These include the results for organic photovoltaic device, light emission device, transparent electrode and memory device, room-temperature ferromagnetism, nonlinear optical limiting, electromagnetic interference shielding and absorbing and photoconducting applications and so on.

References:

[1] "Organic Photovoltaic Devices Based on a Novel Acceptor Material: Graphene", Zunfeng Liu, Qian Liu, Xiaoyan Zhang, Yi Huang, Yanfeng Ma, Shougen Yin* and Yongsheng Chen* Adv Mater. 2008. 20, 3924.

[2] "Evaluation of Solution-Processed Reduced Graphene Oxide Films as Transparent Conductors", Hector A. Becerril, Jie Mao, Zunfeng Liu, Randall M. Stoltenberg, Zhenan Bao, and Yongsheng Chen*, ACS Nano, 2008, 2, 463.

[3] "A Graphene Hybrid Material Covalently Functionalized with Porphyrin: Synthesis and Optical Limiting Property", Yanfei Xu, Zhibo Liu, Xiaoliang Zhang, Yan Wang, Jianguo Tian, Yi Huang, Yanfeng Ma, Xiaoyan Zhang, Yongsheng Chen* Adv Mater. 2009. 21, 1275.

[4] "Molecular-level Dispersion of Graphene into Poly(vinyl alcohol), and Effective Reinforcement of Their Nanocomposites", Jiajie Liang, Yi Huang, Long Zhang, Yan Wang, Yanfeng Ma, Tianyin Guo and Yongsheng Chen*, Adv Funct Mater, 2009,19, 2297

[5] "Polymer photovoltaic cell based on a solution processable graphene and P3HT", Qian Liu, Zunfeng Liu, Xiaoyan Zhang, LiyingYang, Nan Zhang, Guiling Pan, Shougen Yin,* Yongsheng Chen*, and Jun Wei, Adv Funct Mater, 2009, 19, 894

[6] "Photoconductivity of Bulk Films Based on Graphene Sheets", Xin Lv, Yi Huang, Zhibo Liu, Jianguo Tian, Yan Wang, Yanfeng Ma, Jiajie Liang, Shipeng Fu, Xiangjian Wan, Yongsheng Chen*, Small, 2009, 5,1682.

[7] "Room temperature ferromagnetism of graphene", Yan Wang, Yi Huang, You Song, Xiaoyan Zhang, Yanfeng Ma, Jiajie Liang, Yongsheng Chen*, Nano Lett, 2009, 9, 220

[8] "Size-controlled synthesis of graphene oxide sheets on a large scale using chemical exfoliation", Long Zhang, Jiajie Liang, Yi Huang, Yanfeng Ma, Yan Wang, Yongsheng Chen*, Carbon, 2009, 47, 3365

[9] "Supercapacitor devices based on graphene materials",Yan Wang, Zhiqiang Shi, Yi Huang, Yanfeng Ma, Chengyang Wang, Mingming Chen, Yongsheng Chen*; J Phys Chem C, 2009, 113, 13103.

[10] "Infrared-triggered actuators from graphene-based nanocomposites", Jiajie Liang, Yanfei Xu, Yi Huang*, Long Zhang, Yan Wang, Yanfeng Ma, Feifei Li, Tianying Guo, Yongsheng Chen*, J Phys Chem C, 2009, 113, 9921.

[11] "Toward All-Carbon Electronics: Fabrication of Graphene-Based Flexible Electronic Circuits and Memory Cards Using Maskless Laser Direct Writing",Jiajie Liang, Yongsheng Chen, Yanfei Xu, Zhibo Liu, Long Zhang, Xin Zhao, Xiaoliang Zhang, Jianguo Tian, Yi Huang, Yanfeng Ma, Feifei Li; ACS Appl. Mater. Interfaces, 2010, 2, 3310.

[12] "Fabrication and Evaluation of Solution-Processed Reduced Graphene Oxide Electrodes for p- and n-Channel Bottom-Contact Organic Thin-Film Transistors",Hector A. Becerril, Randall M. Stoltenberg,Ming Lee Tang, Mark E. Roberts, Zunfeng Liu,Yongsheng Chen, Do Hwan Kim, Bang-Lin Lee, Sangyoon Lee, and Zhenan Bao ACS Nano, 2010, 4, 6343.

[13] "Flexible, Magnetic and Electrically Conductive Graphene/Fe3O4 Paper and Its Application for Magnetic-Controlled Switches",Jiajie Liang, Yanfei Xu, Dong Sui, Long Zhang, Yi Huang, Yanfeng Ma, Feifei Li, Yongsheng Chen J Phys Chem C, 2010, 114, 17465.

[14] "Towards Flexible All-Carbon Electronics: Flexible Organic Field-Effect Transistors and Inverter Circuits Using Solution-Processed All Graphene Source/Drain/Gate Electrodes",Yongsheng Chen, Yanfei Xu, Kai Zhao, Xiangjian Wan, Jiachun Deng, Weibo Yan Nano Res, 2010, 10, 714.
[15] "Solution-processed bulk heterojunction organic solar cells based on an oligothiophene derivative", Bin Yin, Liying Yang, Yongsheng Liu, Yongsheng Chen, Qingjin Qi, Fengling Zhang, and Shougen Yin Appl. Phys. Lett., 2010, 97, 023303.

THERMAL EXPANSION COEFFICIENT OF SINGLE-LAYER GRAPHENE MEASURED BY RAMAN SPECTROSCOPY

Duhee Yoon,[1] Young-Woo Son,[2] and **Hyeonsik Cheong**[1*]

[1]Department of Physics, Sogang University, Seoul 121-742, Korea,
[2]School of Computational Sciences, Korea Institute for Advanced Study, Seoul 130-722, Korea
hcheong@sogang.ac.kr

Graphene is attracting much interest due to potential application as next generation electronic material as well as its unique physical properties. In particular, its superior thermal and mechanical properties, including high thermal conductivity and extremely high mechanical strength that exceeds 100 GPa, make it a prime candidate material for heat control in high-density, high-speed integrated electronic devices. For such applications, knowledge of the thermal expansion coefficient (TEC) as a function of temperature is crucial, but so far few reliable measurements on the TEC have been reported [1]. Several authors have calculated the TEC using various models [2-6]. Mounet *et al*. estimated the TEC of graphene as a function of temperature by using a first-principles calculation and predicted that graphene has a negative TEC at least up to 2500 K [6]. Bao *et al*. experimentally estimated the thermal coefficient in the temperature range of 300 – 400 K by monitoring the miniscule change in the sagging of a graphene piece suspended over a trench and found that it is negative only up to ~350 K [1]. It is not yet clear whether this discrepancy between theory and experimental data is caused by uncertainties in the accuracy of the experimental measurements or limitations in the theoretical calculation. Since precise knowledge of the TEC in the temperature range around room temperature is crucial in designing graphene-based devices and heat management systems, more precise measurements are needed. In this work, we analyze the temperature-dependent shift of the Raman *G* band of monolayer graphene on SiO_2 to estimate the TEC of graphene. We find that the data can be explained in the temperature range of 200 – 400 K with the help of the calculated temperature dependence of the Raman *G* band of free standing graphene.

When the temperature of a graphene sample fabricated on a SiO_2/Si substrate is raised, two effects should be considered: the temperature dependence of the phonon frequencies and the modification of the phonon dispersion due to strain caused by mismatch of the TEC'ss of the substrate and graphene. The Raman frequency shift of the *G* band of free standing graphene as a function of temperature has been estimated by first-principles calculations [7]. Since most graphene samples are fabricated on SiO_2 substrates or over a trench held at the edges, the pure effect of temperature change on the Raman spectrum cannot be measured directly and compared with the theory. The discrepancy between the experimentally measured Raman frequency shift and the theoretical prediction can be reconciled by accounting for the TEC mismatch between the substrate and graphene.

Graphene samples used in this work were prepared on silicon substrates covered with a 300-nm-thick SiO_2 layer by mechanical exfoliation of natural graphite flakes. The number of graphene layers was determined by inspecting the line shape of the Raman 2*D* band. Temperature-dependent Raman spectra of graphene and graphite were obtained while cooling and heating the samples in a microscope cryostat where the temperature could be controlled between 4.2 K and 475 K. The 514.5-nm line of an Ar ion laser was used as the excitation source, and low power (< 0.3 mW) was used to avoid unintentional heating. A long-working-distance microscope objective (40x, 0.6 N.A.) was used to focus the laser beam onto the sample and collect the scattered light. The Raman scattered light signal was dispersed by a Jobin-Yvon Triax 550 spectrometer (1800 grooves/mm) and detected with a liquid-nitrogen-cooled CCD detector. The spectral resolution was ~0.7 cm^{-1}.

Figure (a) shows the frequency shifts of the Raman *G* band of single-layer graphene (SLG), bilayer graphene (BLG), and graphite samples as functions of temperature. The Raman peaks redshift as temperature rises and blueshift as temperature falls from room temperature. The Raman peak shift of SLG as a function of temperature is largest. Temperature-dependent Raman shift is commonly attributed to thermal expansion of the lattice and an anharmonic effect which changes the phonon self-energy. As the temperature rises, the SiO_2 layer expands whereas the graphene sheet contracts. This TEC mismatch would induce a biaxial tensile strain on the graphene sample. When the sample is cooled, a compressive strain is induced instead. In order to interpret our data correctly, we should

consider the effect of stain on graphene induced by the TEC mismatch between the SiO_2 layer and the graphene sheet.

We estimated the TEC by fitting our data to the theoretical prediction [7] of temperature dependence of the Raman *G* band of *free standing* graphene. Figure (b) shows the temperature dependent TEC obtained from the fitting. TEC at room temperature is estimated to be -9×10^{-6} K^{-1}, which is similar to the previous experimental value of -7×10^{-6} K^{-1} [1].

References:

[1] W. Z. Bao et al., Nat. Nanotechnol. 4 (2009) 562.
[2] P. K. Schelling, and R. Keblinski, Phys. Rev. B 68 (2003) 035425.
[3] Y. K. Kwon, S. Berber, and D. Tomanek, Phys. Rev. Lett. 92 (2004) 015901.
[4] K. V. Zakharchenko, M. I. Katsnelson, and A. Fasolino, Phys. Rev. Lett. 102 (2009) 046808.
[5] J. W. Jiang, J. S. Wang, and B. W. Li, Phys. Rev. B 80 (2009) 205429.
[6] N. Mounet, and N. Marzari, Phys. Rev. B 71 (2005) 205214.
[7] N. Bonini, M. Lazzeri, N. Marzari, and F. Mauri, Phys. Rev. Lett. 99 (2007) 176802.

Figures:

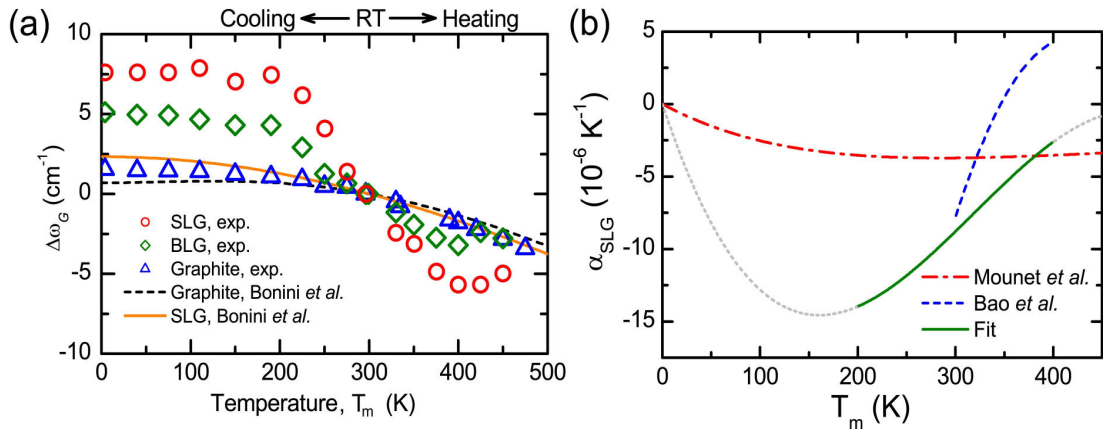

Figure 1: *(a) Raman frequency shifts of graphene and graphite as functions of temperature. (b) Thermal expansion coefficient of single layer graphene that gives the best fit between data and theoretical estimate.*

OPTO-ELECTRONIC PROPERTIES OF GRAPHENE OXIDE

Manish Chhowalla

Rutgers - The State University of New Jersey; Department of Materials Science and Engineering;
607 Taylor Road, Piscataway, NJ 08854, USA

The In this presentation, a solution based method that allows uniform and controllable deposition of reduced graphene oxide (GO) thin films with thicknesses ranging from a single monolayer up to several layers over large areas will be described. The oxidation treatment during synthesis of GO creates sp^3 C-O sites where oxygen atoms are bonded in the form of various functional groups. GO is therefore a two dimensional network of sp^2 and sp^3 bonded atoms, in contrast to an ideal graphene sheet which consists of 100% sp^2 carbon atoms. The most notable difference between GO and graphene is that photoluminescence from blue to red emission can be observed. The atomic and electronic structure along with tunable photoluminescence of graphene oxide at various degrees of reduction will be described.

High temperatures (~ 1000 ºC) are typically required for efficient removal of oxygen functional groups from GO. Furthermore, the attractive properties of graphene are not fully recovered due to creation of structural defects and the presence of residual oxygen in the reduced material. In the second part of the talk, the synthesis and properties of partially oxidized graphene (POG), a material that exhibits significantly different chemical structure to GO will be described. Due to low initial oxygen content, as-synthesized POG can be reduced in mild annealing conditions (< 300 ºC). Our results suggest that fine-tuning the oxidation chemistry of graphene will allow bulk production of highly soluble graphene without extensively compromising its intrinsic properties. We will demonstrate that partial oxidation approach opens up new promising routes to high-performance graphene-based electronics plastic platforms.

UNIFORM MONOLAYER GRAPHENE IN 6-INCH SCALE: ITS ORIGIN AND APPLICATION

Hyun-Jong Chung, David Seo, Sung-Hoon Lee, Jinseong Heo, Heejun Yang, Hyun Jae Song, Seongjun Park

Samsung Advanced Institute of Technology, San 14, Nongseo-dong, Giheung-gu, Yongin-si, Gyeonggi-do Korea

hyunjong.chung@samsung.com

Monolayer graphene has been grown on Cu thin film in 6-inch scale at low temperature using inductive coupled plasma chemical vapor deposition. More than 99% of the film is single layer according to Raman mapping and optical microscopy. [1] Scanning tunneling microscopy and spectroscopy study reveals line structure and undisturbed spectroscopy of graphene which could be the origin of the thinner layer than thermally grown graphene on Cu foil. [2] More than 2000 Hall bars were fabricated on the 6-inch wafer and measured Id-Vg and Id-Vd curves. Also, screening effect for multi-layer graphene was measured using Kelvin probe force microscopy. [3]

References:

[1] J. Lee et al., IEDM (2011).
[2] Jeon et al., ACS Nano, 3 (2011) 1915.
[3] N.J. Lee et al., Appl. Phys. Lett., 22 (2009) 222107.

GRAPHENE FOR BEYOND CMOS DEVICES

Luigi Colombo[1] and Rodney S. Ruoff[2]

[1]Texas Instruments Incorporated, Dallas, TX 75243, USA
[2]Department of Mechanical Engineering and the Texas Materials Institute, 1 University Station C2200, The University of Texas at Austin, Austin, TX 78712-0292, USA
colombo@ti.com

Electronic devices fabricated on silicon, III-V, and II-VI compounds require the highest quality material that can be achieved in order to meet the performance, uniformity, reliability, and cost requirements. The semiconductor industry has demonstrated the ability to produce and provide high quality and reliable devices to the community for many decades as a result of its ability to produce and integrate the highest quality materials. As we move toward trying to replace the basic electronic device, the transistor, with new materials whether it is using Ge, III-Vs or graphene, the highest quality material will be needed to continue meeting the stringent requirements.

Graphene is being studied as a new switch material for devices beyond CMOS. Assuming that the material has the necessary fundamental properties required to fabricate the new switch, namely a Bose-Einstein condensate (BEC), it is will be necessary to grow large area films with the highest quality in order to fabricate these new devices in a manufacturing environment. Graphene will have to be integrated with dielectrics and metals to fabricate the simplest device structures and thus it may be necessary to grow this material defect free. Graphene can be produced by several techniques: 1) exfoliation from bulk graphite [1-3]; 2) chemical reduction of exfoliated graphite oxide [4]; 3) precipitation from bulk metals [5-7]; 4) growth on SiC by silicon desorption [8,9]; and 5) chemical vapor deposition on copper surface [10] or metal surfaces with extremely C solubility of C diffusivity. Growth on very low carbon solubility substrates like copper occurs by a surface mediated process and can cover extremely large areas. Recently Li et al. [11] have also discovered that large single crystals can be grown without domains or grain. The objective of this presentation is to describe the growth process of graphene on metals and how we can use this process to create high quality large area graphene. Figure 1 shows an SEM image of a single graphene domain that according to LEEM (Li et al) is single crystal across the entire domain (400 to 500 □m) [11].

References:

[1] Lu, X. K.; Yu, M. F.; Huang, H.; Ruoff, R. S. Nanotechnology 1999, 10, 269-272.
[2] Novoselov, K. S.; Geim, A. K.; Morozov, S. V.; Jiang, D.; Zhang, Y.; Dubonos, S. V.; Grigorieva, I. V.; Firsov, A. A. Science 2004, 306, 666-669.
[3] Zhang, Y. B.; Small, J. P.; Pontius, W. V.; Kim, P. Appl. Phys. Lett. 2005, 86.
[4] Stankovich, S.; Dikin, D. A.; Piner, R. D.; Kohlhaas, K. A.; Kleinhammes, A.; Jia, Y.; Wu, Y.; Nguyen, S. T.; Ruoff, R. S. Carbon 2007, 45, 1558-1565.
[5] Eizenberg, M.; Blakely, J. M. Surf. Sci. 1979, 82, 228-236.
[6] Hamilton, J. C.; Blakely, J. M. Surf. Sci. 1980, 91, 199-217.
[7] Reina, A.; Thiele, S.; Jia, X. T.; Bhaviripudi, S.; Dresselhaus, M. S.; Schaefer, J. A.; Kong, J. Nano Res. 2009, 2, 509-516.
[8] Van Bommel, A. J.; Crombeen, J. E.; Van Tooren, A. Surf. Sci. 1975, 48, 463-472.
[9] Berger, C.; Song, Z.; Li, T.; Li, X.; Ogbazghi, A. Y.; Feng, R.; Dai, Z.; Marchenkov, A. N.; Conrad, E. H.; First, P. N.; de Heer, W. A. The Journal of Physical Chemistry B 2004, 108, 19912-19916.
[10] Li, X.; Cai, W.; An, J. H.; Kim, S.; Nah, J.; Yang, D.; Piner, R.; Velamakanni, A.; Jung, I.; Tutuc, E.; Banerjee, S. K.; Colombo, L.; Ruoff, R. S. Science 2009, 324, 1312-1314.
[11] Li, X.; Magnuson, C. W.; Venugopal, A.; Tromp, R. M.; Hannon, J. B.; Vogel, E. M.; Colombo, L.; Ruoff, R. S. J. Am. Chem. Soc., 133, 2816-2819.

Figures:

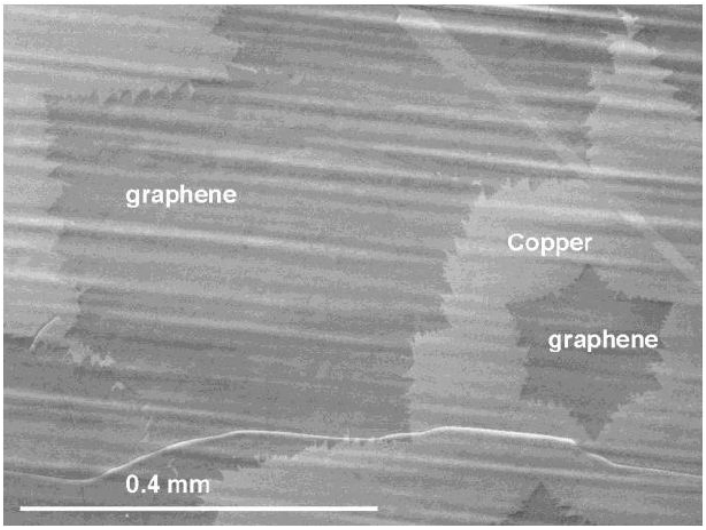

Figure 1: *Large single crystals of graphene grown by low pressure chemical vapor deposition. LEEM analysis has shown that these crystals are mostly single crystals. (Li et al.).*

BAND-GAP ENGINEERING IN GRAPHENE THROUGH FUNCTIONALIZATION WITH FLUORINE

M.F. Craciun[1], F. Withers[2], M. Dubois[3], A. K. Savchenko[2] and S. Russo[2]

[1]Centre for Graphene Science, School of Engineering, University of Exeter, Exeter EX4 4QF, UK
[2]Centre for Graphene Science, School of Physics, University of Exeter, Exeter EX4 4QL, UK
[3]Laboratoire des Matériaux Inorganiques, Clermont Université–UBP, CNRS-UMR 6002, 63177 Aubière, France
M.F.Craciun@exeter.ac.uk

Rece Graphene – a single layer of sp^2 bonded carbon atoms arranged in a honeycomb pattern – is an indefinitely large aromatic molecule, of unique interest in the field of transparent organic electronics. This is a transparent material where charge carriers (relativistic Dirac fermions) exhibit mobilities (>10^6 cm^2/Vs) higher than Si at room temperature. However, the energy dispersion of graphene is gap-less, and this would limit its applications in electronic devices. For instance, in a graphene-based transistor the absence of the gap in the band-structure results in a relatively small resistance difference between the electro-neutrality (Dirac) region and a region with large carrier concentration (i.e., between the "on" and "off" states). Due to this significant limitation in the use of graphene in electronics, intensive research is currently underway aimed at the creation of a (tunable) gap in graphene's energy spectrum.

The ability to chemically functionalize graphene, for instance with fluorine [1] and hydrogen [2] atoms, paved the way towards band-gap engineering. This type of functionalization transforms the graphene planar crystal structure, with sp^2 bonds between the carbon atoms, into a three-dimensional structure with sp^3 bonding between them. Theoretical predictions show that a band gap of 3.8 eV and 4.2 eV is expected for hydrogen and fluorine for 100% functionalization, respectively [3, 4].

Here I will review recent results on fluorinated graphene transistors [1] produced by mechanical exfoliation of natural graphite which is fluorinated to 24% and 100% (as measured by mass uptake). Transport measurements over a wide range of temperatures (from 4.2K to 300K) show a very large and strongly temperature dependent resistance in the electro-neutrality region. The strong temperature dependence of fluorinated graphene is due to the opening of a mobility in gap in the energy spectrum of graphene where electron transport takes place via localised electron states.

Magneto-transport experiments through fluorinated graphene as a function of gate voltage, bias voltage, and temperature show that a magnetic field systematically leads to an increase of the conductance on a scale of a few tesla. This phenomenon is accompanied by a decrease in the energy scales associated to charging effects, and to hopping processes probed by temperature-dependent measurements. All these results demonstrate that disorder induced sub-gap states originate strong localization effects in the transport of charge carriers for energies below the energy-gap of fluorinated graphene.

References:

[1] F. Withers et al., Phys. Rev. B 82 (2010), 073403
[2] D. C. Elias et al., Science 323 (2009), 610
[3] J. O. Sofo, et al., Phys. Rev. B 75 (2007), 153401
[4] D. W. Boukhvalov and M. I. Katsnelson, J. Phys.: Condens. Matter 21 (2009), 344205

EPITAXIAL GRAPHENE GROWN ON SILICON CARBIDE FOR FUNDAMENTAL PHYSICS AND NANOELECTRONICS

Walt de Heer

Georgia Institute of Technology, USA

The invention of graphene based electronics at Georgia Tech (patented in 2003 [1]) was based on carbon nanotube properties of ballistic and coherent transport as well as several other outstanding features of carbon nanotubes, including the possibility of tuning the bandgap in graphene ribbons using the ribbon width. Silicon carbide, with its natural property to produce epitaxial graphene layers after heating in vacuum was considered to be the most promising platform for graphene based electronics.

Considerable advances have since been made in realizing graphene electronics however it is clear that the field is still in its infancy. Graphene devices are not yet competitive with those produced from standard electronic materials. Nevertheless, currently, epitaxial graphene on silicon carbide is still considered to be the most viable platform for high performance graphene based electronics. (In contrast, mechanically transferred CVD graphene is showing potential for low end electronics applications; exfoliated graphene is not scaleable and backgating is not useful for electronics.) There have been demonstrations of extremely high frequency transistors and the possibility of using epitaxial graphene Hall bars as resistance standards. But there remain serious questions whether graphene based nanoelectronics can be realized. The moblities of narrow ribbons produced by standard lithography methods generally show strong localization effects and the apparent band gaps are most likely mobility gaps. Many of these problems can be traced back to edge scattering effects that ultimately result from rough and chemically poorly defined edges.

Recent work at Georgia Tech has demonstrated that many of these problems can be overcome by "growing" graphene on the edges of structures that are directly etched onto the silicon carbide in order to produce interconnected narrow graphene ribbons. These graphene ribbons are demonstrating many of the advantageous properties of carbon nanotubes. Gated ribbons show evidence of single channel ballistic transport, also observed in carbon nanotubes, and PN junctions show evidence of "Klein tunneling" effects. On the other hand, the ribbons produced by this method apparently do not have band gaps. Nevertheless, it is clear that "sidewall" graphene electronics is opening new directions in graphene based electronics, that resembles nanotube based electronics. But this does imply a departure from the standard field effect transistor paradigm of electronics.

This talk will present an overview of these developments as well as providing a survey of the vast fundamental physics that has been accomplished with graphene that it epitaxially grown on silicon carbide.

References:

[1] W.A. de Heer, C. Berger, P.N. First, US Patent No 7015142 (filed 2003, issued 2006)

GRAPHENE PROCESSING FOR ELECTRONICS AND SENSING

Shishir Kumar[1,2], Nikos Peltekis[1], Chan H. Lee[1], KangHo Lee[1], Hye-Young Kim[1],
Georg S. Duesberg[1,2]

[1]Centre for Research in Adaptive Nanostructures and Nanodevices (CRANN), Dublin 2, Irlanda
[2]School of Chemistry, Trinity College Dublin, Dublin 2, Irlanda
duesberg@tcd.ie

The unique electronic properties of graphene of potential applications in future electronic devices. The quality of graphene layers is crucial for those applications, as contamination, impurities, morphology and defects can substantially affect the electronic properties and the performance of these devices. After numerous studies on hand grafted devices CVD growth of graphene yield macroscale samples, opening a pathway to reliably fabricate devices.
Graphene surfaces are ultra sensitive to local chemical environment due to changes in their electrical properties by vicinity doping of adsorbed molecules. Their chemical stability and lithographic manufacturability make them an appealing candidate for next generation biosensors. To exploit the full potential of graphene in sensing, however, selectivity to analytes must be established.
We present a comprehensive study on large scale CVD grown graphene films. Challenges faced in structuring graphene with conventional microfabrication techniques are discussed. Mild plasma treatments for cleaning graphene surfaces and novel hardmasks are introduced, leading reproducible devices with high field effect mobilities. With extensive analysis based on high resolution XPS, Raman spectroscopy and microscopy the metallicity, defect density and contaminations can be clearly identified. This work, therefore, will help high volume processing of graphene using these scalable processes steps, yielding interconnects, FET and sensor device arrays.

ELECTRONIC STRUCTURES OF NANOGRAPHENE WITH ZIGZAG AND ARMCHAIR EDGES

Toshiaki Enoki[1], Ken-ichi Sakai[1], Shintato Fujii[1], Kazuyuki Takai[1], Kenichi Sasaki[2], Katsunori Wakabayashi[2], Takeshi Nakanishi[3], and Ken-ichi Fukui[4]

[1]Chem. Department, Tokyo Institute of Technology, Ookayama, Meguro-ku, Tokyo 152-8551, Japan
[2]International Center for Materials Nanoarchitectonics, NIMS, Namiki, Tsukuba 305-0044, Japan
[3]Nanotube Research Center, AIST, Tsukuba 305-8565, Japan
[4]Dept. of Materials Engineering Science, Osaka University, Toyonaka, Osaka 560-8531, Japan
tenoki@chem.titech.ac.jp

The electronic structure of graphene is described in terms of massless Dirac fermion with two Dirac cones (K and K') in the Brillouin zone, giving unconventional features of zero-gap semiconductor. When a graphene sheet is cut into fractions, the created edges affect seriously the electronic structure depending on the edge shape (zigzag and armchair edges) as observed with the electron wave interference and the creation of non-bonding π-electron state (edge state). We investigated the edgeinherent electronic features by STM/STS observations and Raman spectra. Graphene nanostructures were fabricated using graphene oxide with an AFM tip.

STM/STS observations of hydrogen-terminated graphene edges demonstrate that edge states are created in zigzag edges in spite of the absence of such state in armchair edges [1]. In addition, zigzag edges tend to be short and defective whereas armchair edge is long and continuous in general. These findings suggest that zigzag edge is less energetically stable in comparison with armchair edge, consistent with Clar's aromatic sextet rule. In a finite length zigzag edge embedded between armchair edges, electron confinement is observed in the edge state.

The electron wave scattering takes place differently between zigzag and armchair edges, showing different superlattice patterns in STM lattice images. In the vicinity of an armchair edge, a hexagonal pattern was observed together with a fine structure of three-fold symmetry at the individual superlattice spots [2] (Fig.1), different from the $\sqrt{3}\times\sqrt{3}$ superlattice observed in bulk graphene and also in zigzag edge. At a zigzag edge, the electron wave is subjected to the K-K intra-valley scattering without interference, whereas the K-K' inter-vallery scattering with interference takes place in the scattering event at an armchair edge. Tight binding calculation reproduces the hexagonal superlattice observed in the armchair edge. The three-fold symmetric fine structure is understood as the antibonding coupling between the adjacent spots in the hexagonal superlattice with the mediation of the wave function at the STM tip.

The Raman G-band shows the edge-shape dependence same to that observed in the STM superlattices in relation to the intra-valley/inte-rvalley transition for the scattering at zigzag/armchair edges [3]. The inter-valley scattering at an armchair edge gives specific dependence of the G-band intensity on the polarization direction of the incident beam as expressed by $\cos^2\Theta$ (Θ ; the angle between the polarization and the armchair edge direction). A nanographene ribbon of 8 nm × >1 μm prepared by heat-treatment of graphite step edges shows this angular dependence, being demonstrated to consist of pure armchair edges [4].

Single sheet graphene oxide was found to form a two dimensional arrangement of linear corrugations of oxidized lines running along the zigzag direction with an interline spacing of ca.10 nm [5] (Fig.2). This suggests that zigzag edged nanographene ribbons with a width of ca.5 nm are created between the oxidized lines. Nanofabrication by an AFM tip can allow us to create a nanostructure of graphene sheet intentionally.

References:

[1] T. Enoki, Y. Kobayashi, and K. Fukui, Inter. Rev. Phys. Chem. 26 (2007) 609.
[2] K. Sakai, K. Takai, K. Fukui, T. Nakanishi. and T. Enoki, Phys. Rev. B81 (2010) 235417.
[3] L. G. Cançado, M. A. Pimenta, B. R. A. Neves, G. Medeiros-Ribeiro, T. Enoki, Y. Kobayashi, K. Takai, K. Fukui, M. S. Dresselhaus, R. Saito, and A. Jorio, Phys. Rev. Lett. 93 (2004) 047403.
[4] K. Sasaki, R. Saito, K. Wakabayashi, and T. Enoki, J. Phys. Soc. Jpn.79 (2010) 044603.
[5] S. Fujii and T. Enoki, J. Amer. Chem. Soc. 132 (2010) 10034.

Figures:

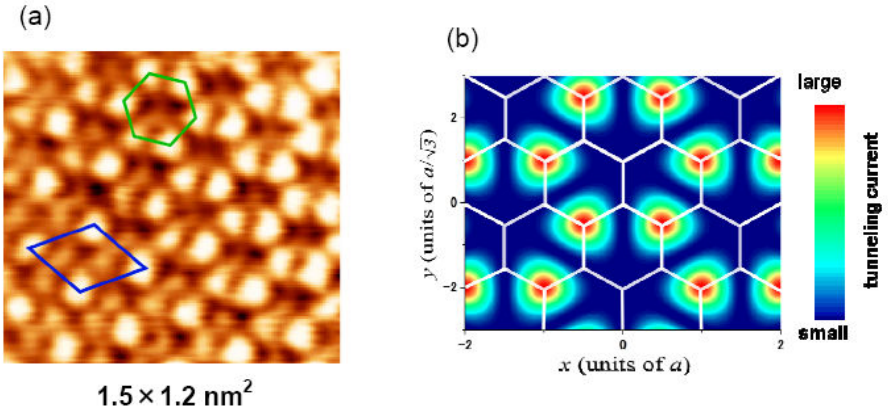

Figure 1: *(a) √3×√3 and hexagonal superlattices near an armchair edge. (b) Calculated current image of the hexagonal superlattice.*

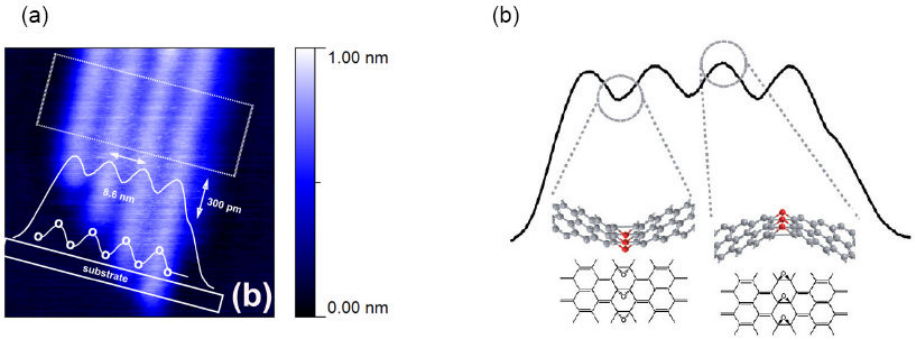

Figure 2: *(a) 1D wrinkles in graphene oxide nanohsheet observed by non-contact AFM. (b) schematic model of graphene oxide consisting of zigzag edged nanographene sheets inter-connected through oxygen bridges.*

GRAPHENE QUANTUM CIRCUITS

F. Molitor, J. Güttinger, S. Schnez, S. Dröscher, A. Jacobsen, C. Stampfer, T. Ihn and **K. Ensslin**

ETH Zurich, Switzerland

Graphene quantum dots and constrictions have been fabricated by mechanical exfoliation of graphene followed by electron beam lithography and dry etching. The single layer quality of graphene has been checked by Raman spectroscopy. The electron hole-crossover can be investigated by linear transport experiments as well as using non-linear effects in three-terminal junctions. A variety of nanostructures such as graphene constrictions, graphene quantum dots and graphene rings have been realized. Of particular interest is the electron hole crossover in graphene quantum dots, spin states as well as the electronic transport through graphene double dots. The goal is to establish the peculiar consequences of the graphene bandstructure with its linear dispersion for the electronic properties of nanostructures.

INTEGER QUANTUM HALL EFFECT IN TRILAYER GRAPHENE

W. Escoffier[1], J.M. Poumirol[1], A. Kumar[1], C. Faugeras[2], D. P. Arovas[3], M. M. Fogler[3], P. Guinea[4], S. Roche[5], M. Goiran[1] and B. Raquet[1]

[1]LNCMI, CNRS, 143 av. de rangueil, 31400 Toulouse, France
[2]LNCMI, CNRS, 25 rue des Martyrs, 38042 Grenoble, France
[3]Department of Physics, Univ. of California - San Diego, 9500 Gilman Drive, California 92093, USA
[4]Instituto de Cienca de Materiales de Madrid, CSIC, Cantoblanco E28049 Madrid, Spain
[5]Centre d'Investigaci en Nanocincia i Nanotecnologia (CSIC-ICN), UAB, 08193 Barcelona, Spain
walter.escoffier@lncmi.cnrs.fr

The Integer Quantum Hall Effect (IQHE) constitutes the hallmark of two-dimensional systems subjected to a strong perpendicular magnetic field. So far, three different realizations of 2D systems displaying distinctive IQHE features have been reported in the literature. These are conventional semiconducting heterostructures, graphene and bi-layer graphene. In the case of graphene-based systems, it has been anticipated that the dynamics of charged carriers drastically change every time an extra graphene layer in added [1,2]. Therefore, the LL spectrum of N-layer graphene systems would display unique IQHE features eventually characterizing their N.π Berry's phase [3]. This property particularly applies to trilayer graphene for which 3π Berry's phase would drastically change the sequence of QH plateaus as compared to mono or bi-layer graphene systems. Making use of both Raman spectroscopy and high field magneto-transport, we report for the first time on a fourth type of IQHE in tri-layer graphene. The sequence of QH resistance plateaus is similar to graphene, however the v=2 QH plateau is missing. The experimental data are supported by a theoretical analysis where both the Bernal and rhombohedral stacking order have been considered. We notice that a nice comparison between theoretical and experimental results is achieved only for the rhombohedral stacking order. At very high magnetic field, the QH resistance tends to vanish as the system is driven close to CNP. We show that the presence of charge puddles is necessary to explain this trend, which is further confirmed by analysing the zero-field temperature and carrier density dependence of the resistance [4].

References:

[1] F. Guinea et. al., Physcal Review B 73 (2006) 245426
[2] Daniel P. Arovas and F. Guinea, Phys. Rev. B 78 (2008) 245416 [3] M. Koshino et. al., Physcal Review B 79 (2009) 125443
[3] J.M. Poumirol et. al., Physical Review B 82 (2010) 121401(R)

Figures:

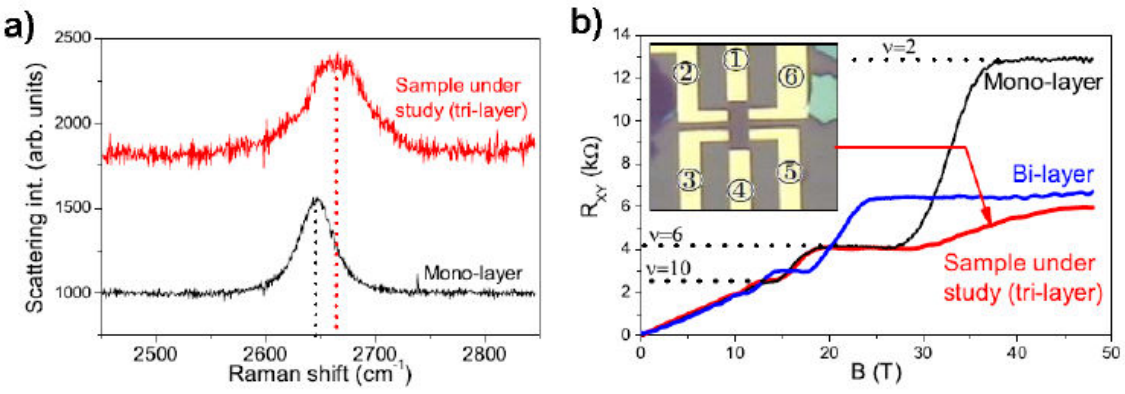

Figure 1: *a) Raman spectra of the sample under study (graphene trilayer) and monolayer graphene for comparison. b) High field Quantum Hall resistance for monolayer, bilayer and trilayer graphene. Inset : optical image of the sample under study.*

POINT DEFECTS ON GRAPHENE ON METALS

D. Fernández-Torre[1], M.M. Ugeda[2], I. Brihuega[2], P. Pou[1], A.J. Martínez-Galera[2], R. Pérez[1], and J.M. Gómez-Rodríguez[2]

[1]Departamento de Física Teórica de la Materia Condensada, Univ Autónoma de Madrid, 28049 Madrid, Spain
[2]Departamento de Física de la Materia Condensada Univ Autónoma de Madrid, 28049 Madrid, Spain
delia.fernandez @ uam.es

Understanding the coupling of graphene with its local environment is absolutely critical to be able to integrate it in tomorrow's electronic devices. Previous studies have shown that highly perfect sheets of graphene can be obtained by epitaxial growth on metal surfaces, and for some transition elements, like Ir or Pt, the interaction is so weak that many characteristic properties of graphene, such as the Dirac cones, are preserved [1,2]. In this work, we show how the presence of a metallic substrate of this kind affects the properties of an atomically tailored graphene layer. After growing a pristine monolayer on a Pt(111) surface, we have deliberately created single carbon vacancies on the graphene sheet, and studied its impact in the electronic, structural and magnetic properties. To this end, we combine low temperature scanning tunneling microscopy (LT-STM) experiments [3] with density functional theory calculations (DFT) and non-equilibrium Green's functions (NEGF) methods to model the electronic transport [4]. The DFT calculations have been performed using the PBE functional empirically corrected to take into account dispersion interactions [5]. Some of our results are displayed in Figure 1. For the non-defective graphene adsorbed on Pt(111), our calculations show that the periodic modulations typically observed by STM on the Moiré patterns can be explained as a purely electronic effect, because the simulated image is anticorrelated with the topmost regions of the corrugated sheet. For the vacancies on graphene/Pt(111), the calculations help us to associate the STM images observed with the positions of the atoms. Our experiments reveal a broad electronic resonance which is shifted above the Fermi energy, and resembles that previously observed near the Fermi level on graphite [6]. Vacancy sites become reactive, leading to an increase of the coupling between the graphene layer and the metal substrate at these points. This gives rise to a rapid decay of the localized state and the quenching of the magnetic moment associated with carbon vacancies in free-standing graphene layers.

References:

[1] Pletikosic et al, Phys. Rev. Lett., 102 (2009) 056808.
[2] P. Sutter et al, Phys. Rev. B, 80 (2009) 245411.
[3] M. M. Ugeda, doctoral thesis, Universidad Autónoma de Madrid (to be published)
[4] J.M. Blanco et al, Prog. Surf. Sci., 81 (2006) 403.
[5] S. Grimme, J. Comp. Chem. 27 (2006) 1787; G. Kresse and J. Furthmüller, Phys. Rev. B 54 (1996) 11169.
[6] M.M. Ugeda et al, Phys. Rev. Lett., 104 (2010) 096804.

Figures:

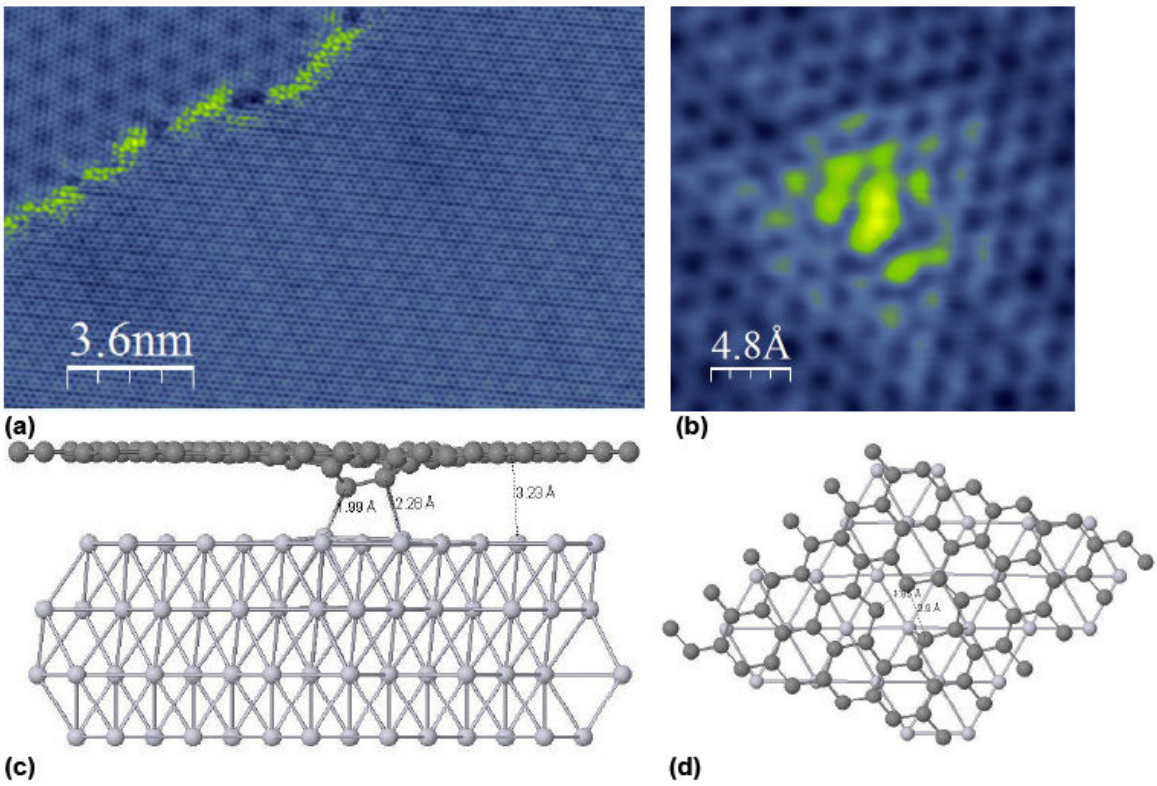

Figure 1: *(a) 14x20 nm2 STM image of the pristine graphene/Pt(111) surface showing two different Moiré structures: an R19xR19 on the upper left side and a 3x3 in the rest of the image. Sample bias: 50 mV, tunneling current: 1.0 nA. (b) STM image of a single vacancy on graphene/Pt(111). Sample bias: -30mV, tunneling current: 0.8 nA. (c) and (d) One of the possible adsorption sites for a single vacancy in graphene on Pt(111). The supercell used is fully displayed in (c). In (d) we show only the topmost Pt layer for clarity.*

RAMAN SPECTROSCOPY OF GRAPHENE: STATE OF THE ART

Andrea C. Ferrari

Department of Engineering, University of Cambridge, Cambridge CB3 OFA, UK
acf26@eng.cam.ac.uk

Raman spectroscopy is the most common and informative characterization technique in graphene science and technology. It is used to determine the number of layers, doping, strain, defects, functional groups, quality and type of edges [1-15]. I will outline the state of the art in this field, the recent developments and future directions of research, focussing on the link between Raman spectra and sample mobility, the quantification and identification of defects, and the role of electron-electron interactions.

References:

[1] A. C. Ferrari et al. Phys. Rev. Lett. 97, 187401 (2006)
[2] C. Casiraghi et al. Nano. Lett. 7, 2711 (2007)
[3] C. Casiraghi et al. Appl. Phys. Lett. , 91, 233108 (2007)
[4] S. Pisana et al. Nat. Mater. 6, 198 (2007)
[5] S. Piscanec et al. Phys. Rev. Lett. 93, 185503 (2004)
[6] C. Casiraghi, et al. Nano Lett. 9, 1433 (2009)
[7] A. C. Ferrari, Solid State Comm. 143, 47 (2007)
[8] A. Das et al. Nature Nano. 3, 210 (2008)
[9] A. Das et al. Phys. Rev. B 79, 155417 (2009)
[10] T. M. G. Mohiuddin et al. Phys. Rev. B 79, 205433 (2009)
[11] J. Yan et al. Phys. Rev. Lett. 98, 166802 (2007)
[12] D Graf et al. Nano Lett. 7, 238 (2007)
[13] A. C Ferrari et al. Phys. Rev. B 61, 14095 (2000); 64, 075414 (2001)
[14] D. M. Basko et al. Phys Rev B 80, 165413 (2009)
[15] F. Schedin et al. ACS Nano (2010)

PHYSICAL CONSEQUENCES OF ELECTRON-ELECTRON INTERACTIONS IN GRAPHENE LANDAU LEVELS

Mark Oliver Goerbig

Laboratoire de Physique des Solides, CNRS, Univ Paris-Sud, Bât. 510, 91405 Orsay cedex, France
goerbig@lps.u-psud.fr

The relative role of electron-electron interactions in graphene can be triggered via the magnetic field. Whereas in the absence of such quantising field, the relative strength of the interactions is given in terms of the "graphene fine-structure constant", the latter is relevant in graphene in a magnetic field only in the integer quantum Hall effect, i.e. when an an integer number of Landau levels is completely filled. In this case, a perturbative treatment of the electron-electron interactions provides valuable insight into the collective excitations of graphene in a magnetic field. In comparison with non-relativistic 2D electron systems, graphene displays a similar upper-hybrid mode (the magnetic-field descendant of the 2D plasmon), but also linear magneto-plasmons (see figure) that are an original feature of Dirac fermions in monolayer graphene [1,2].

However, because of the large Landau-level degeneracy, the situation is drastically different when the levels are only partially filled. In this case, inter-Landau-level excitations constitute high-energy degrees of freedom, due to the level separation, whereas the low-energy physical properties are governed by intra-Landau-level excitations [3]. Since these excitations do not alter the kinetic energy, the latter does not play any dynamical role and may be omitted, such that the remaining energy scale is set by the Coulomb interaction. One therefore obtains the regime of the fractional quantum Hall effect, or generally speaking that of strong electronic correlations. The observed fractional quantum Hall effect in graphene [4] displays the large internal symmetry [SU(4)] due to the fourfold spin-valley degeneracy of the relativistic Landau levels. The SU(4) picture of the fractional quantum Hall effect [5,6] has very recently found an experimental proof in four-terminal measurements on an h-BN substrate [7]. Most saliently, the family of 1/3 states may be stabilised in the case of even very small symmetry-breaking fields, such as the Zeeman effect, and displays novel collective spin-flip excitations beyond the Laughlin state [8].

References:

[1] R. Roldán, J.-N. Fuchs, and M. O. Goerbig, Phys. Rev. B 90 (2009) 085408.
[2] R. Roldán, M. O. Goerbig, and J.-N. Fuchs, Semicond. Sci. Technol. 25 (2010) 034005.
[3] M. O. Goerbig, arXiv:1004.3396 (2010).
[4] X. Du et al., Nature 462 (2009) 192; K. I. Bolotin et al., Nature 462 (2009) 196.
[5] M. O. Goerbig and N. Regnault, Phys. Rev. B 75 (2007) 241405.
[6] C. Töke and J. K. Jain, Phys. Rev. B 75 (2007) 245440.
[7] C. Dean et al., arXiv:1010.1179 (2010).
[8] Z. Papić, M. O. Goerbig, and N. Regnault, Phys. Rev. Lett. 105 (2010) 176802.

Figures:

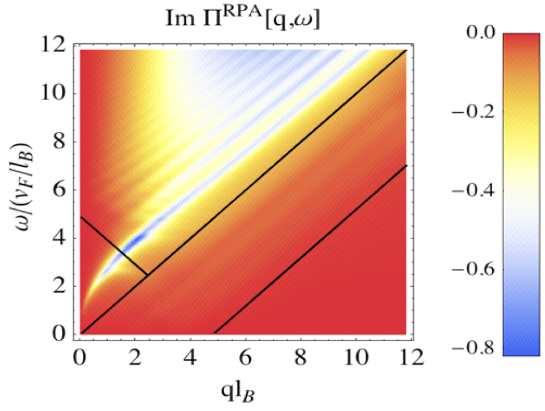

***Figure 1**: Imaginary part of the particle-hole excitation spectrum for graphene in the integer quantum Hall regime, calculated within the random-phase approximation. In addition to the upper-hybrid mode, which disperses as the square root of the wave vector at small values of the latter, one obtains linear magneto-plasmons that disperse roughly linearly parallel to the central diagonal.*

LOW MAGNETIC SIGNALS MEASURED BY A COMBINATION OF MFM AND KPFM

M. Jaafar[1], D. Martínez[1], R. Pérez[2], **J. Gómez – Herrero[1]**, O. Iglesias- Freire[3], L. E. Serrano[4], R. Ibarra[5], J. Mª de Teresa[4] and A. Asenjo[3]

[1] Dpto. Física de la Materia Condensada, Universidad Autónoma de Madrid, Spain
[2]Dpto. Física Teórica de la Materia Condensada, Universidad Autónoma de Madrid, Spain
[3]Instituto de Ciencia de Materiales de Madrid, CSIC, Spain
[4]Instituto de Ciencia de Materiales de Aragón, CSIC, Zaragoza, Spain
[5]Instituto de Nanociencia de Aragón, Zaragoza, Spain
miriam.jaafar@uam.es

The most outstanding feature of the Scanning Force Microscopy (SFM) is the capability to detect different short and long range interactions. In particular, Magnetic Force Microscopy (MFM) is used to characterize the domain configuration in ferromagnetic materials like thin films grown by physical techniques or ferromagnetic nanostructures. It is a usual procedure to separate the topography and the magnetic signal by scanning at a lift distance of 25-50nm so the long range tip –sample interactions dominate. The MFM is nowadays proposed as valuable technique to characterize more complex system such as organic nanomagnets, magnetic oxide nanoislands and carbon based materials [1]. In those cases, the magnetic nanoelements and its substrate present quite different electronic behavior i.e. they exhibit large surface potential differences which causes heterogeneous electrostatic interaction between tip and sample [2] that could be interpreted as magnetic interaction. To distinguish clearly the origin of the tip-sample forces we propose two different methods: (i) by applying *in situ* magnetic field during the MFM operation to detect the variation in the image contrast corresponding to the modification of the magnetic state of the tip or sample [3], (ii) by performing a combination of Kelvin Probe Force Microscopy (KPFM) and MFM to compensate the electrostatic contribution in the frequency shift signal The useful of the KPFM-MFM combination is illustrated by studying Co nanostripes grown by Focused Electron Beam [4] (Figure 1). As another example of this technique we investigate possible ferromagnetic order on the graphite surface [5]. The results show that the tip-sample interaction along the steps is independent of an external magnetic field. By combining KPFM and MFM, we are able to separate the electrostatic and magnetic interactions along the steps obtaining an upper bound for the magnetic force gradient of 16 μN/m (Figure 2). Our experiments suggest the absence of ferromagnetic signal in graphite at room temperature in strong contradiction with [1].

References:

[1] J.Cervenka, M. I. Katsnelson and C. F. J. Flipse, Nature Physics 5, (2009) 840 - 844
[2] R. Schmidt, A. Schwarz and R. Wiesendanger, Nanotechnology 20, (2009) 26400 7
[3] M. Jaafar, J. Gómez-Herrero, A. Gil, P. Ares, M. Vázquez, and A. Asenjo, Ultramicroscopy, 109, (2009) 693
[4] M. Jaafar, O. Iglesias-Freire, L. Serrano-Ramón, M.R. Ibarra J.M. de Teresa and A. Asenjo, in preparation
[5] D. Martínez, M. Jaafar, R. Pérez, J. Gómez - Herrero and A. Asenjo, Phys.Rew.Lett. 105 (2010) 257203

Figures:

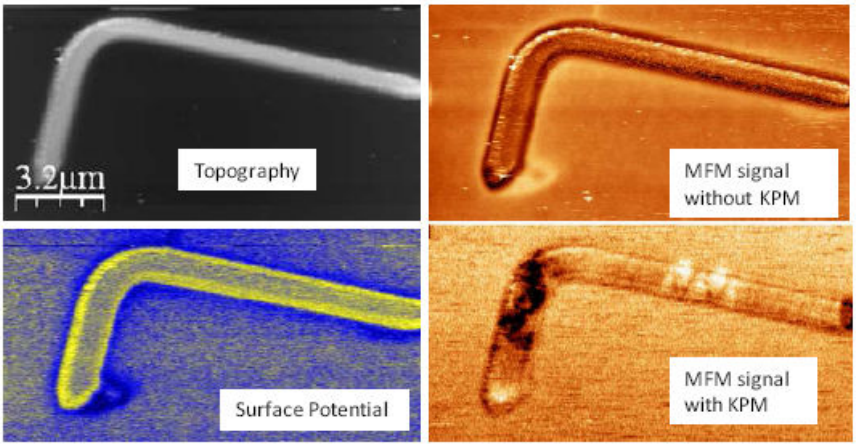

Figure 1: *(a) Topography and (b) MFM signal (frequency shift) of a cobalt nanostripe without electrostatic compensation. The contrast drastically changes when KPM is used simultaneously: (c) Surface potential image and (d) MFM signal with KPFM.*

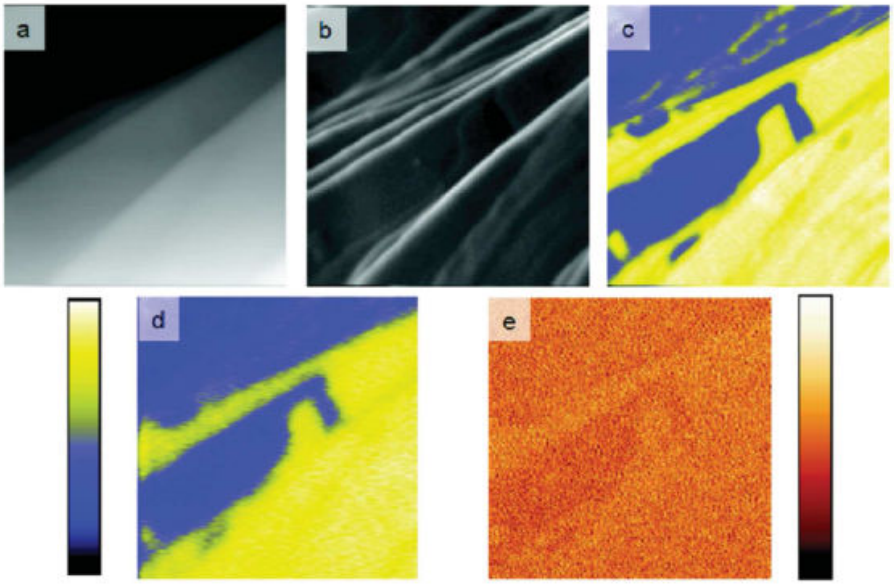

Figure 2: *3 µm x 3 µm AFM, KPFM, and MFM images taken in high vacuum with a cobalt-coated probe on ZYHHOPG. (a) Topography. (b) Edge enhanced image of (a) showing the surface steps. (c) KPFM image simultaneously taken with (a), showing electrostatic domains and steps on the sample surface (the potential difference between bright and dark areas is 200 mV). (d) KPFM image taken in retrace at 50 nm lift distance. (e) Frequency shift image taken simultaneously with (d). The total frequency shift variation in figure (e) is 0.4 Hz.*

IMPURITY SCATTERING IN COHERENT AND INCOHERENT SINGLE AND BILAYER GRAPHENE

Sophie Gueron, M. Monteverde, C. Ojeda Aristizabal, R. Weil, K. Bennaceur, C. Glattli, M. Ferrier, H. Bouchiat, J.N. Fuchs and D. Maslov,

Laboratoire de Physique des Solides, U. Paris Sud Orsay, France
gueron@lps.u-psud.fr

The nature of the scatterers which to this day limit the mobility of graphene, and determine most of its conduction properties, is still highly debated. Some groups attempt to deduce the nature of these scatterers from the effect of the dielectric surrounding the graphene. I will describe our approach in Orsay, which consists in comparing two different scattering times, the elastic scattering time and the transport scattering time, which play different roles in the magnetoresistance of the samples. I will show that the ratio of these two times, as well as their dependence with charge density, point to dominant scattering originating from strong, neutral, short range scatterers, rather than from charged impurities.
I will also present a consequence on quantum transport of the existence of these scatterers, namely, the reproducible conductance fluctuations in these samples at low temperature, when the quantum coherence extends over the entire sample length. We exploit the possibility to control the diffusion constant with gate voltage in monolayer and bilayer graphene to test the theory of mesoscopic fluctuations. We find that the correlation energy is given by the Thouless energy, and that the correlation field corresponds to a magnetic flux quantum threading a coherent area in the sample. But we find that the ergodicity hypothesis is not verified: the gate-voltage dependent fluctuations vary with gate voltage, and are largest near the charge neutrality point, whereas the magnetic field dependent fluctuations do not change with doping. The percolating nature of transport near the charge neutrality point may explain this unexpected result.

In both experiments, we exploit the asset of monolayer and bilayer graphene, namely the fact that the different band structures lead to different gate-voltage dependences of the diffusion coefficients, enabling a quantitative test of heories over broad ranges, impossible to realize with other materials.

References:

[1] C. Ojeda-Aristizabal, R. Weil, M. Ferrier, S. Guéron, H. Bouchiat, J.N. Fuchs, D.Maslov, “Transport and elastic scattering times as probes of the nature of impurity scattering in single and bilayer graphene”, M. Monteverde, Phys. Rev. Lett. 104, 126801 (2010).
[2] C. Ojeda-Aristizabal, M. Monteverde, R.Weil, M. Ferrier, S. Gueron, H. Bouchiat, “Conductance fluctuations and field asymmetry of rectification in graphene”, Phys. Rev. Lett. 104, 186802 (2010).

LARGE INTRINSIC BAND GAPS, FERROMAGNETISM, AND ANOMALOUS MAGNETORESISTANCE OSCILLATIONS DERIVED FROM GRAPHEME EDGE STATES: NANORIBBONS AND ANTIDOT-LATTICE GRAPHENES

Junji Haruyama

Faculty of Science and Engineering, Aoyama Gakuin University, 5-10-1 Fuchinobe, Sagamihara, Kanagawa 252-5258, Japan
J-haru@ee.aoyama.ac.jp

A variety of quantum phenomena observed in graphene is attracting significant attention. In contrast, few works have experimentally reported edge states and related phenomena, although there are so many theoretical reports, which predicted that electrons localize at zigzag edges of graphene due to presence of flat bans and the electron spins strongly polarize. One main reason for lack of experimental reports is high damages at edges introduced by lithographic fabrication.

Here, in the talk, I will present the following two systems fabricated by non-lithographic methods in order to reveal edge-related phenomena; 1. Graphene nanoribbons (GNRs) fabricated by chemical unzipping of carbon nanotubes (CNTs) and 3-stepped annealing [1] and 2. Antidot-lattice graphenes (ADLGs; graphene nano-pore arrays) fabricated using nano-porous alumina templates as etching masks [2, 3].

In the GNRs, we confirm low defects by Raman spectrum, HRTEM, single electron spectroscopy, and also electrical measurements. I present a large an intrinsic energy band gap of 55 meV, which is 7-times larger than those in lithographically fabricated GNRs with defects. It can be understood by calculation for arm-chair edge GNRs.

In the ADLGs, we confirm high electronic density of states at antidot (nano pore) edges by STM. I will show appearance of room-temperature ferromagnetism and anomalous magnetoresistance oscillations derived from edge-localized spins in hydrogen-terminated ADLGs. They can be qualitatively understood by theories for zigzag edges. These results must open a new door to all-carbon (rare-metal free) magnets and also spintronic devices based on spin Hall effects by inducing spin-orbit interaction.

References:

[1] T.Shimizu, J.Haruyama, et al, “Large intrinsic energy bandgaps in annealed nanotube-derived graphene nanoribbons” Nature Nanotech. 6, 45-50 (2011) (Selected for Latest Highlights, News&Views, and Cover index)
[2] T.Shimizu, J.Haruyama, et al, “Edge-state-derived ferromagnetism and anomalous magnetoresistance in antidot-lattice graphenes” To be published on Phys.Rev.Lett.
[3] K. Tada, J.Haruyama, et al, “All-carbon ferromagnetism derived from edges states in graphene nano-pore arrays” Nature Nanotrch. In-depth Review

SUBSTRATE DEPENDENCE IN HYDROGEN-GRAPHENE INTERACTION

L. Hornekær, L. Nilsson, M. Andersen, R. Balog, J. Bjerre, B. Jørgensen, J. Thrower, E. Friis, E. Lægsgaard, F. Besenbacher, I. Stensgaard, P. Hoffman and B. Hammer

Dept. Physics and Astronomy and Interdisciplinary nano-science center, iNANO, Aarhus University, Ny Munkegade Bygn. 1520, Aarhus C, Denmark
liv@phys.au.dk

Theoretical and experimental studies have revealed that the properties of graphene can be changed substantially by hydrogenation. Theoretical calculations show that fully hydrogenated graphene, referred to as graphane, is an insulator [1] and that hydrogen line structures can induce graphene nanoribbon – like band gaps in graphene [2]. Experimental investigations reveal a change of electronic properties of graphene upon hydrogenation [3-6]. The experiments also show that graphene hydrogenation is substrate dependent [6-9]. Here we report on the substrate dependence of hydrogen adsorbate structures on graphene on SiC, Ir(111), Pt(100) and graphite.

Combined STM, TPD, DFT and XPS investigations of the interaction of graphene with atomic hydrogen reveal the formation of different types of hydrogen adsorbate structures on the graphene surface, depending on the degree and type of interaction between graphene and the underlying substrate. In the case of low substrate interaction, dimer like structures, similar to those displayed in figure 1.a. are observed, while in the case of a higher degree of interaction with the substrate, cluster structures with higher stability, similar to those displayed in figure 1.b. are observed. Furthermore, in some systems hydrogenation is observed to lead to increased graphene-substrate interaction.

In e.g. the graphene-Pt(100) system the graphene-substrate interaction is observed to be coverage dependent. At low coverage, hydrogen atoms are observed to form dimer structures similar to those observed previously on graphite, while, at higher coverage the reconstruction of the platinum substrate is lifted and more stable hydrogen adsorbate structures are observed. The experimental data indicate that the Pt substrate plays an active role in stabilizing these adsorbate structures on graphene.

References:

[1] Sofo, J.O., Chaudhari, A.S., & Barber, G.D., Phys. Rev. B, 75 (2007) 153401
[2] Chernozatonskiĭ, L., Sorokin, P., Belova, E., Brüning, J., & Fedorov, A., Jetp. Lett. 85 (2007) 77
[3] Bostwick, A. McChesney, J.L. Emtsev, K.V. Seyller, T. Horn, K. Kevan, S.D. & Rotenberg, E., Phys. Rev. Lett. 103 (2009) 1
[4] Elias, D., Nair, R.R., Mohiuddin, T.M.G., Morozov, S.V., Blake, P., Halsall, M.P., Ferrari, A.C., Boukhvalov, D.W., Katsnelson, M.I., Geim, A.K., & Novoselov, K.S., Science 323 (2009) 610
[5] Guisinger, N., Rutter, G., Crain, J., First, P., & Stroscio, J., Nano Lett. 9 (2009) 1462
[6] Balog, R.; Jorgensen, B.; Nilsson, L.; Andersen, M.; Rienks, E.; Bianchi, M.; Fanetti, M.; Laegsgaard, E.; Baraldi, A.; Lizzit, S.; Sljivancanin, Z.; Besenbacher, F.; Hammer, B.; Pedersen, T. G.; Hofmann, P.; & Hornekaer, L., Nature Materials, 9 (2010) 315
[7] Hornekaer, L.; Sljivancanin, Z.; Xu, W.; Otero, R.; Rauls, E.; Stensgaard, I.; Laegsgaard, E.; Hammer, B.; & Besenbacher, F., Physical Review Letters 96 (2006) 156104
[8] Balog, R., Jørgensen, B., Wells, J., Lægsgaard, E., Hofmann, P., Besenbacher, F., & Hornekær, L., J. Am. Chem. Soc. 131 (2009) 8744
[9] Ng, M. L., Balog, R., Hornekaer, L., Preobrajenski, A. B., Vinogradov, N. A., Martensson, & N., Schulte, K., Journal Of Physical Chemistry C, 114 (2010) 18559

Figures:

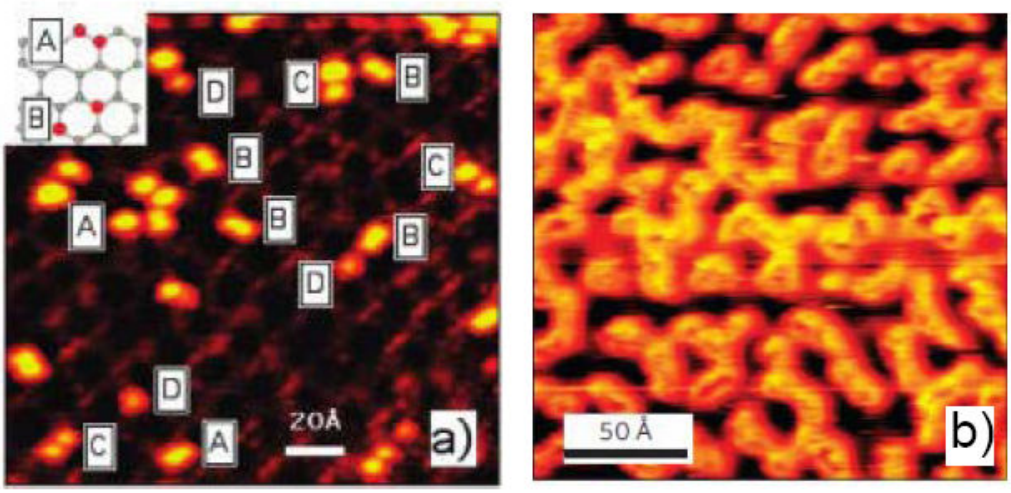

Figure 1: *a) Hydrogen dimer structures on graphene on SiC [8], b) Hydrogen clusters on graphene on Ir(111) [6].*

NANO-CARBON MATERIALS: SYNTHESIS AND CHARACTIRIZATION

Sumio Iijima

Faculty of Science and Technology, Meijo University, Tenpaku, Nagoya, Aichi, Japan
National Institute of Advanced Industrial Science and Technology / Nanotube Research Center
and, NEC Corporation
iijimas@meijo-u.ac.jp

Formation of a large size graphene sheet by a thermal CVD method using a copper substrate foil has been reported. The method requires a high temperature CVD reactor (near 1000ºC), so that it cannot be used in a conventional Si device process and therefore an alternative low temperature synthesis of graphene is needed. For this purpose we utilized a new surface-wave micro-wave CVD method which has been developed originally for the nano-diamond film growth at low temperature down to room temperature. We shall demonstrate the growth of an A4-size graphene sheet formed at 300ºC.

Another subject to be presented is concerned with structural characterization of nano-carbon materials using atom-resolution electron microscopes as well as other characterization methods. The advantage of high resolution electron microscopy (HRTEM) over other techniques is to be able to characterize local atomic structures such as lattice defects and edge structures of nano materials which cannot be studied in conventional techniques. Another emphasis of HRTEM will be on dynamic observation of a reaction process which is not available for other high resolution probe microscope techniques such as STM. A recent progress of HRTEM technology such as aberration correction and EELS, has allowed us to do elemental analysis, distinction of charge valency and more on the individual atom basis. Some latest examples of above mentioned observations on graphene edge structures and electronic states will be demonstrated.

ELECTRONIC TRANSPORT IN GRAPHENE ON HEXAGONAL BORON NITRIDE DEVICES

Pablo Jarillo-Herrero

Massachusetts Institute of Technology
77 Massachusetts Avenue, Bldg. 13-2017; Cambridge, MA 02139, USA
pjarillo@mit.edu

Hexagonal boron nitride (hBN) has been recently shown to be a high quality substrate for graphene devices. In this talk I will review our recent experiments on graphene on hBN devices. In particular I will describe STM measurements that show that electron-hole puddles are much reduced for graphene on hBN compared to graphene on SiO_2, and also our experiments on quantum Hall effect and Landau level crossings of Dirac fermions on high mobility trilayer graphene on hBN.

GRAPHENE SPINTRONICS

Roland Kawakami, Wei Han, Kathy McCreary, Keyu Pi

Department of Physics and Astronomy, University of California, Riverside, CA, 92521, USA
roland.kawakami@ucr.edu

Graphene is an attractive material for spintronics due to the low intrinsic spin-orbit coupling, low hyperfine coupling, and high electronic mobility. These should lead to long spin lifetimes and long spin diffusion lengths. Experimentally, the gate-tunable spin transport at room temperature has been achieved with spin diffusion lengths of ~2 microns. This makes it a very unique and promising material for spin transport. However, the spin injection efficiency has been low and the spin lifetime is still much shorter than expected theoretically. Overcoming these challenges will make graphene a very strong material for spintronics.

In this talk, I will present three of our recent results in graphene spintronics.

(1) **Tunneling spin injection into graphene [1].** We utilized TiO2-assisted deposition of MgO tunnel barriers in order to reduce pinholes, which easily form for thin films on graphene. The use of tunnel barriers enhances the spin injection efficiency by alleviating the conductivity mismatch between the ferromagnetic metal (Co) and the single layer graphene (SLG). The non-local spin signal is found to be as high as 130 ohms at room temperature, with a spin injection efficiency of 30%. This is the highest spin injection efficiency observed in graphene spin valves.

(2) **Long spin lifetimes in graphene [2].** In addition to enhancing the spin injection efficiency, we find that the measured spin lifetime is also enhanced by the tunnel barriers. This indicates that the reported values of spin lifetime are shorter than the actual spin lifetime in graphene due to the invasive nature of the ferromagnetic contacts. Using the tunneling contact to suppress the contact-induced spin relaxation, we investigate the gate and temperature dependence of SLG and bilayer graphene (BLG) spin valves. We find spin lifetimes as high at 771 ps at 300 K in SLG, 1.0 ns at 4 K in SLG, and 6.2 ns at 20 K in BLG (see figure). These are the longest spin lifetimes observed in SLG, and the 6.2 ns is longest spin lifetime observed in a graphene spin valve so far.

(3) **Modification of spin transport properties by surface doping [3].** Because graphene is extremely surface sensitive, there are opportunities to manipulate the spin transport properties by modifying the surface with various dopants. In the initial study, we investigated the effect of gold doping on spin transport and spin lifetime. We find that the spin transport properties such as nonlocal signal and spin lifetime can be enhanced, despite the presence of additional charged-impurity scattering. Mainly, the presence of the gold impurities does not produce a degradation of spin transport, despite greatly reducing the electronic mobility.

These advances are important for the development of spin-based computing with integrated logic and memory.

References:

[1] Wei Han, K. Pi, K. M. McCreary, Yan Li, Jared J. I. Wong, A. G. Swartz, and R. K. Kawakami, Physical Review Letters, 105 (2010) 167202.
[2] Wei Han and R. K. Kawakami, arXiv:1012.3435 (2010).
[3] K. Pi, Wei Han, K. M. McCreary, A. G. Swartz, Yan Li, and R. K. Kawakami, Physical Review Letters, 104 (2010) 187201.

Figures:

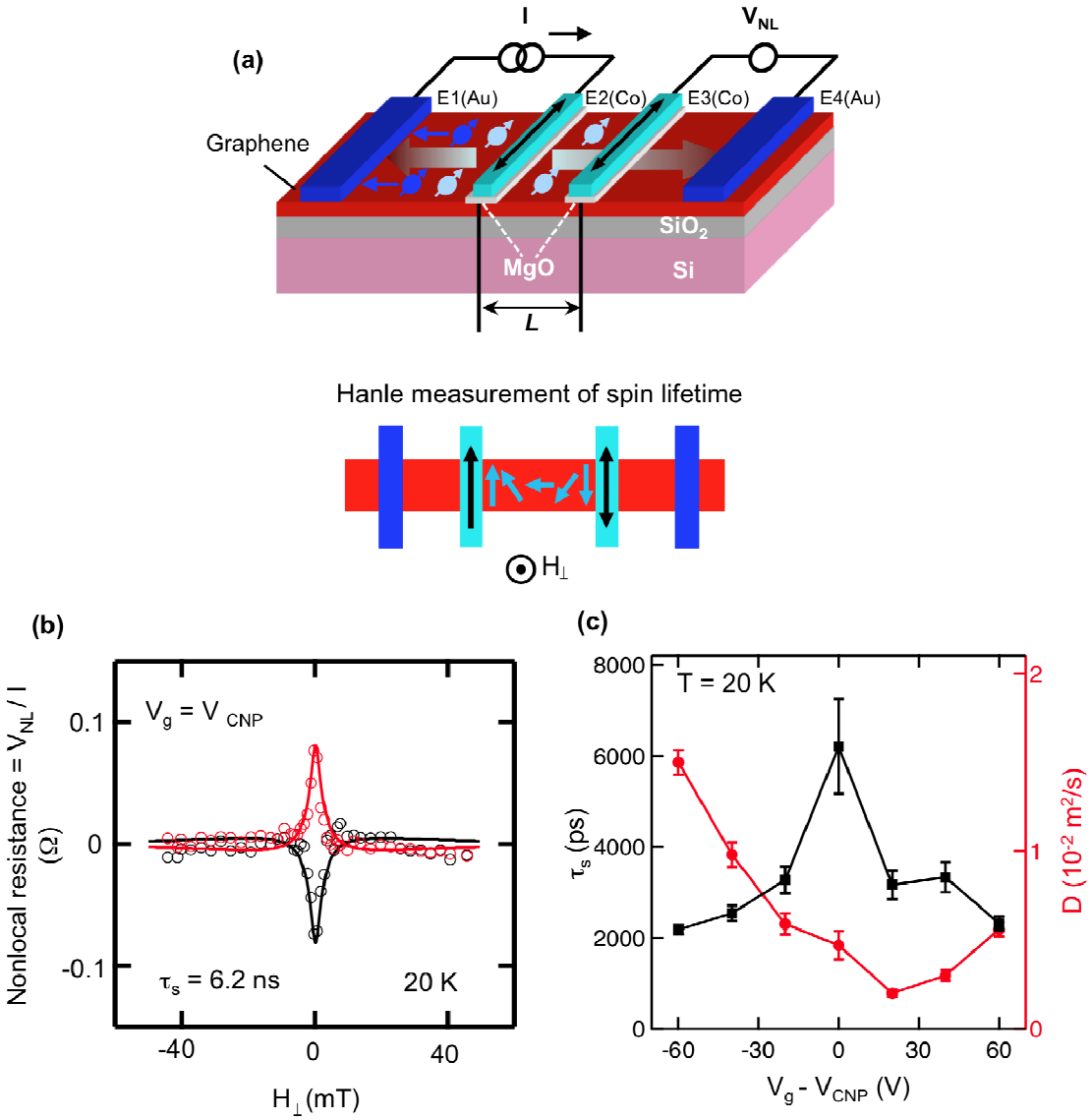

Figure 1: *Long spin lifetimes in graphene. (a) Schematic drawing of a graphene spin valve in the nonlocal measurement geometry. A current source (I) is utilized to inject spin-polarized carriers into the graphene at electrode E2. The spins subsequently diffuse to electrode E3 where they are detected as a voltage V_{NL} measured across electrodes E3 and E4. The spin injection and transport is measured as the nonlocal resistance ($R_{NL} = V_{NL}/I$). Hanle spin precession measurements are performed to determine the spin lifetime. An out-of-plane magnetic field is applied to induce spin precession. (b) Hanle measurement of a bilayer graphene spin valve with L = 3.05 microns, gate voltage (V_g) tuned to the charge neutrality point (CNP), and T = 20 K. The red (black) data is for parallel (antiparallel) alignment of the the Co magnetizations. The narrow Hanle peak corresponds to a spin lifetime of 6.2 ns. (c) Gate dependence of spin lifetime (black) and diffusion coefficient (red) in bilayer graphene at 20 K. Their opposite behaviors indicate the relevance of Dyakonov-Perel spin scattering.*

MANIFEST OF ELECTRON INTERACTIONS IN QUANTUM HALL EFFECT IN GRAPHENE

Philip Kim

Columbia University, USA

The quantum Hall ferromagnetism (QHFM) and fractional quantum Hall effect (FQHE) in 2-dimensional electron gas with multiple internal degrees of freedom provides a model system to study the interplay between spontaneous symmetry breaking and emergent topological order. In graphene, the structure of the honeycomb lattice endows the electron wavefunctions with an additional quantum number, termed valley isospin, which, combined with the usual electron spin, yields four-fold degenerate Landau levels (LLs). This additional symmetry modifies the QHFM and FQHE with intriguing interplay between two different spin flavours. As a consequence, it is conjectured to produce new incompressible ground states in graphene, reflecting strong electron interactions. In this presentation we report multiterminal measurements of the FQHE in high mobility graphene devices fabricated on hexagonal boron nitride substrates. The measured energy gaps of observed FQHE are large, particularly in the second Landau level where they measure up to times larger than those reported in the cleanest conventional systems. In the lowest Landau level, the hierarchy of FQH states reflects the additional valley degeneracy. We will also discuss the implication of QHFM with spin and valley spin degree of freedoms.

UNDERSTANDING THE POTENTIAL OF GRAPHENE WITHIN COMPOSITES: INTERFACIAL STRESS TRANSFER IN IDEAL GRAPHENE COMPOSITES

I.A. Kinloch[1], L. Gong[1], A. Raju[1], I. Riaz[2], R. Jalil[2], K.S. Novoselov[2], R.J. Young[1]

[1]School of Materials, [2]School of Physics and Astronomy, University of Manchester, Manchester, U.K
ian.kinloch@manchester.ac.uk

Graphene is one of the stiffest and strongest known materials with a Young's modulus of the order of 1 TPa and a fracture stress ~ 130 GPa. These properties make graphene an ideal candidate for use as a reinforcement in high-performance composites. However, being one-atom thick crystalline material, graphene poses several rather fundamental questions: (1) Can decades of research on carbon based composites be applied to such ultimately thin crystalline material? (2) Would traditionally used continuous mechanics still be valid at atomic level? (3) How does the macroscopic matrix interact with microscopic graphene crystals (in terms of stress transfer, for instance) and what kind of theoretical description would be appropriate? (4) How does stress transfer between the layers in bilayer and thicker graphene?

We have prepared model composites consisting of single graphene flakes (monolayer and thicker) sandwiched between thin polymer films and employed Raman spectroscopy to monitor stress transfer from the polymer matrix to the graphene during deformation of the composite [1]. Typically, a PMMA beam was coated with 300 nm of epoxy, onto which mechanically exfoliated graphene was placed, finally a 50 nm PMMA coating was then spun onto the graphene. The coated beam was tested in 4-point bending and the Raman spectra were collected to confirm the morphology of the flake being studied and map the strain within it.

The rate of peak shift of the G' peak with applied strain has been shown for carbon reinforcements to be proportional to the effective modulus of the filler in the composite [2]. (This effective modulus takes into account the efficiency of the polymer-filler interface). A shift of ~ 35 cm^{-1}/% was obtained for the monolayer graphene upon initial loading, corresponding to an modulus of ~ 0.6 TPa. The polymergraphene interface was found to fail at high strains but would heal upon relaxation of the sample. The peak shift rate upon unloading, however, was 60 cm^{-1}/%. This shift rate is the highest we have ever observed in any composite system and corresponds to an effective modulus of ~ 1 TPa. This result shows that the full modulus of graphene can be achieved within a polymer matrix.

Mapping the G' peak shift across the flake showed that the strain in a flake was virtually zero at the ends of the flake and built up to the applied, global strain value in the middle. This behaviour was successfully modeled using the continuum shear-lag theory, which is the established model for macroscale fillers. In particular, the diamond shape of the flake that was studied allowed an accurate fit of the model since it meant that the strain data over a range of aspect ratios could be obtained. The maximum shear force at the polymer-graphene interface was calculated as 3 MPa, which is an order magnitude less than that typically achieved in conventional carbon fibre-epoxy composites. Such a low shear force maybe expected, given the weak nature of the van der Waal forces at the interface. One result of these poor interfacial properties is that the critical length of the graphene required to obtain efficient reinforcement was found to be 30 microns. This result implies that in order for graphene to be used in structural composites, the graphene flakes either need to be large (> 30 microns long) or chemically functionalised to improve the interfacial strength with the matrix.

References:

[1] L. Gong, I. A. Kinloch, R. J. Young, I. Riaz, K. S. Novoselov, Advanced Materials, 24 (2010), 2694- 2697.
[2] C. A. Cooper, R. J. Young, M. Halsall, Composites Part A- Applied Science and Manufacturing, 32 (2010), 401-411

Figures:

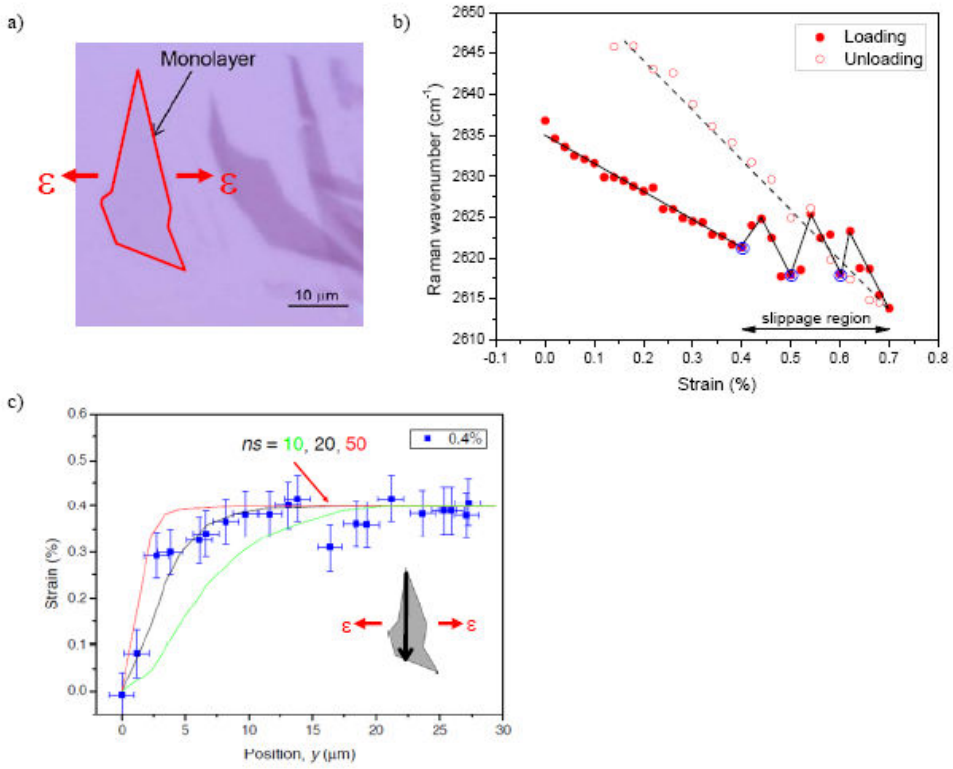

Figure 1: *1a) An optical micrograph showing the flake studied for b) and c), with its outline and the direction the deformation was applied highlighted. b) The position of the G' band at the centre of the flake as function of global strain. The relaxation in the slippage region occurred during mapping of the strain in the flakes. c) The strain distribution down the centre of the flake, scanned perpendicular to the direction of the applied deformation. The curves show the fits of the shear lag model for different values of the factor of stress efficiency transfer, n, and aspect ratio, s.*

LOCAL ON-OFF CONTROL OF A GRAPHENE P-N PHOTODETECTOR

F.H.L. Koppens[1,4], M.C. Lemme[1], A.L. Falk[1], M.S. Rudner[1], H. Park[1,2], L.S. Levitov[3], C.M. Marcus[1]

[1]Department of Physics, Harvard University, Cambridge, MA 02138, USA
[2]Department of Chemistry and Chemical Biology, Harvard University, Cambridge, MA 02138, USA
[3]Department of Physics, Massachusetts Institute of Technology, Cambridge, MA 02139, USA
[4]ICFO, The institute of Photonic Sciences, Barcelona, Spain
frank.koppens@icfo.es

Graphene is a promising photonic material whose gapless band structure allows electron-hole pairs to be generated over a broad range of wavelengths, from UV, visible, and telecommunication bands, to IR and THz frequencies [1]. Previous studies of photocurrents in graphene have demonstrated photoresponse near metallic contacts [2] or at the interface between single-layer and bilayer regions. Photocurrents generated near metal contacts were attributed to electric fields in the graphene that arise from band bending near the contacts and could be modulated by sweeping a global back-gate voltage with the potential of the contacts fixed.

Here, we will discuss the photoresponse of graphene devices with top gates, separated from otherwise homogeneous graphene by an insulator. When the top gate inverts the carrier type under the gate, and a p-n junction is formed at the gate edges, a highly localized photocurrent is observed using a focused scanning laser [3]. Interestingly, a density difference induced by the top gate that does not create a p-n junction does not create local photosensitivity. In this way, by switching from the bipolar to ambipolar regime, our devices allow for on-off control of photodetection (see Figure).

Comparing experimental results to theory suggests that the photocurrent generated at the p-n interface results from a combination of direct photogeneration of electron-hole pairs in a potential gradient, and a photothermoelectric effect in which electric fields result from optically induced temperature gradients. We envision that this type of local on-off control of photodetection allows for the implementation of broadband bolometers with submicron pixelation.

References:

[1] F Bonaccorso, Z Sun, T Hasan, A. C Ferrari, Graphene photonics and optoelectronics. Nature Photonics (2010) vol. 4 (9) pp. 611-622
[2] Lee, E. J. H., Balasubramanian, K., Weitz, R. T., Burghard, M. & Kern, K. Contact and edge effects in graphene devices. Nature Nano. 3, 486 (2008)
[3] M. C Lemme, F. H. L Koppens, A. L Falk, M. S Rudner, H Park, L. S Levitov, C. M Marcus Local On- Off Control of a Graphene p-n Photodetector. arXiv:1012.4745v1 (2010)

Figures:

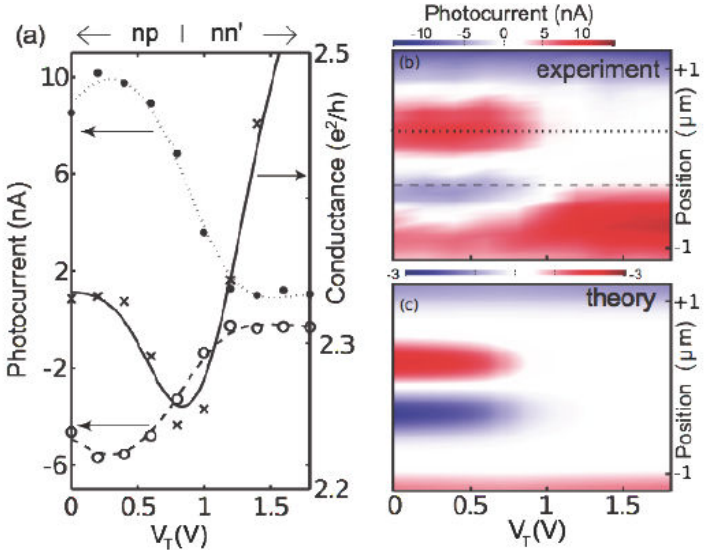

Figure 1: *a) Photocurrent (left axis, circle markers) as a function of top gate voltage with the laser positioned on either side of the top gate. Photocurrents turn on at the charge neutrality point under the top gate, as the device is switched from n-n'-n to n-p-n configuration. Source-drain conductance (right axis, cross markers) of the photodetector measured in FET configuration as a function of top gate voltage with charge neutrality point at V_T = 0.9 V (drain voltage V_D = 0.6 mV). Due to hysteresis when sweeping the top gate voltage, this curve is shifted compared to the data in Fig 1c. b) Photocurrent as a function of top gate voltage taken across the center of the photodetector in Fig 1. The laser wavelength was λ = 600 nm and the power was P = 40 μW. c) Theoretical model of the photocurrent (Eq. 1), plotted as a function of top gate voltage and position along the center of the photodetector. P_0 = 40 μW and we assume 4.6% absorption of the laser light because it passes through the graphene sheet twice due to mirroring at the SiO_2/Si interface.*

TUNABLE MANY BODY INTERACTIONS IN GRAPHENE

Alessandra Lanzara

University California, Berkeley
Materials Sciences Division, Lawrence Berkeley National Laboratory, USA

The discovery of graphene in 2004 has opened a new exciting area of research in condensed matter physics. Not only graphene is the first real two dimensional material ever observed in nature, but it is also characterized by an unusual electronic structure with respect to most condensed matter systems. Indeed, the low energy excitations in graphene behave as Dirac fermions, chiral quasiparticles with zero effective mass, and obey the relativistic Dirac equation, where the speed of light is replaced by the Fermi velocity. This is in striking contrast with most of materials known today, where the low energy excitations obey the non-relativistic Shcroedinger equation and have finite effective mass.

This unusual electronic structure leads to a variety of novel properties and huge potential for applications, the most striking one being the failure of the standard Landau-Fermi liquid picture for quasiparticles.

In this talk I will present an overview of the electronic structure of this amazing two dimensional material and will discuss how this linear dispersion can be easily modified by quantum size effects, substrate interaction, doping and disorder.

Moreover, I'll discuss how fundamental properties such as electron-phonon and electron-electron interactions are modified with respect to a standard metal and do not obey the Fermi liquid picture for quasiparticles.

The implications of our study on the properties of Dirac materials and their potential role for applications are also discussed.

DOUBLE RESONANT RAMAN IN GRAPHENE: ALL YOU WANTED TO KNOW ABOUT

M. Lazzeri[1], P. Venezuela[1,2], F. Mauri[1]

[1]IMPMC, Paris 7, CNRS, Paris, France
[2]Instituto de Fisica, Universidade Federal Fluminense, 24210-346, Niteroi RJ, Brazil
michele.lazzeri@impmc.jussieu.fr

Raman specrtroscopy is the most widely used experimental characterization technique to study graphene samples. Raman lines such as the defect-induced D and D', their overtones and the D'+D'', are usually interpreted within the double resonance mechanism. These lines are very well studied since they can be used as an experimental probe of the presence of defects but, also, to determine the presence of a monolayer in few-layers graphene samples.

Several excellent theoretical works already appeared on this topic providing an overall good understanding of the situation. However, the many different approximations used by different authors (e.g. constant electron-phonon matrix elements, resonant phonons are assumed to be on some high symmetry line, in some cases the electronic dispersion is conic, the electronic life-time is a parameter, etc.) and the several debates still going on leave with the unpleasant sensation that something is missing. Besides, some fundamental questions are basically untouched: Which kind of defects are probed by measuring different lines? Does Raman spectroscopy probe the defects which mostly influence electronic transport?

We determined [1] the DR Raman spectra of graphene by using the most precise available electronic bands, phonon dispersions, and electron-phonon coupling matrix elements (obtained by combining ab-initio density functional theory and many-body GW methods). Three different model defects are considered. The method results in a consistent framework to determine the position, the shape, the width and the intensity of the Raman lines as a function of the laser energy and of the defect concentration. Moreover it allows to treat at the same level defect-induced lines and two-phonon lines. The overall agreement with available experimental data is very good.

References:

[1] P. Venezuela, M. Lazzeri, and F. Mauri, to be published.

MAKING NANO-GRAPHENE

Kian Ping Loh

Department of Chemistry, National University of Singapore, 3 Science Drive 3, Singapore 117543
chmlohkp@nus.edu.sg

In this talk, I will discuss new chemical strategies to synthesize graphene, from large area sheets to nanographene.

Majority of the solution-phase methods produce irregularly-sized and shaped graphene sheets due to the intrinsic randomness in the defect-mediated exfoliation or cutting process of the precursor graphitic flakes. To produce highly regular graphene nanostructures, a fabrication process that is driven by thermodynamics, as in crystal growth, should be more suitable than defect-mediated fragmentation processes. To this end, we will show how we apply templated-directed synthesis to fabricate regular-sized graphene quantum dots. The dynamics of carbon cluster diffusion and aggregation to form nanographene islands is recorded by dynamic Scanning Tunneling Microscopy. The charge transfer interactions between graphene and fullerene, as well as the Van der waals epitaxy of Grapnene on self-assembled C60 will be discussed.

Graphene form functional hybrids with organic molecules, quantum dots and polymers and these can exhibit non-linear optical limiting properties, saturable absorption properties, outstanding photovoltaic and biosensing properties. Some examples of these applications studied in our laboratory will be given in this talk.

Acknowledgement:

This project is funded by the National Research Foundation Competitive Research Funding - Graphene and Related Materials R-143-000-360-281.

References:

[1] Kian Ping Loh, Qiaoliang Bao, Goki Eda, Manish Chhowalla; Graphene oxide as a chemically Tunable Platform for Optical Applications, Nature Chemistry, ASAP (Dec 2010)
[2] Tang LAL, Wang JZ, Loh KP*; Graphene-Based SELDI Probe with Ultrahigh Extraction and Sensitivity for DNA Oligomer, Journal of the American Chemical Society,: 132, 32, 10976-10977 (2010)
[3] J., Yang, J.-X., Xiao, S., Bao, Q., Jahan, M., Polavarapu, L., Wei, J., Xu, Q.-H. and Loh, K.P; A Graphene Oxide–Organic Dye Ionic Complex with DNA-Sensing and Optical-Limiting Properties Balapanuru, . Angewandte Chemie International Edition, 49 (37), 2010, 6549–6553.
[4] Wang SA, Tang LAL, Bao QL, Kian Ping LOH*; Room-Temperature Synthesis of Soluble Carbon Nanotubes by the Sonication of Graphene Oxide Nanosheets, Journal Of The American Chemical Society, 131,46, 16832 (2009)
[5] bAng PK, Chen W, Wee ATS, Kian Ping LOH* et al; Solution-Gated Epitaxial Graphene as pH Sensor, Journal Of The American Chemical Society, 130,44, 14392 (2008)
[6] Zhou Y, Bao QL, Varghese B, Kian Ping LOH* et. al.; Microstructuring of Graphene Oxide Nanosheets Using Direct Laser Writing Advanced Materials, 22, 1 (2010)
[7] Wang SA, Ang PK, Wang ZQ, Kian Ping LOH*; High Mobility, Printable, and Solution-Processed Graphene Electronics; Nano Letters, 10, 1, 92-98 (2010)
[8] Lu J, Kian Ping LOH*, Huang Han, Chen Wei, Andrew Wee TS; Plasmon dispersion on epitaxial graphene studied using high-resolution electron energy-loss spectroscopy Physical Review B 80, 11 113410 (2009)
[9] Bao QL, Zhang H, Wang Y, Kian Ping LOH*; Atomicic-Layer Graphene as a Saturable Absorber for Ultrafast Pulsed Lasers; Advanced Functional Materials, 19 ,19 Pages: 3077-3083 (2009)
[10] Wang Y, Chen XH, Zhong YL, et al.; Large area, continuous, few-layered graphene as anodes in organic photovoltaic devices; Applied Physics Letters, 95, 6, 063302 (2009)

PROBING QUANTUM INTERFERENCE EFFECTS IN EPITAXIAL GRAPHENE BY STM AND MAGNETOTRANSPORT STUDIES

A. Mahmood [1], C. Naud[1], C. Bouvier, F. Hiebel, J.-Y. Veuillen[1], P. Mallet[1], D. Chaussende[2], T. Ouisse[2], L.P. Lévy[1]

[1]Institut Néel, CNRS-UJF, BP 166, 38042, Grenoble Cedex 9, France
[2]Laboratoire des Matériaux et du Génie Physique, CNRS UMR5628 - Grenoble INP, Minatec, 3 parvis Louis Néel BP257 38016 Grenoble, France
ather.mahmood@grenoble.cnrs.fr

A comprehensive understanding of the relationship between growth conditions and the resulting atomic and electronic structure is expected by characterizing the morphology of grown grapheme layers which also allows comparing the mechanisms of electron diffusion in graphene and hence controlling the charge transport through it. The graphitization can be achieved under ultra-high vacuum (UHV) conditions or in controlled atmosphere, starting from either the 6H-SiC(0001) (Si face) or 6H-SiC(000-1) (C face) surfaces. The resulting graphene layers have different disorder and morphologies depending on the growth conditions.

We present the scanning probe characterization of a gently graphitized 6H–SiC (0001) [1] surface prepared under ultra-high vacuum conditions and compare it with low temperature magneto-transport studies. The general surface morphology and atomically resolved Local Density of States (LDOS) is mapped by Scanning Tunneling Microscopy (STM). The differentiation between mono- and bi-layer graphene, presence of defects and interlayer coupling is determined by STM. LDOS mapping demonstrates the observation of quantum interference effects when quasiparticles are scattered off graphene edges, where the later represents line defects. The quantum transport properties are quite sensitive to the nature of disorder in graphene, due mainly to the presence of two additional symmetries: the symmetry between A and B sites in the unit cell (isospin) and the symmetry between the different valleys K-K' (pseudospin). The nature of disorder (local defects or folds in grapheme sheets for example), is responsible for locally breaking either of these symmetries, opening intra- and intervalley scattering processes [2].

Depending on the intrinsic disorder observed in the sample's morphology and on its mobility, the magneto-resistance shows either the conventional weak localization when intervalley scattering is strong or the weak anti localization (WAL), in agreement with the recent WAL theory for graphene [3]. Typically, the feature at small values of magnetic field, show a negative magneto resistance characteristic of weak localization, whereas at larger field a positive magneto resistance typical of antilocalization is observed. The weak localization at small fields depends only upon the phase coherence time, whereas the high field behaviour is dominated by a combination of the intervalley and intravalley scattering time. Each of these scattering times can be extracted from the magneto resistance curves and correlated to the surface morphologies. The consistency of this analysis has been checked using a "universal" scaling for the magneto-transport which will be presented [4].

References:

[1] P. Mallet, F. Varchon, C. Naud, L. Magaud, C. Berger, J.-Y. Veuillen, Phys. Rev. B, 2007, 76, 041403(R)
[2] X. Wu, X. Li, Z. Song, C. Berger, and W. A. de Heer, Phys. Rev. Lett. 2007, 98, 136801 2007.
[3] E. McCann, K. Kechedzhi, V. I. Fal'ko, H. Suzuura, T. Ando, and B. L. Altshuler, Phys. Rev. Lett., 2006, 97, 146805; V. I. Falko, K. Kechedzhi, E. McCann, and B. L. Altshuler H. Suzuura and T. Ando, Solid State Comm, 2007, 143, 33.; K. Kechedzhi, E. McCann, V. I. Falko, H. Suzuura, T. Ando, and B. L. Altshuler, eur. Phys. J. Spec.; Topics, 2008, 148, 39
[4] C. Naud, A. Mahmood, C. Bouvier, F. Hiebel, P. Mallet, J-Y. Veuillen, D. Chaussende, T. Ouisse,
[5] L. Levy, submitted to Phys. Rev. B

Figures:

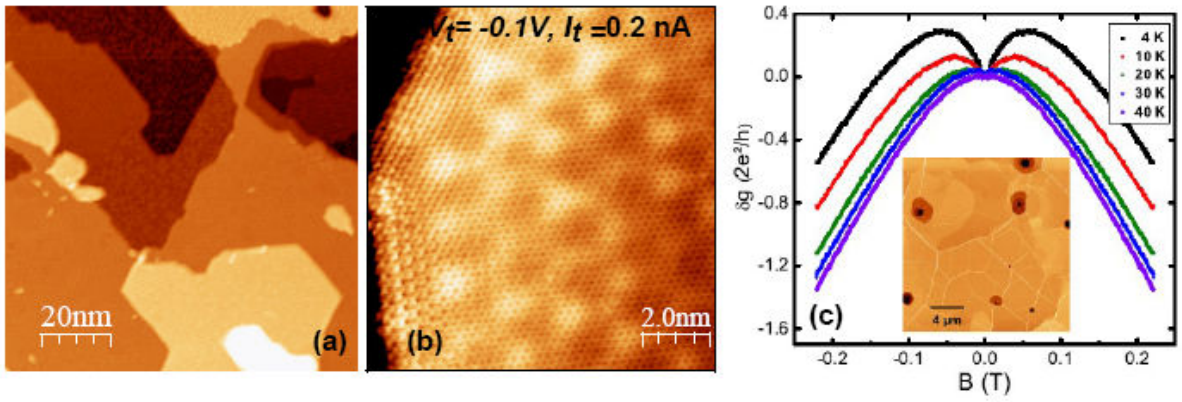

Figure 1: *(a) STM topographic image of graphene on Si face SiC showing terraces of buffer zone, monolayer and bilayer graphene. (b) Low bias STM image of zig-zag and armchair edges present on a monolayer graphene on SiC. (c) Magnetoresistance curves for mulitlayered graphene samples grown under Ar atmosphere (shown in inset).*

DESIGNING ALL-GRAPHENE NANO-JUNCTIONS BY EDGE FUNCTIONALIZATION: OPTICS AND ELECTRONICS

Elisa Molinari[1,2], Caterina Cocchi[1,2], Deborah Prezzi[1], Alice Ruini[1,2] and Marilia J. Caldas[3]

[1]Centro S3 - CNR Istituto Nanoscienze, Via Campi 213/A, 41125 Modena, Italy
[2]Dipartimento di Fisica, Universita' di Modena e Reggio Emilia, Via Campi 213/A, 41125 Modena, Italy
[3]Instituto de Fisica, Universidade de São Paulo, 05508-900 São Paulo, SP, Brazil
elisa.molinari@unimore.it

The recent advances in production techniques of graphene nanostructures call for strategies towards all-graphene nanodevices. We study the effect of covalent edge functionalization on the opto-electronic properties of realistic graphene nano-flakes and junctions.

By means of well tested semi-empirical methods, we compute both mean-field ground state electronic properties and configuration-interaction optical excitations. Our study shows that functionalization can be designed to tune electron affinities and ionization potentials of graphene nanoflakes [1]. This effect can be exploited to realize both *type-I* (straddling) and *type-II* (staggered) all-graphene nano-junctions. At variance to *type-I* [2], we find that *type-II* junctions can display indirect excitations with electrons and holes localized on different sides. The optical properties are characterized in terms of size and functionalization, and the conditions to obtain charge transfer excitons are discussed [3].

References:

[1] C. Cocchi et al. J. Phys. Chem C, in press (2011).
[2] D. Prezzi et al. Phys. Rev. B 77 (2008) 041404(R) and D. Prezzi et al. to be published.
[3] C. Cocchi et al. to be published.

Figures:

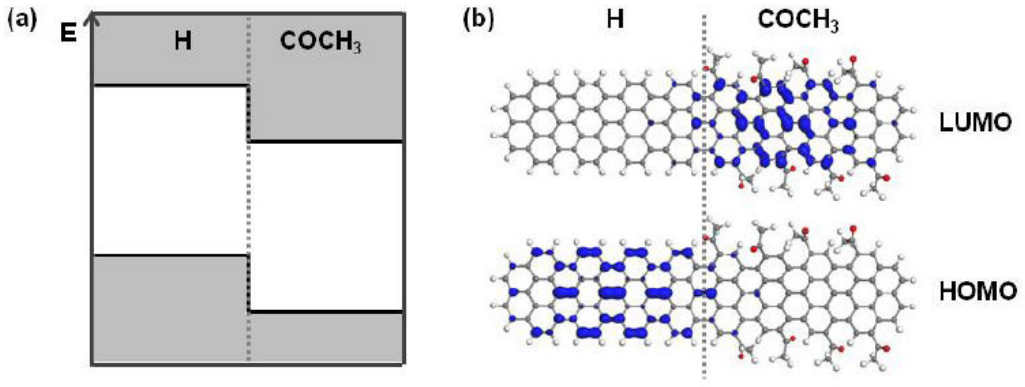

Figure 1: *(a) Scheme for type-II graphene nano-junction: edge covalent functionalization with electron-withdrawing $COCH_3$ groups down shifts the gap region with respect to the hydrogenated side (H); (b) Localized frontier orbitals of H-$COCH_3$ nano-junction.*

THE POLYMER CHEMISTRY OF CARBON MATERIALS AND GRAPHENES

Klaus Müllen

Max-Planck-Institute for Polymer Research, Mainz, 55128, Germany
muellen@mpip-mainz.mpg.de

Research into energy technologies and electronic devices is strongly governed by the available materials. We introduce a synthetic route to graphenes which is based upon the cyclodehydrogenation ("graphitization") of well-defined dendritic (3D) polyphenylene precursors. This approach is superior to physical methods of graphene formation such as chemical vapour deposition or exfoliation in terms of its (i) size and shape control, (ii) structural perfection, and (iii) processability (solution, melt, and even gas phase). The most convincing case is the synthesis of graphene nanoribbons under surface immobilization and in-situ control by scanning tunnelling microscopy.
Columnar superstructures assembled from these nanographene discs serve as charge transport channels in electronic devices. Field-effect transistors (FETs), solar cells, and sensors are described as examples.
Upon pyrolysis in confining geometries or "carbomesophases", the above carbon-rich 2D- and 3D-macromolecules transform into unprecedented carbon materials and their carbon-metal nanocomposites. Exciting applications are shown for energy technologies such as battery cells and fuel cells. In the latter case, nitrogen-containing graphenes serve as catalysts for oxygen reduction whose efficiency is superior to that of platinum.

DEFECTS IN GRAPHENE: A RAMAN SPECTROSCOPIC INVESTIGATION

Zhenhua Ni[1], Zexiang Shen[2], Kostya Novoselov[3] and Andre Geim[3]

[1]Department of Physics, Southeast University, Nanjing, China 211189
[2]Division of Physics and Applied Physics, School of Physical and Mathematical Sciences, Nanyang Technological University, 21 Nanyang Link, Singapore 637371
[3]Centre for Mesoscience and Nanotechnology, University of Manchester, Manchester M13 9PL, U.K
zhni@seu.edu.cn

Graphene, the one monolayer thick flat graphite, has been attracting much interest since it was firstly reported in 2004. Graphene has many unique properties which make it an attractive material for fundamental study as well as for potential applications. Raman spectroscopy has been extensively used to study graphene, i.e. identify graphene layer numbers; probe electronic band structure; determine type of edges (zigzag or armchair); measure the concentration of electron and hole dopants. Here, we present our results on the Raman spectroscopic investigation of defects in graphene.

The Raman D peak (~1345 cm^{-1}) is commonly used to estimate the amount of defects in graphitic materials. However, no such peak has been reported for pristine cleaved graphene, this seems suggest that pristine cleaved graphene is a perfect crystal without defects (or defects are undetectable). Here, we point out that, although small and usually unnoticed under the noise level, the D peak is generally present in cleaved graphene and, typically, reaches ~1.5% in amplitude with respect to the G peak.[1] This small D peak could be due to a certain concentration of sp^3 adsorbates and vacancies in grapheme (in other words, defects), and such resonant scatters can effectively limit the carrier mobility in graphene. By comparing the amplitude of D peak and carrier mobilities obtained in transport measurement; we show that the observed small D peak is sufficient to account for the limited mobilities (~2 m^2/Vs) currently achievable in graphene on a substrate.

We have also monitored graphene sheets with defects that are introduced during insulator layer (such as SiO_2, HfO_2) deposition using different methods (Sputtering, PLD, E-beam evaporation), and our results show that defects were introduced in graphene during deposition and the amounts of defects increase as the graphene thickness decreases. After annealing, the defects in graphene can be greatly reduced.[2] In addition, we also studied the defects in epitaxial graphene grown on SiC substrate [3] and graphene treated by plasma (H_2 and Ar) and electron beam.

References:

[1] Ni ZH, Ponomarenko LA, Nair RR, Yang R, Anissimova S, Grigorieva IV, Schedin F, Shen ZX, Hill EH, Novoselov KS, Geim AK Nano Letters 10, 3868-3872 (2010)
[2] Ni ZH, Wang HM, Ma Y, Kasim J, Wu YH, Shen ZX Tunable stress and controlled thickness modification in graphene by annealing ACS Nano 2, 1033 (2008)
[3] Ni ZH, Chen W, Fan XF, Kuo JL, Yu T, Wee ATS, Shen ZX Raman spectroscopy of epitaxial graphene on a SiC substrate Physical Review B 77, 115416 (2008)

Figures:

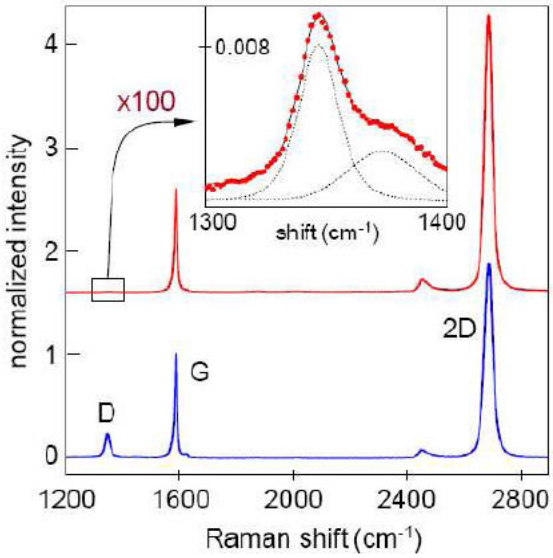

Figure 1: *Raman spectra for pristine and defected graphene (red and blues curves, respectively). In the latter case, the defects were induced by exposure to atomic H. The curves are normalized with respect to the G peak amplitude and shifted for clarity. The inset zooms into the D band region. In our experience, such small D peaks are universally present in Raman spectra of cleaved graphene.*

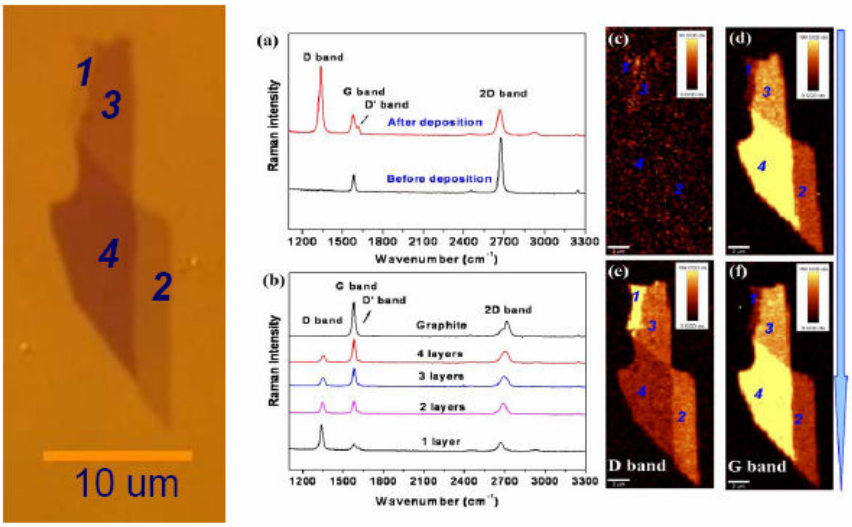

Figure 2: *(a) Raman spectra of single layer graphene before and after the 5 nm SiO_2 deposition. (b) Raman spectra of graphene with different thicknesses as well as that of bulk graphite after 5 nm SiO_2 deposition. Raman images of graphene sheets before SiO_2 deposition generated from the intensity of the D band (c) and G band (d). Raman images of graphene sheets after 5 nm SiO_2 deposition using the intensity of D band (e), and G band (f). The thinner graphene sheets have stronger D band, hence they contain more defects.*

WEAK LOCALIZATION VS WEAK ANTILOCALIZATION IN GRAPHENE

Frank Ortmann, Alessandro Cresti, Gilles Montambaux, Stephan Roche

INAC/SPrAM, CEA Grenoble, 17 Rue des Martyrs, 38054 Grenoble, France
IMEP-LAHC, Minatec, 3 Parvis Louis Neel, 38016 Grenoble, France
Laboratoire de Physique des Solides, UMR 8502 du CNRS, Univ Paris-Sud, 91405 Orsay, France
CIN2 (ICN-CSIC) Barcelona, Campus UAB, 08193 Bellaterra, Spain
ICREA, 08010 Barcelona, Spain
ortmann.f@googlemail.com

The understanding of quantum-transport phenomena in graphene-based materials is the current subject of great excitation. Indeed, low energy excitations can be formally described as massless Dirac Fermions exhibiting a linear dispersion relation together with an additional degree of freedom, namely pseudospin, which stems from the underlying sublattice degeneracy. In the presence of disorder, one of the predicted signatures of pseudospin is the change in sign of the quantum correction to the semiclassical Drude conductivity (1). This phenomenon, referred to as weak antilocalization (WAL), indeed results from complex quantum-interferences effects of charge carriers in a disordered potential landscape, and in grapheme these characteristics are markedly different from ordinary metals.

The effect of WAL has been recently observed experimentally with weak-field magneto-transport measurements in samples of high quality because the quantum-interference effects are preserved when the phase-relaxation length of the electrons is large enough. (2)

In this talk we present a numerical weak-field magneto-transport study of huge graphene samples and the influence of a realistic disorder potential describing charges trapped in the gate oxide causing long-range scattering potentials (3). Our simulations give clearly different magneto-conductance responses in different regimes which are fingerprint of either weak localization or WAL. Depending on the strength of the perturbing potential, the magneto-conductance can be tuned from positive to negative. The energy of the charge carriers as determined by the gate potential provides a second handle to modify these characteristics.

Our results therefore shed new light on experiments and unveil the possible origin of multiple crossovers from positive to negative magneto-conductance.

References:

[1] E. McCann, K. Kechedzhi, V. I. Fal'ko, H. Suzuura, T. Ando, B. L. Altshuler; Phys. Rev. Lett. 97 (2006), 146805
[2] F. V. Tikhonenko, A. A. Kozikov, A. K. Savchenko Phys. Rev. Lett. 103 (2009), 226801
[3] F. Ortmann, A. Cresti, G. Montambaux, S. Roche (submitted)

Figures:

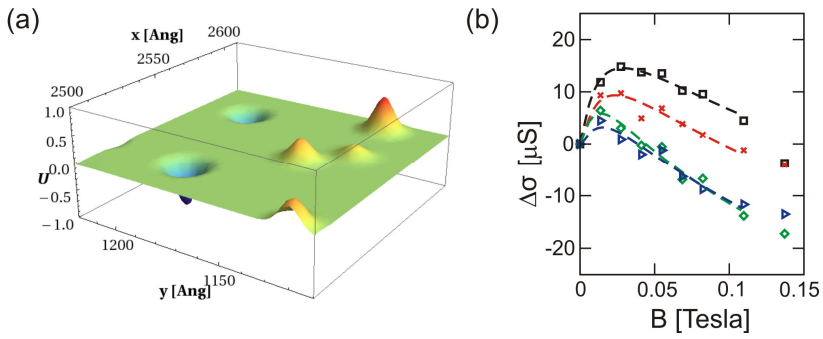

Figure 1: *(a) Typical long-range disorder potential. (b) Magneto-transport response.*

THERMODYNAMICALY STABLE GRAPHENE SOLUTIONS

Alain Pénicaud

Université de Bordeaux, Centre de Recherche Paul-Pascal, CNRS, 115 av. Schweitzer, 33600 Pessac, France
penicaud@crpp-bordeaux.cnrs.fr

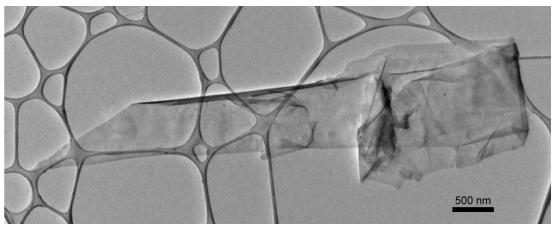

Graphite is insoluble in all media but may be dispersed with surfactants and/or sonication to obtain metastables suspensions. However, some graphite intercalation compounds (GICs) have been shown to be spontaneously soluble in polar organic solvents without the need for any kind of additional energy, such as sonication or high shear mixing.[1-3] Flakes of several μm^2 can be deposited from these solutions.

References:

[1] Solutions of graphene, C. Vallés and A. Pénicaud, patent, WO 2009/087287; FR 07/05803 august 9, 2007.
[2] Solutions of Negatively Charged Graphene Sheets and Ribbons, C. Vallés et al., J. Am. Chem. Soc., 2008, 130, 15802–15804.
[3] Graphene solutions, A. Catheline, C. Vallés, C. Drummond, L. Ortolani, V. Morandi, M. Marcaccio, M. Iurlo, F. Paolucci, A. Pénicaud, submitted.

TRANSPORT SCATTERING TIME PROBED THROUGH RF ADMITTANCE OF A GRAPHENE CAPACITOR

B. Plaçais, E. Pallecchi, A.C. Betz, J. Chaste, G. Feve, B. Huard, T. Kontos, J.-M. Berroir

Laboratoire Pierre Aigrain, Ecole Normale Superieure, 24, rue Lhomond, 75005 Paris, France
placais@lpa.ens.fr

We have investigated electron dynamics in top gated graphene by measuring the gate admittance of a diffusive graphene capacitor in a broad frequency range as a function of carrier density. The density of states, conductivity and diffusion constant are deduced from the low frequency gate capacitance, its charging time and their ratio. The admittance evolves from an RC-like to a skin-effect response at GHz frequency with a crossover given by the Thouless energy. The scattering time is found to be independent of energy in the 0- 200 meV investigated range at room temperature.
This is consistent with a random mass model for Dirac Fermions.

References:

[1] E. Pallecchi et al, arXiv:/1005.3388v1 (2010).

IDENTIFYING REACTIVE SITES ON GRAPHENE SHEETS AGAINST 1,3-DIPOLAR CYCLOADDITION AND AMIDATION REACTIONS

M. Quintana[1], A. Montellano[1], X. Ke[2], G. Van Tendeloo[2], C. Bittencourt[2], and **M. Prato[1]***

[1]Center of Excellence for Nanostructured Materials (CENMAT), INSTM UdR di Trieste, Dipartimento di Scienze Chimiche e Farmaceutiche, University of Trieste, Trieste, Italy
[2]Electron Microscopy for Material Science (EMAT), Physics Department, University of Antwerp, Antwerp, Belgium,

The production of graphene by micromechanical cleavage [1] has triggered an enormous experimental activity. Since then, many studies have demonstrated that graphene monolayers possess novel structural, [2] electrical [3] and mechanical [4] properties. However many important issues need to be addressed before this material can be used in an ideal way. Much workhas been produced that proposes chemical functionalization as a tool for tuning graphene chemical and physical properties. For example, chemical functionalization can render graphene dispersable in different solvents. [5] To exploit the high mobility of graphene, the band gap engineering and controllable doping of semimetal graphene can be achieved by chemical functionalization. [6] Moreover, the non-uniformity of graphene edges and the potential for dangling bonds are thought to have significant influence on their chemical properties and reactivity. [7] Chemical modification of various forms of graphene, including reduced graphene oxide, [8] liquid-phase exfoliated graphite, [9] pristine graphene and its multilayers has been obtained. [5] For instance, the aryl diazonium-based reaction has been extensively studied as a specific radical reaction on graphene layers. [10] In graphene, the edges exhibit a higher reactivity than the interior during this specific reaction. Instead, we have recently reported the functionalization of graphene layers by condensation of a protected α-amino acid and paraformaldehyde, [11] demonstrating that even if the reactivity of graphene differs from that of fullerenes and carbon nanotubes, the 1,3-dipolar cycloaddition can be efficiently performed and yields a highly functionalized material taking place not just at the edges but also at the C=C bonds in the center of graphene sheets. However, further work needs to be performed for understanding the chemical structure of the functionalized graphene and their reaction mechanisms.

In this work we present a detailed study on the reactivity of graphene sheets stabilized in DMF using two different reactions: the 1,3-dipolar cycloaddition reaction and the amide-bond condensation reaction achieved between the free carboxylic groups already present in the exfoliated graphene and the amino functionalities of the attached moieties. Thus, we have functionalized graphene with a first generation polyamidoamine (PAMAM) dendron possessing an anchoring amine point and two terminal Boc-protected amines. Indeed, dendrimers and dendrons containing polar groups in their structures have been widely conjugated to carbon nanostructures in order to increase the solubility, modifying in this way their inherent apolar character to obtain more tunable structures. [12] Even more, the presence of free terminal amino groups can serve as ligands in the stabilization of gold nanostructures. [13] As first step to identify the reactive sites on graphene layers the free amino groups were quantified by the Kaiser test. These amino groups selectively bind to gold nanoparticles, which can then be employed as contrast markers. The interaction between Au nanoparticles and functionalized graphene was followed by UV-Vis spectroscopy, while the morphological changes were characterized by transmission electron microscopy (TEM). The presence of the organic groups and their interaction with Au nanoparticles were verified by X-ray photoelectron spectroscopy. Au nanoparticles distributed uniformly all over the graphene surface were found for functionalized graphene via 1,3-dipolar cycloaddition. Instead, in functionalized graphene by amidation reaction Au nanoparticles were observed mainly at the edges of graphene sheets. All these results confirm that graphene produced by mild sonication of graphite in DMF are relatively free of defects and can be efficiently functionalized by well establish organic reactions.

References:

[1] Novoselov, K. S.; Geim, A. K.; Morozov, S. V.; Jiang, D.; Zhang, Y.; Grigorieva, S. V.; Firsov, A. A.; Science (2004) 306, 666-669.
[2] Meyer, J. C.; Geim, A. K.; Katsnelson, M. I.; Novoselov, K. S.; Booth, T. J.; Roth, S.; Nature (2007) 446, 60-63
[3] a) Castro, N.; Guinea, F.; Peres, N. M. R.; Novoselov, K. S.; Geim, A. K.; Rev. Mod. Phys. (2009) 81, 109-162; b) Berger, C.; Song, Z.; Li, T. X.; Ogbazghi, A. Y.; Feng, R.; Dai, Z.; Marchenkov, A. N.; Conrad, E. H.; First, P. N.; de Heer, W. A.; J. Phys. Chem. B (2004) 108, 19912-19916.
[4] Frank, I. W.; Tanenbaum, D. M.; van der Zande, A. M.; McEuen, P. L.; J. Vac. Sci. Technol. (2007) 25, 2558-2561
[5] Park, S.; Ruoff, R. S.; Nat. Nanotech. (2009) 217-224.
[6] Sharma, R.; Baik, H. J.; Perera, C. J.; Strano, M. S.; Nano Lett. (2010) 10, 398-405
[7] Ritter, K. A.; Lyding, J. W.; Nat. Mater. (2009) 8, 235-242.
[8] Lomeda, J. R. Doyle, C. D. Kosynkin, D. V. Hwang, W. F. Tour, J. M. J. Am. Chem. Soc. (2008) 130, 16201-16206
[9] Hernandez, Y. Nicolosi, V. Lotya,M. Blighe, F. M. Sun,Z. De, S. McGovern,I. T. Holland, B. Byrne, M. GunKo, Y. K. Boland, J. J. Niraj, P. Duesberg, G. Krishnamurthy, S. Goodhue, R. Hutchison, J. Scardaci, V. Ferrari, A. C. Coleman, J. N. Nature Nanotechnology (2008) 3 563-568
[10] Sharma, R.; Huun, B.; Perera. C. J.; Strano, M. S.; Nano Lett. (2010) 10, 398-405.
[11] Quintana, M.; Spyrou, K.; Grzelczak, M.; Browne, W. R.; Rudolf, P.; Prato, M.; ACS Nano (2010) 4, 3527-3533.
[12] Herrero, M. A.; Toma, F. M.; Al-Jamal, K. T.; Kostarelos, K.; Bianco, A.; Da Ros, T.; Bano, F.; Casalis, L.; Scoles, G.; Prato, M.; J. Am. Chem. Soc. (2010) 132, 1731.
[13] Templeton, A. C.; Chen, S.; Gross, S. M.; Murray, R. W.; Langmuir (1999) 15, 66-76.

[14] This work was supported by the Italian Ministry of Education MIUR (cofin Prot. 20085M27SS and Firb RBIN04HC3S).

Figures:

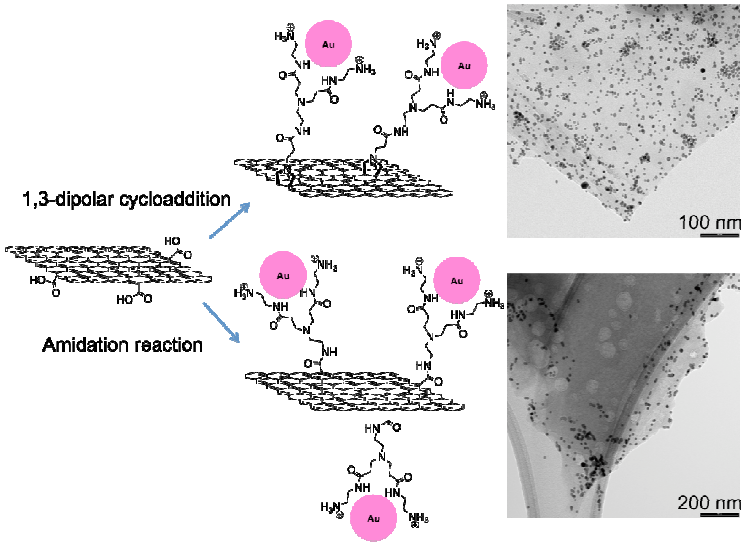

Figure 1: *Schematic representation of functionalized graphene (left). TEM images of reactive sites on graphene marked by Au nanoparticles.*

NON-COVALENT FUNCTIONALISATION OF GRAPHENE USING SELF-ASSEMBLED MONOLAYERS

A.J. Quinn[a], B. Long[a], B. N. Szafranek[b], G. Visimberga[a], M. Manning[a], D. Thompson[a], J.C. Greer[a], I.M. Povey[a], J. MacHale[a], D. Neumaier[b], H. Kurz[b]

[a]Tyndall National Institute, Univeristy College Cork, Lee Maltings, Dyke Parade, Cork, Ireland
[b]Advanced Microelectronic Center Aachen (AMICA), AMO GmbH, Otto-Blumenthal-Str. 25, 52074 Aachen, Germany
aidan.quinn@tyndall.ie

Graphene, monolayer sheets of sp^2-bonded carbon atoms arranged in a honeycomb-like structure, continues to attract intense research interest due to its unique electronic properties and potential applications. As a "surface-only" nanomaterial, the properties of monolayer or few-layer grapheme structures are extremely sensitive to adsorbed ambient contaminants, with a correspondingly severe impact on the electrical characteristics and stability of graphene-based devices. Development of strategies for functionalisation of graphene without adversely affecting its electronic properties are of key importance. Here we report on a simple, versatile functionalisation method based on solution-phase formation of alkane-amine self-assembled monolayers (SAMs) on graphene; see Figure 1a for a schematic.

Ab initio calculations (2^{nd} order Møller–Plesset perturbation theory), applied to a cluster model (methylamine on pyrene) yield a binding energy, E_b = -220 meV for the anchor amine group, when the amine is located above a C-C bond (an "over-bond" site). Similar values were found for calculations with the amine group located over a carbon atom ("over-atom" site, E_b = -223 meV) and for the amine located over the centre of one of the phenyl rings ("over-ring" site, E_b = -215 meV), indicating that there is no strong preferential bonding site to the graphene plane. The results are consistent with a noncovalent amine-graphene interaction (~220 meV binding energy), which is strong enough to enable formation of a stable aminodecane monolayer at room temperature (T = 300 K, E_b ~ 8 kT), but also sufficiently labile to allow the necessary mobility of the molecules required for formation of a closepacked monolayer. Atomistic molecular dynamics simulations for 784 1-aminodecane molecules on a 13 nm x 15 nm graphene substrate (not shown) predict formation of a mobile but stable alkane-amine SAM, with nearest-neighbour distances for the amine anchor groups ~ 0.33 nm.

Measured Raman spectroscopy data for graphene monolayers deposited on thermally oxidised silicon substrates and then functionalized with 1,10-diaminodecane (red data in Fig. 1b) are also consistent with a non-covalent, charge-transfer interaction between the alkane-amine molecules and graphene. The presence of a sharp two-phonon *2D* peak (full-width at half-maximum intensity, FWHM ~ 24.5 cm^{-1}), a characteristic of monolayer graphene, and the absence of a defect (*D*) peak close to 1350 cm^{-1} following functionalization (Fig. 1b, inset) confirms that the layer of 1,10-diaminodecane molecules does not perturb the sp^2-hybridisation of the graphene monolayer and does not introduce additional structural defects. Further, the spectrum for the functionalised monolayer shows several significant differences when compared with data measured for an as-deposited graphene monolayer (Fig. 1b, gray data). Both the shift in the G peak position towards higher energy and the reduction in intensity of the *2D* peak following functionalisation of the exposed graphene surface with 1,10-diaminodecane are consistent with doping, likely via charge transfer from the amine anchor groups to the graphene.

Figure 1c shows two-probe resistance (R_{2P}) vs gate voltage (V_g) data measured in vacuum for a monolayer graphene field-effect device following fabrication. The data show the expected behaviour for unpassivated graphene devices exposed to ambient conditions – hysteretic ambipolar conduction, with minimum conductivity (Dirac Point, $V_{g,DP}$) at positive gate voltage. This positive value of $V_{g,DP}$ indicates unintentional hole doping, likely from contaminants at the graphene surface and the graphene-substrate interface, e.g., adsorbed water and organic residue from the fabrication process. Figure 1d shows the R_{2P}-V_g data for the same device, acquired following ex situ annealing to 250 ºC under nitrogen for 1 hour, functionalisation in solution with 1-aminodecane and transfer under ambient conditions (~ 1 hour) to the vacuum measurement chamber. Several significant changes are evident, including a shift in the Dirac Point to negative gate voltage and a sharper resistance peak (higher carrier mobility) around the Dirac Point for each sweep. These negative values for $V_{g,DP}$ in the functionalised device indicate adsorbate-induced electron doping, presumably from the amine anchor groups in the 1-aminodecane molecular layer. Kim et al. have proposed a simple device model to interpret two-probe R_{2P}-V_g data[25]. Using three fit parameters — the contact resistance (R_c), the impurity carrier density (n_0) and the fieldeffect mobility (μ_{FE}) — the two-probe device resistance can be expressed as

$$R_{2P}(V_g) = R_C(V_g) + \frac{L}{We\mu_{FE}\sqrt{n_0^2 + [n(V_g, V_{g,DP})]^2}} \quad (1)$$

where L (≈ 6μm) and W (≈ 10μm) are the device length and width, respectively, e is the electronic charge and *n* is the gate-induced carrier density, $n \propto |V_g - V_{g,DP}|$ if quantum capacitance effects are excluded. The inset to Fig. 1d shows fits to Equation 1 for the data in the main panel, yielding estimates for both the mobility, $\mu_{FE} \approx 2350–2500 cm^2V^{-1}s^{-1}$, and the impurity carrier density, $n_0 \approx 0.8x10^{12}$ cm^{-2}, assuming a constant contact resistance R_c = 200Ω for both sweeps. In general, devices functionalized with 1-aminodecane following annealing show higher carrier mobilities and also improved stability upon re-exposure to ambient conditions compared with annealed "bare" devices, suggesting that the 1-aminodecane layer can act as a barrier to hinder the readsorption of contaminants, e.g., water.

A key challenge in the development of graphene-based nanoelectronics is the deposition of inorganic dielectrics onto graphene for top-gated devices. "Seeding" processes for atomic layer deposition (ALD) of inorganic dielectrics onto graphene have been reported, including ozone pre-treatment, and also deposition of thin (~10 nm) polymer layers containing appropriate binding groups. Use of selfassembled monolayers represents an attractive complementary process. The smaller thickness of the alkane-amine SAM, compared to polymer layers, would increase the effective total dielectric capacitance, and the defect density in SAM-modified graphene should be lower than for ozone-treated graphene. Figure 1e shows a scanning electron microscopy image of an ultra-thin film of aluminium oxide (5 nm nominal thickness), which was deposited onto highly-oriented pyrolytic graphite that had been functionalised with 1,10-diaminodecane. Uniform coverage of the substrate (including some small defects and a step edge) is evident. Figure 1f shows the edge of the aluminium oxide film following removal of part of the film using adhesive tape. The remaining aluminium oxide shows good adhesion to the substrate. The film is quasi-continuous film arising from coalescence of two-dimensional islands, as expected for the chosen film thickness.

In conclusion, self-assembled monolayers of alkane-amines represent a versatile new route for noncovalent functionalisation of graphene without adversely affecting its unique properties. Advantages for nanoelectronic applications include adsorbate doping, surface passivation and seeded ALD. Selection of suitable terminal groups for binding of target species onto graphene opens up possibilities for selective and sensitive graphene-based electromechanical or electrochemical (bio)sensors.

This work was supported by the European Commission under the FP7 ICT project "GRAND" (215572).

Figures:

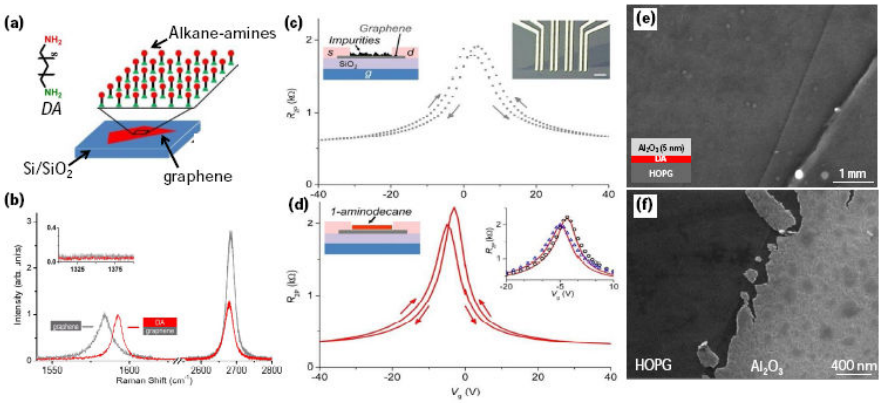

Figure 1: *(a) Left: Structure of 1,10-diaminodecane (DA). Right: Schematic of a graphene layer functionalised with a monolayer of alkane amines. (b) Raman spectra (514.5 nm excitation) for a graphene monolayer deposited onto an unmodified Si/SiO_2 substrate (gray) and also for a graphene monolayer (red) following following functionalisation in solution with 1,10-diaminodecane (DA). Inset: No defect (D) peak ~ 1350 cm^{-1} is observed following functionalisation. (c) Two-probe resistance vs. gate-voltage (R_{2P}–V_g) characteristics measured in vacuum for a back-gated, monolayer graphene device following fabrication.(d) R_{2P}–V_g characteristics for the same device measured following ex situ thermal annealing under nitrogen (200 C) and functionalisation in solution with 1-aminodecane. Fits to the R_{2P}–V_g data for the functionalised device (d, inset) yield estimates for the device mobility, $\mu_{FE} \approx 2350–2500$ $cm^2V^{-1}s^{-1}$. (e) SEM image of a conformal 5 nm thick Al_2O_3 film deposited using atomic layer deposition onto a graphite substrate, which had been functionalised with 1,10-diaminodecane. (f) SEM image of the edge of the Al_2O_3 film and the underlying graphite (HOPG) substrate following removal of part of the Al_2O_3 film using adhesive tape.*

HIGH EFFICIENCY ENERGY STORAGE OF GRAPHENE-BASED COMPOSITES

Wencai Ren, Zhongshuai Wu, Dawei Wang, Guangmin Zhou, Na Li, Jinping Zhao, Songfeng Pei, Feng Li, and Hui-Ming Cheng

Shenyang National Laboratory for Materials Science, Institute of Metal Research, Chinese Academy of Sciences, Shenyang 110016, P.R. China
wcren@imr.ac.cn

Energy storage is vital to meet the challenge of global warming and finite fossil-fuel supplies in modern society [1]. Graphene, a unique two-dimensional carbon material, is predicted to be an excellent electrode material candidate for energy conversion/storage in supercapacitors and lithium ion batteries (LIBs) because of its high specific surface area, good chemical stability, excellent electrical and thermal conductivity as well as remarkably high mechanical strength and Young's modulus [2-4].

Controllable synthesis of graphene sheets (GSs) in a large scale is the prerequisite and essentially important for the energy storage applications of graphene. We proposed a simple and effective strategy to tune the number of graphene layers by selecting suitable starting graphite using a chemical exfoliation method [5], developed a mild oxidation and exfoliation method to prepare large-area graphene oxide with a size up to 200 micrometers and realized the size-controlled synthesis of graphene oxide by simply tuning the content of C-O in graphite oxide [6], proposed a hydrogen arc discharge exfoliation method for the synthesis of GSs with excellent electrical conductivity from graphite oxide [7], and developed a rapid and nondestructive low-temperature reduction method to effectively improve the electrical conductivity of graphene oxide by using HI acid [8].

In order to fully utilize the advantages of GSs for energy storage, we proposed the use of GSs/metal oxide (or conducting polymer) as electrode materials for high performance supercapacitors and LIBs. Based on this idea, we designed and synthesized a series of graphene/metal oxide nanoparticles composites by combining sol-gel and low-temperature annealing processes, including GSs/hydrous RuO_2 composites for high energy supercapacitors [9], GSs/Co_3O_4 and GSs/Fe_3O_4 composites for high energy LIBs [10, 11], and GSs/TiO_2 and GSs/$Li_4Ti_5O_{12}$ composites for high power LIBs [12]. In order to achieve high energy and power densities, we also developed a high-voltage asymmetric electrochemical capacitor based on graphene as negative electrode and a GSs/MnO_2 nanowire composite as positive electrode in a neutral aqueous Na_2SO_4 solution as electrolyte [13]. Moreover, by incorporating with polyaniline, we fabricated GSs/polyaniline composite paper via *in situ* anodic electropolymerization for high performance flexible supercapacitor electrodes [14].

All the above composites show a greatly improved capacity, cycling stability and rate capability compared to solo graphene and metal oxide, demonstrating the positive synergistic effect of GSs and metal oxide on the improvements of electrochemical performance. We believe that the performance of GSs-based composite electrodes can be further improved by optimizing the composition and structure of GSs and particles, and the architecture and synthesis process of composites, to meet the future requirements for high energy and high power energy storage systems.

References:

[1] C. Liu, F. Li, L.P. Ma, H.M. Cheng, Adv Mater 8 (2010) E28.
[2] K.S. Novoselov, A.K. Geim, S.V. Morozov, D. Jiang, Y. Zhang, S.V. Dubonos, I.V. Grigorieva, A.A. Firsov, Science, 306 (2004) 666.
[3] A.K. Geim, K.S. Novoselov, Nature Mater. 3 (2007) 183.
[4] A.K. Geim, Science 5934 (2009) 1530.
[5] Z.S. Wu, W.C. Ren, L.B. Gao, B.L. Liu, C.B. Jiang, H.M. Cheng, Carbon 2 (2009) 493.
[6] J.P. Zhao, S.F. Pei, W.C. Ren, L.B. Gao, H.M. Cheng, ACS Nano 9 (2010) 5245.
[7] Z.S. Wu, W.C. Ren, L.B. Gao, J.P. Zhao, Z.P. Chen, B.L. Liu, D.M. Tang, B. Yu, C.B. Jiang, and H.M. Cheng, ACS Nano 2 (2009) 411.
[8] S.F. Pei, J.P. Zhao, J.H. Du, W.C. Ren, H.M. Cheng, Carbon 15 (2010) 4466.
[9] Z.S. Wu, D.W. Wang, W.C. Ren, J.P. Zhao, G.M. Zhou, F. Li, H.M. Cheng, Adv. Funct. Mater. 20 (2010) 3595.
[10] Z.S. Wu, W.C. Ren, L. Wen, L.B. Gao, J. P. Zhao, Z. P. Chen, G.M. Zhou, F. Li, H.M. Cheng, ACS Nano 6 (2010) 3187.
[11] G.M. Zhou, D.W. Wang, F. Li, L.L. Zhang, N. Li, Z.S. Wu, L. Wen, G.Q. Lu, H.M. Cheng, Chem Mater 18 (2010) 5306.
[12] N. Li, G. Liu, G.M. Zhou, F. Li, H.M. Cheng, Adv Mater In revision.
[13] Z.S. Wu, W.C. Ren, D.W. Wang, F. Li, B.L. Liu, H.M. Cheng, ACS Nano 10 (2010) 5835.
[14] D.W. Wang, F. Li, J.P. Zhao, W.C. Ren, Z.G. Chen, J. Tan, Z.S. Wu, I. Gentle, G.Q. Lu, H.M. Cheng, ACS Nano 7 (2009) 1745.

Figures:

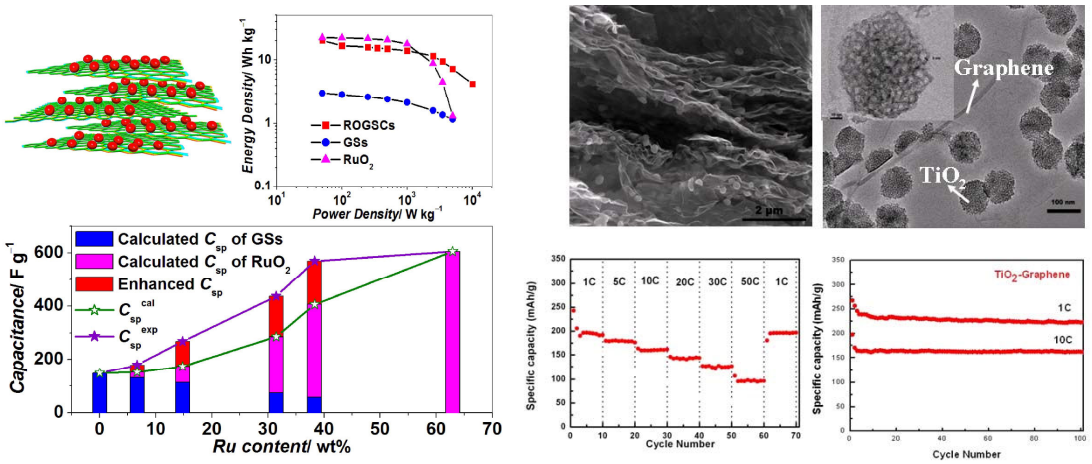

Figure 1: *GSs/hydrous RuO_2 composites for high energy supercapacitors (left panel) [9] and GSs/TiO_2 composites for high power LIBs (right panel) [12].*

DEVELOPMENT OF GRAPHENE FOR HIGH FREQUENCY ELECTRONICS

J. A. Robinson, D. Snyder, Mark Fanton, M. J. Hollander, M. Labella, Z. Hughes, K. Trumbull, R. Cavalero, B. Weiland, E. Hwang, and S. Datta

The Pennsylvania State University, University Park, PA, U.S.A
jrobinson@psu.edu

Graphene's high carrier mobility [1], large saturation current [2], low noise, and superior scalability make it of interest as a channel material for RF-FET applications. The practicality and success of such a technology depends on the ability to, first, regularly and controllably synthesize graphene, second, integrate it with metals and dielectrics in a reproducible manner, and, finally, to develop device designs that take advantage of (or overcome) graphene's unique properties while minimizing performance-limiting parasitics. In this talk, we will provide insight into ultra-large area growth, integration of graphene with ultra-thin dielectrics (EOT ~ 1nm), and how growth and device processing effect the transport properties of epitaxial graphene.

Graphene synthesis is accomplished on SiC (Figure 1) and Sapphire up to 100mm wafers, with excellent uniformity (Figure 2). Graphitization of SiC(0001) is achieved by low-pressure sublimation of Si from the Si-face of semi-insulating 6H-SiC (II-VI, Inc.) at 1600°C and mediated by an Ar atmosphere [3]. Graphene films grown under these conditions are primarily one- to two-layers thick according to Raman spectroscopy and transmission electron microscopy, [4] with a D/G peak ratio of 0.07 ± 0.03. Direct growth of graphene on sapphire is accomplished via the decomposition of methane at 1425 – 1600ºC, where film nucleation and quality are found to be a strong function of methane concentration, growth time, and growth temperature [5]. Raman spectroscopy confirms, for the first time, the formation of monolayer and bilayer graphene on sapphire, with improved structural quality as deposition temperature increases.

In addition to synthesis of large area, high quality graphene, the successful implementation of a graphene-based electronic technology must address low resistance metal/graphene contacts, and the integration of graphene with high-k dielectrics. We have developed a robust method for forming high quality ohmic contacts to graphene, which improves the contact resistance by nearly 6000x compared to untreated metal/graphene interfaces [6]. Optimal specific contact resistance for treated Ti/Au contacts is found to average $5x10^{-8}$ Ohm-cm^2, demonstrating a significant improvement in ultimate resistance compared to current technology. It is found that most metallizations result in similar contact resistances in this work (Figure 3), regardless of the work function difference between graphene and the metal over layer, which is explained by the chemical and structural modification of graphene during device processing.

Finally, we discuss the successful integration of ultra-thin high-k dielectrics and their impact on graphene transport. All oxides deposited via atomic layer deposition require some type of seeding method. Additionally, heterostructures (seed ≠ overlayer) have deleterious effects on Hall mobility while homostructures can lead to an increase in Hall mobility (Figure 4). Doping appears to be material dependent and varies with film thickness. Importantly, 5nm thick EBPVD HfO_2 gate dielectrics with an EOT of ~1nm are successfully demonstrated and show improved Hall mobility, on-off ratio, and transconductance relative to Al_2O_3 gates and heterostructure gates comprised of various dielectrics (Figure 5).

References:

[1] Novoselov, K.S.; Geim, A.K.; Morozov, S.V.; Jiang, D.; Zhang, Y.; Dubonos, S.V.; Grigorieva, I.V.; Firsov, A.A.; Science 2004 306, 666-669
[2] Moon, J.S.; Curtis, D.; Bui, S.; Hu, M.; Gaskill, D.K.; Tedesco, J.L.; Asbeck, P.; Jernigan, G.G.; VanMil, B.L.; Myers-Ward, R.L.; Eddy, C.R.; Campbell, P.M.; Weng, X.; IEEE Electron Device Letters 2010, 31, 4, 260-262
[3] Robinson, J.A.; Labella, M.; Trumball, K.A.; Weng, X.J.; Cavelero, R.; Daniels, T.; Hughes, Z.; Hollander, M.J.; Fanton, M.; Snyder, D.; ACS Nano 4 (5), 2667-2672

[4] Robinson, J.A.; Wetherington, M.; Tedesco, J.L.: Campbell, P.M.; Weng, X.; Stitt, J.; Fanton, M.; Frantz, E.; Snyder, D.; VanMil, B.L.; Jernigan, G.G.; Meyers-Ward, R.L.; Eddy, C.R.; Gaskill, D.K.; Nano Letters 2009, 9, 2873-2876
[5] Fanton, M.; Robinson, J.; Weiland, B.; LaBella, M.; Trumbull, K.; Kasarda, R.; Howsare, C.; Stitt, J.; Snyder, D.; Nano Lett., Submitted Dec 2010
[6] Robinson, J.A.; LaBella, M; Zhu, M.; Hollander, M.; Kasarda, R.; Hughes, Z.; Trumbull, K.; Cavalero, R.; Snyder, D.; Applied Physics Letters, Submitted Dec.2010

Figures:

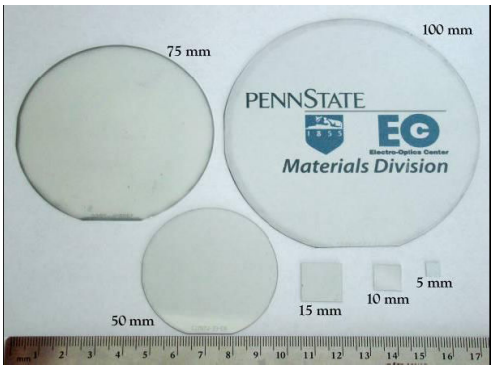

Figure 1: *Photographic image of graphene grown SiC(0001) wafers up to 100 mm*

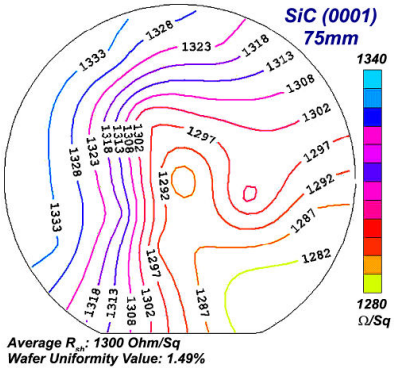

Figure 2: *Sheet resistance (Ohm/sq) map of a 75mm graphene wafer illustrating high uniformity*

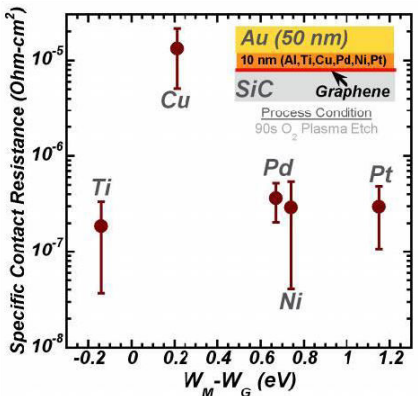

Figure 3: *Specific contact resistance of various metals versus graphene/metal work function difference.*

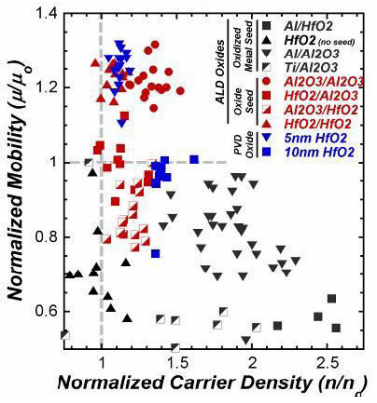

Figure 4: *Normalized Graphene carrier mobility vs. density as a function of dielectric overlayer.*

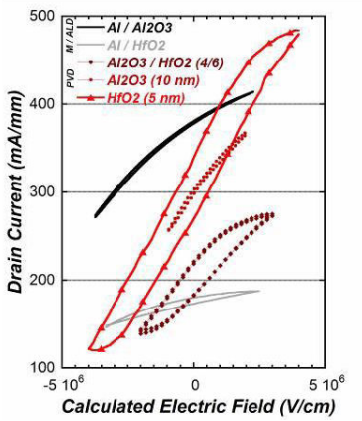

Figure 5: *Graphene transistor drain current vs. gate electric field. 5 nm HfO_2 exhibits superior transport characteristics compared to all other dielectrics.*

NON-ADIABATIC GRAPHENE QUANTUM PUMPS

Pablo San-Jose[1], Elsa Prada[2], Sigmund Kohler[2], Henning Schomerus[3]

[1]Instituto de Estructura de la Materia (CSIC), Serrano 123, 28006 Madrid, Spain
[2]Instituto de Ciencia de Materiales de Madrid (CSIC), Cantoblanco, 28049 Madrid, Spain
[3]Department of Physics, Lancaster University, Lancaster, LA1 4YB, United Kingdom
sanjose@iem.cfmac.csic.es

We present a theoretical study of the non-adiabatic operation of graphene-based quantum pumps, along with a comparison to the semiconductor-based analogues. We show that due to the open nature of graphene contacts resulting from quasiparticle chirality conservation, the current pumped through evanescent modes scales linearly with frequency, and may allow for a competitive advantage respect to the semiconductor-based alternative. Moreover, the scale-free nature of graphene pumps at the neutrality point results in a universal weak-pumping response, reminiscent of that previously identified in the adiabatic regime [1]. In contrast to the latter, however, the differential pumping response becomes maximum at the neutrality point. We provide a full analytical solution of the pumping problem in the weak pumping regime.

References:

[1] E. Prada, P. San-Jose and H. Schomerus, Phys. Rev. B 80, 245414 (2009)

Figures:

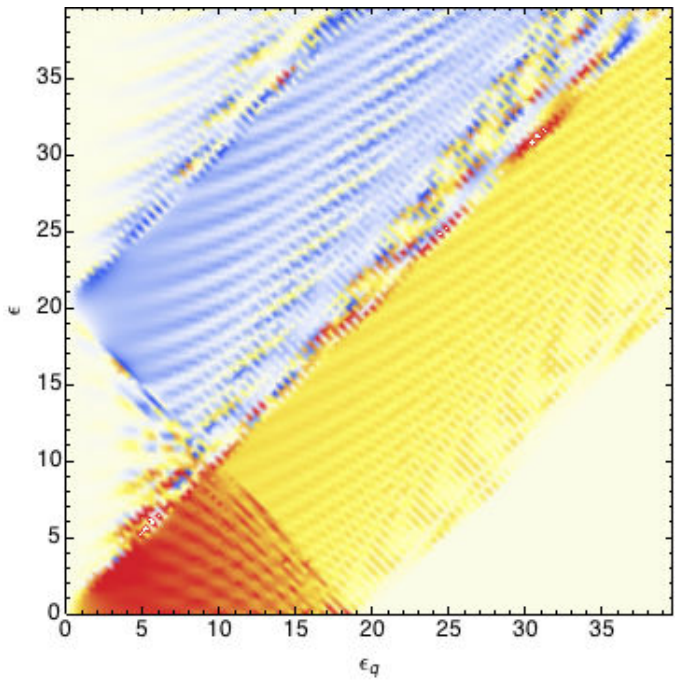

Figure 1: *Differential pumping response $dI/d\epsilon$ as a function of Fermi energy ε and transverse momentum $\varepsilon_q = \hbar v_F q$ in a single parameter graphene quantum pump. The red region, extending up to the pumping frequency $\varepsilon_q=\omega$ at the neutrality point $\varepsilon=0$, represents efficient pumping of evanescent modes.*

MAGNETISM OF COVALENTLY FUNCTIONALIZED GRAPHENE

Elton J. G. Santos, Andrés Ayuela, **Daniel Sánchez-Portal**

Donostia International Physics Center, Paseo Manuel de Lardizabal 4, 20018 San Sebastián, Spain
Centro de Física de Materiales (CFM-MPC), CSIC-UPV/EHU, Paseo Manuel de Lardizabal 5, 20018 San Sebastián, Spain
sqbsapod@ehu.es

We have recently applied *ab initio* density functional calculations to explore the magnetism induced by several types of defects in graphene and graphenic nanostructure, including doping with transition metals [1,2,3] and vacancies [4]. In the present contribution we concentrate on the effect of covalent functionalization on the electronic structure and magnetism of graphene [5] and single-walled carbon nanotubes [6]. We have performed calculations of the functionalization of graphene layer alkanes, polymers, diazonium salts, aryl and alkyl radicals, nucleobases, amide and amine groups, sugar and some organic acids. We find that, independently of the particular adsorbate, whenever a molecule is linked to the carbon layer through single C-C covalent bond, a spin moment of 1.0 μ_B is induced. This is similar to the effect of H adsorption, which saturates the p_Z orbital in the layer, and can be related to the spin moment observed for a single carbon vacancy in a simple π-tight-binding description of the graphene layer. Consistently with this analogy, the calculated spin moment is almost entirely localized in the carbon layer, with an almost negligible contribution from the adsorbate (see Figure 1 below). When the electronegativity of the atom bonded to the layer increases, even if still linked through a single bond, the value of the observed spin moment is modified and eventually goes to zero.

The magnetic coupling between adsorbates has also been studied, using H and CH_3 for graphene [5] and only H for the nanotubes [6], and revealed a key dependence on the sublattice adsorption site (see Figure 2 below): Only molecules at the same sublattice stabilize a ferromagnetic spin order, with exchange coupling decaying quite slowly. When the molecules are adsorbed in different sublattices we always converge to non-magnetic solutions, at least for the supercell sizes used here. Using our previous analogy with a π-vacancy, we can now understand this behavior in terms of the so-called Lieb theorem for bipartite lattices [7]. In the case of the carbon nanotubes, exchange interactions are much larger and have a slower decay for metallic than for semiconducting tubes.

References:

[1] Elton J. G. Santos, A. Ayuela and D. Sánchez-Portal, New Journal of Physics, 12 (2010) 053012
[2] Elton J. G. Santos, D. Sánchez-Portal and A. Ayuela, Phys. Rev. B, 81 (2010) 125433
[3] Elton J. G. Santos et al. Phys. Rev. B, 78 (2008) 195420
[4] Elton J. G. Santos, S. Riikonen, D. Sánchez-Portal and A. Ayuela, arXiv:1012.3304v1.
[5] Elton J. G. Santos, A. Ayuela and D. Sánchez-Portal, submitted
[6] Elton J. G. Santos, D. Sánchez-Portal and A. Ayuela, submitted
[7] E. H. Lieb, Phys. Rev. Lett. 62, (1989) 1201

Figures:

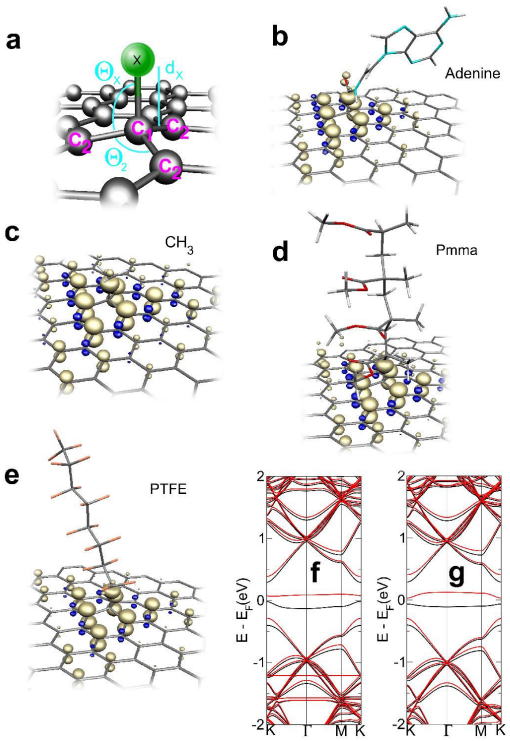

Figure 1: *(a) Scheme of the "on top" adsorption geometry, through single covalent bond to the layer, considered in this work. Panels (b)-(e) show the isosurfaces of the magnetization density induced by the adsorption of the Adenine group, CH_3, Pmma and PTFE on the carbon surface. The cutoff is at ±0.0191431 e/bohr^3. Positive and negative spin densities correspond respectively to light and dark surfaces, which alternate on graphene atoms with a slow decay length in all cases. Panels (f) and (g) show, respectively, the spin polarized band structures for a 8x8 graphene supercell with, respectively, a single Adenine radical and a CH_3 molecule chemisorbed on top of a carbon atom. The black and red lines denote the majority and minority spin bands, respectively. E_F is set to zero.*

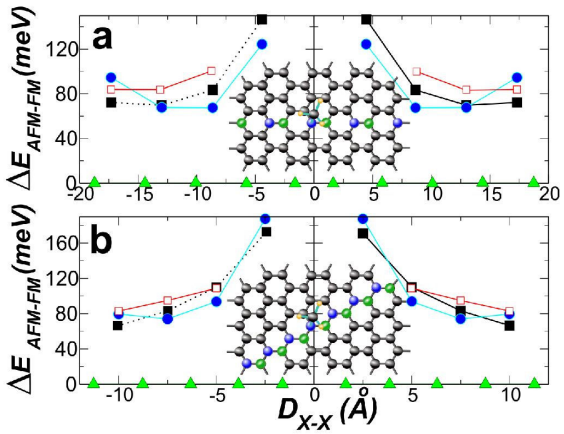

Figure 2: *Exchange coupling as a function of the position of two adsorbates, H and CH3, chemisorbed on top of a C atom in a 8x8 graphene supercell. One of the molecules is moved along (a) the armchair and (b) the zigzag directions, while the other remains at the origin. The filled and empty squares correspond, respectively, to H and CH3 at the same sublattice (e.g. AA). Triangles correspond to both adsorbates at different sublattices (e.g. AB), where it was impossible to stabilize magnetic solutions. The circles correspond to the best fit of the AA data to a Heisenberg model.*

VISUALIZATION OF CHARGE TRANSPORT THROUGH LANDAU LEVELS IN GRAPHENE

Peter Sutter,[1] George Nazin,[1] Yan Zhang,[2] Liyuan Zhang,[3] Eli Sutter[1]

[1]Center for Functional Nanomaterials, Brookhaven National Laboratory, Upton, New York 11973, USA
[2]Department of Physics, Stony Brook University, Stony Brook, New York 11794, USA
[3]Condensed Matter Physics and Materials Science Department, Brookhaven National Laboratory, Upton, New York 11973, USA
psutter@bnl.gov

Band bending and the associated spatially inhomogeneous population of Landau levels play a central role in the physics of the quantum Hall effect (QHE) by constraining the pathways for charge carrier transport and scattering. Spatially inhomogeneous charge distributions, e.g., due to adsorbate-induced surface doping, are expected to be particularly pronounced in graphene due to the proximity of the carrier gas to the surface, and can cause significant deviations from pure edge-state transport. Progress in understanding such effects in low-dimensional carrier gases in conventional semiconductors has been achieved by real-space mapping using local probes. We have recently developed spatially resolved photocurrent microscopy in the QHE regime, i.e., at variable temperature from 300 K to 4 K and at high magnetic fields, to study the correlation between the distribution of Landau levels and the macroscopic transport characteristics in graphene [1].

The conductance of typical two-terminal graphene devices (fig. 1 a) shows series of local extrema associated with individual Landau levels, with maxima predicted to occur at quantized Hall conductances of 2, 4, 6, 10, and 14 e^2/h [2]. The observed maxima are consistently higher (fig. 1 c), suggesting deviations from ideal edge transport in these devices. We find that the gate-voltage dependent photocurrent at fixed locations is oscillatory, with polarity determined by the direction of the magnetic field (fig. 1 d). Such local oscillations are due to a recurring global photocurrent distribution across the device, synchronous with the filling of consecutive Landau levels, which can be used to visualize the gate-voltage dependent distribution of Landau levels in the graphene channel.

Based on an analysis of the photocurrent generation mechanism in graphene subject to a quantizing magnetic field, we conclude that quantum Hall transport in graphene is governed by a non-uniform potential distribution across the channel (fig. 2 a). Multiple inhomogeneously filled Landau levels are populated simultaneously, with the dividing boundaries (traced in the experimental map of fig. 2 b) expected to form incompressible barriers that profoundly affect the electrostatic landscape and current pathways in the device. Besides Landau level mapping at low temperatures, we discuss the extension of photocurrent microscopy to imaging the temperature-dependent quantum Hall transport in graphene up to room temperature, and for characterizing the energy landscape across the graphene channel.

References:

[1] G. Nazin, Y. Zhang, L. Zhang, E. Sutter, and P. Sutter, Nature Physics, 6 (2010) 870.
[2] J.R. Williams, L. DiCarlo, and C.M. Marcus, Science, 317 (2007), 638.

Figures:

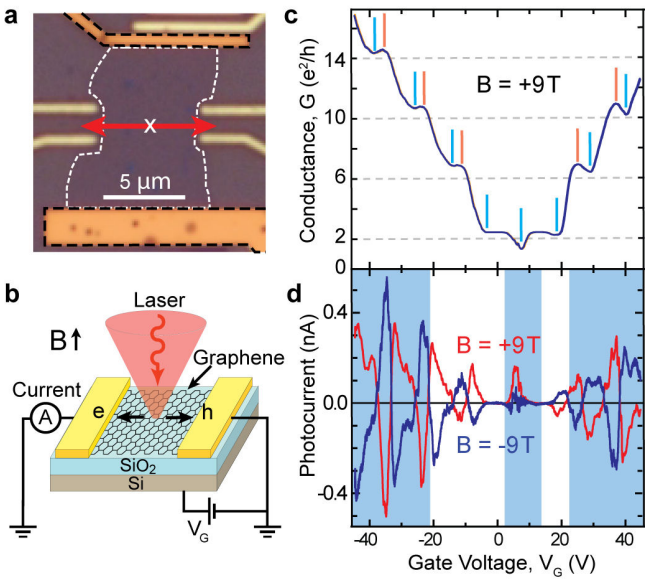

Figure 1: *Low-temperature photocurrent measurements on graphene devices. a – Optical image of a typical two-terminal device. Dashed outlines mark the channel and the two connected electrodes. b – Schematic diagram of the photocurrent measurement. c – Conventional two-terminal conductivity, G, as a function of gate voltage, V_G, measured at T = 4.2 K. Blue and red lines mark local conductivity minima and maxima. d – Photocurrent measured with laser spot at the center of the graphene channel (cross in a) for B = ±9 T.*

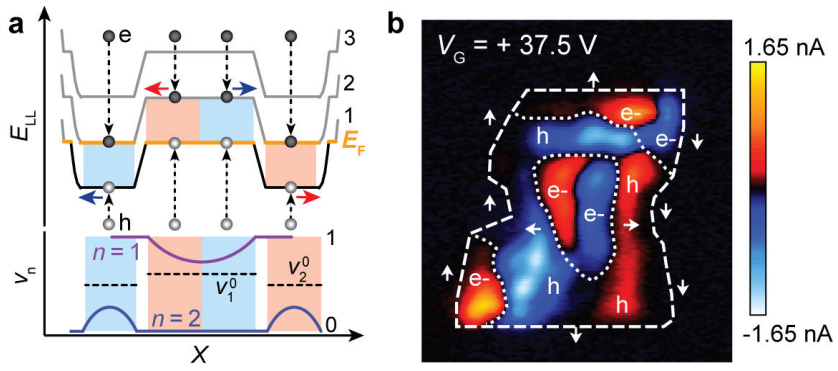

Figure 2: *Mapping photocurrent collection and the distribution of Landau levels in graphene. a – Dominant pathways of charge carrier relaxation and collection across the graphene channel (spatial dimension: X), for n-doped graphene in the case of two Landau levels (n = 1, 2) at E_F inside the channel, and local filling factors, ν_n, of these levels across the device. Colored rectangles connect the Fermi level with the Landau levels responsible for carrier transport; the color indicates the resulting photocurrent polarity. b – Experimental photocurrent map at gate voltage V_G = +37.5 V and magnetic field B = 9 T, measured on the device of fig. 1 a. The distributions of individual Landau levels at E_F, and of the incompressible boundaries between them are indicated as dotted contours.*

LARGE-SCALE ARRAYS OF SINGLE-LAYER GRAPHENE RESONATORS

Arend M. van der Zande, Robert A. Barton, Jonathan S. Alden, B. Rob Ilic, Carlos S. Ruiz-Vargas, William S. Whitney, Phi H. Q. Pham, Jiwoong Park, Jeevak M. Parpia, Harold G. Craighead, and Paul L. McEuen

Cornell University, Department of Physics, Ithaca, NY, USA
amv28@cornell.edu

Graphene's unparalleled strength, small mass per unit area, ultra-high aspect ratio, and unusual electronic properties make it an ideal candidate for nano-electro-mechanical systems (NEMS)[1,2,3,4], but the lack of control over resonance frequency and low quality factor have been major challenges to overcome.

Using graphene grown by chemical vapor deposition (CVD) on copper foils, we developed novel fabrication techniques to produce large arrays of suspended, single-layer graphene membranes on arbitrary substrates. With these fabrication methods, we produced large, high-yield arrays of both doubly-clamped graphene membranes with lengths and widths between 1 and 5 microns, and fully-clamped circular and square graphene membranes with sizes between 2 and 30 microns (See Figure).

With these membranes, we used both optical and electrical actuation and detection techniques to conduct systematic measurements of mechanical resonance as a function of size, clamping geometry, temperature, and electrostatic tensioning. We find that the CVD graphene produces tensioned, electrically-conducting, highly-tunable resonators with frequencies in the megahertz. In addition, we demonstrate that clamping the graphene membrane on all sides reduces the variation in the resonance frequency and makes the resonance frequency more predictable[5].

While doubly clamped resonators typically show quality factors of 25-150, we find that the quality factor of fully clamped membranes show a striking improvement of the membrane quality factor with increasing size[6]. At room temperature, we observe quality factors as high as 2400 ± 300 for a circular resonator 22.5 microns in diameter.

Using electrically-contacted, doubly-clamped, graphene resonators, we find the resonance frequency is tunable with both electrostatic gate voltage and temperature. In addition, the quality factors improve dramatically with cooling, reaching values up to 9000 at 10 K.

These measurements show that it is possible to produce large arrays of CVD-grown graphene resonators with reproducible properties and the same excellent electrical and mechanical properties previously reported for exfoliated graphene. In addition, we also demonstrate that the quality factor of fully clamped graphene resonators relative to their thickness are among the highest of any mechanical resonator demonstrated to date.

References:

[1] Bunch, J. S.; Van Der Zande, A. M.; Verbridge, S. S.; Frank, I. W.; Tanenbaum, D. M.; Parpia, J. M.; Craighead, H. G.; Mceuen, P. L. Science, 315, 5811 (2007) 490-493.
[2] Chen, C.; Rosenblatt, S.; Bolotin, K. I.; Kalb, W.; Kim, P.; Kymissis, I.; Stormer, H. L.; Heinz, T. F.; Hone, J. Nature Nanotech (2009) 1-7.
[3] Robinson, J. T.; Zalalutdinov, M.; Baldwin, J. W.; Snow, E. S.; Wei, Z.; Sheehan, P.; Houston, B. H. Nano Lett, 8, 10 (2008) 3441-3445.
[4] Shivaraman, S.; Barton, R. A.; Yu, X.; Alden, J.; Herman, L.; Chandrashekhar, M.; Park, J.; McEuen, P. L.; Parpia, J. M.; Craighead, H. G.; Spencer, M. G. Nano Lett, 9, 9, (2009) 3100-3105.
[5] van der Zande, A. M.; Barton, R. A.; Alden, J. S.; Ruiz-Vargas, C. S.; Whitney, W. S.; Pham, P. H. Q.; Park, J.; Parpia, J. M.; Craighead, H. G.; McEuen, P. L. Nano Letters 10, 12 (2010) 4869-4873.
[6] Barton, R. A.; Ilic B.; van der Zande, A. M.; Whitney, W. S.; McEuen, P. L.; Parpia, J. M.; Craighead, H. G. In Review

Figures:

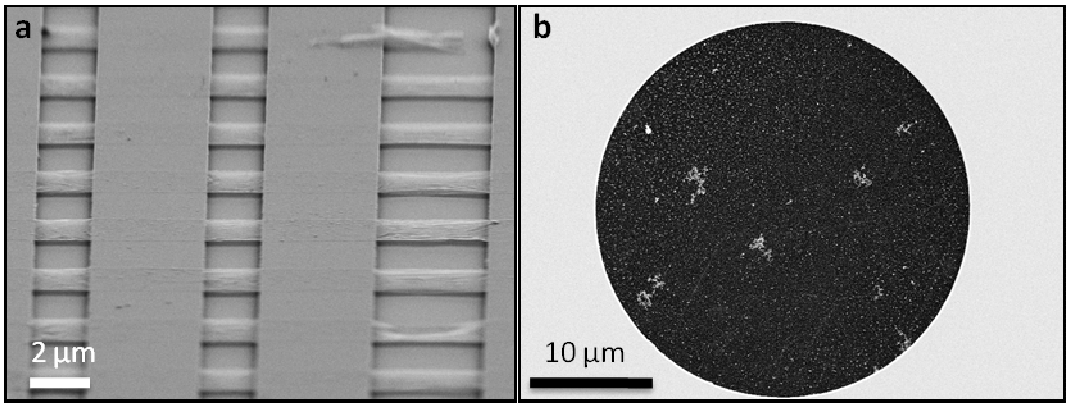

Figure 1: *a) Angled SEM of array of doubly clamped single layer graphene membranes. b) SEM of large, circularly-clamped graphene membrane. Contaminants are clearly visible on the surface.*

QUANTUM TRANSPORT PROPERTIES OF GRAPHENE NANORIBBONS AND NANOJUNCTIONS

Katsunori Wakabayashi

WPI Center for Materials Nanoarchitectonics (MANA), National Institute for Materials Science (NIMS)
Namiki 1-1, Tsukuba 305-0044, Japan
WAKABAYASHI.Katsunori@nims.go.jp

The discovery of graphene and successive fabrication of graphene devices [1,2] have triggered intensive and diverse research on carbon related systems. The honeycomb crystal structure of single layer graphene consists of two nonequivalent sublattices and results in a unique band structure for the itinerant π-electrons near the Fermi energy which behave as massless Dirac fermion. In graphene, the presence of edges can have strong implications for the spectrum of the p-electrons. In graphene nanoribbons with zigzag edges, localized states appear at the edge with energies close to the Fermi level.[3] In contrast, edge states are absent for ribbons with armchair edges. Recent experiments have succeeded to synthesize graphene nanoribbons using lithography techniques [4], chemical techniques.[5,6]

In my talk, we focus on edge and geometry effects of the electronic properties of graphene nanoribbons. The electronic states of graphene nanoribbons crucially depend on the edge orientation and boundary condition [3,7] (1) In zigzag nanoribbons, for disorder without inter-valley scattering a single perfectly conducting channel emerges associated with such a chiral mode due to edge states, i.e. the absence of the localization.[8-10] (2) In armchair nanoribbons, the single-channel transport subjected to long-ranged impurities is nearly perfectly conducting, where the backward scattering matrix elements in the lowest order vanish as a manifestation of internal phase structures of the wavefunction. [10,11] This phase structure can be related to the existence of Berry phase. [12] (3) Nano-graphene junctions are shown to have the zero-conductance anti-resonances associated with the edge states. The relation between the condition of the resonances and geometry is discussed. [13] (4) Finally, we will discuss the effect of edge chemical modification on magnetic properties of nanographene systems. [14]

References:

[1] K. S. Novoselov, A. K. Geim, S. V. Morozov, et.al., Nature, 438 (2005) 197
[2] Y. Zhang, Y.-W.Tan, H.L.Stormer, and P.Kim, Nautre, 438 (2005) 201
[3] M. Fujita, K. Wakabayashi, et.al, J. Phys. Soc. Jpn. 65 (1996) 1920.
[4] M. Y. Han, B. Oezyilmaz, Y. Zhang, and P. Kim, Phys. Rev. Lett. 98 (2007) 206805.
[5] X. Li, X. Wang, L. Zhang, S. Lee, H. Dai, Science 31, (2008) 122.
[6] J. Cai, P. Ruffieux, R. Jaafar, M. Bieri, et.al., Nature 466, (2010) 470
[7] K. Wakabayashi, K. Sasaki, T. Nakanishi, T. Enoki, Sci. Technol. Adv. Mat. 11 (2010) 054504.
[8] K. Wakabayashi, et.al., Phys. Rev. Lett. 99 (2007) 036601
[9] K. Wakabayashi, et.al., CARBON 47 (2009) 124
[10] K. Wakabayashi, New J. Phys. 11 (2009) 095016.
[11] M. Yamamoto, Y. Takane, and K. Wakabayashi, Phys. Rev. B79 (2009) 125421.
[12] K. Sasaki, K. Wakabayashi, T. Enoki, New J. Phys. 12 (2010) 083023.
[13] M. Yamamoto and K. Wakabayashi, Appl. Phys. Lett. 95 (2009) 082109.
[14] K. Wakabayashi, S. Okada et.al., J. Phys. Soc. Jpn. 79 (2010) 034706.

BOTTOM-GATED EPITAXIAL GRAPHENE ON SIC (0001)

Heiko B. Weber, Daniel Waldmann, Johannes Jobst, Florian Speck, Thomas Seyller, Michael Krieger

Lehrstuhl für Angewandte Physik, Universität Erlangen-Nürnberg,
Staudtstraße 7, 91058 Erlangen, Germany
heiko.weber@physik.uni-erlangen.de

We carry out experiments employing epitaxial graphene, fabricated by thermal decomposition on 6H SiC (0001) surfaces [1,2]. A major advantage of this material is the reproducible fabrication of large area and high-quality graphene on an insulating surface. This allows, for example for building graphene Hall bars on atomically flat substrate terraces. However, a disadvantage was so far the absence of a back gate, because the graphene is grown out of the substrate material and an intermediate insulating oxide layer is not possible.

Here we present the controlled fabrication of a bottom gate in the SiC with standard semiconductor technology [3]. A conductive layer at d = 700nm below the surface acts as gate electrode. It is created via implantation of nitrogen ions prior to the graphene growth. It is contacted to the surface with a box-like implantation of a high dose (16 different energies between 30keV and 2MeV). Hence, we define insulating layers and conducting layers by controlling the dopands. The setup is shown in Fig. 1.

A conversion of the graphene layer to quasi-freestanding epitaxial graphene turned out to be mandatory for a working device. This material is hole-filled in contrast to the electron filled standard epitaxial graphene and in magnetotransport measurements it shows the pseudo-relativistic behavior unique for graphene.

A gate voltage applied to the implanted layer enables a variation of the charge carrier density over a wide range. We, find two different regimes of gating mechanisms with strongly different gating efficiency. First for low implanted doses or low temperatures the SiC between gate electrode and surface is insulating and the device behaves like an implanted plate capacitor (IPC). Second we find a Schottky capacitor (SC) regime for high implantation doses or high temperatures. Here the SiC gains a finite conductivity and the capacitance is mainly governed by the Schottky contact between SiC and graphene. The capacitance is higher by a factor of four compared to the IPC regime and is no longer independent from the gate voltage. With this extended Schottky model we can simulate the temperature dependence of the capacitance in Fig. 2. Illumination with ultra violet light extends the SC regime to lower temperatures by generating free carriers in the SiC.

References:

[1] Emtsev et val. Nature materials 8, 203 (2009).
[2] Jobst et al. Phys. Rev. B. 81, 195434 (2010)
[3] Submitted to Nature materials

Figures:

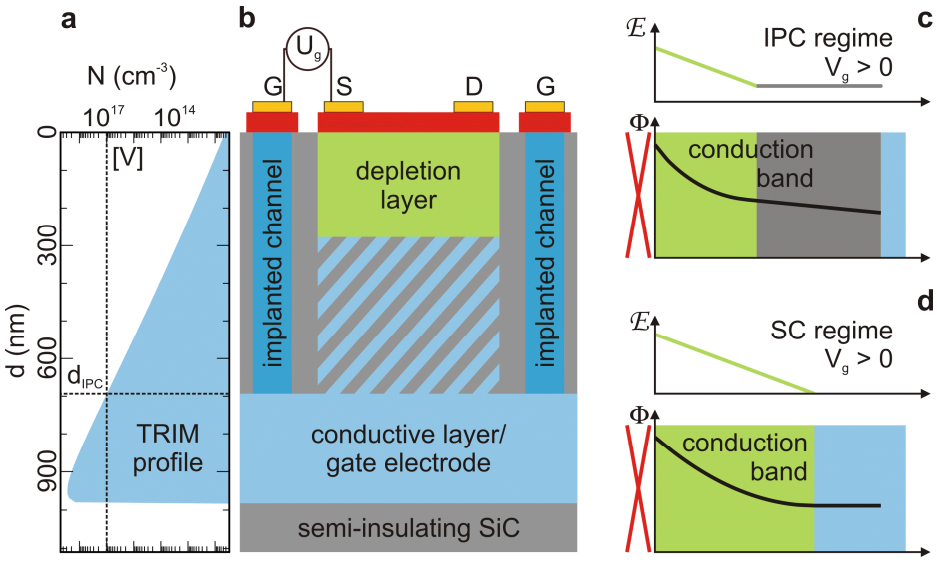

Figure 1: *a) TRIM simulation of the implantation profile. The SiC is conducting where the implanted dose exceeds the vanadium compensation [V] (dotted line) and insulating elsewhere. b) Setup of the bottom gate with source (S), drain (D) and gate (G) electrodes on graphene; conductive gate layer and implanted connections. In the IPC regime the shaded area is insulating, in the SC regime conducting c) Electric field and band diagram for the region between graphene and implanted electrode in the IPC regime, which is self-consistently calculated in our extended Schottky model. A constant external electric field is superimposed onto the built-in field of the depletion layer. d) Electric field and band diagram for the SC regime. The conductive layer extends up to the depletion layer. Hence, the whole applied voltage drops across the depletion layer.*

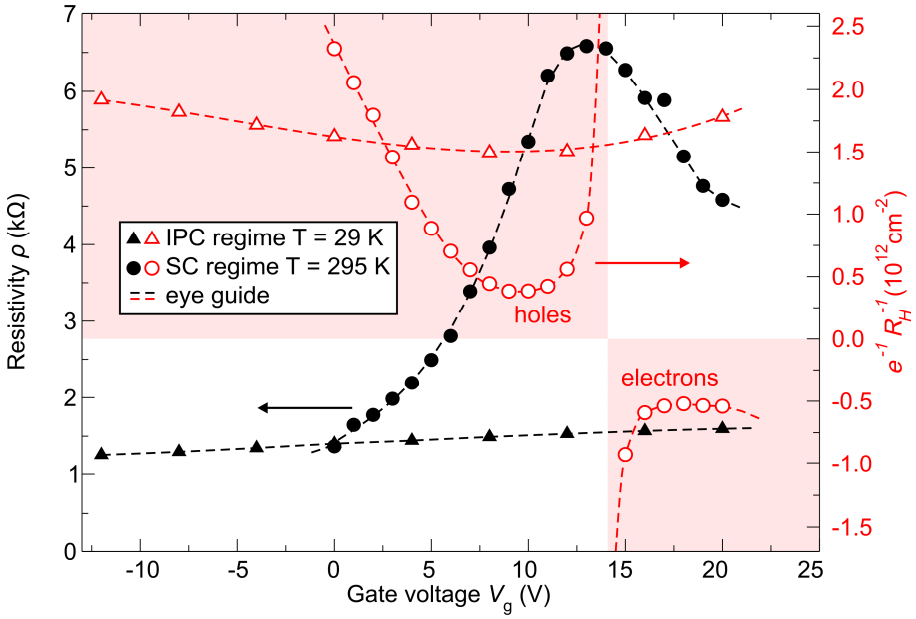

Figure 1: *Gate response of ρ and $1/eR_H$ of sample HD3 in the IPC (triangles) and the SC regime (circles). The capacitance is much higher in the SC than in the IPC regime. In addition the minimal measured charge carrier concentration $n_{min} = (1/eR_H)_{min}$ is much smaller in the SC than in the IPC regime indicating a higher homogeneity.*

MOLECULAR INTERACTIONS ON EPITAXIAL GRAPHENE

Andrew T.S. Wee, Wei Chen, Han Huang, Yuli Huang, Jiatao Sun, Xingyu Gao

Departments of Physics, National University of Singapore, 2 Science Drive 3, Singapore 117542
phyweets@nus.edu.sg

The growth of high quality epitaxial graphene will facilitate the development and commercialization of graphene nanoelectronics devices, and the main substrate-based approaches are chemical vapour deposition (CVD) on metal catalytic thin films and thermal decomposition of silicon carbide (SiC). We have performed detailed studies using in situ scanning tunnelling microscopy (STM), synchrotron photoemission (PES) and density functional theory (DFT) calculations to investigate the structure of the various reconstructions of 6H-SiC(0001) prior to its thermal decomposition to form epitaxial graphene (EG) [1-3] (Fig. 1). We show that the transition from monolayer EG to trilayer EG adopts a bottom-up growth mechanism [4], and x-ray absorption fine structure studies indicate an increase in disorder of Si atoms in the SiC substrate beneath the surface and the formation of Si clusters [5,6].

A major challenge in graphene-based devices is opening the energy band gap and doping. Molecular functionalization of graphene is one approach to modifying its electronic properties. Surface transfer doping by surface modification with appropriate molecular acceptors represents a simple and effective method to non-destructively dope graphene [7-9]. Surface transfer doping relies on charge separation at interfaces, and represents a valuable tool for the controlled and non-destructive doping of semiconductors and nanostructures at relatively low cost, thereby facilitating the development of hybrid organic-graphene nanoelectronics. Molecular self-assembly of bimolecular systems on epitaxial graphene and HOPG is demonstrated [10,11] (Fig. 2). Surface transfer hole doping of epitaxial graphene using oxide thin films is also discussed [12].

References:

[1] W. Chen, H. Xu, L. Liu, X. Y. Gao, D. C. Qi, G. W. Peng, S. C. Tan, Y. P. Feng, K. P. Loh, A. T. S. Wee, Surf. Sci. 596 (2005) 176.
[2] S. W. Poon, W. Chen, E. S. Tok, A. T. S. Wee, Appl. Phys. Lett. 92 (2008) 104102.
[3] S. W. Poon, W. Chen, E. S. Tok, A. T. S. Wee, Phys. Chem. Chem. Phys. 12 (2010) 13522.
[4] H. Huang, W. Chen, S. Chen, A. T. S. Wee, ACS Nano 2 (2008) 25.
[5] X. Y. Gao, S. Chen, T. Liu, W. Chen, A. T. S. Wee, T. Nomoto, S. Yagi, K. Soda, J. Yuhara, Phys. Rev. B 78 (2008) 201404.
[6] X. Y. Gao, S. Chen, T. Liu, W. Chen, A. T. S. Wee, T. Nomoto, S. Yagi, K. Soda, J. Yuhara, Appl. Phys. Lett. 95 (2009) 144102.
[7] W. Chen, S. Chen, D. C. Qi, X. Y. Gao, A. T. S. Wee, J. Am. Chem. Soc. 129 (2007) 10418.
[8] J. T. Sun, Y. H. Lu, W. Chen, Y. P. Feng, and A. T. S. Wee, Phys. Rev. B 81 (2010) 155403.
[9] W. Chen, D. C. Qi, X. Y. Gao, A. T. S. Wee, Prog. Surf. Sci. 84 (2009) 279-321.
[10] H. Huang, S. Chen, X. Y. Gao, W. Chen, A. T. S. Wee, ACS NANO 3 (2009) 3431-3436.
[11] Y.L. Huang, W. Chen, H. Li, J. Ma, J. Pflaum, A. T. S. Wee, Small 6 (2010) 70–75.
[12] Z.Y. Chen, I. Santoso, R. Wang, L.F. Xie, H.Y. Mao, H. Huang, Y.Z. Wang, X.Y. Gao, Z.K. Chen, D.G. Ma, A.T.S. Wee, W. Chen, Appl. Phys. Lett. 96 (2010) 213104.

Figures:

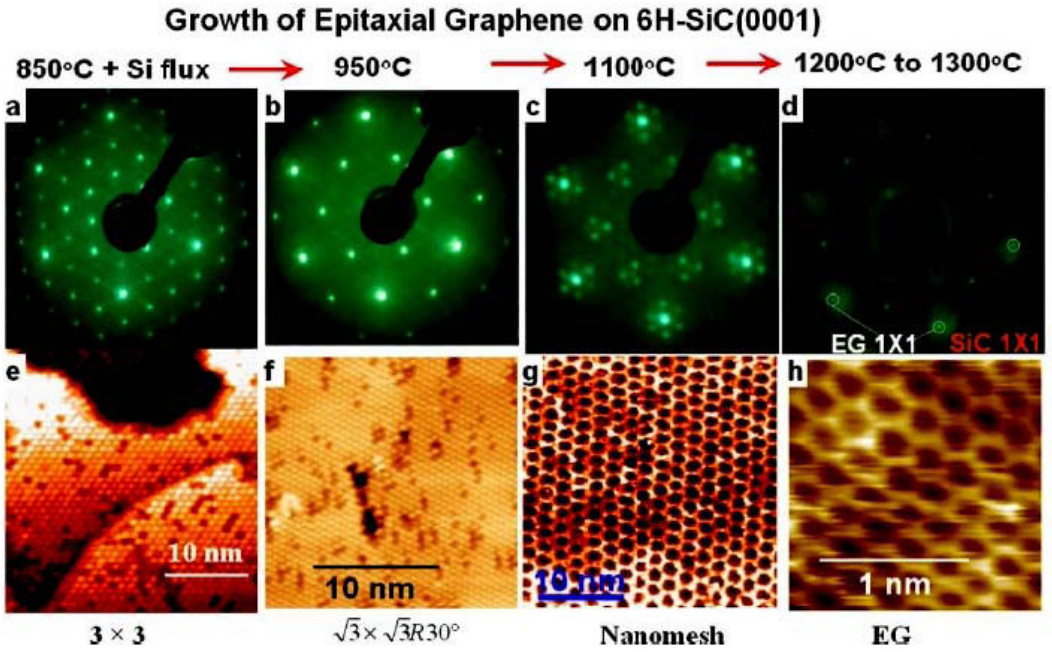

Figure 1: *LEED and corresponding STM images showing the evolution of various superstructures on 6H-SiC(0001) as a function of annealing temperature: 3×3 (panels a and e); (panels b and f); nanomesh (panels c and g); graphene (panels d and g). Incident electron beam energies (LEED) of 100 eV for panels a, b and c, and 175 eV for panel d. Adapted from Ref [9].*

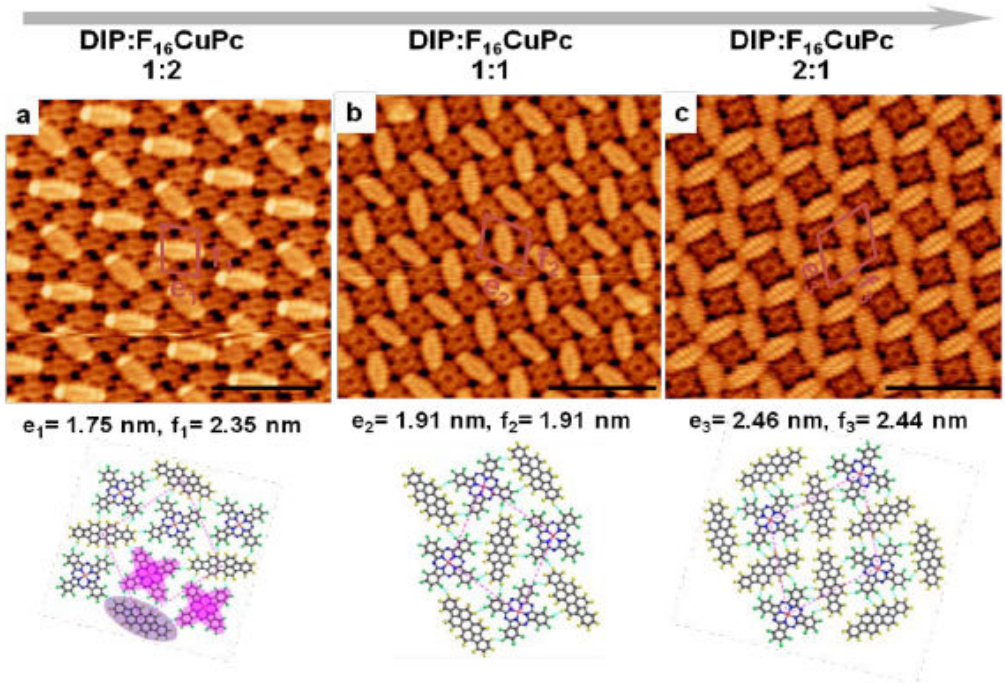

Figure 2: *Molecularly resolved 15x15 nm^2 STM images (top) and DFT simulated molecular models (below) of the F16CuPc molecular dot arrays with tunable intermolecular distance controlled by DIP molecular coverage. The scale bar in each STM image represents 5 nm. (from Ref [11])*

HALL EFFECT IN GRAPHENE NEAR THE CHARGE NEUTRALITY POINT

H. J. van Elferen[1], **S. Wiedmann[1]**, E. V. Kurganova[1], A. J. M. Giesbers[1], U. Zeitler[1], J. C. Maan[1], L. A. Ponamorenko[2], K. S. Novoselov[2], and A. K. Geim[2]

[1]Radboud University Nijmegen, Institute for Molecules and Materials, High Field Magnet Laboratory, Toernooiveld 7, 6525 ED NIJMEGEN, the Netherlands
[2]Department of Physics, University of Manchester, M13 9PL Manchester, United Kingdom
s.wiedmann@science.ru.nl

In single layer grapheme, when the carrier concentration through the charge neutrality point (CNP) is varied from hole-type to electron-type, the measured Hall resistivity ρ_{xy} close to the CNP shows a smooth zero crossing for magnetic fields up to 30 T. In contrast, ρ_{xy} diverges in a conventional semiconductor approaching the CNP from both the electron and the hole side. We explain our results in terms of a two-component carrier system where both electrons and holes with finite concentrations are present simultaneously around the CNP. The Hall resistivity is given by (supposing a similar mobility for electrons and holes) :

$$\rho_{xy} = \frac{n-p}{e(n+p)^2}B \qquad (1)$$

with n and p the charge carrier concentrations for electrons and holes, respectively, e is the electron charge and B the applied magnetic field.

Our samples are monolayer graphene devices deposit on Si/SiO_2 substrate using standard methods [1], and the charge carrier concentration is varied with a back gate from highly electron- to highly holedoped. Fig. 1(a) shows the low magnetic field data for one of our samples measured at T = 0.5 K where the Hall resistance does not yet show the quantum Hall effect (QHE). Knowing the total charge density q=n-p from the back-gate voltage, we have extracted the individual carrier concentrations n and p [Fig. 1(b)] as a function of the total charge with Eq. (1). We find that both types of charge carriers are present both above and below the CNP. For this sample, precisely at the CNP (q=0) we find $n = p = 4.2 \cdot 10^{14}$ m^{-2} only weakly dependent on the magnetic field in this non-quantized regime. Away from the CNP the system remains two-component and the minority carriers only disappear for $|q| > 2 \cdot 10^{15}$ m^{-2}.

When we increase the magnetic field into the quantum Hall regime at T = 4.0 K [2, 3] [Fig. 2(a)], we still observe a zero-crossing of ρ_{xy} and at the CNP in Fig. 2(b), we find that both n and p are present but their number increases with the magnetic field. Plotting charge carrier concentration as a function of *B*, n is found to be constant for $B < 5$ T after which it increases linearly as *B* increases. This behavior is attributed to transport dominated by electron-hole puddles for low magnetic fields evolving into a quantized density of states in high magnetic fields [4].

The observed presence of both electrons and holes near the CNP even deep into the quantized Hall regime may contribute to a better understanding of the nature of electronic states at the lowest Landau level in graphene [5]. In particular, in high magnetic fields it allows to distinguish between different splitting scenarios of the lowest Landau level: valley first where electrons and holes are separated and the Hall resistance is expected to diverge at the CNP, and spin-first where electrons and holes remain present above and below zero-energy and the Hall resistance crosses zero at the CNP [6].

References:

[1] A. K. Geim and K. S. Novoselov, Nat. Mater. 6 (2007) 183.
[2] K. S. Novoselov, A. K. Geim, S. V. Morozov, D. Jiang, M. I. Katsnelson, I. V. Grigorieva, S. V. Dubonos, and A. A. Firsov, Nature (London) 438 (2005) 197.
[3] Y. Zhang, Y. Tan, H. L. Stormer, and P. Kim, Nature (London) 438 (2005) 201.
[4] J. Martin, N. Akerman, G. Ulbricht, T. Lohmann, J. H. Smet, K. von Klitzing, A. Yacobi, Nat. Phys. 4, (2008) 144.
[5] S. Das Sarma and K. Yang, Solid State Commun. 149 (2009) 1502.
[6] A. J. M Giesbers *et al.*, Phys. Rev B 80 (2009) 201403(R).

Figures:

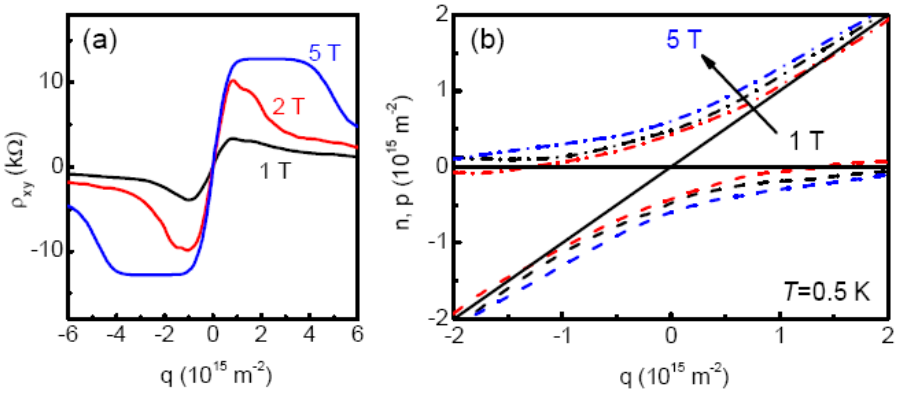

Figure 1: *(a) Low-field Hall resistivity and (b) extracted carrier concentration for electrons n and holes p according to Eq. (1) as a function of total charge q. Both types of charge carriers are present below and above the CNP for $|q| < 2 \cdot 10^{15}$ m^{-2}.*

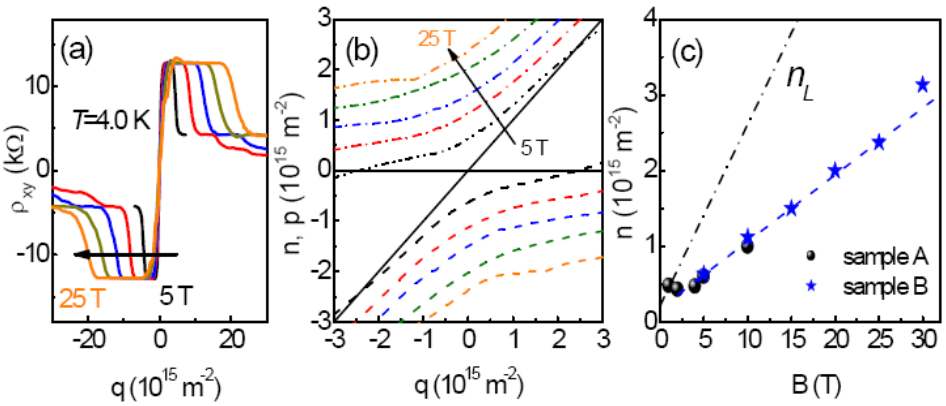

Figure 2: *(a) High-field Hall resistivity in the quantum Hall regime; (b) Extracted carrier concentration for electrons n and holes p according to Eq. (1) as a function of the total charge q; (c) Charge carrier concentration increases with B due to a quantized density of states. Most carriers are localized in the tails of the Landau level and only about 1/3 of the total carrier concentration is measured as free charge carriers.*

EDGE TRANSPORT CHANNEL ON A GRAPHENE NANORIBBON

Sungjong Woo, Young-Woo Son

KIAS Hoegiro 87, Dongdaemun-gu, Seoul 130-722, Korea
nl sjwoo@kias.re.kr

Recently, Scanning Gate Microscopy (SGM) experiment on a graphene nanoribbon by our collaborators has shown a clear evidence of the existence of an edge electronic transport channel; a remarkable SGM signal enhancement has been observed on the ribbon edge.
Charge accumulation on the edge of doped graphene nanoribbons has been studied by Silvestrov et.al.

For such a doped graphene nanoribbon, the effective local Dirac point deviates from the Fermi level depending on the local excess charge density, which is almost constant except the ribbon edge where charge is seriously accumulated.

We have investigated the electronic band structures and transport properties of such doped nanoribbons especially with zigzag edge structures and have further studied their responses to an additional local gate potential given by the SGM tip.
We have found that, once a graphene is doped, the energies of localized edge states of a zigzag graphene nanoribbon, which give a flat band for a neutral one, follow the shifted local Dirac point on the edge bending the corresponding flat band line.

Based on this, we have further showed that one can control the bent edge-state band line using SGM tip gating resulting in single-channel conductance enhancement that was seen in the expriment.
Our theory predicts that such conductance enhancement occurs when the polarity of the local tip potential is against the type of doping which is in good agreement with the experimental results. We have further confirmed that the phenomena persists on general edge structurs.

PROBING THE BANDGAP OF BILAYER GRAPHENE WITH THERMAL AND OPTICAL EXCITATIONS

J. Yan[1], M.-H. Kim[1], G.S. Jenkins[1], A.B. Sushkov[1], D.C. Schmadel[1], J. Melngailis[2], H.D. Drew[1] and M.S. Fuhrer[1]

[1]Center for Nanophysics and Advanced Materials
[2]Department of Electrical and Computer Engineering
University of Maryland, College Park, MD 20742, USA
juny@umd.edu

The opening of a tunable bandgap in bilayer graphene is an interesting problem that has attracted great recent attention. We study the bulk of dual-gated bilayer graphene using a Corbino-disk geometry which excludes the edge conductance channels. The temperature dependence of the maximum resistivity is found to be well described by simple thermal activation at high temperatures and variable range hopping at low temperatures, consistent with other transport studies, from which we conclude that edge transport is not significant [1]. The electric-field-dependent band gap extracted from thermal activation is found to be in good agreement with infrared spectroscopic studies [2, 3]. We further investigate the band gap effect by infrared photoconduction measurements in non-Corbino dual-gated devices. We have measured the photoconductive response as a function of band gap, temperature, incident wavelength, and power. We find that the response is proportional to the source-drain current and that it increases for larger band gap. Interestingly, the signal does not always vanish at zero source-drain voltage and it exists even when the average electric field is zero, corresponding to zero band gap in a disorder-free sample.

References:

[1] J. Yan and M. S. Fuhrer, Nano Lett. 10 (2010) 4521.
[2] Y. Zhang et al., Nature 459 (2009) 820.
[3] K. F. Mak et al., Phys. Rev. Lett. 102 (2009) 256405.

Figures:

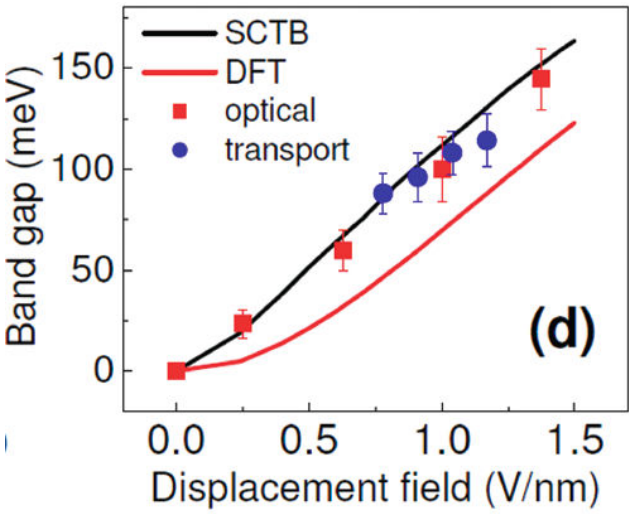

Figure 1: *Bandgap of dual-gated bilayer-graphene Corbino-disk. Transport measurements (blue dots) are from Ref.[1]. Optical data (red squares) and self consistent tight binding (SCTB) as well as density functional theory (DFT) calculations are taken from Ref.[2].*

NANOSPAIN 2011

NanoSpain Conf 2011

NanoIberian Conference

INDEX: INVITED CONTRIBUTIONS

INDEX: INVITED CONTRIBUTIONS (CNANO GSO SESSION)

INDEX: ORALS CONTRIBUTIONS (CNANO GSO SESSION)

INDEX: ORALS CONTRIBUTIONS

ALPHABETICAL ORDER

I: Invited / IC: Invited CNano GSO Session / O: Oral / OC: Oral CNano GSO Session

I: Invited / IC: Invited CNano GSO Session / O: Oral / OC: Oral CNano GSO Session

I: Invited / IC: Invited CNano GSO Session / O: Oral / OC: Oral CNano GSO Session

NANOSPAIN 2011

ABSTRACTS
ALPHABETICAL ORDER

HIGHLY PHOTOSTABLE ORGANIC DISTRIBUTED FEEDBACK LASERS FABRICATED BY THERMAL NANOIMPRINT

I. Alonso[1], V. Trabadelo[1]*, A. Juarros[1], A. Retolaza[1], S. Merino[1], V. Navarro-Fuster[2], M.G. Ramírez[2], P.G. Boj[2], I. Vragovic[2], J.M. Villalvilla[2], J.A. Quintana[2], M.A. Díaz-García[2]

[1]Micro/Nano Engineering Unit, CIC microGUNE, Avda. Otaola 20, 20600 Eibar, Spain
[2]Instituto Universitario de Materiales de Alicante, Universidad de Alicante, 03080 Alicante, Spain
*Present address: EMPA-Swiss Federal Laboratories for Materials Science and Technology, Advanced Materials Processing, CH-3602 Thun, Switzerland.
ialonsovillanueva@tekniker.es

Nanoimprint lithography (NIL) is a promising technique for the fabrication of surface pattern features down to 20 nm, even for future industrial applications, because of its high throughput, low cost and high fidelity pattern transfer. We have used this technique to make distributed feedback (DFB) resonant cavities for solid-state lasers based on semiconducting polymers, an active field of research in the past few years [1].

In this work we present the last results obtained with two kind of devices. First, DFB gratings in SiO_2 (periodicity of 368 nm and equal line and space) on which polystyrene (PS) films doped with 0.5 wt% of a perylenediimide (PDI) derivative were spin-coated afterwards. Using a master grating fabricated by e-beam lithography and plasma etching, the grating was first imprinted onto an mrI-8030E resist layer spin-coated on a thermally oxidized silicon wafer. The embossing was carried out at 180 ºC and the applied force (20000 N) was held for 900 s. The residual layer was removed using an O_2 plasma and the grating was transferred to the SiO_2 by CHF_3/Ar plasma etching. Several grating depths were obtained by varying the etching time.

On the other hand, we also imprinted DFB gratings directly on the active material using the same master stamp. After spin-coating a PS film doped with 0.5 wt% of PDI on a SiO_2 wafer, it was embossed at 155 ºC applying 15000 N for 900 s. This way the dry-etching step can be avoided, so the fabrication process for this second kind of devices becomes more cost-effective.

For the optical characterization of the samples, they were pumped with a circular spot (1.3 mm diameter) provided by a pulsed Nd:YAG laser (10 ns, 10 Hz) operating at 532 nm. The emitted light was collected normal to the surface with a fiber spectrometer. For DFB gratings in SiO_2, the laser showed laser emission at between 569 nm and 572 nm, depending on the grating depth. In the case of imprinted DFB gratings, the emitted wavelength is at around 578 nm. Thresholds were drastically reduced compared with the amplified spontaneous emission of a sample without grating [2]. Moreover, the thresholds of the devices with gratings directly embossed on the doped PS film were even lower than for devices with gratings in SiO_2. Furthermore, this combination of low threshold devices and material properties has shown to be very photostable. The half-life, defined as the number of excitation pulses at which the emission intensity decays at half of its maximum value, is longer than 300000 pump pulses (i.e., more than 8 h at 10 Hz), at a pump intensity twice the threshold (see figure below).

Acknowledgements:

This work is funded by the “Ministerio de Ciencia e Innovación” and the European Community (FEDER) through grant MAT2008-06648-C02. It was also partially supported by the ETORTEK Project MIBIO2 funded by the Basque Government. MGR is supported by a CSIC fellowship within the program JAE.

References:

[1] D.W. Samuel, G.A. Turnbull, Chem. Rev., 107 (2007) 1272.
[2] V. Navarro-Fuster, E. M. Calzado, P. G. Boj, J. A. Quintana, J. M. Villalvilla, M. A. Díaz-García, V. Trabadelo, A. Juarros, A. Retolaza, S. Merino, Appl. Phys. Lett., 97, (2010) 171104.

Figures:

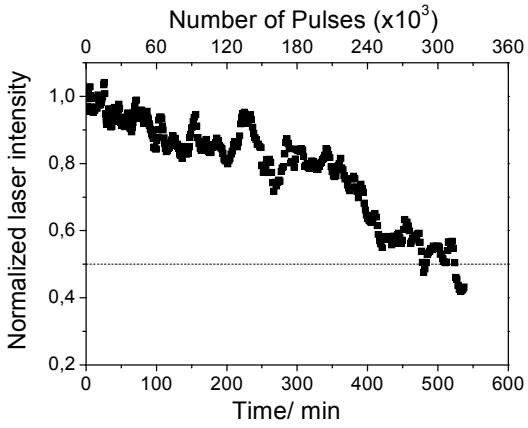

Figure 1: *Normalized laser intensity vs irradiation time (bottomaxis) and vs the number of pump pulses (10 ns, 10 Hz; top axis for a DFB device based on a 0.5 wt % PDI- doped PS film and grating depth of 105 nm at 4 μJ/pulse (twice the threshold)*

PLASMONIC PARTICLES ORGANIZED IN NANOSTRUCTURED POLYMER MATRICES

Ashod Aradian, Clémence Tallet, Julien Vieaud, Olivier Merchiers, Anitha Kumar, Frédéric Nallet, Virginie Ponsinet and Philippe Barois

Université Bordeaux 1 – CNRS, Centre de Recherche Paul Pascal UPR 8641,
Avenue Schweitzer, 33600 Pessac, France
aradian@crpp-bordeaux.cnrs.fr

New “bottom-up” fabrication techniques are now effectively explored for the production of nanostructured functional materials, and specifically for nanophotonic devices and metamaterials. Expected benefits from bottom-up approaches include assembling true three-dimensional metamaterials and synthetizing resonators with sizes appropriate for the optical range. Nanochemistry and self-assembly appear as interesting nanofabrication tools. Among the promising self-assembled systems are the diblock copolymers made of two molecular chains of distinct chemical nature linked together, which present solid state spontaneous structures with long-range order and tunable characteristic sizes between 10 and 50 nm. In particular, alternating lamellar and hexagonally-ordered cylindrical structures are described in many systems. These are, however, organic materials exhibiting moderate susceptibilities and low optical constant contrast. Therefore, in their native state, they should be considered essentially as ‘optically neutral’ templates, used to spatially organize ‘active’ entities. Our work focuses on nanoparticles presenting plasmonic resonances as these ‘active’ entities. Recent developments in the wet chemistry synthesis of plasmonic nanoparticles have allowed for significant improvements in terms of control of composition, surface chemistry, properties and size. In our study, gold nanoparticles are incorporated in polymer matrices with different nanostructures. We wish to correlate the nature, density and spatial organization of the nanoparticles with the optical properties of the nanocomposite materials.

Two different experimental systems are studied. In the first system, 15-nm diameter gold spheres are dispersed randomly in poly(vinyl alcohol) thin films deposited on silicon wafers or glass plates. Volume fraction of gold is varied from 1 to 30% and film thickness from a few nanometers to 300 nm. The structure of the films is studied by atomic force microscopy (Fig. 1) and X-ray reflectivity. In the second system, 10-nm diameter gold nanoparticles are incorporated in the 18-nm thick poly(acrylic acid) layers of the ordered lamellar phase of a poly(styrene)-block-poly(acrylic acid) copolymer. Volume fraction of gold is varied in both thin films on silicon wafer and bulk samples. Small-angle scattering and reflectivity of X-rays, atomic force and electron microscopies (Fig. 2) are used to get a detailled structural description of the nanostructured composites and validate the control of the density and organization of the nanoparticles. The optical properties of the nanocomposites are studied using spectrophotometry and spectroscopic ellipsometry.

The refractive index results, in the visible and infra-red spectral regions, are confronted to effective medium models. As shown in Fig. 3, the classical Maxwell-Garnett model shows an important discrepancy with the measured results, and we will show how the situation can be improved taking into account the appropriate dispersion function for the nanoparticles, as well as substrate effects.
Similar systems using rod-shape gold nanoparticles, developments towards unsual optical properties at high gold fraction, and search for experimental evidence of anisotropic optical properties will also be described in this presentation. The conclusions will allow discussing the use of self-assembly for fabrication of new nanostructured optical materials.

Acknowledgments:

The support of the Région Aquitaine, the French Agence Nationale de la Recherche (NANODIELLIPSO, ANR-09-NANO-003) and the European Union's Seventh Framework Programme (FP7/2008) under grant agreement n° 228762 (METACHEM) is acknowledged.

Figures:

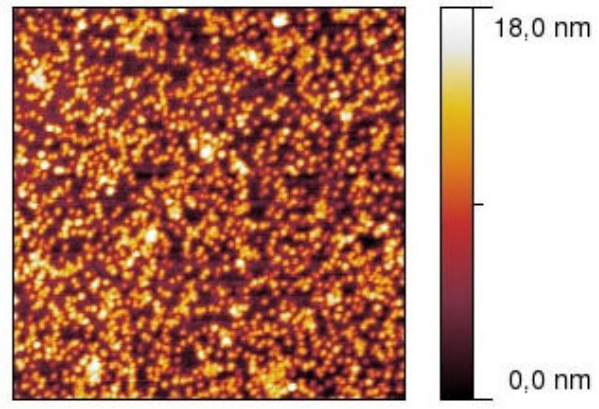

Figure 1: *2 x 2 µm atomic force microscopy topography (upper-view) image obtained on a thin composite film of gold nanoparticles randomly dispersed in poly(vinyl alcohol).*

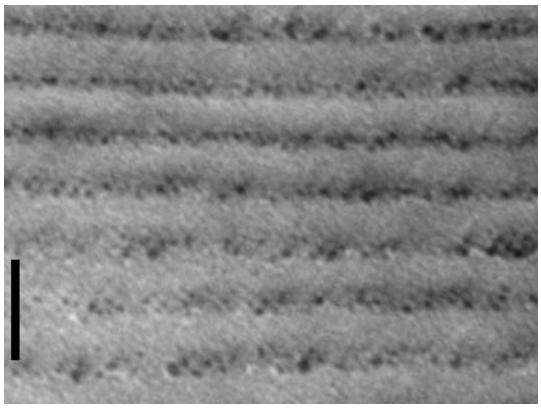

Figure 2: *Transmission electron micrograph (side view) of an ordered lamellar composite film of gold nanoparticles and poly(styrene)-b-poly(acrylic acid) copolymer. Bar = 50 nm.*

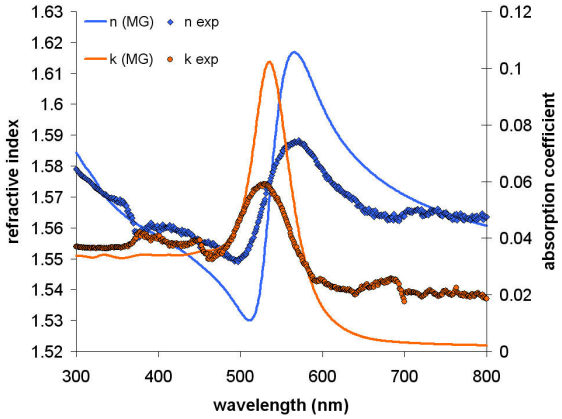

Figure 3: *Optical index n and absoption coefficient k, determined by analysis of spectroscopic ellipsometry data, of a 77nm-thick composite film of gold nanoparticles randomly dispersed in poly(vinyl alcohol), as a function of the wavelength. The discrepancy with a simple Maxwell-Garnett model (full lines) is apparent and motivates the inclusion of other effect such as electron confinement and substrate effects.*

INELASTIC QUANTUM TRANSPORT IN NANOSCALE JUNCTIONS : ROLE OF ELECTRON-PHONON INTERACTIONS ON THE CURRENT-CURRENT NOISE CHARACTERISTICS

V R. Avriller[1], D.F. Urban[2] and A. Levy Yeyati[3]

[1]DIPC (Donostia International Physics Center), Paseo Manuel de Lardizabal, 4, 20018 Donostia-San Sebastián, Spain.
[2]Physikalisches Institut, Albert-Ludwigs-Universität, 79104 Freiburg, Germany
[3]Departamento de Física Teórica de la Materia Condensada C-V, Facultad de Ciencias, Universidad Autónoma de Madrid, E-28049 Madrid, Spain.
remi_avriller@ehu.es

Recent theoretical advances have unveiled the role of electron-phonon (e-ph) interactions in the current-current fluctuations (shot noise) versus voltage characteristics of molecular nano-devices [1,2,3]. For voltages crossing the inelastic threshold, the correction to the noise induced by e-ph interactions was shown to exhibit a crossover between a positive and negative correction, depending on the parameters describing the junction (position of the molecular level, asymmetry of the coupling to the leads) [1,2,3]. More generally the high-bias properties of the noise versus voltage characteristics were shown to result from both electronic and vibronic dynamics [4], the fluctuations of the later being responsible of a dynamical feedback inducing strong non-linear effects in the transport properties [5].

In this work, we would like to review the state of the art of the literature concerning transport properties of molecular junctions (current, noise and full counting statistics) in presence of such inelastic effects. We also would like to address the description of the remaining open questions, as well as some possible directions for further theoretical works.

The aim of such investigations could be to generate simulation tools for computing noise characteristics as efficient as the one available for computing I-Vs [6], and to provide a new way of characterizing experimentally transport properties of molecular junctions [7].

References:

[1] T. L. Schmidt and A. Komnik, Phys. Rev. B. 80, 041307(R) (2009).
[2] R. Avriller and A. Levy Yeyati, Phys. Rev. B. 80, 041309(R) (2009).
[3] F. Haupt, T. Novotny, and W. Belzig, Phys. Rev. Lett. 103, 136601 (2009).
[4] R. Avriller, arXiv:1007.4450 (2010).
[5] D.F. Urban, R. Avriller and A. Levy Yeyati, Phys. Rev. B 82, 121414(R) (2010).
[6] T. Frederiksen, M. Paulsson, M. Brandbyge, and A.-P. Jauho, Phys. Rev. B 75, 205413 (2007).
[7] O. Tal, M. Krieger, B. Leerink and J.M. van Ruitenbeek, Phys. Rev. Lett. 100, 196804(2008).

SPINTRONICS AND BEYOND

S. D. Bader

Materials Science Division and Center for Nanoscale Materials Argonne National Laboratory, Argonne, IL 60439, USA

ialonsovillanueva@tekniker.es

Spintronics encompasses the ever-evolving field of magnetic electronics.[1] It offers the possibility to communicate via pure spin currents as opposed to electric charge currents. [2] The talk provides a brief perspective of recent developments to switch magnetic moments by spin-polarized currents, electric fields and photonic fields. Developments to reinvent today's semiconductor electronics depend on the exploration and discovery of novel nanostructured materials and configurations.

The talk highlights select promising areas, featuring recent work at Argonne, [3] including complex-oxide-based Mott-tronics research [4] ferromagneticsuperconducting heterostructural opportunities, [5] and most strikingly, the realm of new cancer treatment approaches.[6]

Work supported by the U.S. Department of Energy, Office of Science, Basic Energy Sciences, under contract No. DE-AC02-06CH11357.

References:

[1] S. D. Bader and S. S. P. Parkin, "Spintronics," in Annual Reviews of Condensed Matter Physics 1, 71-88 (2010)
[2] O. Mosendz, J. E. Pearson, F. Y. Fradin, G. E. W. Bauer, S. D. Bader, and A. Hoffmann, Phys. Rev. Lett. 104, 046601 (2010)
[3] S. D. Bader, Rev. Mod. Phys. 78, 1-15 (2006).
[4] S. J. May, P. J. Ryan, J. L. Robertson, J.-W. Kim, Tiffany. S. Santos, Elena Karapetrova, J. L. Zarestky, X. Zhai, Suzanne. G. E. te Velthuis, J. N. Eckstein, S. D. Bader, and A. Bhattacharya, Nature Materials 8, 892-897 (2009).
[5] P. Cadden-Zimansky, Ya. Bazaliy, L.M. Litvak, J.S. Jiang, Jiyeong Y. Gu, C.-Y. You, M.R. Beasley, and S.D. Bader, Phys. Rev. B 77, 184501 (2008)
[6] Dong-Hyun Kim, Elena A. Rozhkova, Ilya V. Ulasov, S. D. Bader, Tijana Rajh, Maciej S. Lesniak, and V. Novosad, Nature Materials 9, 165-171 (2010).

OPTIMAL SWITCHING OF A NANOMAGNET ASSISTED BY A MICROWAVE FIELD

Noemi Barros, Mhamed Rassam, Hamid Kachkachi

Université de Perpignan Via Domitia - 52, Avenue Paul Alduy - 66860 Perpignan cedex, France
noemi.barros@univ-perp.fr

Magnetic recording is a key technology in the field of high density information storage. In order to increase thermal stability, small nanoparticles with a high anisotropy may be used. However, high fields are then needed to reverse the magnetization but these are difficult to achieve in current devices. In 2003 Thirion et al. [1] showed that the combination of a constant applied field (DC field), well below the switching field, with a microwave (MW) field pulse can reverse the magnetization of a nanoparticle. Further studies on single domain magnetic nanoelements [2] proved that the effect is stronger if the frequency of the MW field matches the ferromagnetic resonance frequency of the nanoelements. Numerical simulations [3] confirm that chirped MW fields are more efficient than monofrequency fields.

The aim of this work is to find the optimal MW field triggering the switching of a nanoparticle under specified constraints. We consider a single-domain nanoparticle, modelled by a macroscopic magnetic moment (macrospin). The shape of the MW field is then sought by minimizing the absorbed energy, following the trajectory of the macrospin, which is a solution of the damped Landau-Lifshitz equation. The boundary conditions are a given initial state and a specified target state that is supposed to be reached after switching. This boundary value problem is reformulated by defining a cost functional that is then minimized using the Lagrange parameter technique [4]. The problem is then solved numerically using the conjugate gradient algorithm coupled to a simulated annealing scheme.

The calculation is carried out for a nanoparticle with a uniaxial anisotropy in an oblique DC magnetic field and a linearly polarized MW field. According to our results, the optimal MW field is modulated both in amplitude and in frequency (see Fig. 1). Its role is to drive the magnetization from the metastable equilibrium position towards the saddle point, then damping induces the relaxation to the stable equilibrium position. A small magnitude of the MW field is sufficient to induce a substantial reduction of the switching field. For the pumping to be efficient, the MW field frequency must match the proper precession frequency of the magnetization, which equals the ferromagnetic resonance frequency at the early stage of the switching process.

The MW field is optimized for various intensities and orientations of the DC field. The switching field curve (Stoner-Wohlfarth astroid) in presence of a given MW field is then computed. The results are in qualitative agreement with experiments on isolated nanoclusters [1] and on single-domain magnetic elements [2]. The effect of damping is also investigated. The strong dependency of the optimal MW field and the switching curve on the damping parameter provides a means of probing experimentally the latter in nanoclusters.

This study is part of a collaboration with the teams of V. Dupuis (LPMCN, Lyon, France) and E. Bonet (Institut Neel, Grenoble, France), within the ANR project DYSC.

References:

[1] C. Thirion, W. Wernsdorfer, D. Mailly, Nat. Mater. 2 (2003) 524
[2] G. Woltersdorf, C. H. Back, Rhys. Rev. Lett. 99 (2007) 227207
[3] S. Okamoto, N. Kikuchi, O. Kitakami, Appl. Phys. Lett 93 (2008) 142501
[4] N. Barros, M. Rassam, H. Jirari, H. Kachkachi, Phys. Rev. B, submitted

Figures:

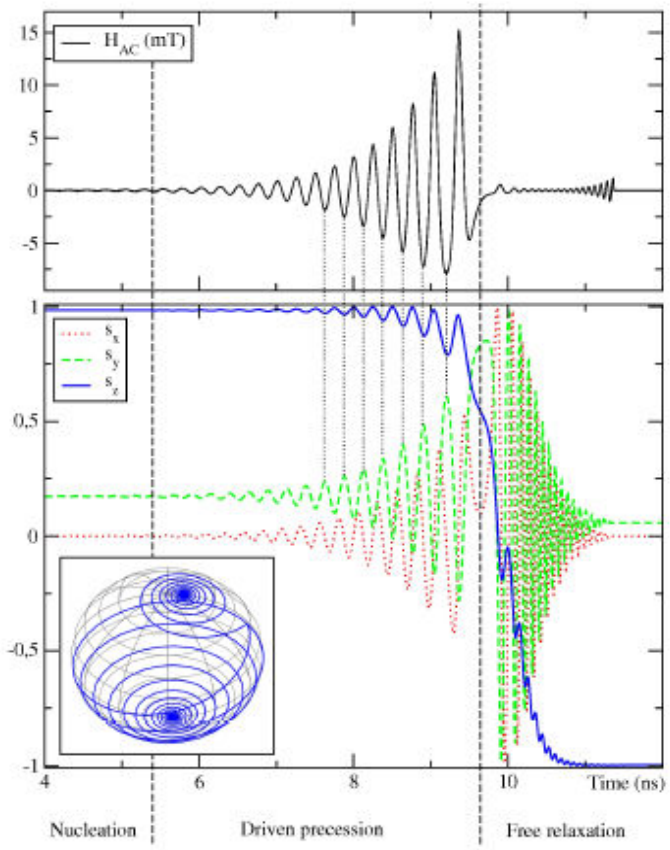

Figure 1: *Optimized MW field (upper panel) and the corresponding spin trajectories (lower panel). The DC field is applied in the yz plane making an angle of 170° with respect to the easy axis (z axis), and its magnitude is 150 mT. The inset is a 3D plot of the spin trajectory on the unit sphere.*

OBSERVATION OF ELECTRONIC RAMAN SCATTERING IN METALLIC CARBON NANOTUBES

H. Farhat[1], **S. Berciaud**[2,3], M. Kalbac[1], R. Saito[4], T. F. Heinz[2], M. S. Dresselhaus[1], and J. Kong[1]

[1]Massachusetts Institute of Technology, Cambridge, MA 02139, USA
[2]Columbia University, New York, NY 10027, USA
[3]IPCMS (UMR 7504), Université de Strasbourg and CNRS, F-67034 Strasbourg, France
[4]Tohoku University, Sendai, 980-8578, Japan
berciaud@unistra.fr

Raman scattering spectroscopy, a powerful tool for studying elementary excitations in materials, has been instrumental in the progress of carbon nanotube research. The Raman features that have been studied to date in carbon nanotubes are associated with the phonon modes that scatter light due to electron-phonon coupling [1]. In metallic nanotubes, low energy electron-hole pairs are another important type of excitation [2], but their inelastic scattering of light [3], via the Coulomb interaction, has not been yet observed. Here, we report on a new feature in the Raman spectrum of individual metallic carbon nanotubes, that we attribute to resonant electronic Raman scattering (ERS) from low-energy electron-hole pairs created across the “graphene-like” linear electronic subbands of metallic nanotubes. The ERS spectra exhibitbroad peaks that appear at a constant photon energy due to a resonance of the scattered photons with the optical transition energies of the metallic nanotube. Our results are consistent with the picture that the mild asymmetry in the lineshape of the Raman G-mode feature [4] is the result of an interference between the overlapping ERS and vibrational Raman scattering by the longitudinal optical (LO) phonon mode.

References:

[1] M. S. Dresselhaus et al., Physics Reports, 409, 47 (2005).
[2] V. V. Deshpande et al., Nature, 464, 209 (2010).
[3] A. Pinczuk, and G. Abstreiter, Light Scattering in Solids V, Springer-Verlag, Berlin, (1989).
[4] Y. Wu et al., Phys. Rev. Lett. 99, 027402 (2007).
[5] M. Y. Sfeir et al., Science, 312, 554 (2006).
[6] J. C. Meyer, M. Paillet et al., Phys. Rev. Lett. 95, 217401 (2005).
[7] S. Berciaud, C. Voisin et al., Phys. Rev. B. 81, 041414(R) (2010).

Figures:

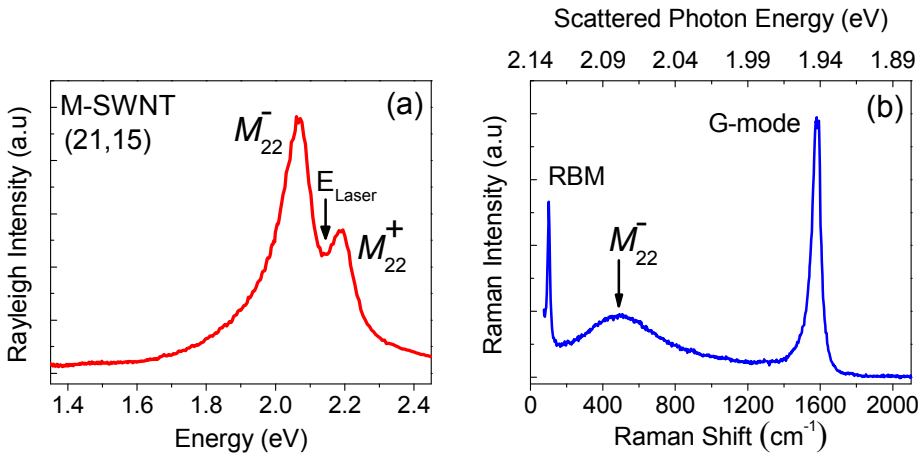

Figure 1: *Electronic Raman Scattering in a structure assigned (21,15) metallic carbon nanotube. The Rayleigh (a) and Raman (b) scattering spectra of an individual, freestanding metallic nanotube are used to determine its (n,m) indices [5, 6]. The labels in a indicate the optical transitions, while the laser energy for the Raman measurement is indicated with arrow. Likewise, the arrow in the Raman spectrum indicate the energies of the optical transitions as obtained from fitting the Rayleigh scattering spectra using an excitonic model [7]. The ERS feature is the broad peak at ~500 cm^{-1} in (b). The corresponding scattered photon energy (2.08 eV, see top axis in (b)) match the energy of the M^-_{22} transition. No ERS features are found in the Raman spectrum of semiconducting nanotubes.*

MANNOSE-TARGETED MESOPOROUS SILICA NANOPARTICLES FOR PHOTODYNAMIC THERAPY

David Brevet,[a] Magali Gary-Bobo,[b] Ouahiba Hocine,[a] Sébastien Richeter,[a] Laurence Raehm,[a] Jean-Olivier Durand,[*a] Bernard Loock,[c] Philippe Maillard,[c] Pierre Couleaud,[d] Céline Frochot,[d] Alain Morère,e Marcel Garcia.[b]

a) Institut Charles Gerhardt Montpellier UMR 5253 CNRS-UM2-ENSCM-UM1, laboratoire CMOS, CC 1701, Place Eugène Bataillon, 34095 Montpellier cedex 05, France
b) INSERM, Unité 896, Montpellier, F 34298 France; Université Montpellier1, Montpellier, F 34298 France; CRLC Val d'Aurelle Paul Lamarque, Montpellier, F 34298 France
c) UMR 176 CNRS/Institut Curie, Institut Curie, Bât 110, Université Paris-Sud, F-91405 Orsay, France; Institut Curie, Section de Recherches, Centre Universitaire, Université Paris-Sud, F-91405 Orsay, France.
d) Département de Chimie Physique des Réactions, UMR 7630, CNRS-INPL, ENSIC, 1, rue Grandville BP 20451, 54001 Nancy Cedex, France
e) UMR 5247 CNRS- UM1-UM2 - Institut des Biomolécules Max Mousseron, Ecole Nationale Supérieure de Chimie de Montpellier, 8 rue de l'Ecole Normale, 34296 Montpellier, France
durand@univ-montp2.fr

Covalent attachment of water-soluble photosensitizers (Figure 1) into mesoporous silica nanoparticles (MSN) for photodynamic therapy (PDT) applications is described. Those MSN were monodispersed with a diameter of 100 nm, a specific surface area of 860 m^2/g and a pores diameter of 2.2 nm. These MSN were proved to be active on breast cancer cells after endocytosis. Moreover, MSN were functionalized on their surface by mannose using an original pathway with diethyl squarate as the linker. Those mannose-functionalized MSN dramatically improved the efficiency of PDT on breast cancer cells. In addition, the involvement of mannose receptors for the active endocytosis of mannose-functionalized MSN was demonstrated (Figure 2).

Figures:

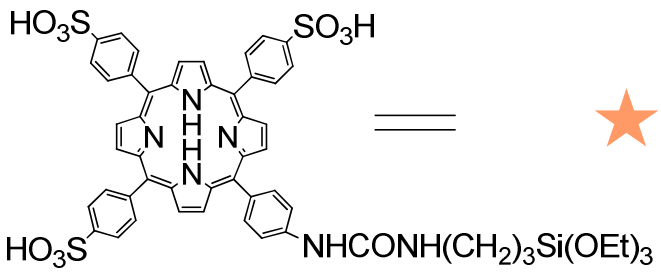

Figure 1

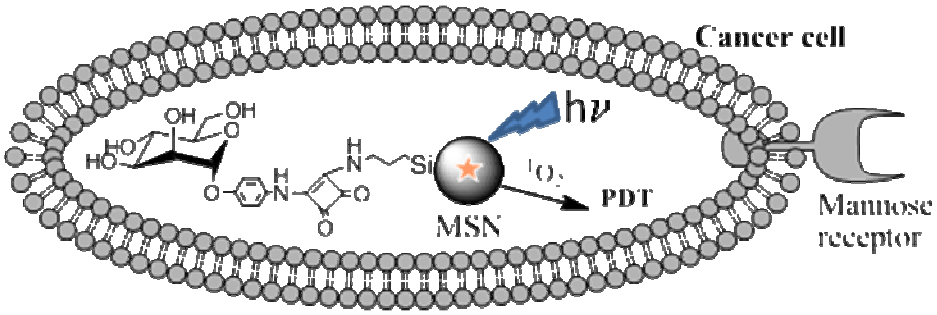

Figure 2

NANOWIRE ARRAYS OF Bi_2Te_3 FOR THERMOELECTRIC APPLICATIONS

O. Caballero-Calero[1], P. Díaz-Chao[1], Deb[2], Y. Shinohara[2], M.S. Martín-González[1]

[1]Thermoelectrics group, IMM-Instituto de Microelectrónica de Madrid (CNM-CSIC), Isaac Newton 8, PTM, E-28760 Tres Cantos, Madrid, Spain
[2]National Institute for Materials Science1-2-1 Sengen, Tsukuba, Ibaraki, 305-0047 Japan
olga.caballero@imm.cnm.csic.es

Thermoelectric materials are those which can convert heat into electricity and vice versa. These materials appear as a promising way to recover power from the heating produced in most of the motors and machines, which is usually wasted [1]. Their main disadvantage is their low efficiency, which depends on their figure of merit (ZT), which is defined as $ZT=(S^2 \cdot \sigma \cdot T)/\kappa$,where S stands for the Seebeck coefficient, σ, κ are the electrical and thermal conductivity, respectively, and T is the absolute temperature. Nowadays, the increase of this ZT is the main objective to optimize them for practical device fabrication. In 1993 a theoretical work presented suggested that a way to enhance their efficiency is by quantum confinement of the electron charge carriers [2]. Therefore, a great effort is being made in demonstrating experimentally this prediction.

One way of achieving this quantum confinement is reducing the dimensions of the material, which can be accomplished by fabricating wires of thermoelectric materials with wire diameters within the nanoscale range. Moreover, nanowire array configuration has some advantages over films, mainly due to a higher freedom in the design of morphology and composition. In our case, we have studied the nanowire formation and properties of Bi_2Te_3, which is a thermoelectric material that has been thoroughly studied in both bulk and film configurations. The fabrication and optimization of these nanowire arrays in order to obtain more efficient thermoelectric devices is the aim of this work.

First of all, Bi_2Te_3 films were grown via electrochemical deposition, following the fabrication procedure described in Martín-González et al. [3,4]. These films were optimized and their morphology (SEM micrographs, see Figure 1), structure (XR-diffraction), and transport properties (Seebeck coefficient and electrical resistivity) were characterized. Finally, films with a well defined crystal orientation (c-axis parallel to the substrate plane, which is the best direction for the thermoelectric performance in this material, see Figure 2) with a homogeneous composition were obtained.

Once this procedure was well established, the method was modified in order to give rise to nanowire arrays in a similar way. To this end, nanoporous anodic aluminium oxide membranes with a nominal pore diameter of 200nm from Whatman® were used. Prior to the growth of the nanowires, all membranes were coated with an evaporated layer of 50 nm Cr and 1500 nm Au. The synthesis of the nanowires was made inside these matrices by electrodeposition. The membrane was placed into electric contact with a Cu plate through the metallic layer, which served as back electrode, forming the working electrode of the electrochemical cell, in a similar arrangement to that described for the growth of Bi_2Te_3 films. Samples grown with different applied potentials between the electrodes and for different time periods were fabricated. SEM micrographs showed that the nanowires have grown along the whole width of the alumina template (Figure 3), giving rise to well oriented wires of Bi_2Te_3. Novel methods developed for the measurement of the thermoelectric-relevant parameters in these structures, comprising the electrical conductivity and thermal conductivity measurement will be presented.

Acknowledgements:

Authors acknowledge financial support from MICINN (FCCI program) ACI PLAN E -JAPON- Grant number PLE2009-0073 and ERC 2008 Starting Grant 240497.

References:

[1] D. M. Rowe, G. Ming, S. G. Willieams, G. K. Kuznetsov, Proceedings of the 17th International Conference on Thermoelectrics (2000), 1499 – 1504.
[2] L. D. Hicks, M. S. Dresselhaus, Phys. Rev. B 47 (1993) 12727 – 12731.
[3] M. Martín-González, J. Electrochem Society 149 11 (2002) C546 – C554.
[4] A.L. Prieto, M.S. Sander, M.S. Martín-González, R. Gronsky, T. Sands, and A.M. Stacy J. Am. Chem. Soc. 123 (2001) 7160.

Figures:

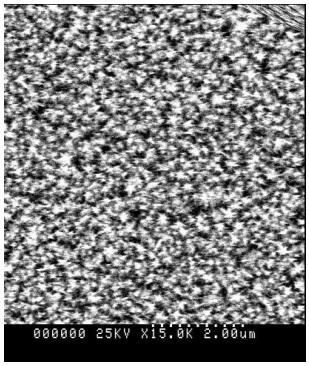

Figure 1: *SEM micrograph a Bi_2Te_3 film grown by electrodeposition.*

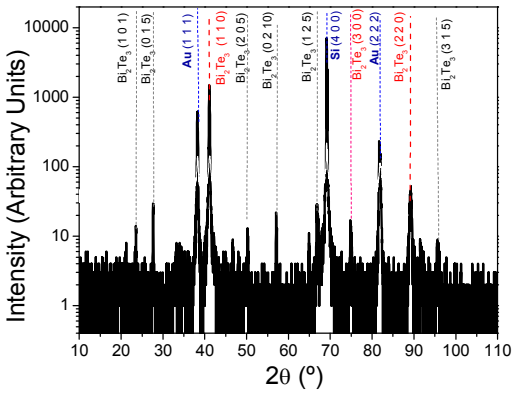

Figure 2: *X-Ray Diffraction data from a Bi_2Te_3 film. Appart from the peaks corresponding to the substrate (Au and Si), the most important diffraction occurs for Bi_2Te_3 oriented along (110), (2 2 0) and (3 0 0), that is, the sample is oriented with the c-axis parallel to the substrate plane (Ref. Natl. Bur. Stand. (U.S.) Monogr. 25,**3** (1964) 16)*

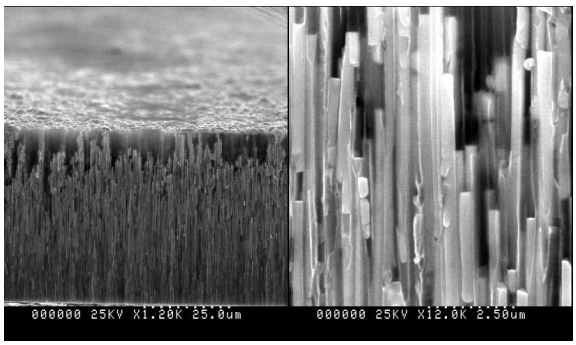

Figure 3: *Different micrographs of the cross-section of nanowire arrays of Bi_2Te_3 grown by electro-deposition in an alumina matrix prepared at IMM.*

QUANTIFYING AND IMAGING MAGNETIZATION REVERSAL OF BURIED INTERFACES BY SOFT X-RAY SPECTROSCOPY AND HOLOGRAPHY

J. Camarero,[1,2],* E. Jiménez,[1] J. Vogel,[3] C. Tieg,[4,5] P. Perna,[2] A. Bollero,[2] F. Yakhou-Harris,[4] C. Arm,[6] E. Gautier,[6] S. Auffret,[6] B. Delaup,[6] G. Gaudin,[6] B. Rodmacq,[6] B. Dieny,[6] and R. Miranda.[1,2]

[1]Departamento de Física de la Materia Condensada and Instituto de Física de Materiales "Nicolás Cabrera", Universidad Autónoma de Madrid, 28049 Madrid, Spain
[2]IMDEA-Nanoscience, Campus de Cantoblanco, 28049 Madrid, Spain
[3]Institut Néel-CNRS, 38042 Grenoble, France
[4]ESRF, F-38043 Grenoble, France
[5]Laboratory Helmholtz-Zentrum Berlin Albert-Einstein-Strasse 15 D-12489 Berlin Germany
[6]SPINTEC, URA2512 CNRS/CEA, 38054-Grenoble, France
julio.camarero@uam.es

The spin arrangement at the interface in layered magnetic nanomaterials is often crucial for the understanding of their magnetic properties and has profound consequences for practical applications. The most striking feature is the unidirectional coupling between the spins in an antiferromagnet (AFM) and those in an adjacent ferromagnet (FM), referred to as exchange bias [1]. FM/AFM structures are at the heart of today's spintronic devices, stabilizing the direction of FM reference layers, while taking advantage of the interfacial exchange interaction effects [2]. In addition, there are a plethora of other magnetic phenomena associated in exchange-coupled FM/AFM systems, such as coercivity enhancement, magnetization reorientation, modified antiferromagnetic spin structures, and asymmetric magnetization reversal, which are not fully understood. Prospects for control, tailor, and enhancement of desirable effects depend upon a clear understanding of the mechanisms governing exchange bias. However, the lack of techniques capable of providing detailed magnetic information of buried interfacial layers with element selectivity and upon external fields is delaying this understanding.

Only very few experimental techniques can address the microscopic magnetization reversal behavior of the different magnetic layers in a multilayered system with element selectivity. Scattering based techniques, such as soft x-ray magnetic resonant scattering (SXMRS) [3] and lensless holographic imaging [4], have been established as a powerful tools for studying magnetic structures in surfaces and thin films on the nanometer length scale. The soft x-ray range hosts the largest magnetic resonances of the magnetically important transition-metal and rare-earth series. Additionally, holographic imaging combines the magnetic sensitivity obtained with x-ray magnetic circular dichroism in transmission geometry with the spatial resolution from a simple Fourier inversion of a reciprocal space soft x-ray interference pattern from an object (sample) and a reference aperture (which defines the final spatial resolution). In addition, the technique can image deeply buried magnetic systems and, as a pure photon-based technique (photon-in/photon-out), can be used in applied magnetic fields. Up to now, soft x-ray holography has focused on [non magnetic/magnetic]n multilayers with perpendicular magnetic anisotropy for both remanence and field-dependent measurements. However, only relatively large (> 5 nm) effective magnetic thicknesses have been studied, and both element-specificity and quantification-availability has not been yet exploited.

We have recently spread out the capabilities of soft x-ray holography for imaging the magnetization reversal, by adding the quantitative aspects of magnetic spectroscopy [5]. We have implemented a unique experimental set-up at beamline ID08 of the European Synchrotron Radiation Facility (ESRF) combining soft x-ray holography and spectroscopy capabilities. This new set-up allows performing element-selective soft x-ray holography measurements for imaging the domain structure of buried magnetic ultrathin films with perpendicular anisotropy under applied magnetic fields, adding the quantitative aspects of magnetic spectroscopy measurements in both total electron yield (TEY) and transmission detection modes. We have investigated ferromagnetic (FM) $[Co/Pt]_n$ multilayers with perpendicular anisotropy exchange coupled with antiferromagnetic (AFM) FeMn and IrMn films. From the spectroscopy analysis, both spectroscopy and element-selective XMCD hysteresis loops measurements confirm the existence of interfacial uncompensated AFM moments, i.e., ~1 ML (monolayer) thick, which behave differently during FM reversal. We have quantified the unpinned (pinned) uncompensated AFM moments, providing direct evidence of its parallel (antiparallel)

alignment with respect to the FM moments. In addition, the Fe-L_3 hysteresis loop reproduces the Co- L_3 one, i.e., it shows a horizontal shift to negative values (opposite to the field cooling FC) direction, exchange bias field $\mu_0 H_E<0$) and, it is slightly shifted vertically downwards (see Fig.1.a). This indicates that the majority (90%) of the uncompensated AFM moments rotates during FM reversal (unpinned moments) whereas a small amount (10%) stays aligned antiparallelly to the FC direction (pinned moments).

The holography experiments allow to image the magnetization reversal of an exchange-biased FM layer with an equivalent Co thickness below 3 nm in real space (1.8 μm diameter field-of-view FOV with 50 nm spatial resolution) and in external magnetic fields [5]. The field dependence images shows that the reversal mechanism of the FM layer is via nucleation, propagation and annihilation of magnetic domains and, in addition, different nucleation sites were found in both hysteresis branches, pointing out a possible deterministic nature of the reversal. A remarkable highlight is that we could image for the first time the magnetization reversal of the uncompensated AFM moments, which correspond to an equivalent thickness of less than one monolayer only [6], and under applied fields [7]. The images show that the uncompensated AFM moments reproduce the magnetic domain structure of the FM layer during the whole hysteresis loop (see Fig1.b), which prove that the FM moments locally drag the unpinned AFM moments during reversal.

Our results provide new microscopic insights into the exchange coupling phenomena and explore the sensitivity limits of these techniques. Future trends will be also discussed.

References:

[1] W. H. Meiklejohn and C. P. Bean, Phys. Rev. 102, 1413 (1956).
[2] J. Nogués and I. K. Schuller, J. Magn. Magn. Mater. 192, 203 (1999).
[3] J. Miguel, J. Camarero, J. Vogel, J. Peters, N. B. Brookes, and J. Goedkoop, Appl. Surf. Sci. 254, 335 (2007).
[4] S. Eisebitt, J. Lüning, W. F. Schlotter, M. Lörgen, O. Hellwig, W. Eberhardt, and J. Stöhr, Nature 432, 885 (2004).
[5] C. Tieg, E. Jiménez, J. Camarero, J. Vogel, C. Arm, B. Rodmacq, E. Gautier, S. Auffret, B. Delaup, G. Gaudin, B. Dieny, and R. Miranda, Appl. Phys. Lett. 96, 072503 (2010).
[6] J. Camarero, E. Jiménez, J. Vogel, C. Tieg, P. Perna, A. Bollero, F. Yakhou-Harris, C. Arm, E. Gautier, S. Auffret, B. Delaup, G. Gaudin, B. Rodmacq, B. Dieny, and R. Miranda, 55th-MMM Conf. invited paper. To appear in J. Appl. Phys. (2011).
[7] E. Jiménez, et al. submitted

Figures:

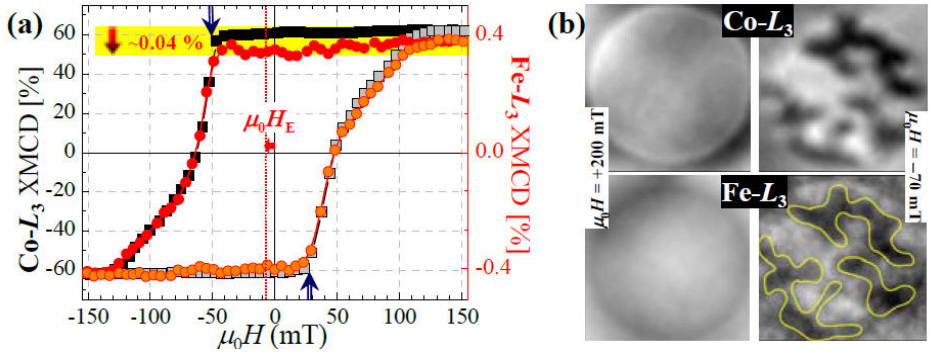

Figure 1: *(a) Element-selective XMCD hysteresis loops of a [1.8 nm Pt/0.6 nm Co]$_8$/10 nm FeMn system recorded in transmission geometry: XMCD data are normalized to their corresponding absorption L_3 peaks. (b) Magnetic domain images of the FM layer (top) and the uncompensated AFM moments (bottom) at selected applied fields. FOV=1.8 μm. The images are retrieved from the Fourier transform of magnetic holograms acquired at the Co-L_3 and Fe-L_3 absorption edges, respectively.*

VIRUS SCAFFOLDS AS ENZYME NANO-CARRIERS (ENCS) TO ORGANIZE BIO-CATALYTIC ENZYME CASCADES. DESIGN OF A SCANNING ELECTROCHEMICAL NANOREACTOR MICROSCOPY DEVICE

Daniela Cardinale[1], Noëlle Carette[1], Amandine Barra[1], Jocelyne Walter[1], Thierry Delaunay[1], Christophe Demaille[2], Agnés Anne[2], Olivier Courjean[3], Nicolas Mano[3], Jean-Paul Salvetat[3], Jean-Pierre Aime[4], Thierry Michon[1]

[1]INRA, UMR 1090 GDPP, IBVM Virologie, 71 Av. Edouard Bourlaux, B.P. 81, 33883 Villenave d'Ornon, France
[2]Laboratoire d'Electrochimie Moléculaire, UMR CNRS – P7 7591, Université Paris Diderot – Paris 7, Bâtiment Lavoisier, 15 rue Jean-Antoine de Baïf, 75205 Paris cedex 13, France
[3]CRPP, Centre de Recherche Paul Pascal, 115 Av. Schweitzer, 33600 Pessac, France
[4]CPMOH, Centre de Physique Moléculaire Optique et Hertzienne, UMR5798,Université Bordeaux 1, 351 Cours de la Libération, 33405 Talence, France
daniela.cardinale@bordeaux.inra.fr

In cellular systems, the association of collaborating enzymes in supramolecular structures enables metabolic processes to be performed more efficiently, accelerating reactions rates and preventing the diffusion of intermediates in the cell medium. The aim of the Cascade project is to create a new experimental tool at the nanoscale level mimicking in vivo enzymatic cascade reactions. The set up will also offer the opportunity to study enzymatic processes at the level of one single or few molecules. To this purpose two model enzymes will be used to build artificial redox cascades: the lipase B (CalB) from *Candida antarctica* and the glucose oxidase (GOX) from *Penicillum amagasakiense*. The free electrons generated by enzymatic activities will be detected by electrochemistry. To this purpose a new nanoelectrochemical technique will be used to confine the clustered enzymes and to measure the final activity. The confined reaction medium will be permitted by a "nanocavity" microelectrode fabricated at the tip of an AFM probe; the combination of AFM/SECM (Scanning Electro Chemical Microscopy) will enable to measure the electrochemical current generated by a few enzyme molecules. Varying the diameter of the nanocavity from few hundreds to about ten nanometers should eventually permit to follow a single enzyme activity.

In order to study one-single enzyme kinetics the very faint signal of the enzyme needs to be amplified. After CalB hydrolysis of p-aminophenyl acetate (pAPA) an electro-inactive substrate to p-aminophenol (pAP) the electro-active product the red-ox couple pAPA/pAP will be continuously recycled between two electrodes amplifying the single enzymatic initial event. Kinetics parameters of pAPA hydrolysis by CALB determined spectrophotometrically and electrochemically are in good agreement. This supports the suitability of pAPA for AFM/SECM single enzyme studies.

In order to control the distribution of enzymes on the electrode we will use virus capsids as Enzyme Nano-Carriers (ENCs). To this aim, two plant viruses, Tobacco mosaic virus (TMV) and potato virus A (PVA) will be tested. Three different strategies will be attempted for the virus to enzyme interfacing: the fusion of leucine zipper (LZ) pairs to enzymes and capsomers, bi-specific antibodies and peptides obtained from phage display screening.

Regarding the first strategy, three pairs of LZ having different characteristics in term of length, affinity and orientation have been selected and the cloning at the N- and C- terminus of CalB is in progress. One assembly CalB (LZKg-CalB) was expressed in Escherichia coli periplasm and we are currently optimizing its purification.

Monoclonal antibodies for CalB have been produced and fusion with antibodies for TMV and PVA will be attempted.

As third strategy, three peptides were selected that recognize PVA. Cloning at the N-terminus of CalB and GOX is in progress.

PLANT VIRUS PARTICLES AS NANOSCAFFOLDS FOR CONTROLLED POSITIONING OF ENZYME CASCADES ON SOLID SUPPORTS

Noëlle Carette[1], Daniela Cardinale[1], Jane Besong[2], Thierry Delaunay[1], Agathe Urvoas[3], Christophe Thibault[4], Jocelyne Walter[1], Amandine Barra[1], Philippe Minard[3], Christophe Vieu[4], Kristiina Mäkinen[2] and Thierry Michon[1]

[1]INRA, UMR BFP, Laboratoire de virologie végétale, 71, Avenue Edouard Bourlaux 81BP, 33883 Villenave d'Ornon, France
[2]University of Helsinki, Applied Biochemistry and Molecular Biology, Department of Food and Environmental Sciences, P.O.Box 27 (Street: Latokartanonkaari 11), Finland
[3]Université Paris Sud, Institut de Biochimie et de Biophysique Moléculaire et Cellulaire, Laboratoire de Modélisation et d'Ingénierie des Protéines, UMR8619, Bât 430, 91405 Orsay, France
[4] LAAS-CNRS, 7, avenue du Colonel Roche, 31077, Toulouse Cedex 4, France
ncarette@bordeaux.inra.fr

In the cell, the close spatial location of enzymes catalyzing consecutive reactions increases the metabolic pathways efficiency, the product of an enzyme becoming substrate of the next enzyme (diffusion limitation or channeling). We intend to design an experimental plateform mimicking this enzyme organization to determine the parameters controlling the cascade reactions. If demonstration is made that a precise positioning of enzymes catalyzing consecutive reactions gives a net advantage upon diffusion controlled processes, the project's outcomes will serve the technology of enzymatically assisted catalysis in organic synthesis with potential applications for the technology of microreactors and biosensors.

Our first goal consists in controlling the distribution of active enzymatic systems on solid supports. The systems concerned are constituted of several enzymes catalyzing a cascade of up to 3 consecutive reactions.

Virus particles are precisely defined nanometer-sized objects, well-ordered, formed by a self-association of capsid proteins monomers. These particles will be used as Enzymes Nano -Carriers (ENCs). Subsequently these ENCs can be finely positioned on solid supports using nanolithography techniques. The rod shaped tobacco mosaic virus (TMV) and the flexuous filamentous potato virus A (PVA) were chosen as ENCs.

Candida Antarctica lipase B (CALB), glucose oxidase (GOx) and horseradish peroxidase (HRP) were chosen as demonstrating enzymes. Three strategies are under investigation for enzymes to virus interfacing.

The first strategy consists in introducing complementary leucine zippers (basic and acid) peptides on TMV (or PVA) and enzymes. We are trying to produce engineered TMV *in planta*. The surface of TMV being negative, acidic leucine zipper (LZecoil) was genetically introduced at the C-terminus part of the capsid protein within the virus genome. A weak systemic infection of *Nicotiana benthamiana* plants by TMV-LZecoil was observed (2 plants/24). The virus progeny eliminated the LZecoil insert in inoculated leaves 15 days after inoculation. Engineered PVA like particles will be reconstituted from an N-terminus fusion between acidic leucine zippers and capsid proteins expressed in *Escherichia coli*.

A second approach consists in the selection by M13 phage display of peptides which present an affinity for the virus surface (TMV or PVA). The sequence of these peptides will be genetically introduced at the N-terminus part of the enzymes.

Three peptide sequences were found to have a specific affinity for PVA particles; their genetic fusion to the enzymes is in progress.

In a third approach, bispecific antibodies will be selected to insure the coupling between virus particles and enzymes. A selection of monoclonal antibodies against either the viruses (TMV, PVA) or the enzymes (CALB, HRP) is in progress. Then a fusion of the cells producing each monoclonal antibody will be attempted.

CELL PENETRATING PEPTIDE-SUPERPARAMAGNETIC IRON OXIDE NANOPARTICLE CONJUGATES AS BIMODAL IMAGING NANOAGENTS

Silvia Cavalli, Daniel Carbajo, Miriam Royo, Fernando Albericio

CIBER-BBN, Networking Centre on Bioengineering, Biomaterials, and Nanomedicine. Barcelona Science Park, Institute for Research in Biomedicine, Baldiri Reixac 10, 08028 Barcelona, Spain.
silvia.cavalli@irbbarcelona.org

Molecular imaging has attracted more and more attention in the past decades. There is a strong interest in developing and validating imaging technologies such as fluorescence imaging and magnetic resonance (MR) to image biological target in vivo. Exploiting the intrinsic properties of superparamagnetic iron oxide nanoparticles (SPION) could result in obtaining medical breakthroughs in diagnosis and therapy. SPION can be used as magnetic contrast agents in magnetic resonance imaging (MRI) as well as hyperthermia agents, where the magnetic particles are heated selectively by application of an high frequency magnetic field (i.e. in thermal ablation/hyperthermia of tumors) or as magnetic vectors that can be directed by means of a magnetic field gradient towards a certain location, such as in the case of the targeted drug delivery. [1] Cell penetrating peptides have been used to increase cellular uptake of these nanoparticles. As an example HIV-1 Tat protein-derived peptide sequences, in particular GRKKRRQR48-57, have been extensively used as an efficient way of increasing internalization into cells. [2]

In this project we developed a bioorthogonal chemical approach [3] to functionalize SPION with a new class of cell-penetrating peptide, cis-g-amino-proline derived peptides, previously developed in our group. [4] A schematic representation of the general approach is shown in Figure 1. Commercially available amino-functionalized SPION (SPION-NH_2) were partially modified with a reacting group (blue triangle, SPION-RG). Fluorescent labelled cell penetrating peptides, previously modified with a complementary reacting group (yellow triangle), were subsequently conjugated to SPION-RG exploiting bioorthogonal chemical reactions that occurred in buffer media close to physiological conditions. A Tat sequence, modified as described above, was included in the study as positive control for cellular uptake, while acetylated peptides were used as negative controls for proving the occurrence of the ligation. An advantage of this approach is that crude peptides could be used during the conjugation thanks to the high chemoselectivity of the reaction. Purification occurred during dialysis of the final nanoconjugate samples.

This study comprised of a synthetic part, in which the peptide-nanoparticle conjugates were prepared and characterized, followed by biological studies conduced to evaluate their cellular uptake and toxicity. In Figure 2 confocal laser microscopy confirmed internalization into HeLa cells of the SPION-CCP obtained by the conjugation of a cis-g-amino-proline derived peptide. Currently, we are performing MRI investigations to validate such new nanodevices as novel bimodal contrast agents for optical imaging as well as MRI.

References:

[1] a) M. J. Kogan, I. Olmedo, L. Hosta, A. R. Guerrero, L. J. Cruz and F. Albericio, Nanomedicine, 2 (2007), 287. b) M. Arruebo, R. Fernández-Pacheco, M. R. Ibarra, J. Santamaría, Nanotoday, 2 (2007), 22. c) C. Carot, P. Robert, J.-M. Idée, M. Port, Adv. Drug Delivery Rev., 58 (2006), 1471.
[2] M. Lewin, N. Carlesso, C.-H. Tung, X.-W. Tang, D. Cory, D. T. Scadden, R. Weissleder, Nature Biotechnology, 18 (2000), 410.
[3] E. M. Sletten, C. R. Bertozzi, Angew. Chem. Int. Ed., 48 (2009), 6974.
[4] J. Farrera-Sinfreu, E. Giralt, S. Castel, F. Albericio, M. Royo, J. Am. Chem. Soc. 127 (2005), 9459.

Figures:

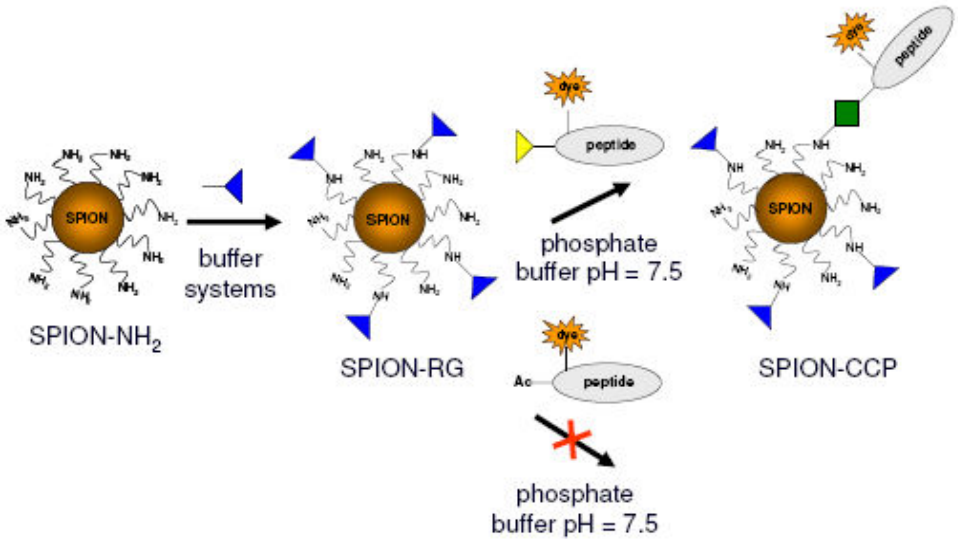

Figure 1: *Schematic representation of the general approach.*

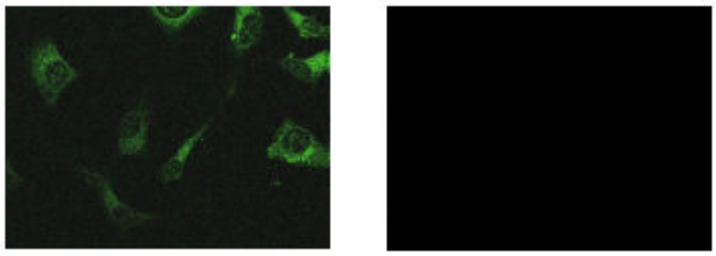

Figure 2: *Confocal laser microscopy images of HeLa cells incubated with 1 μM concentration of SPION-CCP sample (left panel) and negative control with SPION-FG + AcCCP (right panel).*

VIBRATIONAL SUM-FREQUENCY GENERATION SPECTROSCOPY OF SELF-ASSEMBLED AND LANGMUIR-BLODGETT FILMS ON SURFACES: FROM MONOLAYERS TO MODEL LIPID MEMBRANES

Francesca Cecchet, Julien Guthmuller, Benoit Champagne, Yves Caudano, André Peremans, and Dan Lis

Laboratory of Lasers and Spectroscopy (LLS), Research Centre in Physics of Matter and Radiation (PMR), Laboratory of Theoretical Chemistry, FUNDP - University of Namur, Belgium
francesca.cecchet@fundp.ac.be

Investigating the structure and the physico-chemical properties of biomimetic lipid membranes on surfaces is a pre-requisite for a detailed investigation of biological processes occurring within such bio-films, and their selective detection. This also represents a platform to build-up reliable bio-devices mimicking the membrane behaviour. Indeed, the structure and the physico-chemical properties of thin films on surfaces are intrinsically linked. Knowing the organization of organic layers on surfaces is therefore a key element to understand, to control and to tailor their physical, chemical, or biological properties. This requires highly surface/interface sensitive techniques which are able to discriminate interfacial responses from those of the surrounding bulk phases.

The analysis of the physico-chemical properties of bio-interfaces can be achieved by probing their vibrational response. Among the vibrational spectroscopies, sum-frequency generation (SFG) has emerged in the characterization of thin organic layers adsorbed on surfaces [1,2,3]. Indeed, being based on a second order nonlinear optical process, SFG spectroscopy is intrinsically specific to surfaces and interfaces [1,2,3], and therefore it represents an ideal tool to probe organic layers confined at solid surfaces.

In this work, the vibrational signature of (bio)-organic films mimicking the membrane structure has been in order to retrieve information about their structural organization and their molecular orientation. In particular, self-assembled monolayers (SAMs) of thiols (Figure 1a), and solid-supported lipid layers, either in the form of monolayers (Figure 1b), or in that of hybrid bilayers (Figure 1c), have been investigated by SFG spectroscopy (Figure 1, top).

Firstly, we have focused on the analysis of self-assembled monolayers (SAMs) of alkane and of aromatic thiols [4,5], which are models for the interpretation of the vibrational nonlinear optical response of more complex architectures mimicking the lipid membranes. Secondly, we have probed the organization of solid-supported lipid films, prepared either by vesicle fusion or by Langmuir-Blodgett and Langmuir-Schaeffer methods on bare or pre-functionalized substrates. Different lipid molecules have been used to build the model membranes, such as the well-known phosphatidylcholine lipid (PC) or the less-known antigenic 2,4-dinitrophenyl lipid (DNP) [6]. Information about the lipid films order and organization has been obtained, and has indicated that the intimate film organization, which is probed through the analysis of the SFG signature of the lipid hydrophobic chains, strongly depends on the molecular composition and on the surface properties. The SFG responses have been interpreted with the support of DFT calculations, and of experimental measurements of the solid-state IR and Raman activities. This has enabled to predict the SFG active modes of the (bio)-organic films, and therefore to attribute, with high accuracy, the detected signals to vibrational motions.

This analysis is performed in the framework of investigating the structural changes and the physical-chemical interactions induced by recognition processes, which take place within such interfacial layers.

In particular, the high interface/surface sensitivity of SFG spectroscopy may open the way to novel solutions for the detection of biological processes occurring within surface-confined (bio)-organic films.

References:

[1] Shen Y.R., Nature 337 (1989) 519.
[2] Roke, S. ChemPhysChem 10 (2009) 1380.
[3] Chen X., Clarke M.L., Wang, J., Chen Z. Intern. J. Mod. Phys. B 19 (2005) 691.
[4] Cecchet, F., Lis D., Guthmuller J., Champagne B., Caudano Y. Silien, C., Mani A.A., Thiry P., Peremans A. ChemPhysChem 11 (2010) 607.
[5] Cecchet, F., Lis D., Guthmuller J., Champagne B., Fonder G., Mekhalif Z., Caudano Y., Mani A.A., Thiry P., Peremans A. J. Phys. Chem. C 114 (2010) 4106.
[6] Lis D., Guthmuller J., Champagne B., Humbert C., Busson B., Tadjeddine A., Peremans A., Cecchet F. Chem. Phys. Lett. 489 (2010) 12.

Figures:

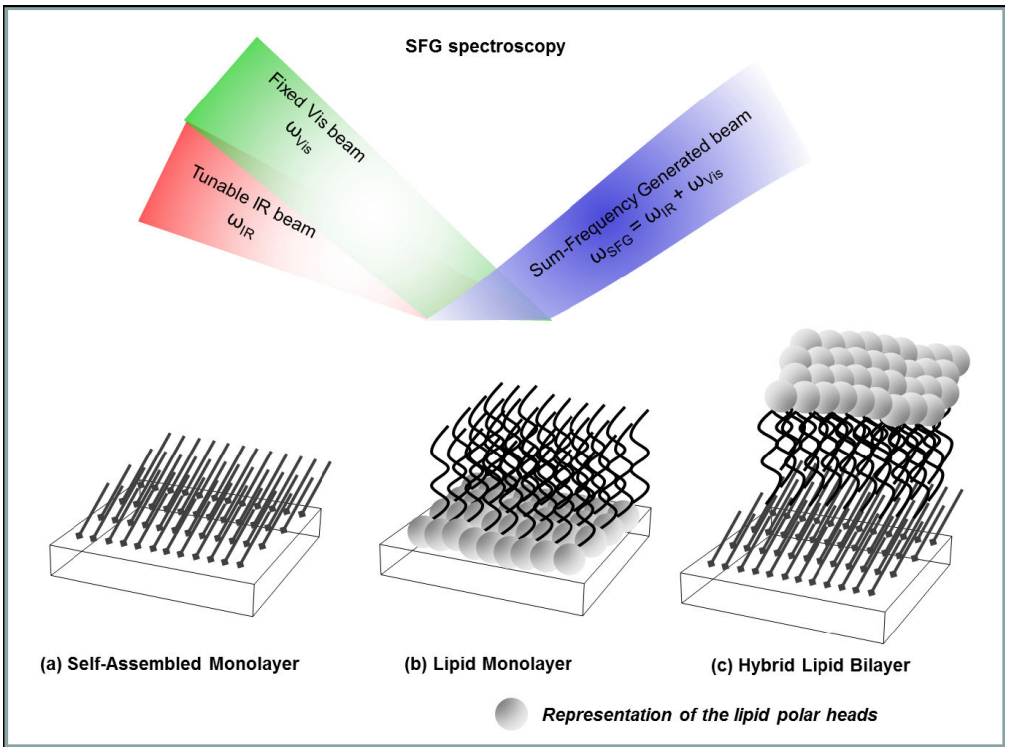

Figure 1: *Schematic representation of the SFG spectroscopy (top), and modeling of the (bio)-organic films which are investigated, namely Self-Assembled Monolayers (a), Lipid Monolayers (b), and Hybrid Lipid Bilayers (c).*

FROM MOLECULAR WIRES TO ORGANIC SEMICONDUCTORS AND BACK - SOME "*DON'T ASK, DON'T TELL*" OF SOFT ELECTRONICS

Gianaurelio Cuniberti

Institute for Materials Science and Max Bergmann Center for Biomaterials,
Dresden University of Technology, 01062 Dresden, Germany
g.cuniberti@tu-dreden.de

Charge migration is a ubiquitous phenomenon with profound implications throughout many areas of chemistry, physics, biology and materials science. The long-term vision of designing functional materials with pre-defined molecular scale properties has triggered an increasing quest to identify prototypical systems where truly inter-molecular conduction pathways play a fundamental role. Such pathways can be formed due to molecular organization of various organic materials and are widely used to discuss electronic properties at the nanometer scale. Many of the mechanisms of charge migration in soft matter nanosystems are common to single molecule electronics and organic electronics. In this talk I will illustrate how recent important contributions of unimolecular electronics research can crossfertilize the field of organic electronics and vice versa how the recent breakthrough in engineering molecular materials in organic semiconductor could inspire new developments in molecular electronics.

References:

[1] C. Gollub et al., Charge migration in organic materials: Can propagating charges affect the physical quantities controlling their motion?, preprint
[2] T. Kawai et al., Mechanically-induced transport switching effect in graphene-based nanojunctions, preprint
[3] H. Kleemann et al., Organic Zener Diodes: Tunneling across the gap in organic semiconductor materials, Nano Letters, 2010, 10, 4929.
[4] R. Gutierrez et al., Physical Review Letters 2009, 102, 208102.
[5] D. Dulic et al., Angewandte Chemie International Edition 2009, 48, 8152.

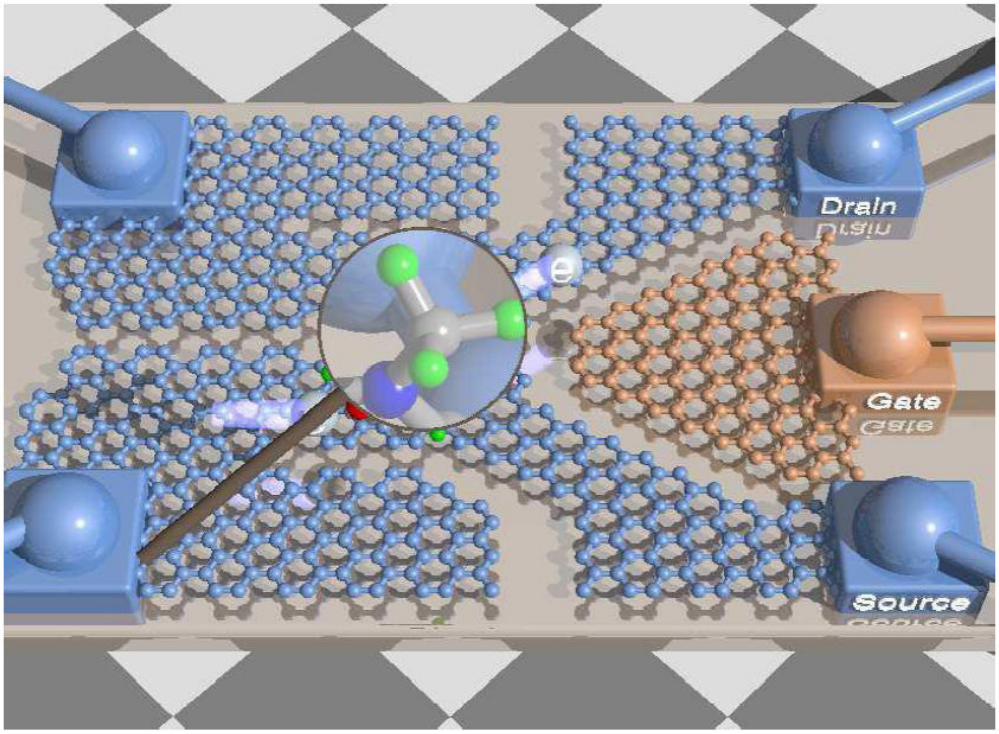

NANOCONTAINERS: PROPERTIES, MANIPULATION AND BIO-MEDICAL APPLICATIONS

Luisa De Cola

Westfälische Wilhelms-Universität, and CeNTech, Mendelstr. 7, 48149 Münster, Germany
decola@uni-muenster.de

The creation of molecular (nano)containers: crystalline or amorphous, rigid or soft is a very fascinating field at the cross point of different disciplines. Our effort, in this talk, focuses on the synthesis and use of crystalline materials, zeolites L, which are transparent, stiff, nanocontainers. They are made of hundreds of parallel aligned unidimensional channels, which can be filled with molecular dyes or other responsive molecules. The selective and spatial resolved functionalization of these nanocontainers can lead to multifunctional systems [1]. Furthermore the selective functionalization of the channel entrances, lead to the self-assembling of the zeolites, and the assembly process can be extended to living organism such as bacteria [2]. The use of appropriate light responsive components in combination with the smallest zeolites (30 nm) has been very successfully applied for the labeling targeting and killing of antibiotic resistant bacteria (see figure) [3].

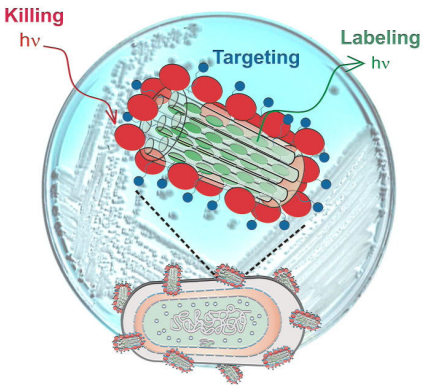

Finally we have realized hierarchical supramolecular organization by optical control of nano-containers that contain highly ordered molecules. Holographic optical tweezers allow for precise, exible, and dynamic 3D position and orientation control of arbitrary shaped multiple container particles. [4].

References:

[1] M. Busby, H. Kerschbaumer, G. Calzaferri, L. De Cola Adv. Mat. 2008, 20, 1614
[2] Z. Popovic, M. Otter, G. Calzaferri, L. De Cola, Angew. Chem. Ind.Ed., 2007, 46, 6188. Z. Popovic, L. De Cola et al. Angew. Chem., Ind. Ed. 2007, 46, 8898.
[3] C. Strassert, M. Otter, R. Albuquerque, A. Höne, Y. Vida, B. Maier, L. De Cola Angew. Chem. Int. Ed. 2009, 48, 7928.
[4] M. Woerdemann, S. Gläsener, F. Hörner, A. Devaux, L. De Cola, C. Denz Adv. Mat., 2010, 22, 4176; OPN Optics & Photonics News, 2010, 21, 40.

FOCUSED ELECTRON BEAM INDUCED DEPOSITION AND ETCHING OF FUNCTIONAL MATERIALS

J.M. De Teresa[1,2], R. Córdoba[2,3], A. Fernández-Pacheco[1,2,3], L. Serrano[1,2], F. Schoenaker[1], M.R. Ibarra[1,2,3]

[1]Inst de Ciencia de Materiales de Aragón, Universidad de Zaragoza-CSIC, Zaragoza, 50009, Spain
[2]Departamento de Física de la Materia Condensada, Universidad de Zaragoza, 50009, Spain
[3]Instituto de Nanociencia de Aragon, Universidad de Zaragoza, Zaragoza, 50018, Spain
deteresa@unizar.es

Many working devices in the field of nanotechnology rely on the top-down approach for their creation. This implies the use of thin-film growth techniques in tight cooperation with micro- and nanolithography techniques. The method of choice should address crucial aspects such as resolution, roughness, shape, materials involved, cost, etc. Optical lithography is normally preferred down to the micron scale and electron-beam lithography below the micron scale. However, some of the involved steps are critical and the final sample nanometric features can be far from ideal. In order to circumvent the annoying use of resists, direct patterning by focused-ion-beam is not rare, but this technique can strongly modify the properties of the materials, restricting its use. It is in this context that focusedelectron-beam-induced-deposition (FEBID) and focused-electron-beam-induced-etching (FEBIE) techniques are becoming promising routes for the direct growth or patterning of functional nanostructures in a single step. These techniques do not involve the painful use of resists, etching or lift-off processes, whereas maintaining the high lateral resolution down to the nanometric scale. In the present contribution, we will show successful examples of the use of FEBID and FEBIE for the creation of functional nanostructures. The deposition or etching experiments have been carried out by means of a field-emission-gun scanning electron microscopy (SEM) and gas injectors which permit to deliver precursor gas to the area of interest.

Cobalt-based nanostructures have been grown by FEBID using $Co_2(CO)_8$ as the precursor gas on Si substrates or insulating $Si//SiO_2$ substrates. Our previous work has shown that Co by FEBID can be grown with high purity, showing remarkable properties for applications in magnetic sensing, storage and logic [1-4]. In the present contribution we show the successful growth of cobalt nanowires with lateral size down to 30 nm, which could be used for highly-integrated domain-wall manipulation. Besides, for the application in Hall sensing, we have grown Co squares with lateral size around 100 nm plus narrower contact lines to permit injection of current from opposite edges of the square and measurement of voltage from the remaining two contacts.

Titanium is a relevant technological material due to its extraordinary mechanical and biocompatible properties, its nanopatterning being an increasingly important requirement in many applications. We report the successful nanopatterning of titanium by means of Focused Electron Beam Induced Etching using XeF_2 as a precursor gas [5]. Etch rates up to 1.25 x 10^{-3} μm^3 s^{-1} and minimum pattern sizes of 80 nm were obtained. Different etching parameters as beam current, beam energy, dwell time and pixel spacing are systematically investigated, the etching process being optimized by decreasing both beam current and beam energy.

References:

[1] A. Fernández-Pacheco et al, J. Phys. D : Appl. Phys. 42, 055005 (2009).
[2] A. Fernández-Pacheco et al, Appl. Phys. Lett. 94, 192509 (2009).
[3] A. Fernández-Pacheco et al, Nanotechnology 20, 475704 (2009).
[4] S. Sangiao et al, Solid State Communications 151, 37 (2011).
[5] F. Schoenaker et al, submitted to Nanotechnology (2011).

Figures:

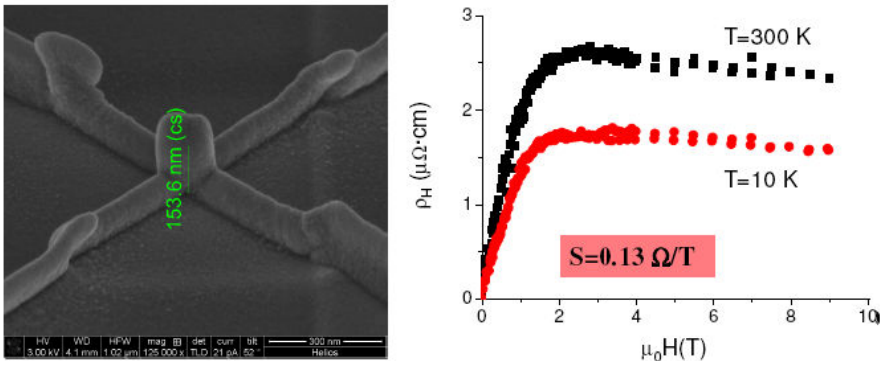

Figure 1: *One of the grown Hall devices based on Co by FEBID and its Hall characterization.*

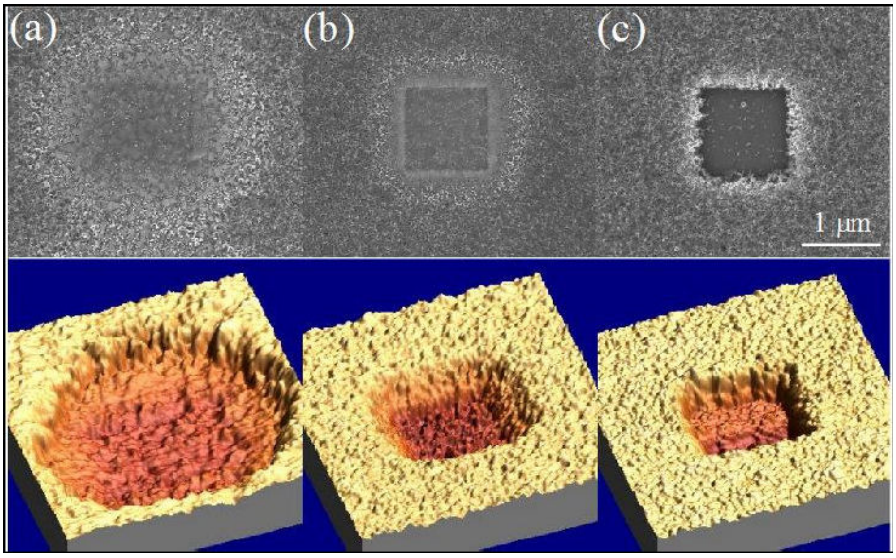

Figure 2: *SEM (top) and AFM (bottom) images of Ti etchings made with 2 kV electron beam energy and different beam currents and etching times. (a) Beam current of 1.35nA and a 30 s etching time. (b) Beam current of 318 pA and a 105 s etching time. (c) Beam current of 5.4 pA and a 600 s etching time.*

DIRECT NEAR-FIELD STUDY OF GENERATION, COUPLING, PROPAGATION AND DESIGN OF SURFACE PLASMONS POLARITONS IN THE MID-INFRARED

Y. De Wilde[1], A. Babuty[1], I. Moldovan-Doyen[1], L. Greusard[1], R. Rungsawang[1], J.-P. Tetienne[2], D. Costantini[2], A. Bousseksou[2], R. Colombelli[2], G. Beaudoin[3] and I. Sagnes[3]

[1] Institut Langevin, ESPCI ParisTech, CNRS, 10 rue Vauquelin, 75231 Paris Cedex 05, France
[2] Institut d'Electronique Fondamentale, Université Paris Sud and CNRS, 91405 Orsay, France
[3] CNRS/LPN, Laboratoire de Photonique et de Nanostructures, 91460 Marcoussis, France
yannick.dewilde@espci.fr

Scattering-type near-field optical microscopy (sNSOM) uses the tip of an atomic force microscope to scatter the electromagnetic near-field towards a detector located in the far-field. Recording the scattered near-field as a function of the position of the tip while it is scanned over the sample surface, allows one to obtain an optical image of the scanned area with subwavelength resolution, at the same time as its topography is recorded. As the scattered light propagates in free space, sNSOM can be applied at any wavelength. Application of sNSOMs at low photon energies such as mid-infrared and terahertz wavelengths is the nanoscale observation of the dielectric contrast between materials [1], or the mapping of the spatial distribution of evanescent waves at the surface of waveguides or devices [2].

Surface plasmons polaritons (SPPs) are propagating electromagnetic modes bound at the interface between a metal and a dielectric, which originate from electron oscillation in the metal. These electromagnetic waves are evanescent in the direction perpendicular to the interface, while they can propagate in a direction parallel to it. sNSOM is a unique tool to perform direct imaging with subwavelength resolution of SPPs propagating on metal surfaces. In this talk, we will give an overview of our recent sNSOM investigations of various types of plasmonic devices which are active, in the sense that they use a mid infrared (midIR) quantum cascade laser (QCL) as an electrical generator of SPPs [3,4].

Due to their dispersion relation, the generation of SPPs generally requires the use of a prism or a grating combined with an external laser source. In situ generation is clearly required to produce compact integrated SPPs devices. We have achieved this goal in a device operating at □≈7.5 μm which includes all the building blocks required for a fully integrated plasmonic active source: an electrical generator of SPPs based on a 1st order distributed feed-back (DFB) metal grating at the surface of the laser cavity, a grating coupler, and a passive metallic waveguide. We have demonstrated the operation of the device by reproducing the analogue in the near-field of the slit-doublet experiment, using the sNSOM to observe directly the standing wave pattern which is formed in the near-field on the passive section of the device, due to the interference of two counter-propagating SPPs [3]. An alternative method to inject SPPs on a passive waveguide is end-fire coupling, which we have used to generate SPPs on a flat metallic strip from the end facet of a QCL at □≈7.5 μm. We demonstrate the propagation of SPPs at distances of several hundreds of micrometers from the end facet of the laser via both far-field and near-field imaging techniques [4]. At midIR wavelength, SPPs propagating on a flat gold surface have a decay-length (perpendicular to the gold surface) of tens of micrometers [4]. The "designer's" or spoof SPPs allow one to dramatically change this behavior by artificially designing the dispersion relation using structured surfaces [5]. The idea is to mimic at IR wavelengths features which in principle are observed at shorter wavelength, and which result in an enhanced confinement of the SPPs at the surface [5,6]. We have achieved this by replacing the flat surface of the SPPs waveguide by a properly designed sub-wavelength metallic groove grating. Increasing the groove depth results in an increased in-plane wavevector and, therefore, long wavelength spoof SPPs have a shorter decay-length and can be manipulated just as their short wavelength counterpart. Based on sNSOM imaging, we demonstrate curved spoof SPPs trajectories and we present our progress towards the realization of a sub-wavelength-sized "hot spot" where local field enhancement occurs (7).

We acknowledge financial support from the French National Research Agency (ANR-07-NANO-039 "NanoFtir" and ANR-09-NANO-020 "Gospel") and from the Centre de compétences NanoSciences Ile-de-France (Project PSTS).

References:

[1] B. Knoll and F. Keilmann, “Near-field probing of vibrational absorption for chemical microscopy”, Nature 399, (1999) 134.

[2] V. Moreau, M. Bahriz, R. Colombelli, P-A. Lemoine, Y. De Wilde, L.R. Wilson, and A.B. Krysa, "Direct imaging of a laser mode via mid-infrared near-field spectroscopy", Appl. Phys. Lett. 90, (2007) 201114.

[3] A. Babuty, A. Bousseksou, J-P. Tetienne, I. Moldovan Doyen, C. Sirtori, G. Beaudoin, I. Sagnes, Y. De Wilde, R. Colombelli, “Semiconductor Surface Plasmon Sources”, 104, (2010) 226806.

[4] J.-P. Tetienne, A. Bousseksou, D. Costantini, R. Colombelli, A. Babuty, I. Moldovan-Doyen, Y. De Wilde, C. Sirtori, G. Beaudoin, L. Largeau, O. Mauguin, and I. Sagnes, “Injection of midinfrared surface plasmon polaritons with an integrated device”,Appl. Phys. Lett. 97, (2010).211110.

[5] J. B. Pendry, L. Martín-Moreno, and F. J. Garcia-Vidal, “Mimicking Surface Plasmons with Structured Surfaces”, Science 305, (2004) 847.

[6] A. I. Fernandez-Dominguez, C. R. Williams, F. J. García-Vidal, L. Martín-Moreno, S. R. Andrews and S. A. Maier, “Terahertz surface plasmon polaritons on a helically grooved wire”, Appl. Phys. Lett. 93, (2008).141109.

[7] M. I. Stockman, “Nanofocusing of Optical Energy in Tapered Plasmonic Waveguides”, Phys. Rev. Lett. 93, (2004) 137404.

Figures:

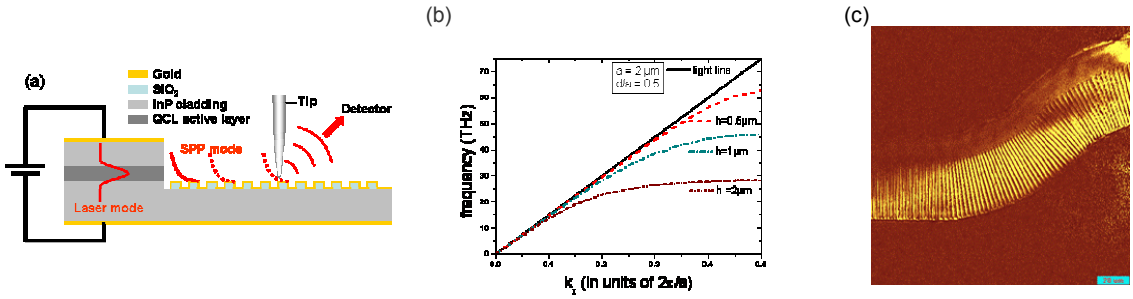

Figure 1: *(a) Schematic cross section of a spoof SPPs device using a mid IR QCL as generator, and schematic view of the sNSOM detection; (b) Dispersion relation of spoof SPPs corresponding to a metal grating with a pitch of 2 μm, duty cycle 0.5, and depth h; (c) sNSOM image measured on a curved spoof SPPs waveguide.*

INTERNALISATION MECHANISMS OF MODIFIED TITANIUM OXIDE NANOPARTICLES IN SKIN CELLS AND MULTICELLULAR LIVING SPECIMENS: RESULTING TOXICITY

M.H. Delville[1], M. Simon[2], A. Girard[1,2], P. Barberet[2], P. Moretto[2], H. Seznec[2], D. Dupuy[3]

[1]CNRS, Université de Bordeaux, ICMCB, 87 avenue du Dr. A. Schweitzer, Pessac, F-33608 Cedex, France
[2]Université Bordeaux, CNRS/IN2P3, Centre d'Etudes Nucléaires de Bordeaux
[3]Gradignan, CENBG, Chemin du Solarium, BP120, 33175 Gradignan, France
Institut Européen de Chimie et Biologie, Univ Bordeaux 1, 2 rue R. Escarpit, 33607 Pessac, France
delville@icmcb-borderaux.cnrs.fr

Nanotechnologies are of great interest from both academic and industrial points of view, with numerous applications in domains such as medicine, catalysis and material sciences. However, their nanotoxicology has also attracted the attention of public and governments' worldwide and established methods of chemical safety assessments have to be modified to address the special characteristics of nanoparticles and more especially to assess the biological effects of these highly reactive materials.

Most of these manufactured nanoparticles have been produced for several decades on an industrial scale. There is an urgent need to evaluate the risks of these particles to ensure their safe production, handling, use, and disposal. Moreover, a comprehensive study is clearly needed to fully explore the toxicity of manufactured nanoparticles, which may help to better understand their deleterious health effects and create environmentally friendly and biologically relevant nanoparticles. In particular, the behavior of nanoparticles inside living cells is still an enigma, and no metabolic responses induced by these particles are understood so far.

This presentation concerns the potential toxicity due to exposure of TiO_2 NPs used in sunscreens and cosmetics. We propose to apply an original imaging methodology (Ion Beam Analysis, TEM, and Confocal microscopy) to in vitro studies, combining technologies for on one hand, the detection, tracking, and quantification of TiO_2 nanoparticles and on the other one, the use of indicators for ion homeostasis, cell metabolism, or cell fate.

The main goal is to precisely identify the molecular and cellular mechanisms involved in the nanotoxicity of TiO_2 nanoparticles in eukaryotic cells and in multi-cellular organisms such as *Caenorhabditis elegans* (*C. elegans*). This study addresses the current knowledge gap of human cells and *C. elegans* responses to TiO_2 nanoparticles exposure. Since the nematodes feed on bacteria and are considered as particle-ingesting organisms, the present study will offer new perspectives in nanoparticles-related risk assessment and food web accumulation modelling.

References:

[1] Marina Simon, Philippe Barberet, Marie-Hélène Delville, Philippe Moretto, Hervé Seznec Nanotoxicology on line 07/15/2010.

ROLE OF THE SURFACE ELECTRONIC STRUCTURE IN THE ENHANCEMENT OF QUANTUM FRICTION BETWEEN PARALLEL SILVER SLABS

Vito Despoja[1;2], Pedro M. Echenique[1], Marijan Sunjic[1;2], and V. M. Silkin[1]

[1]Donostia International Physics Center (DIPC), P. Manuel de Lardizabal, 20018 San Sebastian, Basque Country, Spain and
[2]Department of Physics, University of Zagreb, Bijenicka 32, HR-10000 Zagreb, Croatia

In the framework of the recent debate [1, 7] about the existence and formulation of quantum friction between two moving metallic slabs, we provided a new, more effcient formulation and applied it to the investigation of the role of realistic electronic structure to friction between two silver slabs in relative motion. The results are compared with those of the Drude and jellium models. We show that low energy electronic excitations play a dominant role in the description of quantum friction, i.e. that the Drude model, because of the absence of low energy electronic excitations, is a completely inappropriate model in the description of friction phenomena. On the other hand, the jellium model, because of the absence of surface states (which reduce low energy electron hole intensity), and absence of low energy surface plasmons [9], gives a significant reduction of the frictional force. We show that in the range $0 < v < v_F$, the friction force shows an v^{α} dependence whereas in the jellium model $\alpha = 3$ and for a realistic model potential [10] $\alpha = 4$. Because quantum size effects strongly modifed low energy electronic excitations [8], we provided an analysis of quantum friction as function of slab thicknesses.

References:

[1] J. B. Pendry, J. Phys.: Condens. Matter 9 10301 (1997)
[2] B. N. J. Persson, Phys. Rev. B 57, 7327 (1997)
[3] A. I. Volokitin, B. N. J. Persson, Phys. Rev. B 78, 155437 (2008)
[4] J. B. Pendry, New J. Phys. 12, 033028 (2010)
[5] T. G. Philbin, U. Leonhardt, New J. Phys. 11 033035 (2009)
[6] U. Leonhardt, New J. Phys. 12, 068001 (2010)
[7] J. B. Pendry, New J. Phys. 12, 068002 (2010)
[8] V. M. Silkin, M. Alducin, J. I. Juaristi, E. V. Chulkov and P. M. Echenique, J. Phys.: Condens. Matter 20 (2008) 304209
[9] B. Diaconescu, et al, Nature 448, 57-59 (2007)
[10] E. V. Chulkov, V. M. Silkin and P. M. Echenique, Surf. Sci. 437, 330 (1999)

NANOSTRUCTURED MATERIALS AS DRUG DELIVERY SYSTEMS

Jean-Marie Devoisselle, Syvie Bégu, Anne Aubert-Pouessel, Corine Tourné-Péteilh, Philippe Legrand, D. Tichit, Bruno Alonso, Lydie Viau, A. Vioux

Institut Charles Gerhardt Montpellier, UMR CNRS/UM2/ENSCM/UM1 5253
U.F.R. des Sciences Pharmaceutiques et Biologiques
15 ave Ch. Flahault, BP14491, 34093 Montpellier, France
jm.devoisselle@univ-montp1.fr

Nanotechnology represents a new field of research and includes a wide range of technologies and potential applications. One approach consists on creating new materials which are structured at the nanoscale using sol-gel chemistry. Such materials could be of different pore size or morphology. Nanostructured silicas such as Micelle-Templated Silicas (MTS) materials feature unique textural properties owing to their uniform distribution of mesopores with tunable sizes. Since 2002, we have developed a synthesis strategy to control the particle morphology of MTS at the micro- to millimeter scale. Concerning drug delivery systems, we have evaluated the ability of such mesoporous materials for hosting a non-steroidal anti-inflammatory drug (ibuprofen). Different procedures were evaluated: impregnation of calcined mesoporous materials[1], direct synthesis and drug grafting[2]. We show that it is possible to incorporate ibuprofen in MTS in a range compatible with poorly soluble drugs. The release depends on the way ibuprofen is incorporated. Fast release is observed for the “impregnation” and the “direct synthesis” methods that may indicate that ibuprofen is in a molecular state[3]. We have chosen a second direction that allows in fully investigating the potentialities of sol-gel, self-assembly and spray-drying processes in order to form directly new textured materials acting as DDS with tuneable properties. Spray-drying bears also the advantage of being a scalable process and reducing the number of steps. Furthermore we consider a one-pot synthesis in which organometallic oligomers, drug and surfactant molecules are mixed together in solution. During spray-drying of the solutions, these chemicals interact together, eventually phase-separate inside the droplets and form the final microspheres. Here, we particularly show how a simple tuning of the drug and the surfactant contents can lead to very different drug dispersions at the nanometre scale, and consequently to very different drug release profiles[4]. Finally, we proposed a novel approach to confine drugs in mesoporous silica materials. We first prepared a new ionic liquid ([BMIm][Ibu]) were the drug (Ibuprofenate) is the anion and used this new IL to prepare ionogels. Their silica walls could be functionalized to control the drug release[5].

Another example of nanostructured silica materials as DDS is given by the preparation and release property of hybrid lipid/silica materials. First, we have adapted a typical two-step room-temperature MTS (micelle-templated silica) preparation in which the colloidal solution of amphiphiles is replaced by small unilamellar liposomes[6]. The result is the formation of silica shell nanospheres with non-porous walls and a narrow size distribution. We show that kinetic releases of a hydrophilic fluorescent probes depend on the lipid composition of liposomes. The use of zwitterionic phospholipids (non toxic) as templates requires a modified approach since the liposome structure is sensitive to low pH, high ionic strength. The silica growth is directed by the receptiveness of the quaternary ammonium surface of the phospholipid to the silica. We have also advanced this original report in a number of ways. We have reduced the cluster-like particle aggregation into chain-like aggregates of particles by the use of PEGylated phospholipid. We extended the liposil's shell nature to include hydrophobic modifications. We showed the feasibility of the triggered release of the encapsulated content with two types of remote energy sources[7]. Finally, a new supra-organized hybrid material obtained in “green“ conditions via anionic exchange of self-assembled unilamellar anionic liposomes with the nitrate ions present in the interlayers of layered double hydroxides (LDH), is fully characterized[8]. This material presents original properties linked to the simultaneous presence of a phospholipid bilayer derived from liposomes, still used as vectors for lipophilic drugs, and LDH which protects the bilayer and brings about a pH-sensitivity. The exchange rate is controlled via the added amount of liposomes. TGA, XRD and TEM confirm the organisation of the trapped phospholipids as a bilayer. The presence of the latter allows the material to load lipophilic and neutral drugs which represent the largest fraction of those newly synthesized. Furthermore, in physiological conditions, preliminary tests show a sustained release of phospholipids (1.5% for 7 days and 6% for 14 days) while a fluorescent lipophilic drug-mimic reveals the reorganisation of the phospholipids into liposomes in the release medium. In the

field of biocompatible materials these new hybrid particles have a strong potential for the storage and sustained release of neutral or lipophilic drugs.

References:

[1] C. Charnay, S. Bégu, C. Tourne-Peteilh, L. Nicole, D.A. Lerner, J-M. Devoisselle., European Journal of Pharmaceutics and Biopharmaceutics, (2004) 57, 533-540.

[2] C. Tourné-Péteilh, D. Brunel, S. Bégu, B. Chiche, F. Fajula, D.A. Lerner, J.-M. Devoisselle New Journal of Chemistry (2003) 27, 1415 – 1418.

[3] T. Azais, T. Tourné-Péteilh, F. Aussenac, N. Baccile, C. Coelho, J-M Devoisselle, F. Babonneau, Chemistry of Materials (2006) 18, 6382-6390.

[4] M. Fatnassi, C. Tourné-Péteilh, T. Cacciaguerra, J-M. Devoisselle, B. Alonso, New. J. Chem (2010) 34, 607–610.

[5] L. Viau, C. Tourné-Péteilh, J-M. Devoisselle, A. Vioux. Chem. Comm., 2010, 46, 2, 228-230.

[6] S. Begu, A. Aubert-Pouessel, D.A. Lerner, C. Tourné-Péteilh, J-M Devoisselle. Journal of Controlled Release (2007) 118, 1, 1-6.

[7] Y. Steinberg, A. Schroeder, Y. Talmon, J. Schmidt, R.L. Khalfin, Y. Cohen, y, J-M. Devoisselle, S. Bégu, D. Avnir Langmuir (2007), 23(24), 12024-12031.

[8] S. Bégu, A. Aubert, R. Polexe, E. Leitmanova, D-A. Lerner, C. Tourné-Peteilh, J-M. Devoisselle, D. Tichit. Chem. Mater (2009) 21, 13, 2679–2687.

LAST ADVANCES IN SINGLE-MOLECULE ELECTRIC CONTACTS

Ismael Díez-Pérez, Josh Hihath, Thomas Hines, Zhihai Li, Nongjian Tao

Institute for Bioengineering of Catalonia, Baldiri Reixac 1-5, Barcelona 08028, Spain
Biodesign Institute at Arizona State University, 1001 S. McAllister Ave., Tempe, AZ85287, USA
idiezper@asu.edu, idiez@ibecbarcelona.eu

During the last decade, the first experimental demonstrations of the feasibility to build single-molecule electric contacts [1,2] have led to a huge revolution in the field of Molecular Electronics. The possibility to study charge transport through a single molecule bridged between two macroscopic metal beads has placed this field in an unbeatable position to directly address fundamental questions on the relation between the molecular structure and the charge transport behavior. For example, it has already been described the impact that the presence of certain chemical groups in the single-molecule contact, such as saturated linear chains [3], conjugated blocks [4], electron donor/acceptor groups [5] or redox centers, has in the dominating charge transport mechanism.

In this contribution, we describe our latest advances toward the fundamental understanding of the main parameters dominating the charge transport through organic scaffolds and we demonstrate how the chemical structure can be tailored to achieve a desired electron transport profile in the single-molecule device. In the first part, we will describe the last implemented technical methodologies to univocally identify when a single-molecule contact is formed between two metal electrodes. The methodologies are based on the introduction of small AC perturbations within the electrode-electrode gap separation and the corresponding AC current response detection in the frequency space [6,7]. Together with the AC methods, long pulling programs applied to the molecular contact are also performed at the end of the experiment as a method to evidence the single-molecule nature of the junction. After this technical description, two examples showing how to tailor the single-molecule electron transport through the molecular design will be presented. The first case presents one of the first examples of rectification behavior (diode effect) in a single-molecule device [8]. Here we demonstrate that it is possible to go from a perfectly symmetric to a highly rectifying charge transport behavior by introducing small chemical modifications within the molecular architecture (see Figure 1).

The second case explores the feasibility to design single-molecule field effect transistors (FET) by using a graphene-like molecular structure (coronene derivatives) through the exploitation of the previously introduced electrochemical gate [9] (see Figure 2) in order to modulate the conductance of the single-molecule contact and control the ON-OFF behavior as in conventional FET setups [10]. This last example opens up a bottom-up approach for the future design of functional FET based on graphene materials. The final part of this paper will describe another example of how to modulate the single-molecule conductance in this case by using a mechanical perturbation. This last presented device constitutes the first demonstration of single-molecule electromechanical effect [7].

References:

[1] M. A. Reed, C. Zhou, C. J. Muller, T. P. Burgin, J. M. Tour Science 278 (1997) 252.
[2] B. Q. Xu and NJ. Tao Science 301 (2003) 1221.
[3] X. Li, J. He, J. Hihath, B. Xu, S. M. Lindsay, NJ. Tao JACS 128 (2006) 2135.
[4] L. Venkataraman, J. Klare, C. Nuckols, M. S. Hybertsen, M. Steigerwald Nature 442 (2006) 904.
[5] L. Venkataraman, Y. S. Park, A. C. Whalley, C. Nuckolls, M. S. Hybertsen, M. Steigerwald Nano Letters 7 (2007) 502.
[6] J. Xia, I. Díez-Pérez, NJ Tao Nano Letters 8 (2008) 1960.
[7] I. Diez-Perez, T. Hines, J. Hihath, Z.-S. Wang, G. Zhou, K. Müllen, NJ Tao Nature Nanotechnology, accepted 2011.
[8] I. Diez-Perez, J. Hihath, Y. Lee, L. Yu, L. Adamska, M. A. Kozhushner, I. Oleynik, NJ Tao. Nature Chemistry 1 (2009) 635.
[9] B. Q. Xu, X. Y. Xiao, X. M. Yang, L. Zang, NJ Tao JACS 127 (2005) 2386.
[10] I. Diez-Perez, Z. Li, J. Hihath, J. Li, C. Zhang, X. Yang, L. Zang, Y. Dai, X. Feng, K. Müllen, NJ Tao Nature Communication 1 (2010) 31.

Figures:

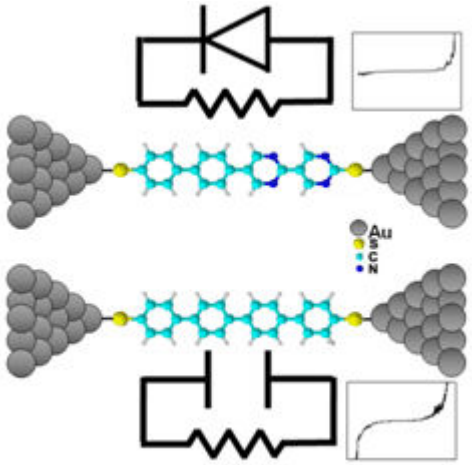

Figure 1: *Representation of two single-molecule devices with similar polyphenyl molecular blocks displaying symmetric (bottom) and diode (top) charge transport behaviors.*

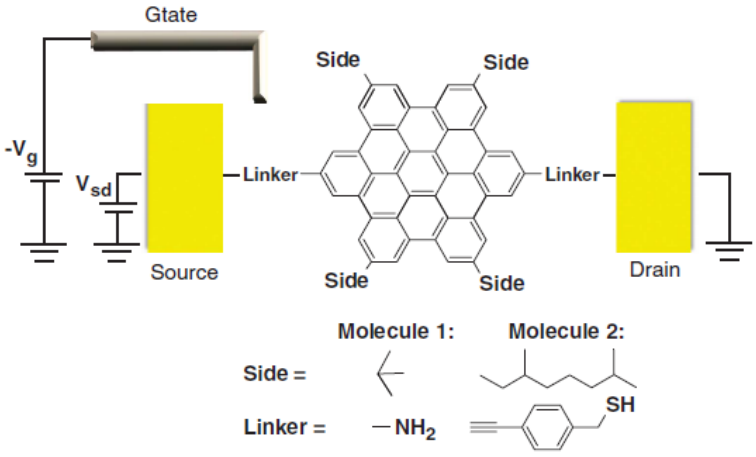

Figure 2: *Representation of a single-molecule FET built with coronene derivatives and gated with a reference electrode in an electrochemical configuration.*

AN O(N^3) IMPLEMENTATION OF HEDIN'S SCHEME FOR MOLECULES IN ORGANIC SEMI CONDUCTORS

D. Foerster[1], P. Koval[2] and D. Sanchez-Portal[2]

[1]CPMOH/LOMA, Bordeaux
[2]CFM/DIPC, San Sebastian
d.foerster@cpmoh.u-bordeaux1.fr

The improved scaling of our method with respect to most published methods is a step forward towards the goal of predicting, prior to their synthesis, the ionization energies and electron affinities of the large molecules that serve as constituents of organic semiconductors.

Here we focus on the principle of locality that previously lead to an efficient solution of the Petersilka-Gossmann-Gross equations of TDDFT and which gives rise to N^3 scaling with the number of atoms N in Hedin's approach for molecules.

For more details on our results, see the contribution by P. Koval on "O(N^3) GW" at the session on HPC.

References:

D. Foerster J. Chem. Phys. 128, 34108 (2008).
P. Koval, D. Foerster and O. Coulaud, J. Chem. Theory Comput. 6, 2654 (2010).
D. Foerster, P. Koval and D. Sanchez-Portal, arXiv:1101.2065v1, submitted to J.Chem.Phys.

NANOPARTICLES FOR TWO-PHOTON INTRACELLULAR THERMAL SENSING

Daniel Jaque [1*], Martinez Maestro[1], E. Martín Rodriguez[1], F. Sanz Rodriguez[2], M.C. Iglesias de la Cruz[2], A. Juarranz[2], F. Vetrone[3], R. Naccache[3], J. A. Capobianco[3] and **José García Solé**[1]

[1] Fluorescence Imaging Group, Departamento de Física de Materiales, C-IV, Universidad Autónoma de Madrid, C/Francisco Tomás y Valiente 7, 28049 Madrid, Spain,
[2] Departamento de Biología, Universidad Autónoma de Madrid, Madrid 28049, Spain
[3] Department of Chemistry and Biochemistry, Concordia University, 7141 Sherbrooke St. W., Montreal, QC H4B 1R6, Canada
daniel.jaque@uam.es

Thermal sensing at the micro and nano scales is one of the most challenging tasks that nanotechnology is nowadays facing. It is required to get a full understanding and characterization of photonic and electrical devices under real operation conditions where relevant local thermal loadings can take place as a consequence of either Joule dissipation or optical activation of non-radiative processes. In biological systems (such as tissues and individual cells) the exact knowledge of the local temperature is essential since it is known that temperature is one of the most important parameter determining the dynamics of the system. During the last years different approaches have been used to achieve thermal sensing with high spatial resolution while ensuring enough temperature sensitivity. Several techniques (such as thermal scanning and molecular fluorescence microscopies) have been already shown to satisfy both requisites simultaneously. Nevertheless, these techniques have limited applications in which, for example, three dimensional thermal imaging or in depth measurements is required.

Very recently a new approach to the thermal imaging at the nanoscale has come into sight. This is based on the incorporation of fluorescent nano-thermometers into the system to be thermally scanned. Fluorescent nano-thermometers are fluorescent nano-particles whose luminescence properties are strongly determined by the local temperature of the environment in which they are hosted. Any luminescent nano-particle whose luminescent properties (in terms of intensity, spectral position, spectral shape or decay time) are strongly dependent on temperature can be considered as a nano-thermometer. Nevertheless, the real application for thermal imaging and sensing in photonic, electrical and biological systems requires additional features such as possibility of multi-photon excitation (for high spatial resolution experiments), possibility of being dispersible in water (for easy incorporation into cells), good thermal stability and, finally, high fluorescence quantum efficiencies for high contrast imaging.

In this work the fluorescence properties of two-photon emitting nano-particles have been systematically investigated as a function of temperature in the 20-70 ºC range. We have focused our attention in two different types of two-photon emitting nano-particles: Semiconductor Quantum Dots and double doped Erbium and Ytterbium doped nano-crystals. From the obtained results the potential thermal sensitivity of these two types of nano-particles has been discussed and the mechanisms at the basis of this thermal sensitivity elucidated. We have concluded that in the case of rare earth doped nano-crystals, thermal sensitivity is based on temperature induced changes in the population of excited states. On the other hand, in the case of Semiconductor Quantum Dots, thermal sensitivity is caused by a complex competition between different mechanism including temperature induced changes in the energy gap of bulk material, thermal induced dilatation and changes in the confinement energy. Although complexes, all these process give the opportunity of improvement and tailoring of the potential thermal sensitivity.

We also include in this work experimental evidence of the potential application of these systems for real intracellular thermal sensing by optical methods. Figure 1 shows a simple experiment designed to test the ability of CdSe Quantum Dots for direct measuring in intracellular thermal loading induced in cancer cells by external air fluxes.

Figures:

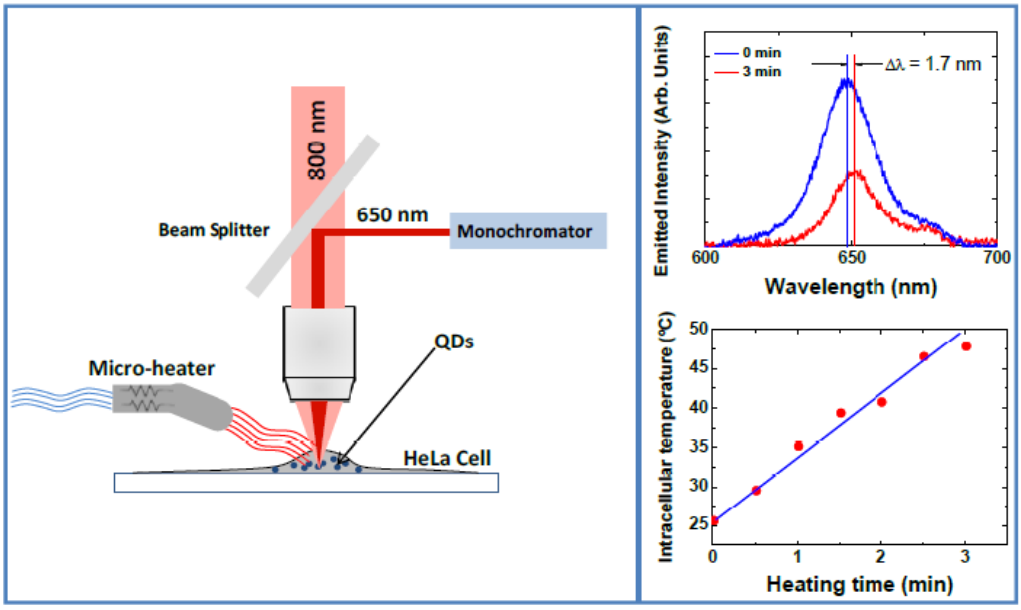

Figure 1: *Experimental set-up and experimental results on the intracellular thermal sensing using two-photon emitting QDs.*

SURVEYING MOLECULAR VIBRATIONS IN SINGLE MOLECULE NANOJUNCTIONS

A. Garcia-Lekue

Donostia International Physics Center (DIPC), Donostia, Spain

Charge transport through metal-molecule junctions is a major subject of study in a rapidly growing interdisciplinary research field. It deals with fundamental and applied aspects of science at the nanoscale aiming to control the electron conductance at the molecular level and the uprising of nanotechnology. One of the major results of this research is that the atomistic arrangement at the junction and the coupling between the molecule and the metal electrodes can significantly alter the electronic and structural properties of the molecule. It is therefore relevant to characterize the influence of the metal contact formation in the electron transport process through a single molecule.

With this aim, we have combined spectroscopic techniques based on scanning tunneling microscopy (STM) with first-principles calculations to achieve a precise characterization of the metal-molecule interaction during the formation of a nanocontact.[1] We use the inelastic tunneling spectroscopy (IETS) signal measured at various molecule-metal distances by approaching the tip of an STM to the CO molecule adsorbed on a Cu(111) metal surface. The vibration modes and inelastic transport have been modeled using density functional theory (DFT) combined with nonequilibrium Green's function methods (NEGF). Both the measured data and the calculations show characteristic shifts of the vibration modes. In particular, we observe a continuous but nonlinear blue shift of the frustrated rotation mode in tunneling with decreasing distance followed by an abrupt softening upon contact formation. This indicates that the presence of the metal electrode sensibly alters the structural and conductive properties of the junction even without the formation of a strong chemical bond.

We have shown that by combining high resolution IETS data and first-principles calculations it is possible to monitor the structural and electronic properties of a molecular nanocontact during its formation. As the tip of the STM can be more widely understood as the presence of any metallic electrode, we believe that these results have a general validity to the measurements of conductance through molecular junctions.

Finally, we report simulated vibrational spectra for CO using chemically functionalized STM tips. Our results indicate that functionalized tips can increase the resolving power of IETS and can yield inelastic signals not observed with a Cu-adatom tip. Such effects are originated by changes in the symmetry of the orbitals involved in the inelastic scattering, and reveal that single-molecule IETS can be optimized by selecting the appropriate tip orbital symmetry.[2]

References:

[1] L. Vitali, R. Ohmann, K. Kern, A. Garcia-Lekue, T. Frederiksen, D. Sánchez-Portal, A. Arnau, NanoLetters 10, 657 (2010).
[2] Garcia-Lekue, D. Sanchez-Portal, A. Arnau, and T. Frederiksen, manuscript in preparation.

SPIN CROSSOVER NANOMATERIALS: TOWARDS SENSOR APPLICATIONS

Illia Guralskyi, Carlos Quintero, Gabor Molnár, Lionel Salmon, Igor Fritsky, Azzedine Bousseksou

Laboratoire de Chimie de Coordination, 205, route de Narbonne, 31077 Toulouse, France
illia.guralskyi@lcc-toulouse.fr

The phenomenon of spin crossover between high-spin (HS) and low-spin (LS) states of $3d^4$-$3d^7$ transition metal ions represents an important area of coordination chemistry. Beside its interesting fundamental aspects, the potential applications of this phenomenon draw much attention but can not be readily exploited in bulk materials. Therefore, we have developed various methods for fabricating spin crossover nanoparticles using polymers[1] or reverse micelles[2] as nanoreactors. We will show their size-dependent spin crossover properties, their patterning using soft lithographic techniques[3] and applications of these novel materials. In particular, we will discuss different strategies for signal transduction in chemical and physical sensors based on spin crossover complexes (see figure for an example of fluorescent transduction)[4].

References:

[1] J. Larionova, L. Salmon, Y. Guari, A. Tokarev, K. Molvinger, G. Molnar and A. Bousseksou, Angew. Chem. Int. Ed., 47 (2008) 8236
[2] A. Tokarev, L. Salmon, Y. Guari, W. Nicolazzi, G. Molnár, A. Bousseksou, Chem. Commun., 46 (2010) 8011
[3] C. Thibault, G. Molnár, L. Salmon, A. Bousseksou, C. Vieu, Langmuir, 26 (2010) 1557
[4] L. Salmon, G. Molnár, D. Zitouni, C. Quintero, C. Bergaud, J.-C. Micheau, A. Bousseksou, J. Mat. Chem., 20 (2010) 5499

Figures:

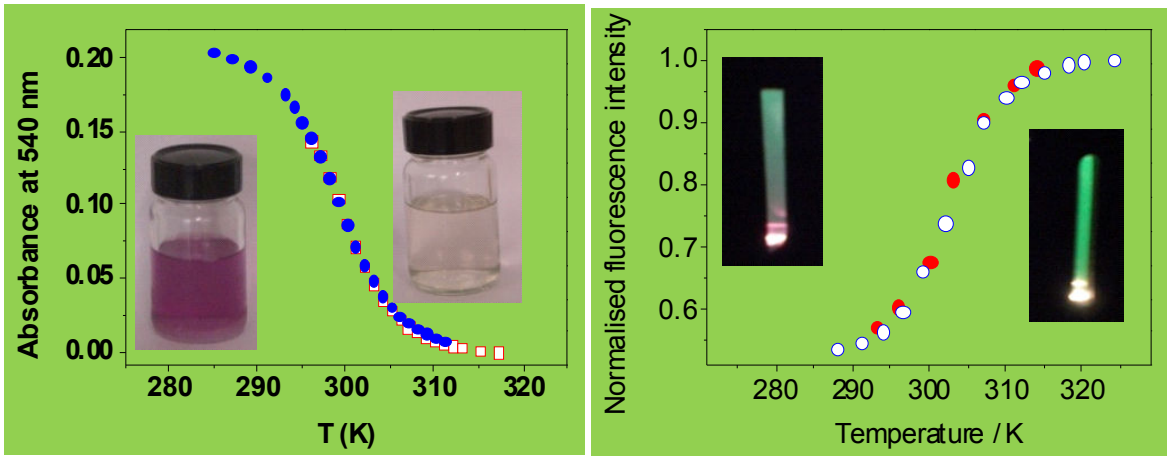

Figure 1: *(Left panel) Temperature dependence of the optical absorbance (recorded at 540 nm) of the $Fe(NH_2Trz)_3(OTs)_2$ spin crossover nanoparticles (3 nm) suspension in the heating (open symbols) and cooling (closed symbols) modes. The inserts show the photographs of the sample at 295 K (violet) and 320 K (transparent). (Right panel) Temperature dependence of the fluorescence intensity (recorded at 540 nm) of the nanoparticle system doped by Rhodamine-110. The inserts show the luminescence of the sample (at 0.001% doping level) under white light excitation at 295 K and 320 K.*

PROBING NANOSCALE SUPERCONDUCTIVITY IN ORGANIC MOLECULAR CHAINS

Abdou Hassanien

Nanosystem Research Institute,AIST, 1-1-1 Umezono, Tsukuba, Ibaraki 8568, Japan.
National Institute of Chemistry, Hajdrihova 19, SI-1001 Ljubljana, Slovenia
Abdou.Hassanien@aist.go.jp

The BSC theory has provided a general framework for understanding the microscopic origin of superconductivity in simple metals. With the emergence of new materials, especially high Tc and organic superconductors, clear deviations from the standard theory are reported. Several theories have been proposed to provide microscopic paring mechanisms and thereby elucidating the macroscopic properties for these unconventional superconductors.

In order to unravel details on the mechanism and test theories one needs to investigate the local nanoscale properties on clean systems. For this purpose we have synthesized high quality single crystals of $(BETS)_2GaCl_4$, where BETS is (ethylenedithio)tetraselenafulvalene, as source materials for engineering sub-monolayers and chain like structure on Ag(111) surface. In bulk $(BETS)_2GaCl_4$ has a superconducting transition temperature Tc of ~8 K and a two-dimensional layered structure that is reminiscent of the high-Tc cuprate superconductor.

We present low temperature scanning tunneling microscopy and spectroscopy to study directly the nanoscale electronic properties of $(BETS)_2GaCl_4$. We show that superconductivity still robust down to a single layer islands and chain like structures. A single chain of $(BETS)_2GaCl_4$ molecules displays a superconducting gap that increases exponentially with the length of the chain. Moreover, we show that a superconducting gap can still be detected for just four of $(BETS)_2GaCl_4$ molecules. Real-space spectroscopic images directly visualize the chains of BETS molecules as the origin of the superconductivity. These findings not only pave the way to study nanoscale superconductivity on other nanosystems, especially high Tc cuprates, but also to investigate paring mechanism versus structural parameters and molecular manipulations.

References:

[1] K. Clark, A. Hassanien, S. Khan, K.-F. Braun, H. Tanaka and S.-W. Hla, "Superconductivity in just four pairs of $(BETS)_2GaCl_4$ molecules", Nature Nanotechnology 5, (2010).261.

Figures:

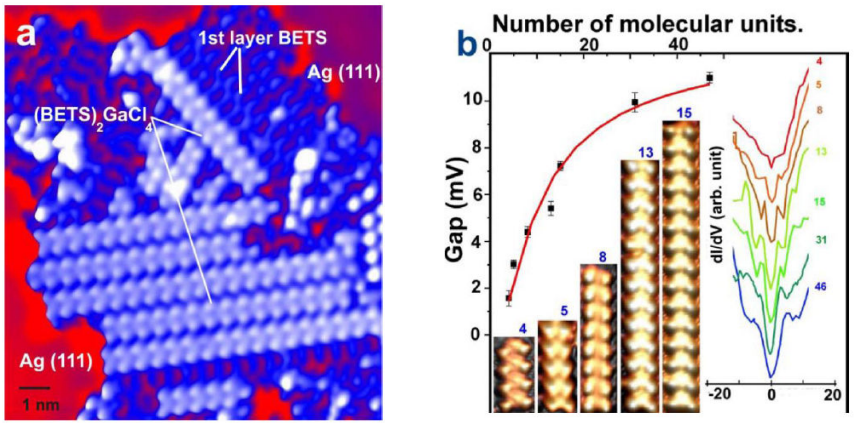

Figure 1: *Size dependent molecular superconductivity. a, An STM image revealing shorter molecular chains at the centre. Light blue are doubled stacked BETS while darker features are the first layer BETS, The superconducting gap as a function of molecular units. The inset shows the molecular chains with 4, 5, 8, 13, and 15 units. The right inset illustrates corresponding dI/dV curves that reveal superconducting gaps of these chains.*

ULTRATHIN PBS SHEETS BY TWO-DIMENSIONAL ORIENTED ATTACHMENT

Beatriz H. Juárez[1], C. Schliehe[2], C. Klinke[2], H. Weller[2]

[1]IMDEA Nanoscience, Fco. Tomás y Valiente 7. 28049. Cantoblanco, Madrid, Spain.
[2]University of Hamburg. Grindelallee 117. Hamburg, Germany
beatriz.hernandez@imdea.org

Nanostructured materials offer a huge range of possibilities for the development of new devices with fascinating optical, magnetic, or electronic properties. The synthesis of colloidal semiconductor nanoparticles has been vastly improved in the last decades. In this work, a novel procedure developed to organize dot-like semiconducting nanocrystals into 2D nano-sheets will be presented. By means of this procedure the nanoparticles initially covered by randomly oriented organic molecules (see illustration on the right) assemble like “lego” bricks to form small aggregates that evolve into crystalline sheets. During this process, the organic molecules densely pack and organize on the surface of the new crystal. This ordered arrangement of the organic molecules allows the formation of these two dimensional crystals.

The work shows the formation mechanism of two-dimensional crystalline structures, based on the interaction among nanocrystals with defined orientations and the self-assembly and packing of the organic molecules on their surface. The results have special relevance to understand and control the shape of colloidal nanostructures, key for the generation of advanced functional materials at the nanoscale. These ordered 2D structures with just 2 nm thicknesses have been integrated in photodetectors. The results may be relevant to generate more efficient devices.

References:

[1] Constanze Schliehe et al. Science, 329, 5991, 2010, 550-553

Figures:

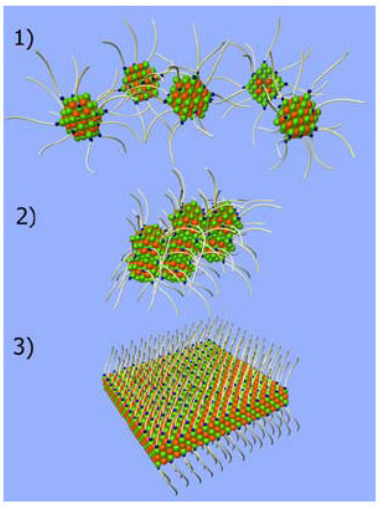

Figure 1: *Scheme of the fusion of nanocrystals to form 2D crystals in three steps: Initially, nanocrystals stabilized by organic molecules in solution (1) form small aggregates by fusing in certain crystallographic directions (2). These aggregates evolve to form the crystalline sheets (3). During this process, the organic molecules self-assemble and densely pack on both sides of the crystal.*

MAGNETIZATION REVERSAL OF UNIAXIAL CO FILMS WITH TUNABLE CRYSTALLOGRAPHIC ORDER

O. Idigoras, A. K. Suszka, P. Vavassori and A. Berger

CIC nanoGUNE Consolider, Tolosa Hiribidea 76, E-20018 Donostia-San Sebastian, Spain
oidigoras@nanogune.eu

It is well established that crystallographic order has a very pronounced relevance for the magnetic properties of materials due to the quantum mechanical spin-orbit coupling, which is responsible for magneto-crystalline anisotropy [1]. The control of magnetic properties and in particular the tuning of magneto-crystalline anisotropy is also essential for technological applications, such as hard disk drive media [2] or magnetic random access memories (MRAMs) [3]. However, most magnetic materials characterization studies have been focused either on nearly perfect crystallographic samples or highly disordered samples in the past, and there are only very few studies, in which the region in between perfect crystalline samples and disordered materials has been explored.

Here, we have studied the influence of crystallographic order onto the magnetization reversal process in granular Co films. In order to allow for a well-defined variation of the crystallographic order a reproducible processing sequence was developed that enables the continuous modification of epitaxial growth for (10$\underline{1}$0) Co films by partially interrupting the epitaxial growth sequence. Specifically, we used the epitaxial growth sequence Ag(11$\underline{0}$)/Cr(211)/Co(10$\underline{1}$0) onto HF-etched Si (110) substrates, which enables the fabrication of high-quality epitaxial Co-films with an in-plane easy axis of magnetization by means of ultra high vacuum (UHV) sputter deposition [4]. In order to disturb or interrupt the epitaxy in a well defined manner we have deposited an ultrathin SiO_2 film of the order of one monolayer thickness on top of the Si substrate prior to the Ag layer deposition. By using different deposition times for this Sioxide layer (t_{ox}), we managed to fabricate Co (10$\underline{1}$0) samples with different crystallographic order level.

Figure 1 shows an X-ray θ-2θ measurement for a fully epitaxial grown sample and a sample with t_{ox}=12s, corresponding to partial epitaxy interruption. While we only observe the Si (220), Ag (220), Cr (211), Co (10$\underline{1}$0) and Co (20$\underline{2}$0) peaks for the fully epitaxial sample, we find multiple Ag peaks that correspond to different crystallographic orientations for the sample with partial epitaxy interruption. Nonetheless, this sample still has a high degree of Ag (220) and Co (10$\underline{1}$0) texture, if one does a quantitative analysis of the X-ray data. The degree of Co (10$\underline{1}$0) texture decreases further in a systematic fashion as t_{ox} is increased.

We have studied the magnetization reversal process in these samples by means of macroscopically and microscopically magneto-optical Kerr effect measurements. Figure 2 shows single domain (SD) vs. multi domain (MD) magnetization state maps, determined from quantitative Kerr microscopy [5], for three samples with different degrees of disorder (fig. 2a t_{ox}=0 s, fig. 2b t_{ox}=12 s and fig. 2c t_{ox}=15 s) as a function of the applied field angle β with respect to the easy axis (EA) and the applied field strength. Here, the blue color indicates a single domain state while other colors reveal the existence of multi-domain structures. We find that while in crystallographically well ordered films no static domain states exist in the entire field size and orientation range, magnetization reversal by means of non-uniform intermediate stable or meta-stable states exists for partially epitaxial samples with sufficient inter-granular misalignment. We also observe that these non-uniform states are more common for intermediate field orientations in between the macroscopic EA and hard axis (HA) directions.

Furthermore, we also observed an anomaly in samples with partial crystallographic alignment, for which conventional HA behavior disappears. When the magnetic field is applied along the nominal HA in such samples, a frustrated magnetic state occurs, which arises from the competition between ferromagnetic exchange and the uniaxial anisotropies of misaligned adjacent grains. The existence of such a frustrated state is related to a non-uniform magnetization reversal in the nominal HA and produces considerably high values of remanent magnetization and coercive field (figs. 3 (b)), while only 2° away from the nominal HA, the magnetization reversal is dominated by coherent rotation, as it is expected for highly uniaxial samples along or near the HA (figs. 3 (a) and (c)). The anomaly has been theoretically explained by means of a two-grain coupled Stoner Wohlfarth model and has been corroborated experimentally by microscopic imaging.

We acknowledge funding from the ETORTEK Program, Project No. IE06-172, the Spanish Consolider-Ingenio 2010 Program, Project No. CSD2006-53 and the Basque Government fellowships No. BFI09.284.

References:

[1] D. Weller et al., Phys. Rev. Lett. 75, 3752 (1995)
[2] B. D. Terris and T. Thomson, J. Phys. D: Appl. Phys. 38, R199 (2005)
[3] A. Chung, J. Deen, J. S. Lee, et al., Nanotechnology 21, 412001 (2010)
[4] W. Yang, D. N. Lambeth, and D. E. Laughlin, J. Appl. Phys. 85, 4723 (1999)
[5] O. Idigoras, P. Vavassori, J. M. Porro, and A. Berger, J. Magn. Magn. Mater., L57-L60 (2010)

Figures:

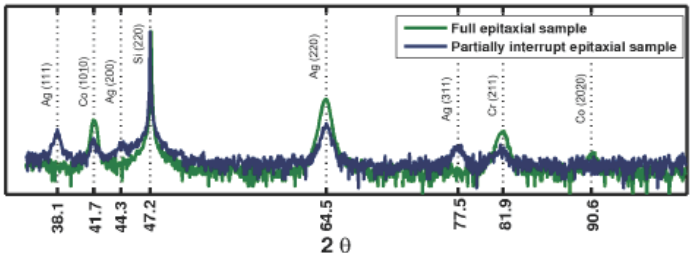

Figure 1: *X-ray diffraction spectra in θ-2θ configuration for a fully epitaxial sample tox=0s (green) and for a partially epitaxial sample with tox=12s (blue).*

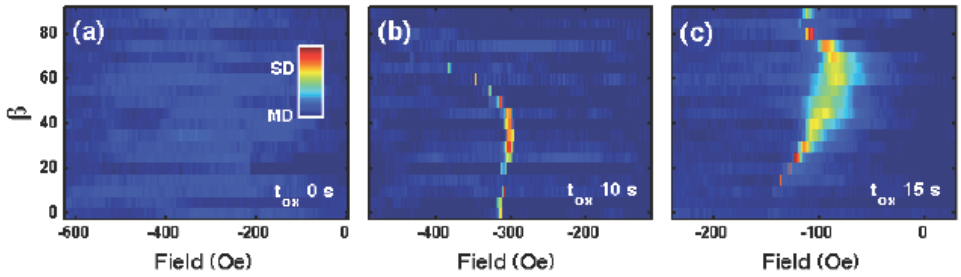

Figure 2: *Single-domain/multi-domain existence map for samples with different degrees of crystallographic order as a function of applied field angle and strength: (a) fully epitaxial (10$\underline{1}$0) Co sample, and partially epitaxial samples, generated by SiO_2 underlayer deposition of (b) 12s and (c) 15s duration.*

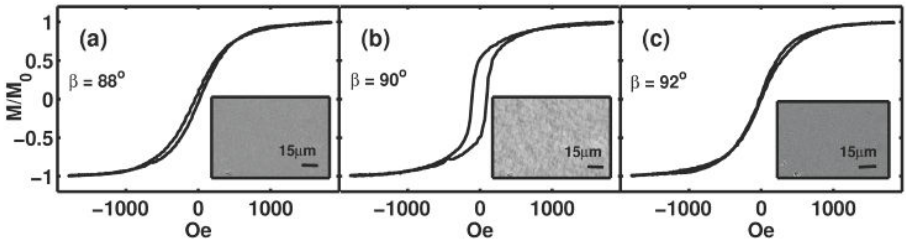

Figure 3: *Hysteresis loop for a partially epitaxial sample, grown with t_{ox}=12 s, for magnetic field orientations ±2° away from the HA (a) and (c) respectively, and along the nominal HA (b). The inset figures show the remanent magnetization states taken by Kerr microscopy after applying a magnetic field along the corresponding field angle.*

OPTICAL FORCES ON SMALL MAGNETODIELECTRIC PARTICLES IN THE FOCAL VOLUME OF HIGH NUMERICAL APERTURE MICROSCOPES

Ignacio Iglesias[1] and Juan José Sáenz[2,3]

[1]Dpto de Física, Universidad de Murcia, Campus de Espinardo (CIOyN Bldg.), E-30100, Murcia, Spain
[2]Dpto de Física de la Materia Condensada, Universidad Autónoma de Madrid, E-28049 Madrid, Spain
[3]Donostia International Physics Center (DIPC), Paseo Manuel Lardizabal 4, 20018 Donostia-San Sebastian, Spain
iic@um.es

A small dielectric particle experiences an optical field gradient and scattering forces caused by the electric-dipolar response. The scattering forces can be modeled as radiation pressure and a nonconservative force term that emerges from the spin curl [1]. In the focal region field generated by a microscope objective, the curl term is a fundamental contribution to the total force when using high numerical apertures [2]. Its presence explains the asymmetry of the trapping potential, which, for linear polarization, has been observed using focused beams (see Fig.1). Additionally, when other polarization structures in the microscope pupil plane are considered, the curl term becomes fundamental for explaining the force field the particle experiences even for moderate numerical apertures.

Recently it has been shown [3] that there are additional force terms when magnetodielectric particles are considered. These correspond to the magnetic-dipolar response, a counterpart to the aforementioned forces, together with additional components emerging from the electric-magnetic dipolar interaction. These new forces should also apply to pure dielectric particles like submicron silicon spheres which present strong magnetic and electric dipolar response in the near infrared [4,5].

Centered on these particles, this presentation will show the characteristics of the force field in the important particular case of tight focused beams generated by microscope objectives, which are frequently used in optical trapping and manipulation experiments.

References:

[1] S. Albaladejo, M. I. Marques, M. Laroche, and J. J. Saenz, "Scattering Forces from the Curl of the Spin Angular Momentum of a Light Field," Phys. Rev. Lett. 102, 113602-113604 (2009).
[2] I. Iglesias and J. J. Saenz, "Non conservative scattering forces in the focal volume of high numerical aperture microscope objectives," Opt. Comm. (in press)(2010).
[3] M. Nieto-Vesperinas, J. J. Sáenz, R. Gómez-Medina, and L. Chantada, "Optical forces on small magnetodielectric particles," Opt. Express 18, 11428-11443 (2010).
[4] A. García-Etxarri, R. Gómez-Medina, L. S. Froufe-Perez, C. Lopez, L. Chantada, F. Scheffold, J. Aizpurua, M. Nieto- Vesperinas, and J. J. Saenz, "Strong magnetic response of silicon nanoparticles in the infrared," ArXiv:1005.5446v1 (submitted 2010).
[5] M Nieto-Vesperinas, R. Gómez-Medina, and J.J. Sáenz, "Angle-suppressed scattering and optical forces on submicrometer dielectric particles," J. Opt. Soc. A 2011 28, 54-60 (2011).

Figures:

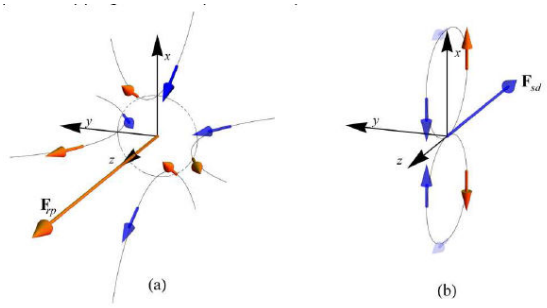

Figure 1: *Scattering forces that a small dielectric particle can experience in the focal region of a high numerical aperture microscope objective. In panel (a) the radiation pressure, in panel (b) the force of the curl term for a linear polarized light beam along the x-axis.*

MOLECULE LOGIC GATE OR SURFACE ATOMIC SCALE CIRCUITS

C. Joachim

Nanoscience Group & MANA Satellite
CEMES-CNRS Toulouse, France
ICT/FET AtMol
VIP Atom Tech, IMRE Singapore

At the atomic scale, there are 2 ways of implementing a complex logic gate: atom by atom at the surface of a material or in a molecule also interconnected at the surface of a material. Quantum designs are leading to gates with a large calculating power and a short calculation time as compared to a classical design. In a quantum design, the complexity increase is based on the manipulation of states in a dual space with no correlation with the expansion in space of the final gate. In a classical design, it is based on the accumulation in space of independent devices following for example Shannon like design rules. We will compare classical and quantum design from the point of view of their intrinsic performances but also from a more practical point of view: how a quantum design resists the interconnection when constructing the calculator.

QUANTUM HALL EFFECT IN EPITAXIAL GRAPHENE ON OFF-AXIS (000-1) SIC

N. Camara [1,2], **B. Jouault[2]**, A. Caboni[1], B. Jabakhanji[2], W. Desrat[2], E. Pausas[1], C. Consejo[2], N. Mestres[3], P. Godignon[1] and J. Camassel[2]

[1]CNM-IMB-CSIC, Campus UAB, Bellaterra, 08193 Barcelona, Spain
[2]GES, UMR 5650, Université Montpellier 2/CNRS, 34095 Montpellier Cedex 5, France
[3]ICMAB-CSIC, Campus UAB, Bellaterra, 08193 Barcelona, Spain

In this presentation, we will discuss on different methods we have used in order to obtain good epitaxial graphene monolayers grown on SiC. Then, we will focus on one of the method, which gives promising results: using high temperature annealing conditions with a graphite cap covering the C-face of an 8° off-axis SiC sample, large and homogeneous single epitaxial graphene layers can be grown. Raman spectroscopy shows evidence of the almost free-standing character of these monolayer graphene sheets. Magnetotransport measurements confirm these results. We find moderate p-type dopings, high carrier mobilities, and half integer quantum Hall effect typical of high quality graphene samples. This opens the way to a fully compatible integration of graphene with SiC devices on wafers that constitute the standard in today's SiC industry. This is also promising for quantum metrology.

References:

[1] N. Camara et al., Applied Physics Letters 97, 093107 (2010).

QUANTUM OPTO-ELECTRONICS IN SEMICONDUCTOR NANOWIRES

Leo Kouwenhoven

Kavli Institute of NanoScience, Delft University of Technology,
POB 5046, 2600GA Delft, The Netherlands

We are experimentalists studying quantum phenomena in nanostructures. By carefully shaping the nanostructures and choosing optimal material properties we design the system in such a way that we obtain desirable electronic and optical properties, i.e. quantum engineering. Particularly, the quantum phenomena of superposition and entanglement are interesting to control at the level of individual electrons and photons. Applications of this control are foreseen in the field of quantum information science. In this field superposition and entanglement are used for encoding information in quantum mechanical bits; the qubits.

Various systems are being investigated for realizing quantum hardware. Our favourite systems consists of nanowires (~40 nm in diameter and micrometers long) made out of various semiconducting materials, such as InAs, InSb, Si, etc. See the figure for nanowire examples.

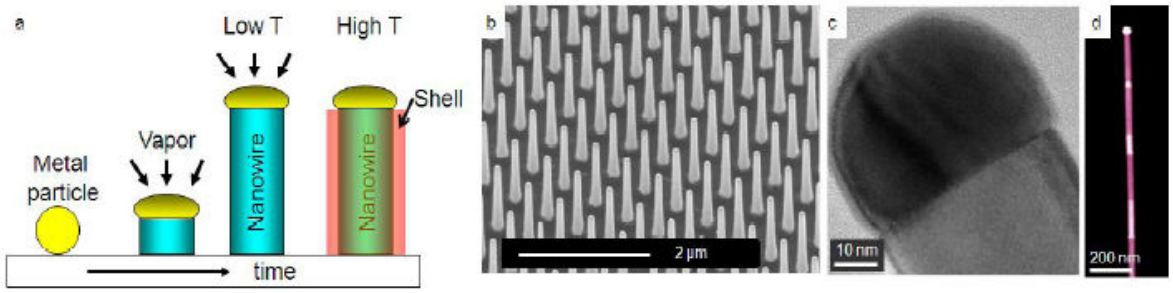

Figure 1: *a) Illustration of the growth mechanism of nanowires. The Au particle catalyses the nanowire growth. After axial growth, radial growth can be initiated covering the wire with a shell of different material. b) SEM image of an array of nanowires grown from a pattern of Au particles. c) TEM image of a nanowire with the Au-particle on top. d) dark field TEM image of a GaP-GaAs heterostructured nanowire.*

For the quantum transport studies we fabricate electronic devices in such a way that we can trap individual electrons. These electrostatic traps, called quantum dots, are highly stable and flexible such we can deplete all mobile electrons except for the last one. We then study the spin properties of this last electron. The spin-up or spin-down states are our qubit states, so quantum control over the spin states provides the qubit control. See figure below.

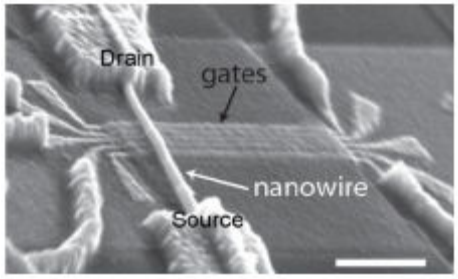

Figure 2: *An InAs nanowire crossing 5 gates (horizontal strips made of Au) with electrical source and drain contacts. This device allows to define two quantum dots each containing one electron. The device has been used to operate qubits based on the spin-orbit interaction in InAs.*

For optical studies we incorporate different materials in the nanowire. For instance in the first figure the GaP sections are optically inactive, whereas the GaAs sections show luminescence. When the GaAs section are made small enough, the optical transitions are determined by the quantum confined states. Such quantum optical transition we have investigated in particular in InAsP quantum dots. In these experiments we have shown that we can control the spin of the electron and holes that determine the polarization of the out coming light. This light, importantly, is demonstrated to be a one-by-one emission of individual photons, each photon polarization determined by the spin of the electron and hole.

We are currently pushing two new directions. First of all we wish to convert electron spin superpositions into photon polarization superpositions. This would demonstrate a transfer of the quantum state from an electron-particle to a photon-particle. Quantum state transfer is important for quantum information.

The second new direction is a hunt for a new particle: Majorana Fermion. In solid state systems one can not only engineer a quantum state, one may also be able to engineer particles. A Majorana Fermion is a fundamental particle but never observed. Now theoretical schemes exist that propose using semiconductor nanowires with strong spin-orbit interaction in order to create states that accommodate Majorana Fermions.

References:

[1] Spin–orbit qubit in a semiconductor nanowire, S. Nadj-Perge, S.M. Frolov, E.P.A.M. Bakkes, L.P. Kouwenhoven, Nature 468, 1084 (2010)

[2] Selective excitation and detection of spin states in a single nanowire quantum dot, M.H.M. van Weert, N. Akopian, U. Perinetti, M.P. van Kouwen, R.E. Algra, M.A. Verheijen, E.P.A.M. Bakkers, L.P. Kouwenhoven and V. Zwiller Nano Letters 9, 1989 (2009)

NANOSENSORS FOR STRUCTURAL MONITORING IN CIVIL ENGINEERING: NEW INSIGHT ON PROMISING CARBON NANOTUBES DEVICES

B. Lebental[1], E. Norman[3], L. Gorintin[4], P. Renaux[2], P. Bondavalli[4], C. S. Cojocaru[3] and A. Ghis[2]

[1]Université Paris-EST, IFSTTAR, Paris, 75015, France
[2]CEA-LETI, Minatec Campus, Grenoble, 38000, France
[3]LPICM, Ecole Polytechnique, Palaiseau, 91128, France
[4]Nanocarb Laboratory, Thales Research and Technology, Palaiseau, 91767, France
berengere.lebental@ifsttar.fr

In recent years, requirements in terms of service-life of civil engineering structures have become more and more stringent, so that the focus of designers and owners is now set on structural durability. Foreseeing structural failures and repairing damaged structures at an early stage has become a major stake. This approach calls for an accurate knowledge of the state of the structure at any point in its lifetime. This is the incentive for the world-wide development of various *in-situ* monitoring techniques for structural materials. However, by measuring global structural quantities only, the existing monitoring techniques provide only indirect information on the structural health of the structure.

To this day, no existing sensor features the resolution required to investigate in-situ structural materials at the micro- and nanoscale. This is a major lack, as micro and nanoscale features play a significant role in the durability of cementitious materials. From this perspective, IFSTTAR working with CEA-LETI and LPICM has set itself the long-term goal to devise innovative nanoscale structural health monitoring solutions based on nanosensors. Two types of single-walled carbon nanotubes (SWNT) devices are currently being studied with highly promising results: ultrasonic nanotransducers for microporosity assessment [1] and field-effect transistors for humidity monitoring [2].

The SWNT-based ultrasonic nanotransducer developed at the CEA-LETI consists in a metallic membrane of aligned nanotubes suspended above an actuation electrode (fig. 1). It vibrates by capacitive effect upon application of a varying voltage on the actuation electrode. Devices were fabricated by SWNT dielectrophoresis, e-beam patterning of anchoring electrodes and HF wet etching release (fig. 2) [3]. Thanks to a breakthrough laser vibrometry experiment, we observed up-to-5 nm amplitude vibrations of the SWNT membrane in air at ultrasonic (3.7 MHz) frequencies (fig. 3).

These high amplitudes of vibration is explained by the very low thickness of the membrane (fig. 4), obtained as a result of an extensive parametric study of SWNT dielectrophoresis. Our detailed numerical model shows that low membrane thickness is essential to the proposed sensing application. The model also indicates that the proposed devices embedded in a cementitious material could determine the volume and content of the microporosity in their vicinity [1]. Such microscale information would be invaluable in the evaluation of structural durability [4].

Structural durability specialists also know that not only size and content, but also humidity and chemical compositions are important for durability assessment [5]. With LPICM, we are focusing on relative humidity measurements based on field-effect transistors devices made with low density singlewalled carbon-nanotubes networks (fig. 5). The CNTFET devices were fabricated on a silicon substrate with silicon oxide layer. A conventional photolithographic process was used to create the electrodes. Mostly semiconducting CNTs were sprayed to form the gate channel [6].

Although the sensitivity of such devices to water vapor has been very often considered a drawback [7], our electrical characterizations (fig. 6) suggest that it could be exploited as a robust, high sensitivity means to probe high relative humidity environment (>60 %) such as concrete. The sensitivity of the devices to water vapor appears even stronger than that of other gases. It might be due to the strong polar nature of water and its affinity to both the metallic and dielectric parts of the CNTFET. This interpretation could lead us to various original device optimizations to improve the sensing features of the CNTFET devices.

With their very promising outputs, these two studies open up the path toward in-situ morphology and composition monitoring of the microporosity of cementitious materials by nanosensors. This

nanosensors-based microscale knowledge is the key to detect and prevent degradations of cementbased structures. As such, it will significantly contribute to an improved sustainability in civil engineering.

References:

[1] B. Lebental et al., Eur. J. Env. Civil. Eng. 2011, accepted
[2] P. Bondavalli et al., Sensors and Actuators B: Chemical, 140(1):304-318, 2009
[3] B. Lebental, PhD Thesis, 2010, University Paris-Est
[4] O. Coussy and S. Brisard, Journal of Mechanics of Materials and Structures, 2009, 4, 263–279
[5] O. Coussy, and P. J. M. Monteiro, Cement and Concrete Research, 2008, 38, 40-48
[6] P. Na et al., Appl. Phys. Lett. 87 (2005) 093101

Figures:

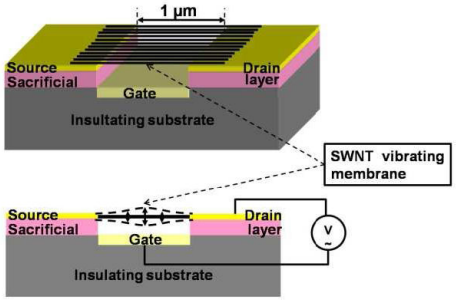

Figure 1: *Schematic view of SWNT-based capacitive ultrasonic nanotransducer*

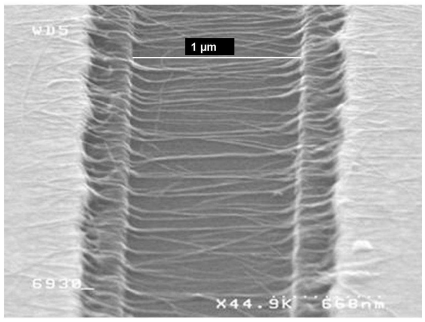

Figure 2: *SEM picture of a thin membrane of aligned SWNT obtained by AC dielectrohoresis*

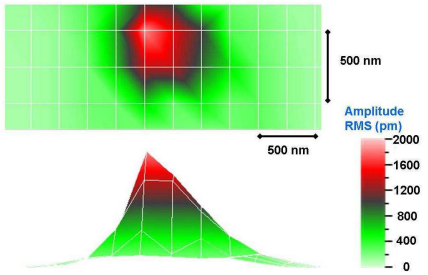

Figure 3: *Topview and sideview of the vibration amplitudes of a 2 µm-large SWNT membrane at 3.7 MHz, as measured by scanning laser vibrometry. Peak to peak amplitude of vibration is 5 nm.*

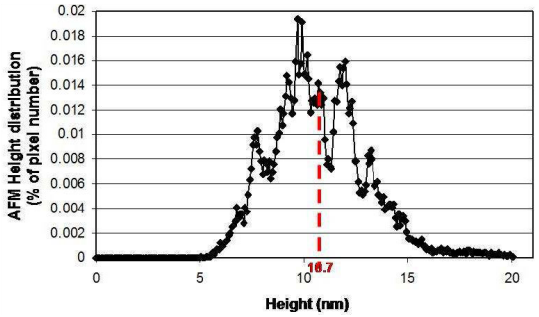

Figure 4: *AFM measured height distribution of a SWNT based membrane before suspension. Membrane thickness is 10.7 nm.*

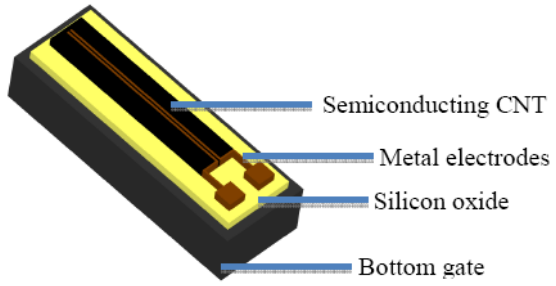

Figure 5: *Schematic view of a field-effect transistor using a low density SWNT network as channel material.*

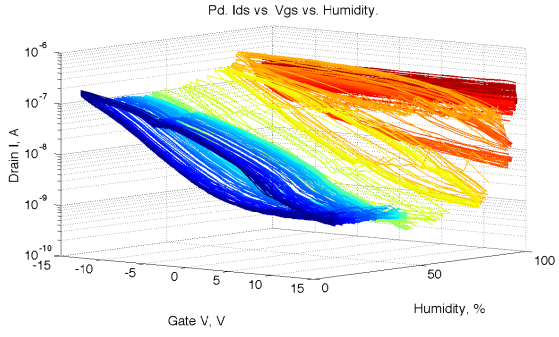

Figure 6: *IV characteristics of a CNTFET device with Pt electrodes: Vds=3V; dual sweep of Vgs from -15 V to +15 V*

CARBON NANOTUBE PHOTOCATHODES FOR OPTICALLY DRIVEN MULTIPLE X-RAY SOURCES

P. Legagneux[1], P. Ponard[2], L. Gangloff[1], S. Xavier[1], C. Bourat[2], J. Martinez[2], C.S. Cojocaru[1], A. Gohier[1], JP Mazellier[1], JP Schnell[1], D. Pribat[1], K.B.K. Teo[3]

[1]Nanocarb, Thales-Ecole Polytechnique, Palaiseau, France
[2]Thales Electron Devices, Thonon, France
[3]Aixtron, Cambridge, UK
Pierre.legagneux@thalesgroup.com

We have demonstrated the first optically driven X-ray source based on carbon nanotube (CNT) photocathodes. It is a compact dual X-ray source and the two sources are accurately and independently controlled with two laser diodes illuminating the photocathodes. Thanks to the emission stability, high quality images have been obtained. This dual source provides two images from two different viewing angles. This concept can be easily extended to multiple X-ray sources. Associated with linear or 2D X-ray detectors, low cost, compact/mobile, efficient and stationary (gantry free) tomosynthesis scanners could be realized. Such systems which provide 3D imaging can be used for security applications, nondestructive inspection in the industry and for medical applications. The innovation is the use of CNT photocathodes [1]. X-ray sources based on these photocathodes exhibit the following features: galvanic insulation for current control, fast switching and accurate control of X-ray emission.

The CNT photocathode is an array of vertically aligned multiwalled CNTs (electron emitters) associated with individual p-i-n photodiodes. These photodiodes act as optically-driven current sources. The emitted current varies linearly with the optical power delivered by the laser diode located under the photocathode.

Figure 1 shows a schematic description and SEM pictures of the fabricated photocathodes which are based on silicon photodiodes. CNTs are grown on n+ doped areas defined by ion implantation in a 5 µm thick intrinsic layer. The p+ doped silicon wafer is thinned to obtain a 7 µm thick membrane and to enable backside illumination of the photocathode. In order to demonstrate the proof of concept of this new system, we have fabricated a dual X-ray source based on two CNT photocathodes (see figures 2-4). The distance between the two sources is 10 cm. Due to the galvanic insulation (optical control), we can use a simple diode configuration with a high voltage applied to the photocathode and with a grounded anode. Compared to the power supply used in a conventional X-ray tube, no high voltage filament transformer is required. Thus our high voltage power supply is compact (see Figure 4). Being grounded, the anode is a tungsten film directly deposited on the X-ray window. The anode cooling is then simply performed by air convection. To obtain X-ray images, we have used a 2D X-ray detector and positioned different objects between the source and the detector. With this dual source, 2 views in parallel are obtained (see Figure 5). Figure 6 shows an image of an animal obtained with one single CNT photocathode.

This work was funded by the ANR project SPIDERS. Through the ANR project NANOSCANNER, we are currently studying the fabrication of CNT photocathodes based on low temperature grown GaAs photoswitches that should exhibit very large ON/OFF ratio (a few hundreds).

References:

[1] L. Hudanski, E. Minoux, L. Gangloff, K.B.K. Teo, J.-P. Schnell, S. Xavier, W.I. Milne, D. Pribat, J. Robertson, P. Legagneux, “Carbon nanotube based photocathode”, Nanotechnology 19 105201 (2008).

Figures:

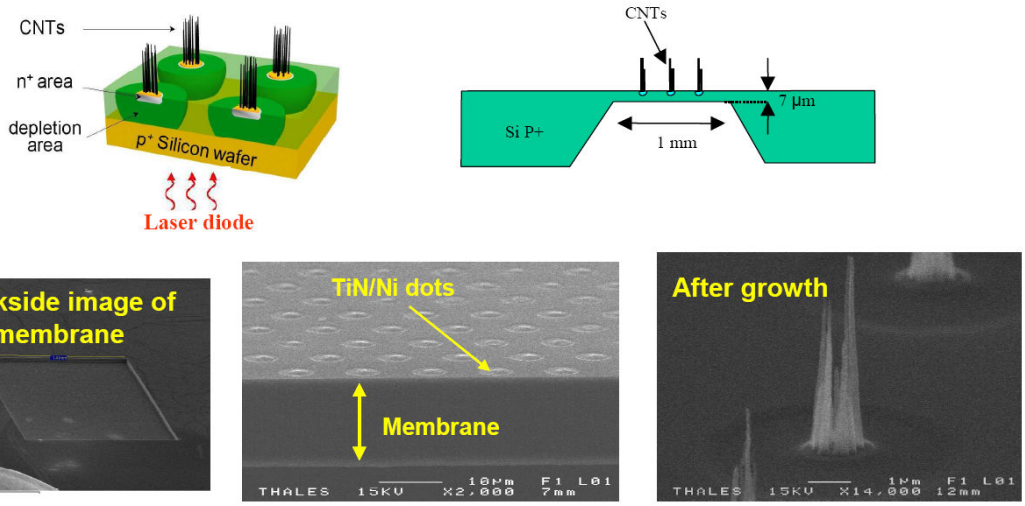

Figure 1: *Schematic description and SEM pictures of the CNT photocathode. The photocathode uses multiwalled CNTs as electron emitters and silicon p-i-n photodiodes to control the emission. CNTs are grown on n+ doped areas defined by ion implantation in a 5 µm thick intrinsic layer. The p+ doped silicon wafer is thinned to obtain a 7 µm thick membrane. This enables backside illumination of the photocathode.*

Figure 2: *Picture showing the two "satellites" holding the CNT photocathodes. The backside of the upper left photocathode is illuminated.*

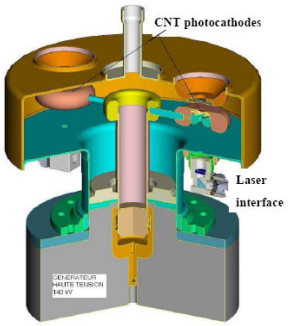

Figure 3: *Schematic description of the optically driven dual X-ray source*

Figure 4: *Picture of the dual Xray source associated with the power supply.*

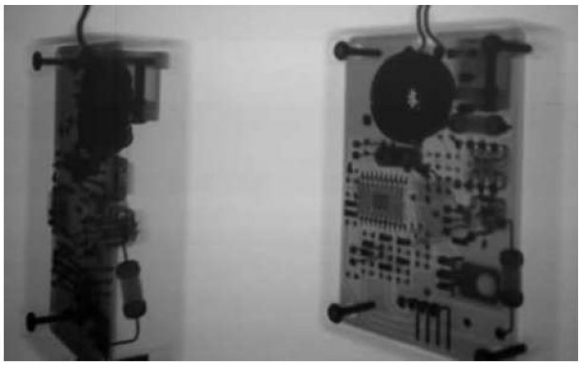

Figure 5: *Images of a printed circuit board obtained on the 2D X-ray detector with the dual source (2 views in parallel)*

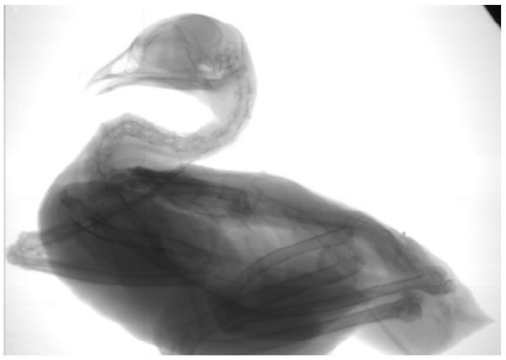

Figure 6: *Image of a bird realised with a single CNT source.*

CHARGE INJECTION AND TRANSPORT IN NANOWIRES

François Léonard

Sandia National Laboratories, Livermore, CA, USA
fleonar@sandia.gov

Semiconductor nanowires show promise in electronic, optoelectronic, and sensing devices. To realize this promise, a fundamental understanding of charge injection and electronic transport in these novel nanomaterials is necessary. In this presentation, I will discuss recent work that couples experiment and theory to address this topic. For example, in GaN and InAs nanowires, we achieve efficient charge injection and find that space-charge-limited currents are unusually strong [1,2]. In contrast, charge transport across individual Au-nanoparticle/Ge-nanowire interfaces is injection-limited, and surprisingly, the conductance increases with decreasing nanowire diameter due to a dominance of electron-hole recombination [3]. Furthermore, we find that transport in GaAs nanowires is governed by charge traps, which can be activated to reveal the nature of the charge injection at the contacts [4]. More generally, our results indicate that a broad range of electronic transport regimes can be observed in semiconducting nanowires depending on the particular material system and growth process.

References:

[1] AA Talin, F Léonard, B Swartzentruber, X Wang, S Hersee. Physical Review Letters 101 (2008) 076802.
[2] A M Katzenmeyer, F Léonard, AA Talin, ME Toimil-Molares, JG Cederberg, JY Huang, and J Lensch-Falk. IEEE Transactions in Nanotechnology 10 (2011) 92.
[3] F Léonard, AA Talin, B Swartzentruber, T Picraux. Physical Review Letters 102 (2009)106805.
[4] AA Katzenmeyer, F Léonard, AA Talin, P-S Wong, and DL Huffaker. Nano Letters 10 (2010) 4935.

Figures:

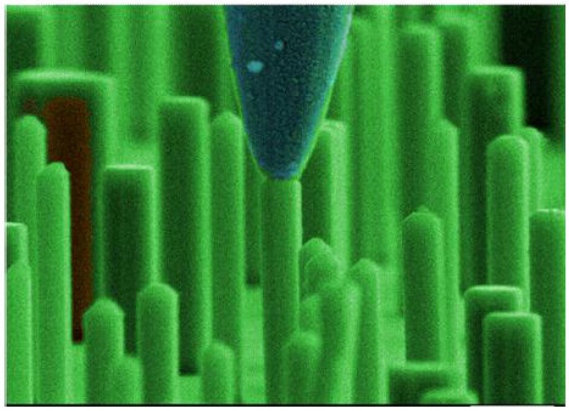

Figure 1: *A conducting tip retrofitted inside of a scanning electron microscope measures the electronic properties of individual nanowires.*

ARTIFICIAL SPIN ICE

J. P. Morgan[1], A. Stein[2], J. Akerman[1,3], C. Sanchez-Hanke[4], D. A. Arena[4], C. J. Kinane[5], R. Fan[5], S. Langridge[5], and **C. H. Marrows**[1]

[1]School of Physics & Astronomy, University of Leeds, Leeds LS2 9JT, United Kingdom
[2]Center for Functional Nanomaterials, Brookhaven National Laboratory, Upton, NY 11973, USA
[3]Instituto de Sistemas Optoelectrónicos y Microtecnología (ISOM), Universidad Politécnica de Madrid, Avda. Complutense s/n, 28040 Madrid, Spain
[4]National Synchrotron Light Source, Brookhaven National Laboratory, Upton, NY 11972m USA
[5]ISIS, STFC Rutherford Appleton Laboratory, Harwell Science and Innovation Campus, Didcot, Oxon. OX11 0QX, United Kingdom

Spin ices are rare earth pyrochlores where the crystal geometry leads to frustration of the rare earth moments [1], which meet at tetrahedra in the lattice. Like water ice, they violate the third law of thermodynamics, and have been extensively studied by neutron scattering. Recently it has been realised that excitations of this system can be described as deconfined emergent monopoles and associated Dirac strings [2]. Nanotechnology allows many of the essential features of this physical system can be reproduced in arrays of patterned nanomagnets where moments meet at the vertices of a square grid [3]. This approach offers the opportunity to continuously tune the various parameters controlling the magnetic microstate, and also to inspect that microstate using advanced magnetic microscopy [4,5]. A significant difference with the naturally occurring spin-ices is that the change in symmetry gives rise to a true long-range ordered ground state, although the frustrated interactions in these athermal systems mean that its observation is extremely difficult [6].

Here I will describe our recent work on such a system, an array of 250 nm × 80 nm Permalloy islands in the square ice geometry (shown in Figure 1), including the achievement of a thermalised ground state during fabrication and the observation of the effects of fractionalised monopoles on excitations out of it (shown in Figure 2) [7], and athermal achievement of the ground state using a suitable field protocol, both observed using magnetic force microscopy. I will also describe some preliminary data from soft x-ray scattering measurements, the effects of dc field reversal, and also the application of an effective temperature formalism [8] to the frozen microstates we observe.

This work was supported financially by EPSRC and the STFC Centre for Materials Physics and Chemistry. Parts of this research were carried out at the Center for Functional Nanomaterials and at the National Synchrotron Light Source, Brookhaven National Laboratory, which are supported by the U.S. Department of Energy, Office of Basic Energy Sciences, under Contract No. DE-AC02-98CH10886.

References:

[1] S. T. Bramwell and M. J. P. Gingras, Science 294, 1495 (2001).
[2] C. Castelnovo, R. Moessner, and S. L. Sondhi, Nature 451, 42 (2008).
[3] R. F. Wang et al., Nature 439, 303 (2006).
[4] S. Ladak et al., Nature Physics 6, 359 (2010).
[5] E. Mengotti et al., Nature Physics 7, 69 (2011).
[6] X. Ke et al., Phys. Rev. Lett. 101, 037205 (2008).
[7] J. P. Morgan, A. Stein, S. Langridge, and C. H. Marrows, Nature Physics 7, 75 (2011).
[8] C. Nisoli et al., Phys. Rev. Lett. 105, 047205 (2010).

Figures:

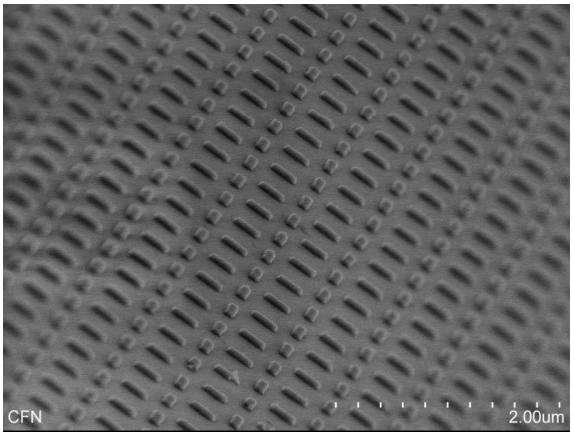

Figure 1: *Scanning electron micrograph of a array of Permalloy nanomagnets, prepared using electron beam lithography, that form a frustrated square ice lattice.*

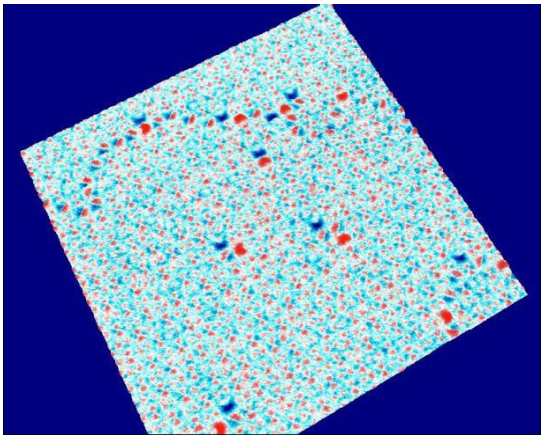

Figure 2: *Rendering of a magnetic force micrograph showing the smeared magnetic charge density: monopole defects in the periodic ground state are clearly visible.*

SELECTIVE LUMINESCENCE SWITCHING IN ENTANGLED METAL-ORGANIC FRAMEWORKS BY INCLUSION OF AROMATIC GUESTS. MOLECULAR SENSOR FOR SUBSTITUTED-BENZENES

Virginia Martínez-Martínez[1], Yohei Takashima[2,3], Shuhei Furukawa[2,4], Susumi Kitagawa[2,3,4] and Iñigo López Arbeloa[1].

[1]Dpto de Química Física, Universidad del País Vasco UPV-EHU, Apdo. 644, 48080-Bilbao, Spain
[2]ERATO Kitagawa Integrated Pores Project, Japan Science and Technology Agency (JST), Kyoto Research Park Bldg#3, Shimogyo-ku, Kyoto 600-8815, Japan
[3]Deparment of Synthetic Chemistry and Biological Chemistry, Graduate School of Engineering, Kyoto University, Katsura, Nishikyo-ku, Kyoto 615-8510, Japan
[4]Inst. for Integrated Cell-Material Sciences, Kyoto Univ., Yoshida, Sakyo-ku, Kyoto 615-8510, Japan
virginia.martinez@ehu.es

Porous coordination polymers (PCPs) or metal–organic framework (MOFs) are recently considered as a functional class of porous materials. The designability by varying the nature of the coordination metals and the organic linkers, the cristallinity in their structures resulting in nanometer-size confined spaces and the flexibility by the entanglement of their frameworks are unique properties for the development of multiple applications such as gas storage and gas separation, heterogeneous catalysts and molecular sensors.

The design of a PCP with photoactive entities as part of the structure and whose luminescent properties are highly sensitive to guests can offer potential application as luminescent sensors.

In this work [1], a new interpenetrated porous coordination polymer with naphthalenediimide (NDI) incorporated as fluorophore linker exhibits an unpredicted turn-on emission upon the incorporation of a class of aromatic compounds (substituted-benzenes). The unexpected luminescent properties are as consequence of the induced-fit structural transformation (framework displacement), checked by single-crystal x-ray diffraction, triggered by the guests incorporation to maximize the interaction with NDI. Non-interpenetrated analog. PCP (frameworks are impossible to slide) shows no luminescence, indicating the importance of the dynamic confined space for the luminescence.

The entangled PCP exhibits different luminescent colour depending on the substitution of the benzene ring as guests. For instance, from strong electron withdrawing (cyano) to electron donating capacity of the substituents (methoxy), the fluorescence can be tuned in the whole visible region (from 400 to 700 nm) or even stabilized radical-ion species (N,N-dimethyl). On the other hand, when halogen atoms are included in the benzene ring, a switching from fluorescence to phosphorescence emission is observed.

In this way, this new PCP can be used as a molecular sensor for benzene derivates which can recognized tiny differences in the substitution of aromatic ring and converted into a detectable signal (even by eye).

References:

[1] Y. Takashima, V. Martínez-Martínez, S. Furukawa, M. Kondo, S. Shimomura, H. Uehara, M. Nakahama, K. Sugimoto and S. Kitagawa. Nature Communications (accepted)

Figures:

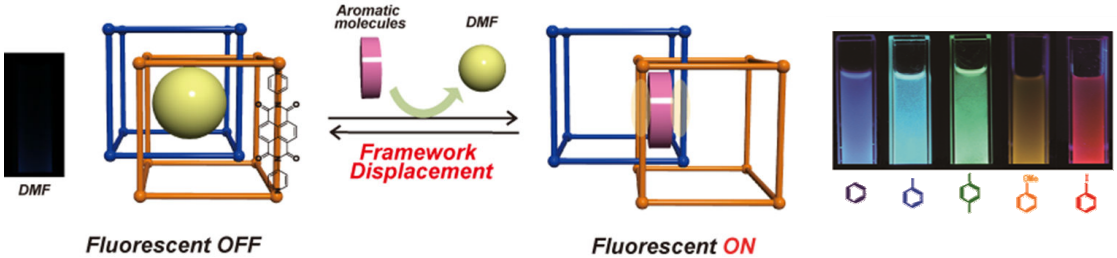

WAFER SCALE FABRICATION OF PASSIVATED CARBON NANOTUBE TRANSISTORS FOR ELECTROCHEMICAL SENSING

I. Martin-Fernandez[1], X. Borrisé[1,2], P. Godignon[1], E. Lora-Tamayo[1], F. Perez-Murano[1]

[1]Instituto de Microelectrónica de Barcelona (IMB-CNM, CSIC), Campus UAB, E-08193 Cerdanyola del Vallès, Spain
[2]Institut Català de Nanotecnologia (ICN), Campus UAB, E-08193 Cerdanyola del Vallès, Spain
inigo.martin@imb-cnm.csic.es

Since the operation of carbon nanotube transistors (CNT-FETs) was demonstrated [1], much progress has been achieved on the knowledge about electronic transport on SWCNTs and on their application for sensing [3]. However, there is still no standard high yield technology to fabricate single CNT-FETs.

In this contribution we present a technological process for the batch fabrication of CNT-FET based chips for electrochemical sensing applications (Figure 1) [2]. The fabrication of the CNT-FET structures is performed by using standard microelectronic steps at wafer level. Optical lithography is the only patterning technique to be used. The overall process can be divided in three main steps: the substrate preparation, the selective synthesis of the single-walled (SW) CNTs and the definition of the metallic contacts, stripes and pads. Recently, we have reported the fabrication of 10,000 functional CNT-FET devices on a 4 inch wafer by this technology [4].

An important requirement for the operation of the CNT-FETs in an electrochemical environment is the electrical contacts to be isolated from the electrochemical solution. With this purpose, we have developed a passivation procedure consisting in a PMMA coating of the CNT-FET and an electron beam lithography (EBL) process to locally remove the PMMA from the top of the CNTs and from the liquid polarization electrodes. The EBL process is programmed for the pattern to be automatically aligned on each device and it is performed at low electron beam energy to avoid any damage to the devices [5].

Figure 2(a-c) shows results on the fabrication of the CNT-FET based sensors. Figure 2(a) shows a 4 inch wafer after the fabrication of the CNT-FET structures. The wafer contains 5,616 CNT-FET structures. Almost 30% of the devices on this wafer were identified as operative and one third of those devices showed a semiconducting characteristic. Figure 2(b) shows an optical image of a sensor-platform into which the CNT-FET structures on the wafer are arranged. Each sensor-platform is composed of 24 CNT-FET structures that are located at the center of the chip for an electrochemical cell to be installed. The SEM image in Figure 2(c) shows a CNT-FET structure which channel length is 1.5 µm and where the width of the trench in the PMMA is 800 nm. Two SWCNTs had been contacted in this case by the metal contacts. The typical IV characteristics of a functional CNT-FET are shown in Figure 2(d). The transistors are p-type, their ON current is ~1 µA and the I_{ON}/I_{OFF} ratio is ~105.

The passivated CNT-FET devices are currently being tested in electrochemical environment.

Acknowledgements:

This work was partially founded by NANOFUN and SENSONAT projects. I.M.F acknowledges financial support through the I3P program.

References:

[1] R. Martel et al., Applied Physics Letters 73 (1998), 2447; S.J.Tans et al., Nature, 393 (1998), 49.
[2] I. Martin-Fernandez et al., J. of Vacuum Science and Technology B 28 (2010), C6P1.
[3] A. Jorio et al., Carbon Nanotubes: Synthesis, Structure, Properties, and Applications (2008), Springer.
[4] I. Martin-Fernandez et al., Microelectronic Engineering 87 (2010), 1554.
[5] G. Rius et al., Microelectronic Engineering 84 (2007), 1596.

Figures:

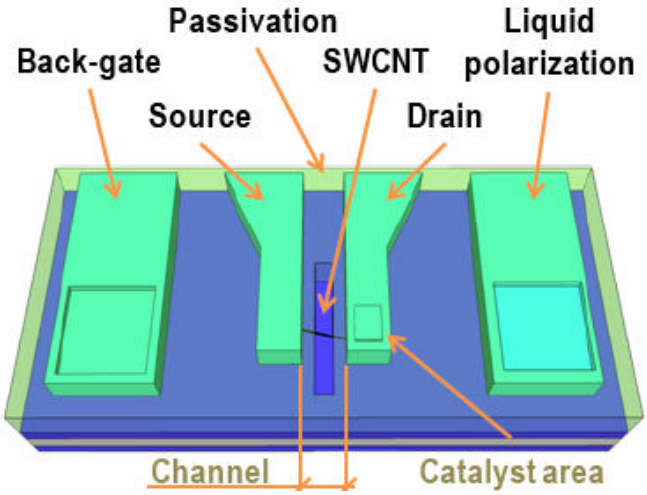

Figure 1: *Schematic of the passivated, back-gated CNT-FET sensor. The sensor consists of one (or more than one) SWCNT that is contacted by two metal electrodes, a back-gate that is actuated through a top metal electrode and a top liquid polarization electrode. The sensor is completely passivated by PMMA except for the channel of the CNT-FET, for part of the liquid polarization electrode and for the contact pads.*

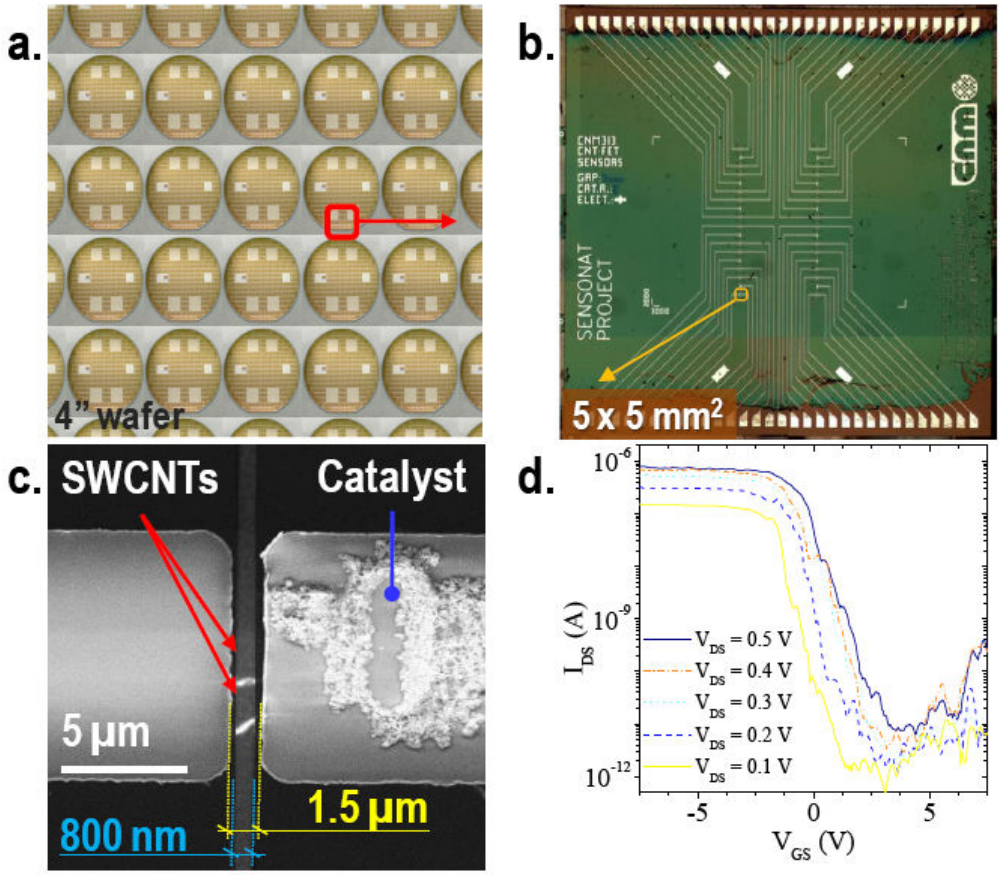

Figure 2: *Images on the fabrication and IV characteristics of the CNT-FETs. (a) Photograph of a batch fabricated 4 inch wafer. (b) Optical image of a sensor chip after the passivation procedure. The sensor is 5 x 5 mm^2. (c) SEM image of a passivated CNT-FET device. (d) Typical IDS vs. VGS characteristics of a CNT-FET formed of a single semiconducting SWCNT.*

PHYSICS OF TWO PHOTON LUMINESCENCE IMAGING IN NANOPLASMONICS

R. Marty[1], G. Baffou[2], A. Arbouet[1], V. Paillard[1], R. Quidant[3,4] and C. Girard[1]

[1]CEMES, UPR 8011, CNRS-Université de Toulouse, 29 rue Jeanne Marvig, BP 94347, F-31055 Toulouse, France
[2]Institut Fresnel-Domaine Universitaire de Saint-Jérôme, Avenue Escadrille Normandie-Niémen, F-13397 Marseille, France
[3]ICFO-The Institute of Photonic Sciences, Mediterranean Technology Park Av. del Canal Olímpic, 08860 Castelldefels (Barcelona), Spain
[4]ICREA-Institucio Catalana de Recerca i Estudis Avançats, 08010 Barcelona, Spain
renaud.marty@cemes.fr

Since the eighties, a tremendous interest has been devoted to the original near-field optical properties of nano-objects (either dielectric or metallic) deposited on surfaces [1]. To investigate these properties, near-field experimental methods such as PSTM and SNOM were initially developed [2]. They however need to accurately locate a near-field detector (tip) in the vicinity of the sample, making the system difficult to describe theoretically since the detector has an influence on the system itself. Recently, an alternative method based on two photon luminescence (TPL) has been developed to give access to near field informations through a far field measurement [3-4]. This technique can be advantageously coupled to optical absorption measurements of isolated nano-objects [5,6].

We investigate here lithographically fabricated gold nanoprisms. Both TPL and scattering by dark-field microspectroscopy were performed on isolated nanoprisms. The signals provided by these experiments are then compared and investigated theoretically.

In a first step, the nanostructure is represented by a single gold nanosphere deposited on a glass substrate and excited by an incident electric field. By using the field susceptibility theory, a simple analytical expression of the scattering signal generated by this nanoparticle is extracted as a function of the experimental parameters (incident wavelength and power, numerical aperture). In a second step, we describe the two photon luminescence signal in this simple configuration. This allows to discuss the origin of the spectral shift of the surface plasmon resonance during the propagation towards the far-field.

Finally we generalize this analytical scheme to realistic gold nanoparticles to simulate our experimental results. This comparison enables us to extract the order of magnitude of the non-linear response function of the nano-object as function of the incident wavelength.

References:

[1] C. Girard, and A. Dereux, Rep. Prog Phys. 59 (1996) 657
[2] P. Dawson, F. de Fornel, and J-P. Goudonnet, Phys. Rev. Lett. 72 (1994) 2927
[3] P. Ghenuche, S. Cherukulappurath, T. H. Taminiau, N. F. van Hulst, and R. Quidant, Phys. Rev. Lett. 101 (2008) 116805
[4] K. Imura, T. Nagahara, and H. Okamoto, J. Phys. Chem. B 109 (2005) 13214
[5] A. Arbouet, D. Christofilos, N. Del Fatti, F. Vallee, J. R. Huntzinger, L. Arnaud, P. Billaud, and M. Broyer, Phys. Rev. Lett. 93 (2004) 127401
[6] M. W. Knight, J. Fan, F. Capasso, and N. J. Halas, Optics Express 18 (2010) 2580.

Figures:

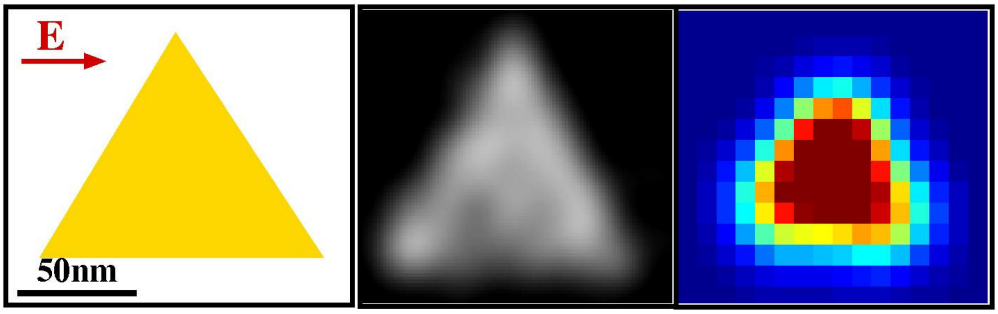

Figure 1: *(a) Investigated configuration: the electric field is parallel to the side of the nanoprism and the propagation of the beam is perpendicular to the triangle (and to the substrate). (b) SEM image of the considered gold nanoprism. The length of its side is 120nm. (c) TPL map of the nanotriangle performed at λ=822nm.*

COMMUNICATION BETWEEN MOLECULES VIA PHOTOCONTROLED IONS

Nathan D. McClenaghan[1], Guillaume Sevez[1], Aurélien Ducrot[1], Robin Bofinger[1], Pinar Batat[1,2], Ren-Wei Chang[1,3], Gediminas Jonusauskas[2], Laura Jonusauskaite[1], Jean-Luc Pozzo[1], Reiko Oda[3]

[1]Institut des Sciences Moléculaires, CNRS/Université Bordeaux I (UMR 5255),
351 cours de la Libération, 33405 Talence Cedex, France
[2]Laboratoire Ondes et Matière d'Aquitaine, CNRS/Université Bordeaux I (UMR 5798),
351 cours de la Libération, 33405 Talence Cedex, France
[3]Institut Européen de Chimie et Biologie, CNRS/Université Bordeaux I (UMR 5248),
2, rue Robert Escarpit, 33607 Pessac Cedex, France
n.mc-clenaghan@ism.u-bordeaux1.fr

Despite intense research, no single strategy has been shown to satisfactorily connect artificial molecular components in networks. This is perhaps the greatest hurdle to overcome if implementation of artificial molecular devices and sophisticated molecule-based arrays are to become a reality. One major goal of our work is to establish a strategy whereby functional molecular devices (e.g. photo-/electroactive) can communicate with one another in solution and in organized, self-assembled media (biotic and abiotic).[1]

Natural systems use chemical communication with small molecules and ions to promote transfer of information in different processes, including vision and neural transmission. In the current case artificial biomimetic systems are being developed integrating photonic and ionic processes, where remote control of ion release from synthetic molecular receptors, and thus the information transfer, is governed by a photonic stimulus in a bottom-up strategy. Ultimately this is anticipated to lead to coded information transfer through ion movement, which when combined with suitable receptors is signalled by fluorescent reporter groups and induced by photomodulated receptor groups in small photoactive molecules.

A range of artificial nanoobjects are presented with have been synthesized where different ion and molecule messengers are considered and are under study using ultrarapid transient absorption spectroscopy and dynamic fluorescence. Fast processes of photoejection and migration of ions are particularly well-suited to studies in real-time (using time-resolved photophysical techniques) with high spatial resolution (using fluorescence confocal microscopy techniques) allowing evaluation of the versatility of this strategy in the treatment and transfer of information and incorporation into devices.

As well as studies in solution, communication between distant sites / molecules considers the use of photoejected ions in nanocapsules and organized media including membranes, thin films, nanostructured hosts. Proof-of-principle of compartimental effects in dynamic micellar nanodomains has recently been demonstrated, see figure 1.[2]

References:

[1] http://mcclenaghan.ism.u-bordeaux1.fr/
[2] M. Cantuel, C. Lincheneau, T. Buffeteau, L. Jonusauskaite, T. Gunnlaugsson, G. Jonusauskas, N. D. McClenaghan, Chem. Commun., (2010) 2468.

Figures:

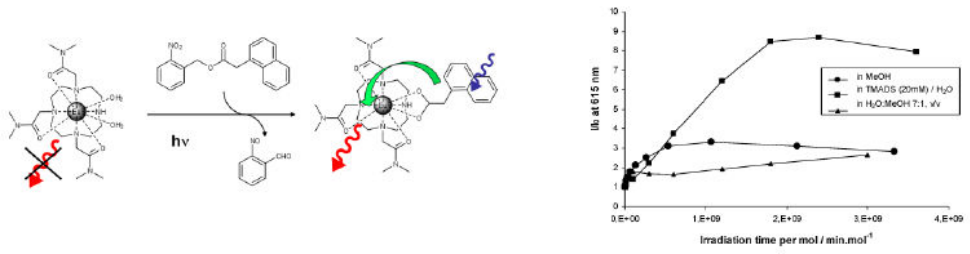

Figure 1: *Rudimentary photocontrolled chemical communication between molecules (left) and enhanced chemical communication in self-assembled surfactant (TMADS) nanodomains (right) as denoted by luminescence.*

ORDERED VACANCY NETWORK INDUCED BY THE GROWTH OF EPITAXIAL GRAPHENE ON PT(111)

G. Otero[1], C. Gonzalez[1], A.L. Pinardi[1], P. Merino[2], S. Gardonio[3], S. Lizzit[3], M. Blanco-Rey[4], K. Van de Ruit[5], C.F.J. Flipse[5], **J. Méndez[1]**, P.L. de Andres[1] and J.A. Martın-Gago[1,2]

[1]Inst Ciencia de Materiales de Madrid (CSIC), C. Sor Juana Ines de la Cruz 3, 28049-Madrid, Spain
[2]Centro de Astrobiologıa, INTA-CSIC, Torrejon de Ardoz, 28850 Madrid. Spain
[3]Sincrotrone Trieste SCpA, Strada Statale 14, Km. 163.5, 34149 Trieste, Italy
[4]Department of Chemistry, University of Cambridge, Cambridge CB2 1EW, United Kingdom
[5]Department of Applied Physics, Eindhoven University of Technology, P.O. box 513, 5600 MB Eindhoven, The Netherlands
jmendez@icmm.csic.es

We have studied large areas of √3×√3R30º graphene commensurate with a Pt(111) substrate. A combination of experimental techniques with ab initio density functional theory indicates that this structure is related to a reconstruction at the Pt surface, consisting of an ordered vacancy network formed in the outermost Pt layer and a graphene layer covalently bound to the Pt substrate. The formation of this reconstruction is enhanced if low temperatures and polycyclic aromatic hydrocarbons are used as molecular precursors for epitaxial growth of the graphene layers.

References:

[1] G. Otero et al., Physical Review Letters, 105 (2010) 216102.

Figures:

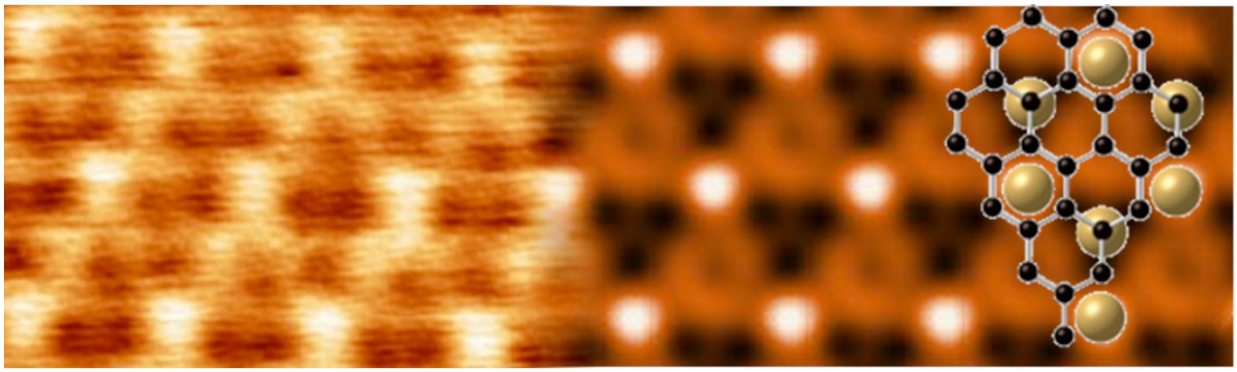

Figure 1: *STM image (left) and DFT simulation (right) of the proposed vacancy model (overlaid).*

PROBING THE ELECTROMAGNETIC FIELD DISTRIBUTION WITHIN A MAGNETOPLASMONIC NANODISK

D. Meneses-Rodríguez, E. Ferreiro-Vila, P. Prieto, J. Anguita, A. García-Martín, M. U. González, J. M. García-Martín, A. Cebollada, and G. Armelles

IMM-Instituto de Microelectrónica de Madrid (CNM-CSIC)
Isaac Newton 8, PTM, E-28760 Tres Cantos (Madrid), Spain
david.meneses@imm.cnm.csic.es

It is well known that localized surface plasmon resonances (LSPRs) greatly influence the optical [1, 2] and magneto-optical [3] properties of metallic nanostructures. It has been reported an enhancement of the magneto-optical (MO) activity when these LSPRs are excited. The key factor for this phenomenon is the high intensity of the electromagnetic (EM) field inside the global nanostructure when a LSPR occurs [4, 5]. In this work we show how the EM profile related to the LSPR can be probed locally inside the nanostructure.

We have studied the MO activity upon plasmon excitation in magnetoplasmonic nanodisk arrays. Such arrays have been fabricated in large area onto glass substrates by combining colloidal lithography with deposition under UHV and lift-off techniques. Each nanodisk is a Au (45nm-X)/Co(7nm)/Au (X)/Cr(2nm) multilayer with height=54nm and diameter=140nm, and for the sake of comparison, continuous thin films with identical composition have been also prepared (see Fig. 1(a) left and right, respectively).

The MO activity has been obtained by measuring the MO Kerr effect in polar configuration upon normal incidence illumination. With the help of extinction spectra, it has been checked that the maximum MO activity is in the same spectral range than the LSPR excitation. Fig. 1(b) shows the maximum MO activity as a function of the Co position for the nanodisk arrays as well as for the continuous films. The MO activity in the nanodisks depends on the position of the Co layers. It exhibits maximum values when the Co layer is located near the top or the bottom of the disks and minimum values in-between due to the LSPR excitation. This behavior is in contrast with the MO activity exhibited by the continuous films, which increases monotonously as the Co layer becomes closer to the top surface. This indicates that the EM field inside the nanodisks exhibits a nonuniform distribution in plasmon resonance conditions. In fact, the Co layer acts as a probe sensing the EM field within the nanodisk, since the MO activity depends on the intensity of such field.

This information could be very relevant for the design of magnetoplasmonic systems offering optimum MO enhancement, for instance for sensing applications where maximum sensitivity is expected in the areas with higher EM field.

References:

[1] S. A. Maier, Plasmonics: Fundamentals and Applications (Springer, Berlin, 2007).
[2] S. A. Maier and H. A. Atwater, J. Appl. Phys. 98, (2005) 011101.
[3] G. A. Wurtz, W. Hendren, R. Pollard, R. Atkinson, L. Le Guyader, A. Kirilyuk, Th. Rasing, I. I. Smolyaninov and A. V. Zayats, New J. of Phys. 10 (2008) 105012.
[4] J. B. González-Díaz, A. García-Martín, J. M. García-Martín, A. Cebollada, G. Armelles, B. Sepúlveda, Y. Alaverdyan and M. Käll, Small 4 (2008) 202.
[5] G. Armelles, A. Cebollada, A. García-Martín, J. M. García-Martín, M. U. González, J. B. González-Díaz, E. Ferreiro-Vila and J. F. Torrado, J. Opt. A: Pure Appl. Opt. 11 (2009) 114023.

Figures:

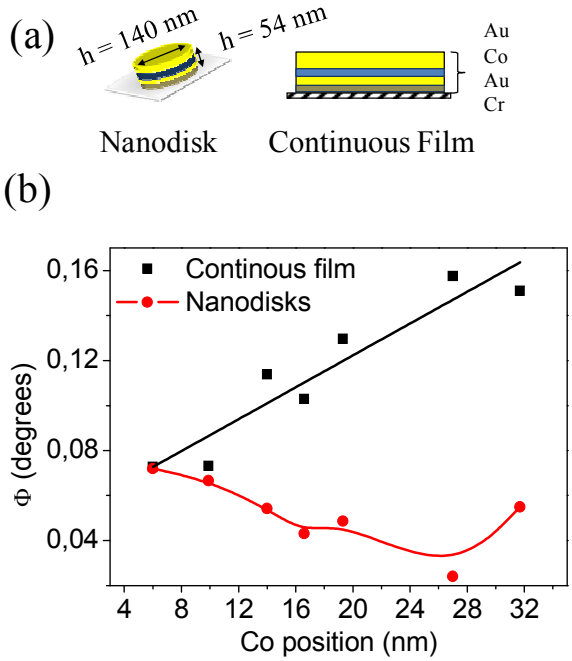

Figure 1: *(a) Schemes of the Au/Co/Au/Cr magneto- plasmonic systems here studied: nanodisks and continuous films, respectively. (b) Maximum magneto-optical activity as a function of the Co position for both kinds of structures.*

NOVEL CARBON NANOTUBE MULTIFUNCTIONAL COMPOSITE FIBERS

Célia Mercader[1], P. Poulin[2], P. Gaillard[1]

[1]CANOE (Consortium Aquitain en Nanomatériaux et électronique Organique),
16 avenue Pey Berland, 33600 Pessac, France
[2]Centre de Recherche Paul Pascal,
115 avenue Albert Schweitzer, 33600 Pessac, France
cmercader@enscbp.fr

Fibers and yarns are among the most promising forms for using carbon nanotubes (CNTs) on a macroscopic scale [1-8]. In analogy with high performance polymer, fiber spinning allows nanotubes to be preferentially oriented along the main axis of the fiber and then weaved into textile structures or used as cables.

We developed a new spinning method to produce fibers with a nanocomposite structure and with a high nanotube fraction. We spin continuous CNT fibers by a coagulation process which consists in injecting an aqueous dispersion of CNTs, polyvinyl alcohol (PVA) and surfactant in a static coagulation bath containing sodium sulphate. The used surfactant plays a critical role as the quality of the dispersion of the carbon nanotubes in the polymer is the key factor for a spinnable mixture. The surfactant leads to a good dispersion of the nanotubes and prevents from their coagulation in the presence of PVA in the dope material. In addition, it can be easily desorbed. The dope exhibits a homogeneous and aggregate free texture when observed with an optical microscope. This reflects the absence of aggregates larger than a micrometer typically. In the coagulation bath, all the nanotubes remain trapped in the coagulated PVA. The fiber is then washed, dried and collected as shown in figure 1. A 300 meters long fiber collected onto a winder is shown in figure 2. The fibers obtained by this continuous and robust process have a composite structure with large fraction of oriented CNTs, which can reach 50%, bound by the polymer, as shown in figure 3.

The diameter of the fibers can be varied from 10 to 100µm by changing the spinning conditions. The nanotubes are homogeneously distributed in the PVA matrix and their orientation along the fiber axis is about ±10°. These fibers are electro conductive fibers with a resistivity of 10Ω.cm and can be used for antistatic applications. CNT fibers exhibit also piezo-resistivity properties. This means that the resistivity of the fiber is sensitive to the mechanical loading. The electrical resistivity strongly increases with strain. This property makes CNT fibers good candidates for sensor applications. In addition, the mechanical properties are promising with a Young's modulus of 40GPa and a high toughness.

In order to validate these different applications, a large quantity of fibers is required but scalingup the process is very challenging. In this way, we are now building a multifilaments fiber spinning pilot unit on CANOE, a platform of technological innovation based in Pessac, near Bordeaux, focused on nanostructured materials. The objectives of the platform are to promote the emergence of an integrated value chain (from raw material to finished product) in the field of nanomaterials and more particularly of carbon nanotubes.

References:

[1] H. Gommans et al., 2000, Journal of Applied Physics, 88, 2509.
[2] B. Vigolo et al., 2000, Science, 290, 1331.
[3] H. Zhu et al., 2002, Science, 296, 884.
[4] K. Jiang et al., 2002, Nature, 419, 801.
[5] Y. Li et al., 2004, Science, 304, 276.
[6] L. Ericson et al., 2004, Science, 305, 1447.
[7] M. Zhang et al., 2005, Science, 306, 1358-1361.
[8] A. B. Dalton et al., 2003, Nature, 423, 703.

Figures:

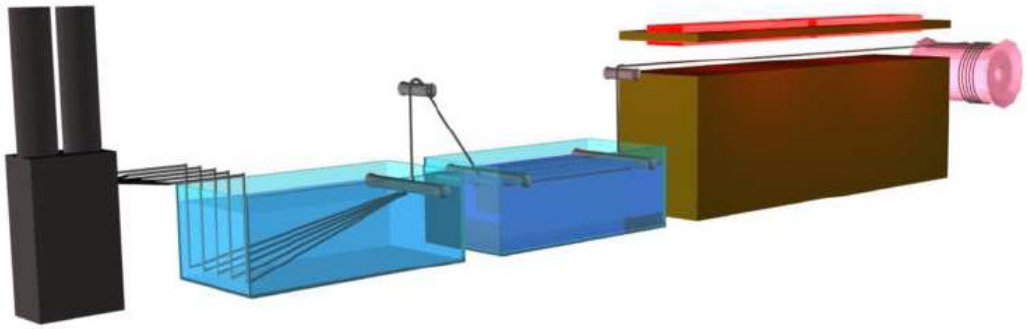

Figure 1: *Scheme of the coagulation wet spinning process*

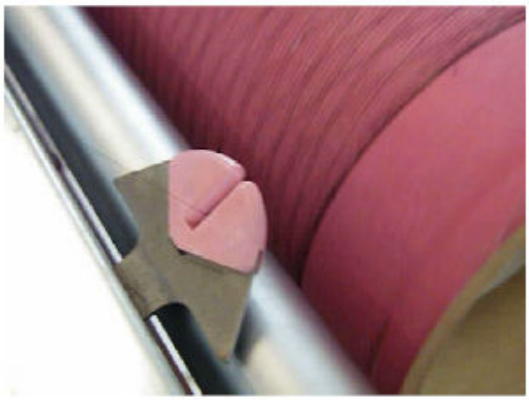

Figure 2: *Collecting the composite CNT fiber on the winder*

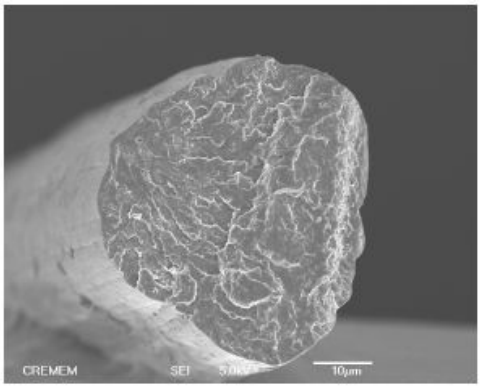

Figure 3: SEM picture o the cross section of the composite CNT fiber

OPTIMISATION OF CNT BASED NANOSTRUCTURES FOR USE AS ELECTRON SOURCES

W. I. Milne[1,2], D. Hasko[1], M. Cole[1], Chi Li[1], Ke Qu[1] and Y. Zhang[1]

[1]Electrical Engineering Division Building, University of Cambridge, 9 JJ Thomson Avenue, Cambridge CB3 0FA, UK
[2]Kyung Hee University, Dept. Information Display, Seoul 130701, South Korea

Semiconductor The aim of this paper is to describe the growth and optimization of carbon nanotube (CNT) based nanostructures to produce novel electron sources for use in a variety of applications including, Electron microscopy, e-beam lithography, travelling wave tubes (TWTs), backlighting and x-ray sources.

Because of their unique properties including their shape and current carrying capabilities Carbon Nanotubes are ideal as electron sources. The emitters studied in this project include spaghetti type layers of CNTs and regular array of vertically aligned CNTs. They will also include CNT/ZnO nanostructures as alternative sources. The objectives of this work are to develop a cathode that is able to deliver a stable current density of > 1A/cm^2 at DC and even higher in pulsed mode and to produce cheap, stable light emission sources for lighting applications such as backlighting which are able to run at comparatively high pressures to provide 1 mA/cm^2. In order to attain the large current densities with reasonable uniformities and long life time required for application to X-ray sources, it is necessary to prevent the best CNT emitters in the array from emitting too large a current by use of an integrated ballast resistor. In this paper we will also describe our recent work in this area.

Although we can get significant emission from the spaghetti type layers of CNTs, which are suitable for use in backlight structures in AMLCDs, as shown in Figure 1 (a), the CNTs we have investigated most frequently are in arrays which are vertically aligned, as previously described in reference [1]. Such a cathode design allows us to minimize the electric field shielding effects and lead to the higher current densities needed in TWTs and X-ray sources. A typical array is shown in Figure 1(b).

A smaller version of such an array consisting of a 22.5 μm x 22.5 μm array of CNTs spaced 2.5 μm apart providing 100 CNTs, produced a current density of 18A/cm^2 at 9V/μ. In order to attain such large current densities with reasonable uniformities and long lifetimes, however, it is necessary to prevent the best CNT emitters in the array from emitting a current larger than the current which induces their destruction (around 100 μA). To solve this problem, a ballast resistor must be integrated.

Our initial efforts to produce the ballast resistor structure was based on an SOI (undoped-Si/SiO_2/Si) substrate employing electron beam lithography and plasma enhanced chemical vapour deposition (PECVD) - see Figure 2. First, a catalyst dot array similar to that shown in Figure 1(b) was produced using e-beam lithography and Ni metal sputtering. Finally, a top-contact layer of tungsten was used to bias the CNTs, with the gap between the tungsten and CNTs of undoped Si acting as the ballast resistor.

However, the fabrication process for this structure is very complex. This may be acceptable for expensive x-ray sources and Travelling Wave Tubes, but is undesirable for lighting applications and thus a novel, but simpler structure, incorporating a combination of Carbon Nanotubes and ZnO nanowires, has been produced for this application.

Firstly a CNT array such as the one shown above in Figure 1(b) was produced and then ZnO nanowires were grown onto these using a simple hydrothermal method to produce the arrays shown in Figure 3. A solution of zinc acetate dehydrate (98%, Aldrich) in 1-propanol (spectroscopic grade) was prepared. The solution was then spin coated onto the VACNF array at 2000 rpm for 30 s. The substrates were then annealed at 100°C fpr 2 minutes after each spin coating step to promote adhesion. A uniform seed layer was obtained after three layers of spin coating. The ZnO nanowires were then grown by dipping the substrates in an equimolar mixture of 25 nM zinc nitrate hexahydrate ($Zn(NO_3)_2 \cdot 6H_2O$, Sigma Aldrich) and hexamethylenetetramine (HTMA, Sigma Adrich) in deionized (DI) water heated in an oven at 80°C.

This presentation will therefore describe the growth and production of the CNT emitters, their optimisation and their use in electron microscope sources, parallel e-beam lithography, travelling wave tubes, portable X-ray sources and backlights.

Figures:

(a) (b)

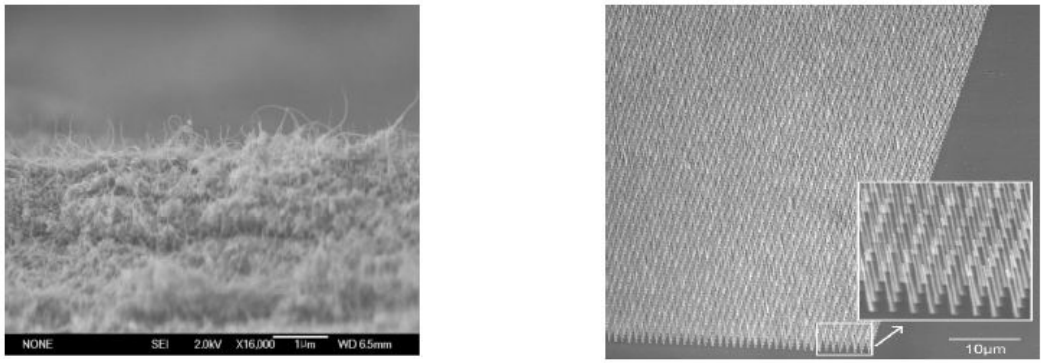

Figure 1: *(a) Spaghetti type CNTs; (b) Vertical array of MWCNTs*

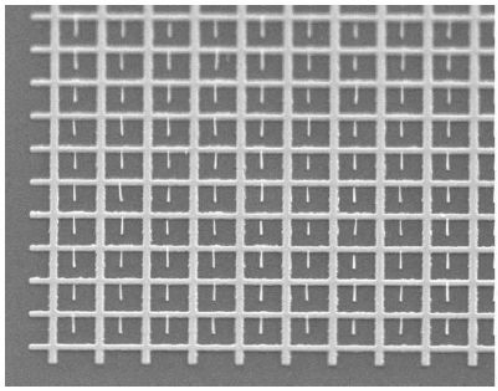

Figure 2: *An array of CNTs grown on undoped SOI*

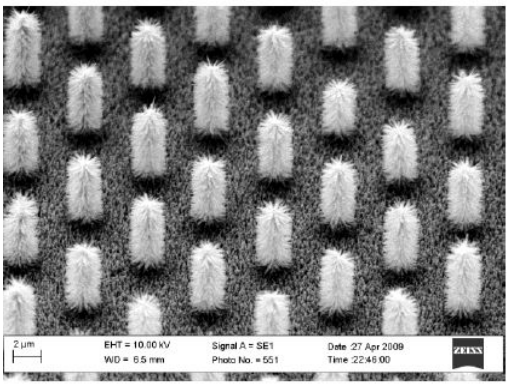

Figure 3: *ZnO coated CNT array*

TUNING WRITING MAGNETIC FIELDS IN MULTI-STATE STORAGE MEDIA

R. Morales[1,2], M. Kovylina[3], Z-P. Li[4], M. Erekhinsky[4], J. E. Villegas[5], A. Labarta[3], X. Batlle[3], and Ivan K. Schuller[4]

[1]Dpto. de Química-Física, Universidad del País Vasco, 48940 Leioa, Spain.
[2]IKERBASQUE, Basque Foundation for Science, 48011 Bilbao, Spain.
[3]Departament de Física Fonamental and Institut de Nanociència i Nanotecnologia, Universitat de Barcelona, 08028 Barcelona, Catalonia, Spain
[4]Physics Department, University of California San Diego, La Jolla 92093 CA, USA
[5] Unité Mixte de Physique CNRS/Thales, Université Paris Sud, 91405 Orsay, France
rafael_morales@ehu.es

Antiferromagnetic/ferromagnetic (AF/FM) bilayers exhibiting both negative and positive exchange bias have been proposed as multi-state storage media [1]. In such media the same magnetic region or element can store more than two digits. Thus, a track length comprising 8 magnetic elements stores up to 2^8 = 256 bytes in regular media, whilst in a threefold multi-state system it could store up to 3^8 = 6561 combinations, that could be called Tits (Ternary Digits). A multi-state digit is defined by the remanent magnetization (M_s) of the magnetic element. M_s is determined by the external field (H_{FC}) applied while cooling the AF/FM bilayer through the AF Néel temperature. A low H_{FC} yields a FM hysteresis loop with negative exchange bias providing a state with the highest Ms value (Fig. 1, H_{FC} = 0.5 kOe). High H_{FC} leads to a loop with positive exchange bias giving a digit with the lowest M_s (Fig. 1, H_{FC} = 5.0 kOe). States in-between can be defined either by a fractional value of M_s or even by a null remanence, by applying intermediate cooling fields (Fig. 1, H_{FC} = 2.0 kOe).

The minimum H_{FC} necessary to obtain positive exchange bias establishes the magnetic field required for multi-state storage writing. In continuous thin films it depends on structural parameters. However, we demonstrate in this work that this minimum H_{FC} yielding positive exchange bias can be tuned by patterning the continuous bilayer. It will be showed that both dots and antidots nanostructures reduce the writing magnetic field of all multi-states. The writing magnetic field decreases either as the dot size decreases or as the antidot density increases. [2,3] These findings are explained upon energy considerations of buried and bare pinned uncompensated spins in the AF.

Work supported by U.S. DOE, Spanish MICINN (MAT2009-08667 and FIS2008-06249), Catalan DURSI (2009SGR856), U.S. Air Force Office for Scientific Research, and IKERBASQUE Basque Foundation for Science.

References:

[1] I. V. Roshchin, O. Petracic, R. Morales, Z.-P. Li, X. Batlle, I. K. Schuller, US Patent Number 7,764,454.
[2] Z.-P. Li, R. Morales, and I. K. Schuller, Appl. Phys. Lett. 94 (2009) 142503
[3] M. Kovylina, M. Erekhinsky, R. Morales, J. E. Villegas, I. K. Schuller, A. Labarta, and X. Batlle, Appl. Phys. Lett. 95 (2009) 152507

Figures:

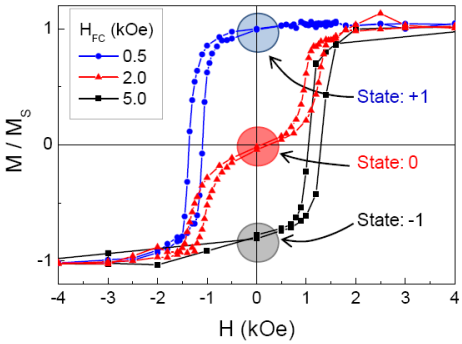

Figure 1: *Three hysteresis loops of a continuous FeF_2/Ni bilayer for different cooling fields. These cooling fields defined a threefold multi-state.*

EULER BUCKLING INSTABILITY AND ENHANCED CURRENT BLOCKADE IN SUSPENDED SINGLE-ELECTRON TRANSISTORS

F. Pistolesi, G. Weick, and F. von Oppen

Laboratoire d'Ondes et Matière d'Aquitaine, Université de Bordeaux 1 and CNRS, Talence France
Fabio.Pistolesi@u-bordeaux1.fr

Single-electron transistors embedded in a suspended nanobeam or carbon nanotube may exhibit effects originating from the coupling of the electronic degrees of freedom to the mechanical oscillations of the suspended structure. Here, we investigate theoretically the consequences of a capacitive electromechanical interaction when the supporting beam is brought close to the Euler buckling instability by a lateral compressive strain (see Fig.1). Our central result is that the low-bias current blockade, originating from the electromechanical coupling for the classical resonator, is strongly enhanced near the Euler instability. We predict that the bias voltage below which transport is blocked increases by orders of magnitude for typical parameters (see Fig. 2). This mechanism may make the otherwise elusive classical current blockade experimentally observable.

References:

[1] G. Weick, F. von Oppen, F. Pistolesi, Phys. Rev. B, in press (2011)
[2] G. Weick, F. Pistolesi, E. Mariani, F. von Oppen, Phys. Rev. B 81, 121409 (R) (2010)
[3] F. Pistolesi, Y. Blanter, and I. Martin, Phys. Rev. B 79 085127 (2008)
[4] F. Pistolesi and S. Labarthe, Phys. Rev. B 76 165317 (2007)

Figures:

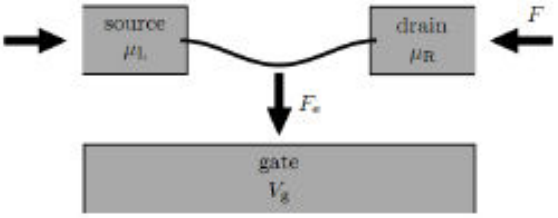

Figure 1: *Sketch of the considered system: a suspended doubly- clamped beam forming a quantum dot electrically connected to source and drain electrodes. The beam is capacitively coupled to a metallic gate kept at a voltage V_g, which induces a force F_e that attracts the beam towards the gate electrode. An additional, externally controlled compressional force F acts on the beam and induces a buckling instability.*

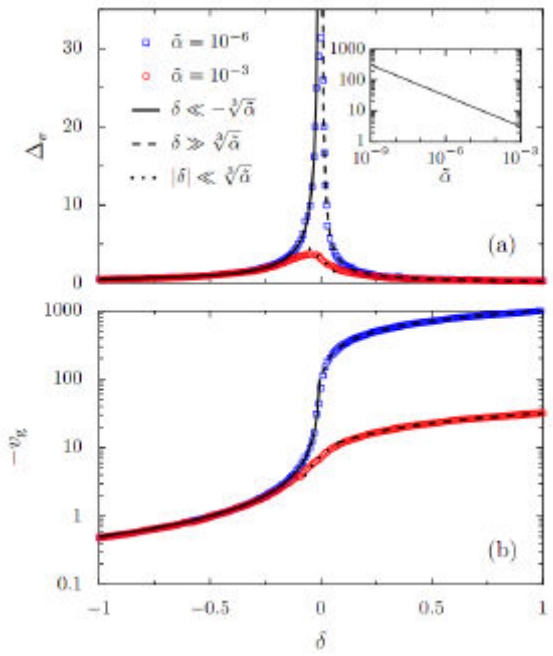

Figure 2: *Gap (a) and gate voltage position of the minimum gap in dimensionless units (b) as a function of the dimensionless distance from the transition point: $\delta = F/F_{c-1}$, where F is the force acting on the rod, and F_c is the critical force. One can clearly see a great enhancement of the gap of the order of 30 times the original value at the transition point. The red and blue curves correspond to different values of the non-linear coupling.*

A NOVEL DNA CHIP FOR SINGLE MOLECULE ANALYSIS

T.Plénat[1,2], C.Tardin[1,2], C.Vieu[3,2], C.Thibault[3,2], E.Trévisiol[3,4] and L.Salomé[1,2]

[1]CNRS; IPBS (Institute of Pharmacology and Structural Biology); 205 route de Narbonne, F-31077 Toulouse, France
[2]University of Toulouse; UPS; IPBS; F-31077 Toulouse, France
[3]LAAS, Nanobiosystems, 7, Avenue du Colonel Roche, F-31077 Toulouse, France
[4]UMR 5504, UMR 792, Ingénierie des Systèmes Biologiques et des Procédés & Plate-forme Biopuces, CNRS, INRA, INSA, 135, avenue de Rangueil, 31077 Toulouse, France
plenat@ipbs.fr salome@ipbs.fr

The last two decades have seen the emergence of single-molecule experiments [1]. By avoiding the ensemble averaging inherent to traditionnal bulk-phase biochemistry, the study of molecular machineries at the single-molecule level permits a better understanding of the behavior of living systems. Indeed the dynamics of the machineries processes can be characterized and rare subpopulations can be identified [2].

One of the main shortcoming of single molecule experiments is that the acquisition of statistically solid data is very time consuming, which explains the fact that they are still not widely used in laboratories.

We will present the development of a new single DNA chip, allowing the simultaneous analysis of hundreds of single DNA molecules by the Tethered Particle Motion (TPM) technique. Our single DNA chip gives high-throughput capabilities to this approach of valuable interest for multiple applications.

The principle of a TPM experiment consists in tracking a bead tethered at the free end of a DNA molecule which is immobilized by the other end to a coverslip thanks to optical videomicroscopy. The amplitude of the Brownian motion of the bead is related to the effective length of the DNA molecule [3]. Any conformational change of the DNA molecule due to external factors (proteins, ions, temperature), that induces a variation of the effective length of the DNA tether, can be thus monitored by TPM [4].

References:

[1] Cornish, P. V.; Ha, T., Acs Chemical Biology 1 (2007) 53
[2] van Oijen, A. M., Nature Chemical Biology, 8 (2008) 440
[3] Yin, H.; Landick, R.; Gelles, J., Biophys J, 6 (1994) 2468
[4] Pouget, N. et al.; Nucleic Acid Res., 9 (2004) e73

QUANTUM TRANSPORT AND HIGH MAGNETIC FIELD PHENOMENA IN CARBON NANOTUBES AND NANO-RIBBONS

Bertrand Raquet

Laboratoire National des Champs Magnétiques Intenses – Toulouse, LNCMI-T
UMR 3228, CNRS, UPS, INSA, Université de Toulouse, France

Over the last two decades, new forms of carbon, fullerenes, carbon nanotubes (CNT), isolated graphene flacks and more recently graphene nanoribbons (GNR) have been synthesized, manipulated and electrically connected. Their fundamental studies unravel remarkable electronic properties resulting from the electronic confinement at nano-scale and the electronic band structure of graphene. The feasibility of room temperature carbon based field effects transistors and inter-connexions have been demonstrated while their industrial integration as elementary bricks of new devices raises severe technological issues.

In this talk, after a brief comparative description of the electronic band structure of carbon nanotubes and graphene nano-ribbons, I will focus on (magneto)-transport experiments performed on individually connected CNTs and GNRs. I will show that magneto-transport in the high magnetic field regime along with an electrostatic control of the electronic doping is an outstanding probe of the 1-D electronic band structure and its unusual magnetic field dependence.

An applied magnetic field along the CNT axis induces giant quantum flux modulation of the conductance due to the periodic energy gap modulation at the charge neutrality point [1]. This so-called Aharonov-bohm effect is also an efficient tool to identify the metallicity of the external shell of a multi-walled carbon nanotube and to infer the locations of the different 1-D subbands [2]. By rotating the CNT perpendicular to the magnetic field, the energy gap of a semiconducting CNT is progressively reduced due to the onset of the first Landau level at zero energy and propagating Landau states develop at the flank of the tube [3]. Concerning (magneto)-transport experiments on GNR, I will present compelling evidences of the 1D transport character in the first generation of chemically derived GNRs with smooth edges and the possibility of tuning backscattering effects by means of an external magnetic field [4]. These experiments enlighten the richness of the electronic transport measurements on an individual nano-object in presence of a large magnetic confinement.

References:

[1] M. Sagnes & al, Phys. Rev. Lett. 94, 066801 (2005); B. Lassagne & al, Phys. Rev. Lett. 98, 176802 (2007)
[2] S. Nanot & al, C. R. Physique 10 (2009).
[3] B. Raquet & al, Phys. Rev. Lett. 101, 046803 (2008); S. Nanot & al, Phys. Rev. Lett. 103, 256801 (2009)
[4] J-M Poumirol et al, Phys. Rev. B 82, 041413(R) (2010)

ONE-STEP SYNTHESIS OF JANUS NANOPARTICLES BY SELF-ASSEMBLY MONOLAYERS

Javier Reguera[1,2], Miao Yu[1,2], Ines Pons-Siepermann[3], Sharon C. Glotzer[3,4], Francesco Stellacci [1,2]

[1]SUNMAG, DMSE, Massachusetts Institute of Technology, 77 Mass. Av., Cambridge, MA (USA)
[2]SUNMIL, IMX, École Polytechnique Fédérale de Lausanne, Lausanne, Switzerland
[3]Department of Chemical Engineering, University of Michigan, Michigan, USA
[4]Department of Materials Science and Engineering, University of Michigan, Michigan, USA
jreguera@mit.edu

Described first by De Gennes[1] Janus Nanoparticles (Janus NPs) are called like the Roman God custodian of universe, God of gates and doors, beginnings and endings and hence represented with a double-faced head. Janus Nanoparticles are therefore particles with two distinct sides. The term Janus has been used to describe different particles such as dendritic macromolecules, block-copolymers micelles, or inorganic materials. The asymmetry generated in these particles is useful in wide range of applications. The most known is probably the one that uses the so-called Pickering effect, [2] that is, particles can be used to stabilize oil-in-water and water-in-oil emulsions. It has been demonstrated theoretically and experimentally that this stabilization is much higher when it is done by amphiphilic Janus nanoparticles instead of homogeneous particles, due to the higher adsorption energy of the particles at the liquid-liquid interface. These stabilized droplets could be used for diverse applications from water-based paints to heterogeneous nanocatalysis. The Janus nanoparticles can also be used in other important fields like electronic displays, nanomotors, drug or gene delivery or as building blocks for assembly of suprastructures. [3]

Up to now a few different strategies to obtain Janus nanoparticles have been described in the literature that can be included in one of these groups: toposelective surface modification that includes: 1. selective masking, use of reactive directional fluxes, microcontact printing or arrangement of the particle along an interface and partial contact with a reactive medium; 2. template-directed self-assembly; controlled phase separation phenomena; 3. and controlled surface nucleation. [3] There are several problems related to these strategies like the difficulty to obtain small nanoparticles (<10nm); the complexity of the synthesis methods that involves first the synthesis of symmetric particles (homogenous or core-shell) and them a posterior modification; and the low yield of this strategies due to the fact that most of them require the use of a surface where the particles are placed to avoid the reaction of one of the sides. To the best of our knowledge none of these strategies has the ability of producing truly large nanoparticle quantities in an easy way, as a direct synthesis can do. [3]

In our group it has been reported previously that when a metallic nanoparticle is synthesized with mixture of dislike ligands, there is a self-assembly with the formation of stripes on the topology of the nanoparticle.[4-7] However this is not the only possible topological conformation, depending on the parameters of the particle (ligand lengths, ligands functionality or surface curvature) other self-assembly structures such as Janus or random domains are also possible. [6] Here we report the synthesis of Janus Nanoparticles with the use of self-assembly monolayers (SAMs) composed of two types of ligand molecules of different length. The particles have been synthesized using a modification of the method described by Zheng et al. [8] extended to mixtures of ligands. This synthesis is an easy one-step, onephase synthesis for monodisperse metallic nanoparticles of small size (<10 nm) that can be scaled up to produce enough particles for useful applications and that can be extended to different functionalities. The two ligands used here were 1-hexanethiol (HT) and 1-dodecanethiol (DDT). TEM images were used to calculate the size and size distribution of the particle. [1] H NMR spectroscopy after particle decomposition was used to calculate the ligand ratio. Once synthesized the particles were deposited on gold-on-mica substrates using Langmuir-Blodget deposition and then imaged using STM. The phase separation calculations were made using mesoscale simulations.

Figure 1 shows a representative STM image of a monolayer of nanoparticles made of 1:2 HT:DDT (ratio in solution). As we can see in the image the particles tend to order in a hexagonal lattice due to the monodispersity of the nanoparticles. The most interesting feature of these NPs is however the existence of two clear phases, a big one that corresponds to the DDT ligand and an small and circular one (on the left size of the particles) that correspond to the HT ligand. To be sure this was a real feature and not an artifact several images were taken in different areas and with different tips, in

addition this features were seen with to different STM microscopes a Veeco Multimode in air and an Omicron in ultra high vacuum (UHV). We have also seen that the amount of Janus NPs depends on the ratio between ligands being bigger for mixtures far from the 1:1 ligands' ratio. Mesoscale simulations have shown the formation of Janus Nanoparticles for high values of the interaction parameter of the ligands. In our case the high difference in ligands length, and therefore high differences in the enthalpic component of the phaseseparation makes this parameter to be high enough to make a complete phase-separation of the two ligands.

This new way to obtain Janus nanoparticles has a really high potential to be used I several applications due to its simplicity, scalability and variability of ligands ant therefore functionalities that can be used.

References:

[1] de Gennes, P. G. Reviews of Modern Physics, 64, (1992), 645.
[2] Pickering, S. U. Journal of the Chemical Society, 91, (1907), 2001-2021.
[3] Perro, A.; Reculusa, S.; Ravaine, S.; Bourgeat-Lami, E. B.; Duguet, E. Journal of Materials Chemistry, 15, (2005), 3745-3760.
[4] Jackson, A. M.; Myerson, J. W.; Stellacci, F. Nature Materials, 3, (2004), 330-336.
[5] DeVries, G. A.; Brunnbauer, M.; Hu, Y.; Jackson, A. M.; Long, B.; Neltner, B. T.; Uzun, O.; Wunsch, B. H.; Stellacci, F. Science, 315, (2007), 358-361.
[6] Singh, C.; Ghorai, P. K.; Horsch, M. A.; Jackson, A. M.; Larson, R. G.; Stellacci, F.; Glotzer, S. C. Physical Review Letters, 99, (2007), 226106.
[7] Carney, R. P.; DeVries, G. A.; Dubois, C.; Kim, H.; Kim, J. Y.; Singh, C.; Ghorai, P. K.; Tracy, J. B.; Stiles, R. L.; Murray, R. W.; Glotzer, S. C.; Stellacci, F. Journal of the American Chemical Society, 130, (2008), 798-799.
[8] Zheng, N.; Fan, J.; Stucky, G. D. Journal of the American Chemical Society, 128, (2006), 6550-6551.

Figures:

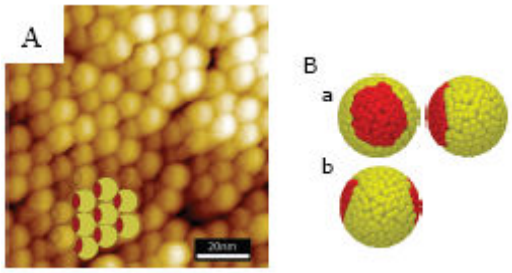

Figure 1: *A) STM image of a monolayer of nanoparticles 1:2 HT:DDT Janus NPs (The cartoon has been drawn to help the reader to identify the Janus NPs). B) Mesoscale simulation of the same particles showing a phaseseparation in equilibrium with distributions in 2 or 3 domains (a and b respectively).*

GAS SENSOR FOR FOOD INDUSTRY AND AGRICULTURE BASED ON ZNO NANOPARTICLES AND NANORODS

Andrey Ryzhikov, Pierre Fau, Myrtil Kahn, Katia Fajerwerg, Bruno Chaudret, Philippe Ménini*, Chang-Hyun Shim*, Alain Gaudon**

Laboratoire de Chimie de Coordination, 205 route de Narbonne, Toulouse, France;
*LAAS-CNRS, UPS, Université de Toulouse; **Alpha MOS
andrey.ryzhikov@lcc-toulouse.fr

Semiconductor gas sensors can be widely used in food industry and agriculture. Measurements of ethylene concentration in vegetable stores and greenhouses allow the control of fruit ripening, whereas detection of H_2S, mercaptans, amines may be used to control of meat, fish and vegetable freshness. In this work we present a new generation of semiconductor gas sensors based on the combination of micromachined silicon substrates [1] and highly sensitive layer of ZnO nanoparticles. ZnO nanoparticles displaying 3 different morphologies (cloudy-like structures, size controlled isotropic particles and nanorods (Fig. 1)) were obtained through the controlled hydrolysis reaction of an organometallic precursor, namely the biscyclohexyl zinc, in the presence of various levels of long-chain amines surfactants [2]. ZnO nanopowders were deposited by a generic ink-jet method on low power consumption silicon substrates. High quality and micron thick layers have been obtained with a low defect level (no cracks, no delamination). The sensor responses to reducing gases (CO, propane, ammonia, ethylene, and acetaldehyde) have been studied in relation with the morphology of ZnO nanocrystals. Cloudy-like ZnO sensors showed a high response to ammonia vapors (20 ppm), whereas isotropic nanoparticles possessed the highest response to acetaldehyde gas (10ppm) and nanorods based layers displayed a higher sensitivity to ethylene (50ppm). These variations can be associated with the different ratios of crystalline faces exposed to reactive gases. These results open the route to the fabrication of a multisensor system based on pure ZnO nanoparticles with different shapes for the detection of reducing gases in complex mixtures.

References:

[1] Ph. Ménini et al., Eurosensors XXII proceedings, 2008, 342
[2] M. Monge et al., Angew. Chem. Int. Ed., 2003, 42, 5321

Figures:

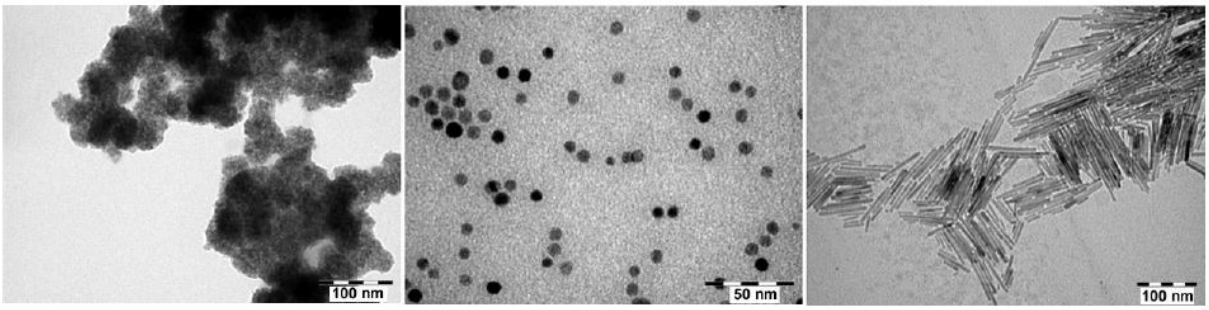

Figure 1: *ZnO cloudy-like structures, isotropic nanoparticles and nanorods*

NEW INSIGHTS INTO NANOMAGNETISM BY SPIN-POLARIZED SCANNING TUNNELING MICROSCOPY AND SPECTROSCOPY

Dirk Sander, Hirofumi Oka, Pavel Ignatiev, Safia Ouazi, Jérôme Borme **, Sebastian Wedekind, Guillemin Rodary*, Larissa Niebergall, Valeri Stepanyuk, and Jürgen Kirschner

Max-Planck-Institute of Microstructure Physics, Halle, Germany
*present address: LPN, CNRS UPR20, Marcoussis, France
**permanent address: Iberian Nanotechnology Laboratory, Braga, Portugal
sander@mpi-halle.de

Spin-polarized scanning tunneling microscopy (SP-STM) allows imaging and spectroscopic characterization of nanostructures with unsurpassed spatial resolution. Its working principle exploits the dependence of the tunnel current on the relative magnetization orientation of a sample and the magnetic STM tip. We present results by SP-STM, where we investigate the correlation between structural, electronic, and magnetic properties of individual nm small Co islands with several hundred to thousands of atoms. We use external magnetic fields of up to 4 T to tune the magnetic state of both tip and sample, and we extract the corresponding change of the differential conductance of the tunnel junction.

A recent example is our measurement of magnetic hysteresis loops of individual nm small Co islands on Cu(111) at 8 K by SP-STM in external magnetic fields. We find switching fields of up to 2.5 T for islands with roughly 8,000 atoms. The quantitative analysis of these results provides novel insights into the magnetization reversal on the nanoscale, and deviations from the venerable Stoner-Wohlfarth model are discussed.

We also exploit the high spatial resolution of SP-STM in magnetic fields to measure maps of the differential conductance within a single nm-small Co island for different magnetization states. In connection with density functional theory calculations we demonstrate that the spin polarization is not homogeneous but spatially modulated within the Co island, as indicated in Fig. 1. We ascribe the spatial modulation of the spin polarization to spin-dependent electron confinement within the Co island [1].

References:

[1] Oka, Ignatiev, Wedekind, Rodary, Niebergall, Stepanyuk, Sander, Kirschner, Science 327(2010) 347

Figures:

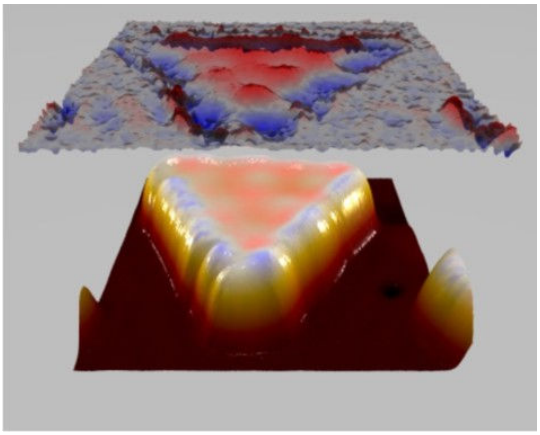

Figure 1: *Superposition of a 3D-topographic representation of a bilayer high Co island with a base length of 12 nm from STM topography (bottom) with a map of the asymmetry of the differential conductance measured at the Fermi energy (top). Blue: negative; red: positive, gray: zero asymmetry. The top map reflects a spatial modulation of the spin-polarization, induced by spin-dependent electron confinement within the Co island [1].*

DOXORUBICIN LOADED MAGNETIC POLYMERSOMES: THERANOSTIC NANOCARRIERS FOR MR IMAGING AND MAGNETO-CHEMOTHERAPY

Olivier Sandre, Charles Sanson, Odile Diou, Julie Thévenot, Emmanuel Ibarboure, Alain Soum, Annie Brûlet, Sylvain Miraux, Eric Thiaudière, Sisareuth Tan, Alain Brisson and Sébastien Lecommandoux

Laboratoire de Chimie des Polymères Organiques (LCPO)
UMR5629 Université de Bordeaux / CNRS / Institut Polytechnique de Bordeaux,
ENSCBP – 16 avenue Pey Berland, 33600 Pessac, France
olivier.sandre@ipb.fr

Hydrophobically modified maghemite (γ-Fe_2O_3) nanoparticles were encapsulated within the membrane of poly(trimethylene carbonate)-b-poly(L-glutamic acid) (PTMC-*b*-PGA) block copolymer vesicles using a nanoprecipitation process. This formation method gives a simple access to highly magnetic nanoparticles (MNPs) (loaded up to 70 wt %) together with a good control over the vesicles size (100 to 400 nm). The simultaneous loading of maghemite nanoparticles and doxorubicin was also achieved by nanoprecipitation. The deformation of the vesicle membrane under an applied magnetic field has been evidenced by small angle neutron scattering. These superparamagnetic hybrid self-assemblies display enhanced contrast properties that open potential applications for Magnetic Resonance Imaging. They can also be guided in a magnetic field gradient. The feasibility of controlled drug release by radio-frequency magnetic hyperthermia was demonstrated in the case of encapsulated doxorubicin molecules, showing the viability of the concept of magneto-chemotherapy. These magnetic polymersomes can be used as efficient multifunctional nano-carriers for combined therapy and imaging.

References:

[1] S. Lecommandoux, O. Sandre, F. Chécot, J. Rodriguez-Hernandez, R. Perzynski, Adv. Mat, 17 (2005), 712-718.
[2] S. Lecommandoux, O. Sandre, F. Chécot, J. Rodriguez-Hernandez, R. Perzynski, Journal of Magnetism and Magnetic Materials 300 (2006), 71-74.
[3] S. Lecommandoux, O. Sandre, F. Chécot, R. Perzynski, Progress in Solid State Chemistry, 34 (2006), 171-179.
[4] C. Sanson, J-F. Le Meins, C. Schatz, A. Soum, S. Lecommandoux, Soft Matter, 6 (2010), 1722-1730
[5] C. Sanson, C. Schatz, J-F. Le Meins, A. Brûlet, A. Soum, S. Lecommandoux, Langmuir 26 (2010), 2751-2760.
[6] C. Sanson, C. Schatz, J-F. Meins, A. Soum, E. Garanger, J. Thévenot, S. Lecommandoux. Journal of Controlled Release, 147 (2010), 428-435.
[7] C. Sanson, O. Diou, J. Thévenot, E. Ibarboure, A. Soum, A. Brûlet, S. Miraux, E. Thiaudière, S. Tan, A. Brisson, V. Dupuis, O. Sandre, S. Lecommandoux, ACS Nano, Published online (2011), doi: 10.1021/nn102762f.

Figures:

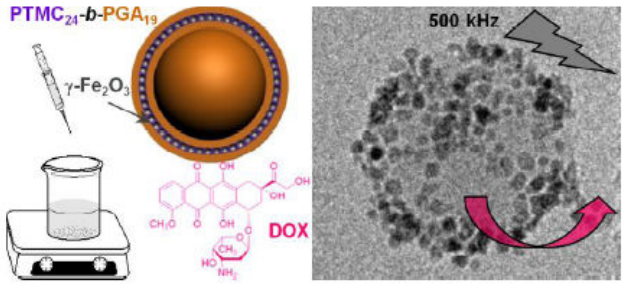

Figure 1: *Left: Sketch of dually-loaded vesicles prepared by addition of an aqueous buffer into a mixture of PTMC-b-PGA copolymer, hydrophobically coated magnetic nanoparticles and doxorucin drug. Right: Cryo-TEM image of vesicle showing the dense mantle of MNPs, which excitation by a radiofrequency magnetic field transmits heat locally to membrane and accelerates the DOX release.*

ATOMIC-SCALE CONTROL OF MOLECULAR CONTACTS

Guillaume Schull[1], Thomas Frederiksen[2], Andrés Arnau[2,3,4], Daniel Sanchez-Portal[2,3], Mads Brandbyge[5], Natalia Schneider[6], Richard Berndt[6]

[1]Institut de Physique et Chimie des Matériaux de Strasbourg, UMR 7504 (CNRS -- Université de Strasbourg), 67034 Strasbourg, France
[2]Donostia International Physics Center (DIPC), 20018 San Sebastian, Spain
[3]Centro de Física de Materiales CSIC-UPV/EHU, Materials Physics Center MPC, 20080 San Sebastian, Spain
[4]Depto. Fisica de Materiales UPV/EHU, Facultad de Quimica, 20080 San Sebastian, Spain
[5]DTU Nanotech, Technical University of Denmark, DK-2800 Kongens Lyngby, Denmark
[6]Inst für Experimentelle und Angewandte Physik, Christian-Albrechts-Universität, 24098 Kiel, Germany
guillaume.schull@ipcms.u-strasbg.fr

The transport of charge through a conducting material depends on the intrinsic ability of the material to conduct current and on the charge injection efficiency at the contacts between the conductor and the electrodes. Exploring the single molecule limit in experiments requires control of the junction geometry. Scanning tunneling microscopy (STM) provides here a way to probe this parameter with atomic scale precision.

Using STM we will see that the current passing through a single molecule can be probed while changing, one by one, the number of atoms in the electrode that are in contact with a single molecule [1]. We show quantitatively that the contact geometry has a strong influence on the conductance. For C_{60}, this revealed a crossover from a regime in which the conductance is limited by charge injection at the contact to a regime in which the conductance is limited by scattering at the molecule. Thus, the concept of “good” and “bad” contacts, commonly used in macro-and mesoscopic physics, can also be applied at the molecular scale. In a second step, the transport properties of small chains made of two C_{60} trapped between the tip and the surface of a STM will be presented [2]. Here the orientation and electronic states of both molecules was characterized before connecting them with atomic-scale precision. The experimental results are complemented by first-principles transport calculations which give access to the distance-dependent nature of the inter-molecular electron transport and predict the evolution of the transport properties with molecular chain length. Finally, the properties of photons that are emitted at junctions bridged by a single metallic atoms [3,4] and the perspectives that it opens for molecular contacts will be evocated.

References:

[1] Schull G, Frederiksen T, Arnau A, Sanchez-Portal D, Berndt R. Nature Nanotec. 6, (2011) 23
[2] Schull G, Frederiksen T, Brandbyge M, Berndt R. Phys. Rev. Lett. 103, (2009) 206803
[3] Schull G, Néel N, Johansson P, Berndt R. Phys. Rev. Lett. 102, (2009) 057401
[4] Schneider N, Schull G Berndt R. Phys. Rev. Lett. 105, (2010) 026601

Figures:

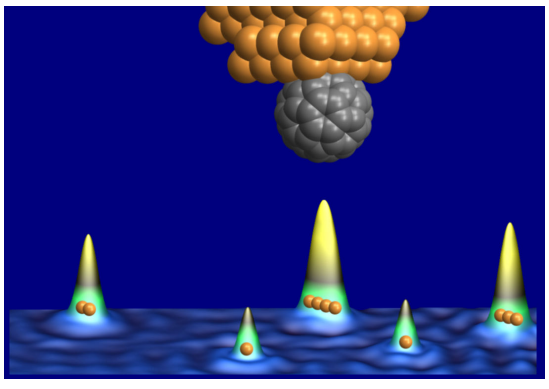

Figure 1: *Graphical representation of a scanning tunnelling microscope tip with a C_{60} molecule fixed to its apex, above a copper sample with five atomic scale electrodes engineered atom per atom.*

EFFECT OF PHONON CONFINEMENT ON HEAT DISSIPATION IN RIDGES

Pierre-Olivier Chapuis[(a),1,*], Mika Prunnila[(b)], Andrey Shchepetov[(b),1], Lars Schneider[(a)], Sampo Laakso[(b)], Jouni Ahopelto[(b)], and **Clivia M. Sotomayor Torres**[(a, c, d)]

[(a)]Institut Català de Nanotecnologia (ICN), Centre d'Investigacio en Nanociencia e Nanotecnologia (CIN2), Campus UAB, 08193 Bellaterra (Barcelona), Spain
[(b)]VTT Technical Research Center of Finalnd, PO Box 1000, 02044 VTT, Espoo, Finland
[(c)]ICREA, Institució Catalana de Recerca i Estudis Avançats, 08010 Barcelona, Spain
[(d)]Dept. of Physics, Universitat Autònoma de Barcelona, 08193 Bellaterra, Barcelona, Spain
[1]These authors contributed equally
olivier.chapuis@cin2.es

We have investigated experimentally the effect of lateral confinement of acoustic phonons in ridges as a function of the temperature. Electrical methods are used to generate phonons in 100nm large nanostructures and to probe the nanostructure temperature in the same time, what allows tracking the heat flux generated and its possible deviation to Fourier diffusive heat conduction.

It is now well-established that Fourier's law of heat diffusion in solids breaks down when device sizes reaches the nanometer-scale [1]. Detailed studies of the characteristic lengths where the law has to be replaced or modified are required as these lengths might depend on the considered device geometries.

We have fabricated special devices made of nanostructured ridges on top of planar substrate as represented on Figure 1. The top of a ridge is a wire made either of metal or of doped silicon that acts as a heater and as a thermometer in the same time. The lower part that supports the wire is made of an etched part of the wafer substrate. This type of structure enables to generate phonons in the ridge and to measure the heat flux flowing to the substrate.

Different electrical methods such as the 3ω method [2] are used to heat the wire. The goal is then to measure a wire-voltage component (dc or ac) proportional to the wire temperature. A model enables then to link the wire temperature to the heat flux transmitted to the substrate. In addition to the localized heat source effect due to the sub-mean free path size of the source [3], we have investigated experimentally the consequences of the fact that the source cannot be considered as a proper heat bath at equilibrium.

We have quantified the effect as a function of the two characteristic numbers that can be associated with the problem, namely the constriction Knudsen number describing the transmission of the phonons and the nanostructure Knudsen number characterizing the nonequilibrium of the source. We compare our results with those of a recent theoretical paper [4] based on the ballistic-diffusive equations. The determination of the mean free paths of phonons as a function of the frequency remains a key point due to the consequences for heat transport and thermal management [1].

We observe a strong decrease of the thermal conductance through the ridge in comparison to a prediction based on the Fourier diffusive as expected. But, more strikingly, we also observe a decrease in comparison to the ballistic prediction. We aim at ascribing part of this decrease to an effect of phonon confinement in the ridge.

Acknowledgements:

We acknowledge the support of EU FP7 projects NANOPACK and NANOPOWER. We also acknowledge the support of Spanish MICINN project ACPHIN.

References:

[1] D. G. Cahill, W. K. Ford, K. E. Goodson, G. D. Mahan, A. Majumdar, H. J. Maris, R. Merlin, S. R. Phillpot, J. Applied Physics 93, 793-818 (2003)
[2] D. Cahill, Rev. Scient. Instr. 61, 802 (1990)
[3] M.E. Siemens, Q. Li, R. Yang, K.A. Nelson, E.H. Anderson, M.M. Murnane, and H.C. Kapteyn, Nature Materials 9, 26 (2010)
[4] S. Volz and P.O. Chapuis, J. Applied Physics 103, 34306 (2008)

Figures:

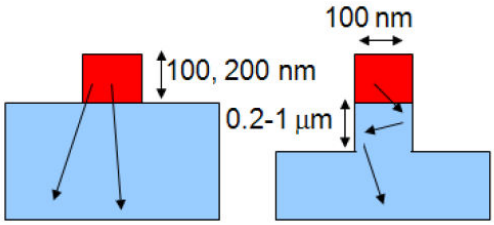

***Figure 1**: Schematic of the nanostructures*

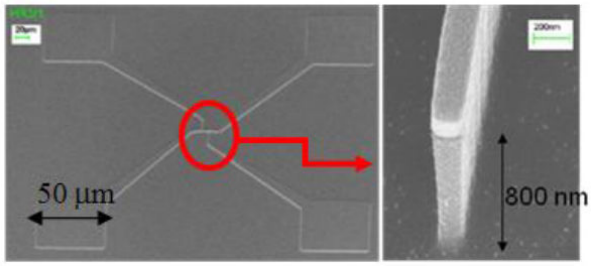

***Figure 2**: Electrical accesses and ridge before mask removal*

ORIGIN AND EVOLUTION OF POSITIVE EXCHANGE BIAS IN EPITAXIAL *(HCP)*CO/COO BI-LAYER STRUCTURES

A. K. Suszka, O. Idigoras and A. Berger

CIC nanoGUNE Consolider, Tolosa Hiribidea 76, E-20018 Donostia-San Sebastian, Spain
a.suszka@nanogune.eu

The phenomenon of unidirectional anisotropy of antiferromagnetic (AF)/ferromagnetic (FM) bi-layers, also referred to as exchange bias, is a prominent scientific and technological topic. Exchange biased magnetic thin films with uniaxial magnetic anisotropy (UA) are currently at the forefront of technology in magnetic recording and represent a challenge for scientific research. A relatively small number of experiments has been dedicated to study the exchange bias for systems with in-plane UA of the FM layer. Specifically, some recent studies focused on the competition of UA and exchange bias and revealed a distinct temperature dependence of uniaxial anisotropy at the interface of the FM layer that is in contact with the AF, for both out-of-plane [1] and in-plane magnetized thin films [2]. So far, however, very little work on the exchange bias has been done for Co/CoO structures in the presence of UA, even though Co/CoO-bilayers are the prototypical exchange bias system, and to our knowledge no previous work was dedicated to the study of (hcp) Co/CoO bi-layers with in-plane c-axis orientation [3].

Two types of multilayers with structure: Si-substrate/Ag(75nm)/Cr(50nm)/Co(12nm)/CoO(3nm) were grown by ultra high vacuum (UHV) sputtering. For one type of the multilayers, we modified the Co texture and consequently the UA by interrupting the epitaxial growth sequence in between the HFetched Si-substrate and Ag underlayer, specifically by exposing the substrate to an ultra-low power SiO_2 plasma for 30s prior to Ag deposition [4]. In this way, we fabricated samples with uniaxial (epitaxial structure) and isotropic (polycrystalline structure) magnetic characteristics as shown in figs. 1(a) and (b) respectively. X-ray diffraction studies confirm the Si(110)/Ag(110)/Cr(211)/Co(10$\underline{1}$0) structure for samples without SiO_2 interlayer [4]. CoO was formed by natural oxidation in both types of multilayers. Samples were characterised using magneto-optical Kerr effect setup (MOKE), superconducting quantum interference device (SQUID), X-ray diffraction, ellipsometry and Kerr microscopy.

We measured hysteresis loops for epitaxial and polycrystalline samples as a function of temperature in the easy (EA) and hard axis (HA) magnetization direction. Epitaxial multilayer shows higher values of exchange bias (H_{ex}) and blocking temperature (T_B) in comparison with polycrystalline structures. In addition to that, a positive exchange bias is measured for the epitaxial structures in a certain temperature window while it is not observed in polycrystalline samples. Increasing the magnitude of the cooling field (FC) results in a decrease of the positive Hex effect and causes a different transition temperature from positive to negative H_{ex}. We also find a direct relation between the asymmetry of the magnetization reversal process, and the enhancement of unidirectional anisotropy. Some previous reports suggested the existence of positive exchange bias due to anisotropic enhancement of the coercivity H_c [5]. This conclusion was originally supported by the existence of a peak in the coercivity around the positive H_{ex}. Here, we find a non-monotonous increase in the coercivity for the epitaxial sample. This is most pronounced in the hard axis magnetization direction (Figs. 2(a) and (b)). Changes in coercivity relate directly to the behavior of positive and negative switching fields as shown on figure 2 (c). Figure 2 (d) shows the extracted dm/dH of our hysteresis loops for different temperatures and reveals switching asymmetry near positive exchange bias. In current work we also analyze the magnetic characteristics of the EA for epitaxial structure and the exchange bias for polycrystalline sample. Each one of these cases shows different and unique evolution of exchange bias with varying temperature. The experimental results are analyzed in the framework of changes in magnetization states near interface of FM/AF and the influence of competition of uniaxial anisotropy and exchange bias on magnetization switching at various temperatures.

Acknowledgements:

We acknowledge funding from the ETORTEK Program, Project No. IE06-172, the Spanish Consolider-Ingenio 2010 Program, Project No. CSD2006-53 and the Basque Government fellowships No. BFI09.284.

References:

[1] E. Shipton, K. Chan, T. Hauet, O. Hellwig, and E. E. Fullerton, Appl. Phys. Lett. 95, 132509 (2009)
[2] M. Grimisditch, A. Hoffmann, P. Vavassori, H. Shi, and D. Lederman, Phys. Rev. Lett. 90, 257201 (2003)
[3] F. Radu, M. Etzkorn, R. Siebrecht, T. Schmitte, K. Westerholt, and H. Zabel, Phys. Rev. B 67, 134409 (2003)
[4] O. Idigoras, A. K. Suszka, J. M. Porro, P. Vavassori, and A. Berger, submitted to Phys. Rev. Lett.
[5] T. Gredig, I. N. Krivorotov, P. Eames and E. D. Dahlberg, Appl. Phys. Lett. 81, 1270 (2002)
[6] O. Idigoras, P. Vavassori, J. M. Porro, and A. Berger, J. Magn. Magn. Mater. 320, L57-L60 (2010)

Figures:

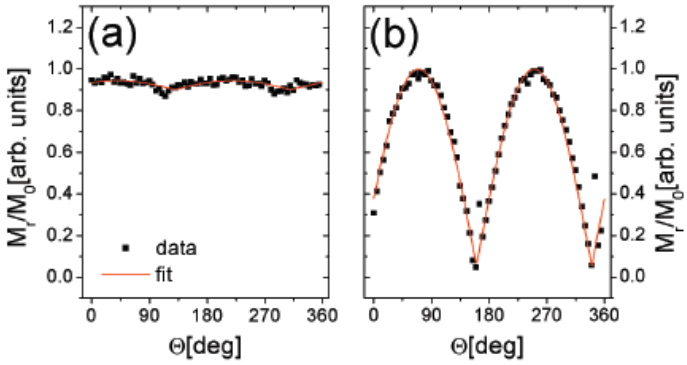

Figure 1: *Normalized remanent magnetization (M_r/M_0) as a function of magnetic field orientation angle Θ for a polycrystalline (a) and an epitaxial (b) Co/CoO sample, measured at room temperature. Red line is a fit to the data (M_r/M_0=a*abs(cos(Θ-ϕ))+c) following reference [6].*

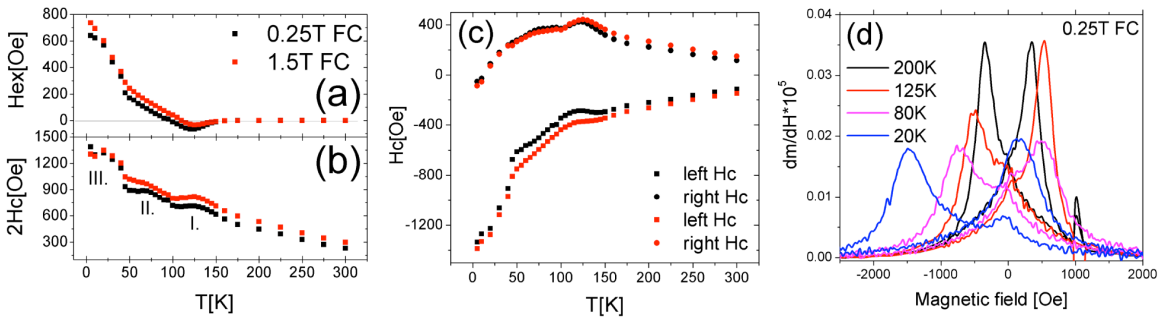

Figure 2: *Exchange bias (a) and coercivity (b) as a function of temperature measured in the hard axis magnetization direction on an epitaxial sample for two cooling field values (0.25T and 1.5T), (c) left and right coercivity as a function of temperature for the same sample and orientation cooled at 0.25T (black) and 1.5T (red). (c) field derivative of hysteresis loops for an epitaxial sample cooled at 0.25T at different temperatures, revealing a substantial switching asymmetry in the region of positive exchange bias.*

NOVEL PARADIGMS FOR BIOLOGICAL SENSING BASED ON NANOMECHANICAL SYSTEMS: FROM MICROCANTILEVERS TO NANOWIRES

Javier Tamayo, Eduardo Gil-Santos, Daniel Ramos, Priscila Kosaka, Valerio Pini, Johann Mertens, Sheila Gónzalez and Montserrat Calleja

Instituto de Microelectrónica de Madrid (CSIC), Isaac Newton 8 (PTM), Tres Cantos, Spain
jtamayo@imm.cnm.csic.es

The development of ultrasensitive protein spectrometers and ultrasensitive biological sensors will speed up the identification of disease biomarkers and their rapid detection [1,2]. Nanomechanical resonators have emerged as promising candidates for ultrasensitive mass sensors [3,4]. The continuous advancements in top-down micro- and nanofabrication techniques has made possible increasingly smaller nanomechanical resonators with detection limits in the subattogram range. Moreover, resonant nanowires and nanotubes fabricated by bottom-up methods can weigh masses below a zeptogram ($1.66\ 10^{-21}$ g). However, the implementation of these devices is hindered by several obstacles such as the need of operation in high vacuum, low specificity and low reproducibility and still little understanding of the effect of biomolecular adsorption on the mechanical properties of nanoresonators.

In this talk, I will present our recent developments oriented to apply nanomechanical systems for biological detection. In particular, I will present two novel paradigms for sensing that opens the door to develop ultrasensitive biological sensors. The first approach that is no longer depending on the extreme miniaturization of the devices is the use of coupled nanomechanical resonators fabricated by standard silicon technology [5,6] (Fig. 1). When the resonators are identical, the vibration of the eigenmodes is delocalized over the array. In a similar way to the Anderson's localization, the addition of the mass on one of the resonators leads to the spatial localization of the eigenmodes. Since vibration localization is insensitive to uniform adsorption, coupled nanomechanical resonators allows decoupling of unspecific and specific molecular adsorption in differentially sensitized resonators.

The second approach uses resonant nanowires/nanotubes and it is based on the fact that if a molecule alights on a perfectly axisymmetric resonant nanobeam, the frequency degeneration of the stochastic two-dimensional orbits is abruptly broken, and the vibration can be described as the superposition of two orthogonal vibrations with different frequency. The measurement of the frequency degeneration breakage enables the determination of the adsorbate's mass and stiffness, and the azimuthal direction from which the adsorbate arrives [7]. We experimentally demonstrate such sensing paradigm with resonant silicon nanowires, which serves to add kPa resolution in Young's modulus determination to their currently established zeptogram mass sensitivity. The proposed method provides a unique asset for ultrasensitive mass and stiffness spectrometry of biomolecules by using nanowire-like resonant structures.

References:

[1] Naik, A., Hanay, M., Hiebert, W., Feng, X. & Roukes, M. Towards single-molecule nanomechanical mass spectrometry. Nature Nanotechnology 4, 445-450 (2009).
[2] Mertens, J., Tamayo, J. et al. Label-free detection of DNA hybridization based on hydration-induced tension in nucleic acid films. Nature Nanotechnology 3, 301-307 (2008).
[3] Tamayo, J. Nanomechanical systems: Inside track weighs in with solution. Nature Nanotechnology 2, 342-343 (2007).
[4] Waggoner, P. & Craighead, H. Micro-and nanomechanical sensors for environmental, chemical, and biological detection. Lab on a Chip 7, 1238-1255 (2007).
[5] Spletzer, M., Raman, A., Wu, A., Xu, X. & Reifenberger, R. Ultrasensitive mass sensing using mode localization in coupled microcantilevers. Applied Physics Letters 88, 254102 (2006).
[6] Gil-Santos, E. et al. Mass sensing based on deterministic and stochastic responses of elastically coupled nanocantilevers. Nano letters 9, 4122-4127 (2009).
[7] Gil-Santos, E., Tamayo, J. et al. Nanomechanical mass sensing and stiffness spectrometry based on two-dimensional vibrations of resonant nanowires. Nature Nanotechnology 5, 641-645 (2010).

Figures:

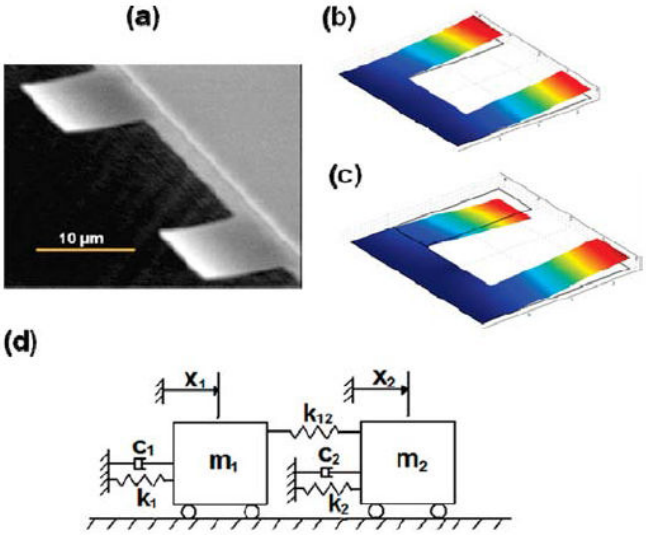

Figure 1: *(a) Scanning electron micrograph of a system of coupled cantilevers. The cantilevers were fabricated in low stress silicon nitride. The length, width, and thickness of the cantilevers were 25, 10, and 0.1 µm, respectively. The gap between the cantilevers is 20 µm. The structural coupling between the cantilevers arises from the overhang connecting the cantilevers at the base, which is about 8 µm long. (b) Symmetric and (c) antisymmetric mode of vibration of this coupled array. (c) A lumped parameter model for this coupled array.*

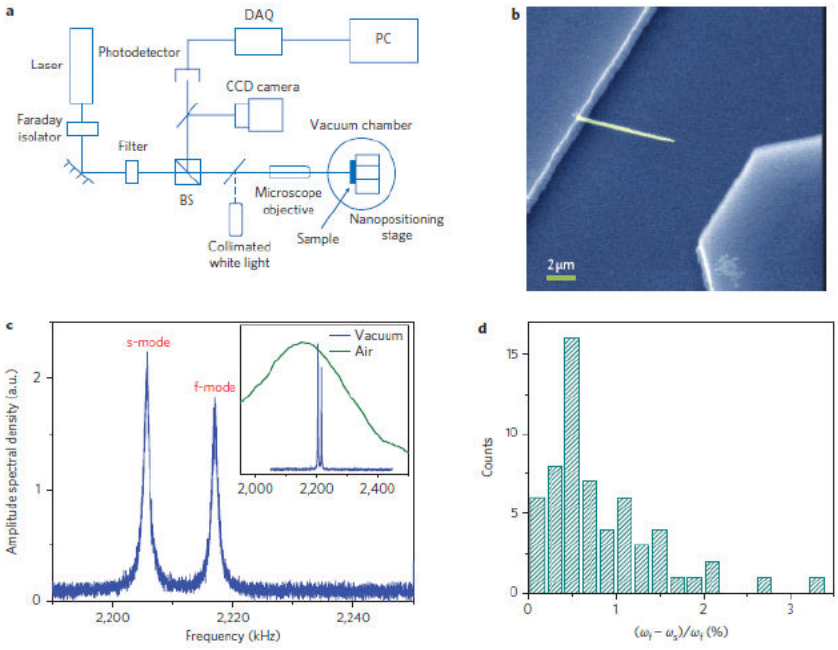

Figure 2: *Thermal displacement fluctuations of silicon nanowires. a, Schematic of the optical interferometer used to detect the out-of-plane nanowire vibrations. The nanowire sample was placed in a vacuum chamber at approximately 1× 10^{-6} torr and room temperature. The spot size was 0.7 µm and the incident power 0.5 mW. Picometre-scale modulation of the height of the nanowire above the substrate results in a measurable intensity modulation due to the interference between the light reflected from the nanowires and from the substrate.b, Scanning electron micrograph (SEM) of a typical nanowire used in this work. Nanowires anchored normal to the trench wall were selected, with lengths and diameters of 5–10 mm and 100–300 nm, respectively. c, A fast Fourier transform of the signal from the photodetector is dominated by the displacement thermal fluctuation of the nanowires. Only a single resonant peak can be seen in air (green line in inset), but two resonant peaks can be clearly seen in vacuum (blue lines). Depending on the nanowire dimensions, the resonance frequencies range from 2 to 6 MHz. s-mode and f-mode refers to the spliting of the resonance frequency into slower and faster vibration modes vibrating at orthogonal directions. d, Histogram of the relative frequency separation between the two close resonance peaks observed in vacuum.*

EXPLORING THE USE OF FILLED CARBON NANOTUBES FOR BIOMEDICAL APPLICATIONS

Gerard Tobias[a], Belén Ballesteros[b], Malcolm L.H. Green[c]

[a]Institut de Ciència de Materials de Barcelona (ICMAB-CSIC), Campus UAB, 08193 Bellaterra, Barcelona, Spain
[b]Centre d'Investigació en Nanociència i Nanotecnologia (ICN-CSIC), Campus UAB, 08193 Bellaterra, Barcelona, Spain
[c]Inorganic Chemistry Laboratory, University of Oxford, South Parks Road, OX1 3QR Oxford, UK
gerard.tobias@icmab.es

Carbon nanotubes (CNTs) have been advocated as promising agents for biomedical applications including *in vivo* imaging, tumour targeting and drug delivery systems. One added advantage of using nanotubes is that their inner cavity can be filled with a chosen payload whilst the outer surface can be modified to improve their dispersability and biocompatibility.

A key step towards the characterisation and application of filled CNTs is the complete removal of the large amount of unwanted external material present after the filling step, whilst preserving the encapsulated payload (of the same nature). An absence of species outside the CNTs will reduce the side effects during targeting. We have developed two complementary methodologies for the containment of materials inside single-walled carbon nanotubes (SWCNTs), namely by closing their ends by thermal annealing[1] and by using fullerenes as corks[2]. These nanocapsules (filled and sealed SWNTs) can then be readily purified by stirring the sample in a suitable solvent.

In the context of drug delivery systems we have investigated methods that allow a controlled discharge of the encapsulated payload by lowering the pH of the media. Here, we demonstrate that removable ''corking'' of SWCNTs in aqueous media using pH sensitive ''corks'' is feasible [3]. As a test for the successful containment and release of the filling material, we chose copper and uranium salts as the cargo, not for medical or related reasons but because the presence of copper into washings can be detected with high sensitivity by UV–vis spectroscopy, and because the heavy atoms of uranium can be easily detected in filled SWCNTs by high resolution transmission electron microscopy (HRTEM). Thus, in this ''proof-of-principle'' study we demonstrate the use of acid-sensitive functionalized fullerenes as removable ''corks'' for the containment and controlled release of the cargo contained within SWCNTs by lowering of the pH in aqueous media (Figure 1). It is well known that the pH of primary tumours and regions of inflammation and infection is lower than physiological.

We will also present recent results on the development of "hot" filled SWCNTs for *in vivo* radioemitter localization and imaging [4]. The nanocapsules were prepared by first filling the SWCNTs with $Na^{125}I$, followed by their sidewall functionalisation with carbohydrates (Figure 2). Short SWCNTs were employed in this study to further improve the biocompatibility of the materials. Effectively, the nanocapsules (filled SWCNTs with closed ends) guaranteed essentially zero leakage of the radionuclide and remained stable *in vivo* for extended periods. The sealing of iodide within single-walled carbon nanotubes enabled its biodistribution to be completely redirected from tissue with innate affinity (thyroid) to lung. Surface functionalization of these nanocapsules offers versatility towards modulation of biodistribution of the radioemitting crystals in a manner determined by the capsule that delivers them.

Acknowledgements:

We acknowledge support by Thomas Swan Ltd. and by a Marie Curie ERG European Community FP7.

References:

[1] L. Shao, G. Tobias, Y. Huh, M. L. H. Green, Carbon 44 (2006), 2855
[2] L. Shao, T.-W. Lin, G. Tobias, M. L. H. Green, Chem. Commun. (2008), 2164
[3] P. Luksirikul, B. Ballesteros, G. Tobias, M.G. Moloney, M.L.H. Green, Carbon 48 (2010) 1912
[4] S.Y. Hong, G. Tobias, K. T. Al-Jamal, B. Ballesteros, et al. Nature Materials 9 (2010), 485 (highlighted in News and Views: Nature Materials 9 (2010) 467)

Figures:

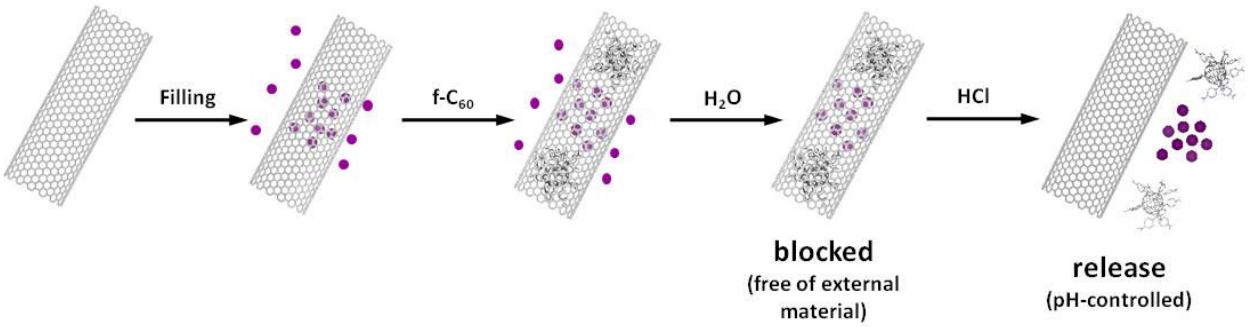

Figure 1: *Schematic representation of the use of functionalized fullerenes as removable corks for SWCNTs [3].*

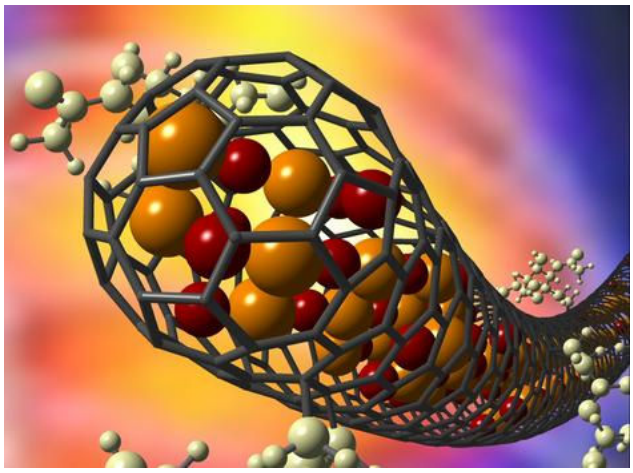

Figure 2: *Schematic representation of the "hot" nanocapsules developed encapsulation $Na^{125}I$ [4].*

NON VOLATILE MOLECULAR MEMORY DEVICES BASED ON SWITCHABLE AND BISTABLE SELF-ASSEMBLED MONOLAYERS OF ELECTROACTIVE ORGANIC RADICALS

Jaume Veciana[a], Cláudia Simão[a], Marta Mas-Torrent[a], Núria Crivillers[a], Vega Lloveras[a]
Juan Manuel Artés[b], Pau Gorostiza[b], Concepció Rovira[a]

[a]Institut de Ciència de Materials de Barcelona (CSIC)-Networking Research Center on Bioengineering, Biomaterials and Nanomedicine (CIBER-BBN), Bellaterra, E-08193, Spain
[b]Institute for Bioengineering of Catalonia (IBEC), Institució Catalana de Recerca i Estudis Avançats (ICREA). Baldiri Reixac 15-21, E-08028 Barcelona, Spain, Networking Research Center on Bioengineering, Biomaterials and Nanomedicine (CIBER-BBN). Universitat de Barcelona. C/ Martí i Franquès, 1. Barcelona, E-08028 Barcelona, Spain.
vecianaj@icmab.es

The increasing interest in miniaturizing electronic devices to achieve denser circuits and memories will eventually entail the utilization of molecules as active components. In particular, self-assembled monolayers attached to substrates appear as suitable candidates in *Molecular Electronics* for the development of switchable and bistable memory devices based on electroactive molecules grafted on surfaces.[1] Polychlorinated triphenylmethyl (PTM) radicals are persistent electroactive organic radicals that can be easily reduced to the corresponding anionic species which also show a high stability in solution. Both species exhibit different optical and magnetic properties and can be reversibly interconverted in solution.[2] In addition such radicals can be covalently grafted on surfaces of different nature (Au, SiO_2) where they keep their bistability and switchability without degradation.[3-5]

Here, we describe the functionalization of transparent and conducting ITO surfaces with appropriately functionalized PTM radicals. Such hybrid organic/inorganic surfaces behave as chemical and electrochemical redox switches with bistable optical (absorption and fluorescence) and magnetic responses exhibiting an exceptionally high long-term stability and excellent reversibility and reproducibility. Moreover, such hybrid surfaces can be patterned as well as electrochemically locally addressed enabling to write-store-read information reversibly on the patterned clusters of electroactive molecules. One example of such a nonvolatile molecular memory device will be presented and discussed.[6]

References:

[1] Liu, Z. et al., Science 302 (2003) 1543
[2] Veciana, J., Ratera, I. in "Stable Radicals: Fundamentals and Applied Aspects of Odd-Electron Compounds", Ch. 2., Ed. by Hicks, R.G., John Wiley & Sons, Ltd, 2010
[3] Mas-Torrent, M. et al., J. Mater. Chem. 19 (2009) 1691
[4] Crivillers, N. et al. J. Am. Chem. Soc., 130 (2008) 5499
[5] Crivillers, N. et al. Adv. Mater. 21 (2009) 1177
[6] Simão, C., et al. Nature Chem., in press (2011)

Figures:

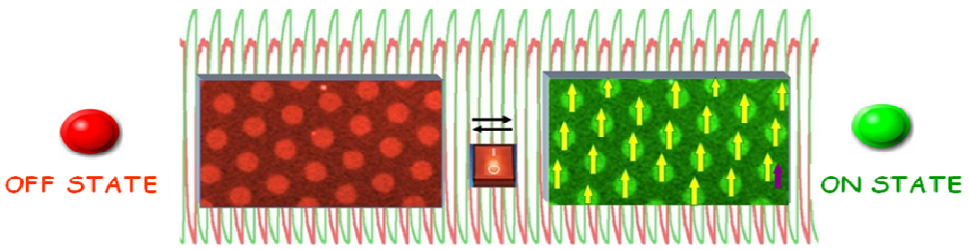

Figure 1: *Schematic representation of the reversible switching between the two states of the hybrid organic/inorganic surfaces based on electroactive organic radicals*

STM AND LEEM CHARACTERIZATION OF THE INTERACTION BETWEEN MAGNESIUM GROWN ON RU(0001) AND HYDROGEN

L. Vergara[1], B. Santos[1], T. Herranz[2], M. Monti[1], K. F. McCarty[3], J. de la Figuera[1]

[1]Instituto de Química-Física "Rocasolano", CSIC, C/ Serrano 119, 28006 Madrid, Spain
[2]Instituto de Catálisis y Petroleoquímica, CSIC, 28049 Madrid, Spain
[3]Sandia National Laboratories, 7011 East Avenue, Livermore, California 94550, USA
lvergara@iqfr.csic.es

Magnesium is a readily available non-toxic metal whose hydride (MgH_2) is being studied as a potential hydrogen storage medium, owing to its large content of 7.6% by weight of hydrogen. Magnesium is known to grow as almost perfect thin films on many substrates; in some instances, like in the case of refractory metals, with very sharp interfaces. Since a layer of $MgO/Mg(OH)_2$ grows onto the magnesium surface when it is exposed to air, changing its reactivity, the understanding of the interaction between the surface of the magnesium layer and hydrogen is of the utmost importance. Most of the few works that have been devoted to the preparation of magnesium on refractory metals study its growth on W(110) substrates [1,2]. A study about the epitaxial growth of magnesium on Ru(0001) using low-energy electron diffraction (LEED) [3] reported that magnesium keeps its own in-plane spacing when growing on such substrate, owing to the large mismatch between their respective in-plane lattice spacings (around 18%). This results in a moiré pattern on the magnesium surface, and an overlayer film without significant strain. Additionally, not much has been published about scanning tunnel microscopy (STM) characterization of epitaxial growth of magnesium up to two monolayers at room temperature.

This work is a continuation of our recent studies about the growth and hydrogenation of magnesium on Ru(0001) substrates in ultra-high vacuum [4,5]. The characterization techniques we have employed are STM and low-energy electron microscopy (LEEM), an in-situ technique that provides real-time observations at different temperatures with spatial resolution of nanometres. Magnesium was grown to a thickness of one to ten atomic layers by evaporating a rod heated by electron bombardment at a pressure in the low 10^{-10} Torr range, with a typical deposition rate of about one monolayer per minute. Up to a temperature of 430 K, the films present a layer-by-layer growth with three levels exposed at the most. The submonolayers of magnesium, detected only by STM and only in the first two atomic layers, show a moiré pattern with a periodicity of 12 Å, as can be seen in figure 1. Dark-field LEEM experiments show that films with a higher number of monolayers present stacking faults and, on stepped areas, screw dislocations are observed by STM (see figure 2), owing to the mismatch of the step heights of magnesium and ruthenium in these areas. Electron reflectivity shows quantum size effects in the unoccupied bands, indicating an abrupt interface between magnesium and ruthenium for the thicker films. Additionally, we have studied the exposure to H and H_2 of the growing films by LEEM and STM. While growth in an H_2 atmosphere produces no significant change in the magnesium films, LEEM measurements have demonstrated the nucleation of dark islands as soon as H is fed into the vacuum chamber; further exposure to H leads to their almost covering completely the field of view. Using a mass spectrometer, we have performed thermal desorption experiments in these dark islands (see figure 3), which show that hydrogen is the only gas desorbed, with a sharp peak around 470 K coinciding with the disappearance of the islands in the LEEM images. At higher temperatures, only a faint trace of them remains on the surface.

References:

[1] F. Schiller, M. Heber, V.D.P. Servedio and C. Laubschat, Phys. Rev. B 70 (2004), 125106.
[2] L. Aballe, A. Barinov, A. Locatelli, T. Mentes and M. Kiskinova, Phys. Rev. B 75 (2007), 115411.
[3] H. Over, T. Hertel, H. Bludau, S. Pflanz and G. Ertl, Phys. Rev. B 48 (1993), 5572.
[4] T. Herranz, K.F. McCarty, B. Santos, M. Monti and J. de la Figuera, Chem. Mat. 22 (2010), 1291.
[5] T. Herranz, B. Santos, K. F. McCarty and J. de la Figuera, Surf. Sci., in press.

Figures:

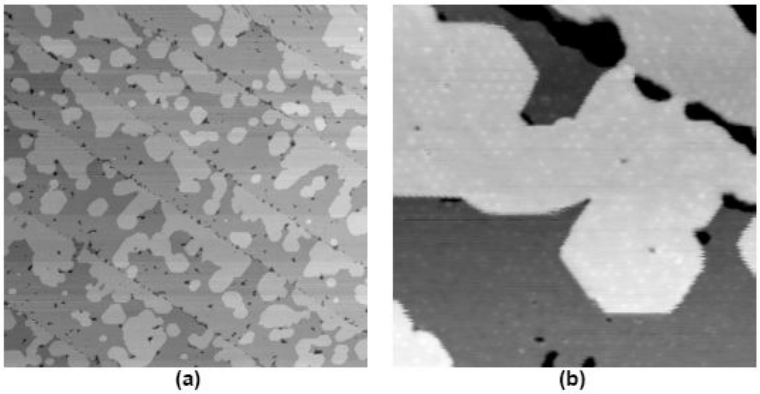

Figure 1: *STM images of a magnesium film with an almost complete first monolayer and islands of the second monolayer. a) 4500-Å wide image, and b) 550-Å wide image, in which the moiré in the islands can be seen.*

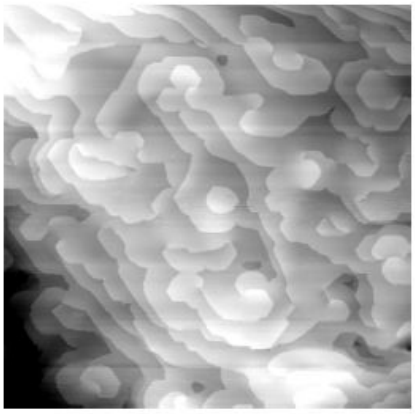

Figure 2: *Screw dislocation in stepped areas seen by STM (image width and height: 3500 Å).*

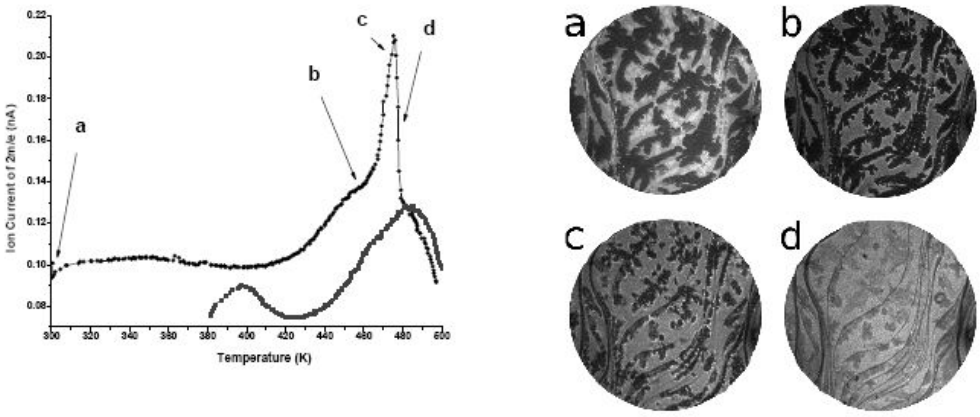

Figure 3: *Thermal desorption measurements carried out in the dark islands of magnesium films with ten atomic layers grown under exposure to H2 (lower curve) and H (upper curve). Labelled temperatures in the upper curve correspond to each of the LEEM images on the left (field of view is of 15 μm).*

NANOBIO&MED 2011

INDEX: INVITED CONTRIBUTIONS

INDEX: INVITED CONTRIBUTIONS (SUDOE TRAIN2 SESSION)

INDEX: INVITED CONTRIBUTIONS (COST BIO-INSPIRED SESSION)

INDEX: INVITED CONTRIBUTIONS (CIBER BBN SESSION)

INDEX: KEYNOTE CONTRIBUTIONS

INDEX: KEYNOTE CONTRIBUTIONS (CIC BIOMAGUNE SESSION)

INDEX: KEYNOTE CONTRIBUTIONS (CIBER BBN SESSION)

INDEX: ORAL CONTRIBUTIONS

INDEX: ORAL CONTRIBUTIONS (CIBER BBN SESSION)

INDEX: ORAL CONTRIBUTIONS (SUDOE TRAIN2 SESSION)

INDEX: ORAL CONTRIBUTIONS (COST BIO-INSPIRED SESSION)

ALPHABETICAL ORDER

I: Invited / IS: Invited SUDOE TRAIN2 Session / IC: Invited COST Bio-Inspired Session / IB: Invited CIBER BBN Session / K: Keynote / KG: Keynote CIC biomaGUNE Session / KB: Keynote CIBER BBN Session / O: Oral / OB: Oral CIBER BBN Session / OS: Oral SUDOE TRAIN2 Session / OC: Oral COST Bio-Inspired Session

I: Invited / IS: Invited SUDOE TRAIN2 Session / IC: Invited COST Bio-Inspired Session / IB: Invited CIBER BBN Session / K: Keynote / KG: Keynote CIC biomaGUNE Session / KB: Keynote CIBER BBN Session / O: Oral / OB: Oral CIBER BBN Session / OS: Oral SUDOE TRAIN2 Session / OC: Oral COST Bio-Inspired Session

I: Invited / IS: Invited SUDOE TRAIN2 Session / IC: Invited COST Bio-Inspired Session / IB: Invited CIBER BBN Session / K: Keynote / KG: Keynote CIC biomaGUNE Session / KB: Keynote CIBER BBN Session / O: Oral / OB: Oral CIBER BBN Session / OS: Oral SUDOE TRAIN2 Session / OC: Oral COST Bio-Inspired Session

NANOBIO&MED 2011

ABSTRACTS
ALPHABETICAL ORDER

TO REACH TRANSLATIONAL OBJECTIVES: THE BIOENGINEERING CHALLENGE WITHIN CIBER-BBN

Jordi Aguiló*, Rosa Villa**

*Departament de Microelectrónica i Sistemas Electrónics, Universitat Autònoma de Barcelona
**Instituto de Microelectrónica de Barcelona, Campus UAB, Bellaterra, Spain
Jordi.Aguilo@uab.es

For years, bioengineers have been trying to bring together knowledge and technologies from the engineering world and knowledge and life sciences from the biomedical world with a clear objective: to contribute to the advancement of health through the adaptation and development of technologies

- For easy, accurate and non invasive diagnoses
- To enhance predictive and preventive know-how and capacities
- To develop high technology based devices for local or remote on-line monitoring of relevant vital parameters by having multimodal functionalities suitable for clinical use
- To develop new instrumentation and models allowing scientific progresses and a more in depth knowledge of living mechanisms. Micro-Nano-Bio systems can help to know and interact with high level behavior such as learning mechanisms or psychological diseases up to, on the micro-nano side, to unlock specific aspects of cellular metabolism, membrane structures or gene behaviors.
- To propose and validate new therapies coming from the new knowledge and new available technologies.
- To propose and validate new devices and systems allowing functional recovery and improvement
- To develop technologies and devices to help developing and emerging fields such as biotechnology, cellular and molecular engineering, etc.

Following these main lines, the Biomedical Applications Group, GAB, today within the CIBER-BBN is trying to take advantage of its own technological facilities and its scientific and technical know-how, to transform the innovation possibilities of micro-devices and related technologies into successful commercial biomedical products and advanced applications.

In the recent past the most relevant work of GAB has been the development of microsystem devices to monitor relevant heart parameters during open heart surgery, to measure graft viability on transplants, to contribute to functional recovery of blind people and to set-up the sensoring modules on a telemedicine application.

Concerning technology, a service of micro and nano fabrication including a carbon nanotube growth service has been set-up.

Concerning applications, today and in the near future we are working on the development of microsystem devices and instrumentation to measure the osteointegration level in implants, the degree of liver steatosis, the corneal endothelial permeability through a non-invasive way, to detect and to remove biofilms and the detection of p53-antibodies for early cancer prognostic. We are also taking the first steps in some other domains such as instrumentation to measure osteoporosis, to give objetive measurement of some psychic and somatic diseases and on the development of micro-nano systems for multifunctional stents and catheters.

HOW USE MICRO STRUCTURED SCAFFOLDS AND NANO TAGS TO CONTROL CELL DIFFERENTIATION AND IMPROVE TISSUE REGENERATION

Jose Iñaki Alava, Nerea Garagorri, Patricia Gracía Parra

Tecnalia Research and Innovation Co. Ciber BBN, ITUS-INASMET group, Paseo Mikeletegui 2, San Sebastián –Donostia, 20009, Spain
inaki.alava@tecnalia.com

Furthermore, the extracellular matrix plays a key role in controlling the differentiation of progenitor cells into the cell lines that will be replaced. Depending on the signals that these cells receive from their environment, their capacity for differentiation is enhanced or limited. In last 15 years, many researchers have tried to control neural growth and differentiation by using a wide range of approaches - micropatterned scaffolds [1], conductive biomaterials [2], electrospining [3] and many others [4,7,8,9] The appearance in 2002-2003 of new micro-technologies such as microcontact printing and others in the field of neurobiology, (we will comment on them in the next paragraph) have led to competition aimed at obtaining optimum micro (or nano) patterning of guidance molecules for neural cell growth and differentiation [4].

With the appearance of nanotechnology on the scene, the biocompatibility and special properties of some nanoparticles have led to the use of single wall carbon nanotubes in cell cultures [5] as a way of improving neural signal transfer [6]. In 2006, multiple-channel biodegradable scaffolds were used to promote spinal cord regeneration [7] with Schwann-cells as feeder-cells

The ability to replicate patterns at the micro to nanoscale is crucially important for the progress of micro and nanotechnologies and the study of nanosciences. The planar manufacturing technology used by the semiconductor industry means that integrated circuits are built by stacking one layer of circuit elements on top of another. Each layer is manufactured according to a sequence of well-characterized processes. Lithography is used over and over again to create desired patterns in all these processes. Considerable industrial effort has been devoted to the leading-edge optical methods and the so-called next generation lithography (NGL) techniques, exposing the material to energy beams from UV, electron beam, ion-beam or x-ray sources. However, there are many other non-traditional microelectronic applications that require nanoscale features and demand low-cost nano and micro patterning technologies. One of the main areas is the biological field, with applications in micro and nanofluidic devices for labs-on-a-chip, biosensors, DNA or protein arrays and the alignment of biomaterials for cell patterning or tissue engineering related applications. Surfaces with micro and nanopatterns are being used as cell culture substrates to develop new assays for monitoring cell adhesion and cell proliferation or differentiation on different surfaces [10,11].

Patterned surfaces and their chemical landscape provide cues for cells to attach, migrate and assemble into functioning tissue. Tissue engineering is a multidisciplinary/interdisciplinary field that applies the principles of biology and engineering to develop tissue substitutes that restore, maintain, or improve the function of diseased or damaged human tissues. One approach to tissue engineering involves seeding biodegradable polymeric scaffolds with donor cells and/or growth factors and then culturing and implanting the scaffold to induce and direct the growth of new, healthy tissue. Unfortunately, current polymeric biodegradable scaffolds have several drawbacks: However, most biodegradable polymers being used in clinical practice do not exhibit clearly biocompatible behaviour and their mechanical properties are usually not enough to allow them to be used for load bearing parts of the body. No single material, however, can satisfy all the goals required for creating optimum scaffolding. On the other hand, the extra cellular matrix (ECM) is a complex and strange material. In fact, is impossible for a single material to mimic all ECM properties. A composite multi-material matrix is the natural solution to the different requirements of the wide range of ECMs needed for tissue regeneration [12]. Therefore, the incorporation of nanoparticles such as carbon nanotubes or carbon nanofibers and nanohidroxiapatite to the polymer matrix for increasing the safety of the polymer appears to be very important [13]. We show some examples of micro-structured scaffolds, with nano-tags (molecular signals), that may be used for cell differentiation and tissue repair.

References:

[1] Schmalenberg, K.E., Uhrich, K.E., Biomaterials 26, (2005), 1423-1430
[2] George, P.M., Lyckman A.W., LaVan, D.A., Hegde, A., Leung, Y., Avasare, R., Testa, C., Alexander, P.M., Langer, R., Sur, M., Biomaterials, 26, ,(2005), 3511-3519
[3] Yang, F., Murugan, R., Wang, S., Ramakrishna, S., Biomaterials, 26, (2005), 2603-2610.
[4] Oliva, A.A. Jr, James C.D., Kingman, C.E.,Craighead, H.G.,Banker, G.A., Neurochemical Research, Vol 28, (2003), 11,1639-1648.
[5] Gheih, M.K., Sinani, V.A., Wicksted, J.P., Matts, R.L., Kotov, N.A. Adv. Mater. 17, (2005), 2663-2670.
[6] Lovat, V. Pantarotto, D., Lagostena, L., Cacciari, B., Grandolfo, M., Righi, M., Spalluto, G., Prato, M., Ballerini, L. Nano Letters, Vol 5, 6, (2005), 1107-1110.
[7] Moore, M.J., Friedman J.A., Lewellyn, E.B., Mantila, S.M., Krych, A.J., Ameenuddin, S., Knight, A.M., Lu, L., Currier, B.L., Spinner, R.J., Marsh, R.W., Windebank, A.J., Yaszemski, M.J., Biomaterials, 27, (2006), 419-429.
[8] Recknor, J.B., Sakaguchi, D.S., Mallapragada, S.K., Biomaterials 27. (2006), 4098-4108.
[9] Tsai, E.C., Dalton, P.D., Shoinet, M.S., Tator C.H., Biomaterials.27. (2006), 519-533
[10] Falconnet D. et al., Biomaterials 27, (2006) 3044-3063.
[11] Zhang SG, et al, Biomaterials 20, (1999), 1213-20.
[12] Alava,J.I., Jurado, M.J., García, A., and Murua O. Joint Meeting of the Tissue Engineering Society International and the European Tissue Engineering Society, Congress Abstracts, Lausanne, Switzerland, (2004).
[13] Meike van der Zande, Balaji Sitharaman, X. Frank Walboomers, Lesa Tran, Jeyarama S. Ananta, Andor Veltien, Lon J. Wilson, Jose Inaki Alava, Arend Heerschap, Antonios G. Mikos, and John A. Jansen. Tissue Engineering: Part C Volume 17, Number 1, (2011), 19-26

THERAPEUTIC NANOCONJUGATES

Fernando Albericio, Miriam Royo

CIBER-BBN, Networking Centre on Bioengineering, Biomaterials and Nanomedicine Barcelona Science Park, 08028-Barcelona, Spain

Therapeutic Nanoconjugates and Drug Delibery Systems are one of the key strategic lines of the CIBER-BBN.

As it is well known, the number of new chemical and biological entities being accepted by the Food and Drug Administration is stabilized around 20-30 every year. This relatively low number is due to several factors, but one of the main reasons in the poor ADME properties showed by compounds that previously had been good in vitro activity

To improve this situation, several approaches have been used: (i) preparation of therapeutic conjugates that are able to protect the drug until it reaches the target; (ii) preparation of conjugates bearing nanovectors with the objetove of reaching more efficiently the target.

Our laboratories have developed a robust synthetic platform mainly based in peptides able to address the problem mentioned above. Herein, multifunctional polyethylenglycol-based dendrimers for drug delivery; γ-proline based foldamers as cell penetrating peptides; and gold nanoparticles; and multifunctionalized gold nanoparticles with peptides targeted to peptide receptor of a tumour cell line will be discussed.

References:

[1] Marcelo J Kogan, Ivonne Olmedo, Leticia Hosta, Ariel R. Guerrero, Luis J. Cruz, Fernando Albericio Peptides And Metallic Nanoparticles For Biomedical Applications. Nanomedecine, 2, 287-306 (2007).

[2] Leticia Hosta, Mateu Pla-Roca, Jordi Arbiol, Carmen López-Iglesias, Josep Samitier, Luis J. Cruz, Marcelo Kogan, Fernando Albericio. Conjugation of Kahalalide F with gold nanoparticles to enhance in vitro antitumoral activity. Bioconjugate Chem., 20, 138-146 (2009).

[3] Leticia Hosta-Rigau, Ivonne Olmedo, Jordi Arbiol, Luis J. Cruz, Marcelo J. Kogan, andFernando Albericio Multifunctionalized Gold Nanoparticles with Peptides Targeted to Gastrin-releasing Peptide Receptor of a Tumour Cell Line. Bioconjugate Chem, 21, 1070-1078 (2010).

[4] Simon Guerrero, Eyleen Araya, Jenny Fiedler, J. Ignacio Arias, Carolina Adura, Fernando Albericio, Ernest Giralt, Jose Luis Arias, M. Soledad Fernández, and Marcelo J. Kogan. Improving the Brain Delivery of Gold Nanoparticles by Conjugation with an Amphipathic Peptide. Nanomedicine, 5, 897-913 (2010).

TISSUE ENGINEERING FOR LUMBAR SPINAL FUSION IN SHEEP

J. Becerra[1,2], MD Cuenca-López[1,2], S. Gómez[3], P. Zamora-Navas[4,2], E. Guerado[5,2], JA Andrades[1,2]

[1]Dep of Cell Biology, Genetics and Physiology, Faculty of Sciences, Univ of Málaga, Málaga, Spain
[2]Networking Biomedical Research Center in Bioengineering, Biomaterials and Nanomedicine (Ciber-bbn)
[3]Department of Pathological Anatomy, Faculty of Medicine, University of Cádiz, Spain
[4]Service of Orthopaedic Surgery and Traumatology, V. Victoria University Hospital, Málaga, Spain
[5]Division of Orthopaedic Surgery and Traumatology, Hospital Costa del Sol. Marbella, Spain
becerra@uma.es

Posterior lumbar spinal fusion is nowadays a very standardized surgical technique worldwide. The intervention consists of two main steps, a firm fixation by a hardwork instrumentation to provide mechanical stability, and the addition of a biological substance for bone formation enhancement. Grafting enhances bone fusion, and therefore permanent stability, being considered bone autograft as the gold standard. The goals for bone-graft substitutes are to match fusion rates with autologous bone grafting techniques, while avoiding the morbidity of bone graft harvest and extending the quantity of available graft material. So far, there is a long list of bone graft substitutes [1], and most of them need a carrier to be administrated in the surgical field. Anyway, spinal fusion models are particularly unique, compared to other types of bone repair. Spinal fusion requires not to recreate original anatomy but the formation of a heterotopic bone bridge where usually bone does not exist. This may be the cause of the high clinical failure rate, above 35% [2]. Allograft as substitute/carrier is an important osteoinductive and osteoconductive agent but it has been especially claimed that it can provoke disease transmission and immunogenicity [3].

Since osteogenesis is exclusively conducted by bone cells, a very important strategy when dealing with bone substitutes, consists of addressing research projects u-sing osteogenic cells as bone marrow (BM) mesenchymal stem cells (MSCs). Two main lines have been maintained during the last years: molecular stimulation by a growth factor-mediation fashion (BMP-2 and BMP-7) [4,5], and transplantation of cells after amplification and committement [6]. BMPs have demonstrated good fusion rates but questions including high cost, high dose needed and some adverse effects, make them a non-definitive therapeutic tools [7]. Regarding cells, since several types of stem cells are susceptible to in vitro differentiate into multiple skeletal lineages, and are able to form bone, when using with the appropriate scaffold, tissue engineering looks like a good substitute for auto- and allograft in orthopedic surgery [8]. Nevertheless, clinical and animal experimental models research have had very important methodological burdens. On the one hand, most of laboratory work have been made in rodent and lagomorphs, species behaving far away, better than human as far as osteogenesis is concerned; further experimental model did not take into account mechanical situations as in human. Anyway, tissue engineering of bone, by combining osteogenic cells with osteoconductive scaffolds, has not yet yielded any clinically useful applications so far.

We have created an experimental model in a large animal model, the sheep, trying to reproduce what is made in human, a mechanical stabilization by a screwed transpedicular lumbar spinal instrumentation, together with the addition of BM committed MSCs adsorbed on hydroxyapatite (HA).

Surgical procedure. Spinal process from L2-L6, laminae, facet joints, and transverse processes were neatly denudated and prepared for arthrodesis. After that, stainless steel pedicular screws (Xia®, Stryker™) were introduced. Bone decortication was acted upon lateral aspect of articular and transverse processes until some bleeding bone could be seen.

Groups. A group of 20 sheep (female, 3-4 year-old, weighing 50-70 kg) received autograft into the right side (AUTO) and allograft on the left one (ALO). Another 20 sheep received HA with MSCs on the right side (HA+cls), and HA alone on the left one (HA) as control.

Cell product. Twenty milliliters of BM aspirates were harvested. The mononuclear cells fraction were plated at a density of 10x106 cells per 100 mm plate in complete culture medium (DMEM, 10% FBS, 1% Penicillin, 0,5% Amphotericin, 1.25% Glutamine, and 1ng/ml FGF-2) and incubated at 37ºC, 95% humidity, and 5% CO_2. The medium was changed three times a week and the cells at passage 1

were cultured for three weeks. At the end of the culture period, the cells were incubated for 3 days in culture medium supplemented with dexametasone and β-glycerophosphate to help with the osteogenic differentiation.

Results have shown that, although autograft obtained better values for fusion than allograft, there was no statistical significance difference between autograft and allograft. Further, autograft and allograft accomplished a better bone formation rate than committed stem cells. Hydroxyapatite alone produced the worst results both in regard to the amount of bone formed as the rate of spinal fusion. Since *in vitro and in vivo* studies with small animal models have shown that this construct displayed a very strong osteogenic commitment, we aim to improve the implant in sheep, perhaps by increasing its, the number of cells per volume unit, and even introducing certain improvements to the scaffold.

References:

[1] Pneumaticos SG, Triantafyllopoulos GK, Chatziioannou S, Basdra EK, Papavassiliou AG. Trends Mol Med. 2010 Dec 30. [Epub ahead of print]
[2] Reid JJ, Johnson JS, Wang JC. J Biomech. 11;44(2) (2011):213-20
[3] Mroz TE, Joyce MJ, Steinmetz MP, Lieberman IH, Wang JC. J Am Acad Orthop Surg. 16(10) (2008):559-65.
[4] Rihn JA, Makda J, Hong J, Patel R, Hilibrand AS, Anderson DG, Vaccaro AR, Albert TJ. Eur Spine J. 18(11) (2009):1629-36.
[5] Leach J, Bittar RG. J Clin Neurosci. 16(11) (2009):1417-20.
[6] Miyazaki M, Zuk PA, Zou J, Yoon SH, Wei F, Morishita Y, Sintuu C, Wang JC. Spine (Phila Pa 1976). 15;33(8) (2008):863-9.
[7] Hsu WK, Wang JC. Spine J 8 (2008): 419–425.
[8] Bianco P, Robey PG, Simmons PJ. Cell Stem Cell 2 (2008): 313–319.

Figures:

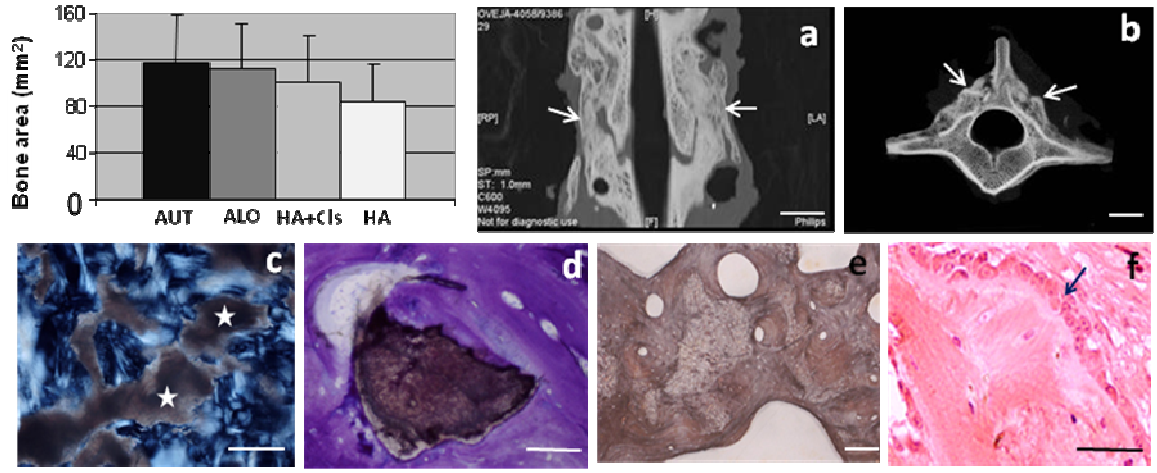

Figure 1: *Graph showing bone area formed in the different types of implants. a) Coronal view (TAC) of the artrodesed segments showing fusion bridges of bone tissue between vertebral bodies (arrows). Bar, 1cm. b) Axial view (TAC) where new bone in the area of the implant can be seen (arrows). Bar, 1cm. c) Tissue section under polarization microscopy showing HA (starts) surrounded by new bone. Bar, 250μm. d) HA fragment (brown color) in resorption surrounded by new bone type woven in an implant with MSCs (section stained with toluidine blue). Bar, 100μm. e) New bone in an implant with MSCs where woven bone types coexist with laminar and haversian types and resorption lacunae (Von Kossa stained). Bar, 200μm. f) Row of osteoblasts (arrow) in active synthesis of new bone (hematoxiline-eosine). Bar, 50μm*

REARRANGING PROTEIN ASSEMBLIES FROM 2D LAYERS TO 1D FIBRES BY ELECTROSPINNING

Alexander Michael Bittner[1,2], Wiwat Nuansing[1], Amaia Rebollo[1], Ulf Baus[3], Thomas Subkowski[4]

[1]CIC Nanogune, Tolosa Hiribidea 76, 20018 Donostia, Spain
[2]Ikerbasque, Alameda Urquijo, 36-5, Plaza Bizkaia, 48011 Bilbo, Spain
[3]BASF SE; Performance Chemicals Division, GVF/C - A030, 67056 Ludwigshafen, Germany
[4]BASF SE; Biotechnology Research, GVF/C - A030, 67056 Ludwigshafen, Germany
a.bittner@nanogune.eu

Natural proteins do usually not assemble to regular structures, which very much impedes their characterisation. However, some of them can be crystallised, i.e. they form regular 3D assemblies. Others assemble in 2D, e.g. membrane proteins, and in 1D, e.g. fibrous proteins and some viruses. Conformational changes inside a protein can change its mode of assembly. Some of the best-known examples are prion proteins, which can change to a conformation with increased beta sheet content, which can result in neuropathogenic fibres. Since Alzheimer disease is based on similar mechanisms, 1D assembly is and will remain a very hot topic in protein science [1,2,3].

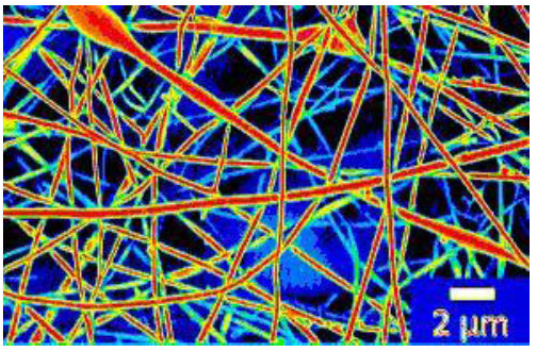

Figure 1: *SEM of electrospun pure hydrophobin. The quasi endless fibre has ca. 300 nm average diameter*

Various proteins, some related to Alzheimer and Parkinson disease, exhibit a surprising in vitro behaviour: Shear forces speed up their assembly to fibres [1,4,5]. We here show that a combination of solvent-induced conformational change and extreme shear induces such severe changes that the assembly mode switches from 2D to 1D. To this end, we dissolved a protein, hydrophobin, at high concentration in an organic solvent, and applied polymer-free (i.e. monomer) electrospinning [6].

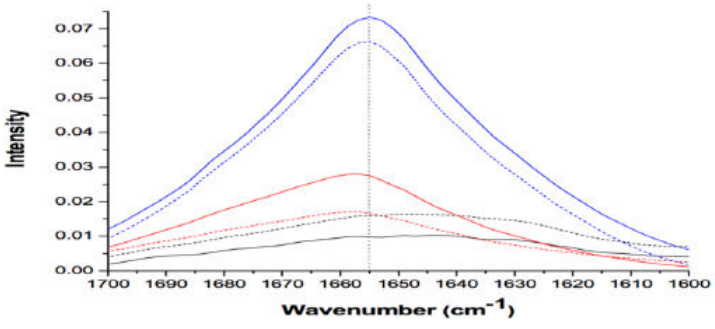

Figure 2: *IR spectra of the amide band region of HP samples. The bottom curves (maxima at 1645 cm^{-1}) correspond to the original state, the top curves with maxima at 1655 cm^{-1} point to an increase in alpha helices in organic solvent.*

Hydrophobins (HPs) exhibit 2D organisation. They are used in the context of "White Biotechnology" as emulsifiers and surface primers (www.hydrophobin.basf.com). HPs are naturally found on fungi, where they determine the very hydrophobic nature of the fungus cap. They can easily be produced in kg amounts by biotechnological fermentation techniques.

Electrospinning requires highly concentrated solutions of HPs in a solvent with high vapour pressure. We showed with electrophoresis (www.hydrophobin.basf.com) and Raman, IR, and circular dichroism spectroscopy that already the dissolution changes the conformation of the HPs, different from contact with water. However, HPs did not assemble in solution. Only during electrospinning the high shear force, together with the evaporation, induced 1D alignment, and we were able to spin extremely long microfibers that consist of pure (polymer-free) proteins. We characterised the fibres with SEM, including environmental SEM in water vapour.

We believe that electrospun fibres of pure proteins can have multiple applications in biotechnology, e.g. as highly biocompatible scaffold materials.

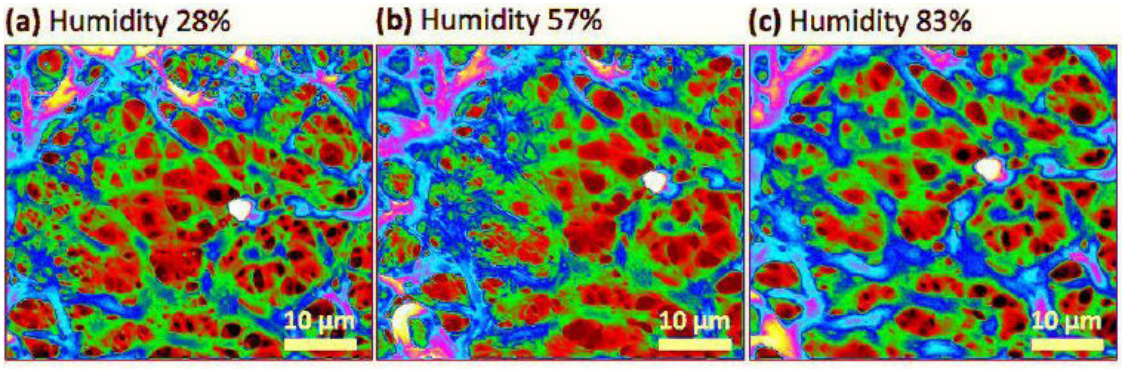

Figure 3: *Environmental SEM of electrospun hydrophobin. The water vapour pressure increases the diameter of the fibres.*

References:

[1] T.P.J. Knowles, C.A. Waudby, G.L. Devlin, S.I.A. Cohen, A. Aguzzi, M. Vendruscolo, E.M. Terentjev, M.E. Welland, C.M. Dobson, Science 326 (2009) 1533
[2] A.M. Bittner, Surf. Sci. Rep. 61 (2006) 383
[3] A.M. Bittner, Naturwissenschaften 92 (2005) 51
[4] G. Bhak, J.-H. Lee, J.-S. Hahn, S.-R. Paik, PLOSone 4 (2009) e4177
[5] P. Hamilton-Brown, I. Bekard, W.A. Ducker, D.E. Dunstan, J. Phys. Chem. B 112 (2008) 16249
[6] G. Singh, A.M. Bittner, S. Loscher, N. Malinowski, K. Kern, Adv. Mater., 20 (2008) 2332

CANTILEVER-LIKE SENSORS FOR USE IN BIO-MEDICAL APPLICATIONS

Anja Boisen

DTU Nanotech, Technical University of Denmark, Lyngby, Denmark
anja.boisen@nanotech.dtu.dk

Small mechanical structures such as cantilevers, bridges and lids can be used as sensitive and label free sensors. A biochemical reaction at the surface of the structure can be monitored as a bending, due to a change in surface stress. Minute temperature changes can be registered by exploring the bimorph effect. Furthermore, mass detection can be achieved by using resonating structures and monitor how the resonant frequency changes as a function of the added mass. In order to obtain high sensitivity the structures need to have micrometer and sometimes nanometer dimensions. They are fabricated by cleanroom processing using either silicon or polymer based materials. We will present examples of our recent advances in the field of sensor development including results on the on-line detection of DNA proteins and nano-particles. Also the strength of combining several independent miniaturized sensors will be discussed and illustrated for the use in explosives detection.

MRI CELL TRACKING USING MAGNETIC NANOPARTICLES

Jeff W.M. Bulte

Russell H. Morgan Department of Radiology and Radiological Science, Division of MR Research, Department of Biomedical Engineering, and Department of Chemical & Biomolecular Engineering, Cellular Imaging Section and Vascular Biology Program, Institute for Cell Engineering, The Johns Hopkins University School of Medicine, Baltimore, MD, USA

jwmbulte@mri.jhu.edu

The clinical use of novel experimental cell therapies calls for suitable methods that can monitor the cellular biodistribution non-invasively following administration. Among the different clinically used imaging techniques, magnetic resonance (MR) imaging has superior spatial resolution with excellent soft tissue contrast. In order for exogenous therapeutic cells to be detected, they need to have a different contrast from endogenous cells. The most sensitive MR label to date are the superparamagnetic iron oxide nanoparticles or SPIOs. SPIOs are clinically approved and create strong local magnetic field disturbances that spoil the MR signal leading to hypo- or hyperintense contrast.

After approximately a decade of animal studies using MRI cell tracking these nanoprobes entered the clinic for cell tracking in 2004. The first phase I trial demonstrated the feasibility and safety of MRI (dendritic) cell tracking in cancer patients. A surprising finding, only observable by MRI, was that misinjection of cells occurred in half the patients. While the injection procedure was performed under ultrasound guidance, neither radionuclide or US imaging was able to reveal the failure of targeted cell delivery. Therefore, MR-guided targeted cell delivery may have significant advantages for clinical implementation of novel treatment paradigms using cellular therapeutics. If the administration is done in real-time under MR guidance, then verification of accurate cell delivery in, adjacent, or remote from the target site is mandatory. As of the end of 2010, 6 clinical trials using SPIO-based cell tracking have now been published, and some of these will be highlighted.

ADVANCED THERAPIES FOR OCULAR SURFACE RECONSTRUCTION: FROM *IN VITRO* RESEARCH TO CLINICAL TRIALS

Margarita Calonge Cano

IOBA (Instituto Universitario de Oftalmobiología Aplicada)
Universidad de Valladolid, Valladolid, Spain

The corneoscleral junction or limbus is the native niche for corneal stem cells (SC), especifically called limbal epithelial SC (LESC). Dysfunction of these cells (LESC deficiency syndrome) usually results in blindness and chronic pain by causing corneal opacity and persistent ocular surface inflammation, notably decreasing quality-of-life.

In these cases, corneal transplantation was the only option to recover vision, but a poor outcome was usually the rule due to the lack of LESC in the donor corneal graft. For the last 15 years, transplantation of pieces of limbal tissue directly from a cadaveric source or a living relative met good short-term results but only in some partial unilateral cases, failing (mainly due to immune rejection) in the more frequent cases of diffuse and/or bilateral disease. A more successful approach is the transplantation of *in vitro* expanded and cultivated LESC, an approach first described in 1997. Since then, progress has been made and at present transplantation of LESC has become the most successful therapy for LESC deficiency syndromes. This actually represents one of the first and clearest successes of regenerative medicine, as our work team is also demonstrating in an on-going clinical study. This study is being performed following good manufacturing practice (GMP) and good clinical practice (GCP) rules, and subsequently LESC are cultivated in a validated clean room (as mandated by the Spanish legislation, transposition of the European directive) and patients are followed under a strict clinical and surgical protocol. To date, 25 patients have been transplanted (mean follow-up, 9.2 months) with 80% global success, substantial quality-of-life improvement, and visual gain in 63% of patients. The 13 autologous and the 12 allogeneic transplants have presented similar results. The required immunosuppression for allogenic cases has been minimal, no sign of immune rejection has been observed, and additionally we have seen lower costs and less surgical morbidity. However, an important drawback remains, which is the dependency of donations in bilateral cases and the fact that an extra-surgical procedure is required in the only good-eye of a unilateral affected patient, increasing potential morbidity and sanitary costs. Therefore, an extraocular source of SC could be extremely valuable. As it is well known, mesenchymal stem cells (MSC) have a remarkably immunomodulatory capacity, and allogeneic transplantation of bone marrow-derived MSC (BM) has been successfully used for experimental ocular surface reconstruction. For this reason, we set out to demonstrate the hypothesis that the transplantation of BM-MSC cells is equal or superior to LESC transplantation through a randomized, double-masked clinical trial.

VIRUS SCAFFOLDS AS ENZYME NANO-CARRIERS (ENCS) TO ORGANIZE BIO-CATALYTIC ENZYME CASCADES. DESIGN OF A SCANNING ELECTROCHEMICAL NANOREACTOR MICROSCOPY DEVICE

Daniela Cardinale[1], Noëlle Carette[1], Amandine Barra[1], Jocelyne Walter[1], Thierry Delaunay[1], Christophe Demaille[2], Agnés Anne[2], Olivier Courjean[3], Nicolas Mano[3], Jean-Paul Salvetat[3], Jean-Pierre Aime[4], Thierry Michon[1]

[1]INRA, UMR 1090 GDPP, IBVM Virologie, 71 Av. Edouard Bourlaux, B.P. 81, 33883 Villenave d'Ornon, France
[2]Laboratoire d'Electrochimie Moléculaire, UMR CNRS – P7 7591, Université Paris Diderot – Paris 7, Bâtiment Lavoisier, 15 rue Jean-Antoine de Baïf, 75205 Paris cedex 13, France
[3]CRPP, Centre de Recherche Paul Pascal, 115 Av. Schweitzer, 33600 Pessac, France
[4]CPMOH, Centre de Physique Moléculaire Optique et Hertzienne, UMR5798,Université Bordeaux 1, 351 Cours de la Libération, 33405 Talence, France
daniela.cardinale@bordeaux.inra.fr

In cellular systems, the association of collaborating enzymes in supramolecular structures enables metabolic processes to be performed more efficiently, accelerating reactions rates and preventing the diffusion of intermediates in the cell medium. The aim of the Cascade project is to create a new experimental tool at the nanoscale level mimicking in vivo enzymatic cascade reactions. The set up will also offer the opportunity to study enzymatic processes at the level of one single or few molecules. To this purpose two model enzymes will be used to build artificial redox cascades: the lipase B (CalB) from *Candida antarctica* and the glucose oxidase (GOX) from *Penicillum amagasakiense*. The free electrons generated by enzymatic activities will be detected by electrochemistry. To this purpose a new nanoelectrochemical technique will be used to confine the clustered enzymes and to measure the final activity. The confined reaction medium will be permitted by a "nanocavity" microelectrode fabricated at the tip of an AFM probe; the combination of AFM/SECM (Scanning Electro Chemical Microscopy) will enable to measure the electrochemical current generated by a few enzyme molecules. Varying the diameter of the nanocavity from few hundreds to about ten nanometers should eventually permit to follow a single enzyme activity.

In order to study one-single enzyme kinetics the very faint signal of the enzyme needs to be amplified. After CalB hydrolysis of p-aminophenyl acetate (pAPA) an electro-inactive substrate to p-aminophenol (pAP) the electro-active product the red-ox couple pAPA/pAP will be continuously recycled between two electrodes amplifying the single enzymatic initial event. Kinetics parameters of pAPA hydrolysis by CALB determined spectrophotometrically and electrochemically are in good agreement. This supports the suitability of pAPA for AFM/SECM single enzyme studies.

In order to control the distribution of enzymes on the electrode we will use virus capsids as Enzyme Nano-Carriers (ENCs). To this aim, two plant viruses, Tobacco mosaic virus (TMV) and potato virus A (PVA) will be tested. Three different strategies will be attempted for the virus to enzyme interfacing: the fusion of leucine zipper (LZ) pairs to enzymes and capsomers, bi-specific antibodies and peptides obtained from phage display screening.

Regarding the first strategy, three pairs of LZ having different characteristics in term of length, affinity and orientation have been selected and the cloning at the N- and C- terminus of CalB is in progress. One assembly CalB (LZKg-CalB) was expressed in Escherichia coli periplasm and we are currently optimizing its purification.

Monoclonal antibodies for CalB have been produced and fusion with antibodies for TMV and PVA will be attempted.

As third strategy, three peptides were selected that recognize PVA. Cloning at the N-terminus of CalB and GOX is in progress.

NANOTECHNOLOGIES AND "SECURITY AT WORK": A NEW CHALLENGE FOR INDUSTRIAL RELATIONS AND SOCIETY

Patrick Chaskiel

CERTOP, UMR 5044 CNRS, UT2, UT3-UPS, 115 rte de Narbonne, 31077 Toulouse cedex 4, France
patrick.chaskiel@iut-tlse3.fr

Nanotechnologies, considered here as a "security at work" theme, raised a new challenge to industrial relations, i.e. relations between employers, state and workers. Nanotechnologies question the social organization of risks control relations, generally based on a single industry-wide approach when the entire cycle of nanoproduct life: from fabrication to disposal, would suppose an inter/multi-industrial approach of risks control.

Historically industrial relations on "security at work" in most industrialized countries fit the shape of general industrial relations, i.e. collective bargaining. The reason for that is not only historical: it relies on the very fact that "security at work" problems (and also working conditions) are linked - and must be referred - to a well identified type of activity, for instance: chemical or nuclear industries. To that extent and as it has been revealed by previous researches, industrial relations on "security at work" combined "shop-floor" day-to-day negotiations, company-wide talks and more formal agreements, these latter appearing quite infrequent in France. Nevertheless, it can be said that "security at work" is mainly a plant-wide issue, but regularly addressed at a wider level. It does not signify that risks, notably nanotechnologies problems, are not assessed at company level before implementing a nanoactivity in a plant. We only said that controlling "security at work" is eventually a shop-floor topic embedded in a larger framework and we need to know if nanotechnologies fit this model.

In France the main industrial relations institution implied in controlling "security at work" is the CHSCT (*Comité d'Hygiène, Sécurité et Conditions de travail*) [1]. Since a couple of years CHSCTs have played an increasing role in industrial relations, and changes have been noticed in the "security at work" topic: this latter is a more and more addressed issue, by employers, unionists and state and by public opinion either [2]. Growing costs of "repairing" industrial accidents (compensations), internal as well as public claims (from state or public opinion) to decrease accidents explain why the "security at work" topic has become that much important in industries and in society as a whole.

References:

[1] Health, Security, and Working Conditions Committee.
[2] Here public opinion is defined as the flow of discussions aiming to build an universal point of view. So it is not to be sought as results of polls published by mass medias.

PHONONIC METAMATERIALS FOR SHAPING FLUID FLOW

Jonathan Cooper

University of Glasgow, UK

The development of microfluidic systems is often constrained both by difficulties associated with the chip interconnection to other instruments, and by mechanisms that can enable fluid movement and processing. Surface acoustic wave (SAW) devices have previously shown promise in allowing samples to be manipulated, although designing complex fluid manipulations involves the generation of mixed signals at multiple electrode transducers.

We now demonstrate a new and very simple interface between a piezoelectric SAW device and a disposable microfluidic chip, involving the use of phononic structures, Figure 1(a) to shape the acoustic field. The surface wave is coupled from the piezoelectric substrate into the disposable chip to allow fluid actuations, including droplet movement, splitting, jetting, nebulisation and centrifugation to be performed. The phononic structure has a band-gap and by showing that the interaction of the fluid within the chip structure is dependent upon the acoustic frequency, we provide providing a method to programme complex fluidic functions into a microchip.

Further, we demonstrate the application of this new technology in a number of new analytical proceedures, including for example, the implementation of digital microfluids, the interface of microfluidics with mass spectrometry (Figure 1(b)), PCR, and the lysis of cells on-chip. We show initial results demonstrating the integration of these methods. In doing so, we propose to create a "tool-box" of different diagnostic functions (sample processing, cell separation, cell lysis, PCR, nebulization for MS, detection) each of which requires a different phononic structure. Just as in electronics, where discrete components are combined to create a circuit, so we will use different combinations of phononic lattices to create fluidic microcircuits, each of which provides a unique diagnostic function.

Figures:

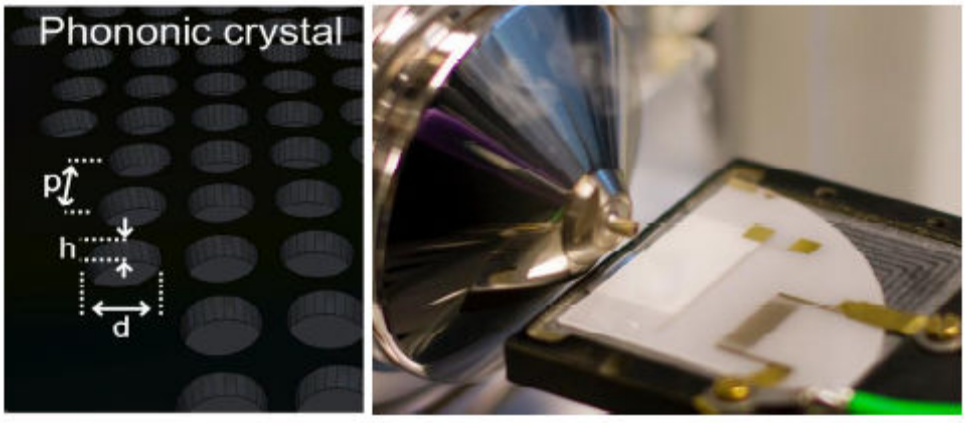

Figure 1: *Left, shows a schematic of a phononic crystal, used for microfluidics whilst, right, shows the interface of a disposable chip with a MS instrument.*

INTERACTIONS OF NANOPARTICLE WITH LIVING ORGANISMS

Kenneth Dawson

University College Dublin, Ireland

Nanoscale materials can interact with living organisms in a qualitatively different manner than small molecules. Crucially, biological phenomena such as immune clearance, cellular uptake and biological barrier crossing are all determined by processes on the nanometer scale. Harnessing these endogeneous biological processes (for example in creation of new nanomedicines or nanodiagnostics) will therefore require us to work on the nanoscale. This ensures that nanoscience, biology and medicine will be intimately connected for generations to come, and may well provide the best hope of tacking currently intractable diseases.

These same scientific observations lead to widespread concern about the potential safety of nanomaterials in general. Early unfocussed concerns have diminished, leaving a more disciplined and balanced scientific dialogue. In particular a growing interest in understanding the fundamental principles of bionaointeractions may offer insight into potential hazard, as well as the basis for therapeutic use.

Whilst nanoparticle size is important, the detailed nature of the nanoparticle interface is key to understanding interactions with living organisms. This interface may be quite complex, involving also adsorbed protein from the biological fluid (blood, or other), leading to a sort of 'protein corona' around the nanomaterial surface. We discuss how this corona is formed, and how it may be a determining feature in biological interactions.

References:

[1] Cedervall T, Lynch I, Lindman S, Berggård T, Thulin E, Nilsson, H, Linse S, Dawson KA. Understanding the nanoparticle protein corona using methods to quantify exchange rates and affinities of proteins for nanoparticles, Proc. Natl. Acad. Sci. USA, 104, 2050-2055 (2007)

[2] Linse S., Cabaleiro-Lago, C., Xue W.F., Lynch I., Lindman S., Thulin E., Radford S.E., Dawson, K.A., Proc. Natl. Acad. Sci. USA, 104 (21); 8691-8696 (2007)

[3] Lundqvist M, Stigler J, Cedervall T, Elia G, Lynch I, and Dawson KA. Nanoparticle Size and Surface Properties determine the Protein Corona with possible implications for Biological Impacts. Proc. Natl. Acad. Sci. USA, 105, 14265-14270 (2008)

[4] Cabaleiro-Lago C., Quinlan-Pluck F., Lynch I., Lindman S., Minogue A.M., Thulin E., Walsh, D.M., Dawson K.A., Linse, S., J. Am. Chem. Soc., 130 (46); 15437-15443 (2008)

[5] Lynch I, Salvati A and Dawson KA. Protein-nanoparticle interactions: What does the cell see? Nature Nanotech. 4, 546-547 (2009)

[6] Cabalerio-Lago C., Quinlan-Pluck F., Lynch I., Dawson K.A., Linse S., ACS Chem. Neurosci., 1 (4), 279 (2010)

[7] Walczyk D, Baldelli Bombelli F, Monopoli PM, Lynch I and Dawson KA. What the Cell "Sees" in Bionanoscience, J. Am. Chem. Soc., 132 (16), 5761–5768 (2010)

TARGETING THE IMMUNE SYSTEM WITH BIODEGRADABLE NANO ENGINEERED POLYMERIC MICROCAPSULES

Bruno G. De Geest, Stefaan De Koker, Chris Vervaet, Jean Paul Remon

Laboratory of Pharmaceutical technology, Ghent University, Ghent, Belgium
br.degeest@ugent.be

Vaccines that can elicit strong T-cell responses are undoubtedly one of the major challenges for medicine today. [1] For this purpose, dendritic cells (DCs) have to internalize antigen, process them into peptide fragments and present them to T-cells. Whereas soluble antigen largely fails to induce potent cellular immune responses, formulation of antigen into microparticles has emerged as an attractive alternative. Here, we demonstrate efficient *in vitro* and *in vivo* antigen delivery to DCs using biodegradable polyelectrolyte capsules as antigen carrier.

Figure 1 schematically shows the encapsulation procedure of antigen into hollow polyelectrolyte capsules. [2,3] In a first step, antigen loaded $CaCO_3$ microparticles (3 µm diameter) are fabricated by co-precipitation of $CaCl_2$ and Na_2CO_3 in the presence ovalbumin (OVA) as model antigen. Subsequently these $CaCO_3$ microparticles are coated (2 bilayers) by sequential deposition of dextran sulfate and poly-L-arginine using electrostatic interaction as driving force. Finally hollow polyelectrolyte capsules are obtained after dissolution of the $CaCO_3$ core templates in aqueous EDTA medium.

As demonstrated by transmission electron microscopy (Figure 2A) and confocal microscopy (figure 2B), polyelectrolyte capsules are efficiently taken up by DCs and both the capsule membrane as well as the encapsulated antigen becomes readily processed. [4,5] Antigen presentation to T-cells was assessed by incubating DCs with OVA loaded capsules followed by co-culturing with respectively OT-I and OT-II cells (Figure 2C). OT-I and OT-II cells are transgenic CD8, respectively CD4 T cells that specifically recognizes the OVA CD8 peptide, respectively CD4 peptide. Compared to soluble antigen a dramatic increase in T-cell presentation is observed. Especially cross-presentation to CD8 T-cells, which are crucial to induce cellular immune responses, is strongly promoted. [4]

In vivo studies show mild tissue reactions [6,7] upon subcutaneous injection [5 while potent humoral and cellular immune responses [8] are induced which show protective immunity against viral infection as well as cancer. Moreover in recent studies we have also demonstrated an easy strategy – involving main stream pharmaceutical technology – to scale the production of polyelectrolyte microcapsules using a one-step procedure which encapsulates antigen with extremely high yields while barely hampering its biological activity. [9]

References:

[1] De Koker, S.; Lambrecht, B.N.; Willart, M.A.; Van Kooyk, Y.; Grooten, J.; Vervaet, C.; Remon, J.P.; De Geest, B.G., Chemical Society Reviews, 40 (2011) 320.
[2] De Koker, S.; De Cock, L.J.; Auzély-Velty, R.; Gil, P.R., Parak, W.J.; Grooten, J.; Vervaet, C.; Remon, J.P.; De Geest, B.G. Advanced Drug Delivery Reviews, in press.
[3] De Cock, L.J.; De Koker, S.; De Geest,B.G.; Grooten, J.; Vervaet, C.; Remon, J.P.; Sukhorukov, G.B.; Antipina, M.N. Angewandte Chemie International Edition, 40 (2010) 6954.
[4] S. De Koker, B.G. De Geest,* S.K. Singh, R. De Rijcke, T. Naessens, K. Van Kooyk, J. Demeester, S.C. De Smedt, J. Grooten, Angewandte Chemie International Edition, 48 (2009) 8485.
[5] P. Rivera-Gil, S. De Koker, B.G. De Geest,* W.J. Parak, Nano Letters, 9 (2009) 4398.
[6] De Koker, S.; De Geest, B.G.; Cuvelier, C.; Ferdinande, L.; Deckers, W.; Hennink, W.E.; De Smedt, S.C.; Mertens, N. Advanced Functional Materials, 17 (2007) 3754.
[7] L.J. De Cock, J. Lenoir , V. Vermeersch, S. De Koker, A.G. Skirtach, P. Dubruel, E. Adriaens, C. Vervaet, J.P. Remon, B.G. De Geest, Biomaterials, 32 (2011) 1967
[8] De Koker, S.; Naessens, T.; De Geest, B.G.; Bogaert, P; Demeester, J.; De Smedt, S.C.; Grooten, J., Journal of Immunology, 184 (2010) 203.
[9] M. Dierendonck, S. De Koker, C. Cuvelier, J. Grooten, C. Vervaet, J.P. Remon, B.G. De Geest* Angewandte Chemie International Edition, 49 (2010) 8620.

Figures:

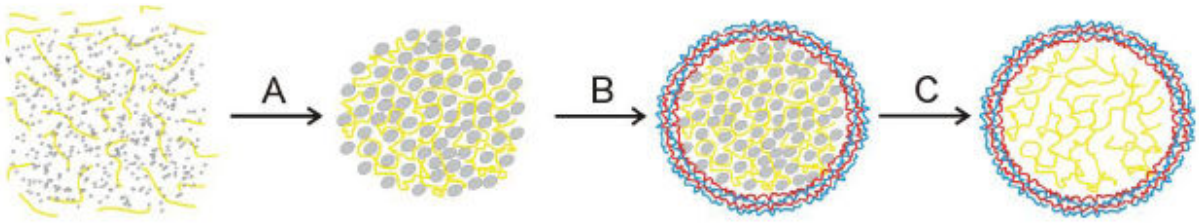

Figure 1: *Polyelectrolyte microcapsule synthesis. (A) Antigen (yellow) is mixed with $CaCl_2$ and Na_2CO_3, resulting in the generation of macromolecule-filled $CaCO_3$ microparticles (gray), which are (B) subsequently coated with alternating layers of dextran sulfate and poly-L-arginine (red, blue). (C) Dissolution of the $CaCO_3$ core by EDTA results in the generation of a hollow microcapsule composed of macromolecules surrounded by the polyelectrolyte shell.*

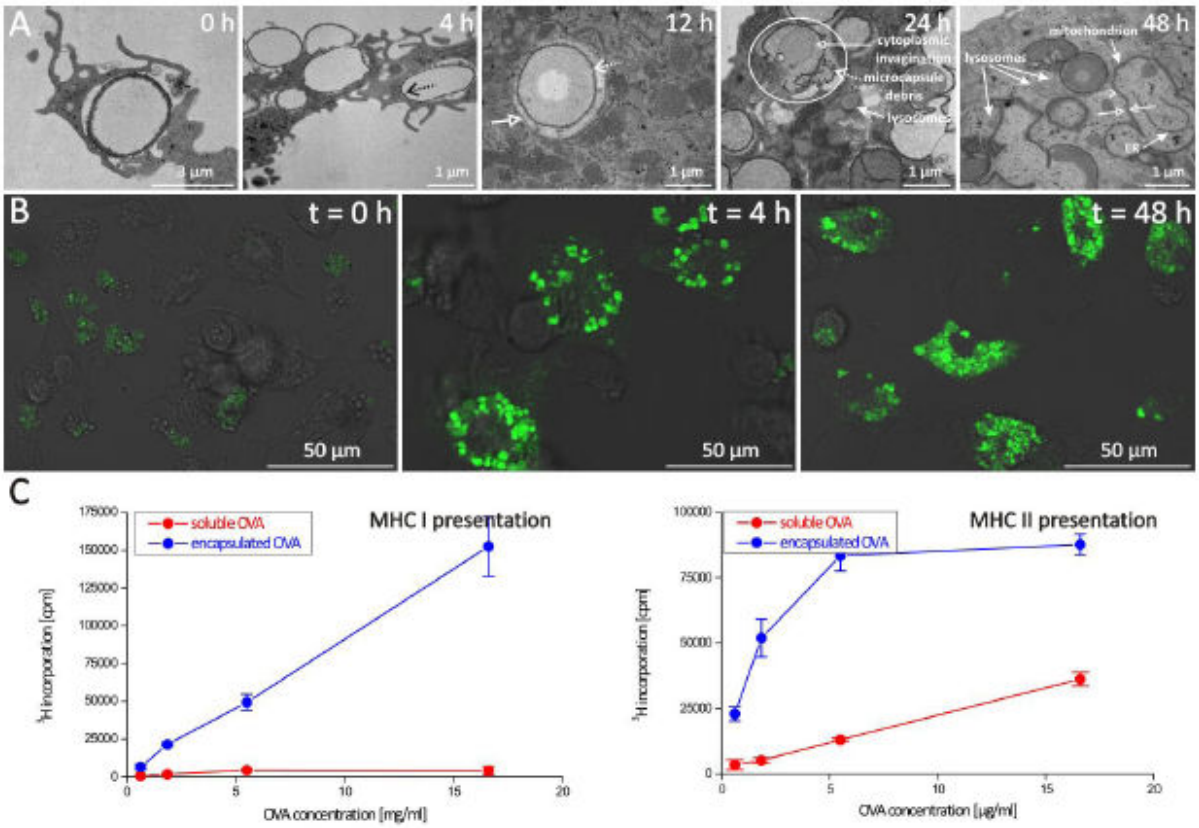

Figure 2: *(A) TEM images of BM-DCs that have internalized dextran sulfate/poly-L-arginine microcapsules at the indicated time intervals. Microcapsule shell: dotted arrows; membranes surrounding the microcapsules: open arrows. In the encircled area, microcapsule rupture and cytoplasmic invagination are clearly distinguishable. Lysosomes, endoplasmatic reticulum (ER), and a mitochondrion are indicated by the solid arrows. (B) Processing of dextran sulfate/poly-larginine microcapsule encapsulated OVA was analyzed using DQ-OVA. Confocal microscopy images of BM-DCs incubated with OVA-DQ microcapsules for 0, 4 and 48 h (overlay of green fluorescence and DIC). (DQ-OVA is ovalbumin oversaturated with BODIPY dyes. Upon proteolytic cleavage, quenching is relieved and green fluorescence appears. (C) Antigen presentation by BM-DCs after uptake of soluble and encapsulated OVA. Proliferation of OT-I cells was used as a measure for MHC-I-mediated cross-presentation of OVA (left graph), proliferation of OT-II cells as a measure for MHC-II mediated presentation (right).*

INTERNALISATION MECHANISMS OF MODIFIED TITANIUM OXIDE NANOPARTICLES IN SKIN CELLS AND MULTICELLULAR LIVING SPECIMENS : RESULTING TOXICITY

M.H. Delville[1], M. Simon[2], A. Girard[1,2], P. Barberet[2], P. Moretto[2], H. Seznec[2], D. Dupuy[3]

[1]CNRS, Univ de Bordeaux, ICMCB, 87 avenue du Dr. A. Schweitzer, Pessac, F-33608 Cedex, France
[2]Université Bordeaux, CNRS/IN2P3, Centre d'Etudes Nucléaires de Bordeaux; France
[3]Gradignan, CENBG, Chemin du Solarium, BP120, 33175 Gradignan, France
Institut Européen de Chimie et Biologie, Univ Bordeaux 1, 2 rue R. Escarpit, 33607 Pessac, France

Nanotechnologies are of great interest from both academic and industrial points of view, with numerous applications in domains such as medicine, catalysis and material sciences. However, their nanotoxicology has also attracted the attention of public and governments' worldwide and established methods of chemical safety assessments have to be modified to address the special characteristics of nanoparticles and more especially to assess the biological effects of these highly reactive materials.

Most of theses manufactured nanoparticles have been produced for several decades on an industrial scale. There is an urgent need to evaluate the risks of these particles to ensure their safe production, handling, use, and disposal. Moreover, a comprehensive study is clearly needed to fully explore the toxicity of manufactured nanoparticles, which may help to better understand their deleterious health effects and create environmentally friendly and biologically relevant nanoparticles. In particular, the behavior of nanoparticles inside living cells is still an enigma, and no metabolic responses induced by these particles are understood so far.

This presentation concerns the potential toxicity due to exposure of TiO_2 NPs used in sunscreens and cosmetics. We propose to apply an original imaging methodology (Ion Beam Analysis, TEM, and Confocal microscopy) to in vitro studies, combining technologies for on one hand, the detection, tracking, and quantification of TiO_2 nanoparticles and on the other one, the use of indicators for ion homeostasis, cell metabolism, or cell fate.

The main goal is to precisely identify the molecular and cellular mechanisms involved in the nanotoxicity of TiO_2 nanoparticles in eukaryotic cells and in multi-cellular organisms such as Caenorhabditis elegans (C. elegans). This study addresses the current knowledge gap of human cells and C. elegans responses to TiO_2 nanoparticles exposure. Since the nematodes feed on bacteria and are considered as particle-ingesting organisms, the present study will offer new perspectives in nanoparticles-related risk assessment and food web accumulation modelling.

REGULATORY ISSUES IN NANOMEDECINE: A FUTURE UNDER CONSTRUCTION

Jean-Marie Devoisselle

Institut Charles Gerhardt Montpellier, UMR CNRS/UM2/ENSCM/UM1 5253 U.F.R. des Sciences Pharmaceutiques et Biologiques 15 ave Ch. Flahault, BP14491, 34093 Montpellier, France
jm.devoisselle@univ-montp1.fr

Research in nanotechnology and specially nanomaterials has gone now to a large commercial undertaking. The scientific literature on environment, health and safety aspects of nanomaterials show clearly how these aspects are now of primary importance. First of all the first question is: how to define nanomaterials and nanomedecine? Several definitions can be found but some initiatives tend to clarify these definitions. The application of nanotechnology to healthcare is already demonstrated by the increasing intensity of research and competition in the pharmaceutical industry. It can be illustrated by the design of new therapeutics and/or diagnostic tools. The field of new drug delivery technologies is also growing rapidly. The research on life sciences applications of nanotechnologies (mainly dedicated to drug delivery and therapeutics) has doubled since 2002. Nanotechnology-based drug delivery systems and devices provide new features and functions that other technologies cannot match. Various nanoscale structures of different size, shapes, texture and chemical compositions has been included as nanopharmaceuticals. Although there are quite a few approved nanopharmaceuticals, several others are under development or close to commercialization. There are currently several challenges and risks concerning the commercialization of nanopharmaceuticals. The most important are environmental, safety, ethical and regulatory issues. These products (drug-loaded nanomaterials or devices) displaying new size-dependent properties and toxicological profiles need new approaches from the regulatory agencies. A global approach is needed. Discussions concern the application of existing regulation and the implementation of new legislation in this field.

References:

[1] Dr. Angela Hullmann, European Commission, Unit “Nano and Converging Sciences and Technologies”, European activities in the field of ethical, legal and social aspects (ELSA) and governance of nanotechnology, october 2008, see http://cordis.europa.eu./nanotechnology
[2] Scientific Committee on Emerging and Newly Identified Health Risks, SCENIHR, 6 July 2010, http://ec.europa.eu/health/ph_risk/risk_en.htm
[3] Office of Pharmaceutical Science, MAPP 5015.9 (6/3/2010)
[4] S.F. Hansen, Nanomed. Nanobiotechnol. (2010) 2 :441-449.
[5] Aida Maria Ponce Del Castillo, CRISP, (2010) n°2065
[6] Bawa, R. Current Drug Delivery, (2011, Feb.3)

IMMUNOLOGICAL PROPERTIES OF ENGINEERED NANOMATERIALS

Marina A. Dobrovolskaia

Nanotechnology Characterization Laboratory, Advanced Technology Program, SAIC-Frederick Inc., NCI-Frederick, Frederick, MD 21702, USA

marina@mail.nih.gov

Nanotechnology is finding growing applications in industry, biology and medicine. The clear benefits of using nanosized products in various biological and medical applications are often challenged by questions regarding toxicity of these materials. One area of interest involves the interactions between nanoparticles and the components of the immune system. Nanoparticles can be engineered to either avoid immune system recognition or to specifically interact with components of the immune responses. This presentation will review data regarding nanoparticle-mediated immunostimulation and immunosuppression; how manipulation of particle physicochemical properties can influence their interaction with components of the immune system (specifically interaction with erythrocytes, effects on blood coagulation system, activation of complement and effects on immune cell function), and discuss challenges with preclinical immunological characterization of engineered nanomaterials (specifically endotoxin contamination, depyrogenation, sterility and sterilization, and nanoparticle interference with traditional immunological tests).

Funded by NCI Contract No.HHSN261200800001E

STUDY OF THE DISTRIBUTION OF MAGNETITE NANOPARTICLES IN AN EXPERIMENTAL MODEL OF HEPATIC METASTASES

J.J. Echevarria[1], I. Garcia-Alonso[2], J.A. Larena[1], F. Sanz-Sanchez[1], F. Plazaola[3], M. Insausti[3], N. Etxebarria[3], J. Salado[3], B. Fernandez-Ruanova[1]

[1]Radiology Department. Galdakao-Usansolo Hospital, Labeaga s/n, 48960 Galdakao, Spain
[2]Experimental Surgery Laboratory, Medicine Faculty, University of the Basque Country (UPV/EHU), 48940 Leioa, Spain
[3]Faculty of Science and Technology, Univ. of the Basque Country (UPV/EHU), 48940 Leioa, Spain
fernando.plazaola@ehu.es

The purpose of this work is to assess a magnetic fluid for its affinity for liver metastases at different stages of tumor development in laboratory rats, prior to its potential use in antitumor thermal therapy. Iron oxide magnetic nanoparticles ranging between 3.8 and 7.1 nm were synthesized using the polyol method. From this synthesis process, magnetic nanoparticles of Fe_3O_4 capped by oleic acid were obtained. The lipid nature of these ligands allows the particles to be suspended in iodized oil Lipiodol, when the mixture is exposed to ultrasonification. A magnetic fluid consisting of suspensions of 2 mg of iron oxide nanoparticles in 0.2 ml of Lipiodol was prepared for transarterial hepatic infusion in each animal.

The magnetic fluid infusion procedure in the selected animals required midline laparotomy to enable the exposure of visceral arterial vessels. The main branches of the celial trunk were clamped, with the exception of the hepatic artery with the aim of driving towards this artery most of the celiac vascular flow. A direct punction of the celiac trunk was carried out using a needle, connected by an elongated catheter to an infusion pump previously filled with the magnetic fluid, and the suspension was slowly and selectively infused into the liver.

The experimental study was carried out using 33 male WAG/RijCrl rats. In order to induce metastases in the liver of laboratory animals, syngenic cells of colon adenocarcinoma, CC-531, were inoculated into the liver of the rats. The splenic reservoir technique was used as a source for the dissemination of tumor cells. A total of 21 rats developed metastases, but six animals died during subsequent surgical procedures. Of the surviving animals, ten were chosen at random to receive the magnetic fluid, via the hepatic artery. The remaining five rats constituted the control group and did not receive the suspension.

Within the first 12 hours after administration of the magnetic fluid, Multi-Detector Computed Tomography (MDCT) and Magnetic Resonance Imaging (MRI) were performed to the animals to check the effectiveness of the infusion procedure. The observation on MDCT of a hyperdense liver due to the presence of Lipiodol in the arterial tree, and the lack of extravasations in the puncture area or the existence of gross intra-arterial contrast media deposits, were considered to be evidence of the correct transarterial administration of the magnetic fluid. MRI studies were carried out on a 1.5 T Siemens Symphony system, using a standard cranial coil and axial Short Time Inversion Recovery (STIR) and gradient-echo (GRE) weighted sequences were performed. The observation on STIR sequences of smooth hyper intense masses into liver was considered as metastatic lesions. The homogeneous decay of signal intensity of liver and metastases on GRE sequences was attributed to the presence of magnetic nanoparticles in the different tissues, and it was considered to be evidence of proper vascular diffusion of the magnetic fluid.

After the imaging studies animals were sacrificed. Livers were extracted, and the number and size of the metastases were determined by visual analysis. Two categories of tumor growth were considered. On the one hand, early stage neoplastic infiltration corresponding to metastases that were smaller than 3 mm, non-overlapping (separated by healthy parenchyma) and with no more than ten visually identifiable lesions. On the other hand, livers that showed extensive neoplastic infiltrations, in an advanced stage, were characterized by having metastases larger than 3 mm or more than ten visually detectable lesions.

Liver and neoplastic tissue were taken to determine iron concentrations, using Inductively Coupled Plasma Mass Spectrometry (ICP-MS). Statistical analysis was performed with non-parametric tests (Wilcoxon test for related samples). Once significant differences between groups had been demonstrated using the Kruskal-Wallis test, comparisons between possible pairs of groups were performed using the U Mann-Whitney test. The minimum level of significance accepted was $P < 0.05$.

Of the ten animals in which surgical procedures and the magnetic fluid infusion were successfully completed, five showed early stage metastatic development while the other five presented advanced stage metastasis. After subtracting the mean endogenous iron values of the control group, from the iron found in animals that had received the magnetic fluid, the mean concentration attributable to exogenous administration in the early stage group was 172.2 mg/g in tumor tissue and 65.2 mg/g in healthy liver tissues, In these animals tumor tissue accumulated 2.6 times more iron than healthy liver tissue. In contrast, exogenous iron values found for the advanced stage group were 22.7 mg/g and 43.1 mg/g in metastatic and healthy tissue, respectively. In this group, metastases of animals with sever tumor infiltrations, accumulated half as much exogenous iron as healthy liver. Moreover, in the comparative study between concentrations of exogenous iron determined in liver and metastases within groups, significant differences were found in the early stage group, but not in the advanced stage group.

Our model of metastatic adenocarcinoma has revealed important differences in the vascularization of metastatic lesions according the stage of development of the disease. Therefore, we should consider the possibility of there being substantial differences in vascular perfusion in neoplastic lesions of similar type, but in different stages of development. The increase in tumor volume does not necessarily lead to a similar development in its vascularization, rather the increase in tumor mass may lead to the appearance of regions with decreased artery supply.

DNA ORIGAMIS: MECHANISMS OF FORMATION AND MELTING, STRUCTURE FLUCTUATIONS

JM. Arbona, **J. Elezgaray** and JP. Aimé

CBMN, UMR5248, 33600 Pessac, France
jm.arbona@iecb.u-bordeaux.fr

In this communication, we focus on the process of DNA-origami formation. In order to do this, several formation-melting experiments have been performed, where we keep track of the UV absorption as a function of the temperature. In parallel, for the melting process, we also image the resulting structures by AFM. These experiments show that, for the usual cooling-heating speed reported in most publications, folding of the origami shows hysteresis. The melting process is characterized by two transition temperatures correlated with the GC content of the staple strands and a third one at a higher temperature that may be correlated with the Origami structure. However, when the origami is prepared under constraint, the third transition disappears. During the formation of the origamis, only two transitions are observed, correlated with the GC content. In order to get further insight in the formation process, we also consider the folding-unfolding properties of a set of three ssDNA as a simplified model of origami (see figure). Using numerical simulations compared to melting experiments, we discuss entropic and defect contributions during the DNA-origami folding and the influence of a cooperative process.

In a separate study, we study the thermal fluctuations of a rectangular origami using a rigid base approximation. To do this, we use a simplified, yet accurate, model of DNA: the Stack of Plates (SOP) model [1], designed to model DNA at the base-pair level. In the SOP model, the right handed DNA structure is the result of the competition between two forces (stacking of the base pairs and a harmonic constraint to mimic sugar-phosphate backbones) and an additional simple geometric constraint. Monte-Carlo simulations show that the equilibrium conformation of the Rothemund origamis is not planar but slightly twisted. The same simulations allow to quantify the predominant elastic modes and the bending elasticity constant. We also discuss how this information can be used to design 'self-constrained' versions of the otherwise 'planar' structures.

References:

[1] Modeling DNA structure, elasticity, and deformations at the base-pair level. Mergell, B.; Ejtehadi, M.R.; Everaers, R

Figures:

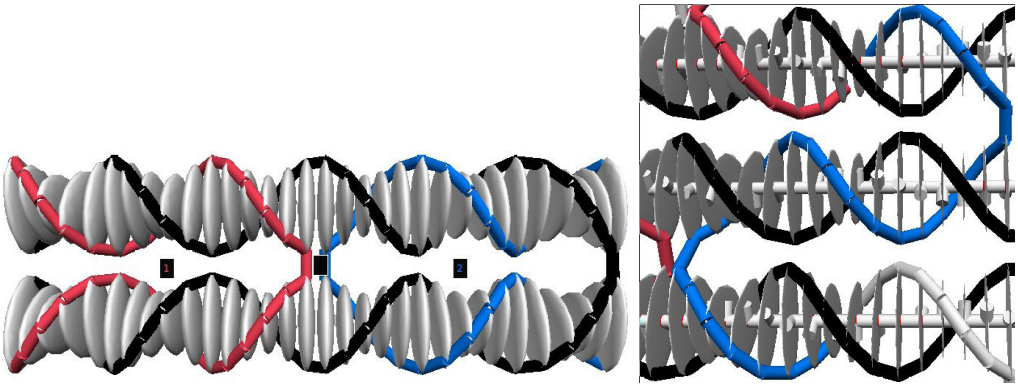

Figure 1: *Left: Simplified Origami made of 64 bases (black line) and two 32 bases long staples (red and blue lines). Right: Rectangular Origami Virus black line, staples red and blue lines.*

SUPRAMOLECULAR STRUCTURAL CHARACTERIZATION OF CHOLESTEROL-RICH VESICLES TO BE USED IN DRUG DELIVERY: INFLUENCE OF THE PREPARATION METHOD

Elisa Elizondo[1,2], Ingrid Cabrera[1,2], Evelyn Moreno-Calvo[1,2], Nora Ventosa[1,2] and Jaume Veciana[1,2]

[1]Department of Molecular Nanoscience and Organic Materials. Institute of Materials Science (ICMAB-CSIC), Campus UAB, 08193 Bellaterra, Spain;
[2]CIBER de Bioingeniería, Biomateriales y Nanomedicina (CIBER-BBN)
ventosa@icmab.es; vecianaj@icmab.es

In the past 30 years, the explosive growth of nanotechnology has promoted challenging innovations in pharmacology, which is currently revolutionizing the delivery of biologically active compounds [1]. Indeed, some existing drugs and new therapeutic compounds emerging from drug discovery processes present special delivery challenges, pushing nanotechnology towards the development of new drug nanocarriers that enhance the bioavailability of drugs [2]. Such nanocarriers or drug delivery systems (DDS) are intended not only to protect drugs from degradation but also to achieve their temporal and spatial site-specific delivery.Vesicles constitute one of the most studied DDS since their discovery in the mid 60s [3]. However, in order to achieve optimal performance of these self-assembled structures as functional materials, a high grade of structural homogeneity is required. For example, the behaviour of vesicles as drug delivery systems (DDS) is highly affected by their homogeneity, not only in size or morphology, but also in their membrane composition and supramolecular organization. Concretely, the vesicular membrane plays an important role in terms of vesicles stability, rigidity, permeability, functionalization or response to external stimuli [4]. In the latter case, the homogeneity in the membrane composition and supramolecular organization between the different vesicles forming a certain system would be a crucial issue in order to have sharp responses that allow homogenous triggering of the drug at the site of action (Figure 1). Attending to this, methods for the preparation of homogeneous vesicular systems, not only in terms of size and morphology, but also regarding the supramolecular organization of the membrane constituents are required for fully exploiting the potential of these self-assembled structures as functional materials.

In the early 90's, compressed fluid (CF)-based processes emerged as an alternative to conventional methods using liquid solvents, attracting enormous interest for the production of micro- and nanoparticulate materials [5]. Our research group has experience in using these novel technologies for the controlled nanostructuration of materials to be used in drug delivery [6,7]. Recently, a CF-based method, DELOS-susp, has been developed for the production of vesicular systems. This one-step process allows the achievement of stable, nanoscopic and unilamellar cholesterol-rich vesicles [8,9], which present higher structural homogeneity regarding size and morphology than those produced by a conventional multi-step hydration method (Figure 2). In this work, by analyzing the membrane composition and supramolecular organization of vesicles prepared by both methodologies, we demonstrate that apart from size and morphology, the superior homogeneity observed for vesicular systems produced by CFs is also present in the molecular assembly of the membrane constituents, which is crucial for an optimum performance of these supramolecular structures as pharmaceutical carriers.

References:

[1] Couvreur, P. and Vauthier, C., Pharmaceutical Research, 23 (2006) 1417.
[2] Peer, D., Karp, J.M., Hong, S., Farokhzad, O.C., Margalit, R. and Langer, R., Nature Nanotechnology, 2 (2007) 751.
[3] Bangham, A.D., Standish, M.M. and Watkins, J.C., Journal of Molecular Biology, 13 (1965) 238.
[4] Guo, X. and Szoka, F.C., Accounts of Chemical Research, 36 (2003) 335.
[5] Davies, O.R., Lewis, A.L., Whitaker, M.J., Tai, H.Y., Shakesheff, K.M. and Howdle, S.M., Advanced Drug Delivery Reviews, 60 (2008) 373.
[6] Elizondo, E., Sala, S., Imbuluzqueta, E., González, D., Blanco-Prieto, M. J., Gamazo, C., Ventosa, N. and Veciana, J, Pharmaceutical Research (2010), doi:10.1007/s11095-010-0248-x.
[7] Imbuluzqueta, E., Elizondo, E., Gamazo, C., Moreno-Calvo, E., Veciana, J. and Ventosa, N., Acta Biomaterialia (2010), doi:10.1016/j.actbio.2010.11.031.

[8] Cano-Sarabia, M., Ventosa, N., Sala, S., Patino, C., Arranz, R. and Veciana, J., Langmuir, 24 (2008) 2433.
[9] Cano-Sarabia, M., Angelova, A., Ventosa, N., Lesieur, S. and Veciana, J., Journal of Colloid and Interface Science, 350 (2010) 10.

Figures:

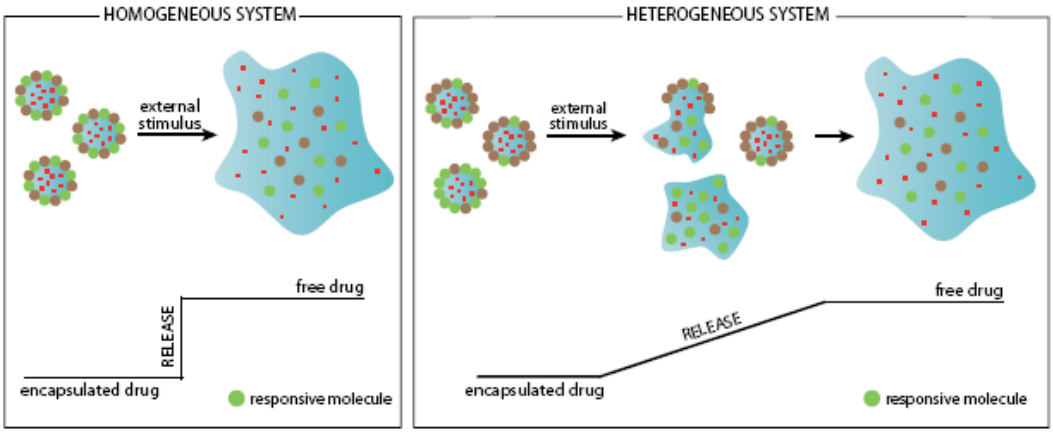

Figure 1: *Schematic illustration of the response to an external stimulus presented by a vesicular DDS with homogeneous (left) and heterogeneous (right) vesicle to vesicle composition and supramolecular arrangement.*

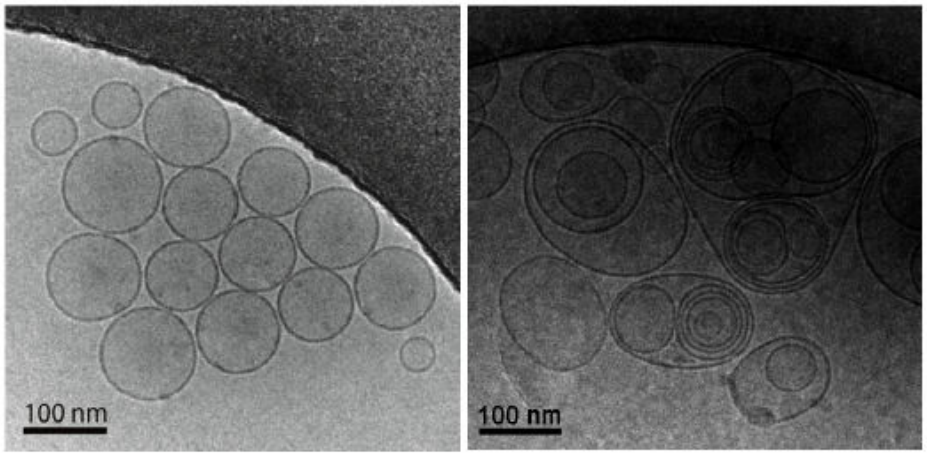

Figure 2: *CryoTEM images corresponding to cholesterol-rich vesicles prepared by DELOS-susp (left) and the hydration method (right).*

QUANTIFICATION OF NANOPARTICLE UPTAKE AND THEIR COLOCALIZATION WITH CELL CONSTITUENTS AT SINGLE CELL LEVEL

I. Estrela-Lopis, J. Fleddermann, M. Dorn, G. Romero, E. Rojas, Sergio Moya, Changyou Gao, Edwin Donath

Institute of Medical Physics & Biophysics, Leipzig University, Härtelstraße 16, 04107 Leipzig, Germany
Irina.Estrela-Lopis@medizin.uni-leipzig.de

The development of nanotechnology in recent years is unprecedented. Understanding the effects of nanoparticles (NPs) on human health is thus of major importance.[1,2] The degree and the mechanism of uptake, localization and distribution of NPs in cells are major issues concerning toxicity and risk assessment, and the effectivity of NPs as delivery devices. A better understanding of the potential effects of nanomaterials on human health is crucial regarding the introduction of nanoproducts into the market and has thus considerable economical importance.

Ion Beam Microscopy (IBM) and Confocal Raman Microspectroscopy (CRM) were therefore employed as label-free techniques capable of detecting and characterizing nanomaterials within single cells. The uptake, intracellular distribution and toxicity of carbon nanotubes (CNTs) and metal oxide nanoparticles in hepatocarcinoma (HepG2) and lung cells (A549) were studied employing these techniques.

By means of IBM the intracellular concentration and distribution of NPs can be established. Overlapping of cell basis element P with CeO_2 NPs can be easily seen in Figure 1. The concentrations of NPs in / or on the cell were calculated in one cell by choosing the mask of cell area. This provides the basis for intracellular dose dependent toxicity studies.

By means of Raman spectra deconvolution and subsequent cross-correlation analysis the colocalization of NPs with different intracellular environments, such as lipid rich regions, cytoplasm and nucleus was quantified. Figure 2 demonstrates the distribution of lipids and poly-(sulfo propyl methacrylate) (PSPM) modified CNTs in HepG2 cell. CRM, furthermore, was capable of detecting nanomaterial induced changes in the secondary nuclear protein structure and nucleobases content. These changes can be used as an indicator of the toxic effect of NPs. This was confirmed with cell proliferation tests. Studies with NPs surface engineered with lipids and polyelectrolytes showed that the nature of the surface of NPs and their modification in biological fluids is crucial for uptake and toxicity.

References:

[1] Lee J, Lilly GD, Doty RC, Podsiadlo P, Kotov NA 2009 Small 5 1213-21.
[2] Hillegass JM, Shukla A, Lathrop SA, MacPherson MB, Fukagawa NK, Mossman BT 2010 Wiley Interdiscip Rev Nanomed Nanobiotechnol 2 219-31.
[3] Romero G, Estrela-Lopis I, Zhou J, Rojas E, Franco A, Espinel CS, Fernandez AG, Gao C, Donath E, Moya SE 2010 Biomacromolecules 11 2993-2999

Figures:

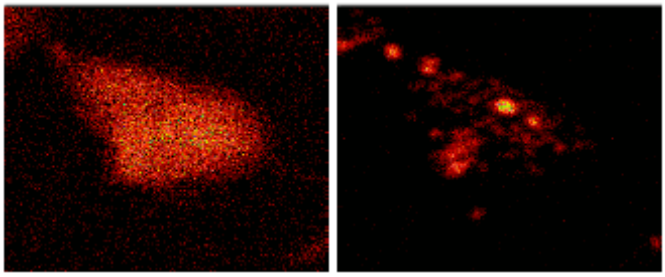

Figure 1: *Proton Induced X-Ray Emission elemental mapping of the cells A549 treated during 72 h with CeO_2 NPs. Left image demonstrate the P distribution and right image – Cerium.*

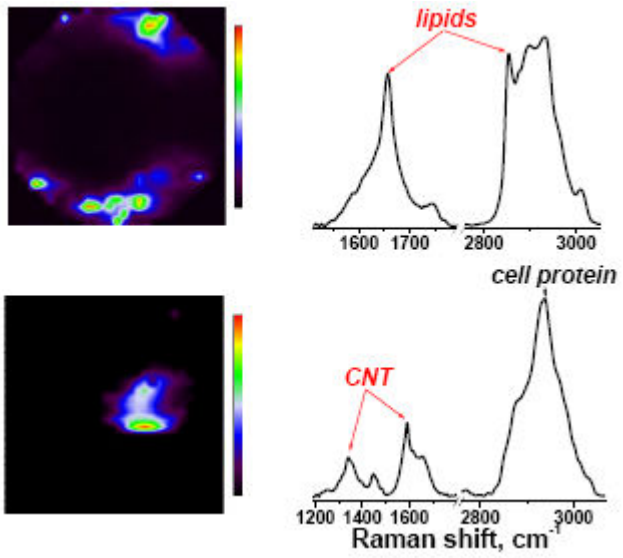

Figure 2: *CRM mappings of a HepG2 cell treated with CNT/PSPM NPs. Top and bottom images show distribution of lipid rich region and CNTs, respectively. The spectra refer to the spot of maximum concentration of both components in corresponding images of the cell.*

UNDERSTANDING INTERACTIONS OF ENGINEERED NANOMATERIALS WITH THE IMMUNE SYSTEM

Bengt Fadeel

Division of Molecular Toxicology, Institute of Environmental Medicine,
Karolinska Institutet, Stockholm, Sweden
bengt.fadeel@ki.se

Engineered nanoparticles may affect the innate or adaptive immune system; such interactions, in turn, could result in adverse outcomes or could potentially be exploited for therapeutic gain. The recognition or non-recognition of engineered nanomaterials by immune-competent cells may determine not only the toxic potential of such materials but also their biodistribution. However, understanding the physico-chemical properties that drive cellular interactions of nanoparticles remains a key challenge. Needless to say, particular attention should be paid to novel, adverse properties arising as a consequence of the nano-scale size. For instance, nanoparticles may escape immune surveillance and translocate to distal sites following entry into the body. In addition to particle size, other aspects including particle shape, and surface charge, may also play an important role for immune recognition and subsequent handling of nanomaterials.

When human subjects are deliberately exposed to engineered nanomaterials, for diagnostic or therapeutic purposes (or both), it becomes critically important to determine the ultimate fate of the nanoparticles: are engineered nanomaterials excreted from the body, or biodegraded by cells of the immune system, or do they bioaccumulate, thereby leading to potentially harmful long-term effects? The surface of nanoparticles can be modified using targeting moieties, etc but as these particles enter into a biological system, for instance via inhalation or injection into the bloodstream, it is likely that the surface of the particles is covered with biomolecules – proteins and lipids – that modify the properties of the nanoparticles and the way in which the particles interact with cells, including immune-competent cells. Moreover, the binding of proteins to nanoparticles may also induce modifications of the proteins. Understanding such nano-bio-interactions is critical for the safe application of nanoparticles in medicine.

Further reading:

[1] Fadeel B, Garcia-Bennett AE. Better safe than sorry: understanding the toxicological properties of inorganic nanoparticles manufactured for biomedical applications. Adv Drug Deliv Rev. 2010;62:362-74.
[2] Feliu N, Fadeel B. Nanotoxicology: no small matter. Nanoscale 2010;2:2514-20.
[3] Shvedova AA, Kagan VE, Fadeel B. Close encounters of the small kind: adverse effects of man-made materials interfacing with the nano-cosmos of biological systems. Annu Rev Pharmacol Toxicol. 2010;50:63-88.

The Use of Nanostructured Microparticles in a Suspension Based Adsorption System for Extracorporeal Blood Purification to Treat Acute Liver Failure and Sepsis

Dieter Falkenhagen, M.Brandl, Jens Hartmann and Viktoria Weber

Department of Clinical Medicine and Biotechnology, Danube University Krems
Krems, Austria

Introduction: Acute liver failure and sepsis are severe diseases that are characterized by high morbidity but also mortality. Especially sepsis as the general inflammatory response of a mainly bacterial infection is characterized by high mortality of 20-60% depending of the stage of the disease. Alone in the US about 200.000 patients die annually (N.Engl.J.2002) on this dangerous disease. Interestingly, also the high mortality of acute liver failure is caused by an inflammatory scenario which is caused by the disturbed liver function which in contrast to a normal liver does not inhibit the transfer of the very toxic endotoxins derived from Gram-negative germs of the intestine into the blood circulation. Therefore, sepsis as well as acute liver failure are characterized by many processes which are based on the activation of cellular mechanisms as well as communication pathways between different blood- and tissue cells which are over stimulated in a very dangerous way. We have developed a technology – the so called MDS (Microspheres based Detoxification System, D.Falkenhagen et al: Therapeutic Apheresis and Dialysis 10, 154, 2006)) which combines membrane separation and adsorption processes in an extracorporeal blood purification (EBP) – device in order to influence by separation specific signaling factors such as cytokines but also toxic substances such as endotoxins as well as liver specific metabolites such as bilirubin but also uremic toxins.

Methodology: For our investigations – neutral microadsorbents based on styrene-divinylbenzene-copolymers with different pore size dimension from 15-20 nm (type 1), 30-40 nm (type 2) and 80 to 100 nm (type 3) as an average have been developed in cooperation with the company Dow Chemical characterized all by an average diameter of 5 respectively 10µm. Those nanostructured microparticles have been analysed in batch tests but also in MDS-systems investigations with respect to the removal of

- endotoxins using the microparticles mentioned coated with polymyxin B just by adhesion forces based on hydrophobic interaction,
- bilirubin and cholic acid using the microparticles coated/uncoated with human serum albumin (HSA)
- Cytokines TNF, IL-1ß, IL-8, IL-10 investigating all microparticle mentioned coated/uncoated with human seumalbumin (HSA)

Finally systems investigation using the complete MDS with 1.2 L whole blood were performed. The microspheres containing suspension was based on 100 ml HAS coated neutral resins sized 10µm in average having an inner pore size structure of 30-40 nm.

Results: 1. Endotoxin removal from heparinized plasma was optimal using PS-resins – type 3 having an inner pore size of 80-100 nm in comparison to smaller pore size containing resins.

The immobilization of PM-B by just physical forces demonstrated highest efficiency for endotoxin removal which was not negatively influenced by autoclavation.

HSA – coated PS-resins type 2 having an inner pore size of 30-40 nm were optimal adsorbents for bilirubin being characterized by significant less protein C and S as well as fibrinogen adsorption in comparison to the HSA-non-coated resins interestingly not loosing their efficiency for bilirubin – an HSA – bound liver-specific substance.

HSA-pre-treated PS-resins type 1 characterized by an inner pore size of 10-20 nm showed nearly an untouched adsorption of different cytokines (except TNF) avoiding the adsorption of considerable amounts of protein C and S as well as fibrinogen.
HSA-coating of type 1 and 2 - resins demonstrated a significant improvement of blood compatibility especially related to the adsorption of protein C and also fibrinogen which is essential for the use of microparticles in EBP.

Systems investigations clearly demonstrated the efficiency of MDS especially in case of the removal of strongly bound biirubin but also of many cytokines such as IL 6,8,10 despite the fact that the inner filtration rate in the suspension circuit connected to the plasmafilter (FMC, P1) was by far not optimal.

Conclusion: Optimization of inner pore size structure of hydrophobic resins for adsorption seems to be a useful way to develop efficient microadsorbents for the elimination of different substances being relevant for acute liver failure and sepsis. The extracorporeal blood purification technology MDS applying the microparticles in suspension and not in a column is closed to become clinically used.

Key words: Adsorption, therapy, extracorporeal blood purification, sepsis, liver failure

IN SITU DELIVERY OF TROPHIC FACTORS AND MOLECULES IN THE HUMAN BRAIN BY CONVECTION TECHNOLOGIES

Massimo S. Fiandaca, Adrian P. Kells, Dali Yin, Ernesto Aguilar Salegio, R. Mark Richardson, Piotr Hadaczek, John Bringas, Mitchell S. Berger, John Forsayeth, and Krystof S. Bankiewicz

UCSF Neurosurgery, San Francisco, California, USA
massimo.fiandaca@ucsf.edu

Convection-enhanced delivery (CED) is a direct method of distribution for therapeutic agents within the central nervous system (CNS) that bypasses the blood-brain barrier (BBB). CED allows the homogenous distribution of a variety of molecular species within the CNS extracellular space (ECS) by developing a pressure gradient between the tip of the infusion catheter and the surrounding ECS [1]. The propagation of therapeutic materials within the resulting bulk flow of infusate is not size dependant, as it is for delivery technologies that are based upon diffusion. This fact allows the transmission of macromolecules and viruses in addition to small molecular species within the CNS via CED [2-5].

Our laboratory has been actively involved in developing a delivery platform that combines MRI and CED technologies (real-time convective delivery, RCD) [6]. We currently utilize RCD for our preclinical investigations and stress the importance for its use in clinical applications for neurodegenerative diseases [7], neuro-oncology [8], and inherited metabolic disorders [9] affecting the CNS, since it allows us to directly monitor the infusion of therapeutics within the target site. This direct visualization may not only help improve treatment efficacy for a therapeutic, by standardizing the volumetric distribution, but is also important in preventing reflux and leakage associated with CED [10].

In this presentation, we aim to review the how CED technologies function and how they may impact future treatments of human brain disorders.

References:

[1] Bobo, R. H.; Laske, D. W.; Akbasak, A.; Morrison, P. F.; Dedrick, R. L.; Oldfield, E. H., Proc Natl Acad Sci U S A 91 (1994) 2076-2080.
[2] Bankiewicz, K. S.; Eberling, J. L.; Kohutnicka, M.; Jagust, W.; Pivirotto, P.; Bringas, J.; Cunningham, J.; Budinger, T. F.; Harvey-White, J., Exp Neurol 164 (2000) 2-14.
[3] Lonser, R. R.; Schiffman, R.; Robison, R. A.; Butman, J. A.; Quezado, Z.; Walker, M. L.; Morrison, P. F.; Walbridge, S.; Murray, G. J.; Park, D. M.; Brady, R. O.; Oldfield, E. H., Neurology 68 (2007) 254-261.
[4] Morrison, P. F.; Lonser, R. R.; Oldfield, E. H., . J Neurosurg 107 (2007) 74-83.
[5] Szerlip, N. J.; Walbridge, S.; Yang, L.; Morrison, P. F.; Degen, J. W.; Jarrell, S. T.; Kouri, J.; Kerr, P. B.; Kotin, R.; Oldfield, E. H.; Lonser, R. R., J Neurosurg 107 (2007) 560-567.
[6] Fiandaca, M. S.; Forsayeth, J. R.; Dickinson, P. J.; Bankiewicz, K. S., Neurotherapeutics 5 (2008) 123-127.
[7] Fiandaca, M. S.; Bankiewicz, K. S., Curr Opin Mol Ther 12 (2010) 519-529.
[8] Dickinson, P. J.; LeCouteur, R. A.; Higgins, R. J.; Bringas, J. R.; Roberts, B.; Larson, R. F.; Yamashita, Y.; Krauze, M.; Noble, C. O.; Drummond, D.; Kirpotin, D. B.; Park, J. W.; Berger, M. S.; Bankiewicz, K. S., J Neurosurg 108 (2008) 989-998.
[9] Aguilar-Salegio, E.; Kells, A. P.; Richardson, R. M.; Hadaczek, P.; Forsayeth, J.; Bringas, J.; Sardi, P. S.; Passini, M. A.; Shihabuddin, L. S.; Cheng, S. H.; Fiandaca, M. S.; Bankiewicz, K. S., Hum Gene Ther 21 (2010) 1093-1103.
[10] Varenika, V.; Dickenson, P.; Bringas, J.; LeCouteur, R.; Higgins, R.; Park, J.; Fiandaca, M.; Berger, M.; Sampson, J.; Bankiewicz, K. S., J Neurosurg 109 (2008) 874-880.

Figures:

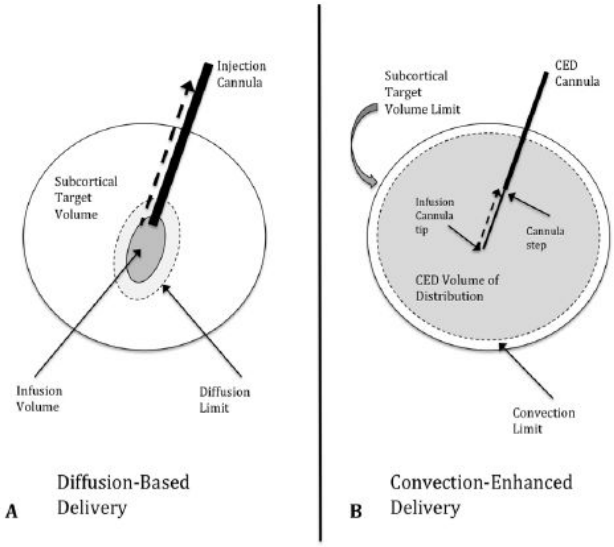

Figure 1: *Cannula-based delivery options utilized with gene therapy. (A) Diffusion-based delivery system: A characteristically large injection cannula is used to deliver the infusion volume within the target region. The infusion volume typically displaces the surrounding parenchyma at the tip of the cannula and forms a small cavity from which diffusion occurs into the surrounding brain, eventually expanding to the diffusion limit, but falling significantly short of filling the subcortical target volume. Multiple factors influence the diffusion limit for infused substances, with molecular size being one of the most significant factors. Macromolecules, proteins and viral particles are limited significantly in their ability to diffuse beyond the infusion volume. Another factor that limits the effectiveness of this technique is the development of backflow or reflux (dashed black arrow) of the infusate out of the target region, along the path of the injection cannula. (B) Convection-enhanced delivery (CED) system: Optimal CED cannulae consist of an outer guide cannula and an inner fused-silica infusion cannula that is attached to the pump mechanism that controls the rate of infusion. The infusion cannula extends beyond the guide cannula, with the transition between the two referred to as the cannula step. The infusate is delivered with a constant flow rate (most commonly 0.5 to 1.0 µl/min) from the infusion cannula tip. This flow rate establishes a pressurized extracellular bulk flow that allows the homogenous distribution of molecules of various sizes, including liposomes, proteins and viral particles, for significant distances (multiple centimeters, if necessary) from the infusion cannula tip. Reflux (dashed black arrow) typically only occurs up to the cannula step, and major backflow along the cannula and out of the target region is prevented by central placement of the step within the target volume. The convection limit can approach the subcortical target volume limit more easily compared with the diffusion-based delivery system. (Adapted with permission from Massimo S Fiandaca. © 2010 Massimo S Fiandaca)*

BIOMEDICAL APPLICATIONS OF DOUBLE-WALLED CARBON NANOTUBES AND QUESTIONS RELATED TO THEIR POTENTIAL IMPACT ON HUMAN HEALTH AND THE ENVIRONMENT

E. Flahaut, B. Pipy, L. De Gabory, L. Bordenave, F. Mouchet, L. Gauthier, A-M. Galibert, B. Soula, P. Lukanov, C. Tilmaciu, S. Benderbous, I. Loubinoux, L. Vaysse, A. Beduer, C. Vieu

Universite Paul Sabatier, France

Carbon nanotubes (CNT), with an annual world production reaching several hundreds of tons, represent a special category of nanomaterials with exceptional characteristics. In particular, they are currently investigated for many biomedical applications, ranging from medical imaging (MRI, Raman) to targeted drug delivery and cancer treatment. Tissue engineering is a field in which CNT could bring many improvements as compared to existing biomaterials, and especially for regeneration of neuronal tissues as they provide a unique combination of useful electrical and mechanical properties at the nanometer scale. Double-walled CNT [1], at the frontier between SWNT and MWNT, are very promising for applications in the biomedical field.

Recent results will be presented, showing that through surface engineering, we can direct and guide the growth and differentiation of neural cells. Topographical grooves obtained by a moulding process against a silicon master turned efficient for both neural lines cells and adult neural stem cells. Double-walled CNT [1] patterns obtained by soft lithography were also found very efficient and have the advantage of possible electrical stimulation due to their metallic electrical behaviour. In both cases, low cost fabrication processes (moulding or soft-lithography) are developed, enabling further large scale applications for biological or medical purposes. Potential application of DWNT for medical imaging (MRI) and gene delivery will also be presented.

Although the toxicity and the environmental impact of CNT have now both been investigated by many different groups (although the latter never focused much attention until very recently), there is yet a controversy about the results and still no answer to the simple question: "are CNT toxic?" The fact is that the large range of kinds of CNT and methods to produce and then (in most cases) process them make any comparison almost impossible. The results presented here were obtained with the same batch of CCVD-produced DWNT [1] investigated for biomedical applications, and concern both the investigation of their potential impact on human health (*in vitro* / *in vivo* models) [2, 3] and the environment (*in vivo* models) [4]. They lead to the conclusion that all the experimental parameters (dealing both with CNT and biological models used) play a very important role and can easily explain the large differences between the results obtained by the different researchers.

References:

[1] E. Flahaut et al., Chem. Comm. (2003) 1442.
[2] E. Flahaut, M.C. Durrieu, *, Ch. Baquey, Carbon, 44, (6), (2006), 1093-1099
[3] J. C. Debouzy, D. Crouzier, E. Flahaut, Env. Toxicol. Pharmacology, 30, (2), (2010), 147-152 [4] E. Flahaut, Nanomedicine, 5, (6), (2010), 949-590

ELECTROCHEMICAL APTASENSORS BASED ON CARBON NANOTUBES AND CONDUCTING POLYMERS

Tibor Hianik[1], Maja Šnejdarková[2], Alexandra Poturnayová[2], Anna Porfireva[3], Gennady Evtugyn[3], Anna Miodek[4], Hafsa Korri-Youssoufi[4], Isabel Neudlinger[5], Ivana Karpisova[1], Christian Rankl[5], Peter Hinterdorfer[5], Andreas Ebner[5]

[1]Faculty of Mathematics, Physics and Informatics, Comenius University, Mlynská dolina F1, 842 48 Bratislava, Slovakia
[2]Institute of Animal Biochemistry and Genetics, Slovak Academy of Sciences, 900 28 Ivanka pri Dunaji, Slovakia,
[3]Analytical Chemistry Department, Kazan Federal University, 18 Kremlevskaya Street, Kazan, 42008, Russian Federation,
[4]Equipe de Chimie Bioorganique et Bioinorganique, CNRS UMR 8182, Institut de Chimie Moléculaire et de Matériaux d'Orsay, Université Paris-Sud, Bâtiment 420, 91405 Orsay, France,
[5]Biophysics Institute, Johannes Kepler University Linz, Altenbergertrasse 69, 4040 Linz, Austria
tibor.hianik@fmph.uniba.sk

DNA and RNA aptamers are single stranded oligonucleotides with high affinity to proteins or other ligands, comparable to those of antibodies. The aptamers are selected in vitro by the SELEX method [1]. In solution, the aptamers maintain an unique configuration that contains specific binding site to the ligand. Aptamers can be easily modified by biotin, SH or amino- groups, leading to a variety of immobilization strategies on solid supports. Using simple molecular engineering based on DNA hybridization it is possible to create aptamer dimers with two binding sites like that in antibodies [2]. These aptamer dimers (aptabodies) are characterized by improved sensitivity to the analyte, for example to thrombin. We have shown that typical guanine quadruplexes that form binding site for thrombin are stable in aptamer dimers [3]. Currently there is increased interest in development of aptamer based biosensors for detection proteins and other molecules using various methods of detection, such us optical, acoustical and electrochemical [4,5]. These biosensors could be used in fast and low cost medical diagnostics. The sensitivity of detection depends not only on the selectivity of binding site, but also on supporting part of the aptamer that serve for immobilisation onto a solid support. Using multiwalled carbon nanotubes (MWCNTs) as an immobilization matrix we developed high sensitive biosensor for detection human thrombin [2] and cellular prions (PrP^C) [6] in biological liquids. In this work we analyzed in detail the properties of DNA aptasensors sensitive to thrombin, immobilised either on a gold support covered by neutravidin or on a surface of MWCNTs. We have shown that immobilisation of aptamers and aptamer dimers at MWCNTs improved the sensitivity of the sensor for thrombin and allowing detection in a complex matrix such as blood plasma. Using single molecule force spectroscopy (SMFS) we studied in detail the forces between enhanced single stranded aptamers (BFA) and aptamer dimers (BFF) immobilised on an AFM tip and the thrombin immobilised on a mica surface. By varying the pulling velocity in force distance cycles the formed thrombin – aptamer complexes were ruptured at different force loading allowing determination of the energy landscape. It turned out that the BFA aptamer shows a higher binding force at the investigated loading rates and a significant lower dissociation rate constant, k_{off}, compared to BFF. The lower binding strength of BFF in comparison with those of BFA may be due to certain sterical hindrance between two G-quadruplexes of this aptamer dimer. However, the potential of the aptabody BFF to form more stable double bound complex could clearly be shown.

Using thickness shear mode acoustic method (TSM) we analyzed in detail the interaction of thrombin with DNA aptamers of various configurations immobilised at the neutravidin layer chemisorbed on TSM quartz crystal transducer and showed enhanced sensitivity for detection thrombin by aptamer heterodimer (BFH) [8]. The obtained results agree well with those of SMFS studies.

By means of electrochemical quartz crystal microbalance method (EQCM) we performed comparative analysis of the sensitivity of DNA aptamers and antibodies specific to human cellular prions (PrP^C) immobilised on a surface of MWCNTs (Fig. 1). We found that the detection limit (LOD) for both aptamers (50 pM) and antibodies (20 pM) was rather low indicating high, but comparable sensitivity (Fig. 2). The LOD was also much better in comparison with immobilisation of aptamers on a surface of conducting co-polymers and using QCM and surface plasmon resonance (SPR) as detecting

methods. Higher stability of aptamers in comparison with antibodies and possibility to easy regenerate aptasensors make them rather promising candidates for practical applications.

Acknowledgements:

Financial support of Agency for Promotion Research and Development under the projects No. LPP-0341-09 and SK-FR-0025-09, Slovak Academy of Sciences under the project mnt-era.net (proposal No. 2009-50), VEGA 1/0794/10 and COST TD1003 is gratefully acknowledged.

References:

[1] A.D. Ellington, J.W. Szostak, Nature, 346 (1990) 818.
[2] T. Hianik, A. Porfireva, I. Grman, G. Evtugyn, Protein and Peptide Letters, 15 (2008) 799.
[3] S. Ponikova, K. Tlučková, M. Antalík, V. Víglaský, T. Hianik, Biophys. Chem., 2011, in press
[4] T. Hianik, J. Wang, Electroanalysis, 21 (2009) 1223.
[5] M. Mascini (Ed.) Aptamers in Bioanalysis, Wiley, New Jersey, 2009.
[6] T. Hianik, A. Porfireva, I. Grman, G. Evtugyn, Protein and Peptide Letters, 16 (2009) 363.
[7] T. Hianik, I. Grman, I. Karpišová, Chem. Commun. (2009) 6303.

Figures:

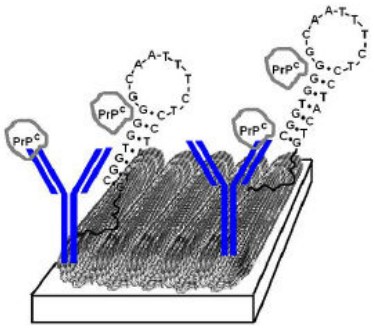

***Figure 1**: Schematic representation of the sensor surface composed of MWNTs and immobilised DNA aptamers and antibodies with bounded PrP^c.*

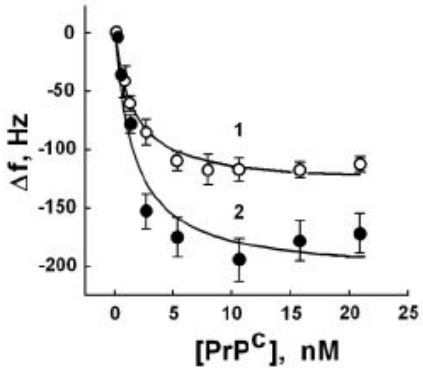

***Figure 2**: The plot of the frequency changes as a function of PrPC concentration for biosensor based on: 1 – single-stranded aptamer and 2 – BAR 223 antibody immobilized on the surface of MWCNTs. The points are experimental results and the lines are fit according to Langmuir isotherm (error bars: SD, N = 3) [7].*

FIELD FLOW FRACTIONATION COUPLED WITH LIGHT SCATTERING AND ICP-MS FOR QUANTITATIVE BIO-NANO MEASUREMENTS

Erik H. Larsen, Katrin Löschner, Bjørn Schmidt

Technical University of Denmark, National Food Institute, 19, Mørkhøj Bygade, DK-2860, Denmark
Ehlar@food.dtu.dk

An instrumental platform based on asymmetric flow field flow fractionation (AFFF) coupled with classical multi angle light scattering (MALS), dynamic light scattering (DLS) and ICP-MS was established and applied to the study of silver, gold and selenium NPs in biological materials.

Using the platform, gold nanoparticles (10-60 nm o.d.) were separated and quantified with respect to their size and mass concentration (Fig. 1), and figures of merit including LOD, recovery and repeatability were established [1]. The bare gold NPs adhered to instrument surfaces, as demonstrated by electron microscopy, and caused incomplete recoveries. Gold NPs were administered by intravenous injection and recovered from rats' livers following alkaline solubilisation of the tissue. The gold NPs were successfully stabilised with bovine serum albumin (BSA) in the alkaline suspension, but TEM imaging showed that the NPs were associated with un-digested tissue residues, which precluded appropriate separation by AFFF.

The platform was used to the study absorption, distribution, metabolism and excretion (ADME) in rats of BSA-stabilised Se^0 NPs (20 nm o.d.) using selenite as positive control. The results (Fig. 2) showed that selenium as nano-Se^0 particles or as selenite both were highly bio-available and mainly were deposited in liver and kidney or excreted via urine and feces. Se^0 was detected in tissues of rats following in situ reaction with sulphite to form the selenosulfate anion, which was determined by HPLC-ICP-MS. The finding of Se^0 both in tissues from nano- Se^0 and selenite dosed animals brings new information to the current knowledge about metabolic pathways of selenium.

Research on dedicated methods for sample preparation of food prior to silver NP detection is underway in the NanoLyse project, funded by the European Commission (www.nanolyse.eu)

The general conclusion of our work on biological research with nanoparticles is that access to a variety of tools and methods, including appropriate sample preparation, separation and atomic spectrometric detection and electron microscopy, are necessary for trouble shooting and acquisition of robust data.

References:

[1] Bjørn Schmidt, Katrin Loeschner, Niels Hadrup, Alicja Mortensen, Jens J. Sloth, Christian Bender Koch and Erik H. Larsen, Quantitative Characterization of Gold Nanoparticles by Field-Flow Fractionation Coupled On-line with Light Scattering Detection and Inductively Coupled Plasma Mass Spectrometry, Anal. Chem., (submitted)

Figures:

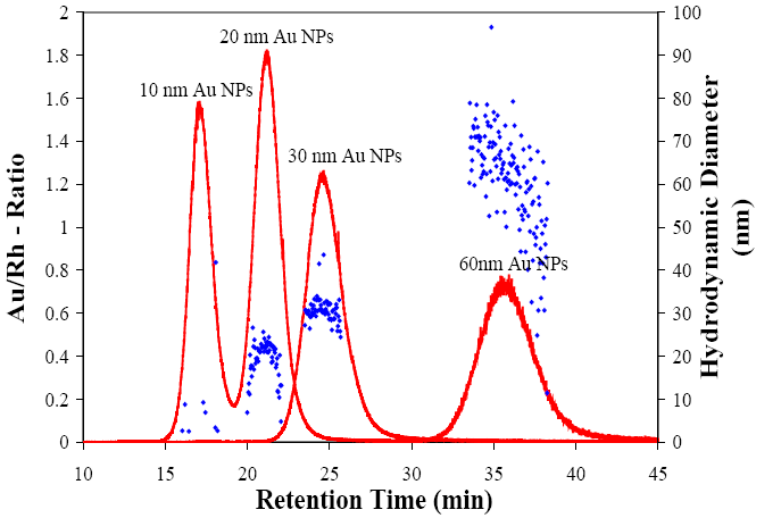

Figure 1: *AFFF-LS-ICP-MS fractogram and hydrodynamic diameter of a mixture of 4 gold nanoparticles*

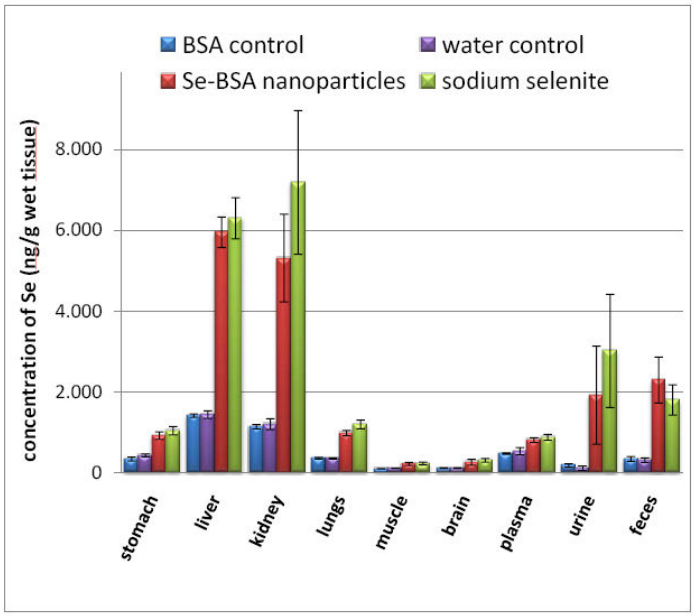

Figure 2: *Distribution of selenium in biological samples from rats administered selenium at 0.4 mg/kg b.w./day for 28 days as BSA-stabilised nano-Se^0 or selenite*

FUNCTIONALIZED NANOPARTICLES FOR BIOMOLECULAR IMAGING AND SENSING

Raphaël Lévy, Yann Cesbron, Chris Shaw, Umbreen Shaheen and Daniel Nieves

Institute of Integrative Biology, Crown Street, L69 7ZB Liverpool, United Kingdom
http://raphazlab.wordpress.com/, rapha@liverpool.ac.uk

Gold nanoparticles have been used for several decades as labels in immuno-electron microscopy. In the last decades, progress in the synthesis, functionalization and optical detection of these particles have opened a range of new applications in imaging and sensing. For most of these applications, the capping layer is a critical feature as it provides colloidal stability and control specific and unspecific interactions.

The presentation will cover three related themes of research. First, I will present the synthesis and characterization of peptide-capped gold nanoparticles [1] and discuss our efforts to generate complex and controlled nanomaterials based on self-assembly of these small molecules at the surface of the particles. Then, I will report on the entry and fate of the particles in live cells, with a particular focus on the fate of the capping layer [2]. Finally. I will discuss our current attempts to break the barrier of endocytotic trapping of the nanoparticles using a variety of methods including toxins, signalling peptides and direct injection.

References:

[1] Rational and combinatorial design of peptide capping Ligands for gold nanoparticles; Lévy, R., Thanh, N.T.K., Doty, R.C., Hussain, I., Nichols, R.J., Schiffrin, D.J., Brust, M. and Fernig, D.G. (2004) . J. Am. Chem. Soc. 126, 10076-10084

[2] Cathepsin L Digestion of Nanobioconjugates upon Endocytosis; Violaine Sée, Paul Free, Yann Cesbron, Paula Nativo, Umbreen Shaheen, Daniel J. Rigden, David G. Spiller, David G. Fernig, Michael R. H. White, Ian A. Prior, Mathias Brust, Brahim Lounis and Raphaël Lévy, ACS Nano, 2009, 3, 2461-2468

DIAGNOSTIC AND THERAPEUTIC CHALLENGES IN NEURODEGENERATIVE DISEASES

Gurutz Linazasoro

INBIOMED Foundation, San Sebastián, Spain

Nanotechnology will play a key role in developing new diagnostic and therapeutic tools. Nanotechnologies use engineered materials with the smallest functional organization on the nanometre scale in at least one dimension. Some aspects of the material can be manipulated resulting in new functional properties.

Neurodegenerative diseases of the elderly currently represent a major challenge to the health care system. With the increasing longevity of the general population, the predicted figures for the prevalence of these disorders and their global financial impact are truly staggering. For example, it has been estimated that by 2030 as many as 7.7 million people in the US will have Alzheimer's disease, and by 2050 this number will reach approximately 13.5 million, with total annual costs for care rising from $172 billion in 2010 to $1.08 trillion in 2050. This analysis does not take into account the value of unpaid care provided by families and others, estimated to have been $144 billion in 2009. In the UK, the cost of dementia is now estimated to exceed the combined cost of cancer, heart disease and stroke. The prevalence of Parkinson's disease is expected to double by the year 2030, and, given the greater risk of Parkinson's disease dementia in elderly individuals with Parkinson's disease, it is expected that the health care costs for this disorder will increase even more relative to the prevalence of the disease. These concerns highlight the urgent need for the development of effective disease-modifying therapies. Effective treatment would have a major influence on the economic and social burden of these age-related disorders. For example, in the case of Alzheimer's disease, it has been estimated that a delay in onset by 5 years would translate into a 50% decrease in disease prevalence, and a delay of 10 years would result in a virtual disappearance of the disease. Unfortunately, despite considerable investment, to date all attempts at developing such treatments have failed. In summary, there is an urgent need of developing reliable biomarkers of very early phases of the neurodegenerative process and to discover effective therapies directed at the core of the biological process in order to stop disease progression.

Besides this general and urgent need, there are many other key points in the diagnosis and tretatment of neurodegenerative diseases that can be targeted by nanotechnologies. Among them it is worth mentioning:

1. - Early diagnosis:
   a) To monitor the rate of cell loss in brain nuclei and alert the defence system and the compensatory mechanisms systems (neurogenesis included) when the rate is exceeding the normal expected decline.
   b) To monitor the state of defence and compensatory mechanisms.
   c) To create biosensors to monitor neurotransmitter levels in precise locations within the brain which can be reduced long before the appearance of symptoms.
   d) To improve image technologies (Fluorophores and quantum dots) which may also facilitate surgical approaches.
   e) Systems to detect abnormalities in plasma, thus avoiding the need of invasive tools.

2. - Study of pathogenetic mechanisms. To increase our knowledge about the mechanisms of cell death, thereby opening the doors to new drug targets.

3. - Treatment
   - To direct drugs to their target in a very specific way: Smart targeted drug delivery systems. Drugs can act on signalling pathways required for neurotransmission (symptomatic effect) or in signalling pathways involved in neurodegeneration (neuroprotection and neurorescue). (eg. Nanoparticles, drug encapsulation strategies, multifunctional nanotherapeutics, ablation of areas with nanoparticles, DNAbots to identify and destroy pathogenic proteins,...)
   - To develop systems able to overcome the blood brain barrier (eg, biobar codes)
   - To create biosensors to monitor neurotransmitter levels in precise locations within the brain.

- Intracellular manipulations and interventions: To repair DNA and other damages, cleaning of deposits of aggregated abnormal proteins,…
- To introduce genes and proteins required for normal functioning in a highly controlled way (durable and controlled expression of the gene) avoiding the needs of viral vectors and complex control systems or of infusion pumps (Eg organic silica particles)
- To create bridges between different nuclei affected by the degenerative process and to favour their development by blocking the expression of antireparative signals (no-go, etc)
- Creation of media to push the development of functional specific type of neurons from stem cells.

All these points can be considered as opportunities for nanotechnologies. Indeed, the NEURONANO era is here.

LAYER-BY-LAYER ASSEMBLY OF BIOMOLECULE-SILICA NANOPARTICLE HYBRIDS FOR ELECTROCHEMICAL BIOSENSORS

Sven Christian Feifel and **Fred Lisdat**

Biosystems Technology, Technical University Wildau Bahnhofstrasse1, 15745 Wildau, Germany
flisdat@th-wildau.de, feifel@th-wildau.de

Biomolecule-nanoparticle hybrid systems have excellent prospects for interfacing biological recognition events with electronic signal transduction so as to design a new generation of bioelectronic devices with high sensitivity. Direct electron transfer between redox proteins and electrodes is of practical and theoretical interest and can be improved by electrode or protein modification. Communication between proteins immobilized in multiple layers on the electrode can be achieved by in situ generation of small shuttle molecules or more advantageously by direct interprotein electron transfer. This allows the construction of new sensing electrodes.[1,2] As a new approach we have tested the use of modified silica nanoparticles (SiNPs) for the built up of fully electro-active cytochrome c (CytC) multilayer assemblies. For this purpose silica nanoparticles of different size are synthesized by adjustment of the Stöber method[3] and the SiNPs were modified by silan-based chemistry[4], to be applied for assembly formation by the layer-by-layer deposition technique.

In this study we use carboxy-modified SiNPs to provide an artificial environment - similar to that of the redox protein in the native system - to construct fully electro-active CytC multilayer architectures. The particles are characterized by dynamic-light-scattering (DLS), zeta-potential and FT-IR. The conditions of assembly formation and stability are determined by QCM. The electrochemical properties of the multilayer assemblies are analyzed by cyclic voltammetry (CV). Special focus is on the size influence of the SiNPs and the electron transfer ability of the multilayer assembly, in dependence on the deposited protein layers. This novel approach may provide a general way to fabricate enzyme multilayers useful in practical applications for biosensors. A future aim is the embedment of specific enzymes into these assemblies to obtain sensorial signal chains.

References:

[1] F. Lisdat, R. Dronov, H. Möhwald, F. W. Scheller, D. G. Kurth,; Chem. Commun. 2009, 274-283.
[2] S. M. Bonk, F. Lisdat; Biosens. Bioelectron. 2009, 25, 739-744.
[3] W. Stöber, A. Fink, E. Bohn; J. Colloid Interface Sci. 1968, 26, 62-69.
[4] R. D. Badley, W. T. Ford, F. J. McEnroe, R. A. Assink; Langmuir 2006, 22, 4357-4362.

Figures:

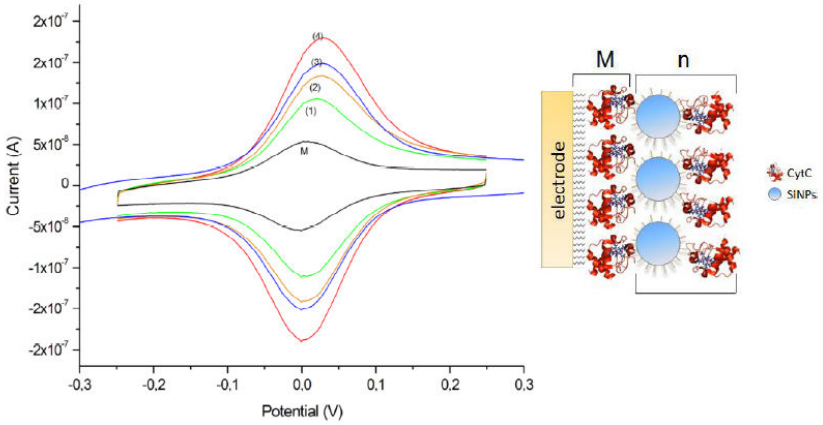

Figure 1: *Cyclic voltammetry of SiNPs/CytC multilayer assemblies, (M) Au-MU/MUA-CytC, (1) M-[SiNPs/CytC]$_1$, (2) M-[SiNPs/CytC]$_2$, (3) M-[SiNPs/CytC]$_3$, (4) M-[SiNPs/CytC]$_4$ for comparison (scan rate100 mV/s, KPP pH7).*

SYNTHESIS OF POSITRON EMITTER LABELED METAL OXIDE NANOPARTICLES FOR BIODISTRIBUTION STUDIES BY DIRECT ACTIVATION WITH HIGH ENERGY PROTONS

Jordi Llop[1], Carlos Pérez Campaña[1], Vanessa Gómez-Vallejo[1], Eneko San Sebastián[1], Abraham Martín[1], Torsten Reese[1], R.Ziolo[3], Sergio E. Moya[2]

[1]Molecular Imaging Unit, CIC biomaGUNE, Paseo Miramon 182, San Sebastian, Spain
[2]Biosurfaces Unit, CIC biomaGUNE, Paseo Miramon 182, San Sebastian, Spain
[3]Advanced Materials Dept. CIQA, Blvd. Enrique Reyna Hermosillo 140, Saltillo, Mexico
jllop@cicbiomagune.es

Nanoparticles (NPs) are widely used and have potential applications in different areas like health care, electronics, manufacturing, food industry, etc. The widespread use of NPs raises several issues regarding their possible toxicological end points. A key issue regarding the study of the possible toxicological effects of NPs is to determine their biological fate and biodistribution. For this, the use of animal models and the application of techniques such as Magnetic Resonance Imaging (MRI) and Positron Emission Tomography (PET) become highly necessary. There is, therefore, an increasing interest for the development of radiolabeling strategies of such NPs, either to determine their pharmacokinetic properties or to assess potential toxicological effects related to long term exposure.

The objectives of the present work are:

1. To develop a new strategy for the introduction of a radioactive atom (positron emitter) in the core of metal oxide NPs.
2. To characterize NPs before and after irradiation to evaluate the effects of activation in the physic-chemical properties.
3. To perform preliminary in vivo biodistribution studies in rodents.

Aluminum oxide NPs incorporating Oxygen-18 in their crystalline structure (which can be activated to the positron emitter Fluorine-18, half-life = 110 min) were synthesized by dissolving an aluminum salt ($AlCl_3$, $Al_2(SO_4)_3$) in [^{18}O]H_2O in the presence of a base (NH_4OH, Urea). NPs were irradiated with 18 MeV protons in an IBA cyclone 18/9 cyclotron. The activated NPs were introduced in a specifically designed phantom and measured with a PET camera (eXplore Vista-CT, GE Healthcare) for 6 hours in 1-20 minutes frames. Time-Activity Curves were obtained and the percentage of the activity as ^{18}F was determined. In the best scenario ($AlCl_3$ / NH_4OH) up to 570 MBq/g of ^{18}F were produced in 6 minutes (Beam intensity on target: 5 μA, beam current: 0.5 μAh). Characterization by means of TEM, light Scattering and X-Ray showed no significant changes in crystal structure, crystal size and NP size after irradiation. In vivo studies were performed using PET after administration of the radioactive NPs to mice and rats (I.V. and oral). Images were co-registered with MRI to localize anatomically regions of interest (ROIs) and Time-Activity curves were determined for liver, kidneys, brain, lungs, stomach, intestine and bladder.

In conclusion, metal oxide NPs containing ^{18}O could be synthesized and activated by bombardment with high energy protons. The irradiation process did not introduce significant changes in particle size and crystal structure. Final amount of radioactivity was sufficient to perform whole body in vivo biodistribution studies in rodents.

ANIMAL MODELS OF DISSEMINATED DISEASE FOR THE DEVELOPMENT OF NANOPARTICLE-DIRECTED DELIVERY OF CANCER THERAPY

R Mangues[1,2], P Álamo[1,2], R Bosch[1,2], R Diéguez[1,2], MJ Moreno[1,2], U Unzueta[1,2], Neus Ferrer-Miralles[1,3], A Villaverde[1,3], M Trias[1,4], J Pavía[1,5], S Rojas[1,5], R Herranz[1,5], L Mondragón[1,6], I Abasolo[1,7], M Royo[1,8], R Martinez[1,6], S Schwartz[1,7], F Albericio[1,8], E Vázquez[1,3], I Casanova[1,2], MV Céspedes[1,2]

[1]CIBER de Bioingeniería, Biomateriales y Nanomedicina (CIBER-BBN) Bellaterra, Barcelona, Spain
[2]Grup d'Oncogènesi i Antitumorals, Institut de Recerca, Hospital de Sant Pau, Barcelona, Spain
[3]Institut de Biotecnologia i de Biomedicina, Universitat Autònoma de Barcelona, Bellaterra, Spain
[4]Departament de Surgery, Hospital de la Santa Creu i Sant Pau, Barcelona, Spain
[5]Grupo de Imagen Biomédica, Universidad de Barcelona, Spain
[6]Grupo de Química Molecular Aplicada, Universidad de Valencia, Spain
[7]CIBBIM Nanomedicine, Vall d'Hebron University Hospital, Spain
[8]Grupo de Química de Péptidos y Nanopartículas del Parc Cientific de Barcelona-UB, Spain
rmangues@santpau.cat

Nanomedicine offers an unprecedented opportunity for targeted drug delivery. The ability of nanometric size particles to enter cells through receptor-mediated endocytosis opens the possibility of designing vehicles for the specific delivery of therapy to disease cells. This directed delivery will highly increase the therapeutic window, by reducing the toxicity on normal cells whereas achieving an enhanced therapeutic response. Even rational therapies (e.g. monoclonal antibodies (mAb)) have limiting toxicities because they are biodistributed to both normal and diseased cells [1]. Thus, the combined effect of a specific delivery vector and a targeted drug, loaded into it, promises to improve current therapeutic approaches.

Most cancer patients have macroscopic or subclinical metastases at diagnosis. Moreover, therapy for metastatic cancer is faced with high level of recurrence, acquired resistance and systemic toxicity [2]; thus, most patients nowadays still die because of metastases [3]. Novel targeted therapies, including mAbs have not significantly improved outcome in this disease [4]. Existing cancer therapies, including mAbs have been developed to block the primary tumor rather than the metastatic process. However, it is known that the same tumor displays a differential regulation of the cell cycle and cell death pathways [5] and a dramatically different response to the same drug [6] depending on the organ where it is growing. The fact that currently used preclinical drug development models (mainly subcutaneous xenografts) do not predict clinical response to antitumor drugs [7] could be in part due to these differences.

Animal models of disseminated disease can be used to assess the efficacy of targeted delivery systems as well as antimetastatic effect. We have developed orthotopic xenograft models of human colorectal and pancreatic tumors, as well as human lymphoma and leukemia, which closely reproduce the metastatic pattern observed in humans [8-11]. We are characterizing tumor cells for their mutational spectrum, to define targets for therapy, as well as the over-expression of membrane receptors, to identify target receptors for the selective delivery of therapy. The design of targeted vectors able to undergo receptor-mediated endocytosis in tumor cells and their ability to selectively deliver targeted therapy, against the oncogenes driving the tumor, inside tumor cells is being tested in such models. This approach may have a significant impact on cancer therapy [12]. Our capacity of using non-invasive radioactive, fluorescent or optical methods, to assess nanoparticle biodistribution and antimetastatic effect, will greatly facilitate our ability to evaluate the effectiveness of these novel therapies.

References:

[1] Adams GP, Weiner LM. Monoclonal antibody therapy of cancer. Nat Biotechnol 2005, 23(9):1147-57

[2] Guyot F, Faivre J, Manfredi S, Meny B, Bonithon-Kopp C, Bouvier AM. Time trends in the treatment and survival of recurrences from colorectal cancer. Ann Oncol. 2005, 16(5):756-61

[3] Coia LR. Cancer Management, 4th ed. Huntington, NY: PRR.Inc, 2000:273-99;

[4] VanCutsem E et al. Cetuximab and Chemotherapy as Initial Treatment for Metastatic Colorectal Cancer. N Engl J Med 2009, 360(14):1408-17.

[5] Farre L, Casanova I, Guerrero S, Trias M, Capella G, Mangues R. Heterotopic implantation alters the regulation of apoptosis and the cell cycle and generates a new metastatic site in a human pancreatic tumor xenograft model. FASEB J. 2002 Jul;16(9):975-82. (IF: 6,820) PMID: 12087058

[6] Teicher BA. Xenografts of EMT-6 mouse mammary tumor cells. Mol Cancer Ther 5(10):2435, 2006

[7] Johnson JI et al. Relationships between drug activity in NCI preclinical in vitro and in vivo models and early clinical trials. Br J Cancer. 2001 May 18;84(10):1424-31.

[8] Guerrero S, Figueras A, Casanova I, Farre L, Lloveras B, Capella G, Trias M, Mangues R. Codon 12 and codon 13 mutations at the K-ras gene induce different soft tissue sarcoma types in nude mice. FASEB J. 2002 Oct;16(12):1642-4.

[9] Céspedes MV, Espina C, García-Cabezas MA, Trias M, Boluda A, Gómez del Pulgar MT, Sancho FJ, Nistal M, Lacal JC, Mangues R. Orthotopic microinjection of human colon cancer cells in nude mice induces tumor foci in all clinically relevant metastatic sites. Am J Pathol 170 (3):1077-1085, 2007.

[10] Cespedes MV, Casanova I, Parreño role in M, Mangues R. Mouse models in oncogenesis and cancer therapy. Clin Transl Oncol. 2006 May;8(5):318-29.

[11] Céspedes MV, Larriba MJ, Alamo P, Casanova I, Parreño M, Feliu A, Sancho FJ, Muñoz A and Mangues R. Site-dependent E-cadherin cleavage and nuclear translocation in a metastatic colorectal cancer model. Am J Pathol. 177(4):2067-79, 2010.

[12] Vazquez E, Ferrer-Miralles N, R. Mangues, J. L. Corchero, Schwartz S Jr, and A. Villaverde, Modular protein engineering in emerging cancer therapies, Curr. Pharm. Des, 15 (2009) 893-916.

MICROFLUIDICS & MINIATURIZATION - THE TEENAGE YEARS ARE OVER...

Andreas Manz

KIST Europe, Saarbruecken, Germany
manz@kist-europe.de

After a brief overview of historic micro- and nanotechnology for “lab on chip” devices, I will focus on 2 examples of near market applications: Bacteria causing infections can be identified by detecting specific DNA sequences. This method is widely used and has a high degree of specificity. However, for this purpose, the micro organisms will have to be captured, and it is not clear whether they are dead or alive. Metabolite studies have the advantage that remote evidence for live cells can be identified.

I will present portable equipment for volatile metabolite quantification, based on multi-capillary GC and ion-mobility detection [1]. The raw data is mathematically treated to receive best discrimination of patient groups. Applications for diagnostics of lung infections and lung cancer will be shown. In addition, a chip-based hand held real-time PCR instrument will be presented. A "virtual reactor" approach, i.e., a free droplet in oil, is used for thermal cycling and subsequent melting temperature profiling of the PCR product [2].

References:

[1] Perl, T., Vautz, W., Nolte, J., Baumbach, J.I. & Quintel, M. Ion mobility spectrometry of human pathologic bacteria - metabolic profiling by volatile organic compounds. Infection 37, 24-24 (2009).

[2] Pavel Neuzil, Chunyan Zhang, Juergen Pipper, Sharon Oh, Lang Zhuo, Ultra fast miniaturized real-time PCR: 40 cycles in less than six minutes. Nucleic Acids Research, 2006, Vol. 34, doi:10.1093/nar/gkl416

New Nanobiotechnological Approaches For The Diagnostic Of Infectious And Cardiovascular Diseases

M.-Pilar Marco, Carme Pastells, Pablo Salvador, Gloria Colom, Nuria Sanvicens and Nuria Pascual

Applied Molecular Receptors Group (AMRg). Institute for Advanced Chemistry of Catalonia (IQAC) of the Spanish Council for Scientific Research (CSIC)
CIBER de Bioingeniería, Biomateriales y Nanomedicina, Spain
pilar.marco@cid.csic.es

Future trends in medicine demand for rapid, reliable diagnostic technologies able to assist doctors on a more personalized and efficient medicine. At the same time, the so-called “omic” technologies have accelerated the number of candidate biomarkers discovered pointing to a future in which the heath status or disease of an individual will be established based on molecular signatures or footprints showing if there is any alteration on the biomarker expression profiles. Biotechnology, microtechnology and more recently nanotechnology are the most promising emerging technologies of the last decades. At the interface of these sciences lies the nanobiotechnology (or the micro/nanobiotechnology) which makes use of the knowledge from these fields to create biological micro/nanosystems and biofunctional devices. The Nanobiotechnology and Biomolecular Diagnostics research line of the CIBER-BBN supports research in this direction with a clear aim to translate the results into the clinical arena. With this final goal, several ongoing projects are addressing the possibility to develop a new generation of improved diagnostic devices and biosensing systems based on novel nanobiotechnological approaches.

Examples illustrating the use of nanoparticles, nanostructured materials and microelectronic devices to create functional biohybrid materials for the detection of bioactive substances will be presented in this oral communication. Thus, reliable methods for rapid, selective detection of pathogens for diagnosing infectious diseases, being necessary single-cell detection for certain types of body fluids (ex. blood or cerebrospinal fluid) and microorganisms (Pseudomonas aeruginosa, Staphylococcus aureus, etc), causing nosocomial diseases. On the other hand, cardiovascular diseases (CVD) are a major cause of death in Europe. The disease develops through a series of consecutive steps in which several validated and candidate biomarkers have been identified. Development of diagnostic methods able to simultaneously detect a panel of representative biomarkers of each of these stages would allow early-diagnosis before heart failure occurs. Regarding multiplexation, an interesting approach is the use of nanoparticles with distinct optical or electrical properties, such nobel metal nanoparticles, quantum dots (QDs) or other types of nanoparticles that show great potential for multiplexation. As an example, a fluorescent quantum dot (QD)-based antibody array has been developed to detect Escherichia coli in serum samples. The microarray reaches a detectability of 1CFU mL^{-1}, three order of magnitude lower than the ELISA (enzyme-linked immunosorbent assay) using the same immunoreagents [1,2]. On the other hand, the localized surface plasmon resonance of noble metal nanorods with different aspect ratio allows envisaging the possibility to develop cost-effective multiplexed devices [3]. Similarly, in respect to electrochemical nanoprobes made of metal sulfides with distinct redox potentials. Finally, strategies for creating universal diagnostic devices based on DNA-directed immobilization approaches will also be discussed.

References:

[1] Sanvicens, N.; Pascual, N.; Fernandez-Arguelles, M. T.; Adrian, J.; Costa-Fernandez, J. M.; Sanchez-Baeza, F.; Sanz-Medel, A.; Marco, M. P. Analytical and Bioanalytical Chemistry 399, 2011, , 2755.
[2] Sanvicens, N.; Pastells, C.; Pascual, N.; Marco, M. P. TrAC - Trends in Analytical Chemistry 28, 2009, 1243.
[3] Mannelli, I.; Marco, M. P. Analytical and Bioanalytical Chemistry 399, 2011, 1923.

Figures:

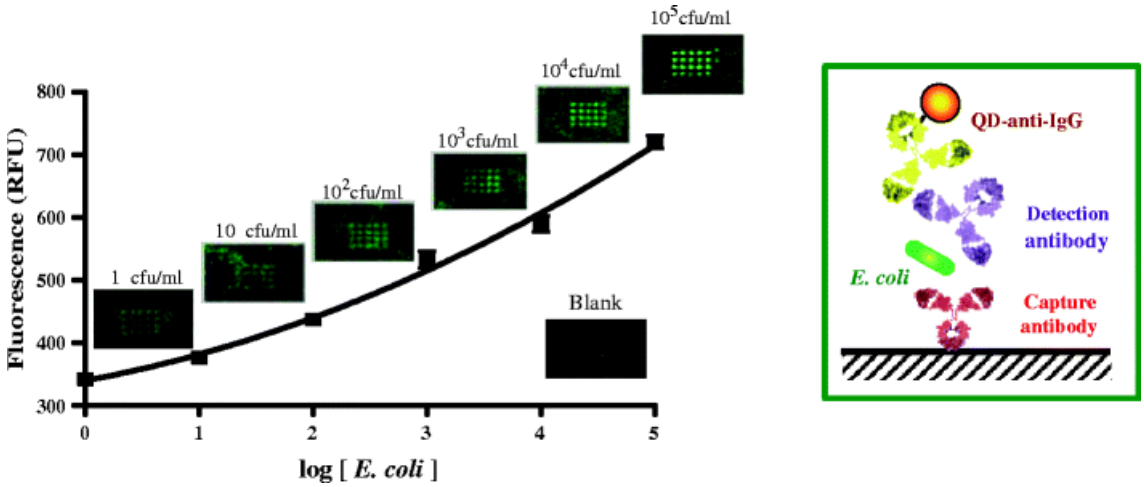

Figure 1: *Dose-response curve for E. coli O157:H7 in a sandwich array-based assay. The standard curve was fitted to a quadratic polynomial equation as indicated by Herman et al [20] and the LOD was calculated using the statistical approach reported by Long and Winefordner [21]. Results correspond to the average and standard deviation of four assays run on 4 different days in duplicate (n = 12)*

TARGETING CANCER AND ACTIVATION OF THE IMMUNE SYSTEM WITH QUANTUM DOTS

Carlos Juan C. Mareque-Rivas[1,2,3], Nina Gomez-Blanco[1], Malou Henriksen-Lacey[1], Carmen Rodriguez-Maldonado[3], Martin Krembuszewski[3], Tom Barr[4] and David Gray[4]

[1]CIC biomaGUNE, Biofunctional Nanomaterials Unit, Paseo Miramón 182, 20009 San Sebastian, Spain
[2]Ikerbasque, Basque Foundation for Science, 48011 Bilbao, Spain
[3]School of Chemistry, University of Edinburgh, Edinburgh, United Kingdom EH9 3JJ
[4]Institute of Immunology & Infection Research, School of Biological Science, University of Edinburgh, Edinburgh, United Kingdom EH9 3JT
jmareque@cicbiomagune.es

The use of inorganic nanoparticles for molecular imaging applications has attracted considerable interest in the last few years. Semiconductor nanocrystals (quantum dots, QDs) in particular have become important tools in biology as alternatives to traditional organic and genetically-encoded fluorophores [1]. For optical imaging, QDs offer high molar extinction coefficients and high quantum yields, strong resistance to photobleaching and degradation, continuous absorption spectra spanning the UV to the near infrared (depending on the size and elements forming the semiconductor core), narrow emission and large Stokes shifts. In addition, QDs have large two-photon cross-sectional efficiency (2-3 orders of magnitude that of organic dyes), which makes them ideal also for *in vivo* deep-tissue imaging using two-photon excitation [2].

However, QDs could potentially become more than passive bio-probes. New risks and new opportunities may arise when QDs are combined and interact with other molecules. We are particularly interested in the interactions between QDs and components of the immune system, and between QDs and photoactive molecules which can target/damage DNA.

The immune system has the essential task of controlling host defenses against infections and can be used to recognize and kill cancer cells. For these functions activation of a family of highly conserved and recently discovered receptors termed Toll-like receptors (TLRs) appears to be critically important [3]. The recognition/activation of each TLR is a complex event, and it is mediated by a specific pathogen-associated molecular pattern (PAMP) –a conserved molecular motif which is present in a bacteria and/or a virus and is absent in mammalian cells. We have found that QDs biofunctionalised with PAMPs provide strong stimulation of the mammalian immune system via TLR activation in both *in vitro* and *in vivo* experiments [4]. Moreover, when the nanoparticle carries both an antigen and a TLR ligand the magnitude and quality of the immune response is significantly improved. These results suggest that QDs and other traceable nanoscopic materials can, as pathogen-mimetic materials, make important contributions in fundamental and applied research pertinent to the development of safer and more effective vaccines.

The site-directed generation of cytotoxic effects upon targeted light irradiation to convert photosensitive inert chemical compounds into toxic tumour-killing agents is, on the other hand, becoming an increasingly successful treatment for some forms of cancer. Currently this new anticancer technique – photodynamic therapy (PDT) – requires an organic dye to absorb the radiation and use it to generate cytotoxic singlet oxygen, which has considerable limitations [5]. Our recent studies suggest that it may be possible to develop alternative PDT methodologies by combining suitable QDs with suitable photoactive metal complexes and light of a specific wavelength [6]. Moreover, we have found that the same type of combination can significantly enhance DNA damage [7]. Thus, in the context of targeting cancer there could be an opportunity for the interaction between QDs and small photoactive molecules to be exploited to generate or release in a controlled fashion anticancer drugs or other cytotoxic species using light.

References:

[1] Michalet, X. et al. Science, 307 (2005) 538; Bruchez, M. J et al Science, 281 (1998) 2013; Gao, X. et al. Curr. Opin Biotech.,16 (2005) 63; Medintz, I. L et al Nat. Mater., 4 (2005) 435.
[2] Larson, D. R et al. Science, 300 (2003) 1434.
[3] Hennessy E. J. et al. Nat Rev. Drug Discovery, 9 (2010) 293.
[4] Barr, T. A. et al. Molecular Biosystems, 6 (2010) 1568.
[5] Dougherty T. J. et al. J. Natl. Cancer Inst.,90 (1998) 889; Brown S. B. et al. Lancet Oncol., 5 (2004) 497; Moore C. M. et al. Nat. Clin Pract. Urol., 6 (2009) 18.
[6] Gomez-Blanco, N et al. Chem. Commun., 35 (2009) 5257.
[7] Hernandez-Gil, J. et al. Chem. Commun., (2011), Advance article, DOI: 10.1039/C0CC04163G

MICRO-ORDERING OF LUMINESCENT NANOPARTICLES BY TARGETING OF BIOMOLECULES

Emma Martin Rodriguez[1], Nicoleta Bogdan[1], Jorge Lamela[2], Daniel Jaque[2], Francisco Jaque[2], José García Solé[2] and John A. Capobianco[1]

[1]Department of Chemistry and Biochemistry, Concordia University, 7141 Sherbrooke St. W, H4B 1R6 Montreal, Canada
[2]Departamento de Física de Materiales, C-IV, Universidad Autonoma de Madrid, C/Francisco Tomas y Valiente 7, 28049 Madrid, Spain.
emma.martin@uam.es

Nowadays a great effort has been directed towards the early detection of pathogenic agents or cancer cells by optical methods. One of the most investigated approaches is the use of inorganic luminescent nanoparticles (quantum dots, gold nanorods and lanthanide doped nanoparticles), which have been used to obtain high resolution images of cancer cells in in-vitro and in-vivo assays. The specificy of bioassays can be improved by using the interactions between ligands found on cell surfaces and protein receptors as they are involved in several biological processes such as bacteria and virus adhesion, cancer diseases, inflammation, immunology, and cell-cell communications. Thus, it is of vital importance to develop nanoparticles exposing multiple copies of these ligands to be potentially used in highly sensitive assays for the detection of bacteria or virus infections, or cancer tumors.

As natural polysaccharide, chitosan (containing glucosamines groups) is used in many biological applications as it is nontoxic, biocompatible and biodegradable. It display multiple biochemical functions at its surface chitosan so could serve as support to bind luminescent nanoparticles with the above mentioned ligands, so it would be possible to develop luminescent markers for the detection of specific biomolecules. Thus in this study chitosan molecules were patterned at the surface of epoxy-silane modified slides and, it was demonstrated that the chitosan labeled at the surface of these modified-slides is able to strongly interact with water dispersible $NaGdF_4:Er^{3+},Yb^{3+}$ up-converting luminescent nanoparticles.

Chitosan molecules have been directly patterned on modified slides using microcontact printing, a method that has been very successfully adopted for the precise and gentle transfer of biomolecules (proteins, DNA and lipid bilayers) from stamp a to a substrate. This occurs in a few seconds and without loss of biological activity. The stamps were fabricated using Polydimethylsiloxane (PDMS) (Sylgard 184). PDMS was molded using a prefabricated master, consisting in a grating with 250 lines/mm. The stamp was then inked with a chitosan /acetic acid solution and pressed after drying in the silane coated slide allowing for a conformal contact between the stamp and the surface of the glass-slide. The transfer of the chitosan molecules from the stamp to the glass-slide could be observed by using an optical microscope under reflection illumination (see Figure 1(a)). The fabricated chitosan patterns were then submerged in a water solution of $NaGdF_4:Er^{3+},Yb^{3+}$ (1mg/mL) nanoparticles. These nanoparticles were synthesized by acidic treatment of the nanoparticles previously synthesized via the thermal decomposition procedure.

After removing the sample from the solution, it was abundantly washed with distilled water. To ensure the presence of the nanoparticles in the sample after the washing process, the sample was illuminated by a laser diode with 980 nm wavelength. A strong green signal was observed with the naked eye. The emission spectrum of the sample was then characterized, corresponding to the Er^{3+} emission spectrum. To ensure the binding of the nanoparticles to the patterns, the washing procedure was repeated 10 times. The intensity emitted by the nanoparticles was not observed to significantly decrease after the washing process, indicating a strong binding chitosan-nanoparticles.

The characterization of the samples has been carried out by two different optical techniques. By Near-field Scanning Optical Microscopy (NSOM) optical contrast could be observed between the lines with chitosan and the surrounding regions, the higher brightness corresponding to the chitosan lines. Then we use fluorescence microscopy to detect the distribution of the nanoparticles in the sample. For this purpose we focused a 980 nm wavelength laser beam by means of a 100X objective, and the variation of the luminescence intensity of the sample was mapped. Although we could detect Er^{3+} emission from

the nanoparticles along the entire sample (see Figure 1(b)), the intensity of emission was higher along the chitosan lines, showing that the nanoparticles bind preferably to the chitosan molecules.

In conclusion, we have demonstrated that luminescent nanoparticles can bind to chitosan molecules. We have demonstrated this preference by the fabrication of chitosan micropatterns where the nanoparticles are preferently bound. In addition to the biological applications of the nanoparticles to targeting of specific biomolecules, the work describes a fast and easy technique for the fabrication of luminescent micro arrays, with applications in other fields of science and technology, as for instance biosensing, chromatography, diagnostic immunoassays, cell culturing, DNA microarrays, and other analytical procedures.

Figures:

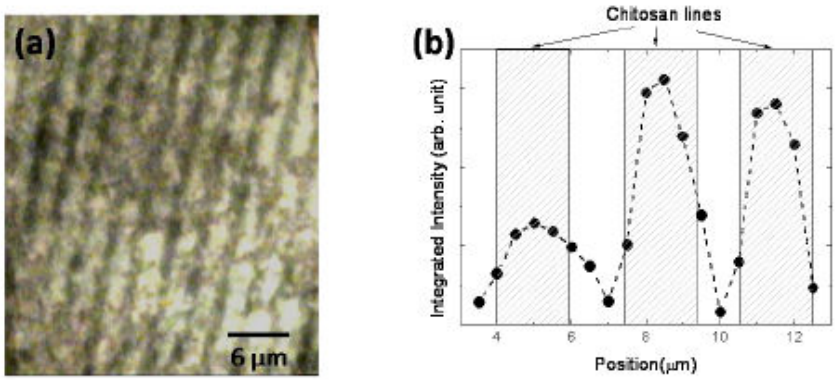

Figure 1: *(a) Optical microscope image of the micropatterned sample, white ones correspond to chitosan; (b) Er^{3+} luminescence intensity across three chitosan lines showing the preferent binding of $NaGdF_4:Er^{3+},Yb^{3+}$ nanoparticles to chitosan. Dotted lines are guides for the eyes.*

SYNTHETIC STRUCTURES TO AID REGENERATION IN THE CENTRAL NERVOUS SYSTEM

Manuel Monleón Pradas

Centro de Biomateriales e Ingeniería Tisular, Universidad Politécnica de Valencia, Spain
Centro de Investigación Príncipe Felipe, Valencia, Spain
CIBER-Biomateriales, Bioingeniería, Nanomedicina
mmonleon@upvnet.upv.es

Trauma brain injury, stroke and several neurodegenerative processes entail the loss of neuronal populations and of tissue structures. The very limited regeneration ability of the central nervous system has represented an unsurmountable obstacle for the overcoming of the ensuing disabilities. In this context, the discovery of the pluripotency of various cell types has opened wider possibilities for new therapeutic strategies. Nonetheless, cells supplied to injured or degenerated sites, and even cells migrating to those sites from nearby proliferative regions have proved to be short-lived and have failed to achieve significant improvements. This may be due to an impossibility for these cells to rebuild or restore lost neuronal circuitry connections, and also to the loss of viability of those cells in an aggressive microglial environment at the lesion site. It is in this situation where synthetic biomaterial structures may be of help, in that they may *(i)* host and supply in a neuroprotective environment cell populations for transplant; *(ii)* deliver neurotrophic factors; *(iii)* sustain and stimulate neural progenenitor cell differentiation and axonal growth; *(iv)* provide targeted guidance to axon outgrowth. Success of these synthetic structures has as a prerequisite their biocompatibilty, their integration in the host tissue without eliciting a glial scar that would invalidate their functions, and, possibly, their ability to be vascularized in order to maintain the viability of the biohybrid construct. These demands condition the choices of chemistries and the development of inner architectures and morphologies of the synthetic materials. Our group has been working in the identification of brain-compatible biomaterials and has developed different types of structures suited for implantation in the cortex and in the nigrostriatal tract [1]. The presentation discusses some of the results obtained *in vitro* and *in vivo* in rat model, with special reference to cell differentiation and migration, glial scar formation and angiogenesis.

References:

[1] Martínez-Ramos et al. Tissue Engineering A 14 (2008) 1365; Soria J M et al. J Biomed Mater Res Part A 97 A (2011) 85; Martínez-Ramos et al. (2011, to appear)

Figures:

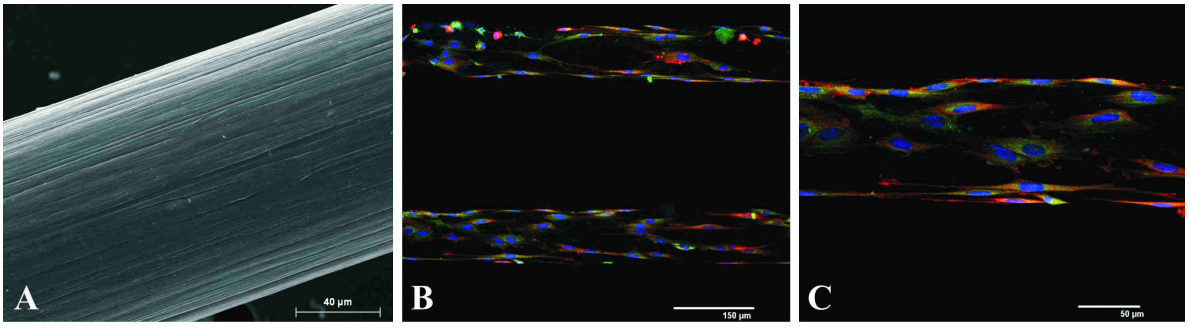

Figure 1: *Textured PCL microfilament (A) and olfactory ensheathing glial cells grown on them (B and C)*

GLYCONANOTECHNOLOGY TO DEVELOP MULTIFUNCTIONAL AND MULTIMODAL NANOMATERIALS FOR BIOMEDICAL APPLICATIONS

Soledad Penadés

Laboratory of GlycoNanotechnology, Biofunctional Nanomaterials Unit, CICbiomaGUNE and CIBERBBN, Parque Tecnológico, Pº de Miramon 182, 20009 San Sebastian, Spain
spenades@cicbiomagune.es

During the last years our laboratory has developed a new technology (*Glyconanotechnology*) for tailoring - in a simple and versatile way – bio-functional gold nanoclusters (*glyconanoparticles*). [1,2,3] The manipulation of the metallic cluster to obtain magnetic nanoparticles for in vivo application in cellular labeling and imaging by magnetic resonance (MRI), is comprised within the potential of this novel technology. [4, 5]

Glyconanoparticles (GNPs) bearing biological significant carbohydrates (antigens) in varying density have been prepared to study biological mechanisms [6, 7] and to intervene in cell adhesion processes. [8] The methodology includes the preparation of *hybrid* GNPs incorporating carbohydrates and other molecules such as fluorescent probes, biotin as well as biological molecules such as peptides, DNA and RNA.

The design and preparation of complex bio-functional GNPs and their application as polyvalent tools to study and intervene in carbohydrate mediated biological interactions will be highlighted. As examples of application in Nanomedicine, the preparation and study of GNPs as anti-adhesion agents in inhibition of metastasis, [8] as potential microbicides for blocking HIV-1 infection, [9] or as magnetic probes for in vivo labeling and tracking specifically cells by means of magnetic resonance imaging (MRI) will be also reviewed.

References:

[1] J. M. de la Fuente et al., Gold Glyconanoparticles as Water-Soluble Polyvalent Models To Study Carbohydrate Interactions, Angew. Chem. Int. Ed., 40 (2001) 2258-2261.
[2] A. G. Barrientos et al., Gold Glyconanoparticles: Synthetic Polyvalent Ligands Mimicking Glycocalyx- Like Surfaces as Tools for Glycobiological Studies, Chem. Eur. J. 9 (2003), 1909-1921.
[3] I. García et al., Glyconanoparticles: multifunctional nanomaterials for biomedical applications. Nanomedicine, 5, (2010) 777-792
[4] J. Gallo et al., Water-soluble magnetic glyconanoparticles based on metal-doped ferrites coated with gold: Synthesis and characterization. J. Mat. Chem.20 (2010) 10010-10020
[5] I. García et al., Magnetic Glyconanoparticles as a Versatile Platform for Selective Immunolabeling and Imaging of Cells. Bioconjugate Chem. doi.org/10.1021/bc1003923
[6] M.-J. Hernáiz et al., A Model System Mimicking Glycosphingolipid Clusters to Quantify Carbohydrate Self-Interaction by Surface Plasmon Resonance, Angew. Chem. Int. Ed. 41 (2002) 1554-1557.
[7] J. M. de la Fuente et al., Thermodynamic Evidence for Ca2+ mediated self-aggregation of Lewis X gold glyconanoparticles. A model for cell adhesion via carbohydrate-carbohydrate interaction, J. Am. Chem. Soc. 127 (2005) 6192-6197.
[8] J. Rojo et al., Gold Glyconanoparticles as New Tools in Anti-adhesive Therapy, ChemBioChem. 5 (2004) 291-297.
[9] O. Martínez-Ávila et al., Multivalent Manno-Glyconanoparticles Inhibit DC-SIGN Mediated HIV-1 trans-Infection of Human T-cells. ChemBioChem. 10 (2009) 1806-1809.

A NOVEL DNA CHIP FOR SINGLE MOLECULE ANALYSIS

T.Plénat[1,2], C.Tardin[1,2], , C.Vieu[3,2], C.Thibault[3,2], E.Trévisiol[3,4], and L.Salomé[1,2]

[1]CNRS; IPBS (Institute of Pharmacology and Structural Biology); 205 route de Narbonne, F-31077 Toulouse, France
[2]University of Toulouse; UPS; IPBS; F-31077 Toulouse, France
[3]LAAS, Nanobiosystems, 7, Avenue du Colonel Roche, F-31077 Toulouse, France
[4]UMR 5504, UMR 792, Ingénierie des Systèmes Biologiques et des Procédés & Plate-forme Biopuces, CNRS, INRA, INSA, 135, avenue de Rangueil, 31077 Toulouse, France
plenat@ipbs.fr, salome@ipbs.fr

The last two decades have seen the emergence of single-molecule experiments [1]. By avoiding the ensemble averaging inherent to traditionnal bulk-phase biochemistry, the study of molecular machineries at the single-molecule level permits a better understanding of the behavior of living systems. Indeed the dynamics of the machineries processes can be characterized and rare subpopulations can be identified [2].

One of the main shortcoming of single molecule experiments is that the acquisition of statistically solid data is very time consuming, which explains the fact that they are still not widely used in laboratories.

We will present the development of a new single DNA chip, allowing the simultaneous analysis of hundreds of single DNA molecules by the Tethered Particle Motion (TPM) technique. Our single DNA chip gives high-throughput capabilities to this approach of valuable interest for multiple applications.

The principle of a TPM experiment consists in tracking a bead tethered at the free end of a DNA molecule which is immobilized by the other end to a coverslip thanks to optical videomicroscopy. The amplitude of the Brownian motion of the bead is related to the effective length of the DNA molecule [3]. Any conformational change of the DNA molecule due to external factors (proteins, ions, temperature), that induces a variation of the effective length of the DNA tether, can be thus monitored by TPM [4].

References:

[1] Cornish, P. V.; Ha, T., Acs Chemical Biology 1 (2007) 53.
[2] van Oijen, A. M., Nature Chemical Biology, 8 (2008) 440.
[3] Yin, H.; Landick, R.; Gelles, J., Biophys J, 6 (1994) 2468.
[4] Pouget, N. et al.; Nucleic Acid Res., 9 (2004) e73

BIO-TEMPLATED SYSTEMS FOR NANOELECTRONICS

Danny Porath

Institute of Chemistry and Center for Nanoscience and Nanotechnology,
The Hebrew University of Jerusalem, Israel
porath@chem.ch.huji.ac.il

In our research we use bio-templated systems to realize one-dimensional conducting nanowires and nanodevices for scientific investigation of electrical charge transport in these systems, for nanoelectronics and for nanotechnology applications. One example is dsDNA and its synthetic derivatives. Within this frame we measured electrical charge transport in dsDNA, measured the energy level spectrum of dsDNA, showed polarizability of DNA derivatives and more. I will briefly review our previous results and our ongoing activity in this direction. Another example for bio-templated systems is the SP1 protein which is hybridized with various nanoparticles to form memory units and protein-particles conducting chains. We demonstrate the construction of various building blocks, acquiring specific attachment to gold or Si surfaces, array formation and finally charging and logic operations in hybrid SP1-nanoparticle systems. I will review this activity in more details. The research is conducted by my group in close collaboration with several groups from complementary fields.

References:

[1] “Direct Measurement of Electrical Transport Through Single DNA Molecules of Complex Sequence”, Hezy Cohen, Claude Nogues, Ron Naaman and Danny Porath, PNAS 102, 11589 (2005).
[2] “Electrical characterization of self-assembled single- and double-stranded DNA monolayers using conductive AFM”, Hezy Cohen et al., Faraday Discussions 131, 367 (2006).
[3] “Long Monomolecular G4-DNA Nanowires”, Alexander Kotlyar, Nataly Borovok, Tatiana Molotsky, Hezy Cohen, Errez Shapir and Danny Porath, Advanced Materials 17, 1901 (2005).
[4] "Polarizability of G4-DNA Observed by Electrostatic Force Microscopy Measurements", Hezy Cohen et al., Nano Letters 7(4), 981 (2007).
[5] “High-Resolution STM Imaging of Novel Poly(G)-Poly(C)DNA Molecules”, Errez Shapir, Hezy Cohen, Natalia Borovok, Alexander B. Kotlyar and Danny Porath, J. Phys. Chem. B 110, 4430 (2006).
[6] “Electronic structure of single DNA molecules resolved by transverse scanning tunneling spectroscopy”, Errez Shapir et al., Nature Materials 7, 68 (2008).
[7] “SP1 Protein Based Nanostructures and Arrays”, Izhar Medalsy et. al., Nano Letters 8, 473 (2008).
[8] "Float And Compress: A Honeycomb Like Array Of A Highly Stable Protein Scaffold", Arnon Heyman et al., Langmuir 25, 5226 (2009).
[9] “Protein Scaffold Engineering Towards Tunable Surface Attachment”, Arnon Heyman et al., Angewandte Chemie Int. Ed., 48, 9290 (2009).
[10] “A DNA sequence scanned”, Danny Porath, Nature Nanotechnology 4, 476 (2009).
[11] "Logic implementations using a single nanoparticle-protein hybrid", Izhar Medalsy et. al., Nature Nanotechnology 5, 451 (2010).

Figures:

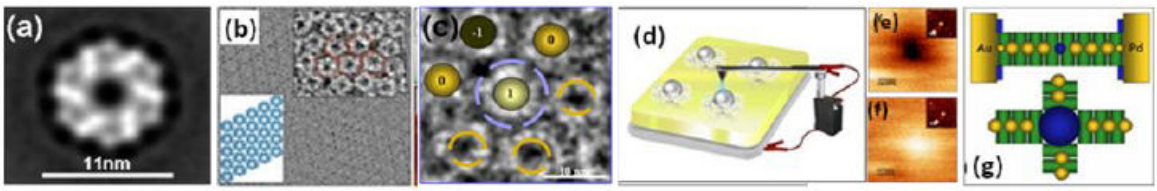

Figure 1: *SP1 protein as a basis for nanoelectronic applications: (a) TEM of a single SP1 protein. (b) A large packed ordered array of SP1 molecules. Lower inset: a scheme of the array, upper inset: enlargement of part of the array, where the hexagonal packing is marked. (c) Overlaid scheme of the suggested memory array. (d) Scheme of the suggested implementation, where the writing is by charging individual particles with AFM and reading by EFM. (e-f) Two charged states of the hybrid and topography (inset). (g) Scheme of chain structures.*

SURFACE CELL GROWTH ENGINEERING ASSISTED BY A NOVEL BACTERIAL NANOMATERIAL AND THE IMPACT OF GENETIC TAILORING ON THEIR PROPERTIES

Imma Ratera[1,2], César Díez-Gil[1,2], Sven Krabbenborg[1,2], Elena García-Fruitós[2,3], Esther Vázquez[2,3,4], Escarlata Rodríguez-Carmona[2,3], Rosa M. Ferraz[2,3,4], Nora Ventosa[1,2], Joaquín Seras[2,3,4], Olivia Cano[2,3], Neus Ferrer-Miralles[2,3,4], Antonio Villaverde[2,3,4], and Jaume Veciana[1,2]

[1] Department of Molecular Nanoscience and Organic Materials. Institut de Ciencia de Materials de Barcelona (CSIC) Bellaterra, Barcelona, Spain
[2]CIBER de Bioingeniería, Biomateriales y Nanomedicina (CIBER-BBN) Bellaterra, Barcelona, Spain
[3]Institut de Biotecnologia i de Biomedicina, Universitat Autònoma de Barcelona, Bellaterra, Spain
[4]Department of Genetics and Microbiology Universitat Autònoma de Barcelona, Bellaterra, Spain
iratera@icmab.es

Bacterial inclusion bodies (IBs) are highly pure protein deposits in the size range of a few hundred nanometers produced by recombinant bacteria.[1] Although IBs were supposed to be undesirable side products on protein transcription processes it has been recently probed that those intriguing nanoparticulate proteic materials retain part of their original functionality and further more that it is possible to tailor its properties during biological production. The polypeptide chains that form IBs fold into an unusual amyloid-like molecular architecture compatible with their native structure, thus supporting the biological activities of the embedded polypeptides (eg fluorescence or enzymatic activity).[2] Therefore, a wide spectrum of uses as functional and biocompatible materials might arise upon convenient engineering.[3] Although theoretically feasible through adjusting genetic and production conditions, the biophysical features of these proteinaceus nanoparticles, such as activity and size, have been never engineered and very few is known about their physicochemical properties.

As IBs are biofunctional by nature, engineering of IBs might have wide applications in different nanomedical scenarios. In this study (Figure 1), we have characterized the relevant nanoscale properties of IBs as particulate materials using Scanning Electron Microscopy (SEM), Dynamic Light Scattering (DLS), Atomic Force Microscopy (AFM) and Confocal Microscopy (CM). We have demonstrated that these particles are mechanically stable and fully biocompatible, and that their size and biological activities can be tailored by appropriate genetic and process engineering.[4-6] Moreover, wettability and nanomechanical studies developed on IBs produced in different Escherichia coli genetic backgrounds depict distinguishable characteristics within the proteinaceous nanoparticles. (Figure 2 and 3).[5] As a proof of concept of the biomedical potential of IBs we have modified the topology of surfaces suitable for mammalian cell culture by adsorbing these particles, resulting in a dramatic stimulation of cell proliferation.[6] Furthermore, IB-grafted surfaces have been produced by using the microcontact printing (mCP), on which cell growth has been driven in desired patterns (Figure 1 g-i). Furthermore it was possible to observe how cultured mammalian cells respond differentially to inclusion body variants when used as particulate materials to engineer the nanoscale topography, proving that the actual range of referred mechanical properties is sensed and discriminated by biological systems.[5] The unique properties of this proteinaceous material including biocompatibility, manipulability and functionality make it especially appealing for regenerative medicine.

References:

[1] A. Villaverde, M. M. Carrio, Biotechnol. Lett., 25 (2003) 1385-1395
[2] (a) N. Gonzàlez-Montalbán , E. García-Fruitós, A. Villaverde, Nat. Biotechnol. 25(7) (2007) 718-720 (b) E. Garcia-Fruitos, E. Aris, A. Villaverde, Appl. Environ. Microbiol., 73 (2007) 289-294
[3] E.Garcia-Fruitos, M. Martínez-Alonso, N. Gonzàlez-Montalbán, M. Valli, D. Mattanovich, A. Villaverde, J. Mol. Biol. 374 (2007) 195-205
[4] (a) Garcia-Fruitos E, Martinez-Alonso M, Gonzalez-Montalban N, Valli M, Mattanovich D, Villaverde A. Divergent Genetic Control of Protein Solubility and Conformational Quality in Escherichia coli. J.Mol.Biol. 2007;374:195-205. (b) E. Vazquez, Mónica Roldán, C. Diez-Gil, U. Unzueta, J. Domingo-Espín, J. Cedano, O. Conchillo, I. Ratera, J. Veciana, Xavier Daura, N. Ferrer-Miralles & A. Villaverde, Nanomedicine, 5(2) (2010), 259–268

[5] C. Díez-Gil, S. Krabbenborg, Elena García-Fruitós, Esther Vázquez, Escarlata Rodríguez-Carmona, Rosa M. Ferraz, Nora Ventosa, I. Ratera Joaquín Seras, Olivia Cano, Neus Ferrer-Miralles, Antonio Villaverde, Jaume Veciana, Biomaterials, 31 (2010) 5805-5812

[6] (a) Patent ES- P200900045 (b) E. García-Fruitós, E. Rodríguez-Carmona, C. Diez-Gil, R. M. Ferraz, E. Vázquez, J. L. Corchero, M. Cano-Sarabia, I. Ratera, N. Ventosa, J. Veciana, A. Villaverde, Adv. Mater., 21 (2009) 4249–4253

Figures:

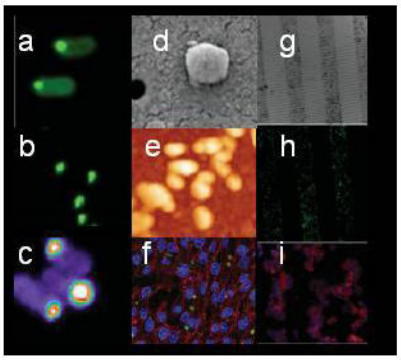

Figure 1: *IBs formed by the green fluorescence protein (GFP) when produced in bacteria (a), after purification (b), and under confocal analysis for florescence mapping (c). In (d) and (e), purified inclusion bodies observed by SEM and AFM respectively. In (f), BHK21 cells growing on polystyrene plates decorated with GFP IBs. In (g), a silica surface patterned with pure GFP IBs, that still being fluorescent (h), drive the growth of BHK 21 cells under the same lineal pattern (i).*

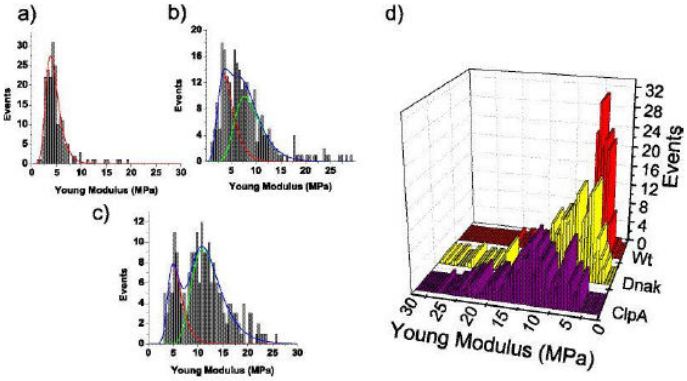

Figure 2: *Histogram representation of the number of events vs. Young modulus for IBs produced in bacterial mutants. a) Wt IBs showing only one peak at 3.73 MPa; b) DnaK- IBs show two overlapped Young modulus distributions which centered at 3.56 and 7.75 MPa; c) ClpA- IB show the presence of two different young modulus distributions, at 5.01 and 10.99 MPa; d) 3D representation of the later histograms.*

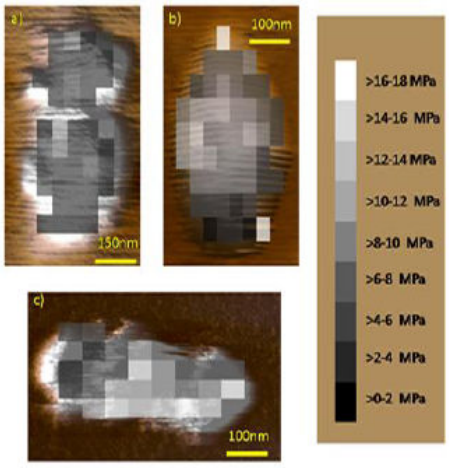

Figure 3: *2D software developed reconstruction of the elasticity maps of selected IBs from the three genetic backgrounds. a) wt IBs, b) DnaK- IBs, c) ClpA- IBs. Observations infer the existence of a homogeneously spread distribution of Young modulus values over the wt IBs. On the other hand, maps obtained for DnaK- and ClpA- IBs indicate the existence of two elasticity populations, with the harder areas segregated and localised on the centre of the DnaK- IBs and on the right side of ClpA- particles.*

STUDYING SURFACE-ADSORBED COLLOIDAL PARTICLES WITH QUARTZ CRYSTAL MICROBALANCE: HYDRODYNAMIC EFFECTS

I. Reviakine

Centro de Investigación Cooperativa en Biomateriales, Parque Tecnológico de San Sebastián, E-20009 San Sebastián, Spain
Department of Biochemistry and Molecular Biology, University of the Basque Country, 48940 Leioa, Spain

Quartz crystal microbalance (QCM) is widely used for studying soft interfaces in liquid environments. Many of these interfaces are heterogeneous in nature, in the sense that they are comprised of isolated entities adsorbed at a surface. When characterizing such interfaces, one is interested in determining parameters such as surface coverage and size of the surface-adsorbed entities. Currently this information is obtained by fitting QCM data—shifts in resonance frequency, ΔF, and bandwidth $\Delta\Gamma$ (also referred to as dissipation shifts)—with the model derived for smooth, homogeneous films using the film acoustic thickness and shear elastic moduli as fitting parameters. This is the so-called continuum approach. Experimentally, we investigated adsorption of proteins, liposomes, and icosahedral virus particles on inorganic surfaces with QCM and with a combined atomic force microscopy (AFM)-QCM setup. Theoretically, we modeled the QCM response with finite element method (FEM) calculations based on the incompressible Navier-Stokes equation to incorporate hydrodynamic effects.

The results of our studies can be summarized as follows. Experimentally, the relationship between the surface coverage and the frequency shift is not linear. This non-linearity can be modeled with the FEM calculations clarifying the contribution of the solvent to the frequency shift and the origin of dissipation in these heterogeneous films. In particular, our results show that the dissipation in these heterogeneous layers occurs mostly in the solvent and arises due to the motion of the adsorbed particles. In other words, it is not a measure of the elastic properties of the adsorbed particles, but rather of the particle-surface contact.

To directly compare the predictions of the continuum approach with the experimental results, we focus on the ratio between the bandwidth and frequency shifts, $\Delta\Gamma/\Delta F$ (the *Df* ratio). The continuum model predicts that this should increase both with surface coverage and particle size. Instead, we observe that this ratio increases with increasing particle size, but decreases with increasing surface coverage. This behavior is again consistently modeled with the FEM calculations: in other words, this is a hydrodynamic effect.

Finally, we find that the size of the adsorbed colloidal particles can be recovered from a model-independent analysis of the plot of the $\Delta\Gamma/\Delta F$ ratio vs. the frequency shift on many overtones (Figure1).

References:

[1] Tellechea, E.; Johannsmann, D.; Steinmetz, N. F.; Richter, R.; Reviakine, I. Langmuir 2009, 25, 5177 - 5184.
[2] Johannsmann, D.; Reviakine, I.; Richter, R. P. Anal.Chem. 2009, 81, 8167-8176.
[3] Johannsmann, D.; Reviakine, I.; Rojas, E.; Gallego, M., Effect of sample heterogeneity on the interpretation of qcm(-d) data: Comparison of combined quartz crystal microbalance/atomic force microscopy measurements with finite element method modeling. Analytical Chemistry 2008, 80, (23), 8891-8899.
[4] Rojas, E.; Gallego, M.; Reviakine, I. Analytical Chemistry 2008, 80, (23), 8982-8990.
[5] Bingen, P.; Wang, G.; Steinmetz, N. F.; Rodahl, M.; Richter, R. P. Analytical Chemistry 2008, 80, 8880-8890.
[6] Carton, I.; Brisson, A. R.; Richter, R. P. Analytical Chemistry 2010, 82, (22), 9275-9281.

Figures:

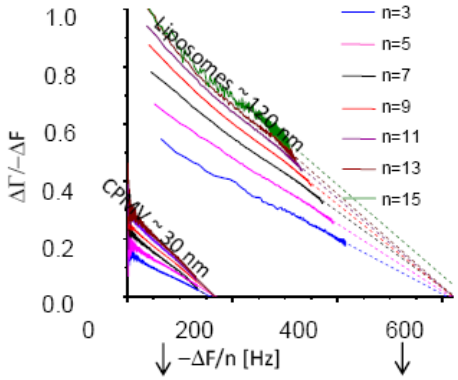

-ΔF/n [Hz]	175 ± 5	448 ± 32	616 ± 61
Calculated height, nm	29 ± 0.8	81 ± 6	111 ± 11
Particle diameter, nm	28	83 ± 4	114 ± 8

Figure 1: *The plot of the ΔΓ/-ΔF ratio vs. the frequency shift, -ΔF /n, for liposomes and cowpea mosaic virus (CPMV) particles adsorbing on inorganic surfaces. Different overtones are represented by different colors. The ratio decreases with the frequency shift (~ surface coverage), but is greater for larger objects. The curves are nearly linear and extrapolate to frequency shifts that can be converted into object heights via the Sauerbrey relationship. These are found to correlate with the crystallographic dimensions of the CPMV particles and liposome sizes measured by dynamic light scattering.*

NANOSCALE FILMS OF BIOMOLECULAR HYDROGELS – A NOVEL PLATFORM TO INTERROGATE THE RELATIONSHIP BETWEEN SUPRAMOLECULAR ORGANIZATION AND DYNAMICS, AND BIOLOGICAL FUNCTION

Nico B. Eisele[1,2], Patricia M. Wolny[1,3] and **Ralf P. Richter**[1,3]

[1]CIC biomaGUNE, Biosurfaces Unit, Paseo Miramon 182, 20009 San Sebastian, Spain
[2]Max-Planck-Institute for Biophysical Chemistry, Am Fassberg 11, 37077 Göttingen, Germany
[3]Max-Planck-Institute for Metals Research, Heisenbergstrasse 3, 70569 Stuttgart, Germany
rrichter@cicbiomagune.es

Nature has evolved complex materials that are exquisitely designed to perform specific functions. Certain proteins and glycans self-organize in vivo into soft and dynamic, strongly hydrated gel-like matrices. Illustrative examples of such biomolecular hydrogels are cartilage or mucus. Even though biomolecular hydrogels are ubiquitous in living organisms and fulfill fundamental biological tasks, we have today a very limited understanding of their internal organization, and how they function. The main reason is that this type of assemblies is difficult to study with conventional biochemical methods.

In order to study biomolecular hydrogels directly on the supramolecular level, we have developed an unconventional approach that draws on knowledge from several scientific disciplines. Exploiting surface science tools, we tailor-make model films with thicknesses in the nanometer range by directed selfassembly of purified components on solid supports. With a toolbox of biophysical characterization techniques, these model systems can be investigated quantitatively and in great detail down to the nanometer scale. The experimental data, combined with polymer theory, allow us to develop a better understanding of the relationship between the supramolecular organization and dynamics of biomolecular hydrogels, their physico-chemical properties and their biological function. To illustrate this concept, I will present two examples of our recent research. They relate to (i) a nanoscopic protein hydrogel that is responsible for the regulation of all macromolecular transport between the nucleus and the cytosol of eukaryotic cells [1] (Figure 1), and (ii) a microscopic glycoconjugate hydrogel that is involved in fertilization as well as cancer progression [2, 3].

References:

[1] N. B. Eisele, S. Frey, J. Piehler, D. Görlich and R. P. Richter, Ultrathin nucleoporin FG repeat films and their interaction with nuclear transport receptors. EMBO Rep., 11 (2010), 366-372.
[2] R. P. Richter, K. K. Hock, J. Burkhartsmeyer, H. Boehm, P. Bingen, G. Wang, N. F. Steinmetz, D. J. Evans and J. P. Spatz, Membrane-Grafted Hyaluronan Films: a Well-Defined Model System of Glycoconjugate Cell Coats. J. Am. Chem. Soc., 127 (2007), 5306-5307.
[3] P. M. Wolny, S. Banerji, C. Gounou, A. R. Brisson, A. J. Day, D. G. Jackson and R. P. Richter, Analysis of CD44-hyaluronan interactions in an artificial membrane system: insights into the distinct binding properties of high and low molecular weight hyaluronan. J. Biol. Chem., 285 (2010), 30170-30180.

Figures:

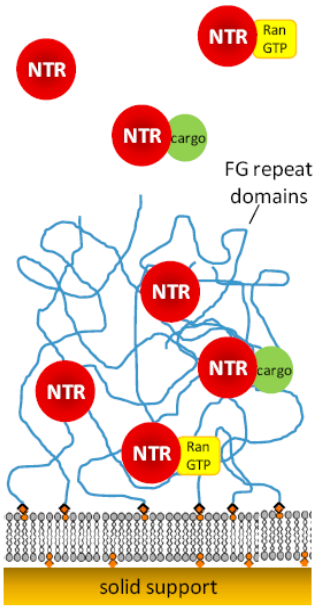

Figure 1: *Macromolecular transport between the cell's nucleus and the cytosol occurs through nuclear pore complexes (NPCs). The transport is selective: objects (cargo) beyond a certain size (30 kDa) need to attach to soluble nuclear transport receptors (NTRs) in order to be channeled efficiently through the pore. A supramolecular assembly of specialized and natively unfolded protein domains within the NPC is thought to be the key component of the NPC´s permeability barrier. The mechanism behind transport selectivity is at present only poorly understood. We have developed ultrathin FG repeat domain films as a surface-confined model system of the permeability barrier. In this contribution, we will present how such model systems can provide insight into the mechanism of transport across the permeability barrier.*

NANOSCALE PROPERTIES OF IMPLANTABLE BIOMATERIALS

Federico Rosei

INRS, Univ. of Quebec, Canada

Modifying the nanoscale structure/chemistry of materials allows to tailor and optimize their properties [1]. Our strategy rests on creating nanopatterns that act as surface cues [2,3] and affect cell behavior. We developed a chemical treatment of Ti-based materials that produces a unique nanostructured topography [4], showing that chemical oxidation is a general strategy that affects biocompatibility [5]. Our treatment generates multifunctional surfaces that promotes the growth of certain cells while inhibiting that of others, without using any growth factors. Nanostructured Ti surfaces selectively inhibit fibroblastic cell growth [4] and promote osteogenic cell activity [6] in vitro. Controling nanoscale features and functionalizing surfaces with molecular overlayers [7] will lead to a new generation of intelligent biomaterials that selectively influence cell behavior at the tissue-biomaterial interface, for example by controlling the adsorption of proteins [9]. Further enhancement of mechano-biocompatibility may be provided by coating with spider silk, whose structural/functional properties are currently being studied [10, 11].

References:

[1] F Rosei, J Phys Cond Matt 16, 1373 (2004).
[2] F Cicoira, F Rosei, Surf Sci 600, 1 (2006).
[3] F Variola et al, Small 5, 996 (2009).
[4] F Variola et al, Biomaterials 29, 1285 (2008).
[5] F Vetrone et al, Nanolett 9, 659 (2009).
[6] L Richert et al, Adv. Mater. 20, 1488 (2008).
[7] S Clair et al, J. Chem. Phys. 128, 144705 (2008).
[8] F. Variola et al., Adv. Eng. Mater. 11, B227 (2009).
[9] L. Richert, F. Variola, F. Rosei, J.D. Wuest, A. Nanci, Surf. Sci. 604, 1445 (2010).
[10] C. Brown, F. Rosei, E. Traversa, S. Licoccia, Nanoscale in press (2011).
[11] C Brown et al, in preparation.

NANOBIOTECHNOLOGIES: DISRUPTING THE LOGIC OF THE DRUG INDUSTRY

Valérie Sabatier, Vincent Mangematin

Grenoble Ecole de Management, 12 rue Pierre Sémard - BP 127 F-38003 Grenoble cedex 01, France
Valerie.sabatier@grenoble-em.com

The emergence of nanobiotechnologies in the drug industry is not only a scientific challenge, it is also challenging corporate strategy and business models. Based on an analysis of recent changes in the drug industry, we identify which are the triggers of change in an industry's dominant logic, defined as the general scheme of value creation and capture shared by its actors. Breakthrough innovations leading to technological discontinuities are a necessary, but not sufficient, condition for the disruption of such dominant logics. The emergence of new business models questions an industry's existing value chain and the relations between its actors.

We argue that in the drug industry, experiencing strong discontinuities and with high technological uncertainties, business models will tend to fit into the dominant logic of the industry and value chains will remain unchanged. But, as the new technologies evolve and uncertainty decreases, disruptive business models will emerge and challenge dominant industry logics and reshape established value chains, especially if they involve new and diversifying players joining the industry.

As technologies emerge and converge, they are leading us towards a more holistic healthcare industry. New approaches to healthcare – such as personalized medicine, nanobiotechnology, theranostics, or systems biology – are opening new business opportunities that build on new ways to address patients' needs and that provide physicians and hospitals with new therapeutic principles. Nanobiotechnologies, defined as the applications of nanotechnologies in the life sciences [1], promise improvements in diagnostics and drug delivery, particularly in the quantity and toxicity of drugs injected into patients. It offers the promise of a convergent approach that can merge diagnosis, treatment and monitoring.

We observe here the beginnings of a new industry that will emerge from the upheaval of the established drug industry and its merging with the diagnostics and other industries. We will discuss the new business opportunities and what firms are doing today in order to prepare tomorrow, in a new drug industry being transformed by nanobiotechnologies.

References:

[1] Briquet-Laugier V, Ott M.O., Biofutur, 265 (2006) 57-62.

NANOBIOPLATFORM BASED ON OLFACTORY RECEPTORS FOR DIAGNOSTIC PURPOSES

Josep Samitier

UCSF Institute for Bioengineering of Catalonia (IBEC)
CIBER of Bioengineering, biomaterials and nanomedicine
University of Barcelona, Barcelona, Spain
jsamitier@ibecbarcelona.eu

The use of smell in different fields has been rediscovered due to major advances in odour sensing technology and artificial intelligence. However, current electronic noses, based on electronic sensors, have significant limitations relating sensitivity, reliability and selectivity, amongst others. These limitations are at the basis of recurrent troubles of the electronic nose technology to reach essential applications in different areas, such as food safety, disease diagnosis, security, environment.

An electronic nose (E-nose) can be regarded as a modular system comprising: a set of active materials that detect the odour; associated sensors that transduce the chemical response into electrical signals, and an appropriate signal conditioning and processing to classify known odours or identify unknown odours, through the processing system (done by the brain in the human nose).

Similar concepts as in the case of the E-nose, but for analysis in liquids have been described recently. These systems are related in similar ways to the sense of taste, so for them the terms 'electronic tongue' or 'taste sensor' have been created. Such systems use as sensors lipid/polymer membranes on a multichannel electrode, resonant sensors, sensor beads or the principle of voltammetry.

Recently, a number of cell-based biosensors have been designed, using yeasts, or more specialized taste or olfactory sensory neurons, or even cells recombinantly expressing olfactory receptors (ORs), to measure changes of electrical parameters in the presence of volatile chemical compounds. These findings will allow the development of a new generation of nanobiosensors to detect chemical volatiles.

The BOND project proposes a new bioelectronic nose based in olfactory receptors in order to mimic the human nose. For this aim, micro/nano, bio and information technologies will converge to develop an integrated bioelectronic analytical nanoplatform platform based on olfactory receptors for odour detection. The general objective of the BOND project is to develop an array of smart nanobiosensor based on olfactory receptors for the detection of odorant signatures.

Briefly, the basis of the nanobioplatform will be the olfactory receptors (OR), proteins specifically sensitive to the odorants belonging to the odorant disease signature prepared in the form of small vesicles immobilized onto the nanotransducers. An array of smart nanotransducers will acquire and process electronically the odour detected. Such an easy-to-use nanobioplatform, with user-friendly interface and odorant identification algorithm, will detect and discriminate the production profiles of odour compounds.

DOXORUBICIN LOADED MAGNETIC POLYMERSOMES: THERANOSTIC NANOCARRIERS FOR MR IMAGING AND MAGNETO-CHEMOTHERAPY

Olivier Sandre, Charles Sanson, Odile Diou, Julie Thévenot, Emmanuel Ibarboure, Alain Soum, Annie Brûlet, Sylvain Miraux, Eric Thiaudière, Sisareuth Tan, Alain Brisson and Sébastien Lecommandoux

Laboratoire de Chimie des Polymères Organiques (LCPO)
UMR5629 Université de Bordeaux / CNRS / Institut Polytechnique de Bordeaux,
ENSCBP – 16 avenue Pey Berland, 33600 Pessac, France
olivier.sandre@ipb.fr

Hydrophobically modified maghemite (γ-Fe_2O_3) nanoparticles were encapsulated within the membrane of poly(trimethylene carbonate)-b-poly(L-glutamic acid) (PTMC-*b*-PGA) block copolymer vesicles using a nanoprecipitation process. This formation method gives a simple access to highly magnetic nanoparticles (MNPs) (loaded up to 70 wt %) together with a good control over the vesicles size (100 to 400 nm). The simultaneous loading of maghemite nanoparticles and doxorubicin was also achieved by nanoprecipitation. The deformation of the vesicle membrane under an applied magnetic field has been evidenced by small angle neutron scattering. These superparamagnetic hybrid self-assemblies display enhanced contrast properties that open potential applications for Magnetic Resonance Imaging. They can also be guided in a magnetic field gradient. The feasibility of controlled drug release by radio-frequency magnetic hyperthermia was demonstrated in the case of encapsulated doxorubicin molecules, showing the viability of the concept of magneto-chemotherapy. These magnetic polymersomes can be used as efficient multifunctional nano-carriers for combined therapy and imaging.

References:

[1] S. Lecommandoux, O. Sandre, F. Chécot, J. Rodriguez-Hernandez, R. Perzynski, Adv. Mat, 17 (2005), 712-718.
[2] S. Lecommandoux, O. Sandre, F. Chécot, J. Rodriguez-Hernandez, R. Perzynski, Journal of Magnetism and Magnetic Materials 300 (2006), 71-74.
[3] S. Lecommandoux, O. Sandre, F. Chécot, R. Perzynski, Progress in Solid State Chemistry, 34 (2006), 171-179.
[4] C. Sanson, J-F. Le Meins, C. Schatz, A. Soum, S. Lecommandoux, Soft Matter, 6 (2010), 1722-1730
[5] C. Sanson, C. Schatz, J-F. Le Meins, A. Brûlet, A. Soum, S. Lecommandoux, Langmuir 26 (2010), 2751-2760.
[6] C. Sanson, C. Schatz, J-F. Meins, A. Soum, E. Garanger, J. Thévenot, S. Lecommandoux. Journal of Controlled Release, 147 (2010), 428-435.
[7] C. Sanson, O. Diou, J. Thévenot, E. Ibarboure, A. Soum, A. Brûlet, S. Miraux, E. Thiaudière, S. Tan, A. Brisson, V. Dupuis, O. Sandre, S. Lecommandoux, ACS Nano, Published online (2011), doi: 10.1021/nn102762f.

Figures:

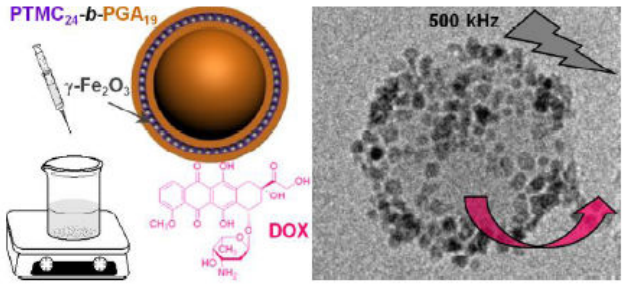

Figure 1: *Left: Sketch of dually-loaded vesicles prepared by addition of an aqueous buffer into a mixture of PTMC-b-PGA copolymer, hydrophobically coated magnetic nanoparticles and doxorucin drug. Right: Cryo-TEM image of vesicle showing the dense mantle of MNPs, which excitation by a radiofrequency magnetic field transmits heat locally to membrane and accelerates the DOX release.*

SPECIFIC IMMOBILIZATION AND PURIFICATION OF RECOMBINANT PROTEINS USING DIETHYLAMINOETHYL-FUNCTIONALIZED MAGNETIC NANOPARTICLES

Jesús M. Sanz[1], Gracia Retamosa-Hernández[1], Beatriz Maestro[2], María J. Rodes-Martínez[1], M. Luisa Ferrer[3] and M. Puerto Morales[3]

[1]Instituto de Biología Molecular y Celular. Universidad Miguel Hernández. Avda. Universidad, s/n. Elche-03202, Spain
[2]Instituto de Electroquímica. Universidad de Alicante. 03690 - San Vicente del Raspeig, Spain
[3]Instituto de Ciencia de Materiales de Madrid - CSIC, 28049-Madrid, Spain
jmsanz@umh.es

The affinity of proteins for their ligands is usually employed in several biotechnological processes that involve their immobilization on solid surfaces, among which affinity chromatography is perhaps the best known application. In this sense, the choline-binding modules (CBMs) such as the CLytA protein, have been used in these tasks with appreciable success [1-4]. CBMs constitute a family of polypeptides that are part of several enzymes such as the murein hydrolases from *Streptococcus pneumoniae* (pneumococcus) [5-6] and that present a high affinity for choline and other tertiary and quaternary amines [7], as well as for supports that contain these groups, such as diethylaminoethyl (DEAE)-cellulose. Fusion proteins containing one of these choline-binding modules as affinity tags can be immobilized and/or purified in a single chromatographic step by means of a simple, gentle, noncovalent procedure [1-4,8].

With the aim of checking the performance of the CBM system on the immobilization of proteins in nanostructures, we have evaluate the binding of the C-LytA and C-LytA fusion proteins on several classes of magnetic nanoparticles. Firstly, we carried out the synthesis of Fe_2O_3 magnetic nanoparticles by coprecipitation methods which were subsequently coated with DEAE-dextran, with a resulting diameter of ~ 10 nm. On the other hand, we also assayed commercial magnetite nanoparticles coated with DEAE-starch (Fig. 1) (200 nm diameter) or with DEAE-silica (750 nm diameter). In all cases we observed a very efficient binding of the C-LytA module, either isolated or fused to the green fluorescent protein (C-LytA-GFP) or to the β-galactosidase (C-LytA- β -gal). Bound proteins could withstand strong washes with up to 1 M NaCl, conserved their structure and activity, and could be specifically eluted upon addition of 150 mM choline as a competitor ligand (Fig. 2). With this in mind, we set up a simple purification procedure of recombinant proteins from a bacterial extract using the 200-nm particles and the protocol depicted in Fig. 3. Proteins could be purified this way to electrophoretic homogeneity (Fig. 4), with a yield of 50 mg per gram of nanoparticles, and the whole procedure could be accomplished in as low as 20 minutes.

The procedure described here displays a series of advantages with respect to other current methods: DEAE nanoparticles are easy to synthetize and the protein immobilization is fast, efficient and strong although, due to its non-covalent nature, the regeneration of the particles can be easily carried out. Moreover, buffers are simple and do not contain components that may potentially inactivate enzymes or be harmful to the human body. Besides the rapid purification of proteins, DEAE-containing magnetic nanoparticles may act as protein carriers to be used in a wide panoply of applications, such as the construction of enzymatic electrodes, recyclable enzymatic bioreactors, or *in vivo* delivery of proteins to specific tissue targets by means of the application of an external magnet.

References:

[1] Sánchez-Puelles, J.M. et al. Eur. J. Biochem. 203, (1992),153-159.
[2] Ortega, S. et al Bio/Technology 10 (1992), 795-798.
[3] Akerstrom, B. et al. Biochim. biophys. Acta 1482 (2000),172-184.
[4] Caubin, J.et al. Biotechnol. Bioeng. 74 (2001), 164-171.
[5] García,P.et al. J. Appl. Biomed. 8, (2010), 131–140.
[6] CW_binding_1 family: Pfam code PF01473; http://pfam.sanger.ac.uk/family?PF01473
[7] Sanz,J.M. et al. FEBS Lett. 232, (1988), 308-312.
[8] LYTAG and LYTAG-Two-Phase user manuals. Biomedal, S.L. http://www.biomedal.es

Figures:

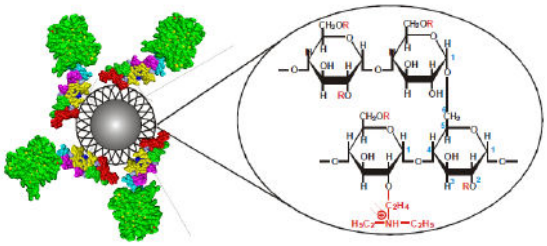

Figure 1: *Scheme of magnetic nanoparticles derivatized with DEAEstarch (taken from Chemicell GmbH) coated with C-LytA-GFP.*

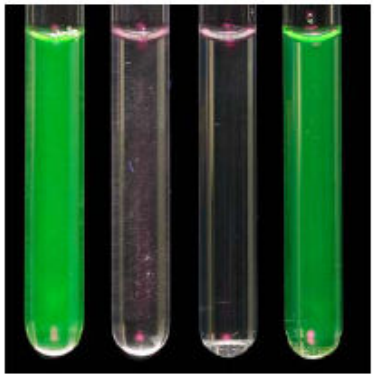

Figure 2: *Left to right: C-LytA-GFP solution prior to binding to magnetic nanoparticles; two washes with 1M NaCl; elution of protein from the particles with choline.*

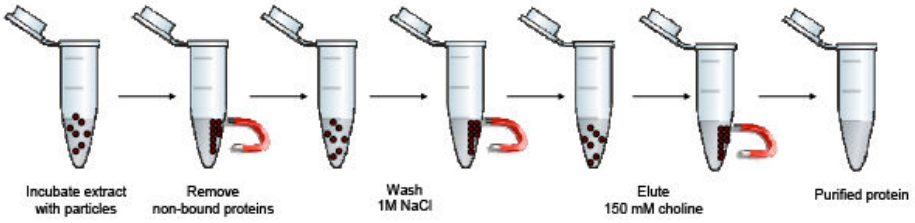

Figure 3: Scheme *of the purification method of CBM-tagged proteins*

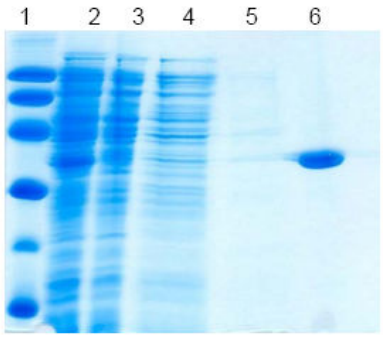

Figure 4: *Polyacrylamide gel electrophoresis in the presence of SDS showing the purification of C-LytA-GFP. Lane 1, protein molecular weight markers; Lane 2, total extract of Escherichia coli RB791 overproducing CLytA-GFP; Lane 3, non-bound proteins upon incubation with magnetic nanoparticles; Lane 4, first wash with NaCl; Lane 5, last wash with NaCl; Lane 6, protein eluted with choline.*

APTAMERS FOR NANOSTRUCTURED BIOSENSORS

Beate Strehlitz, Christine Reinemann, Regina Stoltenburg

Helmholtz-Centre for Environmental Research – UFZ, Permoserstr 15, D-04318 Leipzig, Germany
beate.strehlitz@ufz.de

Aptamers are ssDNA or RNA oligonucleotides featured by a very high affinity of their target binding, offer new possibilities for nanotechnological applications. Aptamers are suitable as molecular recognition elements in a wide range of analytical systems with the goal of separation and purification of molecules from complex mixtures or of detection of molecules in complex matrices. In this context, aptamers will play an important role as new receptors in biosensors [1, 2]. Moreover, aptamers have a great potential for their use in the field of medical and pharmaceutical basic research as well as clinical diagnostic and therapy (e.g. inhibition of enzyme activities, blocking of receptor binding sites).

Aptamers as nucleic acids are very attractive compounds for combinatorial chemistry. They are able to fold into defined secondary and tertiary structures, and they can easily be amplified by PCR. Very complex libraries of random sequence oligonucleotides with about 10^{15} different molecules can be produced by chemical synthesis and screened in parallel for a particular functionality, such as recognition and high affinity binding to a given target or catalytic activity. In 1990, three laboratories independently described a method for the identification of nucleic acid sequences, exhibiting predetermined properties, within large pools of randomised synthetic oligonucleotides [6-8]. This method is known as SELEX (Systematic Evolution of Ligands by Exponential enrichment) and is now widely used for the selection of aptamers, which bind their target with high affinity and specificity.

The functionality of aptamers is based on their stable 3D-structure, which depends on the primary sequence, the length of the nucleic acid molecule (smaller than 100 nt) and the ambient conditions. Typical structural motives are stems, internal loops, bulges, hairpin structures, tetra loops, pseudoknots, triplicates, kissing complexes, or G-quadruplex structures. In presence of the target, the aptamers undergo adaptive conformational changes and their three-dimensional folding creates a specific binding site for the target. The intermolecular interactions between aptamer and target are characterised by a combination of complementarity in shape, stacking interactions between aromatic compounds and the nucleobases of the aptamers, electrostatic interactions between charged groups, and hydrogen bondings [6-8].

The aptamer selection process (SELEX) is an iterative process (Fig. 1). Starting point is a chemically synthesised random DNA oligonucleotide library consisting of about 10^{13} to 10^{15} different sequence motifs. Several rounds (typically 6 to 20 rounds) of in vitro selection (binding, partitioning) and enzymatic amplification of oligonucleotide variants result in the enrichment of relatively few sequence motifs with the highest affinity and specificity for the target. This evolution is driven by the selection conditions (target features and concentration, buffer, temperature, incubation time, efficiency of the partition method, negative selection steps ...). The stringency strongly affects the affinity and specificity of the aptamers to be selected, and is typically progressively increased in the course of a SELEX process.

The SELEX technology has been applied to different classes of targets. Inorganic and small organic molecules, peptides, proteins, carbohydrates, antibiotics as well as complex targets like target mixtures or whole cells and organisms were used for an aptamer selection [9-13]. Aptamers can also be selected for toxic or non-immunogenic targets. Once selected, they can be produced by chemical synthesis in high amount and with high reproducibility. Multiple modifications are possible e.g. to enhance their stability or to permit the quantification and immobilisation of the aptamers. Denatured aptamers can be regenerated. Because of these properties aptamers represent an alternative to antibodies regarding analytical applications.

With this presentation we will show several results of our aptamer selections and some examples of their application in biosensors and assays.

References:

[1] O'Sullivan, C. K., Anal. Bioanal. Chem. 372 (2002) 44-48.
[2] Tombelli, S., Minunni, A.Mascini, A., Biosens. Bioelectron. 20 (2005) 2424-2434.
[3] Ellington, A. D., Szostak, J. W., Nature 346 (1990) 818-822.
[4] Tuerk, C., Gold, L., Science 249 (1990) 505-510.
[5] Robertson, D. L., Joyce, G. F., Nature 344 (1990) 467-468.
[6] Hermann, T., Patel, D. J., Science 287 (2000) 820-825.
[7] Patel, D. J., Curr. Opin. Chem. Biol. 1 (1997) 32-46.
[8] Patel, D. J., Suri, A. K., Jiang, F., Jiang, L. C., Fan, P., Kumar, R. A.Nonin, S., J. Mol. Biol. 272 (1997) 645-664.
[9] Famulok, M. Curr. Opin. Struct. Biol. 9 (1999) 324-329.
[10] Göringer, H. U., Homann, M.Lorger, M., Int. J. Parasitol. 33 (2003) 1309-1317.
[11] Klussmann, S. (2006) The Aptamer Handbook. Functional Oligonucleotides and Their Applications, WILEY-VCH Verlag GmbH & Co. KGaA, Weinheim.
[12] Stoltenburg, R., Reinemann, C., Strehlitz, B., Biomol. Eng. 24 (2007) 381-403.
[13] Wilson, D. S., Szostak, J. W., Annu. Rev. Biochem. 68 (1999) 611-647.

Figures:

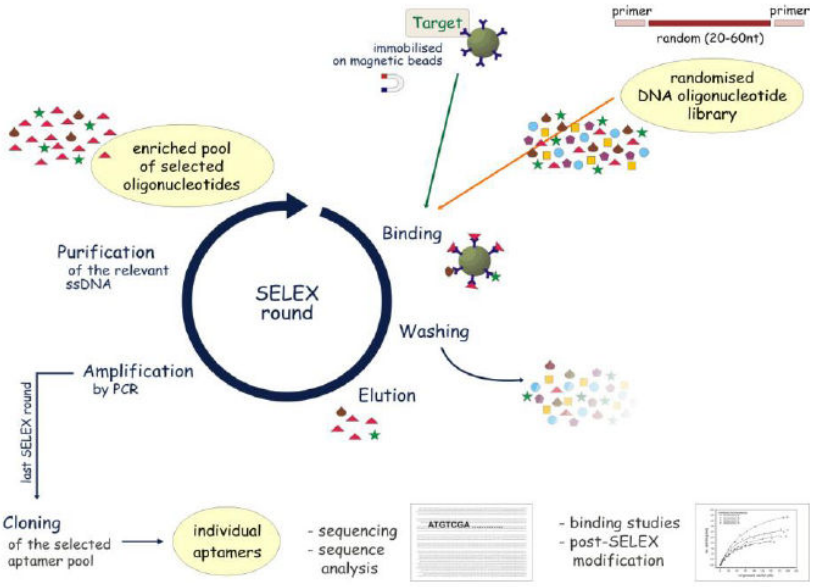

Figure: 1: *SELEX process for the selection of target-specific DNA aptamers. The starting randomised oligonucleotide library is directly used for binding with the target molecules (in this case immobilised on magnetic beads) in the first SELEX round. Unbound oligonucleotides are removed by several stringent washing steps of the binding complexes. The target-bound oligonucleotides are eluted and subsequently amplified by PCR. A new enriched pool of selected oligonucleotides is generated by purification of the relevant ssDNA from the PCR products. This selected new oligonucleotide pool is then used for the next selection round. If an enrichment of target-specific oligonucleotides is observed the last SELEX round is finished after the amplification step. The enriched aptamer pool is cloned and several individual aptamers have to be characterised.*

BISPHOSPHONATE-SUPERPARAMAGNETIC IRON OXIDE NANOPARTICLES CONJUGATES FOR DUAL-MODALITY PET/SPECT-MR MEDICAL IMAGING

Rafael Torres Martin de Rosales, Richard Tavaré, Arnaud Glaria, Maite Jauregui-Osoro, Rowena L. Paul, Gopal Varma, Andrea Protti, Istvan Szanda and Philip J. Blower

Department of Imaging Chemistry and Biology - Division of Imaging Sciences & Biomedical Engineering - King's College London - London, United Kingdom

rafael.torres@kcl.ac.uk

The combination of radionuclide-based imaging modalities such as single photon emission computed tomography (SPECT) and positron emission tomography (PET) with magnetic resonance imaging (MRI) is likely to become the next generation of clinical scanners. Hence, there is a growing interest in the development of SPECT- and PET-MRI agents [1]. These dual-modality agents may allow users to make the most of the high sensitivity of PET/SPECT and the high anatomical resolution and soft tissue contrast of MRI in a synergistic fashion. To this end, we have developed a new class of SPECT/PET-MR imaging agents based on the conjugation of radiolabeled bisphosphonates (BP) directly to the surface of superparamagnetic iron oxide (SPIO) nanoparticles (Figure 1) [2]. We demonstrate the high potential of the BP-iron oxide conjugation using radiolabeled BPs (^{64}Cu for PET or ^{99m}Tc for SPECT), and Endorem/Feridex, a liver MRI contrast agent based on SPIO. The labeling of SPIOs with BPs can be performed in one step at room temperature if the SPIO is not coated with an organic polymer. Heating is needed if the nanoparticles are coated, as long as the coating is weakly bound as in the case of dextran in Endorem. The size of radiolabeled Endorem was characterised by TEM (5 nm, Fe_3O_4 core) and DLS (106 ± 60 nm, Fe_3O_4 core + dextran). EDX, Dittmer-Lester and radiolabeling studies demonstrate that the BP is bound to the nanoparticles and that it binds to the Fe_3O_4 cores of Endorem, and not its dextran coating. The bimodal imaging capabilities and excellent stability of these nanoparticles were confirmed *in vivo* using MRI and nanoSPECT-CT or nanoPET-CT imaging, showing that the radionuclides and Endorem co-localise in the reticuloendothelial system (liver and spleen) and the lymph nodes, as expected for particles of the composition and size of Endorem. To the best of our knowledge, these are the first examples of radiolabeling SPIOs with BP conjugates and the first examples of radiolabeling SPIO nanoparticles directly onto the surface of the iron oxide core, and not its coating. This work lays down the basis for a new generation of SPECT/PET-MR imaging agents in which the BP group could be used to attach functionality to provide targeting, stealth/stability and radionuclides to Fe_3O_4 nanoparticles and other inorganic materials of biomedical interest using very simple methodology readily amenable to GMP.

References:

[1] a) A. Louie, Chem. Rev. 110, (2010), 3146; b) L. E. Jennings, N. J. Long, Chem. Commun. (2009), 3511; c) S. Lee, X. Chen, 8, Mol. Imaging (2009), 87; d) J. Kim, Y. Piao, et al., Chem. Soc. Rev. 38, (2009), 372; e) J. Cheon, J. H. Lee, Acc. Chem. Res. 41, (2008), 1630.

[2] a) R. Torres Martin de Rosales, R. Tavaré, et al., Submitted, (2010); b) R. Torres Martin de Rosales, C. Finucane, et al. Chem. Commun. (2009), 4847.; c) R. Torres Martin de Rosales, C. Finucane, et al., Bioconjugate Chem. 21, (2010), 811.

Figures:

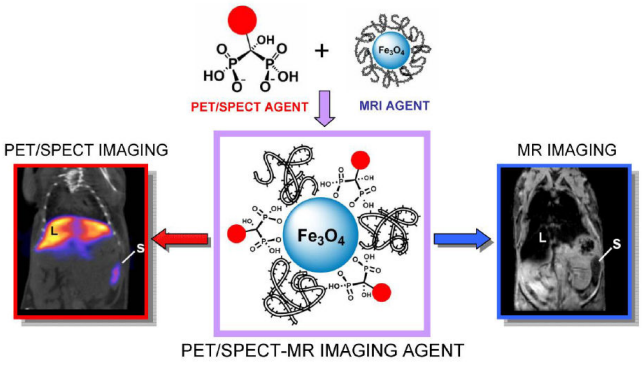

APTAMERS FOR DIAGNOSTIC

Jean-Jacques Toulmé[1], Eric Dausse[1], Carmelo Di Primo[1], Michèle Allard[2], Julie Miguel[2] and Sonia Da Rocha[3]

[1]Inserm, European Institute of Chemistry and Biology, University of Bordeaux, Bordeaux, France
[2]General Hospital, Bordeaux, France
[3]Novaptech, 2 rue R. Escarpit, Pessac, France
jean-jacques.toulme@inserm.fr

Aptamers are oligonucleotides identified through a combinatorial process known as SELEX (Systematic Evolution of Ligands by EXponantial enrichment). They exhibit both high affinity and specificity for a pre-determined taget of interest. They can be raised against a wide range of molecules -even living cells- including marker proteins for major diseases. Following association to various devices aptamers can signal the presence of their cognate ligand (fluorescence, SPR, ...).

We developped an automated platform that speeds up the selection of apatmers and designed a high throughput screening method for the identification of aptamers to various proteins, including human matrix metalloproteases and viral components. Aptamer-based tools were subsequently synthesized for imaging human brain tumors by scintigraphy and detecting viral proteins on micro-arrays.

NANOSCIENCE NANOTECHNOLOGIES: A NEW IMAGINERY IN SCIENCE AND PHILOSOPHY

Daniel Truong Loï

France

The buzz about nanosciences and technologies can be explained in reference to the imaginery they invite and disrupt; by changing the scheme of visibility, by producing objets, they activate some mythical characters of mastery (Faust, Prometheus, Frankenstein for example), and their fate are thought of as misfortunes. In the same mind the NBIC give rise to a dissenting picture of an enclosed science, to plot against and destabilize society. To objectivize this imaginary can help to assess the link between science and society.

DEVELOPMENT OF AN ELECTROCHEMICAL IMMUNOSENSOR BASED ON SPECIFIC ANTIBODIES LABELLED WITH CDS NANOPARTICLES DEVOTED TO THE PARAQUAT RESIDUES DETECTION IN SPIKED POTATO SAMPLES

Enrique Valera[a,b], Raül García-Febrero[a,b], Isabel Pividori[c], Francisco Sánchez-Baeza[a,b], M.-P. Marco[a,b]

[a]Applied Molecular Receptors Group (AMRg), IQAC-CSIC, Jordi Girona 18-26, 08034 Barcelona, Spain
[b]CIBER de Bioingeniería, Biomateriales y Nanomedicina (CIBER-BBN), Barcelona, Spain
[c]Unitat de Química Analítica, Grup de Sensors i Biosensors. Edifici C - Campus de la UAB 08193 Bellaterra (Cerdanyola del Vallès), Barcelona, Spain
enrique.valera@iqac.csic.es

The analysis of the presence of potentially hazardous chemicals (e.g. pesticides, antibiotics) in food remains a major concern in the European Community. However, to ensure quality and traceability, there is a great need to increase the continuous control and monitoring of foodstuff at critical steps in the food chain, such as for example after the recollection of the raw materials, after the food processing (monitoring of storage and logistics), as well as of final products.

Fast, reliable and cost-effective analytical methods are necessary to ensure the safety of the food products. Following the flexibility, sensitivity, specificity and efficiency of analysis demonstrated by the numerous immunochemical and biological tests today available, research is now intending to go forward by developing devices capable of working out of laboratory, i.e. in the different steps of the food chain. With this idea the concept arises of biosensor as a miniaturized analytical devices, consisting of an immobilized biological component (antiody, enzyme, receptor, DNA, etc.) in intimate contact with a transducer (optic, electrochemical, piezoelectric, etc.) that may convert the biorecognition process into a quantifiable electrical signal.

With regards to the use of biosensors as a method to verify compliance of legislation, most of the devices reported until now, rely on the use of labels to reach the necessary detection limits required. Likewise, the use of inorganic nanocrystals tracers as labels for electrochemical immunoassays have recently received great attention because the possibility of obtain simultaneous detection/measurements of DNA targets and proteins [1,2].

In this work, the potential of a new electrochemical immunosensor to detect residual amounts of paraquat (PQ) in a complex matrix, such as potatoes, is evaluated. The immunosensor presented is based on graphite composite electrodes (GECs), immunoreagents specifically developed to detect paraquat, magnetic µ-particles, and CdS nanoparticles labelled to the specific antibodies. The assay relies on the immunochemical competitive reaction between the pesticide residues and a fixed amount of the immobilized antigen on the magnetic beads for a small amount of the specific antibody. At the end of the reaction the amount of antibody captured by the free antigen is evacuated (Figure 1). By means of the well-known anodic stripping techniques, CdS nanoparticles are read, and the amounts of its metal ions are expressed as a signal of current or charge. Due to the amplification of the amperometric/coulombimetric signal, produced by the presence of the CdS nanoparticles, PQ can be detected in spiked potato samples. The results obtained showed that after the extraction and dilution of the matrix, PQ can be determined in potato samples with limits of detection of 0.64 µg L^{-1} and 0.39 µg L^{-1}, depending of the chosen parameter for the detection (current or charge), and taking into account the dilution used. Hence, the LODs obtained are far below the Maximum Residue Level (0.02 mg Kg^{-1}) established by EU for most crops.

References:

[1] Wang, J.; Liu, G.; Merkoçi, A., Journal of the American Chemical Society, 125 (2003) 3214-3215.
[2] Liu, G.; Wang, J.; Kim, J.; Jan, M.-R., Analytical Chemistry 76 (2004) 7126-7130.

Figures:

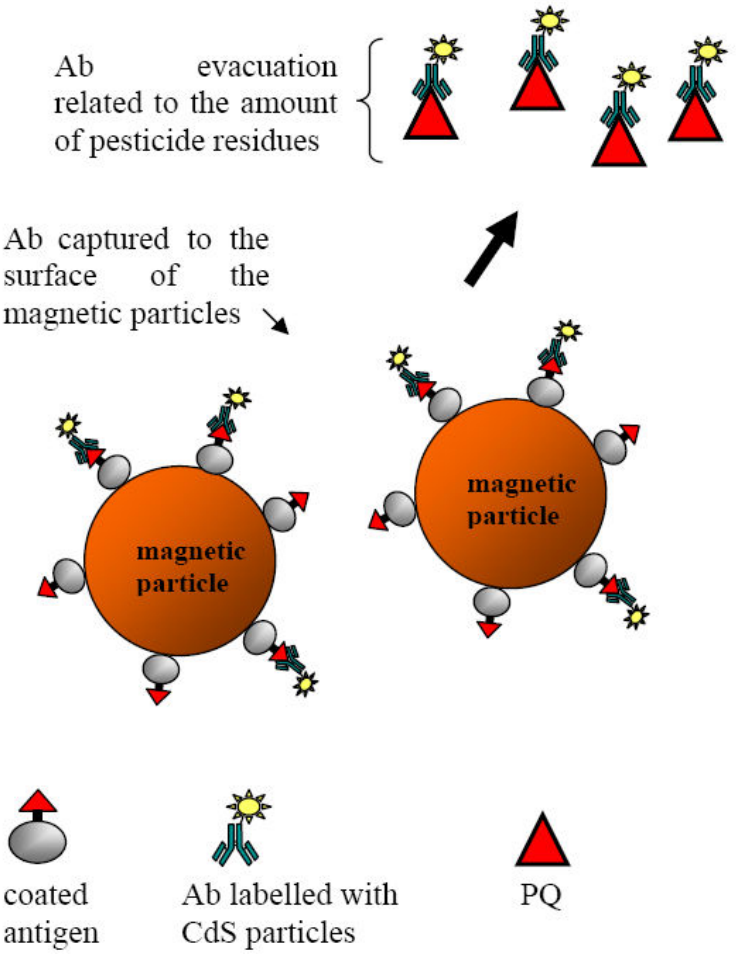

Figure 1: *Electrochemical immunosensor reaction. An amount of the specific antibody is captured by the coated antigen. Likewise, the amount of Ab bound to the pesticide was evacuated. The amount of CdS particles is indirectly related to the PQ residues concentration.*

POLYMERSOME NANOREACTORS AS ARTIFICIAL ORGANELLES

J.C.M. van Hest, S.F.M. van Dongen, W.P.R. Verdurmen, R.J.R.W. Peters, R.J.M. Nolte, R. Brock

Radboud University Nijmegen,Heyendaalseweg 135, 6525 AJ Nijmegen, The Netherlands
j.vanhest@science.ru.nl

Compartmentalisation is one of the techniques that cells adopt to enable a high level of control over (bio-)chemical processes, for instance the order in which enzymes react. In many cases, the compartment also serves to protect the cell from the action of its degrading contents, as is the case with lysosomes. It furthermore serves as a scaffold for the precise positional assembly of enzymes that work together in a multistep cascade reaction.

In an effort to mimic these complex enzyme systems, many studies concerning enzyme encapsulation or assembly have been reported in the literature. The focus of this research initially was on phospholipid liposomes. However, the relative fragility of liposomes limits their potential applicability. Like liposomes, polymersomes are spherical aggregates that contain a bilayer architecture. They are formed by the self-assembly of amphiphilic block copolymers in an aqueous environment and their polymeric bilayer shows a greater stability, mainly due to the lower critical aggregation concentration of amphiphilic macromolecules. A drawback of polymersome membranes is their low permeability even to water, which hampers application as nanoreactors.

To overcome this problem, block copolymers have to be used that give an intrinsically porous bilayer when self assembled. One such copolymer is PS-PIAT. On dispersal in water it forms porous polymersomes that possess a relatively high degree of Small molecules can move across their membranes while larger molecules, such as proteins, cannot.

In a first line of research, we have positioned enzymes at three different locations on these polymersomes, namely, in their lumen (glucose oxidase, GOx), in their bilayer membrane (Candida antarctica lipase B, CalB) and on their surface (horseradish peroxidase, HRP, see figure 1). The surface coupling was achieved by ‘click’ chemistry between acetylene-functionalised anchors on the surface of the polymersomes and azido functions of HRP, which were introduced by using a direct diazo transfer reaction to lysine residues of the enzyme [1].

To determine the encapsulation and conjugation efficiency of the enzymes, they were decorated with metal-ion labels and analysed by mass spectrometry. This revealed an almost quantitative immobilisation efficiency of HRP on the surface of the polymersomes and a more than statistical incorporation efficiency for CalB in the membrane and for GOx in the aqueous compartment. The enzyme-decorated polymersomes were studied as nanoreactors in which glucose acetate was converted by CalB to glucose, which was oxidised by GOx to gluconolactone in a second step. The hydrogen peroxide produced was used by HRP to ABTS to $ABTS^{\cdot+}$ (figure 2). Kinetic analysis revealed that the reaction step catalysed by HRP is the fastest in the cascade reaction.

In a second line of research, artificial organelles were created. For this purpose we modified the outer surface of the polymersome nanoreactors with cell-penetrating peptides, in particular the tat sequence. As a result, the polymersomes obtained the property to enter cells. Enzymes which were encapsulated in the polymersomes could be transported into mammalian cells and perform their biological activity in a living system. This was demonstrated via the introduction of HRP, which could neutralize hydrogen peroxide and therefore protect the cell against oxidative stress (figure 3) [2].

References:

[1] S. F. M. van Dongen, M. Nallani, J.J. L. M. Cornelissen, R. J. M. Nolte, J. C. M. van Hest Chemistry - a European Journal 15 (2009) 1107-1114.

[2] S. F. M. van Dongen, W. P. Verdurmen, R. J.R.W. Peters, R. J.M. Nolte, R. Brock, and J. C.M. van Hest. Angew. Chem. Int. Ed Engl 49 (2010) 7213-16

Figures:

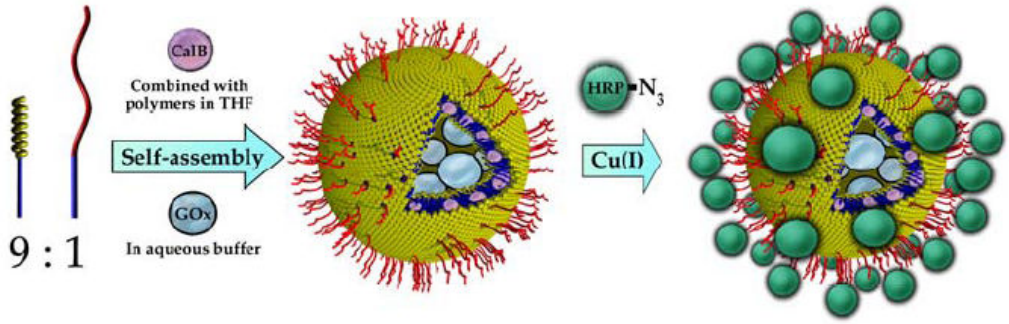

Figure 1: *Positional assembly of enzymes in a polymersome.*

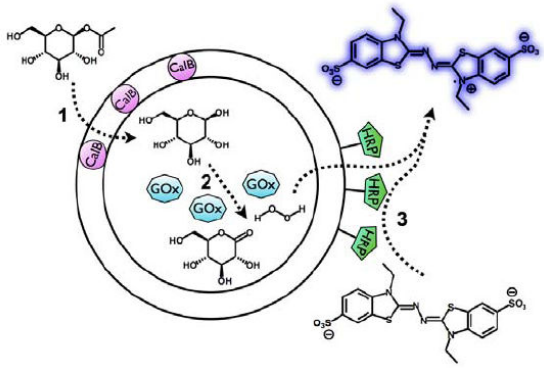

Figure 2: *Schematic representation of the multistep reaction. 1) Monoacetylated Glucose is deprotected by CalB, which is embedded in the polymersome membrane. 2) In the inner aqueous compartment, GOx oxidises glucose to gluconolactone, providing a molecule of hydrogen peroxide. 3) Hydrogen peroxide is used by HRP to convert ABTS to $ABTS^{\cdot+}$. HRP is tethered to the polymersome surface.*

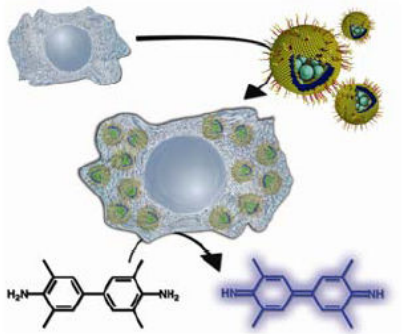

Figure 3: *Schematic representation of the introduction of polymersomes into cells. Polymersomes filled with HRP and functionalized on the periphery with cell penetrating peptides are taken up by mammalian cells. They display their activity as artificial organelles by the oxidation of TMB with hydrogen peroxide.*

PARTICULATE MOLECULAR MATERIALS FOR DRUG DELIVERY: CHALLENGES IN ITS LARGE-SCALE PREPARATION

Jaume Veciana, Nora Ventosa, Santi Sala, Maria Muntó, Mary Cano-Sarabia, Elisa Elizondo, Ingrid Cabrera, Alba Córdoba

Institut de Ciència de Materials de Barcelona (CSIC) and Networking Research Center on Bioengineering, Biomaterials and Nanomedicine (CIBER-BBN), Campus Universitari de Bellaterra, E-08193 Cerdanyola, Spain

vecianaj@icmab.es

The obtaining of particulate micro and nanostructured molecular materials and the understanding of how to manipulate them at nanoscopic and supramolecular level are currently playing a crucial role in drug delivery and clinical diagnostics [1-3]. It has been observed that polymeric nanoparticles, micelles, microemulsions, nanosuspensions, nanovesicles, and nanocapsules are efficient drug carriers that can significantly help to develop new drug delivery routes, more selective and efficient disease-detection systems, drugs with a higher permeability to biological membranes with controlled released profiles, and to enhance their targeting towards particular tissues, cells or intracellular compartments.

The potential of «bottom-up» strategies, based on molecular self-assembling, is much larger than that of «top-down» approaches for the preparation of such micro- and nanostructures. For instance, by precipitation from conventional liquid solutions it should be possible to control particle formation, and hence particle size and size distribution, morphology and particle supramolecular structure. However, this is still a dream up to now when conventional liquids are used.

The solvent power of compressed fluids (CFs), either in the liquid or supercritical state, can be tuned by pressure changes, which propagate much more quickly than temperature and composition solvent changes. Therefore, using compressed solvent media, it is possible to obtain supramolecular materials with unique physicochemical characteristics (size, porosity, polymorphic nature morphology, molecular self-assembling, etc.) unachievable with classical liquid media [4,5]. Small changes in temperature and pressure of CFs result in large but homogenous changes in the fluid's density, and hence in its solvent power. This tunable range in density (solvation ability) cannot be achieved so easily with any conventional solvent. The most widely used CF is compressed CO_2 (cCO_2), which is non-toxic, non-flammable, cheap and easy recyclable. It has gained considerable attention, during the past few years as a «green substitute» to organic solvents and even to water in industrial processing. During the past few years, CFs based technologies, in particular precipitation procedures, are attracting increasing interest for the preparation of particulate molecular materials with application in the field of drug-delivery and nanomedicine [6-8].

In this presentation a few examples of particulate drugs and encapsulated medicines inside vesicles, prepared in a large scale, with CFs will be presented.

References:

[1] M. E. Davis, Z. Chen, D. M. Shin, Nature Reviews-Drug Discovery 2008, 7, 771-782.
[2] P. Couvreur, C. Vauthier, Pharmaceutical Research 2006, 23, 1417-1450.
[3] D. Peer, J. M. Karp, S. Hong, O. C. Farokhzad, R. Margalit, R. Langer, Nature Nanotechnology 2007, 2, 751-760.
[4] E. Reverchon, R. Adami, Journal of Supercritical Fluids 2006, 37, 1-22.
[5] H.M. Woods, M.M.C.G. Silva, C. Nouvel, K.M. Shakesheff, S.M. Howdle, Journal of Material Chemistry 2004, 14, 1663-1678.
[6] M. Cano-Sarabia, N. Ventosa, S. Sala, C. Patiño, R. Arranz, J. Veciana, Langmuir 2008, 24, 2433-2437.
[7] K. Mishima, Advanced Drug Delivery Reviews 2008, 60, 411–432
[8] E. Elizondo, S. Sala, E. Imbuluzqueta, D. González, M. J. Blanco-Prieto, C. Gamazo, N. Ventosa, J. Veciana Pharmaceutical Research 2010, DOI 10.1007/s11095-010-0248-x

LANTHANIDE-DOPED UPCONVERTING NANOPARTICLES: FROM SYNTHESIS TO APPLICATIONS IN BIOLOGY

Rafik Naccache[1], Laura Martinez Maestro[2], Emma Martin Rodriguez[1,2], Daniel Jaque[2], José García Solé[2], John A. Capobianco[1], **Fiorenzo Vetrone**[3]

[1]Concordia University, Department of Chemistry and Biochemistry, 7141 Sherbrooke St. W., Montréal, Québec, Canada, H4B 1R6
[2]Universidad Autónoma de Madrid, Fluorescence Imaging Group, Departamento de Física de Materiales, Madrid, 28049, Spain
[3]Université du Québec, Institut National de la Recherche Scientifique – Énergie, Matériaux et Télécommunications, 1650 Boul. Lionel-Boulet, Varennes, Québec, Canada, J3X 1S2
vetrone@emt.inrs.ca

The recent development of novel highly sensitive and specific luminescent probes with optical properties superior to organic dyes and fluorescent proteins have attracted a diverse group of researchers in a number of key areas. Luminescent nanoparticles such as semiconductor quantum dots (QDs) are emerging as useful tools in diagnostic medicine and therapeutics and are finding widespread applications [1]. However, the majority of these probes require high-energy (UV or blue) light as the excitation source. This has considerable disadvantages resulting in increased background fluorescence (auto-fluorescence), decreased penetration depths in biological tissues as well as photo-induced damage to the specimen under study [2]. To alleviate such issues, multi-photon excited biolabels, including nanoparticles, being more widely used [3]. In particular QDs and gold nanorods (GNRs) are being extensively studied. These nanoparticles are excited with near-infrared (NIR) light, and thus have considerable advantages. For example, NIR light is silent to tissues thus minimizing autofluorescence, possesses greater tissue penetration capabilities and does not cause damage to the sample. Moreover, the nanoparticles require ultrafast (femtosecond) excitation light to induce the multi-photon excited luminescence, which results in increased spatial resolution.

An exciting recent development is the adaption of upconversion for biological applications including biosensing and multi-photon imaging [4-6]. Upconversion is a process inherent to lanthanide-doped materials whereby two (or more) low energy NIR photons are absorbed and in turn, emit higher energy radiation (in the UV-visible-NIR region). This is a very common phenomenon in Ln^{3+}-doped insulating materials because their energy level scheme is favorable for serial addition of multiple isoenergetic photons. Due to the multiphoton nature of the process where “real” long-lived electronic energy states participate, intense upconversion can be observed with low-power commercial cw laser diodes. As a result, inorganic Ln^{3+}-doped nanoparticles are very promising materials and can be used to develop new biocompatible ultra-highly sensitive fluorescent upconverting probes for advanced biomedical applications. Ln^{3+}-doped nanoparticles offer high output, stability with respect to photobleaching, reasonably small size, and flexibility in surface chemistry, which should facilitate their delivery and targeting in biological applications.

Here, we present the synthesis of lanthanide-doped fluoride nanoparticles and subsequent strategies to impart biological functionality. Finally, we show relevant biological applications of these nanoparticles including their ability to be used as imaging probes for malignant cancer cells.

References:

[1] W. C. W. Chan, D. J. Maxwell, X. Gao, R. E. Bailey, M. Han, S. Nie, Curr. Opin. Biotechnol., 13 (2002) 40.
[2] nig. J. Microsc., 200 (2000) 83.
[3] D. Larson, W. Zipfel, R. Williams, S. Clark, M. Bruchez, F. Wise, W. Webb. Science, 300 (2003) 1434.
[4] F. Wang, Y. Han, C. S. Lim, Y. Lu, J. Wang, J. Xu, H. Chen, C. Zhang, M. Hong, X. Liu, Nature, 463 (2010) 1061.
[5] F. Vetrone, R. Naccache, A. Zamarrón, A. Juarranz de la Fuente, F. Sanz-Rodríguez, L. Martinez Maestro, E. Martín Rodriguez, D. Jaque, J. García Solé, J. A. Capobianco, ACS Nano, 4 (2010) 3254.
[6] F. Vetrone, R. Naccache, A. Juarranz de la Fuente, F. Sanz-Rodríguez, A. Blazquez-Castro, E. Martín Rodriguez, D. Jaque, J. García Solé, J. A. Capobianco, Nanoscale, 2 (2010) 495.

Figures:

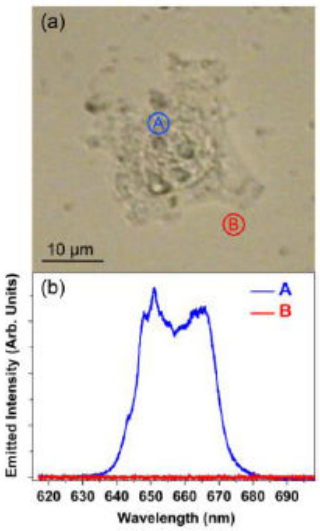

Figure 1: *(a) Optical transmission image of a single HeLa cancer cell after 1.5 h incubation in a water solution containing $NaYF_4:Er^{3+}$, Yb^{3+} nanoparticles. (b) Visible two-photon micro-fluorescence spectra obtained when the fs NIR laser is focused inside and outside the HeLa cell (points A and B in the optical transmission image, respectively).*

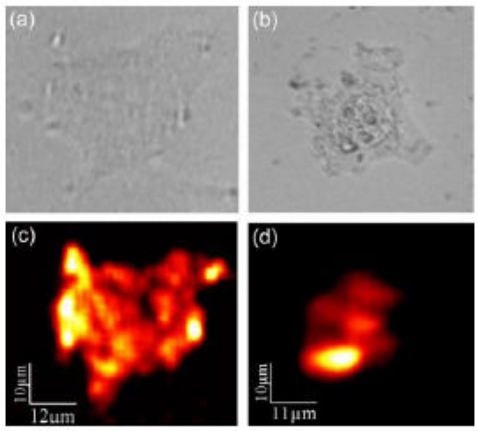

Figure 2: *Top – optical transmission images of two HeLa cells after incubation with $NaYF_4:Er^{3+}$, Yb^{3+} nanoparticles during (a) 1.5 and (b) 3 h. Bottom – confocal fluorescence images of the same HeLa cells ((c) and (d) for 1.5 and 3 h incubations, respectively).*

TOWARDS A TUNABLE ARCHITECTURE OF PROTEIN-ONLY ARTIFICIAL VIRUSES

A. Villaverde[1,2,3], U. Unzueta[1,2,3], J. Cedano[1,4], J. Domingo-Espín[1,2,3], R. Cubarsí[5,3], M. Roldán [6], Valérie Petegnief[7], A. Planas[7], I. Ratera[8,3], O Conchillo[1], E García-Fruitós[1,2,3], C. Diez-Gil[8,3], X. Daura[1,9], P. Saccardo[1,2,3], N. Gonzalez-Montalbán[10], J Ganz 11,12, R. Mangues[3,13], J. Veciana[8,3], H. Peluffo[11,12], N. Ferrer-Miralles[1,2,3], E. Vázquez[1,2,3]

[1]Institut de Biotecnologia i de Biomedicina, Universitat Autònoma de Barcelona, Bellaterra, Spain
[2]Department of Genetics and Microbiology Universitat Autònoma de Barcelona, Bellaterra, Spain
[3]CIBER de Bioingeniería, Biomateriales y Nanomedicina (CIBER-BBN) Bellaterra, Barcelona, Spain
[4]Departament de Bioquímica i Biologia Molecular, Univ Autònoma de Barcelona. Bellaterra, Spain
[5]Departament de Matemàtica Aplicada IV. Universitat Politècnica de Catalunya. Barcelona, Spain
[6]Servei de Microscòpia, Universitat Autònoma de Barcelona, Bellaterra, Spain
[7]Dep d'Isquèmia Cerebral i Neurodegeneració. Inst d'Investigacions Biomèdiques de Barcelona (IIBB), CSIC-Institut d'Investigacions Biomèdiques August Pi i Sunyer (IDIBAPS), Barcelona, Spain
[8]Department of Molecular Nanoscience and Organic Materials. Institut de Ciencia de Materials de Barcelona, CSIC, Bellaterra, Barcelona, Spain
[9]Catalan Institution for Research and Advanced Studies (ICREA), 08010 Barcelona, Spain
[10]Center for Biomedical Engineering and Technology (BioMET), University of Maryland Baltimore (UMB), Baltimore, USA
[11]Neurodegeneration Laboratory, Institut Pasteur de Montevideo, CP 11400 Montevideo, Uruguay
[12]Dept of Histology and Embryology, Faculty of Medicine, UDELAR, CP 11800 Montevideo, Uruguay
[13]Grup d'Oncogènesi i Antitumorals, Institut de Recerca, Hospital de la Santa Creu i Sant Pau, Barcelona, Spain
antoni.villaverde@uab.cat

Nucleic Arginine-rich peptides are well known in molecular medicine by their abilities to condense DNA, to cross cell membranes and as efficient nuclear localization signals [1-4]. Altogether, these properties make them very useful functional elements of artificial viruses [5] for gene therapy and drug delivery. Very recently, we have shown that the homogeneous peptide R9 acts, in addition, as an unexpected architectonic agent at the nanoscale, promoting the self-assembling of a multifunctional protein that contains it, as protein-only, planar nanoparticles of 20 nm in diameter [6]. These particles, that show a strong nuclear avidity and accumulate in the cell nucleus a few minutes after exposition [7], are able to bind, condense and deliver expressible DNA [6].

As the self-organizing properties of R9 seemed to result in much more regular nanoparticles that those offered by conventional self-assembling amyloidogenic peptides, that render either fibers [8] or amorphous aggregates [9], we explored if cationic peptides other than R9 could also promote the self-assembling of holding building blocks. A series of unrelated peptides with diverse amino acid sequences and structures were tested as architectonic tags by using an EGFP as convenient building block. Interestingly, all these peptides were able, at different extents, to promote the spontaneous formation of protein nanoparticles of different sizes, ranging from 20 to 100 nm, in a process in which the arginine residues are critical for the final geometry of the resulting particles. On the contrary, Lysine-rich peptides, although very useful as DNA condensers, do not show any architectonic ability when incorporated to artificial viruses [10].

The use of arginine-rich peptides as structural agents of protein-only nanoparticles opens intriguing possibilities to the tailoring particle geometry through conventional protein engineering, a possibility so far unapproachable in bionanomedicine [11].

References:

[1] E. Vazquez, N. Ferrer-Miralles, R. Mangues, J. L. Corchero, Schwartz S Jr, and A. Villaverde, Modular protein engineering in emerging cancer therapies, Curr. Pharm. Des, 15 (2009) 893-916.

[2] P. Saccardo, A. Villaverde, and N. Gonzalez-Montalban, Peptide-mediated DNA condensation for non-viral gene therapy, Biotechnol. Adv., 27 (2009) 432-438.

[3] E. Vazquez, N. Ferrer-Miralles, and A. Villaverde, Peptide-assisted traffic engineering for nonviral gene therapy, Drug Discov. Today, 13 (2008) 1067-1074.

[4] N. Ferrer-Miralles, E. Vazquez, and A. Villaverde, Membrane-active peptides for non-viral gene therapy: making the safest easier, Trends Biotechnol., 26 (2008) 267-275.

[5] E. Mastrobattista, M. A. van der Aa, W. E. Hennink, and D. J. Crommelin, Artificial viruses: a nanotechnological approach to gene delivery, Nat. Rev. Drug Discov., 5 (2006) 115-121.

[6] Vazquez, E., Roldán, M, Diez-Gil, C, Unzueta, U., Domingo-Espin, J., Cedano, J, Conchillo-Sole, O., Ratera, I, Veciana, J, Ferrer-Miralles, N, and Villaverde, A. Protein nanodisk assembling and intracellular trafficking powered by an arginine-rich (R9) peptide. Nanomedicine 5 (2010).259-268.

[7] E. Vazquez, R. Cubarsi, U. Unzueta, M. Roldan, J. Domingo-Espin, N. Ferrer-Miralles, and A. Villaverde, Internalization and kinetics of nuclear migration of protein-only, arginine-rich nanoparticles, Biomaterials, 31 (2010) 9333-9339.

[8] Y. Zhao, M. Tanaka, T. Kinoshita, M. Higuchi, and T. Tan, Self-assembling peptide nanofiber scaffolds for controlled release governed by gelator design and guest size, J. Control Release, 147 (2010) 392-399.

[9] W. Wu, L. Xing, B. Zhou, and Z. Lin, Active protein aggregates induced by terminally attached self-assembling peptide ELK16 in Escherichia coli, Microb. Cell Fact., 10 (2011) 9.

[10] J. Domingo-Espin, E. Vazquez, J. Ganz, O. Conchillo-Sole, E. García-Fruitós, J. Cedano, U. Unzueta, V. Petegnief, N. Gonzalez-Montalban, A. M. Planas, X. Daura, H. Peluffo, N. Ferrer-Miralles, and A. Villaverde, The nanoparticulate architecture of protein-based artificial viruses is supported by protein-DNA interactions, Nanomedicine, In press, DOI 10.2217/NNM.11.28 (2011).

[11] E. Vazquez and A. Villaverde. Engineering building blocks for self-assembling protein nanoparticles, Microb. Cell Fact., 9 (2010) 101.

USING PARALLEL-STRANDED DUPLEXES TO DIRECT CONTROLLED FORMATION OF PARALLEL-STRANDED G-QUADRUPLEX STRUCTURE

Liliya A. Yatsunyk[1,2] and Jean-Louis Mergny[2]

[1]Swarthmore College, Swarthmore PA 19081, INSERM U869, Bordeaux, France
[2]InstitutEuropéen de Chimie et Biologie, INSERM U869, Bordeaux, France

Nucleic acids are gaining quick popularity and utility for creating new nanomaterials. G-quadruplexes are an attractive alternative to regular B-DNA to assemble nucleic acids, but suffer from a fatal flaw: the rules of pairing, i.e. formation of a G-quartet, in which four identical bases are paired, prevent the controlled assembly between different strands. Complex mixtures are obtained instead of well-defined objects.

In this report, we propose a solution to this problem.Three carefully designed parallel stranded duplexes were used to direct the formation of all parallel G-quadruplex DNA from four different strands. G-quadruplex core can serve as a 'knot' due to its known unusual stability. The presence of multiple points of attachments allows for additions of DNA sequences that are prone to formation of desired specific structures: Watson-Crick duplexes, i-motifs, other G-quadruplexes, etc adding to the versatility of the structure. The correct formation of the overall structure was assessed using gel electrophoresis; the presence of four strands within the structure was demonstrated using fluorescent labels. The presence of the G-quadruplex core was demonstrated through Uv-vis and fluorescent titrations with G-quadruplex specific ligands. The thermal properties of the target structure as well as its duplex components were thoroughly analyzed. The structure obtained displayed unusual but expected stability under denaturing conditions. Attempts to extend the design to one and two dimensional materials are underway in our laboratory.

NANOENGINEERED SELF-ASSEMBLED MONOLAYERS FOR SENSING BIOINSPIRED RECOGNITION

Jing-jiang Yu

Nanotechnology Measurement Division, Agilent Technologies, Inc., Chandler, AZ 85226, USA
Jing-jiang_yu@agilent.com

Self-assembled monolayers (SAMs) have attracted tremendous attention due to their highly ordered structure, stability and rich terminal group chemistry and they offer very promising applications in development of biocompatible materials, solid-phase bioanalytical techniques and biosensors. Particularly, nanometer-scaled mixed self-assembled monolayers (SAMs) are better systems than pure SAMs in mimicking biomembranes because of the presence of segregated domain structures and variety of surface functionalities. In nature, the collective properties and biofunctionalities of these ensembles depend not only on the individual molecular unit but also on the organization at the molecular or nanoscopic level. It has been demonstrated that high-resolution nanofabrication of mixed SAMs with sub-10 nm precision can be achieved readily using either lithography or natural growth approaches [1]. These artificially engineered organic thin films with both desired surface chemistry and designed spatial distribution provide a unique scaffold to investigate bioinspired molecular recognition in the fields of biosensors and immunoassays. For example, HIV infection of CD4 negative cells is initiated by the binding of the viral envelope glycoprotein gp120 to galactosylceramide (GalCer), a glycosphingolipid that serves as the cellular receptor for viral adhesion. By constructing a series of GalCer nanostructures with various geometries via AFM-based lithography and using high-resolution AFM imaging as an in situ, real-time and label-free detection approach to directly monitor the subsequent binding of recombinant gp120 molecules to those engineered carbohydrate ligand nanostructures, the polyvalent interactions between HIV-gp120 protein and GalCer nanostructures are revealed both qualitatively and quantitatively and a better understanding of HIV viral infection process at single molecular level is gained [2]. In addition, our recent studies on advanced strategies to generate thiol-exposing SAMs [3,4] that can serve as highly selective bio-platforms for development of biosensors will be discussed.

References:

[1] Yu et al. A Nanoengineering Approach to Regulate the Lateral Heterogeneity in Mixed Self-Assembled Monolayers. J. Am. Chem. Soc. 2006, 128, 11574-11581.
[2] Yu et al. Polyvalent Interactions of HIV-gp120 Protein and Nanostructures of Carbohydrate Ligands. NanoBiotechnology 2005, 1,201-210.
[3] Yu et al. Nanografting versus Solution Self-Assembly of α,ω-Alkanedithiols on Au(111) Investigated by AFM. Langmuir 2008, 24, 11661-11668.
[4] Li et al. Engineering the Spatial Selectivity of Surfaces at the Nanoscale Using Particle Lithography Combined with Vapor Deposition of Organosilanes. ACS Nano 2009, 7, 2023- 2035.

PPM 2011

INDEX: INVITED CONTRIBUTIONS

INDEX: INVITED CONTRIBUTIONS (NANOMAGMA SESSION)

INDEX: ORAL CONTRIBUTIONS

INDEX: ORAL CONTRIBUTIONS

INDEX: ORAL CONTRIBUTIONS (NANOMAGMA SESSION)

ALPHABETICAL ORDER

I: Invited / IN: Invited NANOMAGMA Session / O: Oral / ON: Oral NANOMAGMA Session

I: Invited / IN: Invited NANOMAGMA Session / O: Oral / ON: Oral NANOMAGMA Session

		pag
Emmanuel Hadji (CEA, France) *"On chip light handling with single and twinned nanobeam cavities"*	I	**433**
Evelyn Hu (Harvard SEAS, USA) *"Gap-Mode Plasmonic Cavities: Engineering Light-Matter Interactions in Metallic Structures"*	I	**435**
Mitsuteru Inoue (Toyohashi Univ of Technology, Japan) *"Magnetophotonics and its applications"*	I	**-**
Kuntheak Kheng (CEA-Grenoble and Univ. of Grenoble, France) *"Bright CdSe/ZnSe nanowire-quantum dots for single photons emission"*	O	**437**
Thomas F Krauss (University of St. Andrews, UK) *"Photonic crystal nanocavities: Efficient light-matter interaction at the nanoscale"*	I	**439**
Christoph Langhammer (Chalmers University of Technology, Sweden) *"Indirect Nanoplasmonic Sensing for Nanomaterials Science"*	O	**441**
Marco Leonetti (CSIC, Spain) *"Measuring light diffusion in thin leaky systems"*	O	**443**
Fred Lisdat (Technical University Wildau, Germany) *"Photobioelectrochemical sensors based on the combination of quantum dot electrodes with enzyme reactions"*	O	**445**
Luis M. Liz-Marzan (Universidad de Vigo, Spain) *"Hot spots and confinement in metal nanoparticles and assemblies"*	I	**447**
Enrique Macia (UCM, Spain) *"Exploiting aperiodic order in photonic devices"*	O	**449**
Maria Grazia Manera (CNR-IMM Lecce, Italy) *"Magneto-Plasmonic Nanostructured Materials For Gas Sensors Applications"*	O	**451**
Tetyana Nychyporuk (Lyon Institute of Nanotechnology (INL), France) *"Strong photoluminescence enhancement of Si and SiC quantum dots by their resonant coupling with multi-polar plasmonic hot spots"*	O	**453**
John Pendry (Imperial College London, UK) *"Transformation Optics at Optical Frequencies"*	I	**455**
Theo Rasing (Radboud Univ, The Netherlands) *"Ultrafast optical manipulation of magnetic order: challenges and opportunities"*	I	**457**
Ida Ros (University of Padova, Italy) *"Surface Enhanced Raman Spectroscopy of different chain length PEP+ moiety bound to Nanorods"*	O	**459**
Juan Jose Saenz (Universidad Autonoma de Madrid, Spain) *"Magneto-Optical properties of nanostructured thin films"*	ON	**461**
Jose A. Sánchez-Gil (CSIC, Spain) *"Designing plasmon nanoparticles tailored for applications in nanophotonics"*	O	**463**
Titus Sandu (National Institute for Research and Development in Microtechnologies, Romania) *"The effect of shape and structure variation of metallic nanoparticles on localized plasmon resonances"*	O	**465**
Thierry Taliercio (University Montpellier 2, France) *"Nanostructured arrays of doped semiconductors for IR nanophotonics"*	O	**467**
Alexei Tchelnokov (CEA, France) *"Title not available"*	I	**-**
Vasily Temnov (MIT, USA) *"Ultrafast acousto-magneto-plasmonics in hybrid metal-ferromagnet multilayer structures"*	IN	**469**
Veronica Toccafondo (Universidad Politécnica de Valencia, Spain) *"Development of high sensitivity biosensors using SOI photonic crystal waveguides"*	O	**471**
Paolo Vavassori (CIC nanoGUNE Consolider, Spain) *"Magnetic information in the Light Diffracted by Arrays of Nanometer-scale Magnets"*	I	**473**
Rémi Vincent (Institut Langevin, ESPCI ParisTech, France) *"Controlling fluorescence resonant energy transfer with a magneto-optical nanoantenna"*	ON	**475**

PPM 2011

ABSTRACTS
ALPHABETICAL ORDER

LIGHT LOCALIZATION ON A GOLD NANODISK ARRAY PROBED BY NEAR-FIELD OPTICS

L. Aigouy[1], L. Lalouat[1], P. Prieto[2], A. Vitrey[2], A. Cebollada[2], M.U. González[2], A. García-Martín[2]

[1]LPEM, UMR 8213 CNRS-ESPCI, 10 rue Vauquelin, 75231 Paris cedex 5, France
[2]IMM (CNM-CSIC), Isaac Newton 8, PTM, Tres Cantos, E-28760 Madrid, Spain
lionel.aigouy@espci.fr

By near-field optics, we have studied the localization of light on an array of metallic nanoparticles illuminated in a transmission mode. The array is made of 286 nm-wide and 50 nm-high gold nanodisks with a period of 500 nm. The SNOM probe is a fluorescent particle which detects the near-field on the surface. We will show that the measured local field is situated between adjacent nanodisks and in a direction parallel to the polarization of the incident light. By performing scans in a direction perpendicular to the surface, we have also observed that the light intensity strongly decays above the sample surface showing a 3D localization. All the experimental results are in very good agreement with numerical simulations performed by the FDTD method and by taking into account the size of the near-field probe.

Figures:

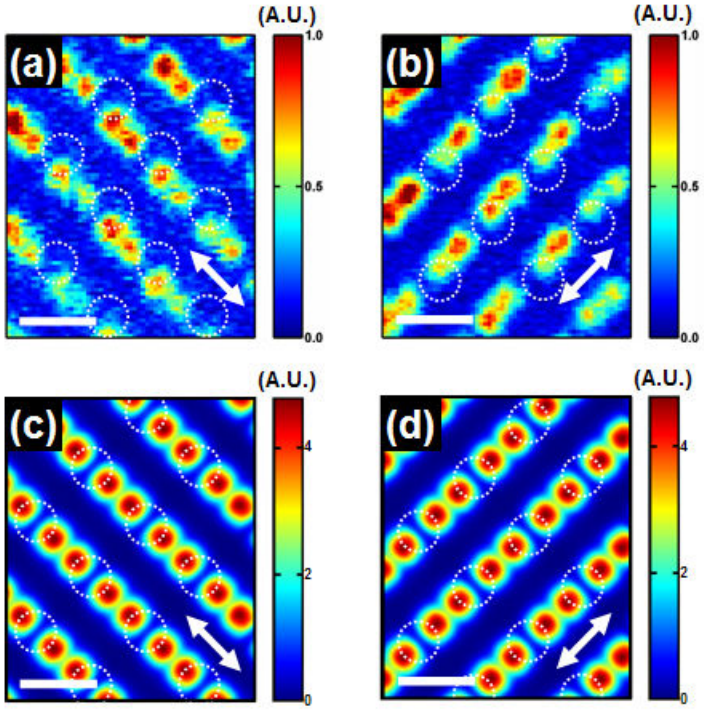

Figure 1: *(a,b) SNOM images measured in a non-contact mode on the nanodisk array at a wavelength of 975 nm. The dotted circles indicate the position of the disks. (c,d) FDTD calculations of the near-field distribution on the structures. The calculation represents the square of the intensity of the total field which is the quantity measured with the near-field fluorescent probe used in the experiments. The calculations has been performed by taking into account of the probe size (a 160 nm large cube).The white arrows indicate the incident polarization direction. The scale bar is 500 nm-long.*

PLASMONIC NANONOANTENNAS:
BUILDING BLOCKS FOR NANOSCALE CONTROL OF OPTICAL FIELDS

Javier Aizpurua

Center for Materials Physics CSIC-UPV/EHU and Donostia International Physics Center DIPC,
Paseo Manuel Lardizabal 5, Donostia-San Sebastián 20018, Spain
aizpurua@ehu.es

Optical antennas or plasmonic antennas are nanoscale metallic structures which act as effective receivers, transmitters and receivers of visible light. Different canonical nanostructures such as metallic nanorings [1], nanorods [2], nanowires [3], dimers [4] or nanoshells [5] are commonly used as optical nanoantennas. These nanoatennas show the ability to focus electromagnetic radiation into tiny spots of nanometer-scale dimensions allowing for more effective field-enhanced visible spectroscopies such as in surface-enhanced Raman spectroscopy (SERS) or in SEIRA. We will address here the optical response of these nanoantennas in a variety of configurations.

We will show theoretically and experimentally how the optical response of a nanoantenna can be engineered through the manipulation of the antenna gap, bridging together concepts of optics and circuit theory [6-9]. With use of similar concepts, we also analyze theoretically the concept of ultrafast optical switches based on nonlinear plasmonic nanoantennas. We explore the use of a photoconductive load at the antenna gap to act as an effective optical nanoswitcher. The principle of switching is based on the transition from capacitive to conductive coupling between two plasmon modes when bringing two nanoparticles into physical contact, as schematically shown in Fig. 1a. We show that photoexcited free carriers in a semiconductor material can be used as a load to short circuit the antenna arms, leading to a strong modification of both the spectral resonance structure (Fig 1b) and near-field mode-profile (Fig 1c-d). As the plasmonic antenna switch is based on a strong confinement of optical fields in space rather than in time, the nanoantenna switch can operate at very low switching energy while potentially reaching a much faster response than microphotonic switching devices.

Another spectroscopy where the role of plasmonic resonances plays an important role is Raman-Brillouin scattering of single metallic nano-objects [10]. The interaction between the vibrations of a metallic nano-object and the plasmons induced on it determine the activation and deactivation of certain vibrational modes in the Raman scattering. To illustrate the wide range of applications of plasmonic interactions in totally different systems, we will conclude by analysing the forces originated from the excitation of plasmons by the fast electron beam in Scanning Transmission Electron Microscopy (STEM) [11]. Our model calculations show that metallic nanoparticles experience attractive or repulsive forces as a function of the position of the electron beam. This ability to manipulate the forces on the particles can be used in gold nanoparticles for example to produce coalescence.

From the overview and the examples shown here, it is straightforward to conclude that an understanding of the interactions occurring at the optical nanoantennas in such a variety of systems, and the knowledge on the electromagnetic response occurring in the different spectroscopy and microscopy configurations are crucial to engineer and design plasmonic devices for improved detection and controlled optical response.

References:

[1] J. Aizpurua et al. Phys. Rev. Lett. 90 (2003) 057401.
[2] J. Aizpurua et al. Phys. Rev. B. 71 (2005) 235420.
[3] F. Neubrech et al. Appl. Phys. Lett. 89 (2006) 253104.
[4] I. Romero et al. Optics Express 14, (2006) 9988.
[5] B. Lassiter et al. Nano Letters 8, (2008) 1212.
[6] A. Alù and N. Engheta, Nat. Phot. 2, (2008) 307-310.
[7] M. Schnell et al. Nature Photonics 3, (2009) 287-291.
[8] N. Large, M. Abb, J. Aizpurua, and O. Muskens, Nano Letters. (2010) 10, 1741-1746.
[9] O. Pérez-González et al. Nano Letters. 10, (2010) 3090.
[10] N. Large et al. Nano Letters 9 (2009) 3732.
[11] A. Reyes-Coronado et al. Phys. Rev. B 82 (2010) 235429.

Figures:

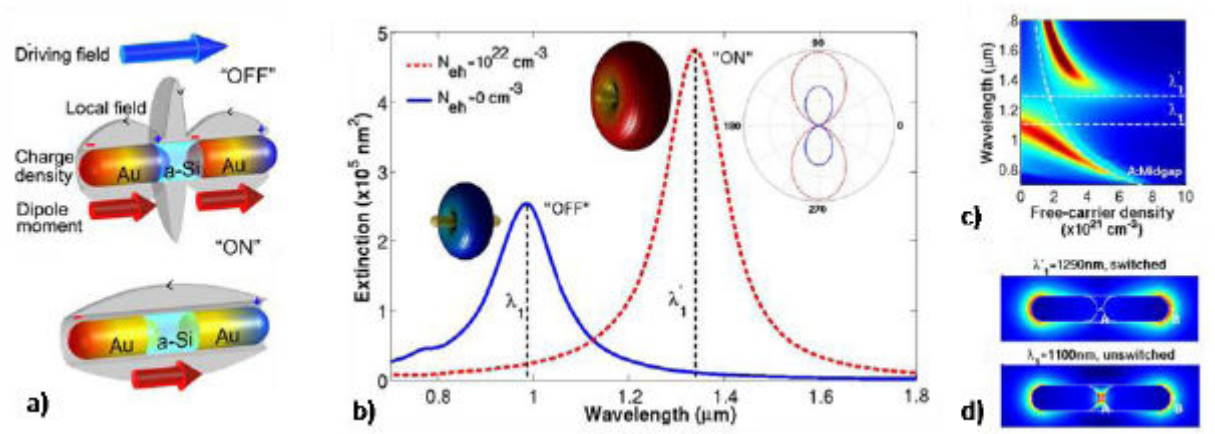

Figure 1: *Figure: a) Schematics of the surface charge density in an "OFF" and "ON" nanoantenna switching situation. b) Extinction spectrum for "OFF" and "ON" switches. c) Near-Field peaks positions as a function of free-carrier concentration. d) Near-field distribution for the "ON" situation at λ=1290nm and "OFF" situation at λ=1100nm.*

MAPPING NEAR-FIELD COUPLING EFFECTS IN INFRARED GAP ANTENNAS

P. Alonso-González[1], P. Albella[1,2], L. Arzubiaga[1], M. Schnell[1], J. Chen[1,2], F. Huth[1], F. Golmar[1], F. Casanova[1,3], L. Hueso[1,3], J. Aizpurua[2], and R. Hillenbrand[1,3]

[1]CIC nanoGUNE Consolider, 20018 Donostia-San Sebastián, Spain
[2]Centro de Fisica de Materiales (CSIC-UPV/EHU) and Donostia International Physics Center (DIPC), 20018 Donostia-San Sebastián, Spain
[3]IKERBASQUE, Basque Foundation for Science, 48011 Bilbao, Spain
palonso@nanogune.eu

The vector near-field distribution of infrared gap antennas (linear dipole antennas coupled via a nanometric gap) is mapped by scattering-type scanning near-field microscopy (s-SNOM). The images provide direct experimental evidence of strong in-plane near-field localization inside a gap as small as 50 nm. By measuring the gap fields as a function of the total antenna length (near-field spectroscopy), we observe a clear resonance shift compared to uncoupled linear dipole antennas, thus verifying strong near-field coupling via the gap. We also find significant differences between near-field and far-field spectra of the antennas and discuss their implications.

Vector near-field imaging of the infrared antennas [1, 2] was carried out with s-SNOM where s-polarized laser light is used for antenna excitation. A dielectric Si tip scatters the local near fields of the antennas. Interferometric and polarization-resolved detection of the tip-scattered light yields amplitude E and phase φ of the in- (x) and out-of-plane (z) near-field components (Ex, φx) and (Ez, φz).

Fig. 1 shows the near-field patterns obtained for a single gap antenna with a gap width of about 50 nm. The out-of-plane near-field component (Ez, φz) shows large near-field amplitudes at both sides of the gap, while a phase jump of about 180º occurs at the gap center [3]. The in-plane near-field component (Ex, φx), in contrast, is strongly enhanced exactly inside the gap and directly verifies field concentration inside the gap.

To provide experimental evidence of near-field coupling in the infrared gap antennas, we perform near-field spectroscopy. We fabricate gap antennas of different total length (but constant gap size) and measure the in-plane gap field as a function of the antenna length. A comparison with near-field spectra of single dipole antennas (continuous nanorods) shows a pronounced resonance shift, which clearly verifies near-field coupling across the antenna gap.

Our results show that vector near-field mapping is a powerful tool for measuring spectral resonance shifts in the near field of infrared antennas, in both amplitude and phase. This enables detailed studies of near-field coupling signatures, including the mapping of strongly localized field enhancement (“hot spots”) and resonance shifts of near-field spectra, which are not accessible by far-field spectroscopy.

References:

[1] Schnell, M.; García-Etxarri, A.; Alkorta, J.; Aizpurua, J.; Hillenbrand, R. Nano Lett., 10 (9) (2010), 3524–3528.
[2] Olmon R. L., Rang, M.; Krenz, P. M.; Lail, B. A.; Saraf, L. V.; Boreman, G. D.; Raschke, M. B. Phys. Rev. Lett., 105 (2010), 167403.
[3] Schnell, M.; García-Etxarri, A.; Huber, A. J.; Crozier, K.; Aizpurua, J.; Hillenbrand, R. Nat. Photonics, 3 (2009), 287-291.

Figures:

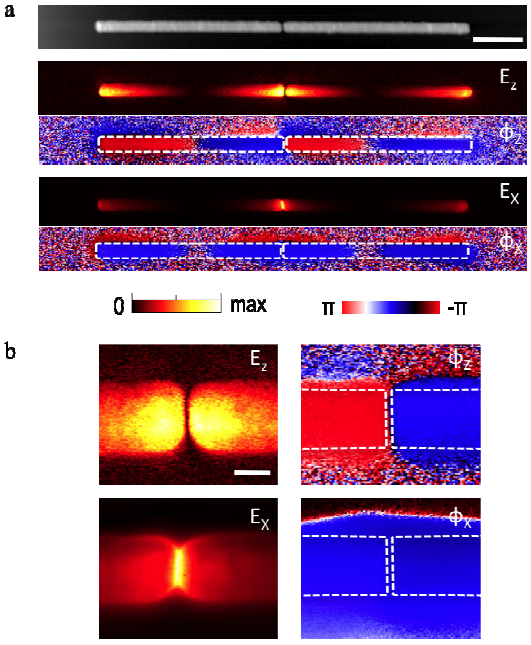

Figure 1: *Near-field images of an infrared gap-antenna recorded at λ=11.06μm. (a) Out-of-plane near-field amplitude Ez and phase φz (top). In-plane near-field amplitude Ex and phase φx (bottom). Scale bar is 1 μm. (b) Enlarged near-field images of the gap region, showing amplitude and phase of the out-of-plane and in-plane near-field components. Scale bar is 100 nm.*

UNUSUAL SPECTRAL RESPONSE OF LOSS-COMPENSATED PLASMONIC NANOPARTICLES IN ACTIVE GAIN MEDIA

A. Veltri, **A. Aradian**

Centre de Recherche Paul Pascal - CNRS & University of Bordeaux
115 av. du Dr Schweitzer 33600 Pessac, France
veltri@crpp-bordeaux.cnrs.fr; aradian@crpp-bordeaux.cnrs.fr

While based on phenomena recognized and described almost one and a half century ago [1], the physics of plasmons in metal nanoparticles has been recently fueled by the rapid development of new techniques for producing small particles and by the applicability of these structure in the realization of visible range metamaterials. One of the main issues in using metallic nano-structures for metamaterial applications at optical frequencies is their high level of losses. A most promising strategy to circumvent this obstacle is loss compensation, where the structures are coupled to active compounds (such as pumped dye molecules or quantum dots) which are able to transfer them energy and therefore amplify the desired response. Research along this line has recently gained momentum, resulting for example in the first demonstration of a nanoscale spaser using gain-assisted core-shell nanoparticles [2]. In this work, we study the apparently simple situation of a single metallic nanoparticle immersed in a gain medium with a focus on the plasmonic response, and show that interesting effects already arise with surprising modifications of the plasmonic spectral response.

We studied the behavior of a metallic nanosphere of radius *r* made of a metal of permittivity $\varepsilon_1 = \varepsilon_1' + i\varepsilon_1''$ (based on the experimental data from [3]) surrounded by an active (externally pumped) dielectric host with permittivity $\varepsilon_2 = \varepsilon_2' + i\varepsilon_2''$ (with $\varepsilon_2'' < 0$ for gain). We here focus on the polarisability of the particle with respect to the outside medium. In the presence of gain, this is given in the quasi-static limit as:

$$\alpha = \alpha' + i\alpha'' = 4\pi r^3 (\varepsilon_2' + i\varepsilon_2'') \frac{(\varepsilon_1' + i\varepsilon_1'') - (\varepsilon_2' + i\varepsilon_2'')}{(\varepsilon_1' + i\varepsilon_1'') + 2(\varepsilon_2' + i\varepsilon_2'')}$$

The plasmon resonance appears at the frequency ω_0 where $2\varepsilon_2' = -\varepsilon_1'$. As proposed in [4], perfect loss compensation is then obtained when the gain level is exactly adjusted ($2\varepsilon_2'' = -\varepsilon_1''$) at this same frequency: one then recovers a singular response. It is obviously highly desirable to obtain such a high amplitude plasmon in order to exacerbate the overall metamaterial response. However, our work points out that this singular behavior is intrinsically different from the ideal plasmon obtained from a lossless metal: in the latter case, the imaginary response $\alpha''(\omega)$ is a Dirac peak (resonant losses are confined to a very narrow spectral region), while in the perfectly-compensated plasmon $\alpha''(\omega)$ takes on a spectrally wide, $1/(\omega - \omega_0)$ behavior (Fig. 1-b and 1-f). To the best of our knowledge, this has remained unnoticed but has important implications, since it means that even with perfect loss compensation, resonant losses can be mitigated but they do *not* simply vanish away.

Moving away from the perfect compensation point by adding or removing gain, more unusual, and sometimes surprising features appear. Mathematically, this comes from the fact that the equations for the real and the imaginary part of polarizability are more similar in presence of external gain than in the absence of it, which gives rise to new behaviours. One striking example happens if, at the Plasmon frequency, we have $\varepsilon_2''(\omega_0) = -\varepsilon_2'(\omega_0)$ as shown in Fig. 1-c and 1-e. In this situation, the real part $\alpha'(\omega)$ takes on a bell shape, while the imaginary part $\alpha''(\omega)$ has a zig-zag shape. This is exactly opposite to the usual plasmon case (Fig.1-a and 1-d) where – as is well-known from textbooks for any type of passive resonator – the *real* part should be zig-zagging and the *imaginary* part should be bell-shaped. We call this new behavior an “anti-plasmon”.

Beyond the peculiarity of this “anti-plasmon” behaviour, an interesting point is that where the real part of the polarisability is maximum, losses are zero (again in contrast with conventional plasmons, Fig. 1-a and 1-d). In Fig. 1-c, for example, one observes strongly negative response with low loss around the plasmon resonance, a property that could be most interesting if one is interested in metamaterials with negative properties based on such resonant elements. Note that the “anti-plasmons” can have either positive or negative real parts (Fig. 1-e and 1-c): this depends if, for the specific system considered,

the condition for the anti-plasmon ($\varepsilon_2'' = -\varepsilon_2'$) is met at gain levels higher (Fig. 1, upper row) or lower (lower row) than the condition for perfect loss-compensation ($\varepsilon_2'' = -1/2\varepsilon_1''$).

Although our approach relies on a very simple theoretical description, it is worthwile noting that related behaviour appears, although left unnoticed by the authors, in much more sophisticated approaches (full FDTD simulations of split-ring resonators in active medium) [5].

Our work therefore underlines that the behaviours of loss-compensated plasmonic particles can be both unusual and richer than the usual case without gain, and that some of these could find, if confirmed in experiments, some potential applications in metamaterial designs.

This work was supported by the FP7-NMP-2008 European project METACHEM and the SAMM project of the GIS-Advanced Materials in Aquitaine network.

References:

[1] M. Faraday. Philos. Trans. R. Soc. London, 147 (1857).
[2] M. A. Noginov et al., Nature, 460 (2009) 1110.
[3] P. B. Johnson and R. W. Christy, Phys. Rev. B, 6 (1972) 4370.
[4] N. M. Lawandy. Appl. Phys. Lett., 85 (2004) 5040.
[5] A. Fang et al., J. Optics, 12 (2010) 024013.

Figures:

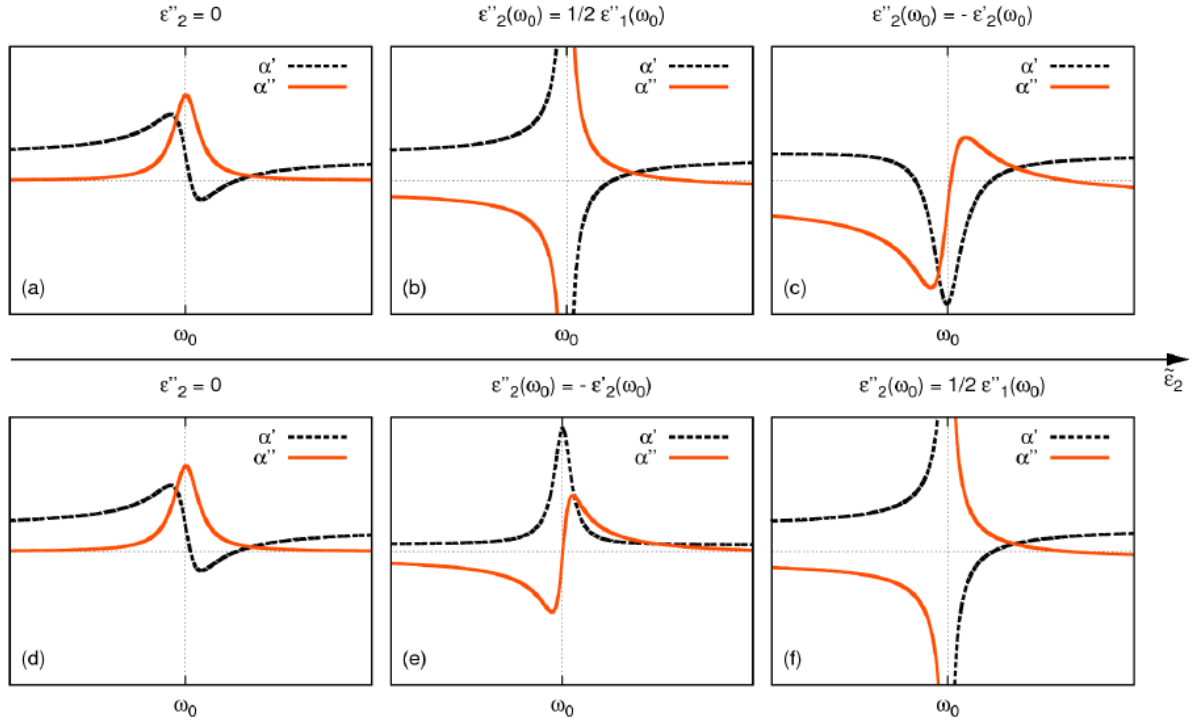

Figure 1: *Polarisability of a spherical nanoparticle in an active gain medium, with increasing gain levels from left to right. (a) and (d): Conventional plasmon resonance without gain. (b) and (f): when perfect loss compensation is obtained a $1/(\omega - \omega_0)$ behavior is obtained both for the real and the imaginary part. (c) and (e): when $\varepsilon_2''(\omega_0) = -\varepsilon_2'(\omega_0)$ an anti plasmon appear. The sign of the real part of the polarizability in a anti-plasmon resonance depends if it appears after the perfect loss compensation (a-c) or before it (d-f).*

ARTIFICIAL PHOTONIC MATERIALS TO CHALLENGE CONVENTIONAL LIMITS TO LIGHT TRAPPING AND SOLAR ENERGY CONVERSION

Harry A. Atwater, Jeremy N. Munday, Dennis M. Callahan, Emily Kosten

Kavli Nanoscience Institute and Thomas J. Watson Laboratories of Applied Physics,
California Institute of Technology, Pasadena, CA, USA

Solar energy is currently enjoying substantial growth and investment, owing to worldwide sensitivity to energy security and climate change, and this has spurred basic research on light-matter interactions relevant to solar energy. Artificial photonic materials can enhance light-trapping and absorption, as well as increase the open circuit voltage and enhance quantum efficiency in solar photovoltaic structures. We describe photonic approaches for designing thin film and wire array solar cells that have light-trapping intensity and absorption enhancements that can exceed the conventional ergodic light-trapping limit using both wave optics and ray optics methods.

From thermodynamic arguments, Yablonovitch and Cody in 1982 determined the maximum absorption enhancement in the ray optics limit for a bulk material to be $4n^2$, where n is the index of refraction of the absorbing layer [1]. Stuart and Hall in 1997 expanded this approach to study a simple waveguide structure; however, for the waveguide structures they considered, the maximum absorption enhancement was $<4n^2$ [2]. Using a combination of analytical and numerical methods, we describe why these structures do not surpass the conventional ergodic limit, and show how to design structures that can.

We present here a physical interpretation in terms of the waveguide dispersion relations and describe the necessary criteria for surpassing the conventional limit. In particular, the wavevector □ needed for a mode to surpass the ergodic limit is given by $\beta > (2n^2h\omega^2)/(\Gamma\pi c^2)$, where Γ is the waveguide confinement factor and h is the waveguide thickness.

Another perspective on this issue is that the conventional light trapping limit can be exceeded in waveguide-like structures when the active region has an elevated local density of optical states (LDOS) compared to that of the bulk, homogeneous material. Additionally, to practically achieve light trapping exceeding the ergodic limit, the modes of the structure must be appreciably populated via an appropriate incoupling mechanism. We find using full wave simulations that ultrathin solar cells incorporating a plasmonic back reflector can achieve spatially averaged LDOS enhancements of 1 to 3, and a metal-insulator-metal (MIM) structure can achieve enhancements over 50 at a wavelength of 1100 nm, the bandedge of Si. Interestingly, incorporating the active solar cell material within a localized metallodielectric plasmonic or metamaterial resonator can lead to nearly spatially uniform LDOS enhancements above 1000 within the active material. We also have examined the possibility of structuring and combining ultrathin solar cells with dispersive dielectric structures such as photonic crystals to exceed the ergodic light trapping limit. We find that LDOS enhancements of ~2-5 inside an untextured, planar solar cell can be achieved by simply placing a photonic crystal above or below the active material.

We have also developed a ray optics model for high aspect ratio wire array light trapping that suggests intensity enhancements within the wires can exceed the conventional limit for arrays with low wire area fractions on a Lambertian back reflector. We have applied this model to wire arrays with area fractions from .1% to 90%, and with aspect ratios between 30 and 200. The intensity enhancement at low wire area fraction can increase cell open circuit voltage, but low wire fraction results in a reduced short circuit current per unit area, and we explore optimizing cell efficiency within this parameter space. We compare with experimental Si wire array optical absorption data for wavelengths between 500 and 1100 nm for Si wires of varying sizes. We find reasonable agreement for large Si wires (radius 4um) but the model underpredicts optical absorption for smaller wires (radius 1um), suggesting that wave optics effects are important for the strong absorption observed in the small wire arrays.

Overall, we find many opportunities for exceeding the previously anticipated intensity enhancement and light trapping factor in dispersive dielectric and metallodielectric photovoltaic structures. These results can guide future solar cell designs that incorporate dispersive dielectric structures, plasmonics and metamaterials to achieve unprecedented light trapping.

References:

[1] Yablonovitch and Cody. IEEE Trans. Elect. Dev. 29 300 (1982)
[2] Stuart and Hall J. Opt. Soc. Am A 14 3001 (1997)

TWO-PHOTON LASER FABRICATION OF 3D SILVER NANOWIRE MICROSTRUCTURES AND THEIR PLASMONIC APPLICATIONS

Patrice Baldeck[1], S. Zaiba[1,2,3], T. Kouriba[1], O. Stéphan[1], O. Ziane[1,2], J. Bosson[4], G. Vitrant[5]

[1]Laboratoire Interdisciplinaire de Physique, CNRS UMR 5588, Université Joseph Fourier Grenoble, BP 87 38220 Saint Martin d'Hères Cedex, France
[2] Laboratoire d'Electronique Quantique, Faculté de physique, Université des sciences et de la technologie Houari Boumediene, Alger, Algérie
[3]Université M'hamed Bouguera, Boumerdes, Algérie
[4] Laboratoire de Physique Fondamentale et appliquée, Université d'Abobo-Adjamé, Côte d'Ivoire
[5] IMEP-LACH, CNRS 5130, Grenoble INP Minatec, 38016 Grenoble, France
patrice.baldeck@ujf-grenoble.fr

We have developed a laser photochemistry process to fabricate, by direct writing, 3D metallic microstructures using a two-photon microfabrication machine (http://www.teemphotonics.com). In this work we report the optical properties of silver nanowire microstructures. Typical nanowire diameter and length are 300 nanometers and 10 microns, respectively.

In the first part of the presentation we will present the diffraction properties of parallel nanowires with inter-distances in the 0.8 to 4 microns range. The interference of individual interference patterns gives rises to focusing effects that have the characteristics of ideal ultrasmall microlens with focal lengths in the micron range and with resolution limited by diffraction, i.e. in the 300 nm range in the visible. We will show that a 3D arrangement of such nanowires lead to an efficient chromatic spatial dispersion that may open a new route for RGB separation of colors at the micron scale.

In the second part of the presentation we will describe the optical properties of arrays of vertical nanowires with interdistances in the 0.8 to 4 microns range. The re-organized incident electromagnetic field is concentrated along the nanowires as shown by 3D wide-field microscopy and FDTD calculations.
We will present how we have used this electromagnetic field enhancement to improve the detected signals from Raman and fluorescences nanoprobes.

References:

[1] L. Vurth, P. Baldeck, O. Stéphan, G. Vitrant, "Two-photon induced fabrication of gold microstructures in polystyrene sulfonate thin films using a ruthenium(II) dye as photoinitiator", Appl. Phys. Lett. 92, 171103 (2008)

Figures:

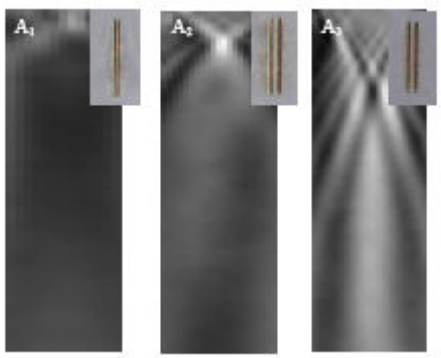

Figure 1: *Focusing effects obtained by the diffraction of silver nanowire pairs separated by 1, 2 and 4 microns for A_1, A_2 and A_3, respectively*

SYNTHETIC OPALS AND SANDCASTLES: EXPLORING WATER AT THE NANOSCALE

Alvaro Blanco, F. Gallego-Gómez, V. Canalejas, C. López

Instituto de Ciencia de Materiales de Madrid and Unidad Asociada CSIC-UVigo, C/ Sor Juana Inés de la Cruz 3, 28049 Madrid, Spain
ablanco@icmm.csic.es

Humid granular media are everyday systems present in pharmaceutics, construction or agriculture. Sandcastles are built with wet sand, where water forms necks between grains, highly improving their mechanical stability [1]. Synthetic opals can be considered as sandcastles at the nanoscale. It is well known that the amorphous silica surface can adsorb a significant amount of water from the surrounding. The characteristics of systems based on silica structures can be greatly affected by the presence of adsorbed water, like the photonic properties of artificial opals formed by silica spheres. Previous work was focused on irreversible change of the water content in the spheres (e.g., by annealing at high temperatures) and its influence on the resulting silica opal [2]. However, studies on in situ water changes in the opal by e.g. due to alterations of the operating temperature or humidity are missing.

In this direction, we have performed a complete characterization of water content in silica artificial opals for different conditions of composition, temperature and growth. We investigate the reversible modification of the water content in the opal (principally by moderate heating but also in vacuum) and the simultaneously changes in the photonic bandgap (PBG). We observe, due to removal of interstitial water, large blue-shifts up to 30 nm and a predominantly decrease of the bandgap width up to 7%. In this study, we make a novel use of the optical properties of the opal to infer quantitative information about water distribution within silica beads and dehydration phenomena from simple reflection spectra. Taking advantage on the well-defined opal morphology, our approach offers a simple tool for straightforward investigation on generic adsorption-desorption phenomena, which might be extrapolated to other humid granular media.

In addition, we also demonstrate that photoswitching can be induced by low cw-visible-irradiation in lightabsorbing hydrophilic silica opals due to local heating, in which large and fast bandgap shift (15 nm in 5 milliseconds) is obtained (Figure 1) [3]. This very simple and cost-effective approach provides high switchability in conventional silica photonic crystals, promising an inexpensive solution for a number of applications.

References:

[1] D. J. Hornbaker, et al., Nature, 387, 765 (1997).
[2] H. Míguez et al. Advanced Materials 10, 480 (1998).
[3] F. Gallego-Gómez et al. submitted (2011).

Figures:

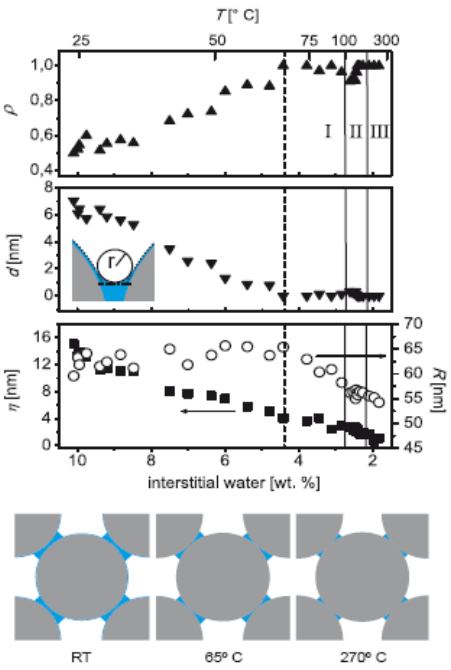

Figure 1: *Water distribution as a function of humidity for different temperatures in an artificial opal formed by silica spheres of 335 nm.*

INTERNAL ELECTROMAGNETIC FIELD DISTRIBUTION AND MAGNETO-OPTICAL ACTIVITY OF METAL AND METAL-DIELECTRIC MAGNETOPLASMONIC NANODISKS

D. Meneses-Rodríguez, E. Ferreiro-Vila, J.C.Banthí, P. Prieto, J. Anguita, A. García-Martín, M. U. González, J. M. García-Martín, **A. Cebollada**, and G. Armelles

IMM-Instituto de Microelectrónica de Madrid (CNM-CSIC)
Isaac Newton 8, PTM, E-28760 Tres Cantos (Madrid), Spain.
david.meneses@imm.cnm.csic.es

Localized surface plasmon resonances (LSPRs) greatly influence the optical [1-4] and magneto-optical (MO) [5-10] properties of fully metallic and metal-dielectric nanostructures. The observed enhancement in the MO activity when these LSPRs are excited is attributed to the high intensity of the electromagnetic (EM) field inside the global nanostructure when the LSPR occurs [5,11]. Unfortunately, it is not straightforward to experimentally determine the intensity of the EM field inside a nanostructure. Here we show how the EM profile related to the LSPR can be probed locally inside the nanostructure by measuring the MO activity of the system as a function of the position a MO active probe (a Co nanolayer). This will be done in full detail in metallic systems, and preliminary results will also be presented in more complex metal-dielectric magneto-plasmonic nanodiscs.

The magnetoplasmonic nanodisk arrays have been fabricated in large area onto glass substrates by combining colloidal lithography with sputter, thermal and electron beam deposition and lift-off techniques. Typical nanodisk structures are Au/Co/Au/Cr and Au/SiO_2/Co/SiO_2/Au/Ti, for the fully metallic and the metal-dielectric structures respectively, with total heights between 50 and 70 nm and diameters between 110 and 140nm (Figure 1(a)). For the sake of comparison, continuous thin films with identical composition have been also prepared.

The MO activity (Φ) has been obtained by measuring the MO Kerr effect in polar configuration upon normal incidence illumination, previously identifying the optical resonances through extinction spectra. In the fully metallic nanostructures, we find a distinctive evolution as a function of Co position of the MO activity in the nanodiscs compared with that of the continuous layers, with maximum values when the Co layer is located near the top or the bottom of the disks and minimum values in-between due to the LSPR excitation. This behavior is in contrast with the MO activity exhibited by the continuous films, which increases monotonously as the Co layer becomes closer to the top surface (Figure 1(b)). This indicates that the EM field inside the nanodisks exhibits a nonuniform distribution in plasmon resonance conditions. In fact, the Co layer acts as a probe sensing the EM field within the nanodisk, since the MO activity depends on the intensity of such field. Preliminary results on the possible influence of multiple resonances in metal-dielectric magnetoplasmonic nanodiscs will be also presented (Figure 1(c)).

This information could be very relevant for the design of magnetoplasmonic systems offering optimum MO enhancement, for instance for sensing applications where maximum sensitivity is expected in the areas with higher EM field.

References:

[1] S. A. Maier, Plasmonics: Fundamentals and Applications (Springer, Berlin, 2007).
[2] S. A. Maier and H. A. Atwater, J. Appl. Phys. 98, (2005) 011101.
[3] K.H.Su, Q.H.Wei, and X.Zhang, Appl. Phys. Lett. 88 (2006) 063118.
[4] T.Pakizeh, A.Dimitriev, M.S.Abrishamian, N.Granpayeh, and M.Häll, J. Opt. Soc. Am. B 25 (2008) 659.
[5] J. B. González-Díaz, A. García-Martín, J. M. García-Martín, A. Cebollada, G. Armelles, B. Sepúlveda, Y. Alaverdyan and M. Käll, Small 4 (2008) 202.
[6] G. A. Wurtz, W. Hendren, R. Pollard, R. Atkinson, L. Le Guyader, A. Kirilyuk, Th. Rasing, I. I. Smolyaninov and A. V. Zayats, New J. of Phys. 10 (2008) 105012.
[7] P.K.Jain, Y.Xiao, R.Walsworth, and A.E.Cohen, Nanolett. 9 (2009) 1644.
[8] G.X.Du, T.Mori, M.Suzuki, S.Saito, H.Fukuda, and M.Takahashi, Appl. Phys. Lett. 96 (2010) 081915.
[9] L.Wang, K.Yang, C.Clavero, A.J.Nelson, K.J.Karroll, E.E.Carpenter, and R.A. Lukaszew, J.Appl. Phys. 107 (2010) 09B303.
[10] G.X.Du, T. Mori, M.Suzuki, S.Saito, H.Fukuda, and M.Takahashi, J.Appl. Phys. 107 (2010) 09A928.
[11] G. Armelles, A. Cebollada, A. García-Martín, J. M. García-Martín, M. U. González, J. B. González-Díaz, E. Ferreiro-Vila and J. F. Torrado, J. Opt. A: Pure Appl. Opt. 11 (2009) 114023.

Figures:

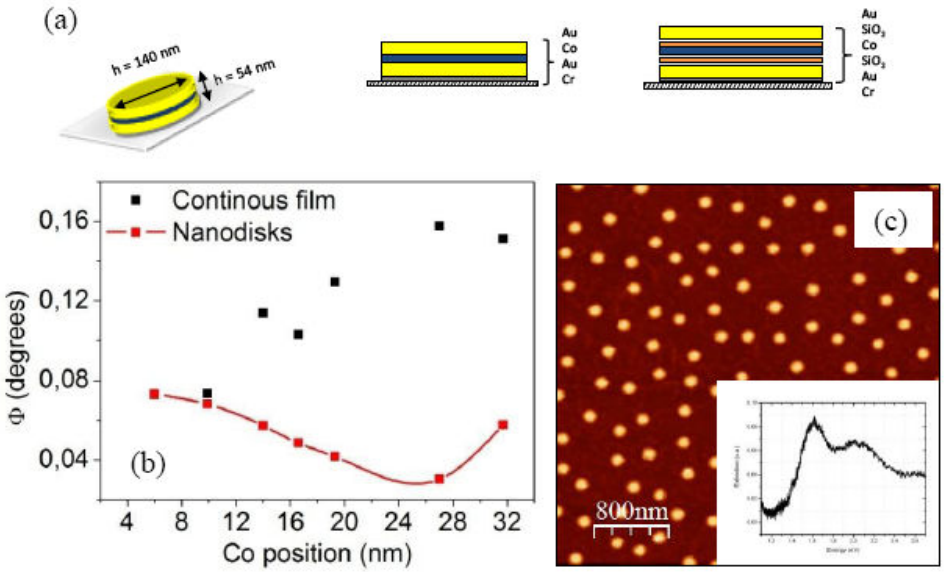

Figure 1: *(a) Sketch of the fully metallic and metal/dielectric nanodiscs (b) Maximum magneto-optical activity as a function of the Co position for fully metallic continuous films and nanodiscs (c) AFM image of an array of metal-dielectric nanodisc array (Inset: extinction spectrum showing two characteristic peaks).*

FERROMAGNETIC PLASMONIC NANOANTENNAS

J. Chen[1,2], P.Albella[1,2], Z. Pizadeh[3], P. Alonso-González[1], F. Huth[1], P. Vavassori[1,4], A. Dmitriev[3], J. Aizpurua[2] and R. Hillenbrand[1,4]

[1]CIC nanoGUNE Consolider, 20018 Donostia-San Sebastián, Spain
[2]Centro de Fisica de Materiales (CSIC-UPV/EHU) and Donostia International Physics Center (DIPC), 20018 Donostia-San Sebastián, Spain
[3]Department of Applied Physics, Chalmers University of Technology, 41296 Göteborg, Sweden
[4]IKERBASQUE, Basque Foundation for Science, 48011 Bilbao, Spain

Optical antennas are devices designed to efficiently convert optical radiation into localized energy and vice versa [1]. Currently, there is great interest in the development of magnetic optical nanoantennas that combine optical nanofocusing properties with magnetic functionality. Such antennas would be interesting for bioseparation, drug targeting and cell isolation [2]. However, plasmons in ferromagnetic materials are typically strongly damped. A common strategy to overcome this problem is to develop hybrid structures consisting of noble metals and ferromagnetic materials [3]. Plasmon properties of pure ferromagnetic nanostructures are a widely unexplored terrain, although pure ferromagnetic structures offer the advantage of stronger magnetic polarization and less demanding fabrication.

Here we report an experimental and theoretical study of the optical properties of ferromagnetic nanostructures fabricated purely of nickel. By farfield extinction spectroscopy (Fig. 1a) we provide direct experimental evidence of particle Plasmon resonances in nickel disks and ellipsoids. In order to identify the mode associated with the resonance peak, we imaged amplitude (Fig. 1b) and phase (Fig. 1c) of the vertical near-field component using a scattering-type scanning near-field optical microsocpe (s-SNOM) operating at 633 nm wavelength. In the amplitude image we observe two bright spots aligned along the polarization direction, which are oscillating out of phase for 180°. Such a near-field pattern provides direct experimental evidence of a dipole mode, which has been observed earlier for plasmon-resonant gold disks [4,5]. We emphasize that we also clearly observe the transverse plasmon mode in the elliptical antenna.

Performing numerical calculations, we find significant differences between far- and near-field spectra of plasmonic nickel antennas, which are indicated experimentally by comparing single wavelength near-field images and far-field spectra. We find that the near-field resonance is dramatically red shifted compared to the far-field resonance. This is a fundamental behavior already reported earlier for gold nanoantennas [6], but which is not fully understood yet. We will discuss these shifts theoretically. We also discuss a simple harmonic oscillator model revealing that a major contribution to the shift between near- and far-field resonances is a consequence of the Plasmon damping.

References:

[1] Muhlschlegel, P.; Eisler, H. J.; Martin, O. J. F.; Hecht, B.; Pohl, D. W. Science 2005, 308, (5728), 1607-1609.
[2] Insin, N.; Tracy, J. B.; Lee, H.; Zimmer, J. P.; Westervelt, R. M.; Bawendi, M. G. ACS Nano 2008, 2, (2), 197-202.
[3] Levin, C. S.; Hofmann, C.; Ali, T. A.; Kelly, A. T.; Morosan, E.; Nordlander, P.; Whitmire, K. H.; Halas, N. J. ACS Nano 2009, 3, (6), 1379-1388.
[4] Hillenbrand, R.; Keilmann, F.; Hanarp, P.; Sutherland, D. S.; Aizpurua, J. Appl. Phys. Lett. 2003, 83, (2), 368-370.
[5] Esteban, R.; Vogelgesang, R.; Dorfmuller, J.; Dmitriev, A.; Rockstuhl, C.; Etrich, C.; Kern, K. Nano Lett. 2008, 8, (10), 3155-3159.
[6] Bryant, G. W.; De Abajo, F. J. G.; Aizpurua, J. Nano Lett. 2008, 8, (2), 631-636.

Figures:

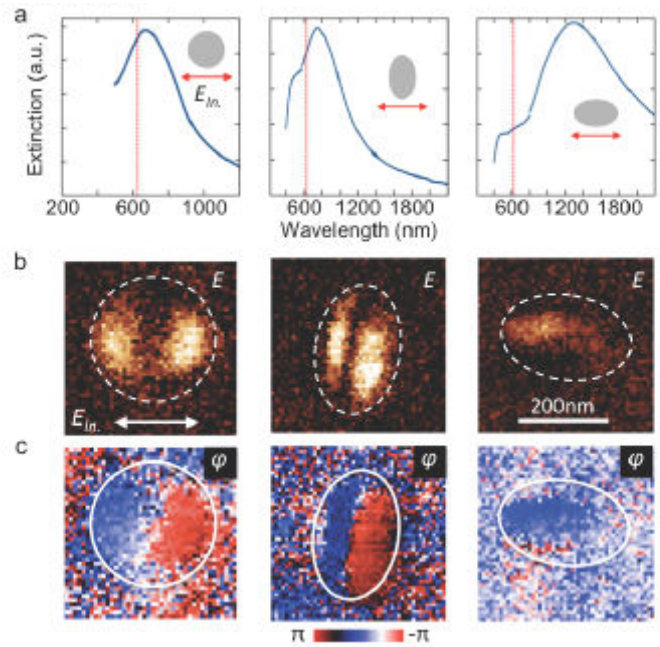

Figure 1: *Plasmonic nickel nanoantennas. (a) Extinction spectra of circular and elliptical nickel antennae. The red line in the spectra marks the wavelength λ=633 nm where near-field imaging was performed. The arrows indicate polarization of incident light. (b) Near-field optical amplitude images E. The arrow and bar denote the polarization of incident laser and scale of the images. (same for all three particles) (c) Near-field optical phase images φ.*

MAGNETO-OPTICAL STUDY OF MAGNETIC MICROWIRES: DOMAIN STRUCTURE, DOMAIN WALLS MOTION, MAGNETIZATION REVERSAL

Alexander Chizhik[1], Arcady Zhukov[1], Julián González[1], Juan Mari Blanco[2]

[1]Dpto. Física de Materiales, Fac. de Química, Universidad del País Vasco, San Sebastian, Spain
[2]Dpto. Física Aplicada I, EUPDS, UPV/EHU, 20018 San Sebastián, Spain
oleksandr.chyzhyk@ehu.es

The investigation of the magnetization reversal process, domain structure and domain walls motion in magnetic microwires is one of the most important tasks related to the use of magnetic wires in different technological devices. In particular, intensive studies of magnetic properties of glass coated microwires have been performed to enhance the giant magnetoimpedance (GMI) effect used in magnetic sensing technology.

The present abstract is devoted to the recent results on magneto-optical Kerr effect (MOKE) study of the surface magnetization reversal and surface domain structure in glass covered amorphous microwires.

The full cycle of the magnetization reversal between two circularly magnetized mono-domain states has been fixed using MOKE microscope in longitudinal configuration. The process of circular domains nucleation and propagation strongly depends on the dc external axial magnetic field. The comparative analysis of the magnetometry and optical microscopy results shows that the magnetization reversal consists mainly of the nucleation of circular domains and transformation to multi-domain structure when the dc axial field is relatively small. It was found also that the dc axial field suppresses the nucleation process putting in the forefront the propagation of circular domain walls.

Also the surface domain wall (DW) motion has been studied using the MOKE modified Sixtus-Tonks method when two reflections of the broken laser beam from the microwire surface were used instead of the pickup coils [1].

The surface circular DW motion was induced by the pulsed circular magnetic field. The single domain wall motion along the wire was registered as two successive jumps of the MOKE signal. This motion is associated with the circular magnetic bistability related to the giant Barkhausen jump of circular magnetization. During the experiments our attention was focused of the influence of the dc axial magnetic field on the surface circular DW motion.

It was found the influence of the axial magnetic field on the shape of the MOKE jump. Depending on the value of the axial field there are three stage of the jump transformation. At the first stage, the time duration of the jump decreases with axial field increase. At the second stage, the specific transformation of the shape of the jump was observed. We consider that this transformation is related to the transformation of the form of the DW. Finally, the absolute value of the MOKE jump decreases following by the total disappearance of the MOKE signal. This disappearance is reasonable because the dc axial filed of the relatively high value directs the magnetization along the axial direction of the microwire eliminating the transversal projection of the surface magnetization.

Based on the series of the time dependences of the MOKE jumps related to the surface DW motion along the wire, the dependence of the DW velocity on the dc axial field has been plotted (Fig. 1). The results have been obtained for the pulsed circular field of the value of 0.2 Oe.

This dependence has been analyzed jointly with the dc axial field induced transformation of the MOKE jumps. The general growth of the velocity with dc axial field is observed. Nevertheless, three specific parts of the dependence could be marked out. There are two pars with clearly defined increase of the velocity – in the beginning and in the end of the of the curve. Also the local decrease of the velocity value exists in the middle part of the field dependence.

We consider that the first part of the field dependence is related to the DW transformation form inclined one to DW perpendicular to the wire axis, that confirmed by the MOKE signal transformation. When the dc axial field is high enough the magnetization inside the transformed DW is directed

probably more along the axial direction that decelerates the motion of DW between two circular domains. The successive DW acceleration observed in the final part of the curve is clearly related to the field induced decrease of the angle of the turn of the magnetization in the DW. Finally, DW collapses when this angle is reduced to zero.

In frame of the task of the miniaturization of active elements of magnetic sensors the investigation of the magnetization reversal has been performed in nano-scale amorphous microwires for the first time. The arrays of glass covered microwires (nominal composition (Fe97Co3)75B15Si10, diameter of metallic nucleus 1000 nm) have been studied by magnetic and magneto-optical techniques. The results of PPMS magnetic (4 microwires array) and longitudinal magneto-optic Kerr effect (10 microwires array) experiments are presented in the Figs. 2(a) and 2(b). The clear jumps of magnetization could be observed in volume and surface hysteresis loops. These jumps are related to the giant Barkhausen jumps associated with the magnetization reversal in single microwire as a consequence of the interaction between the microwires. Based on the obtained results we can conclude that the magnetic behaviour of the glass covered microwires with such extremely tiny diameter keeps magnetically bistable and could be considered in the frame of core-shell model.

References:

[1] A. Chizhik, R. Varga, A. Zhukov, J. Gonzalez, and J. M. Blanco, J. Appl. Phys. 103, 07E707 (2008).

Figures:

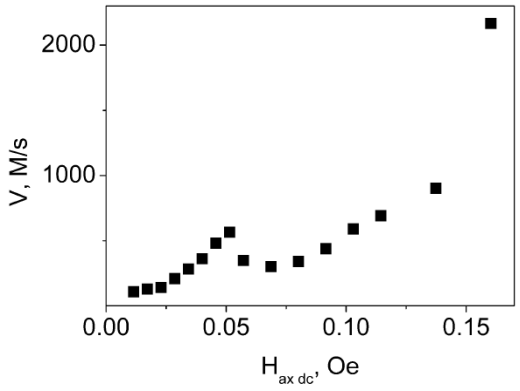

Figure 1: *Dependence of the velocity of the circular surface domain wall on dc axial magnetic field. The value of the pulsed circular magnetic field is 0.2 Oe.*

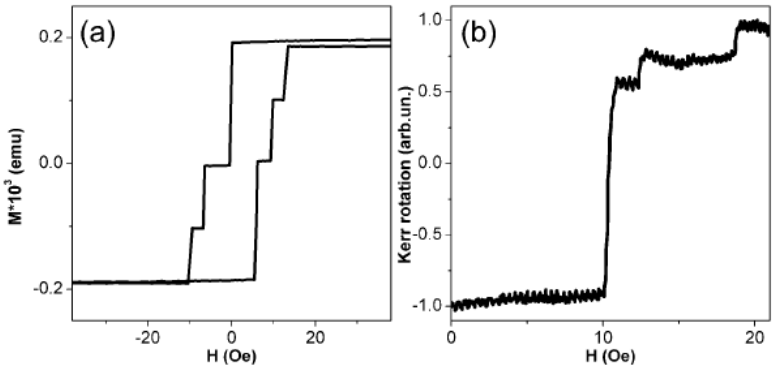

Figure 2: *Magnetization reversal curves obtained by magnetic (a) and magneto-optic (b) techniques.*

NANOGAP RING ANTENNAE AS PLASMON COUPLED, DICHROIC SERRS SUBSTRATES FOR BIOSENSING

Dr. Alasdair William Clark, Prof. Jonathan M. Cooper

University of Glasgow, Biomedical Engineering, Rankine Building, Oakfield Avenue, Glasgow, UK
alasdair.clark@glasgow.ac.uk

We explore the use of engineered nano-gap plasmonic ring systems in biosensing. By employing cutting edge nanofabrication methods we seek to exploit the extraordinary optical properties of metallic nanostructures in a range of novel ways targeted toward extremely sensitive molecular detection.

Surface enhanced (resonance) Raman spectroscopy (SE(R)RS) is a powerful sensing tool which relies on molecular interaction with the fluctuating plasmon field of a resonating nanoparticle. Using this method it has been shown that SERRS can rival the sensitivity of fluorescence techniques, enabling single molecule detection and characterisation.[1] As nanoengineering techniques have become more advanced in recent years there has been a move toward fabricating ever more complex nanoparticle geometries, with the aim of creating functional, tunable sensing substrates with a uniform distribution of intense localised plasmon fields.

In this work, we explore the use of nano metallic split-ring antenna as powerful, multifunctional biosensors with dichroic optical properties. Fabrication via electron-beam lithography allows for the strict control over structural geometry that is necessary to accurately tune the ring's multiple, polarisation dependant plasmon resonances to particular wavelengths.[2] In doing so, we demonstrate that we can tune their optical response such that they exhibit two independently addressable high frequency plasmon resonance modes, each tuned to the absorption wavelength of a differently coloured Raman reporter molecule and its corresponding laser excitation wavelength (Figure 1).[3, 4] This allows the single geometry ring structures to act as tailored SERRS sensors for low concentration DNA analyses at two distinct wavelengths.[4]

We go on to report on the fabrication, optical characterisation and application of a new generation of ultra-small multiple-split nanoring antenna.[5, 6] Using electron-beam lithography, splits of ca. 6 nm are engineered into silver nanophotonic ring structures to create concentrated areas of localised field coupling, which can be exploited for enhanced plasmonic applications. We compare the plasmonic properties of three devices, containing 3, 4 and 5 splits respectively, which have been spectrally tuned to 532 nm. Using finite element analysis, we explore the distinct plasmonic characteristics of each structure, and describe how variations in surface charge distribution effect inter-segmental coupling at different polarisation angles (Figure 2). The impact these changes have on the sensory functionality of each device was determined by a competitive DNA hybridisation assay measured using surface enhanced resonance Raman spectroscopy. The geometry of these novel, circular, multiple-split rings leads to unique plasmon hybridization between the numerous segments of a single structure; a phenomena we demonstrate is applicable to extreme Raman sensitivity, and may also find use in metamaterial applications.

References:

[1] S. M. Nie, S. R. Emery, Science, *275*, (1997) 1102.
[2] A. W. Clark, A. K. Sheridan, A. Glidle, D. R. S. Cumming, J. M. Cooper, Applied Physics Letters, 91 (2007) 093109.
[3] A. W. Clark, A. Glidle, D. R. S. Cumming, J. M. Cooper, Applied Physics Letters 93 (2008) 023121.
[4] A. W. Clark, A. Glidle, D. R. S. Cumming, J. M. Cooper, Journal of the American Chemical Society, 131 (2009) 17615.
[5] A. W. Clark, J. M. Cooper, Small, 7 (2011) 119.
[6] A. W. Clark, J. M. Cooper, Advanced Materials, 22 (2010) 4025.

Figures:

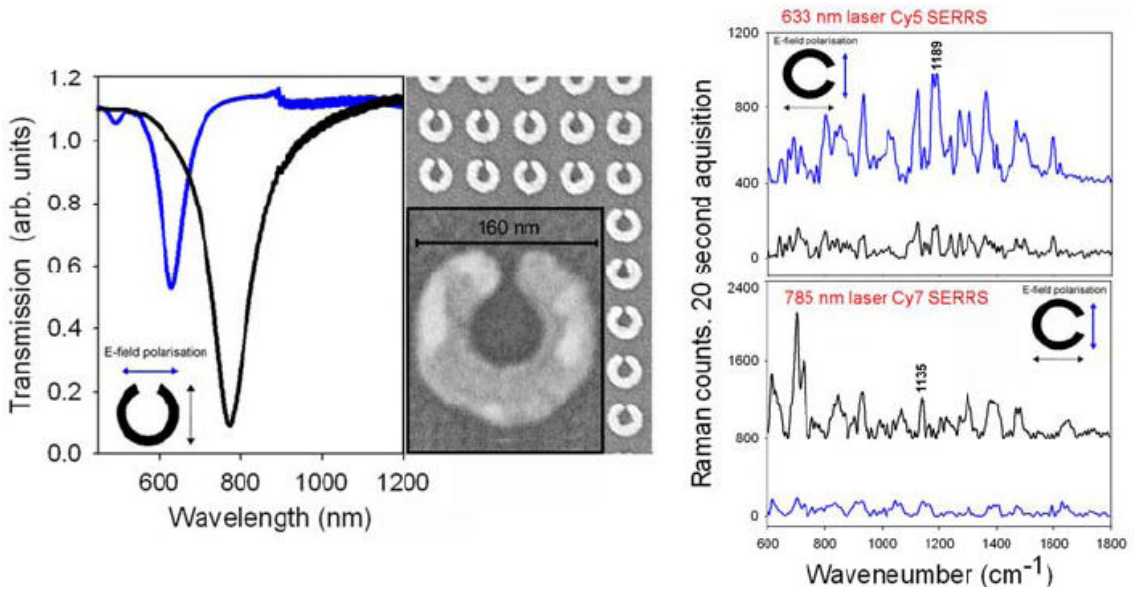

Figure 1: *Left – SEM and transmission spectra of an 80 nm radius Ag split-ring resonator sensor array with 2nd and 3rd order resonances tuned to 785 and 633 nm respectively. Right –SERRS from an identical array modified with a 1:1 ratio of Cy5 and Cy7 labelled oligonucleotide sequences hybridized to complimentary strands attached to the sensor surface. Measurements were performed at 633 and 785 nm and data was collected when the electric field vector of each laser was orientated both parallel and perpendicular to the split in the ring geometry.*

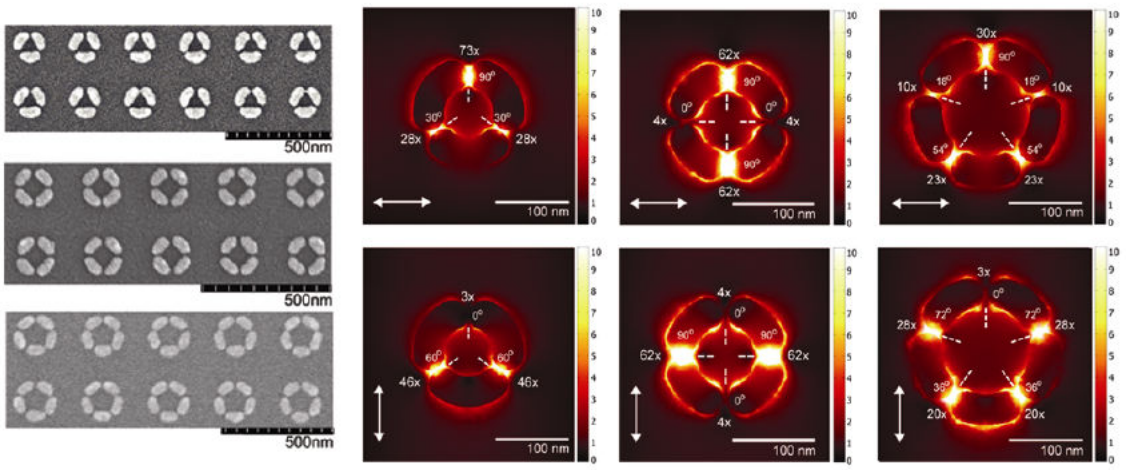

Figure 2: *Left – SEM of multiple-split nanoring antenna with average gap sizes of 6nm or less. Right – Finite element analysis of the plasmonic field distribution around each structure at resonance.*

COUPLING BETWEEN LOCALIZED SURFACE PLASMON RESONANCE AND MAGNETIC PROPERTIES OF NANOPARTICLES, THE EFFECT IN THE REVERSAL PROCESS

C. de Julián Fernández[1], L. Bogani[1,2], L. Cavigli[3], R. Novak[1,4], F. Pineider[1,5], C. Sangregorio[1,6], G. Campo[1], G. Mattei[7], M. Gurioli[3], R. Sessoli[1], A. Caneschi[1] , P. Mazzoldi[7] and D. Gatteschi[1]

[1]INSTM- Università di Firenze, via della Lastruccia 3, 50019 Sesto Fiorentino, Italy; [2] Physikalisches Institut, Universität Stuttgart, Pfaffenwaldring 57, 70550, Stuttgart, Germany; [3]LENS – Università di Firenze, via G. Sansone 1, 50019 Sesto Fiorentino, Italy; [4]LPMC-CNRS, Route de Saclay, 91128 Palaiseau,France; [5]CNR- ISTM, Via Marzolo 1, 35131 Padova, Italy; [6]CNR-ISTM, Via C. Golgi 19, 20133 Milano, Italy,[7]Dipartimento di Fisica –Università di Padova, via Marzolo 8, 35125 Padova, Italy
cesar.dejulian@unifi.it

Magneto-optical (MO) techniques are well-established procedures to characterize the dynamics and reversal process of nanostructured materials and surfaces. At the same time MO properties include information on the band structure because MO effects are produced by the spin-orbit coupling. This interaction is largely modified in nanomaterials due to quantum confinement effects, changes in the electronic structure and surface contribution. Electronic plasmon excitations, typical of metal nanostructures, can also affect the MO response and the magnetic dynamics. Moreover the interaction between femtosecond light and magnetic materials can produce changes in the dynamic of the reversal process. As a consequence MO studies are emerging as fundamental methods to investigate the correlations between the magnetic, optical and electronic properties of nano-sized materials with an important role for understanding the possibility of manipulation of the magnetic information with light.

In our presentation we illustrate our research activity on the study on the interactions of the light with magnetic nanomaterials using magneto-optical techniques. We use a home-made magneto-optical set-up built around an optical cryostat with superconducting coils. This allows to measure the magneto-optical signal in the temperature range of 1.5 K to 300 K and with magnetic field of ± 5 T. We record the magnetic Circular Dichroism using beams with discrete wavelengths covering the 400 nm to 1000 nm range. We investigated the wavelength dependence of the MO hysteresis loops and the dynamics of of two families of alloy based nanoparticles: Co-Ni alloy nanoparticles prepared by sol-gel route [1] and Fe-Au nanoparticles prepared by ion implantation [2].

Co-Ni nanoparticles with different compositions have been investigated and in general they exhibit MO hysteresis loops larger of the magnetometric one (Figure 1) and mainly the coercive fields are wavelength dependent. The largest effect is observed in nanoparticles with composition Co33Ni66 in which the coercive field decreases from 0.25 T at 904 nm to 0.17 T at 400 nm being the magnetometric value 0.12 T. MO dynamic measurements confirm that near the UV, where Plasmon resonance can be excited in the metallic CoNi nanoparticles, the reversal dynamics is accelerated. Temperature dependence of the MO coercive field experiments exclude that the effect be related to the selectivity of the radiation at different ensemble of nanoparticles. In the case of Au-Fe nanoparticles with composition Au:Fe near SPR appears strongly dumped in the Vis-nIR spectral region due to the electronic hybridization of Au and Fe [3]. In fact pure Fe and AuFe nanoparticles present similar MO lineshape and extinction spectra due to the similarity electronic structure. However experiments made by recording the MO hysteresis loops with light at 632.8nm and simultaneously pumping with the Ar-laser line of 514 nm show one decreasing of the coercive field as function of the pumping power[4].

In both cases we observe changes in the reversal process due to the excitation of localized surface Plasmon excitation in the magnetic nanoparticles. The possible mechanisms and the correlation with the magnetic properties of the nanoparticles are discussed.

It unlocks the possibility of observing spin-plasmonic effects in the visible region, and thus opens a new area of fundamental research and interesting applicative possibilities in all fields requiring the mixing of spin and electronic properties, like magneto-optics, spintronics and spin-plasmonics.

References:

[1] C. de Julián Fernández *et al.* Inorganica Chimica Acta 361 (2008) 4138.
[2] G. Mattei et al. Nucl. Instr. and Meth. B. 250 (2006) 225
[3] C de Julián Fernández *et al* Nanotechnology 21 (2010) 165701
[4] L. Bogani *et al.* Advanced Materials 22 (2010) 4054

Figures:

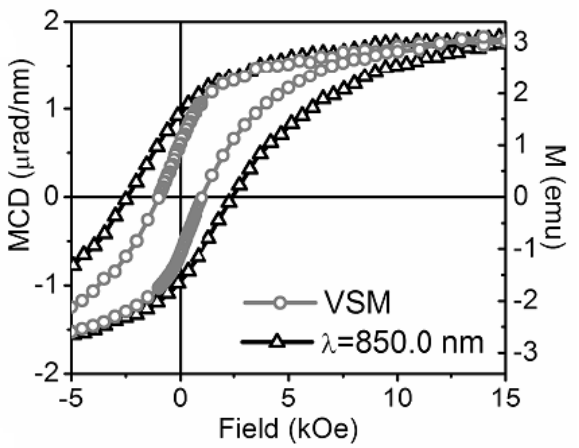

Figure 1: *Hysteresis loops recorded by magnetometric (VSM) and MO measurements at 1.5 K.*

SIGNATURE OF THE ANISOTROPY OF TWO-PHOTON EXCITED LUMINESCENCE OF NEARLY SPHERICAL GOLD PARTICLES DIFFUSING IN SOLUTION

L Anne Débarre[1], Matthieu Loumaigne[1], Priya Vasanthakumar[1,2]

[1]Laboratoire Aimé Cotton, CNRS, University Paris-Sud, Bâtiment 505, Campus d'Orsay, F-91405 Orsay cedex, France.
[2]Nanolab, Department of Physics "Enrico Fermi", University of Pisa, Largo Bruno Pontecorvo, 3, I-56127 Pisa, Italy
anne.debarre@u-psud.fr

Here, we report on the properties of the two-photon excited luminescence of gold nanobeads dispersed in solution.

Nanometallic objects derive their optical properties from an ability to support collective electronic excitations, known as surface plasmons. In the case of gold, a further interest of the particles is their biocompatibility and their ability to be suitable platforms for biophotonics. A lot of studies have been recently devoted to functionalise gold particles to create sensitive hybrid probes for molecular recognition and biosensing. The corresponding approach generally takes advantage of the modulation of the fluorescence properties of a chromophore in close vicinity to the gold core. The emission properties, enhancement or quenching, depend on the photophysical properties of the linked molecules, on the plasmon resonances of the core and on their interaction [1, 2]. The potential of such hybrid probes relies on the tuning the plasmon resonances by shaping the gold core.

Apart from fluorescent functionalisation with linked chromophores, a growing field of research is dedicated to targeted imaging with gold particles as contrast agents because of reduced photoxicity and versatility of excitation, in particular. The optical process involved in imaging is the emission of luminescence, following either one or two photons absorption. Excitation in the near-infrared domain is the rule under two-photon excitation [3] but it can be used even with one photon excitation in the case of nanorods for example. It combines the advantages of being less toxic for the samples and of deeper penetration into the tissues. Another interesting application is the thermal effect related to absorption when the excitation wavelength is close to their plasmon resonance peaks. The latter has been demonstrated to be of interest for therapeutic purposes [4].

The initial aim of our studies was to determine if the two-photon excited luminescence process could be efficient enough to track small spherical gold nanobeads diffusing in aqueous solutions. It implied to work at the single particle level. In fact, luminescence of gold nanoparticles has been mainly studied on deposited samples, eventually at the single particle level but very few experiments have been performed on liquid samples, generally with a rather high concentration of particles.

To understand the optical behavior of gold nanobeads, we have used Fluorescence Correlation Spectroscopy (FCS) implemented on a two-photon microscope comprising imaging capabilities. As is displayed on the Figure 1, the cross-correlation profile of the two-photon excited luminescence of golds beads of 20 nm diameter presents an unexpected component in the microsecond temporal range. This contribution has been attributed to the signature of the Brownian rotation of the beads, using an original dual method correlating luminescence and Rayleigh scattering signals [5]. We will report on a multiparameter analysis of the two-photon excited luminescence of gold nanobeads, which reveals the role played by the ligands capping the particles in the anisotropy of the emission. The latter is closely related to the temperature increase at the water-ligands interface following absorption. The effects of the polarization and of the excitation wavelength will be discussed.

References:

[1] Dulkeith E., Morteani A. C., Niedereichholz T., Klar T. A., Feldmann J., Levi S. A., Van Veggel F. C. J. M., Reinhoudt D. N., Möller M. and Gittins D. I., Phys. Rev. Lett., 89 (2002) 203002.
[2] Loumaigne M., Praho R., Nutarelli D., Werts M. H. V. and Débarre A., PCCP, 12 (2010) 11004.
[3] Wang H., Huff T. B., Zweifel D. A., He W., Low P. S., Wei A. and Cheng J.-X., PNAS, 102 (2005) 15752.
[4] Huang X., El-Sayed I. H., Qian W. and El-Sayed M. A., JACS, 128 (2006) 2115.
[5] Loumaigne M., Richard A., Laverdant J., Nutarelli D. and Débarre A., Nano Lett., 10 (2010) 2817.

Figures:

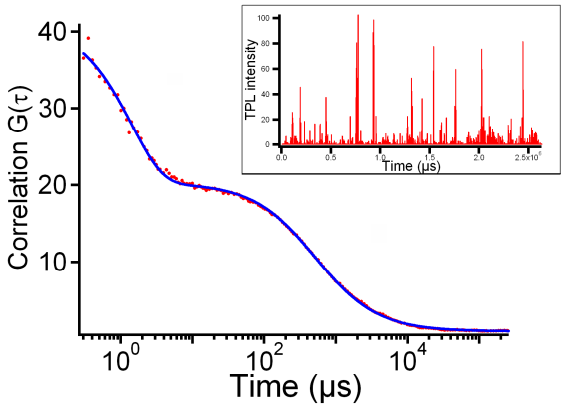

Figure 1: *Cross-correlation profile of two-photon excited luminescence of gold beads of 20 nm diameter; excitation wavelength 815nm; power 6mW; In inset, histogram of bursts.*

MERGING ELECTRONICS AND PHOTONICS USING METAMATERIALS

Nader Engheta

University of Pennsylvania, Department of Electrical and Systems Engineering, Philadelphia, PA, USA
Engheta@ee.upenn.edu

In my group, we have been developing the concept of "metatronics", i.e. metamaterial-inspired optical nanocircuitry, in which the three fields of "electronics", "photonics" and "magnetics" can be brought together seamlessly under one umbrella – the "Unified Paradigm of Metatronics". In this optical circuitry, the nanostructures with specific values of permittivity and permeability may act as the lumped circuit elements such as nanocapacitors, nanoinductors and nanoresistors. Nonlinearity in metatronics can also provide us with novel nonlinear lumped elements. We have investigated the concept of metatronics through extensive analytical and numerical studies, computer simulations, and in a set of experiments at the IR wavelengths. We have shown that nanorods made of low-stressed Si_3N_4 with properly designed cross sectional dimensions indeed function as lumped circuit elements at the IR wavelengths between 8 to 14 microns. We have been exploring how metamaterials can be exploited to control the flow of photons, analogous to what semiconductors do for electrons, providing the possibility of one-way flow of photons. We are now extending the concept of metatronics to other platforms such as graphene, which is a single atomically thin layer of carbon atoms, with unusual conductivity functions. We study the graphene as a new paradigm for metatronic circuitry and also as a "flatland" platform for IR metamaterials and transformation optics, leading to the concepts of one-atom-thick metamaterials, and one-atom-thick circuit elements and optical devices. I will give an overview of our most recent results in these fields. For more information, please see the references given below.

References:

[1] N. Engheta, Physics World, 23 (2010), 31.
[2] N. Engheta, Science, 317 (2007), 1698.
[3] N. Engheta, A. Salandrino, A. Alu, Phys. Rev. Lett. 95 (2005), 095504.
[4] A. Alu, N. Engheta, Nature Photonics, 2, (2008) 307.
[5] M. G. Silveirinha, A. Alu, J. Li, N. Engheta, J. Appl. Physics, 103, (2008) 064305.
[6] A. Alu, N. Engheta, Phys. Rev. Lett., 103, (2009) 143902.
[7] A. Alu, M. E. Young, and N. Engheta, Phys. Rev. B, 77, (2008) 144107.
[8] A. Alu and N. Engheta, Phys. Rev. Lett., 101, (2008) 043901.
[9] A. Vakil and N. Engheta, http://arxiv.org/abs/1101.3585

NANOSTRUCTURED SILICON SURFACES BY SELF-ASSEMBLED NANOPOROUS ANODIC ALUMINA FOR PHOTONIC APPLICATIONS

Josep Ferré-Borrul, Mohammad Mahbubur Rahman, Abel Santos, Pilar Formentín, Josep Pallarès, Lluis F. Marsal

Universitat Rovira I Virgili, Nano-electronic and Photonic Systems, NePhoS Av. Paisos Catalans 26, ETSE-DEEEA, 43007, Tarragona, Spain
josep.ferre@urv.cat

Nanoporous anodic alumina (NPAA) [1] has become a very interesting material in nanotechnology because of its cost-effective production and its geometrical properties that can be tuned in a wide range. The main application of NPAA is in templating to achieve different nanostructures with different functionalities: [2-4]. Furthermore, the structure of nanoporous anodic alumina is a two-dimensional self-assembled structure with a triangular arrangement of the pores. If no pre-patterning techniques are used, the triangular pore arrangement is broken into domains, giving rise to a quasi-random structure. By adequately tuning the fabrication conditions, the size of the domains can be increased. Such triangular pattern reminds that of a triangular Photonic Crystal [5], although it lacks the perfect periodicity. However, it can be demonstrated [6] that the NPAA pattern can show photonic stop bands in the same way it happens with photonic quasicrystals [7] or even in random structures [8].

Silicon is a good candidate to obtain two-dimensional photonic crystals [9] for different applications, mainly because its compatibility with the wide-spread silicon technology. In order to obtain such photonic crystals, a lithography-based pre-patterning technique and further wet- or dry-etching techniques are required. This makes the cost relatively high, especially if the lattice constants have to be reduced to a few hundreds of nanometers. However, some applications may only need to benefit from the existence of a stop band, and thus, in this case, the NPAA pattern could be adequate.

In this work we focus on the transfer of the NPAA pattern to the silicon surface for further electrochemical etching. Such nanostructured silicon substrate will enable a great variety of applications that take benefit from the existence of a photonic band gap onto a conductive substrate that provides electrical contact: efficient light emitters (both diode or lasers), solar cells with more efficient light harvesting, sensors with enhanced sensitivity. With this aim, the process parameters concerning aluminum deposition, etching conditions and processing steps are optimized. We present results on fabrication and characterization of the structures fabricated. One of the main issues is the optical characterization of the resulting Si nanostructure by angular-dependent reflectance spectroscopy and polarimetry [10,11]. Such measurements require a good surface finish between the pores on the silicon. Consequently the process will be optimized to obtain such a surface quality.

The figures show some of the achievements up to date. Figure 1 shows the current transients and the SEM pictures of the surface and of the cross-section of a NPAA layer grown onto p-Si by a two-step electrochemical etching process with a 0.3 M oxalic acid electrolyte and under potentiostatic conditions with an applied voltage of 40 V. Figure 1a shows the current-time curve for the first and the second steps of the anodization processes, Figure 1b shows an ESEM picture of the sample surface and finally, Figure 1c shows the cross section of the sample, showing the alumina and the silicon regions. Figure 2 shows the same information but for a sample obtained with a 0.3 M phosphoric acid electrolyte and an applied voltage of 160 V.

Acknowledgments

This work was supported by the Spanish Ministry of Science and Innovation (MICINN) under grant number TEC2009-09551, CONSOLIDER HOPE project CSD2007-00007, AECID project A/024560/09 and by the Catalan Authority under project 2009SGR549.

References:

[1] W. Lee, R. Ji, U. Gosele, K. Nielsch, Nature Materials, Vol. 5 (2006) 741.
[2] A. Santos, L. Vojkuvka, J. Pallares, J. Ferre-Borrull, L.F. Marsal, Nanoscale Research Letters, Vol. 4 (2009) 1021.
[3] b A. Santos, P. Formentin, J. Pallares, J. Ferre-Borrull, L.F. Marsal, Materials Letters, Vol. 64 (2010) 371.
[4] b A. Santos, P. Formentin, J. Pallares, J. Ferre-Borrull, L.F. Marsal, Solar Energy Materials & Solar Cells, Vol. 94 (2010) 1247.
[5] J. D. Joannopoulos, S. G. Johnson, J. N. Winn, R. D. Meade: Photonic Crystals: Molding the Flow of Light, Princeton Univ. Press, Princeton, New Jersey (2008).
[6] M. M. Rahman, J. Ferré-Borrull, J. Pallarès, L. F. Marsal, Physica Status Solidi-c, In Press (2011).
[7] M. E. Zoorob, M.D.B. Charlton, G:J. Parker, J.J Baumberg, M.C Netti, Nature, Vol. 404 (2000) 740.
[8] D. S. Wiersma, A. Lagendijk, Physical Review E, Vol. 54 (1996) 4256.
[9] T. Trifonov, M. Garin, A. Rodriguez, L. F. Marsal, R. Alcubilla, Physica Status Solidi-a, Vol. 204 (2007) 3237.
[10] Z. Kral, L. Vojkuvka, E. Garcia-Caurel, J. Ferre-Borrull, L. F. Marsal, J. Pallares, Photonics and Nanostructures – Fundamentals and Applications, Vol. 7 (2009) 12.
[11] Z. Kral, J. Ferre-Borrull, T. Trifonov, L. F. Marsal, A. Rodriguez, J. Pallares, R. Alcubilla, Thin Solid Films, Vol. 512 (2008) 8059.

Figures:

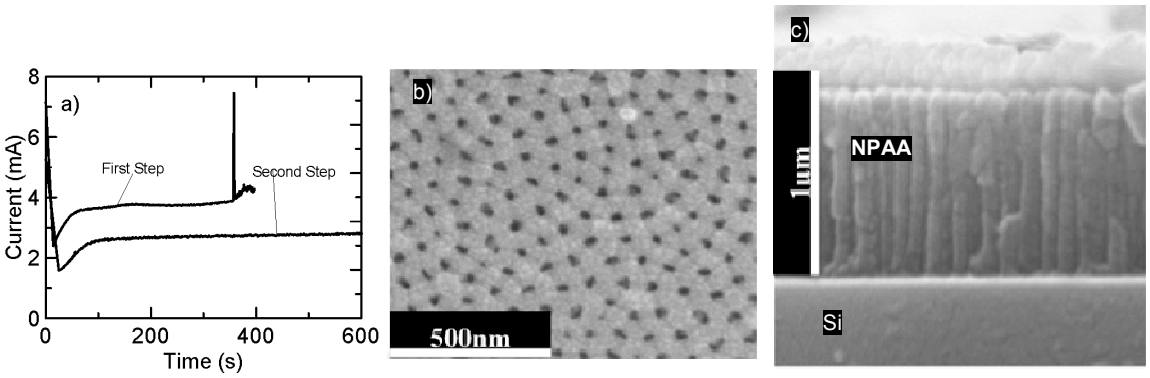

Figure 1: *NPAA template on Si obtained with an 0.3 M oxalic acid electrolyte, under potentiostatic conditions with an applied voltage of 40V. a) current-time curve for the first and the second anodization. b) ESEM picture of the sample surface. c) ESEM picture of the sample cross-section.*

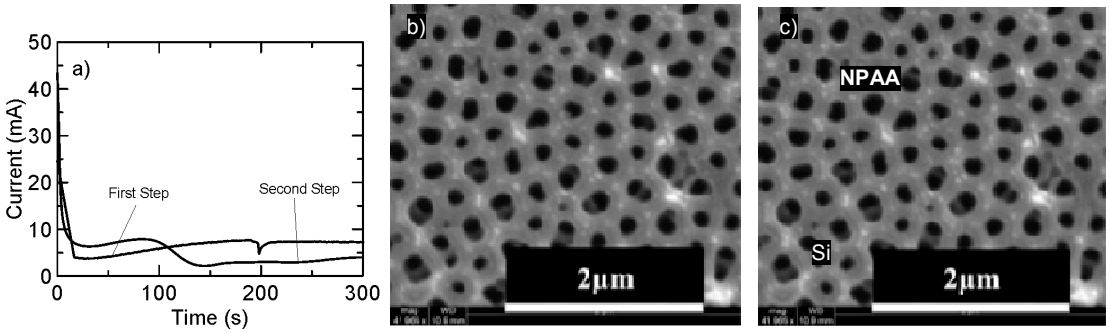

Figure 2: *NPAA template on Si obtained with an 0.3 M phosphoric acid electrolyte, under potentiostatic conditions with an applied voltage of 160V. a) current-time curve for the first and the second anodization. b) ESEM picture of the sample surface. c) ESEM picture of the sample cross-section.*

LIMITS OF LIGHT FOCUSING THROUGH TURBID MEDIA

Luis S. Froufe-Pérez, J. J. Sáenz

Condensed Matter Dept. Autonomous University of Madrid, Av. Tomás y Valiente 7,
Edificio Ciencias, 28049 Cantoblanco, Spain.
luis.froufe@uam.es

Wave emission and propagation in random media has been a matter of intense research during the last decades. Effects induced by coherent multiple scattering of waves explain to a large extent phenomena such as enhanced coherent backscattering, universal conductance fluctuations, strong Anderson localization of waves and random lasing, to cite a few. [1]

Contrary to what intuition may suggest, the introduction of scattering sources in a system can enhance the focusing ability of an optical system. A simple heuristic argument shows that scattering can efficiently open new propagating channels which are closed otherwise. As has been demonstrated in the microwave regime [2], the inclusion of scatters in the near field of a selected focusing point can even enable subwavelength focusing.

By using wavefront shaping techniques, it has been recently shown [3] in the optical range that, despite experimental limitations, it is possible to achieve the best theoretical focus as predicted by Cittert-Zernike theorem. Using a different approach, it has been shown that the full transmission matrix of a thick turbid medium can be measured both in amplitude and phase [4]. Hence, using an appropriate inversion algorithm, any intensity pattern can be transfered through the sample.

In this work, we theoretically analyze the focusing capabilities of a system with varying amounts of disorder. In particular we shall deal with scalar wave models in confined (guided) geometries.

In this kind of systems, several transport regimes appear depending on the ratio of the system length to the scattering mean free path and the propagating number of channels. For lengths small compared with the mean free path, transport is quasi-ballistic. Diffusive transport is dominant for lengths ranging from about a mean free path up to the so-called localization length. For larger lengths, the system undergoes a crossover to the deep localized regime where transport is exponentially inhibited.

It has been shown [5] that the averaged conductance of the system can account for many transport statistical properties in a universal manner, all the way from quasi-ballistic to deep localization regimes. On the other hand, conductance can be properly defined not only in electronic systems but on optical ones [6]. Being hence conductance a key parameter describing the optical transport properties of a disordered system.

By generating random scattering matrices corresponding to previously defined number of propagating channels, scattering mean free path and system length [7]. We are able to determine all the relevant optical transport parameter of the system. Also, through the use of different inversion algorithms, we can determine the set of appropriate incoming amplitudes for each channel in order to focus light at the other side of the system. In figure 1 we show an example of diffraction-limited focusing by using a Montecarlo algorithm through a system of one mean free path thickness.

It can be shown that, if incoming amplitudes can present an arbitrary dynamic range while keeping a sufficiently small signal-to-noise ratio, focusing is diffraction limited for any transport regime including localization. Nevertheless, the amount of transmitted power in strongly reduced as the scattering increases. It is worth stressing that the transmittance in the focusing mode is much smaller than the channel-averaged transmittance of the sample. Hence, one of the limitations we find is that the transmitted power can be negligible even prior to the onset of localization. As can be seen in figure 2.

On the other hand, if we consider a finite signal-to noise ratio for the incoming amplitudes, focusing ability deteriorates as scattering increases.

In conclusion, we show that, although some amounts of disorder provide an effective coupling to new propagating channels, hence increasing the effective numerical aperture of the optical system.

Focusing capabilities of the system and the effective power transmission are severely reduced if disorder is further increased.

Authors acknowledge fruitful and stimulating discussions with Prof. C. López, Dr. M. Leonetti and Prof. J. S. Dehesa. This work has been supported by the spanish MICINN Consolider Nanolight project (CSD2007-00046).

References:

[1] P. Sheng, Introduction to Wave Scattering, Localisation, and Mesoscopic Phenomena (Academic Press, New York, 1995).
[2] G. Lerosey, A. Tourin, and M. Fink, Science 315, (2007) 1120.
[3] M. Vellekoop, A. Lagendijk, and A. P. Mosk, Nature Photonics 4, (2010) 320.
[4] S. M. Popoff, G. Lerosey, R. Carminati, M. Fink, A. C. Boccara, and S. Gigan ,Phys. Rev. Lett. 104, (2010)100601.
[5] L. S. Froufe-Pérez, P. García-Mochales, P. A. Serena, P. A. Mello, and J. J. Saenz , Phys. Rev. Lett. 89, (2002) 246403.
[6] S. Albaladejo, M. Lester, L.S. Froufe-Pérez, A. Garcia Martín y J.J. Sáenz, App. Phys. Lett. 91, (2007) 061107.
[7] L. S. Froufe-Pérez, M. Yépez, P. A. Mello y J. J. Sáenz,Phys. Rev. E 75, (2007) 031113.

Figures:

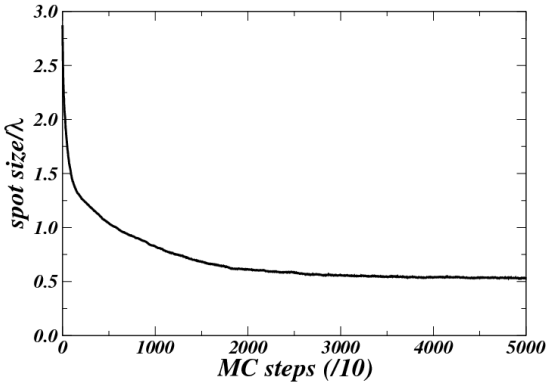

Figure 1: *Focusing through a disordered system of 1 mean free path thickness. a) Spot size as a function of the Montecarlo step. b) intensity map in the focusing plane for a random pattern of incoming field amplitudes. c) intensity map in the focusing plane after incoming amplitudes have been adapted for focusing through a Montecarlo procedure.*

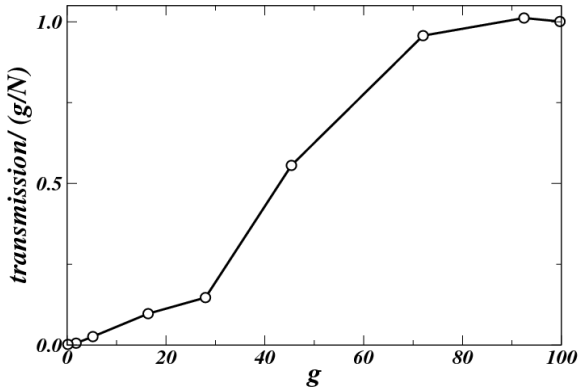

Figure 2: *Power transmission of the focused beam normalized to the average one-channel transmittance (conductance divided by the number of channels) as a function of the waveguide conductance.*

REAL TIME, MULTIPLEX AND LABEL-FREE BIO-INTERACTION ANALYSIS (BY SURFACE PLASMON RESONANCE IMAGING)

Chiraz Frydman

HORIBA Scientific, Chilly-Mazarin, France
chiraz.frydman@horiba.com

For the last two decades, the Surface Plasmon Resonance (SPR) technology is demonstrated as a powerful tool for the bio-molecular interactions investigations and analysis.

The SPR imaging technology is a ideal solution for rapid, label-free and multiplexed bio-assays and investigations. It's a high sensitive detection method for bio-molecular interactions, using a micro-array biochip format to rapidly monitor multiplex kinetic interactions in real time. This technology allows direct visualization of biomolecular interactions and is suitable for determination of real time physico-chemical interactions and kinetics. Thanks to SPRi, analytes can be detected in the range of the femto-mol.

Surface Plasmon Resonance (SPR) is an optical detection process that can occur when a polarized light hits a prism covered by a thin metal layer. Briefly, a broad monochromatic polarized light (at a specific wavelength) illuminates the whole functionalized area of the SPRi-Biochip™, which is combined with a detection chamber. A CCD video camera gives access to array format by image capture of all local changes at the surface of the SPRi-Biochip™.

SPR imaging has the capacity to record simultaneously the interaction of any ligand to every single spot on the golden surface of the reaction chamber without any label addition. The signals obtained are able to identify, by the spot position in the chip, which probes are recognized by the ligand but also, by analysing the on and off rates of ligand binding, the mean affinity (or avidity) of these ligand to probes can be calculated.

Main applications involve interactions between DNA-DNA, protein-DNA, protein-ligand, peptide-ligand, antibody-cell in the fields of health (aid to diagnosis and treatment), environmental control, new drug discovery and development in pharmaceutical and cosmetic research, quality-control in agro-food etc…

LIGHT PROPAGATION IN SELF-ASSEMBLED HYBRID METALLODIELECTRIC STRUCTURES

J. F. Galisteo-López[1], M. López-García[1], A. García-Martín[2], A. Blanco[1], C. López[1]

[1]Instituto de Ciencia de Materiales de Madrid (ICMM-CSIC), c/ Sor Juana Inés de la Cruz 3, 28049 Cantoblanco, Madrid, Spain
[2]Instituto de Microelectrónica de Madrid (IMM-CSIC), c/ Isaac Newton 8, 28049 Tres Cantos, Madrid, Spain
galisteo@icmm.csic.es

Self assembly is a well established approach to fabricate photonic structures able to manipulate light propagation and emission at the nanoscale [1]. Beyond its use as a means to fabricate photonic crystals or resonant disordered structures such as photonic glasses, recent reports have shown how self assembly techniques can be used to fabricate hybrid photonic-plasmonic crystals [2, 3] which optical properties allow for a strong modification of the spontaneous emission of internal sources [2]. Further, the sensitivity of their optical response to their environment has been proposed as a means to use this kind of systems of optical sensors [3], and means to control their optical properties by modifying the dielectric components have been demonstrated [4].

In these hybrid structures, where periodic arrays of dielectric colloids are deposited on metallic substrates, electromagnetic fields undergo a strong spatial redistribution and strong field enhancements can be achieved. Depending on the spectral range under consideration electromagnetic fields can be localized close to the metal substrate (plasmon-like modes) or within the dielectric array (waveguidedlike modes) (see Fig. 1a).

Several metallodielectric structures have been fabricated employing gold or silver substrates and their optical response has been compared to reference samples grown on dielectric substrates in order to better appreciate the effect of the metallic component. The dispersion relation of such structures has been probed by means of angle and polarization resolved reflectivity measurements (see Fig. 1b).

As in any photonic structure, losses degrade the optical response of these systems and hence its applicability; therefore knowledge is needed on how such losses can be minimized. In this work we explore the optical response of self-assembled plasmonic-photonic structures having different configurations and fabricated from different materials and explore how one can minimize intrinsic losses due to leakage and absorption. The effect of the optical constants of the metallic substrates has been explored. Further, the role of extrinsic losses originating at residual disorder generated during the growth process is discussed.

References:

[1] J. F. Galisteo-López, M. Ibisate, R. Sapienza, , L. S. Froufe-Pérez, A. Blanco and C. López, Advanced Matererials, 23 (2011) 30.
[2] M. López-García, J. F. Galisteo-López, A. Blanco, A. García-Martín and C. López, Small 6 (2010) 1757.
[3] X. Yu, L. Shi, D. Han, J. Zi and P.V. Braun, Advanced Functional Materials, 20 (2010) 1910.
[4] M. López-García, J. F. Galisteo-López, A. Blanco, A. Garcia-Martin and C. Lopez, Advanced Functional Materials, 20, (2010) 4338.

Figures:

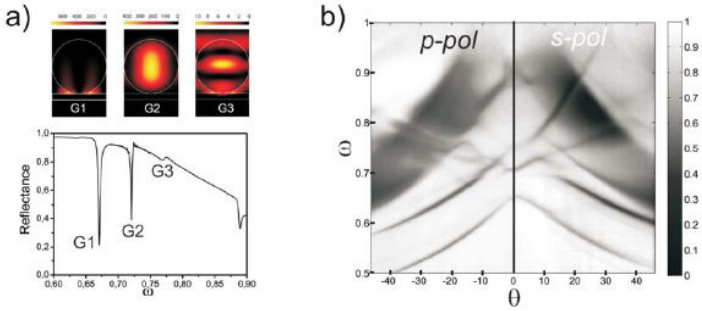

Figure 1: *a) Normal incidence reflection spectrum for a dielectric array of 520nm diameter polystyrene spheres deposited on a gold substrate (bottom) and total field intensity profiles of the modes highlighted (top). b) Angle and polarization resolved reflection for the same sample.*

THREE-DIMENSIONAL OPTICAL METAMATERIALS AND NANOANTENNAS: CHIRALITY, COUPLING, AND SENSING

Harald Giessen

4th Physics Institute, University of Stuttgart; D-70569 Stuttgart, Germany
giessen@physik.uni-stuttgart.de

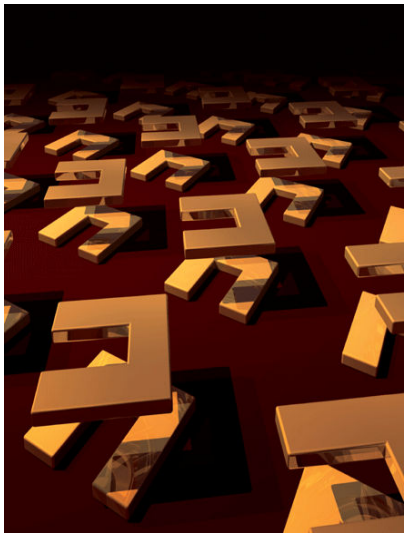

Metallic metamaterials have shown a number of fascinating properties over the last few years. A negative refractive index, negative refraction, superlenses, and optical cloaking are some of the ambitious applications where metamaterials hold great promise.

We are going to present fabrication methods for the manufacturing of 3D metamaterials [1]. We are investigating their coupling properties and the resulting optical spectra. Hybridization of the electric [2] as well as the magnetic [3] resonances allows us to easily understand the complex optical properties. Lateral as well as vertical coupling can result in Fano-resonances [4] and EIT-like phenomena [5, 6]. These phenomena allow to construct novel LSPR sensors with a figure of merit as high as five [7].

The connection between structural symmetry and their electric as well as magnetic dipole and higher-order multipole coupling will be elucidated. It turns out that stereometamaterials [8], where the spatial arrangement of the constituents is varied (see figure), reveal a highly complex rotational dispersion. The chiral properties are quite intriguing and can be explained by a coupled oscillator model.

Our three-dimensional stacking approach allows also for the fabrication of 3D nanoantennas, which are favorable for emitting and receiving radiation from quantum systems [9].

References:

[1] Na Liu, Hongcang Guo, Liwei Fu, Stefan Kaiser, Heinz Schweizer, and Harald Giessen: Three-dimensional photonic metamaterials at optical frequencies, Nature Materials 7, 31 (2008).
[2] N. Liu, H. Guo, L. Fu, S. Kaiser, H. Schweizer, and H. Giessen: Plasmon Hybridization in Stacked Cut-Wire Metamaterials, Advanced Materials 19, 3628 (2007)
[3] Na Liu, Liwei Fu, Stefan Kaiser, Heinz Schweizer, and Harald Giessen: Plasmonic Building Blocks for Magnetic Molecules in Three-Dimensional Optical Metamaterials, Advanced Materials 20, 3859 (2008).
[4] B. Lukyanchuk, N. I. Zheludev, S. A. Maier, N. J. Halas, P. Nordlander, H. Giessen, and C. T. Chong: The Fano resonance in plasmonic nanostructures and metamaterials, Nature Materials 9, 707 (2010).
[5] Na Liu, Stefan Kaiser, and Harald Giessen: Magnetoinductive and Electroinductive Coupling in Plasmonic Metamaterial Molecules, Advanced Materials 20, 4521 (2008).
[6] Na Liu, N. Liu, L. Langguth, T. Weiss, J. Kästel, M. Fleischhauer, T. Pfau, and H. Giessen: Plasmonic EIT analog at the Drude damping limit, Nature Materials 8, 758 (2009).
[7] Na Liu, T. Weiss, M. Mesch, L. Langguth, U. Eigenthaler, M. Hirschner, C. Sönnichsen, and H. Giessen: Planar metamaterial analog of electromagnetically induced transparency for plasmonic sensing, Nano Lett. 10, 1103 (2010).
[8] Na Liu, Hui Liu, Shining Zhu, and Harald Giessen: Stereometamaterials, Nature Photonics 3, 157 (2009).
[9] H. Giessen and M. Lippitz: Directing light emission from quantum dots, Science 329, 910 (2010).

INTERFERENCE BETWEEN ELECTRIC AND MAGNETIC DIPOLES IN DIELECRIC SPHERES: SCATTERING ANISOTROPY AND OPTICAL FORCES

V. R. Gómez-Medina[1,2], M. Nieto-Vesperinas[1], J. J. Sáenz[2]

[1]Instituto de Ciencia de Materiales de Madrid, Consejo Superior de Investigaciones Científicas (CSIC), Campus de Cantoblanco, Madrid 28049, Spain.
[2] Departamento Física de la Materia Condensada UAM, Madrid 28049, Spain
rgomezmedina@icmm.csic.es

Electromagnetic scattering from nanometer-scale objects has long been a topic of large interest and relevance to fields from astrophysics or meteorology to biophysics, medicine and material science [1-5]. In the last few years, small particles with resonant magnetic properties are being explored as constitutive elements of new metamaterials and devices. Magnetic effects, however, cannot be easily exploited in the visible or infrared regions due to intrinsic natural limitations of optical materials and the quest for magnetic plasmons and magnetic resonant structures at optical frequencies [6] has then been mainly focused on metallic structures. The unavoidable problems of losses and saturation effects inherent to these metamaterials in the optical and near infrared regimes have stimulated the study of high-permittivity particles as their constitutive elements [7-9]: For very large permittivities, small spherical particles present well defined sharp resonances [1]; either electric or magnetic resonant responses can then be tuned by choosing the appropriate sphere radius.

In the presence of both electric and magnetic properties, the scattering characteristics of a small object present markedly differences with respect to pure electric or magnetic responses. Even in the simplest case of small or of dipolar scatterers, remarkable scattering effects of magnetodielectric particles were theoretically established by Kerker et al. [10] concerning suppression or minimization of either forward or backward scattering. Intriguing applications in scattering cancellation and cloaking [11] and magneto-optical systems [12-14] together with the unusual properties of the optical forces on magnetodielectric particles [15-17] have renewed interest in the field.

The striking characteristics of the scattering diagram of small (Rayleigh) magnetodielectric particles [10,18] were obtained assuming arbitrary values of electric permittivity and magnetic permeability. Nevertheless, no concrete example of such particles that might present those interesting properties in the visible or infrared regions had been proposed.

Very recently, it has been shown [19] that submicron silicon spheres present dipolar magnetic and electric responses, characterized by their respective first-order Mie coefficient, in the near infrared, in such a way that either of them can be selected by choosing the illumination wavelength. We will show that Si spheres constitute such a previously quested real example of dipolar particle with either electric and/or magnetic response, of consequences both for their emitted intensity and behavior under electromagnetic forces [16,17]. These properties should not be restricted to Si particles but should also apply to other dielectric materials with relatively moderate refraction index. Furthermore, we will discuss the effects associated to the interference between electric and magnetic dipoles in germanium spheres [20]. As we will demonstrate the extinction cross section and the scattering diagrams of these submicron dielectric particles in the infrared region can be well described by dipolar electric and magnetic fields, being quadrupolar and higher order contributions negligible in this frequency range. Specifically, the scattering diagrams calculated at the generalized Kerker's conditions are shown to be equivalent to those previously reported [10,18] for hypothetical ($\varepsilon \neq 1$, $\mu \neq 1$) magnetodielectric particles. Finally we will analyze the consequences of the strong scattering anisotropy on the radiation pressure on these particles showing the electric-magnetic dipolar interaction plays an active role in spinning the particles either in or out of the whirls sites of the interference pattern, leading to trapping or diffusion[17].

References:

[1] H. C. van de Hulst, Light Scattering by small particles (Dover, New York, 1981). C. F. Bohren and D. R. Huffman, Absorption and Scattering of Light by Small Particles (John Wiley&Sons, New York, 1998).

[2] M. I. Mishchenko, L. D. Travis and A. A. Lacis, Scattering, Absorption, and Emissionof Light by Small Particles (Cambridge Univ. Press, 2002). L. Novotny and B. Hecht, Principles of Nano-Optics, (Cambridge University Press, Cambridge, 2006). E. M. Purcell and C. R. Pennypacker, Astrophys. J. 186 (1973) 705. B. T. Draine, Astrophys. J. 333 (1988) 848.

[3] S. J Oldenburg, R. D Averitt, S. L Westcott, N. J Halas. Chem. Phys. Lett., 288 (1998) 243.

[4] P. K. Jain, X. Hunag, I. H. El-Sayed and M. A. El-Sayed, Acc. Chem: Res. 41(12) (2008) 1578.

[5] E. S. Day, J. G. Morton and J. L. West, J. Biomech. Eng. 131(7) (2009) 074001.

[6] A. Alú and N. Engheta, Opt. Express 17, 5723-5730 (2009). Phys. Rev. B 78 (2008) 085112.

[7] K. C. Huang, M. L. Povinelli, and J. D. Joannopoulos, Appl. Phys. Lett. 85 (2004) 543.

[8] C. L. Holloway, E. F. Kuester, J. Baker-Jarvis, and P. Kabos, IEEE Trans. Antennas Propag. 51 (2003) 2596. M. S. Wheeler, J. S. Aitchison, and M. Mojahedi, Phys. Rev. B 72 (2005) 193103.

[9] V. Yannopapas and A. Moroz, J. Phys.: Condens. Matter 17 (2005) 3717. A. Ahmadi, and H. Mosallaei, Phys. Rev. B 77 (2008) 045104. M. S. Wheeler et al, Phys. Rev. B 79 (2009) 073103. L. Jyhl□a, I. Kolmakov, S. Maslovski and S. Tretyakov, J. Appl. Phys. 99 (2006) 043102. L. Peng et al, Phys. Rev. Lett. 98 (2007) 157403. J. A. Schuller et al., Phys. Rev. Lett. 99 (2007) 107401. K. Vynck, et al, Phys. Rev. Lett. 102 (2009) 133901.

[10] M. Kerker, D. S. Wang, and C. L. Giles, J. Opt. Soc. Am. 73 (1983) 765767.

[11] U. Leonhardt, Science 312 (2006) 17771780. J. B. Pendry, D. Schurig, and D. R. Smith, Science 312 (2006) 17801782. A. Alú and N. Engheta, J. Nanophoton. 4 (2010) 041590.

[12] A. Lakhtakia, V. K. Varadan and V. V. Varadan, J. Mod. Optics 38 649 (1991). B. García-Cámara, F. Moreno, F. González and O. J. F. Martin, Opt. Express 18 (2010) 10001.

[13] S. Albaladejo,R. Gómez-Medina, L. S. Froufe-Pérez, H. Marinchio, R. Carminati, J. F. Torrado, G. Armelles, A. García-Martín and J.J. Sáenz, Opt. Express 18 (2010) 3556.

[14] V. V. Temnov, G. Armelles, U. Woggon, D. Guzatov, A. Cebollada, A. García-Martín, J.-M. García-Martín, T. Thomay, A. Leitenstorfer and R. Bratschitsch, Nat. Phot. 4 (2010) 107.

[15] M. Nieto-Vesperinas, J. J. Sáenz, R. Gómez-Medina and L. Chantada, Opt. Express 18 (2010) 11428.

[16] M. Nieto-Vesperinas, R. Gómez-Medina, and J. J. Sáenz, J. Opt. Soc. Am. A 28 (2011) 54.

[17] R. Gómez-Medina, M. Nieto-Vesperinas and J. J. Sáenz, Phys. Rev. A (submitted 2010).

[18] B. García-Cámara, F. Moreno, F. Gonzalez and J. M. Saiz, J. Opt. Soc. Am. A 25 (2008) 28752878. J. Opt. Soc.Am. A 25 (2008) 2875.

[19] A. García-Etxarri, R. Gómez-Medina, L. S. Froufe-Pérez, C. López, L. Chantada, F. Scheffold, J. Aizpurúa, M. Nieto-Vesperinas and J. J. Sáenz, Opt. Express (submitted 2010), ArXiv:1005.5446v1.

[20] R. Gómez-Medina, B. García-Cámara, I. Suárez-Lacalle, F. González, F. Moreno, M. Nieto-Vesperinas, J. J. Sáenz, J. Eur. Opt. Soc, Rapid Publ. (submitted 2011).

ON CHIP LIGHT HANDLING WITH SINGLE AND TWINNED NANOBEAM CAVITIES

B. Cluzel[1], K. Foubert[1,2], L. Lalouat[1], E. Picard[2],D. Peyrade[3], F. de Fornel[1] and **E. Hadji[2]**

[1]LICB/OCP, Unité mixte de recherche n°5209 CNRS - Université de Bourgogne, France
[2]INAC /SP2M - Laboratoire SiNaPS, UMR-E 9002, CEA-Grenoble, France
[3]Laboratoire des Technologies de la Microélectronique, CNRS, Grenoble, France

Optical information processing at the chip level has been a long standing dream. However it requires both on chip light generation and manipulation at sub-wavelength scale which remains challenging. In this context, nanobeam cavities appeared as one of the key players thanks to their field confinement capability and their ridge waveguide integrated geometry. In this context, we showed that strong light localization within nanobeam cavities was possible and was moreover tuneable by near-filed interaction with an external nanometric tip. We showed as well that twinned high Q nanobeam cavities placed in the near-field of each other can optically couple to form a new optical system with discrete field maps addressable by wavelength selection.

The nanobeam cavities presented here integrate tapered mirrors [2]. Thanks to the mirror Bloch mode - cavity wave guided mode mismatch decrease; they allowed achieving record high Q/V ratios [1]. For those nanobeam cavities, near-field scanning optical microscopy (NSOM) is an effective tool to evidence sub-wavelength sized features in the light localization [3]. But it appeared also as a mean to achieve lossless cavity tuning [4]. The evanescent part of the strongly localized optical field can indeed interact with the NSOM nanometric tip [5]. As a result wavelength shifts larger than the cavity line width were observed under the presence of the NSOM tip leading to drastic change of the cavity transmission at the resonant wavelength. On/off ratios (with and without the tip above the nanobeam cavity) larger than 30 db were observed with Q = 50.000 nanobeam cavities.

Then, if two of these cavities are moved within the near-field of each other, the optical fields can evanescently couple to each other. The easiest way to observe this near-field coupling effect is to fabricate two parallel ridge wave-guides separated by a thin air-slot spacer. A careful recording of optical fields above the structure by NSOM clearly demonstrate the field enhancement in the air slot [6] that result from the coupling effects. Now, if nanobeam cavities, instead of simple optical waveguides, are evanescently coupled, an entirely new optical system can be achieved.

In order to understand the coupling mechanism, we first set two cavities, called twinned cavities since they are strictly identical to each other, at lateral coupling distances ranging from 50 to 500 nm. We observed that the original optical field distribution of one single cavity is now reconfigured over the system made by the twinned cavities. The fundamental mode appears to be splitted into two new modes of different parities [7]. This property means that the light localization within the system of twinned cavities is now wavelength dependent, and thus wavelength addressable.

In order to further exploit this effect, we fabricated structures for which the spacing between nanobeam cavities is maintained constant at 100 nm but the number of coupled cavities is varied from 2 to 4 and 8 cavities.

We then recorded the optical field evolution as a function of the number of coupled cavities and observed that the more we increase the number of cavities the more we generate splitted optical modes [8].As a result, since each mode carries its own wavelength, we create for n coupled cavities a set of n different field localizations or field maps over the sample, each of them being addressable by a specific wavelength.

So we evidence here that the electromagnetic field distribution within the reported nanosystems can be engineered on demand at the sub-wavelength scale giving access to a whole range of fields map distribution as a function of the input wavelength.

This new architecture offers an unprecedented opportunity to mold on a chip the morphology of the optical field and opens therefore exciting new perspectives for the future development of configurable optical traps, sensors or opto-mechanical oscillators at the nanoscale.

The authors gratefully acknowledge their fruitful discussions with Dr. Philippe Lalanne from Laboratoire Charles Fabry - Institut d'Optique Graduate School, who pioneered the development of the nanobeam cavities.

References:

[1] P. Velha, J. C. Rodier, P. Lalanne, J.P. Hugonin, D. Peyrade, E. Picard, T. Charvolin, E. Hadji, "Ultracompact silicon-on-insulator ridge-waveguide mirrors with high reflectance", Appl. Phys. Lett. 89, 171121 (2006).

[2] P.Velha, E.Picard, T.Charvolin, E.Hadji, J.C.Rodier, P.Lalanne, D.Peyrade, "Ultra-High Q/V Fabry-Perot microcavity on SOI substrate", Optics Express 15 (24), 16090 (2007).

[3] L. Lalouat, B. Cluzel, P. Velha, E. Picard, D. Peyrade, J.C Rodier, T. Charvolin, P. Lalanne, F. de Fornel, E. Hadji, "Sub wavelength imaging of light confinement in high Q small V photonic crystal nanocavity", Appl. Phys. Lett. 92, 111111 (2008).

[4] B.Cluzel, L.Lalouat, P.Velha, E.Picard, D.Peyrade, J.C Rodier, T.Charvolin, P.Lalanne, F. de Fornel, E. Hadji, "A near-field actuated optical nanocavity", Optics Express, 16 (1), 279 (2008).

[5] L.Lalouat, B.Cluzel, P.Velha, E.Picard, D.Peyrade, J.P Hugonin, P.Lalanne, E.Hadji, F. de Fornel, "Near-field interactions between a subwavelength tip and a small-volume photonic-crystal nanocavity", Phys. Rev. B 76, 041102 (2007).

[6] K. Foubert, L. Lalouat, B. Cluzel, E. Picard, D. Peyrade, E. Delamadeleine, F. de Fornel et E. Hadji, "Near-field modal microscopy of the subwavelength confinement in multi-mode silicon slot waveguides", Appl. Phys. Lett. 93, 251103 (2008).

[7] K. Foubert, L. Lalouat, B. Cluzel, E. Picard, D. Peyrade, F. de Fornel et E. Hadji, "An air-slotted nanoresonator relying on coupled high-Q small-V Fabry Perot nanocavities", Appl. Phys. Lett. 94, 251111 (2009).

[8] B. Cluzel, K. Foubert, L. Lalouat, J. Dellinger, D. Peyrade, E. Picard, E. Hadji e t F. de Fornel, "Addressable sub-wavelength grids of confined light in a multi-slotted nanoresonator", Appl. Phys. Lett. 98, 081101 (2011).

Figures:

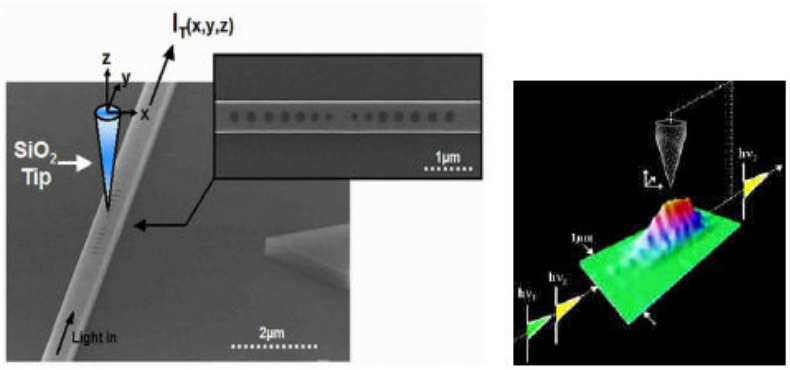

Figure 1: *(left) schematic of tip-nanobeam cavity interaction, (inset) details of the nanobeam cavity; (right) resonant optical field as recorded by NSOM.*

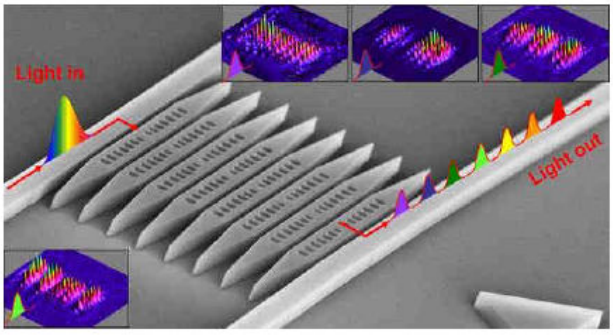

Figure 2: *An array of nanobeam cavities generates sub-wavelength grids of confined light. The spatial distribution of the grids can be modified on demand by changing the wavelength in the nanosystem.*

GAP-MODE PLASMONIC CAVITIES: ENGINEERING LIGHT-MATTER INTERACTIONS IN METALLIC STRUCTURES

Evelyn L. Hu, Kasey J. Russell, Kitty Yeung, Tsung-Li Liu, Shanying Cui

School of Engineering & Applied Sciences; Harvard University
29 Oxford Street; Cambridge, MA 02138, USA
ehu@seas.harvard.edu

Optical cavities can tightly confine light in the vicinity of optical emitters, enhancing the interaction of light and matter. The modes or optical states of the cavity can be precisely designed and engineered, and in recent years there has been remarkable progress in demonstrations of 'cavity quantum electrodynamics (cQED)' in solid state platforms. Such progress has been primarily for cavities fabricated in dielectric materials, with a steady improvement in cavity quality, with quality factors, Q, in excess of 10^4 – 10^6 realized for cavities with coupled emitters [1],[2]. These high Q-coupled emitter systems have demonstrated heralded single photon emission [3], ultra-low threshold lasing [4] and strong light-matter coupling [5],[6].

Metal-based optical cavities would have inherently lower Q's (and greater loss) than dielectrics; however, metal cavities utilizing surface plasmon polaritons (SPPs) can have sufficiently small mode volume to produce a substantial Q/V, the quantity relevant for high Purcell factors, a measure of the light-matter interaction. This talk will focus on such *plasmonic cavities*, with optical modes formed within the gap of the two metal layers which defined the cavity [7]. Initial structures comprised silver (Ag) nanowires (NW), 70 nm in diameter and 1 - 3 μm in length, placed into close proximity to a Ag thin film substrate, with the NW axis parallel to the substrate surface. Optically active material was interposed between the nanowire and the Ag substrate: this comprised one to two monolayers of PbS colloidal quantum dots, clad on top and bottom by thin dielectric layers of varying composition and thickness. A representation of the cavity geometry is shown in Figure 1.

The fluorescence spectrum of PbS quantum dots within the gap was strongly modified by the cavity mode, with peak position in quantitative agreement with numerical calculations, and demonstrating Q values of ~ 60. Figure 2 shows the different modal signatures as a function of nanowire length.

The ability to tune the optical modes into resonance with the emitters is important in achieving the optimal light-matter coupling, and geometry of these cavities lends itself to a relatively simple and straightforward tuning approach. Carefully controlled deposition of dielectric layers formed by Atomic Layer Deposition (ALD) resulted in the systematic shift of the optical modes, as shown in Figure 3.

The high Q/V possible for these cavities, and the range of organic and nanocrystalline emitters they can accommodate make these important building blocks for the exploration of light-matter interaction in the solid state.

References:

[1] S. Noda, M. Fujita, and T. Asano, Nature Photonics 1 (2007) 449.
[2] B.-S. Song, S.-W. Jeon, and S. Noda, Optics Letter 36 (2011) 91.
[3] P. Michler., et al. Science 290 (2000) 2282.
[4] S. Strauf et al., Phys. Rev. Lett. 96 (2006) 127404.
[5] J. Reithmaier et al.. Nature 432(2004) 197.
[6] K. Hennessy, A. Badolato, et al. Nature 445 (2007) 896.
[7] K. Russell and E. Hu, Appl. Phys. Lett.97 (2010) 163115.

Figures:

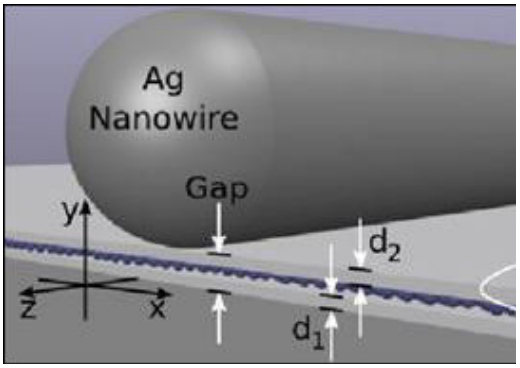

Figure 1: *Schematic diagram of plasmonic nanocavity with quantum dot optical emitters (not to scale).*

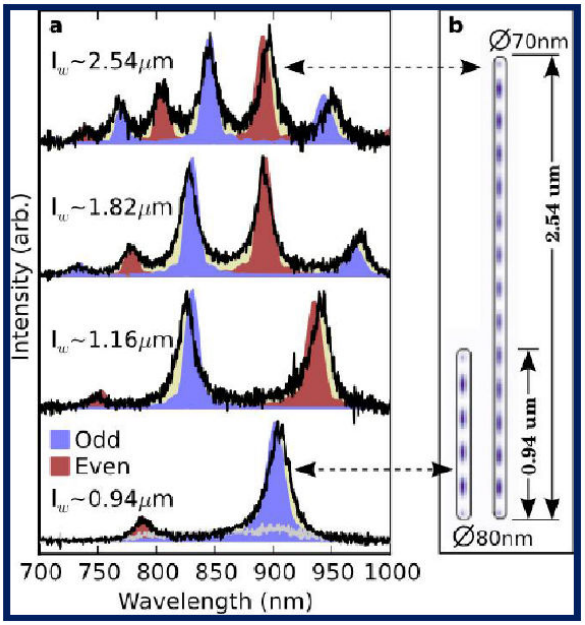

Figure 2: *(a) Measured (lines) modes and FDTD calculated resonances (filled curves) from four cavities of different lengths, indicated in (b) Calculated modal profile for the two indicated cavities. The cavity lengths are indicated by the numbers on the upper-left of each spectrum.*

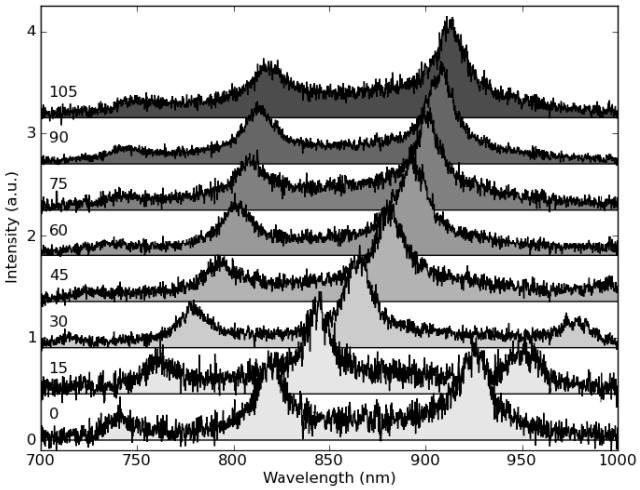

Figure 3: *Systematic shift in modes with increased dielectric deposition on cavity.Numbers on the upper left of each spectrum indicate the number of 'cycles' of atomic layer deposition. Approximately 1 nm/cycle of Al_2O_3 is deposited.*

BRIGHT CDSE/ZNSE NANOWIRE-QUANTUM DOTS FOR SINGLE PHOTONS EMISSION

S. Bounouar, M. Elouneg-Jamroz, G. Sallen, M. Den Hertog, C. Morchutt, E. Bellet-Amalric , R. André, C. Bougerol, J.P. Poizat, S. Tatarenko and **K. Kheng**

Nanophysics and Semiconductors Group, INAC and Institut NEEL, CEA/CNRS/University Joseph Fourier CEA-Grenoble, 17 rue des Martyrs, 38054 Grenoble, France
kkheng@cea.fr

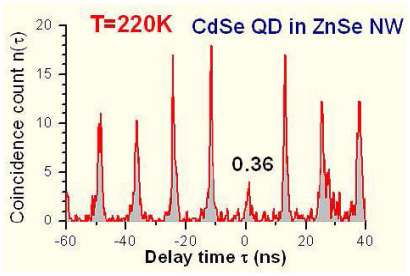

Figure 1: *Single photon emission at 220K [2]*

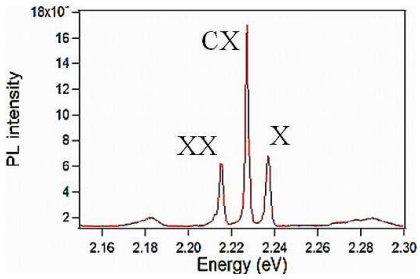

Figure 2: *Exciton, biexciton and charged exciton emission in single CdSe/ZnSe NW-QD [3]*

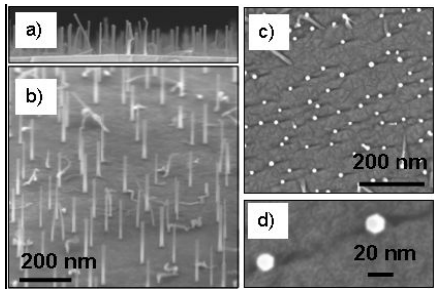

Figure 3: *SEM images ZnSe NWs grown on a ZnSe (111)B buffer layer. Side (a,b) and top (c,d) views.*

Semiconductor nanowires (NW) are appealing structures that allow designing quantum structure with unprecedented freedom. With NW, new type of quantum dot (QD) heterostructures (NW-QD) can be directly grown on defined positions without the necessity of self-assembly, as well as more complex structures such as coupled QDs or core-shell structure. However, the quantum confinement requires growing NW with very small lateral size (of the order o the Bohr radius) with high crystalline structure and clean surfaces (to prevent quenching of the exciton emission through non radiative recombination.

Using MBE in the vapour-liquid-solid growth mode (VLS) we have developed the growth of very high quality ZnSe nanowire [1] with typical diameter of 10 nm (strong confinement regime). We have demonstrated recently that a single CdSe quantum dot embedded in such a ZnSe NW can emit single photons up to 220K [2]. We will present our recent progress over the growth and optical studies on ZnSe/CdSe NW-QD. The quality of our NW is good enough to allow investigating very fine optical properties in single NWs. In pure ZnSe NW, we can observe the band edge emission at 442nm. In ZnSe/CdSe NW-QD, photon correlations measurements have allowed to unambigously identify exciton, biexciton and trion [3] as well as to study the dynamics, in the nanosecond scale, of the spectral diffusion mechanism [4].

References:

[1] T. Aichele et al., Appl. Phys. Lett. 93, 143106 (2008)
[2] A. Tribu, et al., Nano Lett., 8 (12), 4326 (2008)
[3] G. Sallen et al., Phys. Rev. B 80, 085310 (2009)
[4] G. Sallen , A. Tribu , T. Aichele, R. Andre, L. Besombes , C Bougerol , M. Richard , S. Tatarenko, K. Kheng, JP Poizat, Nature Photonics 4, 696 (2010)

PHOTONIC CRYSTAL NANOCAVITIES: EFFICIENT LIGHT-MATTER INTERACTION AT THE NANOSCALE

Thomas F Krauss

SUPA, School of Physics and Astronomy, University of St Andrews, UK
tfk@st-andrews.ac.uk

Controlling light on the nanoscale is an equally exciting and challenging goal, and it allows us to strongly enhance light-matter interactions. Photonic crystals offer such control without inherent losses; they allow us to slow light down, confine it to wavelength-scale spaces and considerably enhance nonlinear interactions. These abilities are enabled by the careful engineering of the photonic crystal's properties and their nanofabrication. Here, we discuss three examples of enhanced light-matter interaction, namely a) farfield-optimised cavities for harmonic wavelength generation, b) substantial control of defect-based light emission via the Purcell factor and c) the strong confinement of light in air for sensing, all enabled by the photonic crystal toolkit.

I. Cavities. High-Q photonic crystal nanocavities have become very popular in recent years, as they offer a unique way for enhancing light-matter interaction due to their ability of combining very high Q-factors with very small volumes [1] thus allowing us to achieve strong enhancement of optical nonlinearities such as harmonic generation. In particular, we have observed both second and third-harmonic generation using only mW-level diode pump sources [2]. A major issue with the design of such high-Q cavities is their off-plane radiation pattern, which makes vertical in- and out-coupling difficult. We have investigated the possibility of modifying the far-field radiation pattern in order to achieve simultaneously high quality factor and high coupling efficiency to an external laser beam in a vertical-coupling configuration [3].

II. Light emission. While studying the nonlinear behaviour of these cavities, we also noted significant levels of light emission in the 1.4 µm - 1.6 µm band, even at room temperature. The emission is understood to arise from the H_2 – based defects, the H_2 being introduced by the implantation process that occurs during SOI manufacturing. We observe sharp and intense photoluminescence peaks that correspond to the resonant modes of the photonic crystal nanocavities, with an up to 300-fold enhancement of the emission from the nanocavity compared to the background, corresponding to a Purcell factor of around 12 [4]. The weak temperature dependence is one of the most striking features, i.e. there is a less than 2-fold reduction between 10 K and room temperature, which makes this approach suitable for the realization of efficient room-temperature light sources at telecom wavelengths as well as providing a quick and easy tool for the broadband optical characterization of SOI-based nanostructures.

III. Slotted cavities. While the above techniques have provided the means for engineering the cavity mode inside the material, they can also be adopted for confining light in air, thus affording opportunities for very strong light-matter interaction in a range of dielectric materials. To this end, we have modified the well-known slotted waveguide configuration [5] and embedded it into the photonic crystal environment. This geometry affords us significant control over the waveguide mode, even outside the dielectric material. As a result, we have been able to achieve confinement in air and reached Q-factors as high as 50,000, which has obvious implications for environmental sensing [6].

In conclusion, it is clear that photonic crystals offer a host of opportunities in confining light at the nanoscale, especially for applications in nonlinear optics, light emission control and environmental sensing.

References:

[1] Y. Akahane, T. Asano, B-S. Song, S. Noda, “High-Q photonic nanocavity in a two-dimensional photonic crystal”, Nature 425 (2003) pp. 944-947.

[2] M. Galli, D. Gerace, K. Welna, T. F. Krauss, L. O’Faolain, G. Guizzetti, and L. C. Andreani, “Low-power continuous-wave generation of visible harmonics in silicon photonic crystal nanocavities”, Opt. Express 18 (2010) 26613.

[3] S.L. Portalupi, M. Galli, C. Reardon, T. F. Krauss, L. O’Faolain, L. C. Andreani, and D. Gerace, “Planar photonic crystal cavities with far-field optimization for high coupling efficiency and quality factor”, Opt. Express 18 (2010) 16064.

[4] R. Lo Savio, S. L. Portalupi, D. Gerace, A. Shakoor, T. F. Krauss, L. O’Faolain, L. C. Andreani, and M. Galli, “Room-temperature emission at telecom wavelengths from silicon photonic crystal nanocavities”, submitted for publication (2011).

[5] V. R. Almeida, Q. Xu, C. A. Barrios and M. Lipson, “Guiding and confining light in void nanostructure,” Opt. Lett. 29 (2004) pp. 1209-1211.

[6] A. Di Falco, L. O’Faolain and T. F. Krauss, “Chemical sensing in slotted photonic crystal heterostructure cavities,” Appl. Phys. Lett. 94 (2009) 063503.

[7] M. G. Scullion, T. F. Krauss and A. Di Falco, “High efficiency interface for coupling into slotted photonic crystal waveguides” IEEE Photonics Journal, in press (2011).

Figures:

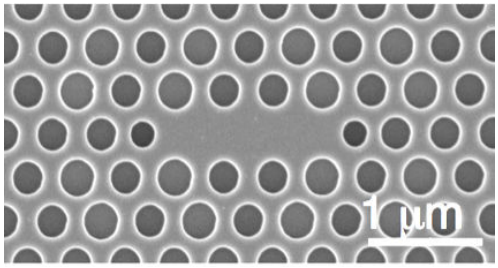

Figure 1: *Photonic crystal cavity with farfield engineering. The alternating smaller and larger holes act as a superimposed second order grating that much improves the farfield radiation pattern without overly compromising the Q-factor; in the best case, for example, the Q-factor drops from 120k to 80k while the extraction efficiency increases by an order of magnitude.*

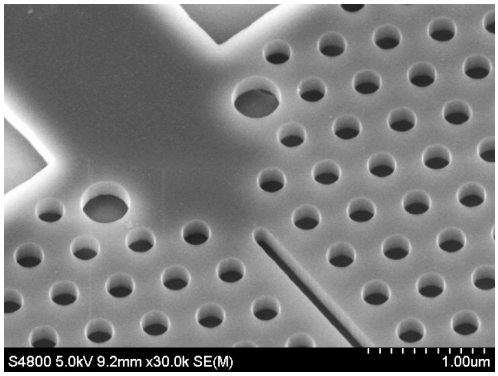

Figure 2: *Interface between slotted photonic crystal and conventional waveguide; careful engineering of this interface affords an injection efficiency of better than 1dB. [7].*

INDIRECT NANOPLASMONIC SENSING FOR NANOMATERIALS SCIENCE

Christoph Langhammer[1,4], Carl Wadell[1], Timur Shegai[2], Elin M. Larsson[3,4], Mikael Käll[2] and Igor Zoric[1]

[1]Chemical Physics, Chalmers University of Technology, Göteborg, Sweden
[2]Bionanophotonics, Chalmers University of Technology, Göteborg, Sweden
[3]Competence Center for Catalysis, Chalmers University of Technology, Göteborg, Sweden
[4]Insplorion AB, Ekmansgatan 3, 411 32 Göteborg, Sweden
clangham@chalmers.se

Nanosized systems (particles and films) are essential ingredients in many established or envisioned technological applications, including sensors, heterogeneous catalysts, photovoltaics, electronic and photonic devices, batteries and hydrogen storage systems. In many of these applications the nanosized systems are in contact with gaseous or liquid environments and desired (e.g. in catalysis) or undesired (e.g. corrosion) interactions between gas or liquid molecules and the nanosized system may occur. In this context it is of particular importance to develop experimental tools for fast, sensitive and reliable measurements of processes on/in nanosized systems under realistic, close-to-application, conditions. The latter often means working at high temperatures, at ambient or higher pressure and in harsh and corrosive environments. Furthermore, sometimes measurements would preferably be done on a single nanoparticle to avoid ensemble-averaging related effects.

Indirect Nanoplasmonic Sensing (INPS) [1-3] is a novel experimental technique fulfilling the above criteria (in analogy to “traditional” nanoplasmonics for biosensing applications [4]). The remarkably sensitive and very versatile INPS platform consists of plasmonic sensor nanoparticles (Au nanodisks or nanocones, prepared on a transparent substrate by Hole-Mask Colloidal Lithography [5]), covered by a thin dielectric film onto which the nanosized system to be studied is deposited (Figure 1). The key to the sensing is utilization of localized surface plasmon resonances (LSPR) in the Au sensor nanoparticles. The latter, via shifts in their extinction spectra, sensitively measure, for example, changes in the surface coverage of adsorbed reactant species (sensitivity <0.1 ML) on [1], or the formation of new phases in [2,3] the adjacent studied nanosystems on the spacer layer. These already demonstrated examples open a whole new field of nanoplasmonic sensing for nanomaterials science due to the generic nature of the INPS approach.

Here, we demonstrate how INPS, (i) in a simple optical transmission/reflection or (ii) dark-field scattering experiment, can be used to monitor and quantify size effects in metal hydride formation on the particle ensemble (i) and, for the first time, single particle level (ii) in Mg and Pd nanoparticles, ranging in size from 1 nm to 50 nm. The latter are ideal model systems to scrutinize how nano-sizing of the hydrogen storage entities influences phase diagram, thermodynamics and kinetics of nanoscopic metal hydrides. Furthermore, Mg is a very interesting system for commercial solid-state hydrogen storage due to its lightweight and low cost. The versatility of the INPS method in this context is illustrated with the following examples:

1) INPS measurements of activation energies for rate limiting steps during hydrogen sorption/desorption in Pd nanoparticles (1-10 nm) illustrate, for the first time, the size dependence of the activation energy for hydrogen diffusion through nanosized Pd hydride and hydrogen desorption from the nanosized Pd particles, respectively. These results are compared to the ab-initio DFTbased calculations for the respective systems.
2) Measurements of hydride formation thermodynamics and kinetics in Mg nanoparticles illustrate how complex INPS nanostructures (i.e. Au/Ti/Mg/Ti/Pd layered nanodisks) can be studied quantitatively in a convenient way and how nanosizing can be efficiently used to engineer storage thermodynamics and kinetics in storage systems relevant for applications.
3) Single particle dark-field scattering INPS experiments on the two above-described systems, i.e. studies of hydride formation in single Mg and Pd nanoparticles, illustrate the possibility to completely eliminate problems caused by inhomogeneous size-distributions and temperature or mass-transport gradients present in studies of ensembles of nanosized entities.

References:

[1] E. M. Larsson, C. Langhammer, I. Zoric, B. Kasemo, Science, 326 (2009), 1091.
[2] C. Langhammer, E. M. Larsson, B. Kasemo, I. Zoric, Nano Letters, 10 (2010), 3529.
[3] C. Langhammer, V. P. Zhdanov, I. Zoric, B. Kasemo, Physical Review Letters, 104 (2010), 135502.
[4] J. N. Anker, W. P. Hall, O. Lyandres, N. C. Shah, J. Zhao, R. P. Van Duyne, Nature Materials, 7 (2008), 442.
[5] H. Fredriksson, Y. Alaverdyan, A. Dmitriev, C. Langhammer, D. S. Sutherland, M. Zaech, B. Kasemo, Advanced Materials 19 (2007), 4297.

Figures:

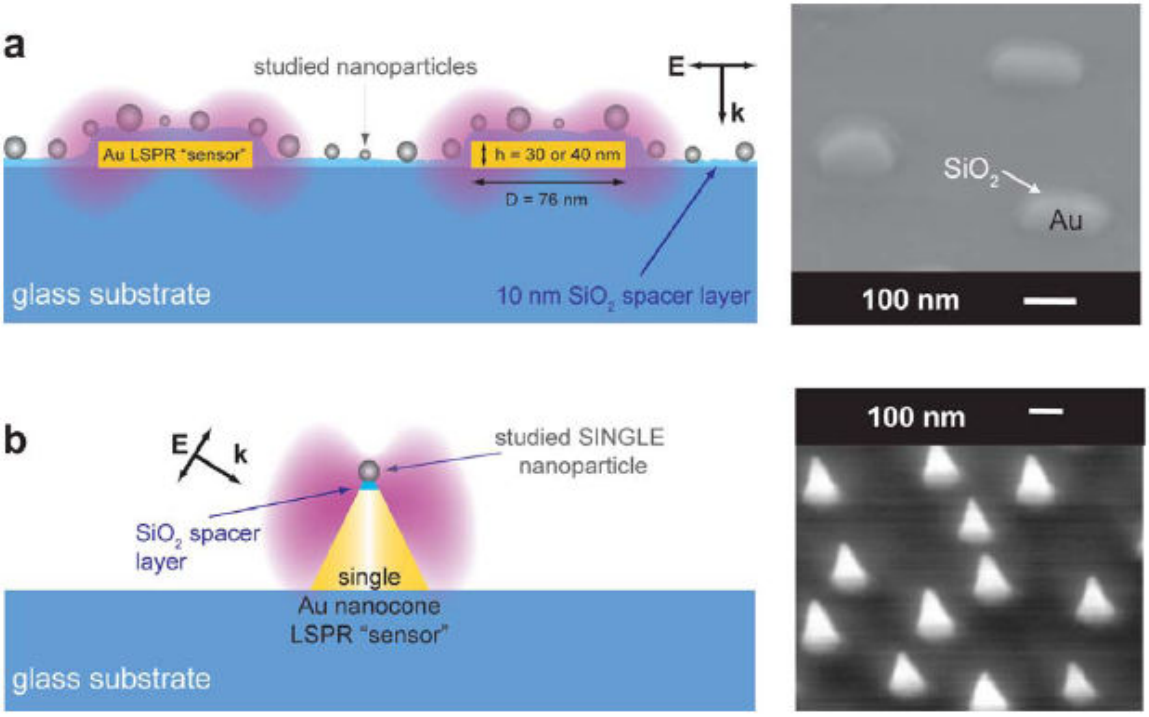

Figure 1: *Schematic depictions of (a) a standard INPS platform and (b) single-particle nanocones sensors. The SEM pictures to the right show the respective real nanostructures.*

MEASURING LIGHT DIFFUSION IN THIN LEAKY SYSTEMS

Marco Leonetti, Cefe López

ICMM, Sor Juana Inés de la Cruz, 3, Cantoblanco, 28049 Madrid, Spain
marco.leonetti@icmm.csic.es

We developed a new experimental technique that allows to study light diffusion in thin leaky systems, allowing to estimate transport mean free path in samples previously inaccessible.

When a pencil of light shines in a white material (a disordered material with no absorption like e.g. a foam), photons entering in different point of the sample follow different paths and their propagation direction is randomized after a few scattering events. The intensity distribution inside the sample may be predicted in the framework of the diffusion approximation[1] that is, disregarding the ondulatory nature of the electromagnetic field to approximate light like intensity packets performing random walk inside the diffusive material. The critical length describing this phenomena is the transport mean free path ℓ, that is the length after which the packet loses the memory of the incoming direction being completely randomized. A few technique (like Enhanced Backscattering Cone[2] and, total transmission measurement[3]) are able to measure this parameter. Here we propose a new approach that is feasible to measure ℓ in thin (nearly 2d) systems in which light injected in plane and has a large probability of exit on the sides of the sample.

A typical sample consists in a drop of water containing dispersed latex beads, enclosed between microscopy coverslips spaced 100 μm. By using a novel strategy to inject the light between coverslips and collecting side emitted photons as a function of the z coordinate (see figure 1), we obtain a measure of how much deep, diffusing light can penetrate inside the sample before being expelled at the lateral side. By fitting [figure 2] this Lateral Leakage Tail (LLT) with results from random walk simulation we are able to estimate the mean free path of the sample.

ℓ measured by fitting LLT on dispersions of micron sized latex beads, and photonic glasses, are in satisfactory agreement with measurements from literature. Our approach opens the way to new applicative (for example biological and lithographic structures) studies on light diffusion and gives a new instrument to address open fundamental questions on light propagation in disordered structures.

References:

[1] Sheng P., Introduction to Wave Scattering, Localization and Mesoscopic Phenomena, Springer; 2nd ed. Edition, Berlin (2010)
[2] Wiersma, D. S., van Albada, Meint P., Lagendijk, Ad, Rev. Sci. Instr., 66 (1995) 5473.
[3] Garcia N., Genack A.Z, Lisyansky A.A., PRB, 46 (1992) 14475.

Figures:

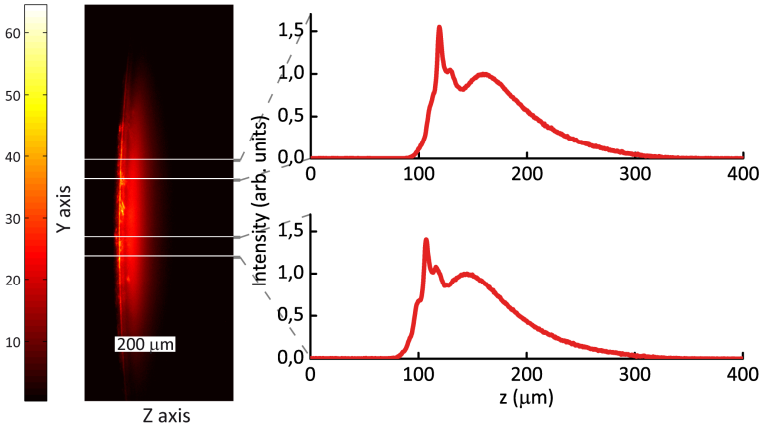

Figure 1: *(On the left) Intensity outgoing from the side of the sample, measured by making an image one of the coverslips enclosing the drop of latex particles on a CCD camera. (On the right), the two graphs represent intensity as a function of z retrieved after integrating on the y direction (the integrated area is the one enclosed by white lines on the figure on the right)*

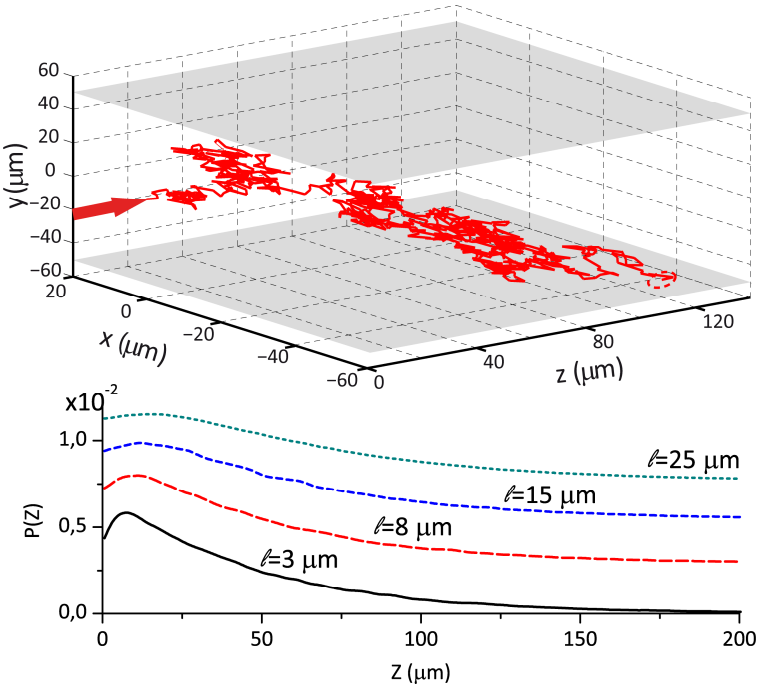

Figure 2: *Results from random walk simulations. On the top the trajectory of a single intensity bunch with a random walk step of R=3 µm. On the Bottom P(z) (Probability for a diffusive photon Injected at coordinates (0,0,0) photon to exit laterally from the sample at a length Z) calculated for different values of random walk step size for . Graphs are translated vertically of an arbitrary amount.*

PHOTOBIOELECTROCHEMICAL SENSORS BASED ON THE COMBINATION OF QUANTUM DOT ELECTRODES WITH ENZYME REACTIONS

F. Lisdat[1], W. Parak[2], K. Schubert[1], J. Tanne[1]

[1]Biosystems Technology, Technical University Wildau, Bahnhofstr. 1, 15475 Wildau, Germany
[2]Biophotonics, Philipps University Marburg Renthof 6, 35032 Marburg, Germany
flisdat@th-wildau.de

Quantum dots, immobilized on electrodes, allow the generation of a photocurrent which is dependent on the applied potential and thus, can work as a light-switchable layer on the sensor surface. The quantum dots can not only interact with the electrode upon illumination but can also exchange electrons with reaction partners in solution allowing the construction of signal chains starting from analyte molecules to be detected [1; 2].

In this work the oxygen dependence of the photocurrent of gold electrodes modified with CdSe/ZnS-quantum dots has been studied. QD immobilisation on the electrode is achieved using a dithiol compound. It has been found that the cathodic photocurrent is enhanced in the presence of oxygen; the current is also influenced by the polarization of the electrode (-500 to +100mV vs Ag/AgCl) and the pH of the solution. It can be also shown that the photocurrent follows the absorption properties of the immobilized QD.

The QD-modified electrode can be used to detect enzyme reactions in solution, this can be shown with lactate dehydrogenase and glucose dehydrogenase [2-4] allowing the analysis of the respective substrate. Here we use the electrode to monitor the activity of the oxygen consuming glucose oxidase (GOD) in solution. Rather small GOD activities (0.025 U/ml) can be detected by photocurrent measurements.

In order to develop a photoelectrochemical biosensor, GOD is immobilized on top of the CdSe/ZnS-electrode. Two different approaches have been followed. The first method is based on the covalent cross-linking of GOD with a bifunctional agent. It can be shown that the consumption of oxygen near the QD surface is a function of the concentration of glucose. The second immobilization strategy uses the layer-by-layer-technique to assemble GOD and poly(allylamin hydrochloride) (PAH). Mass sensitive analysis proves the assembly of $[GOD/PAH]_n$-layer systems (n=2,4,6) on the surface. Photocurrent measurements demonstrate an increased glucose sensitivity with an increase in the number of GOD layers. High enzyme concentrations results in a well detectable photocurrent change between 100µM and 5mM glucose ($[GOD/PAH]_4$-layer-QD-electrode). This allows substrate detection by illumination of the respective sensor surface and thus provides the basis for a spatial read out of the sensing electrode.

References:

[1] C. Stoll, S. Kudera, W. Parak, F. Lisdat, Small 2(6) (2006) 741.
[2] E. Katz, M. Zayats, I. Willner, F. Lisdat, Chem. Comm. 13 (2006) 1395.
[3] C. Stoll, C. Gehring, K. Schubert, M. Zanella, W. Parak, F. Lisdat Biosens. & Bioelec. 24 (2008) 260.
[4] K. Schubert, W. Khalid, Z. Yue, W. J. Parak, F. Lisdat Langmuir 26(2) (2010) 1395.

HOT SPOTS AND CONFINEMENT IN METAL NANOPARTICLES AND ASSEMBLIES

Ramón A. Alvarez-Puebla, F. Javier García de Abajo, **Luis M. Liz-Marzán**

Departamento de Química Física and Unidad Asociada CSIC-Universidade de Vigo, Vigo, Spain
lmarzan@uvigo.es

Gold nanoparticles display extremely interesting optical properties, due to their efficient coupling with visible and NIR light, through localized surface plasmon resonances (LSPR). One of the important effects of LSPR is the huge enhancement of the electromagnetic field at the particles surface, which is in turn the main factor behind the so-called surface enhanced spectroscopies (SES) and in particular of surface enhanced Raman scattering (SERS).

It has been predicted that such enhancing ability can be increased at metal surfaces with acute apexes, where LSPR can be strongly confined. Experimental demonstration of this effect has been recently reported, through the colloidal synthesis of so-called gold nanostars, i.e. nanoparticles covered with a significant number of sharp spikes, which display two plasmon resonances, associated to the central core and the spikes themselves. In this talk we shall present a variety of examples regarding the growth of spikes from different gold nanoparticles, as well as their optical characterization (through UV-vis and EELS spectroscopies). Additionally, we have been able to explore the SERS efficiency of these novel nanostructures, through several experiments that demonstrate maximum enhancement when the probe molecules are adsorbed precisely at the tips.

Additionally, examples will be shown of the possibility of creating organized assemblies of metal nanoparticles, with an extremely high density and uniformity of hot spots, in agreement with numerical simulations.

EXPLOITING APERIODIC ORDER IN PHOTONIC DEVICES

Enrique Maciá

Dpto. Fisica de Materiales, Facultad CC. Fisicas, Universidad Complutense de Madrid,
E-28040, Madrid, Spain
emaciaba@fis.ucm.es

During the last few years a growing number of papers considering the role of deterministic aperiodic order in the optical response of different physical systems has progressively appeared in the literature [1]. Most of these works address the fundamental question concerning whether the specific aperiodic order present in the considered devices results in a better performance than that obtained for more usual periodic arrangements in some specific applications. The inspiring basic principle at work can be easily grasped by considering a layered structure consisting of a number of films aperiodically stacked. In this way, two kinds of order are introduced in the same sample at different length scales. At the atomic level we have the usual periodic order determined by the crystalline arrangement of atoms in each layer, whereas at longer scales we have the quasiperiodic order determined by the sequential deposition of the different layers. This long-range aperiodic order is artificially imposed during the growth process and can be precisely controlled. Since different physical phenomena have their own relevant physical scales, by properly matching the characteristic length scales we can efficiently exploit the aperiodic order we have introduced in the system. Thus, the possibility of growing devices based on an aperiodic stacking of different layers introduces an additional degree of freedom, related to the presence of two different kinds of order in the same sample at different length scales, hence opening new avenues for technological innovation [2]. For instance, one can use sandwiched arrays of aperiodic dielectric multilayers to design optical microcavities [3-5], omnidirectional mirrors [6], multi-stop band filters [7,8], photonic bandgaps [9-12], waveguide structures [13] and many other optical systems of practical interest.

In the case of nonlinear optics, quasiperiodic multilayers can provide more reciprocal vectors to the quasi-phase-matching optical process, and this ultimately results in a more plentiful spectrum structure than that of a periodic multilayer [14,15]. On this basis, the possibility of designing aperiodic structures able to simultaneously phase matching any two nonlinear interactions by properly introducing an aperiodic modulation of the nonlinear coefficient in ferroelectric devices has been proposed in one [16] and two dimensions [17]. The nonlinear properties of optical heterostructures can also be used to fabricate compact-sized compressors for laser pulse. This compression is physically determined by the group velocity dispersion in the material, so that one can expect that by adding more layers to a periodic multilayer one should obtain narrower optical bands and the compression effect will be increased. However, this is inevitably accompanied by an increase of the total thickness of the structure, which is undesirable. In this context, the recourse to aperiodic structures, exhibiting a significantly larger fragmentation of their optical spectrum for similar system sizes, appears as a natural choice.

New approaches in order to obtain innovative optical systems are also based on the construction of modular devices composed of both periodically and aperiodically arranged multilayers Such devices can be viewed as hybrid order systems made of two different kinds of subunits, each one exhibiting a different kind of topological ordering [18]. The introduction of these subunits endows the system with an additional design parameter, bridging the gap between the atomic level characteristic of the microstructural domain of each layer and the mesoscale level associated to the long-range order of the entire device as a whole [19-21].

References:

[1] E. Maciá, “Aperiodic Structures in Condensed Matter: Fundamentals and Applications” (CRC Press, Boca Raton, FL, 2009).
[2] E. Maciá, Rep. Prog. Phys. 69 (2006) 397
[3] Maciá E, Appl. Phys. Lett. 73 (1998) 3330.
[4] V. Agarwal, M. E. Mora-Ramos, and B. Alvarado-Tenorio, Photon. Nanostruct. 7 (2009) 63
[5] S. V. Zhukovsky and S. V. Gaponenko, Phys. Rev. E 77 (2008) 046602
[6] A. G. Barriuso, J. J. Monzón, L. L. Sánchez-Soto, and A. Felipe, Appl. Opt. 46 (2006) 2903
[7] S. Golmohammadi, M. K. Moravvej-Farshi, A. Rostami, and A. Zarifkar, Appl. Opt. 47 (2008) 6477
[8] Y. Trabelsi, M. Kanzari, and B. Rezig, Optica Applicata 39 (2009) 320
[9] P. W. Mauriz, M. S. Vasconcelos, and E. L. Albuquerque, Phys. Lett. A 373 (2009) 496
[10] V. R. Tuz, J. Opt. Soc. Am. B 26 (2009) 627
[11] J. A. Monsoriu, R. A. Depine, and E. Silvestre, J. Eur. Opt. Soc. 2 (2007) 07002; J. A. Monsoriu, R. A. Depine, M. L. Martínez-Ricci, E. Silvestre, and P. Andrés, Opt. Lett. 34 (2009) 3172
[12] X.-H. Deng, J.-T. Liu, J.-H. Huang, L. Zou, and N.-H. Liu, J. Phys.: Condens. Matt. 22 (2010) 055403
[13] Zhu S N, Zhu Y Y, Qin Y Q, Wang H F, Ge C Z, and Ming N B, Phys. Rev. Lett. 78 (1997) 2752
[14] Y. Sheng, K. Koynov, J. Dou, B. Ma, J. Li, and D. Zhang, Appl. Phys. Lett. 92 (2008) 201113
[15] Fradkin-Kashi K, Arie A, Urenski P, and Rosenman G, Phys. Rev. Lett. 88 (2002) 023903
[16] Lifshitz R, Arie A, and Bahabad A, Phys. Rev. Lett. 95 (2005) 133901
[17] Maciá E, Phys. Rev B 63 (2001) 205421
[18] Y. Bouazzi and M. Kanzari, Optica Applicata 39 (2009) 489
[19] J Chen, Bo Qin, H. L. W. Chan, Solid State Comm. 146 (2008) 491
[20] E. M. Nascimento, F. A. B. F. de Moura, and M. L. Lyra, Photon. Nanostruct. 7 (2009) 101

MAGNETO-PLASMONIC NANOSTRUCTURED MATERIALS FOR GAS SENSORS APPLICATIONS

M.G. Manera[a], G.Montagna[a], R. Rella[a], E.Ferreiro-Vila[b] ,A. Garcia-Martin[b], G. Armelles[b], A. Cebollada[b], J.M. Garcia-Martin[b], L. González-García[c], J. R. Sánchez-Valencia[c], A. R. González-Elipe[c]

[a]Istitute for Microelectronic and Microsystems, unit of Lecce, Via Monteroni, 73100 Lecce (Italy)
[b]Instituto de Microelectronica de Madrid, Consejo Superior de Investigaciones Cientificas, Isaac Newton, Tres Cantos, Madrid, Spain
[c]Instituto de Ciencia de Materiales de Sevilla (CSIC-Univ. Sevilla). Avda. Américo Vespucio 49. 41092 Sevilla, Spain
mariagrazia.manera@le.imm.cnr.it

Surface plasmon resonance (SPR) spectroscopy has emerged as a powerful technique which permits real-time monitoring of chemical and bio-chemical interactions occurring at the interface between a thin gold film and a dielectric interface, without the need for labelling of reagents [1]. In recent years it has been used for detection and analysis of chemical and biological substances in many research areas and industrial applications, such as surface science, biotechnology, medicine, environment, and drug and food monitoring. In all these applications, improving the resolution and limits of detection is of vital importance and is the primary goal of the research in this field in the last years.

The sensitivity and limits of detection of the SPR sensors can show variations depending on the method used to excite the surface plasmon (prism coupling, grating coupling, optical fibers etc.).In the widely used Kretschmann configuration, a prism is coated with a metal of suitable thickness. A beam of p-polarized light is allowed to fall on the metal–dielectric interface and the intensity of the reflected light is detected as a function of the angle of incidence. At a particular angle of incidence the resonance condition is satisfied and the resonance is observed as a sharp fall in the reflectivity. The plasmon resonance is extremely sensitive to the changes in the refractive index and the thickness of the dielectric medium adjacent to the metal layer. In the intensity-interrogated configuration, the most widely employed, such changes are monitored by measuring the intensity of the reflected p-polarized monochromatic light at a fixed angle of incidence.

In order to boost up SPR detection sensitivity, various efforts have been made, including construction of SPR equipment and setups with improved measurement modes: incorporation of fluorescent spectroscopy into SPR, signal amplification using functionalized nanoparticles, localized SPR (LSPR) using periodic nanowires and nanoposts, phase-sensitive detection schemes [2-4].

Recently, it has been proposed in the literature a novel Magneto-Optic Surface Plasmon Resonance (MOSPR) sensor [5] which sensor performances can be greatly enhanced with respect to traditional SPR sensors (an improvement by a factor of 3 in the limit of detection is demonstrated) . The novel device is based on the combination of the magneto-optic (MO) effects of the magnetic materials and the surface plasmon resonance. This combination can be achieved by realizing a transducing sensing layer constituted by a multilayer Au/Co/Au deposited onto glass substrates. A magnetic actuator is used to control the magnetization state of the magnetic layer in the transversal configuration, and the relative variations of the reflectivity are detected. By this way, a great enhancement of the magneto-optic effects in the p-polarized light is produced when the resonant condition is satisfied. Such enhancement is strongly localized at the surface plasmon resonance and strongly depends on the refractive index of the dielectric medium, allowing its use for optical sensing and to greatly improve the sensitivity with respect to “standard” SPR sensors. Since this MOSPR seems very promising, we have undertaken the analysis of this configuration both for biosensing purposes and for gas sensing (for the first time in a MOSPR sensor).

In this work, some preliminary results for gas sensing scheme are shown. TiO_2 thin film have been deposited by GLAD (Glancing Angle deposition) onto the last gold surface and its interaction with Volatile Organic Compounds has been monitored both in a standard SPR and in MOSPR configurations in order to compare their sensing performances. Measurements performed in controlled atmosphere demonstrate that the sensitivity results greatly improved in MOSPR sensor for ethanol, methanol and isopropanol vapours. These first results represent a good starting point for the demonstration of the use of the prepared magneto-plasmonic materials in thin film form as candidates

for sensitive optical gas sensors, by greatly enhancing the performances of traditional SPR optical sensors operating at the same conditions.

References:

[1] A J. Homola, S. Yee, D. Myszka, in: F.S. Ligler, C.A.R. Taitt (Eds.), Elsevier, The Netherlands, 207, (2002).
[2] F. Yu, B. Persson, S. Lofas, W. Knoll, Jacs comm, 126, (2004) 8902
[3] L. Malic, B. Cui, T. Veres, and M. Tabrizian, Opt. Lett. 32 (2007) 3092
[4] S. Y. Wu, H. P. Ho, W. C. Law, C. Lin, and S. K. Kong, Opt. Lett. 29 (2004) 2378
[5] B. Sepúlveda, A. Calle, L. M. Lechuga and G. Armelles, Opt. Lett. 31, (2006) 1085.

Figures:

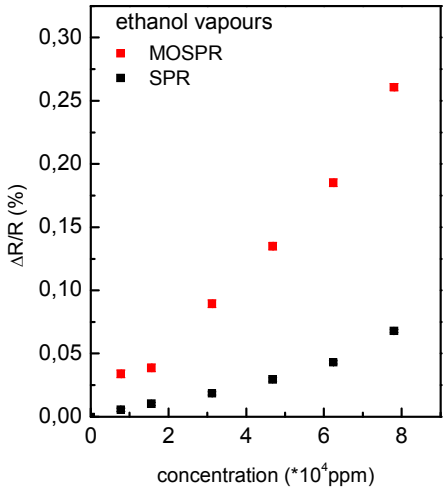

Figure 1: *Sensor response towards ethanol alcohol vapours corresponding to the "standard" SPR configuration and to the MO-SPR configuration demonstrating an increase in sensitivity.*

STRONG PHOTOLUMINESCENCE ENHANCEMENT OF SI AND SIC QUANTUM DOTS BY THEIR RESONANT COUPLING WITH MULTI-POLAR PLASMONIC HOT SPOTS

Tetyana Nychyporuk, Yu. Zakharko, Tetiana Serdiuk, M. Lemiti, Vladimir Lysenko

Lyon Institute of Nanotechnology (INL), CNRS UMR-5270, INSA de Lyon, 7 av. Jean Capelle, Bat.Blaise Pascal, Villeurbanne F-69621, France
tetyana.nychyporuk@insa-lyon.fr

Since the observation in 1990 of strong room-temperature photoluminescence (PL) from nanostructured porous Si [1,2], significant scientific interest has been focused on Si-based nanomaterials (quantums dots (QDs), nanowires, nano-porous layers, etc.) emitting light in a wide spectral range from near infra-red up to ultra-violet regions [3]. However, even for Si QDs of few nanometers with sufficiently broken-down wave-vector selection rules due to spatial and quantum confinements of charge carriers, the luminescence quantum efficiency is rather low (1-10% [4,5,6]) compared to direct band-gap semiconductors [7,8,9], and its considerable enhancement remains an important challenge.

Currently, one of the most intensely studied approaches allowing a significant enhancement of the photo-stimulated emission of various QDs is their localization in the vicinity of metal nanoparticles (NPs) [10,11,12]. Indeed, optically excited collective oscillations of conducting electrons (known also as localized plasmons [13]), appearing in the metal NPs at the spectral ranges corresponding to the plasmon resonance bands allow strong increase of: (i) effective absorption cross-section of the QDs and (ii) their radiative recombination rates. Both reasons provoke an important luminescence enhancement. Moreover, to render much stronger the electrical field in the vicinity of the photoexcited metal NPs and thus to ensure enhancement of the QD photoluminescence intensity by several orders of magnitude, the QDs must be localized in the regions (called hot spots) where the photo-induced electrical fields from several metal NPs are superimposed [14].

Plasmon induced PL amplification was mainly reported for II-VI core/shell QDs [15,16]. In particular, using various configurations of metal (most often: gold and silver) nanostructures, the obtained PL amplification gain varied from 30 to 240 [15,16]. Despite these important recent advances achieved on II-VI QDs, only a seven-fold photoluminescence enhancement was reported for Si QDs [17].

In our present work we show that the plasmon-induced strong local photoluminescence enhancement of Si QDs in SiN matrix can reach 60-fold gain level. This important result was achieved by our team developing original tunable “nano-Ag/SiNX” plasmonic structures. In particular we show that, (i) localization of Si QDs in hot spot regions created by several randomly arranged Ag nanoparticles and (ii) careful tuning of the multi-polar plasmon bands of Ag nanoparticles to match resonantly absorption and emission wavelengths of Si QDs, lead to the important enhancement of their photoluminescence intensity. By exploiting the same physicals mechanisms we were also able to achieve high values of PL enhancement of SiC QDs coupled with plasmonic nanostructures, reaching 20-fold level.

References:

[1] Canham, L. T., Silicon quantum wire array fabrication by electrochemical and chemical dissolution of wafers, Appl. Phys. Lett. 57, 1046-1048 (1990)
[2] Cullis, A. G., Canham, L. T., Visible light emission due to quantum size effects in highly porous crystalline silicon, Nature 353, 335-338 (1991)
[3] Kumar, V., Nanosilicon, Elsevier, Oxford, 2007
[4] Credo, G. M., et al, External quantum efficiency of single porous silicon nanoparticles, Appl. Phys. Lett. 74, 1978-1980 (2008)
[5] Wilson, W. L., et al, Quantum confinement in size-selected, surface-oxidized silicon nanocrystals, Science, 262, 1242-1244 (1993)
[6] Efros, Al. L., et al, Nonlinear optical effects in porous silicon: photoluminescence saturation and optically induced polarization anisotropy, Phys. Rev. B, 56, 3875-3884 (1997)
[7] Talapin, D. V., et al, Highly luminescent monodisperse CdSe and CdSe/ZnS nanocrystals synthesized in a hexadecyamine –tryotylphosphine oxide – trioctylphosphine mixture, Nano Lett. 1, 207-211 (2001)
[8] Chan, W. C. W., et al, Quantum dot bioconjugates for ultrasensitive nonisotopic detection, Science, 281, 2016-2018 (1998)
[9] Bruchez, M., et al, Semiconductor nanocrystals as fluorescent biological labels, Science, 281, 2013-2016 (1998)
[10] Schuller J.A., et al, Plasmonics for extreme light concentration and manipulation, Nature Materials, 9, 193- 204 (2010)
[11] Jin, Y., et al, Plasmonic fluorescent quantum dots, Nature Nanotechnology, 4, 571-576 (2009
[12] Anger, P., et al, Enhancement and quenching of single-molecule fluorescence, Phys. Rev. Lett. 96, 113002 (2006)
[13] Kreibig, U., Vollmer , M. Optical properties of metal clusters; Springer Verlag: Berlin, Heidelberg, 1995
[14] Bek., A., et al, Fluorescence enhancement in hot spots of AFM – designed gold nanoparticles sandwiches, Nano Lett. 8, 485-490 (2010)
[15] Song, J.-H., et al, Large enhancement of fluorescence efficiency from CdSe/ZnS quantum dots induced by resonant coupling to spatially controlled surface plasmons, Nano Lett. 5, 1557-1561 (2005)
[16] Langhuth. H, et al, Strong photoluminescence enhancement from colloidal quantum dot near silver nano-island films, J. Fluores. DOI 10.1007/s10895-010-0740-z
[17] Biteen, J. S., et al., Spectral tuning of plasmon-enhanced silicon quantum dot luminescence, Appl. Phys. Lett. 88, 131109 (2006)

TRANSFORMATION OPTICS AT OPTICAL FREQUENCIES

JB Pendry

Department of Physics, Imperial College, London, SW7 2AZ, UK
j.pendry@imperial.ac.uk

When designing macroscopic optical components such as camera lenses the ray approximation is an excellent design tool. However plasmonic systems function on a scale smaller than the wavelength of light and the ray approximation is of no use to us. In this talk I shall show that the new technology of transformation optics, exact at the level of Maxwell's equations, offers the same intuitive understanding as the ray approximation. The power of the method will be illustrated by showing how to construct 'light harvesting' devices. Starting from a simple well understood system comprising slabs of silver, transformation optics is deployed to generate a whole family of structures that inherit the intrinsic electromagnetic structure of the original but whose geometry is radically transformed from the original.

ULTRAFAST OPTICAL MANIPULATION OF MAGNETIC ORDER: CHALLENGES AND OPPORTUNITIES

Theo Rasing

Department Radboud University Nijmegen, The Netherlands
Institute for Molecules and Materials

The interaction of sub-picosecond laser pulses with magnetically ordered materials has developed into an extremely exciting research topic in modern magnetism and spintronics. From the discovery of sub-picosecond demagnetization over a decade ago to the recent demonstration of magnetization reversal by a single 40 femtosecond laser pulse, the manipulation of spins by ultra short laser pulses has become a fundamentally challenging topic with a potentially high impact for future spintronics, data storage and manipulation and quantum computation.

Recent single-shot pump-probe magneto-optical imaging results show that circularly polarized subpicosecond laser pulses steer the magnetization reversal in a Transition Metal-Rare Earth alloy along a novel and ultrafast route, which does not involve precession but occurs via a strongly nonequilibrium state. However, the nature of this phase and the dynamics of the individual TM and RE moments remained elusive so far. Experiments indicate a possible difference in the dynamics of the TM and RE moments at time scales that are currently limited by the pulse widths of the optical excitations employed (~100fs). To investigate such highly nonequilibrium phases requires both excitation and probing at ultra short time scales and selectivity for the individual moments.

In addition, when the time-scale of the perturbation approaches the characteristic time of the exchange interaction (~10-100 fs), the magnetic dynamics may enter a novel coupling regime where the exchange interaction may even become time dependent. Using ultrashort excitations, we might be able to manipulate the exchange interaction itself. Such studies will require the excitation and probing of the spin and angular momentum contributions to the magnetic order at timescales of 10fs and below, a challenge that might be met by the future fs X-ray FEL's.

References:

[1] A.V.Kimel, A.Kirilyuk, P.A.Usachev, R.V.Pisarev, A.M.Balbashov and Th.Rasing, Ultrafast nonthermal control of magnetization by instantaneous photomagnetic pulses, Nature 435 (2005), 655-657

[2] C.D.Stanciu, F.Hansteen, A.V.Kimel, A.Kirilyuk, A.Tsukamoto, A.Itoh and Th.Rasing, All-optical Magnetic Recording with Circularly polarized Light, Phys.Rev.Lett.99, 047601 (2007)

[3] A.V.Kimel, B. A.Ivanov, R. V.Pisarev, P. A.Usachev, A.Kirilyuk and Th.Rasing, Inertia-driven spin switching in antiferromagnets, Nature Physics 10, 727-731 (2009)

[4] K.Vahaplar, A.M.Kalashnikova, A.V.Kimel, D.Hinzke, U.Nowak, R.Chantrell, A.Tsukamoto, A.Ithoh, A.Kirilyuk and Th.Rasing, Ultrafast Path for Optical Magnetization Reversal via a Strongly Nonequilibrium State, Phys.Rev.Lett.103, 117201 (2009)

[5] A.Kirilyuk, A,V.Kimel and Th.Rasing, Ultrafast Optical Manipulation of Magnetic Order, Rev. Mod. Phys. 82, 2731-2784 (2010)

[6] I. Radu, K. Vahaplar, C. Stamm, T. Kachel, N. Pontius, H. A. Dürr, T. A. Ostler, J. Barker, R. F. L. Evans, R. W. Chantrell, A. Tsukamoto, A. Itoh, A. Kirilyuk, Th. Rasing and A. V. Kimel, Transient ferromagnetic state mediating ultrafast reversal of antiferromagnetically coupled spins, accepted for Nature(2011)

Figures:

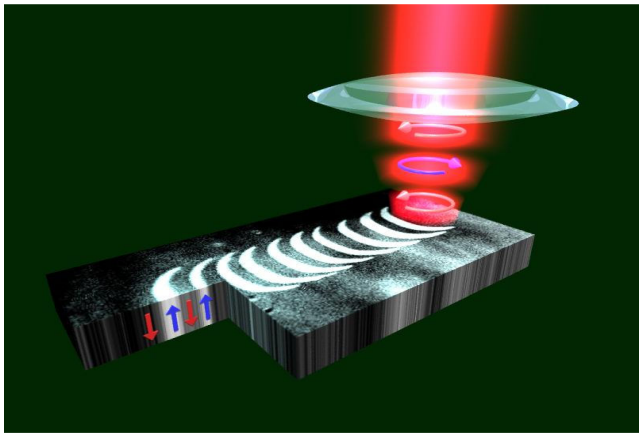

Figure 1: *Demonstration of compact all-optical recording of magnetic bits by femtosecond laser pulses. This was achieved by scanning a circularly polarized laser beam across the sample and simultaneously modulating the polarization of the beam between left and right circular. White and black areas correspond to 'up' and 'down' magnetic domains, respectively. How and how fast does this work?*

SURFACE ENHANCED RAMAN SPECTROSCOPY OF DIFFERENT CHAIN LENGTH PEP+ MOIETY BOUND TO NANORODS

Ros Ida, Placido T., Comparelli R., Marinzi C., Curri L.; Abbotto A., Bozio R.

University of Padova, via Marzolo 1, Padova, Italy
ida.ros@unipd.it

In recent years, Surface Enhanced Raman Spectroscopy (SERS) has become one of the most important technique for characterizing the chemical structure and monitoring structural changes at the single-molecule level.[1] The key effect for the observation of enhanced Raman signals is the favorable optical properties of metal nanostructures, based on their local surface plasmon. The enhancement depends on the type of metal and nanostructures. Several examples of nanostructures of different shape, metal and, eventually, regularly assembled are reported in the literature, resulting in SERS enhancement factors up to 108.[2-6] For example, rod-shaped nanoparticles present a highly tunable longitudinal plasmon band which should be exploited to amplify both the exciting laser and the scattered field in SERS measurements. Despite the desirable characteristics of metallic nanorods, as SERS substrates, only few reports exist for SERS on nanorods where the Raman excitation occurs at a wavelength that overlaps with nanorod plasmon resonances [7-12].

In this presentation, we report our recent results on the amplification of the Raman signals of 1-(N-methylpyrid-4-yl)-2-(N-methylpyrrol-2-yl)ethylene (**PEP+**)) using gold nanorods (NRs) as substrate. The dipolar positively charged dye **PEP+** is a push-pull molecule composed by a π-deficient (pyridinium ion) as acceptor group A and a π-excessive (pyrrole) heterocycle as donor group D.[13] **PEP+** or its derivatives present resonant and non-resonant nonlinear optical properties, such as two-photon absorption or second harmonic generation.[14-15] We have synthesized thiol-acetyl terminated **PEP+** chromophores spaced by two linear alkyl chains of different length, containing 3 or 12 carbon atoms.

The basic idea is to control the intensity of the Raman signals as a function of the distance between the dye and the metallic surface of the metal nanostructure and to study both the effect of the laser resonance with the absorption band of **PEP+** moiety and with the two plasmon modes.

Raman characterization of NRs, functionalized with **PEP+C3SH** and **PEP+C12SH**, both deposited on glass substrates and in solution, is realized using different laser excitation lines. The 488-nm and the 514-nm laser excitation lines are in resonance with the absorption band of the molecules, performing Surface Enhanced Resonance Raman Scattering (SERRS), whereas the 785-nm laser excitation line is out of resonance. Moreover, the 514-nm and the 785-nm lines are resonant with the transverse and longitudinal modes of gold nanorods, respectively, suggesting a further enhancement of the Raman signals.

Comparing Raman spectra, for the same dye bound to NRs, at different laser excitation lines, turns out that data measured by exciting at 514 and 785-nm present a higher signal-to-noise ratio than that at 488 nm. This consideration suggests that the amplification is higher when the laser excitation wavelength is resonant with the two plasmon modes than, exclusively, with the absorption band of the dye, as for the 488-nm radiation.[10] Anyway, the resonance condition of the 514-nm laser excitation with the absorption band of the dye strongly contributes to the amplification of the Raman signal. In fact, DDA calculations, performed on our nanorods, reveal that the local field is about 10 times higher when the longitudinal plasmon mode is excited instead of the transverse one. This means that, in resonance with the longitudinal and transverse plasmon modes, we predict an enhancement of the Raman signal of about 10^4 and 10^2, respectively, which is not confirmed by the measurements if we don't take into account the resonance with the absorption band of the dye.

To compare the amplification of Raman response when the transverse and longitudinal plasmon modes are excited, we evaluated the enhancement factor (EF) using 4-mercaptopyridine (**4-MPy**) as a standard analyte.[10] **4-MPy**, unlike **PEP+** moiety, is not fluorescent and allows us to perform experiments using both 514 nm and 785 nm laser excitation. At 514-nm laser excitation, no signal is observed for **4-MPy** bound to NRs due to the rather low EF. This result clearly agrees with the DDA model prediction for the local field when the transverse mode is excited and further supports our

hypothesis of a strong contribution to the SERRS response from the resonance with the absorption band of **PEP+** moiety.

On the other hand, some Raman bands of **4-MPy** bound to NRs are strongly amplified when excited with 785-nm laser excitation. Characteristic ring breathing modes are observable at 1004 cm^{-1} (v(C–C) mode) and at 1119 cm^{-1} (v(C–S) mode). The latter is remarkably shifted in **4-MPy** bound to NRs (1094 cm^{-1}) and experiences a dramatic increase in intensity compared with the corresponding Raman signal in solution. The evaluated EF for the v(C–C) ring breathing mode at 1004 cm-1 and the v(C–S) ring breathing mode at 1119 cm^{-1} are 4.0×10^{4} and 1.2×10^{5}, respectively, perfectly comparable with the DDA calculation.

These preliminary results show as it is important to control the resonance condition with both the plasmon mode and with the electronic transitions of the molecules. In this way, it is possible to obtain a higher amplification and to detect lower levels of chemical species required for sensoristic applications.

References:

[1] Kneipp, K.; Kneipp, H.; Manoharan, R.; Itzkan, I.; Dasari, R. R.; Feld, M. S. Bioimaging 6 (1998) 104.
[2] Kneipp, K.; Kneipp, H.; Kneipp, J. Acc. Chem. Res. 39 (2006) 443.
[3] Diebold, E. D.; Mack, N. H.; Doorn, S. K.; Mazur, E. Langmuir 25 (2009) 1790.
[4] Yan, B.; Thubagere, A.; Ranjith Premasiri, W.; Ziegler, L. D.; Dal Negro, L.; Reinhard, B. M. ACS Nano 3 (2009) 1190.
[5] Yang, M.; Alvarez-Puebla, R. A.; Kim, H. S.; Aldeanueva-Potel, P.; Liz-Marzan, L. M.; Kotov, N. A. Nano Lett. 10 (2010) 4013.
[6] Bechelany, M.; Brodard, P.; Elias, J.; Brioude, A.; Michler, J.; Philippe, L. Langmuir 26 (2010) 14364.
[7] Nikoobakht, B.; Wang, J.; El-Sayed, M. A. Chem. Phys. Lett. 366 (2002) 17.
[8] Nikoobakht, B.; El-Sayed, M. A. J. Phys. Chem. A 107 (2003) 3372.
[9] Orendorff, C. J.; Gole, A.; Sau, T. K.; Murphy, C. J. Anal. Chem. 77 (2005) 3261.
[10] Orendorff, C. J.; Gearheart, L.; Janaz, N. R.; Murphy, C. J. Phys. Chem. Chem. Phys. 8 (2006) 165.
[11] Aroca, R. F.; Goulet, P. J. G.; dos Santos, D. S.; Alvarez-Puebla, R. A.; Oliveira, O. N. Anal. Chem. 77 (2005) 378.
[12] Guo, H.; Ruan, F.; Lu, L.; Hu, J.; Pan, J.; Yang, Z.; Ren, B. J. Phys. Chem. C 113 (2009) 10459.
[13] Bradamante, S.; Facchetti, A.; Pagani, G. A. Journal of Physical Organic Chemistry 10 (1997) 514.
[14] Facchetti, A.; Abbotto, A.; Beverina, L.; Van Der Boom, M. E.; Dutta, P.; Evmenenko, G.; Pagani, G. A.; Marks, T. J. Chem. Mater. 15 (2003) 1064.
[16] Abbotto, A.; Beverina, L.; Bradamante, S.; Facchetti, A.; Pagani, G. A.; Bozio, R.; Ferrante, C.; Pedron, D.; Signorini, R. Synth. Metals 136 (2003) 795.

MAGNETO-OPTICAL PROPERTIES OF NANOSTRUCTURED THIN FILMS

J.J. Sáenz

Departamento Física de la Materia Condensada
Universidad Autónoma de Madrid, Madrid 28049, Spain
juanjo.saenz@uam.es

Electromagnetic scattering from nanometer-scale objects has long been a topic of large interest and relevance to fields from astrophysics or meteorology to biophysics, medicine and material science [1-5]. In the last few years, small particles with resonant magnetic properties are being explored as constitutive elements of new metamaterials and devices. The studies in the field often involve randomly distributed small elements or particles where the dipole approximation may be sufficient to describe the optical response. We will discuss the optical response of disordered nano-materials where the constitutive nanoparticles can have a non-negligible response to static (**Magneto-Optical active nanoparticles**) or dynamic (**Magneto-dielectric nanoparticles**) magnetic fields.

We will first analyse the peculiar scattering properties of single nanoparticles. In particular, we derive the radiative corrections to the polarizability tensor of anisotropic particles, a fundamental issue to understand the energy balance between absorption and scattering processes [1]. As we will show, Magneto optical Kerr effects in non-absorbing nanoparticles with magneto-optical activity arise as a consequence of radiative corrections to the electrostatic polarizability tensor.

We will also explore the properties of high-permittivity dielectric particles with resonant magnetic properties as constitutive elements of new metamaterials and devices [2]. Magnetic properties of low-loss dielectric nanoparticles in the visible or infrared are not expected due to intrinsic low refractive index of optical media in these regimes. Here we analyze the dipolar electric and magnetic response of lossless dielectric spheres made of moderate permittivity materials. For low material refractive index there are no sharp resonances due to strong overlapping between different multipole contributions. However, we find that Silicon particles with index of refraction $\sim$ 3.5 and radius $\sim$ 200nm present strong electric and magnetic dipolar resonances in telecom and near-infrared frequencies, (i.e. at wavelengths $\approx$ 1.2 – 2 μm) without spectral overlap with quadrupolar and higher order resonances. The light scattered by these Si particles can then be perfectly described by dipolar electric and magnetic fields.

As we will see, the striking characteristics of the scattering diagram of small magneto-optical and magnetodielectric particles [3,4] lead to a number of non-conventional effects in the optical response of nanostructured magneto-optical structures.

References:

[1] S. Albaladejo,R. Gómez-Medina, L. S. Froufe-Pérez, H. Marinchio, R. Carminati, J. F. Torrado, G. Armelles, A. García-Martín and J.J. Sáenz, Opt. Express 18 (2010) 3556.
[2] A. García-Etxarri, R. Gómez-Medina, L. S. Froufe-Pérez, C. López, L. Chantada, F. Scheffold, J. Aizpurúa, M. Nieto-Vesperinas and J. J. Sáenz, Opt. Express 19, 4815 (2011)
[3] M. Nieto-Vesperinas, R. Gómez-Medina, and J. J. Sáenz, J. Opt. Soc. Am. A 28 (2011) 54.
[4] R. Gómez-Medina, B. García-Cámara, I. Suárez-Lacalle, F. González, F. Moreno, M. Nieto-Vesperinas, J. J. Sáenz, to be published (2011).

DESIGNING PLASMON NANOPARTICLES TAILORED FOR APPLICATIONS IN NANOPHOTONICS

R. Rodríguez-Oliveros*, R. Paniagua-Domínguez*, F. López-Tejeira*, D. Macías[+], **J. A. Sánchez-Gil***

*Instituto de Estructura de la Materia, Consejo Superior de Investigaciones Científicas,
Serrano 121, 28006, Madrid, Spain
[+]Laboratoire de Nanotechnologie et d'Instrumentation Optique (ICD-LNIO),
Université de Technologie de Troyes, France
j.sanchez@csic.es

Complex metal nanostructures exhibit surface plasmon resonances that play a crucial role in a variety of electromagnetic phenomena relevant to Nanophotonics. We are interested in the electromagnetic properties of metal nanoparticles of complex shape, with localized plasmon resonances (LPR) yielding large local electromagnetic fields or enhanced emission: such as dimers/trimers playing the role of nanoantennas; or nanoparticles of complex shape (nanostars/nanoflowers); both of interest in enhanced optical emission (Raman, fluorescence, photoluminescence,…) [1-5]. In this regard, it is crucial first to fully characterize the LPR for a variety of metal nanoparticles of arbitrary shape. To this end, we have developed an advanced numerical formulation to calculate the optical properties of 2D and 3D nanoparticles (single or coupled) of arbitrary shape and lack of symmetry [6,7]. The method is based on the (formally exact) surface integral equation formulation. Thus the 3D version is based on the same equations as that of Ref. [8]; nonetheless, it has been implemented for parametric surfaces describing particles with flexible shape through a unified treatment (Gieli's formula), which makes it far more versatile [7,9]. On the basis of these methods, we have indeed calculated the scattering cross sections for nanowires [1-4] and nanoparticles [7] of various shapes (triangles, rectangles, cubes, rods, stars, see i.e. Fig. 1), either isolated or interacting, including far-field patterns and spectra, near-field intensity maps (with corresponding enhancement factors), decay rates, and surface charge distributions.

Furthermore, the optimal design of nanoantennas with specific properties is an aspect of the inverse problem that has not received too much attention until recently, despite being crucial from the point of view of applications. In order to find the optimal nanoparticle geometry that maximizes/minimizes a given optical property, we have made use of a bio-inpired stochastic technique based on genetic algorithms [9], which exploits the above mentioned formulations for flexible surfaces [6,7] to solve the direct scattering problem. We show how this stochastic procedure converges to optimized nanoparticles in some configurations of interest in Nanophotonics: nanoflower/nanostar geometry that exhibits a LPR at or near a given wavelength (see Fig. 2) for SERS (surface-enhanced Raman scattering) substrates [9]; dimer nanoantennas that yield maximum field enhancements and radiative decay rates within the gap for enhanced fluorescence/photoluminescence; long nanoantennas with third-order resonances at given wavelengths for non-linear optical processes (SHG, TPL). With regard to the latter, indeed, the occurrence of Fano resonances at the $L \sim 3\lambda/2$ resonance of the nanorod will also be discussed.

The authors acknowledge support both from the Spain Ministerio de Ciencia e Innovación through the Consolider-Ingenio project EMET (CSD2008-00066) and NANOPLAS (FIS2009-11264), and from the Comunidad de Madrid (grant MICROSERES P009/TIC-1476). R. Paniagua-Domínguez acknowledges support from CSIC through a JAE-Pre grant.

References:

[1] O.L. Muskens, V. Giannini, J.A. Sánchez-Gil, and J. Gómez Rivas, Nano Lett., 7, (2007) 2871-2875.
[2] V. Giannini, J.A. Sánchez-Gil, O.L. Muskens, and J. Gómez Rivas, J. Opt. Soc. Am. B, 26 (2009) 1569-1577.
[3] V. Giannini, R. Rodríguez-Oliveros, and J. A. Sánchez-Gil, Plasmonics, 5 (2010) 99-104.
[4] V. Giannini, A. Berrier, S. A. Maier, J.A. Sánchez-Gil, and J. Gómez Rivas, Opt. Express, 18 (2010) 2797-2807.
[5] L. Guerrini, I. Izquierdo-Lorenzo, R. Rodríguez-Oliveros, J.A. Sánchez-Gil, S. Sánchez-Cortés, J.V. García-Ramos, and C. Domingo, Plasmonics, 5 (2010) 99-104.
[6] V. Giannini and J. A. Sánchez-Gil, J. Opt. Soc. Am. A, 24 (2007) 2822-2830.
[7] R. Rodríguez-Oliveros, J.A. Sánchez-Gil, "Localized plasmon resonances on single and coupled nanoparticles through surface integral equations for flexible surfaces," submitted to Opt. Express.
[8] A.M. Kern and O.J.F. Martin, J. Opt. Soc. Am. A, 26 (2009) 732–740.
[9] A. Tassadit, D. Macías, J. A. Sánchez-Gil, P.-M. Adam, R. Rodríguez-Oliveros, Superlattices & Microstructures, 49 (2011) 288–293.

Figures:

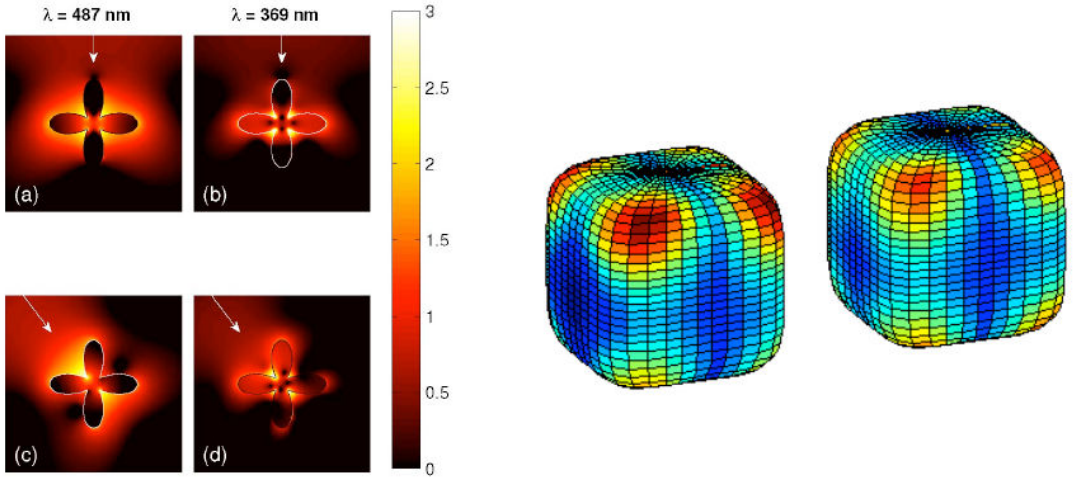

Figure1: *Left-panel: Near-field distributions of the electric field intensities in a log10-scale for the Ag four-petal nanoflower with mean radius ρ=30 nm and deformation parameter β=2/3, illuminated with a monochromatic plane wave with wavelength equal to either one of the two main LPRs (dipolar and quadrupolar, respectively) at λ=487 nm (a,c) and at λ=369 nm (b,d): (a,b) θ_i=0°; (c,d) θ_i=45° [3]. Right-panel: Electric field intensity on the surface of a Ag rounded-cube dimer (L=30 nm, gap=20 nm) with plane wave illumination matching the longitudinal LPR [7].*

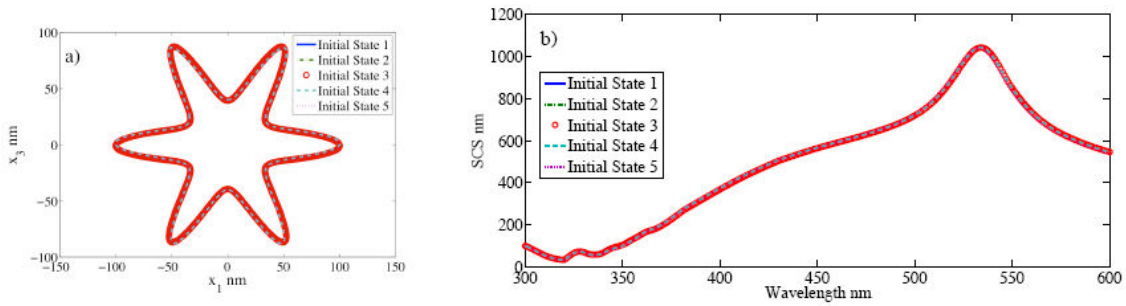

Figure 2: *a) Optimized star-like geometries obtained with Gielis' Superformula. Each line corresponds to an initial state of the optimization algorithm. b) SCSs (optimized to yield a maximum at λ=532 nm) for each of the star-like nanostructures depicted in Fig. 2a (same curve styles in both figures) [9].*

THE EFFECT OF SHAPE AND STRUCTURE VARIATION OF METALLIC NANOPARTICLES ON LOCALIZED PLASMON RESONANCES

Titus Sandu

National Institute for Research and Development in Microtechnologies,126A, Erou Iancu Nicolae street, 077190, Bucharest, Romania
titus.sandu@imt.ro

Localized plasmon resonances (LPRs) in metallic nanoparticles have been now studied extensively for more than a decade. They have a wide range of applications like sensing and waveguiding [1,2] or high throughput communications [3] to name a few. To calculate the LPR properties one has to find the solutions of Maxwell's equations with boundary conditions determined by the interface between nanoparticles and the surrounding medium.

Complex computational schemes like discrete-dipole approximation (DDA) [4] or finite-difference time domain (FDTD) [5] are successfully used to predict optical response of arbitrarily shaped nanoparticles. These aforementioned methods offers, however, little inside about the formation, nature, and the behavior of the LPRs with respect to parameters like the shape (geometry) or complex dielectric functions of nanoparticles. To overcome some of these shortcomings, it has been proposed a hybridization model [6], which works very well in the quasi-static limit. On the other hand, in the quasi-static limit, the Maxwell's equations reduce to Poisson equation which can be solved with the Neumann-Poincare operator associated with the Dirichlet and Neumann problems in potential theory [7]. In plasmonic applications, the method based on the Neumann-Poincare operator has been proposed for some time [8]. The method relates the LPRs to the eigenvalues of the Neumann-Poincare operator, but explicit relations are still lacking. Moreover, the method is similar to the operator method applied for calculation of electric polarizability of biological cells in radiofrequency [9].

I use the operator method outlined in Ref. 9 to define the LPRs in metallic nanoparticles. The LPRs are characterized by the eigenvalues of the Neumann-Poincare operator and their weights to the total polarizability of the nanoparticles. Compact formulas, that contain the complex dielectric functions of nanoparticles and the embedding medium, are given not only for homogeneous but also shelled metallic nanoparticles. The effect of geometry is included in both the eigenvalues of the Neumann-Poincare operator and in their weights to the polarizability. Various trends in LPRs, which otherwise are calculated more expensively with DDA and FDTD, are predicted by simple analysis of these formulas. The effect of geometry variation on LPRs is considered by analyzing the variation of the eigenvalues of the Neumann-Poincare operator and their weights to the nanoparticle polarization. Finally, I consider the case of graded nanoparticles, where their complex dielectric function is not homogeneous but may have a space variation.

References:

[1] P. K. Jain and M. A. El-Sayed, Chem Phys. Lett. 487 (2010) 153.
[2] S. Lal, S. Link, and N. J. Halas, Nature Photonics, 1 (2007) 641.
[3] N. Engheta, 317 (2007) 1698.
[4] B. T. Draine and P. J. Flatau, J. Opt. Soc. Am. A, 11 (1994) 1491.
[5] C. Oubre and P. Nordlander J. Phys. Chem. B 108 (2004) 17740.
[6] E. Prodan, C. Radloff, N. J. Halas, and P. Nordlander, Science, 302 (2003) 419.
[7] O. D. Kellogg, Foundations of Potential Theory, Springer, Berlin, 1929.
[8] D. R. Fredkin and I. D. Mayergoyz, Phys. Rev. Lett. 91 (2003) 253902.
[9] T. Sandu, D. Vrinceanu and E. Gheorghiu,Phys. Rev. E 81 (2010) 021913.

NANOSTRUCTURED ARRAYS OF DOPED SEMICONDUCTORS FOR IR NANOPHOTONICS

Thierry Taliercio[1], Vilianne N'tsame Gulengui[1], Jérôme Leon[2]

[1]Institut d'Electronique du Sud, CNRS-INSIS-UMR 5214, Université Montpellier 2, 34095 Montpellier cedex 05, France
[2]Laboratoire Charles Coulomb, CNRS-UM2 UMR 5221, Département Physique Théorique, CC 070 Université Montpellier 2, 34095 Montpellier cedex 05, France
Thierry.taliercio@univ-montp2.fr

Recent developments of plasmonic have opened new prospects in the control of light-matter interactions. The surface plasmons (SP), at the origin of this new topic, result from the coupling of the electromagnetic wave with the collective oscillation of the electrons supported by the metal/dielectric interface. SP have unique physical properties based on enhanced nanolocalized optical fields. Engineering of surface plasmons using nanostructured materials (nanoparticle, nanostructured film, fishnet etc) made it possible to develop a new range of materials with remarkable properties like, e.g., extraordinary optical transmission (EOT) [1]. A lot of theoretical investigations have been made in the case of one dimensional periodic arrays of slits [2,3]. All these studies focus on the low energy part of the plasmon polariton dispersion, that is, below the plasma frequency. In a recent work [4], we have proposed a model which describes the optical properties of an infinitely periodical nanostructure in a large range of frequencies around the plasma frequency wp. The elementary period of the structure, quite similar to a slit, is composed of two layers: a metal, or doped semiconductor, and a dielectric or un-doped semiconductor, considered in its dielectric range (Figure 1). The index of the periodic structure is defined as (1):

$$n^2(z,\omega)=\begin{cases}\varepsilon_1 \quad for \quad z\in[-b,0]\\ \varepsilon\left[1-\dfrac{1}{\omega(\omega+i\gamma)}\right] \quad for \quad z\in[0,a]\end{cases} \quad (1)$$

where a Drude dielectric function is used to model the behavior of the doped semiconductor. In this work all frequencies are normalized to the plasma frequency wp, the wave numbers to $k_p = \omega_p /c$, the lengths to k_p^{-1} (including spatial variables), and time to w_p^{-1}. In the range of validity of the long wavelength limit, that is, typically a and b < 0.1 λ_p, we prove that under transverse magnetic wave (TM) irradiation, the structure can be modeled by means of the following single effective dielectric function of a ionic-crystal type

$$\varepsilon_{eff}=\tilde{\varepsilon}\frac{\omega(\omega+i\gamma)-1}{\omega(\omega+i\gamma)-\omega_r}$$

where $$\tilde{\varepsilon}=\frac{(a+b)\varepsilon_1\varepsilon}{a\varepsilon_1+b\varepsilon}, \quad \omega_r^2=\frac{b\varepsilon}{a\varepsilon_1+b\varepsilon} \quad (2)$$

where γ is the damping due to losses. In the case of transverse electric (TE) illumination the nanostructure behaves like a metal but with a new plasma frequency, ω_t, which depend on a, b, ε and ε_1, see ref. [4] for more details.

This work presents original optical properties of the nanostructure for different geometrical or physical parameters. Indeed, by modifying the thickness of both layers and the plasma frequency through electrons density, it is possible to highlight a strong coupling between the incident light and the free electrons of the doped semiconductor. This strong coupling results in a broad photonic band gap ($\Delta\omega = 1-\omega_r$) near the plasma frequency. Figures 2 and 3 show respectively the reflectance in TE and TM polarization in normal incidence for different values of a and b. The sizes vary from 0.1 to 0.3 µm. ω_p is defined at a value of 54 THz (corresponding to 6 µm) and γ = 0.03 ω_p. These values are realistic in the case of a layer of InAs doped by silicon atoms at 10^{20} cm^{-3}. We can see on figure 3 that increasing the ratio between a and b increases considerably the stop band since $\Delta\omega$ (green line) reaches an incredible value of 55 % of ω_p. In the same time, figure 2 shows an increase of ω_t which approaches ω_p. Both behavior are awaited. Indeed a reduction of b versus a corresponds to an increase of the metallic part with respect to the dielectric one. In the extreme case, that is b = 0 µm, pure metallic regime is reached. In this case the plasma frequency just depends of the electron density (ω_t = ω_p) and ω_r reaches 0, we are dealing with a free electron gas. On the contrary, if a/b

decreases, ω_t and ω_r tend respectively towards 0 and ω_p. In the same time $\Delta\omega$ (red line on figure 3) decreases denoting a reduction of the light-matter coupling, that is, the equivalent “oscillator strength”. For a ~ 0 µm, the nanostructure gives an optical response similar to that of a dielectric containing oscillators of frequency ω_p.

The interesting aspect of this simple nanostructure is the possibility offered to control the light matter coupling just by adjusting the geometry of the nanostructure or its electrons density. We obtain a metamaterial equivalent to an ensemble of oscillators of which we can control the optical properties, that is, oscillator strength, frequency, broadening, etc. The polaritonic nature of the surface plasmon is at the origin of this specific behavior.

References:

[1] T. W. Ebbesen, H. J. Lezec, H. F. Ghaemi, T. Thio, and P.A. Wolff, Nature 391 (1998) 667.
[2] J.A. Porto, F.J. Garcia-Vidal, and J.B. Pendry, Phys. Rev. Lett. 83 (1999) 2 845.
[3] U. Schröter and D. Heitmann, Phys. Rev B58 (1998) 15 419.
[4] J. Léon and T. Taliercio, Phys. Rev B82 (2010) 195 301.

Figures:

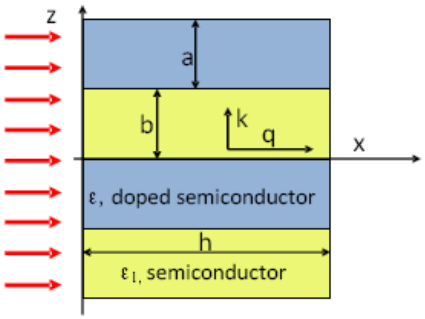

Figure 1: *Scheme of the nanostructure, infinitely periodic in direction z and infinite in direction y.*

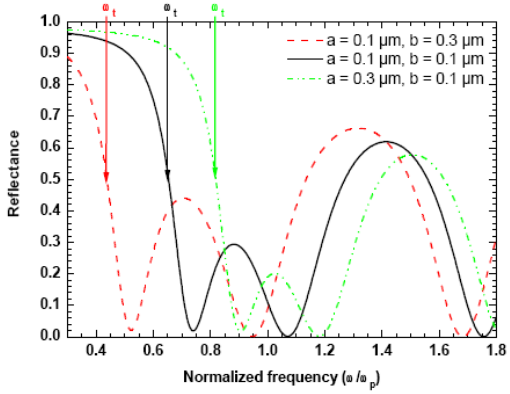

Figure 2: *Calculated reflectance spectra in normal incidence and TE polarization for different size of doped (a) and undoped (b) semiconductor layers. The characteristic plasma frequency (wt) of the different layers are indicated by the vertical arrows.*

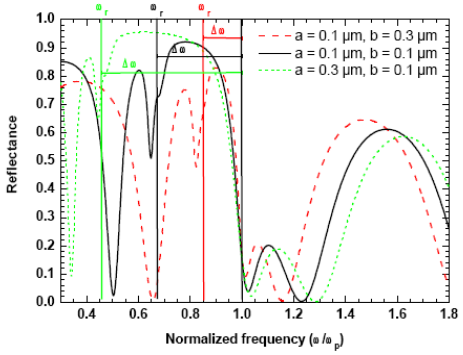

Figure 3: *Calculated reflectance spectra in normal incidence and TM polarization for different size of doped (a) and undoped (b) semiconductor layers. The characteristic frequency (wr) and stop band (Dw) of the different layers are respectively indicated by the vertical and horizontal barres.*

ULTRAFAST ACOUSTO-MAGNETO-PLASMONICS IN HYBRID METAL-FERROMAGNET MULTILAYER STRUCTURES

Vasily Temnov

MIT Chemistry Department, 77 Massachusetts Avenue, 02139 Cambridge, MA, UK
temnov@mit.edu

Nanostructured metal surfaces are presently used to effectively couple light to surface plasmons. This technology is also key to on-chip miniaturization of plasmonic sensors. We present a new plasmonic sensor, based on a tilted slit-groove interferometer, milled into a single noble metal film [1] or into a hybrid metal-ferromagnet structure [2]. Surface plasmons are excited at the groove and propagate towards the slit, where they interfere with incident light (Fig. 1). Due to the tilt angle the optical transmission through the slit shows a pronounced periodic interference pattern. A modulation of the complex surface plasmon wave vector results in a measurable change of the contrast and phase shift of the plasmonic interference pattern [1]. The wave vector of surface plasmons in our hybrid magneto-plasmonic gold-cobalt-gold system can be changed by switching in-plane magnetization using a weak external magnetic field (Fig. 1). Magneto-plasmonic modulation depth of up to 2% is achieved is this geometry. It can be further increased by covering the microinterferometer with high-index dielectric material [3].

When combined with time-resolved optical pump-probe spectroscopy, femtosecond surface plasmon interferometry captures the dynamics of ultrafast electronic excitations and coherent lattice vibrations within δ_{skin}=13nm skin depth in gold with femtosecond time resolution [1]. Using a sapphire/cobalt/gold multilayer structure we generate ultrashort acoustic pulses by thermal expansion of a cobalt film impulsively heated by femtosecond laser pump pulses through sapphire substrate (Fig. 2a). The compressive acoustic pulse propagates through the gold layer at the speed of sound and is converted into a tensile pulse upon reflection from the gold-air interface. The wave vector of femtosecond surface plasmon probe pulses propagating along the gold-air interface serves as a sensitive probe to the local perturbations of the electron density within the skin depth δ_{skin}=13nm induced by the acoustic pulse. Varying the pump-probe delay time makes it possible to monitor the dynamics of acoustic reflection in the plasmonic pump-probe interferogram (Fig. 2c) and extract the pump induced modulation $\delta\varepsilon'+i\delta\varepsilon''$ of surface dielectric function ε (Fig. 2d). On top of the slowly increasing thermal background due to the temperature rise of gold-air interface the apparent acoustic echo in $\delta\varepsilon'$ is observed indicating the change of surface plasmon wave vector $\delta k_{sp}=\delta\varepsilon'/2|\varepsilon|^2$. Straightforward mathematical analysis delivers the exponential shape of the acoustic strain pulse with the amplitude of ~10^{-4}. The 300 fs temporal resolution in our experiment is limited by the duration of femtosecond laser pulses and the roughness of the gold surface.

Using much thinner cobalt transducers we were able to generate sub-picosecond acoustic pulses and use them to study the intrinsic ultrasonic attenuation of longitudinal phonons in gold in the THz frequency range. The observed surprisingly long mean free path of THz phonons in gold at room temperature opens the door to the nanometer resolved acoustic microscopy in metals and a new type of acoustic spectroscopy in solids with ultrahigh (μeV) spectral resolution over the entire Brillouin zone [4].

References:

[1] V.V. Temnov, K.A. Nelson, G. Armelles, A. Cebollada, T. Thomay. A. Leitenstorfer, R. Bratschitsch, Optics Express 17 (2009) 8423.
[2] V.V. Temnov, G. Armelles, U. Woggon, D. Guzatov, A. Cebollada, A. Garcia-Martin, J.M. Garcia-Martin, T. Thomay, A. Leitenstorfer, R. Bratschitsch, Nature Photonics 4 (2010) 107.
[3] D. Martin-Becerra, J.B. Gonzalez-Diaz, V.V. Temnov, A. Cebollada, G. Armelles, T. Thomay, A. Leitenstorfer, R. Bratschitsch, A. Garcia-Martin, M. Ujue-Gonzalez, Appl. Phys. Lett. 97 (2010) 183114.
[4] V.V. Temnov, C. Klieber, K.A. Nelson, T. Thomay, A. Leitenstorfer, D. Makarov, M. Albrecht, R. Bratschitsch (to be published)

Figures:

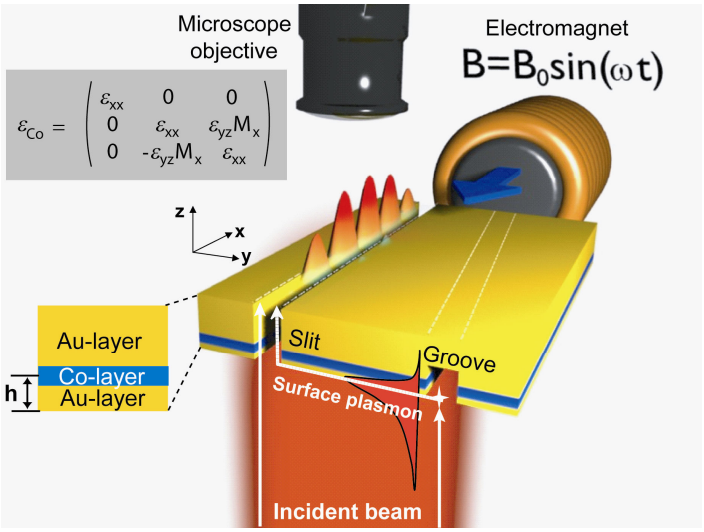

Figure 1: *Active magneto-plasmonic interferometry in tilted slit-groove interferometers patterned in Au/Co/Au multilayer structures. The magnetic field of an electromagnet switches the magnetization in a cobalt layer and thus changes the wave vector of a surface plasmon propagating between the slit and the groove, see Ref. [2] for details.*

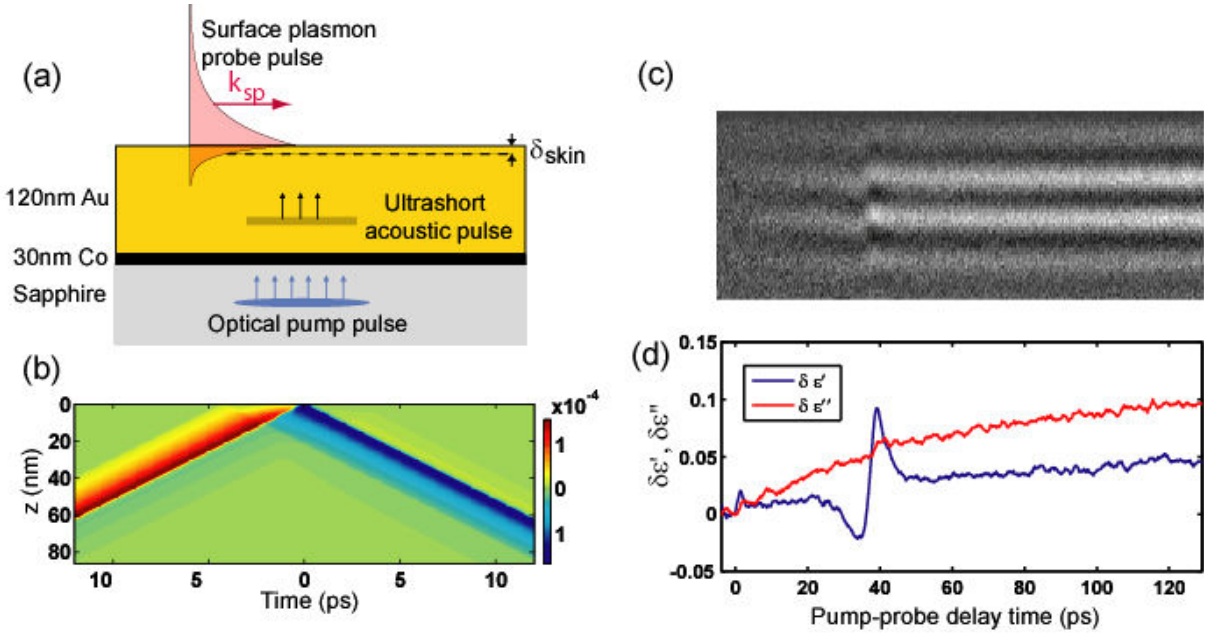

Figure 2: *Femtosecond ultrasonics probed with ultrashort surface plasmon pulses. An ultrashort compressive acoustic pulse is generated by thermal expansion of fs-laser heated cobalt transducer and propagates through the gold film at the speed of sound (a). Upon reflection from gold-air interface the compressive acoustic pulse (layer with high electron density) is converted into the tensile pulse (layer with low electron density) (b). The dynamics of acoustic reflection is captured in a plasmonic pump-probe interferogram (c) and results into the pronounced modulation of the wave vector for a time-delayed femtosecond surface plasmon probe pulse (d).*

DEVELOPMENT OF HIGH SENSITIVITY BIOSENSORS USING SOI PHOTONIC CRYSTAL WAVEGUIDES

J. García-Rupérez[1], **V. Toccafondo[1]**, M. J. Bañuls[2], A. Griol[1], J. G. Castelló[1], S. Peransi-Llopis[2] and A. Maquieira[2]

[1]Nanophotonics Technology Center, Universidad Politécnica de Valencia, Camino de Vera s/n, Valencia (Spain)
[2]Instituto de Reconocimiento Molecular, Dpto de Química, Universidad Politécnica de Valencia, Camino de Vera s/n, Valencia (Spain)
vertocca@ntc.upv.es

Integrated planar photonic devices have become one of the main candidates for the development of high performance lab-on-a-chip devices [1]. Two main advantages of these devices for sensing applications are their high sensitivity and their reduced size, which makes it possible both to detect very small analytes without the need of markers (label-free detection) and to integrate many of these devices on a single chip to perform a multi-parameter detection. Moreover, the CMOS-compatibility when fabricating these planar photonic devices on silicon-on-insulator (SOI) allows a huge reduction of their costs and increase of their production volume.

In this work, we report experimental biosensing results using SOI planar photonic crystal waveguides (PCW). The experimental results comprise refractive index (RI) sensing, label-free detection of antibodies [2] and label-free detection of single strand DNA (ssDNA) [3]. In these experiments, we have used Fabry-Perot fringes appearing in the slow-light regime near the edge of the guided band. These fringes become very sharp as we get close to the band edge, making the determination of their position more accurate, thus allowing a reduction in the limit of detection.

For the refractive index sensing experiments, we flowed several dilutions of ethanol in DIW (Deionized Water), having a RI variation between dilutions of $1.3x10^{-3}$ RIU (Refractive Index Units). By tracking the shift of one of the Fabry-Perot fringes at the band edge, we have obtained a sensitivity of 174.8nm/RIU and an estimated detection limit of $3.5x10^{-6}$ RIU (from the noise in the peak position).

For the label-free detection of antibodies, we bio-functionalized the PCW with bovine serum albumin (BSA) antigen probes (we have used 3-isocyanatepropyl triethoxysilane (ICPTES) in vapour phase for the activation of the surface). Then, we flowed the complementary anti-BSA antibody with a concentration of 10 µg/ml during enough time to achieve a monolayer on the top of the BSAfunctionalized chip. From the wavelength shift of the tracked peaks, together with the noise level of the peak position and the surface density for a close-packed anti-BSA monolayer, we have calculated a surface mass density detection limit below 2.1 pg/mm^2. Concerning the total mass detection limit, if the active region of the PCW is considered, a value of ~0.2 fg is obtained.

Finally, for the label-free detection of ssDNA, we used a similar bio-functionalization strategy in order to attach biotinylated ssDNA probes on the PCW surface. Then, we flowed ssDNA 0.5 µM complementary to the probes in the PCW surface. We have measured a peak shift of 47.1 pm. Using the noise level of the peak position, we estimated a detection limit of 19.8 nM for the ssDNA hybridization detection.

Funding from the European Commission under contract FP7-ICT-223932-INTOPSENS and from the Spanish MICINN under contracts TEC2008-06333 and CTQ2007-64735/BQU is acknowledged. Support from the Universidad Politécnica de Valencia through program PAID-06-09 and the Conselleria d'Educació through program GV-2010-031 is also acknowledged.

References:

[1] X.D. Fan, I.M. White, S.I. Shopova, H. Zhu, J.D. Suter, Y. Sun, Anal. Chim. Acta, 620 (2008) 8-26.

[2] J. García-Rupérez, V. Toccafondo, M. J. Bañuls, J. G. Castelló, A. Griol, S. Peransi-Llopis, and Á. Maquieira, Opt. Express, 18 (2010) 24276-24286.

[3] V. Toccafondo, J. García-Rupérez, M. J. Bañuls, A. Griol, J. G. Castelló, S. Peransi-Llopis, and A. Maquieira, Opt. Lett., 35 (2010) 3673-3675.

Figures:

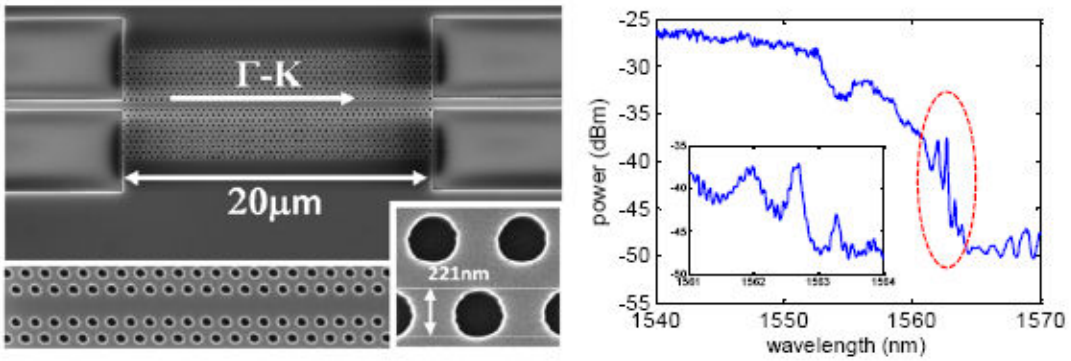

Figure 1: *(Left) SEM image of one of the SOI photonic crystal waveguides used in the experiments, where a row of holes is removed in the Γ-K direction (W1-type), with close-up view of the sensor area and photonic crystal holes (insets). (Right) Spectrum of the PCW in the region of the band edge when having DIW as upper-cladding. Fabry-Perot transmission fringes at the band edge are marked with dashed red line and enlarged in the inset.*

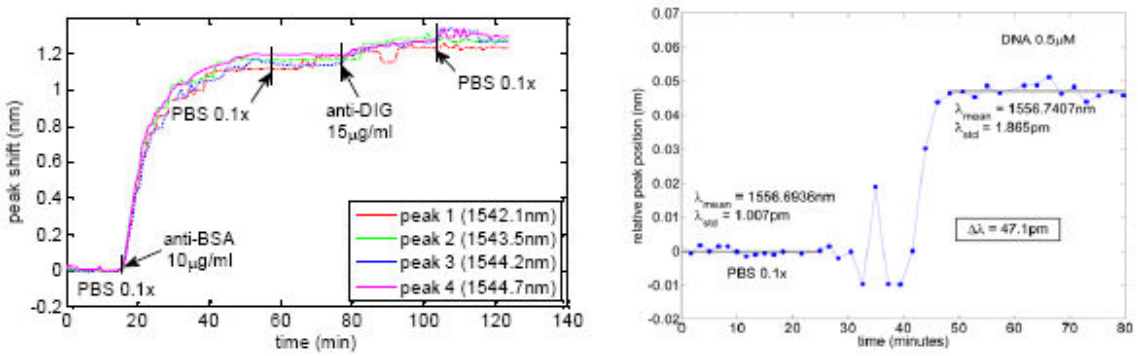

Figure 2: *(Left) Wavelength shift vs time for the label-free anti-BSA 10 μg/ml detection experiment. Each line (color and style identified in the legend) correspond to the relative shift of each tracked peak respect its initial wavelength position. (Right) Wavelength shift vs time for the label-free ssDNA 0.5 μM sensing experiment.*

MAGNETIC INFORMATION IN THE LIGHT DIFFRACTED BY ARRAYS OF NANOMETER-SCALE MAGNETS

P. Vavassori

CIC nanoGUNE Consolider, Tolosa Hiribidea 76, E-20018, Donostia-San Sebastián and IKERBASQUE, Basque Foundation for Science, E-48011, Bilbao, Spain
p.vavassori@nanogune.eu

A key issue in fundamental physics and data storage technology is to understand and control magnetic phenomena, which appear when systems are confined to the nano-scale. The magnetic properties of nano-scale magnetic materials are continuously investigated using a variety of experimental techniques and the ever-increasing efforts devoted to their study are leading to the development of novel systems.

Magneto-optical measurement techniques, especially the Magneto-Optical Kerr effect (MOKE), are established and widely used characterization techniques for the study of fundamental magnetism issues in thin and ultrathin film/multilayered samples. The basic observation in magneto-optics is that the optical properties of a magnetic material change with an alteration of the magnetization state.

So far the vast amount of work done using MOKE has been in a simple reflection geometry, which limits its applicability to planar structures and physical geometries. Only recently, several successful attempts have been made to extend MOKE to diffraction techniques (see Fig. 1), in order to exploit the interference effects of light being diffracted by arrays of nano-structures. This technique, called diffracted magneto optic Kerr effect (D-MOKE), in conjunction with micromagnetic simulations, demonstrated to be a powerful and non-destructive technique for investigating the spatial correlation of the magnetic spin distribution at the nano-scale in a periodic matrix of nano-structures [1].

D-MOKE has been applied to the study of broad variety of magnetic phenomena occurring in arrays of nano-particles as, e.g.,: correlation of the magnetic spins distribution to effects of magnetostatic self energy and dipolar interactions [2]; magnetization reversal path and magnetic configurations in arrays subjected to competing interactions (magnetic frustration) [3].

In this talk, the experimental and theoretical aspects of obtaining the magnetic information carried by laser beams diffracted from an array of nanosized magnetic objects are reviewed. Experimentally it will be shown that MOKE hysteresis loops recorded from diffracted beams (see Fig. 2) are proportional to the magnetic form factor or, equivalently, to the Fourier component of the magnetization corresponding to the reciprocal lattice vector of the diffracted beam. It is finally shown a particular experimental implementation of D-MOKE based on magneto-optical ellipsometry techniques, which allow for the extraction of the unit cell magnetic configuration directly from D-MOKE loops without the aid of micromagnetic simulations. Evidence is given that this recent extension of D-MOKE capabilities provides a vastly improved far-field optical characterization method of the microscopic collective magnetic behavior of arrays of nano-magnets.

We acknowledge funding of the Department of Industry, Trade, and Tourism of the Basque Government and the Provincial Council Gipuzkoa under the ETORTEK Program, Project No. IE06-172, as well as the Spanish Ministry of Science and Education under the Consolider-Ingenio 2010 Program, Project CSD2006-53, IKERBASQUE, the Basque Science Foundation.

References:

[1] M. Grimsditch and P. Vavassori, J. Phys.: Condens. Matter., 16 R275, (2004).
[2] P. Vavassori, et al., Phys. Rev. B 67, 134429 (2003); P. Vavassori, et al., Phys. Rev. B 69, 214404 (2004); P. Vavassori, et al., Phys. Rev. B 78, 174403 (2008).
[3] R. F. Wang et al., Nature 439, 303 (2006).

Figures:

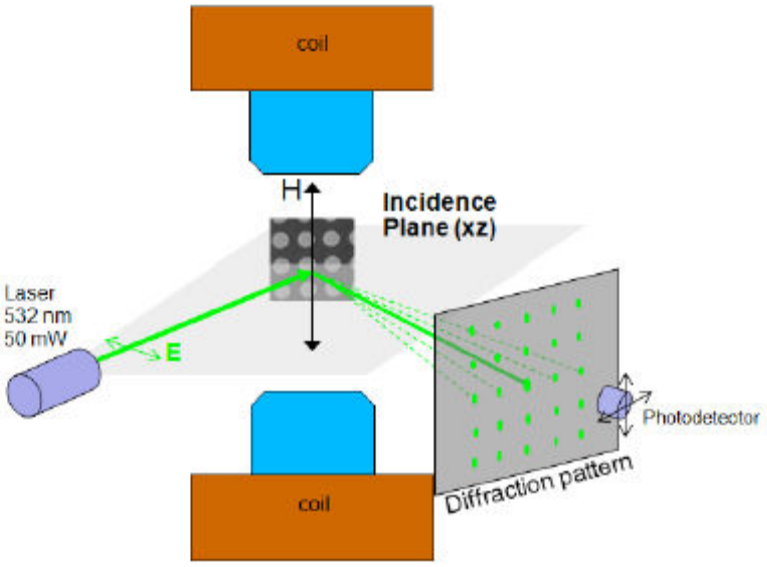

Figure 1: *Schematic drawing showing the transverse MOKE configuration for recording magnetization loops at specularly reflected and diffracted beams*

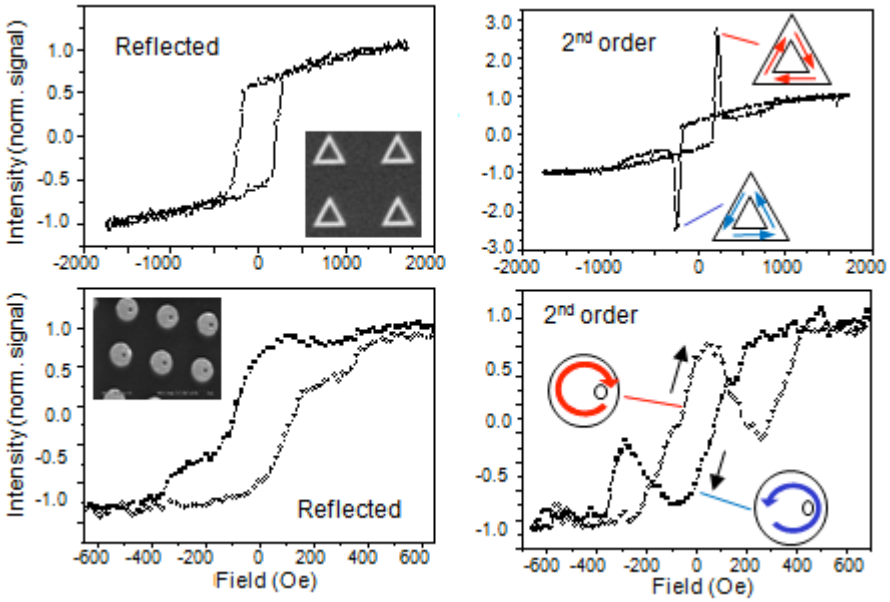

Figure 2: *Examples of hysteresis loops from arrays of dots shown in the scanning electron microscopy images in the insets, showing the unusual shapes of D-MOKE with respect to conventional MOKE loops measured from the reflected beam. In the specific cases shown, the unusual shape of D-MOKE loops is related to the nucleation of magnetic vortex states of well defined chirality.*

CONTROLLING FLUORESCENCE RESONANT ENERGY TRANSFER WITH A MAGNETO-OPTICAL NANOANTENNA

R. Vincent and R. Carminati

Institut Langevin, ESPCI ParisTech, CNRS, 10 rue Vauquelin,
75231 Paris Cedex 05, France

Energy transfer between a molecule in an excited state (donor) and a molecule in the ground state (acceptor) underlies many significant photophysical and photochemical processes, from photosynthesis to fluorescence probing of biological systems. Depending on the separation between the donor (D) and the acceptor (A), the process can be described accurately by various theories accounting for the electromagnetic interaction between the two species. For a D-A distance range on the order of 2 - 10 nm, which is relevant for photochemical studies and nanophotonics, the well established Förster theory [1] based on quasi-static dipole-dipole interaction has been very successful. It shows that while Förster Resonant Energy Transfer (FRET) is a very useful process which can be used, for example, as a ruler for spectroscopic measurements [2], it is a rather weak process which goes down as the inverse sixth power R^6 of the D-A separation [3].

In the present work, we use an established general framework for dipole-dipole energy transfer between an emitter and an absorber in a nanostructured environment [4]. The theory allows us to address FRET between a donor and an acceptor in the presence of a nanoparticle with an anisotropic electromagnetic response. Using Green function formalism [5], we show that the angular contribution, the distance behavior and the influence of the polarizability tensor of the nanoparticle can be identified and separated.

We also compare the contribution of the different non-radiative energy transfer channels: The direct (standard) Förster transfer and the energy transfer mediated by the nanoparticle. In this comparative study a new distance arise, in the spirit of the Förster radius, named polarization coupling radius Rp, which depends of the polarization properties of the nanoparticle.

We illustrate the formalism for the well known metallic nanoparticle, showing that this formalism could furnish insight in the understanding of the good quantities controlling this process and also for nanoparticle with anisotropic dielectric responses [6], e.g., nanoparticle made of a ferromagnetic material exhibiting a magneto-optical response. For which the degree of anisotropy can be controlled by an external static magnetic field. We discussed potential application for FRET tuning.

References:

[1] T. Förster, Ann. Phys. 437, 55 (1948); Discuss. Faraday Soc. 27, 7 (1959).
[2] L. Stryer, Annu. Rev. Biochem. 47, 819 (1978).
[3] L. Novotny, B. Hecht, Principles of Nanooptics, Cambridge University Press, (2006).
[4] R. Vincent, and R. Carminati, Magneto-optical control of Förster energy transfer, Phys. Rev. B, in press, (2011).
[5] R. Carminati, J.-J. Greffet, C. Henkel and J.M. Vigoureux, Optics Communications, 261, 2, 368 - 375, (2006).
[6] S. Albaladejo, R. Gómez-Medina, L. S. Froufe- Pérez, H. Marinchio, R. Carminati, J. F. Torrado, G. Armelles, A. García-Martín, and J. J. Sáenz, Opt. Express 18, 3556-3567 (2010).

TNA 2011
Trends in NanoApplications
Energy

TNA ENERGY 2011

INDEX: INVITED CONTRIBUTIONS

INDEX: INVITED CONTRIBUTIONS (OMNT SESSION)

INDEX: KEYNOTE CONTRIBUTIONS

INDEX: KEYNOTE CONTRIBUTIONS (OMNT SESSION)

INDEX: ORAL CONTRIBUTIONS

ALPHABETICAL ORDER

I: Invited / IM: Invited OMNT Session / K: Keynote / KM: Keynote OMNT Session / O: Oral

		pag
Roger Amade Rovira (Universitat de Barcelona, Spain) *"Carbon nanotubes lined by anodic deposition of MnO_2 for supercapacitor application"*	O	**485**
Franck Artzner (CNRS – IPR, France) *"Bio-inspired scaffolds to manufacture nanomaterials :nanotubes & Quantum Dots arrays"*	KM	**487**
Juan Bisquert (Universitat Jaume I, Spain) *"Dynamics and distribution of photogenerated carriers in organic solar cells and in dye solar cells"*	K	**489**
Fernando Briones (IMM-CNM-CSIC, Spain) *"Molecular Beam Epitaxy (MBE), a versatile tool to integrate model semiconductor nanostructures into advanced solar cell concepts"*	K	**491**
Annalisa Bruno (Imperial College London, United Kingdom) *"Exciton diffusion Length and morphology TFB/ fullerene blends"*	O	**493**
José C. Conesa (Instituto de Catálisis y Petroleoquímica, CSIC, Spain) *"Intermediate band materials for more efficient solar energy use: quantum modeling and experimental realizations"*	O	**495**
Anderson Dias (Universidade Federal de Ouro Preto, Brazil) *"Microwave synthesis and Raman scattering of nanostructured lanthanide-doped $NaTaO_3$ thermoelectric materials"*	O	**497**
Frédéric Favier (CNRS – ICG, France) *"Title not available"*	KM	**-**
Alejandro A. Franco (CEA-LITEN, France) *"Title not available"*	K	**-**
David Fuertes Marron (UPM, Spain) *"Chalcopyrite-based nanostructures: new prospects for highly efficient photovoltaic devices"*	K	**499**
Arnaldo Galbiati (Solaris Photonics, United Kingdom) *"A Novel Ultra Thin Film Photovoltaic Technology with Alkali Metal Active Region"*	O	**501**
Marcin Gorzny (CIC nanoGUNE, Spain) *"Synthesis of High-Surface-Area Platinum Nanotubes Using a Viral Template"*	O	**503**
Michaël Grätzel (EPFL, Switzerland) *"The advent of mesosocopic solar cells"*	I	**505**
Ladislav Kavan (J Heyrovsky Institute of Physical Chemistry, Czech Republic) *"Optically Transparent Cathode for Dye Sensitized Solar Cells Based on Graphene Nanoplatelets"*	O	**507**
Kazuhito Kinosita (Waseda Univ., Japan) *"A rotary molecular motor with amazing performance"*	IM	**-**
Elin Larsson (Applied Physics, Sweden) *"Indirect Nanoplasmonic Sensing in Catalysis: Sintering, Reactant Surface Coverage Changes and Optical Nanocalorimetry"*	O	**509**
Christophe Lethien (CNRS – IEMN, France) *"Silicon nanowires and nanopillars arrays for lithium-ion battery and micro-battery: overview, challenges and perspectives"*	KM	**511**
Antonio Luque (Univ Politécnica de Madrid, Spain) *"Nanotechnology for more efficient photovoltaics: the quantum dot intermediate band solar cell"*	I	**513**
Enrique Macia (UCM, Spain) *"Optimizing the thermoelectric figure of merit of aperiodic solids"*	O	**515**
Marisol Martin-Gonzalez (IMM-CSIC, Spain) *"Nanoengineering Thermoelectrics for Energy Harvesting."*	O	**517**
Jordi Martorell (ICFO, Spain) *"New routes for the fabrication of Organic Photovoltaic Cells"*	K	**519**
Emilio Mendez (Brookhaven National Laboratory, USA) *"Nanotechnology for the Energy Challenge"*	I	**-**

I: Invited / IM: Invited OMNT Session / K: Keynote / KM: Keynote OMNT Session / O: Oral

TNA ENERGY 2011

ABSTRACTS
ALPHABETICAL ORDER

CARBON NANOTUBES LINED BY ANODIC DEPOSITION OF MnO_2 FOR SUPERCAPACITOR APPLICATION

Roger Amade, Eric Jover, Shahzad Hussein and Enric Bertran

Department of Applied Physics and Optics, FEMAN Group, Universitat de Barcelona,
c/ Martí i Franquès 1, 08028 Barcelona, Spain
r.amade@ub.edu

Supercapacitors are energy storage devices that fill the gap between batteries and conventional capacitors, i.e. they have a specific power as high as conventional capacitors and a specific energy close to that of batteries [1]. They store electrical energy using either double-layer charging or fast surface redox reactions (pseudo-capacitors) [2]. Due to their outstanding properties (mechanical, electrical and thermal) and large surface area (1 to > 2000 $m^2 \cdot g^{-1}$) carbon nanotubes (CNTs) are suitable materials for the development of supercapacitors.

A dielectric layer of MnO_2 was anodically deposited lining the surface of CNTs (20-30 nm in diameter and about 10 μm long) previously grown by means of plasma enhanced chemical vapor deposition (PECVD) (Figure 1). This new method is characterized by the anodic deposition of MnO_2 on CNTs in conditions of low Mn^{2+} concentration, providing a slow diffusion that warrants an homogeneous lining of the CNTs. On the other hand, this method avoids the kite growth of manganese dioxide on CNTs. The electrochemical properties of the obtained electrodes were characterized using cyclic voltammetry with scan rates ranging from 10 to 150 $mV \cdot s^{-1}$, galvanostatic charge-discharge techniques and impedance spectroscopy (in the range 10^{-1} - 10^4 Hz). The improvement of the electrochemical characteristics of the electrodes (showing up to 642 $F \cdot g^{-1}$ of specific capacitance) has been discussed in terms of the morphology and structure of the samples analyzed by scanning electron microscopy (SEM) and transmission electron microscopy (TEM).

References:

[1] C. Peng, S. Zhang, D. Jewell and G.Z. Chen, Prog. Nat. Sci., 18 (2008) 777.
[2] P. Simon, Y. Gogotsi, Nature Mat., 7 (2008) 845.

Figures:

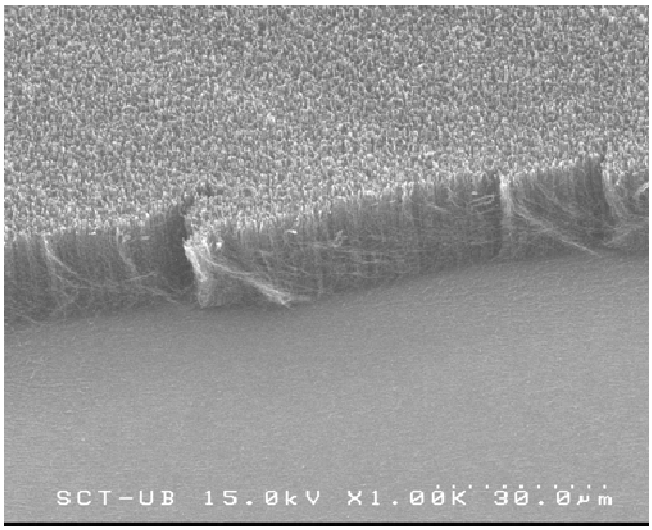

Figure 1: *Vertically aligned CNTs (VACNTs) obtained by means of PECVD. Fe catalyst thickness layer: 3 nm, annealing temperature: 680ºC.*

BIO-INSPIRED SCAFFOLDS TO MANUFACTURE NANOMATERIALS: NANOTUBES & QUANTUM DOTS ARRAYS

Franck Artzner

Biomimetic Self-Assemblies – UMR 6251 CNRS- Université Rennes1, France
franck.artzner@univ-rennes1.fr

Nature is an unlimited source of inspiration for the development of materials presenting original optical properties. The current structural knowledge of some of these biological assemblies is promising as an inspiration source to try to mimics their supramolecular organizations. The development of simplified system presenting properties close to biological assemblies is of great interest. To this end, there is still a long way in order to understand not only the structures, but also their formation mechanisms.

Lanreotide molecules self-assemble in water into highly monodisperse supramolecular nanotubes, the diameter and wall thickness of which are 244Å and 18Å respectively. [1] Following biomineralization principles, we show that the self-assembled nanotubes can be used as a template to produce micron-long, bilayered silica nanotubes having a monodisperse diameter of 29 nm. The nanotubes organize spontaneously into centimeter-size, highly ordered bundles. Furthermore, the formation mechanism was elucidated using a range of techniques, including X ray diffraction, optical and electron microscopy [2].

Lamellar hybrid condensed phase in which the QDs are densely packed in the plane of the layers can be prepared [3]. The 3D crystallization of the QDs can be achieved by the addition of actin proteins that polymerize into filaments with well defined pitch and diameter. New photophysical properties will be presented.

These examples of bio-inspired technologies demonstrate the possibility of solving the challenge of efficiency, less expensive and environmental technologies.

References:

[1] Biomimetic organization : octapeptide self assembly into nanotubes of viral capsid like dimension C. Valéry, M. Paternostre, B.Robert, T. Gulik-Krzywicki, T. Narayanan, J.-C. Dedieu, G. Keller, M.-L. Torres, R. Cherif-Cheikh, P. Calvo & F. Artzner Proc. Natl. Acad. Sci. USA, 2003,100(18), 10258-10262.

[2] Hierarchical architectures by synergy between dynamical template self-assembly and biomineralization, E. Pouget, E. Dujardin, A. Cavalier, A. Moreac, C. Valéry, V. Marchi-Artzner, T. Weiss, A. Renault, M. Paternostre, F. Artzner Nature Materials, 2007, 6, 434-439.

[3] Interaction between water-soluble peptidic CdSe/ZnS nanocrystals and vesicles: formation of hybrid vesicles and condensed lamellar phases, A. Dif, E. Henry, F. Artzner, M. Baudy-Floc h, M. Schmutz, M. Dahan, V. Marchi-Artzner, J. Am. Chem. Soc., 2008, 130(26), 8289-8296.

DYNAMICS AND DISTRIBUTION OF PHOTOGENERATED CARRIERS IN ORGANIC SOLAR CELLS AND IN DYE SOLAR CELLS

Juan Bisquert

Grup de Dispositius Fotovoltaics I Optoelectrònics, Dep. de Física,
Avda Sos Baynat sn, 12071 Castelló, Spain
bisquert@fca.uji.es

Based on large experience on DSC characterization by Impedance Spectroscopy (IS), we are now interested to provide detailed understanding of the factors determining the cell performance.[1] I discuss here the relation between recombination resistance and capacitance of the cell measured by IS, with the j-V curve both in the dark and under (1 sun) illumination. The most challenging aspect of the analysis is to separate the change of conduction band position from an array of charge transfer kinetics factors. This is not trivial since surface changes induced by the presence of the dye may affect both the beta parameter that modifies the fill factor, and slow the charge transfer kinetics, by surface blocking or other factors. We can provide a detailed energetic map that allows to explore innovations such as the new redox couple with more positive potential, or alternative nanostructure. Similar methods can be applied in quantum dot sensitized solar cell to speed up the progress oh these cells that is developing strongly in the last few years.[2]

In organic solar cells, it is important to obtain a picture of the carrier distribution, first in the dark, when the system is in equilibrium, and then at progressive illumination, and as a function of the potential.[3] We discuss our views on this which is obtained from measurement, specifically by scanning the capacitance over a broad set of conditions. This has been done in the standard PCM/P3HT configuration, some important informations about the carrier distribution can be obtained, and implications for open-circuit voltage are discussed.

References:

[1] Fabregat-Santiago, F.; Garcia-Belmonte, G.; Mora-Seró, I.; Bisquert, J. "Impedance spectroscopy of hybrid and organic solar cells". Physical Chemistry Chemical Physics 2011, 10.1039/C1030CP02249G

[2] Gónzalez-Pedro, V.; Xu, X.; Mora-Seró, I.; Bisquert , J. "Modeling High-Efficiency Quantum Dot Sensitized Solar Cells". ACS Nano 2010, 4, 5783–5790

[3] Boix, P. P.; Ajuria, J.; Etxebarria, I.; Pacios, R.; Garcia-Belmonte, G.; Bisquert, J. "Role of ZnO Electron-Selective Layers in Regular and Inverted Bulk Heterojunction Solar Cells". Journal of Physical Chemistry Letters 2011, 2, 407–411

Figures:

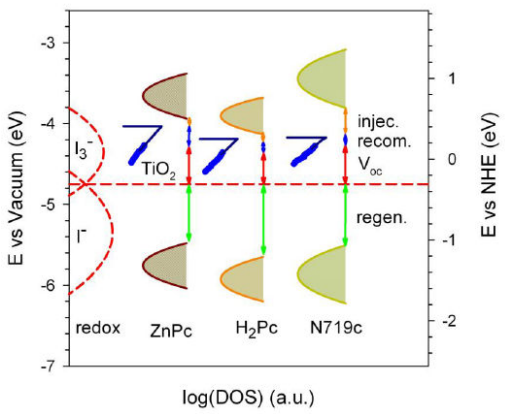

Figure 1: *Energetocs of dye solar cells with different types of dyes.*

MOLECULAR BEAM EPITAXY (MBE), A VERSATILE TOOL TO INTEGRATE MODEL SEMICONDUCTOR NANOSTRUCTURES INTO ADVANCED SOLAR CELL CONCEPTS

F.Briones, J. M. Ripalda, D. Alonso-Álvarez, B. Alén, J. M. Llorens, A. G. Taboada, M. L. Dotor, Y. González

IMM-Instituto de Microelectrónica de Madrid (CNM-CSIC),
Isaac Newton 8, 28760 Tres Cantos, Spain
briones@imm.cnm.csic.es

Semiconductor quantum nanostructures are at the base of advanced designs for high efficiency photovoltaic solar cells. MBE technology is an advanced and versatile technique to create highly perfect single-crystalline semiconductor heterostructures with superb control of dimensions, composition and doping in the nanoscale. In particular, this technique is perfectly adequate to epitaxialy grow complete device structures containing tailor designed nanostructures, due to its compatibility with a variety of in-situ control and characterization techniques. We will describe how MBE is applied at IMM to create model solar cell structures incorporating self-assembled Quantum Dots stacks and Quantum Posts in the InAs/GaAs or InAs/InP systems, together with sharp tunnel junctions, that should allow to test ideas, to study physics of novel structures and to obtain realistic estimations on the feasibility of advanced designs for high efficiency solar cells as the IB concept [1]

After a brief introduction on the peculiarities and applications of MBE, a more detailed description will be given of the principles and techniques used to design, monitor and control the strain distribution, accumulation and compensation. Examples will be presented of cells containing heterostructures and materials with large lattice parameter mismatch and corresponding large local strains. The incorporation of Phosphorus or Antimony as strain creating or compensating elements results in interesting device properties [2]. As a particular case of extreme difficulty, the fabrication of GaAs solar cells, with a large number of stacked QDs layers in the intrinsic zone to enhance QD absorption characteristics without generating dislocations, will be considered. [3]

As a further example, the techniques to grow a new type of nanostructures, Quantum Posts, will be considered. Main interest of using quantum posts instead of quantum dots to form the intermediate band is intimately related with their elongated shape, and hence their potential to tailor the absorption of the photons that cause transitions from the IB to the CB. Typical QDs grown in the Stranski-Krastanov mode have a flat shape with the vertical dimension shorter than the lateral ones. Producing QDs with increased vertical dimension can increase the transition element related to IB to CB transitions and therefore increase the absorption associated to this transition. Stacking several QDs (that is, creating a QP) can be a way to produce the desired aspect ratio. On the other hand, it is of interest to research on the non delta-like density of states introduced by the QPs to investigate the limits in which the extra density of states introduced does not jeopardize the voltage preservation predicted for the IBSC.

Quantum posts are assembled by epitaxial growth of closely spaced quantum dot layers, modulating the composition of a semiconductor alloy, typically InGaAs. In contrast with most self-assembled nanostructures, the height of quantum posts can be controlled with nanometer precision, up to a maximum value limited by the accumulated stress due to the lattice mismatch. Here we present a strain compensation technique based on the controlled incorporation of phosphorous, which substantially increases the maximum attainable quantum post height. The luminescence from the resulting nanostructures presents giant linear polarization anisotropy.

Finally, novel process techniques, derived from the understanding of MBE growth kinetics in the research environment, but applicable to other materials and polycrystalline thin film structures, will be discussed in view of their application to solar cell commercial fabrication.

We conclude that in the next future, similarly to what has been happening in the microelectronics field, a remarkable photovoltaic cell sophistication and efficiency will be compatible with a large scale, low cost industrial scenario.

References:

[1] A. Luque and A. Marti, Phys. Rev. Lett. 78, (1997) 5014
[2] Diego Alonso-Álvarez, Benito Alén, Jorge M. García, J. M. Ripalda, Appl. Phys. Lett. 91, (2007) 263103
[3] D. Alonso-Álvarez, A. G. Taboada, J. M. Ripalda, B. Alén, Y. González, L. González, J. M. García, F. Briones, Appl. Phys. Lett. 93, (2008)123114

Figures:

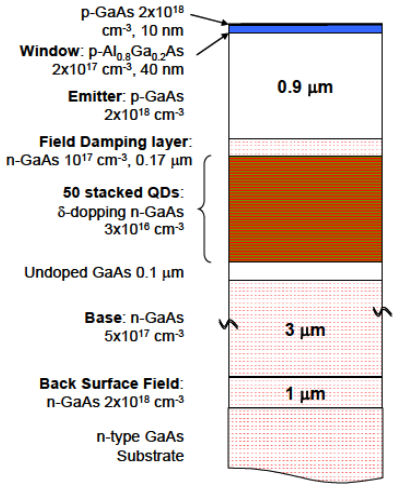

Figure 1: Solar Cell structure

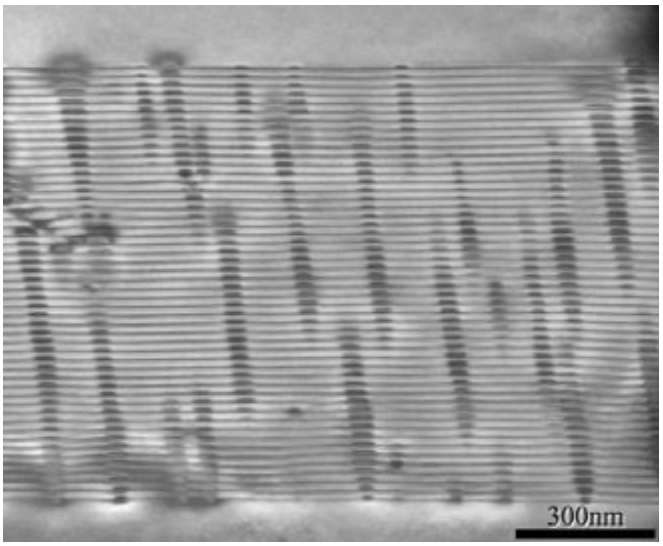

Figure 2: TEM image (<1-10> plane) of the 50 stacked QDs solar cell with SC

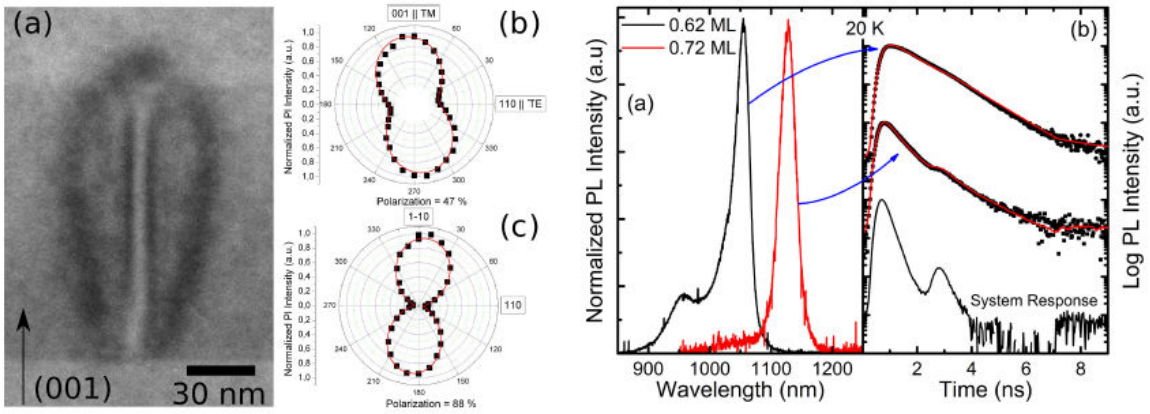

Figure 3: Lef : (a) TEM detail of a QP. Middle: Linear polarization of light emitted along the (b) cleaved edge and (c) growth direction. Right: (a) PL of QPs with different In content and (b) their corresponding time resolved PL decay curves.

EXCITON DIFFUSION LENGTH AND MORPHOLOGY IN TFB/ FULLERENE BLENDS

Annalisa Bruno[1], Luke Reynolds[1], Clare Dyer-Smith[2], Jenny Nelson[2], Saif Haque[1]

[1]Department of Chemistry, Imperial College London, London, United Kingdom;
[2]Department of Physics, Imperial College London, London, United Kingdom
abruno@ic.ac.uk

Organic materials present a promising direction for potentially cheaper solar cells and to allow the construction of mechanically flexible cells. Although recent bulk-heterojunction devices have given really encouraging performances, reaching efficiencies around 8% [1], more work is needed in order to be able to understand the energy losses within these devices, and so increase their efficiency.

As many recent studies have outlined, the excited state dynamics and the processes occurring at the donor-acceptor (D/A) interface [2-4] are critical to the performance of solar cells. The efficiency of charge separation at the D/A interface is crucial to the photocurrent generation in organic solar cells, and a complete understanding of this process is essential in order to be able to maximize the power generation efficiency.

In fact in a polymer-based photovoltaic device light absorption by the polymer usually results predominantly in formation of excitons that diffuse through the polymer layer to reach the interface with the electron acceptor, there they can dissociates into a electrostatically bound charge pair. The pair then separates into a positive polaron in the donor and a negative polaron in the acceptor, which are then transported to the respective electrodes. [5,6].

Here we present a recent work performed using a fluorescence up-conversion technique to systematically study the effect of using three different types of acceptors as [6,6]-phenyl-C61 butyric acid methyl ester (mono-PCBM) and its multi-adduct analogues bis-PCBM and tris-PCBM on the emission quenching and morphology in [9,9-dioctylfluorene-co-N-(4-butylphenyl)-diphenylamine] (TFB) blends. All molecular structures are reported in figure 1.

The innovative experimental set up allows us to probe the ultrafast (<1 ps) excited state dynamics of photo-generated species with a high resolution (<200 fs). This means that we are able to follow the formation of the excited state in the polymer and the charge separation process at the interface with the acceptor.

The ultrafast fluorescence quenching for the three different acceptors has been correlate with the different blends morphologies. Moreover a new excitons dynamic model has been developed to reproduce the experimental quenching rates and in order to evaluate their diffusion length, for the first time from the ultrafast fluorescence measurements. We also present independent measurements of diffusion length to support our evaluation.

When coupled with other standard spectroscopic techniques the exciton recombination dynamics of such systems allow quantitative design rules to be formalized which is essential for the continued development of highly efficient organic bulk hetero-junction PV devices.

References:

[1] Y Liang, Z. Xu, J. Xia, S. Tsai, Y. Wu, G.Li, C. Ray, L. Yu, Advanced Materials 22 (2010) 2696
[2] J.J.Benson-Smith, H. Ohkita, S. Cook, J.R. Durrant, D.D.C. Bradley, J.Nelson, Dalton Transactions, 2009 (2009)10000.
[3] D Veldman, S.C.J. Meskers, R.A.J. Janssen, Advanced Functional Materials 19 (2009) 1
[4] M.A. Faist, P.E. Keivanidis, S. Foster, P.H. Wöbkenberg, T.D. Anthopoulos, D.D.C. Bradley, J. Durrant, J. Nelson, Journal of Polymer Science Part B: Polymer Physics 49 (2010) 45
[5] V, Mihailetchi, L. J. A Koster, J. C. Hummelen, P.W.M. Blom, Physical Review Letters 93 (2004) 216601.
[6] E. Hendry, J.M. Schins, L.P. Candeias, L.D.A. Siebbeles, M. Bonn, Physical Review Letters 92 (2004) 196601.

Figures:

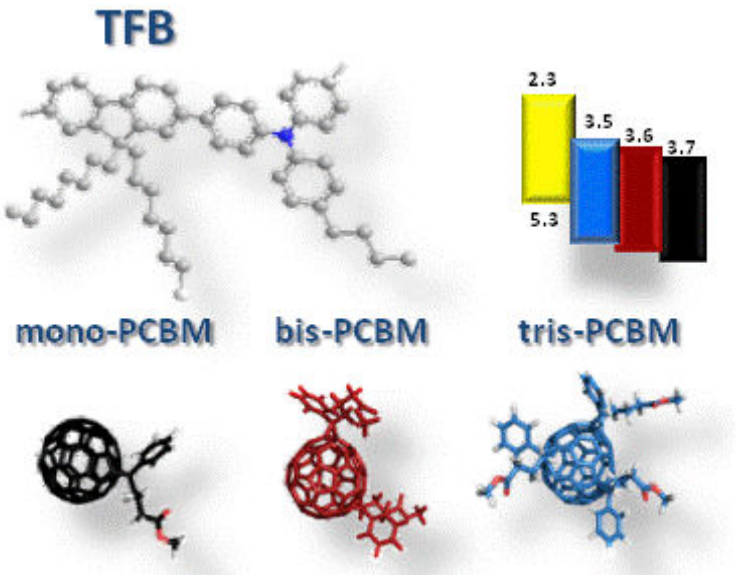

Figure 1: *TFB molecular structure and energy levels are reported in the upper part. MonoPCBM, bisPCBM, and trisPCBM molecular structures are in the lower part.*

INTERMEDIATE BAND MATERIALS FOR MORE EFFICIENT SOLAR ENERGY USE: QUANTUM MODELING AND EXPERIMENTAL REALIZATIONS

J. C. Conesa, P. Wahnón, R. Lucena, P. Palacios, I. Aguilera, F. Fresno, Y. Seminovski

*Instituto de Catálisis y Petroleoquímica, CSIC, Marie Curie 2, 28049 Madrid, Spain
#Instituto de Energía Solar, Univ. Politécnica de Madrid, Ciudad Universitaria s/n, Madrid, Spain
jcconesa@icp.csic.es

The intermediate band (IB) solar cell (Fig. 1) has been proposed [1] to increase photovoltaic efficiency by a factor above 1.5, based on the absorption of two sub-bandgap photons to promote an electron across the bandgap. To realize this principle, that can be applied also to obtain efficient photocatalysis with sunlight, we proposed in recent years several materials where a metal or heavy element, substituting for an electropositive atom in a known semiconductor that has an appropriate band gap width (around 2 eV), forms inside the gap the partially filled levels needed for this aim. After studying Ga(As,P) with Ga partially substituted by Ti or Cr [2], we proposed several systems that could be made in thin film form:

a) Ti- or Cr- substituted $CuGaS_2$ or similar chalcopyrite (Fig. 2), where the thermodynamics of formation is seen to be less disfavourable than e.g. insertion of Mn in GaAs [3];

b) In_2S_3 and other sulphides containing octahedral In, which when doped with Ti or V form also the IB according to quantum calculations [4] (Fig. 3). The V-doped In_2S_3 material is particularly promising. Being based on a binary compound host, controlling its stoichiometry should be easy. In addition In_2S_3, with E_g= 2.0 eV, is used as buffer layer in thin film CIGS PV cells, so that the known technology to make it in thin film form could be used. Besides, we have synthesized it in nanocrystalline form [5] and shown that its optical absorption spectrum has the features predicted by quantum calculations for the IB structure (Fig. 4). Furthermore, recent photocatalytic tests made with it [6] show that the V dopant extends its spectral response down to the IR range without increasing recombination, which would decrease its efficiency.

c) Octahedral Sn^{IV} sulphide and other similar compounds show also, according to DFT modeling (Fig. 5), the formation of an IB with the desired characteristics when V, Nb or similar metals are introduced at Sn sites [7]. The experimental synthesis of such sulphide is in progress, and first results obtained show optical absorption spectra matching again the expectations for an IB material (Fig. 6).

d) Another class of IB materials consists of Si heavily doped with certain elements. With Ti as dopant the desired IB electronic structure appears (Fig. 7) if Ti lies at interstitial sites [8]. Such material has been prepared by ion implantation methods, and its electrical properties [9] show uncommon features that can be explained assuming the formation of a partially filled band a few tenths of eV below the conduction band, as predicted by the DFT calculations. Although its band gap is not optimum to get high efficiency, it can serve as benchmark to study the behaviour of IB materials in single-crystal form. We could also show that substitution of Si by S or Se, accompanied by hole doping, provides an IB material as well [10].

e) Finally we showed with DFT calculations that a clathrate-type silicon polymorph, that in pure form has E_g=1.9 eV and for which some thin film preparation recipes exist, forms an IB material when a metal as Ag is occluded in its cavities or some of its Si atoms are substitued by a transition metal as V [11] (Fig. 8).

References:

[1] Luque and A. Martí, Phys. Rev. Lett. 78 (1997) 5014
[2] P. Palacios et al. Phys. Rev. B 73 (2006) 085206; ibid. J. Chem. Phys. 124 (2006) 014711
[3] P. Palacios et al. Thin Solid Films 515 (2007) 6280; ibid. J. Phys. Chem. C 112 (2008) 9525
[4] P. Palacios et al. Phys. Rev. Lett. 101 (2008) 046403
[5] R. Lucena et al. Chem. Maters. 20 (2008) 5125
[6] R. Lucena and J.C. Conesa, in preparation

[7] P. Wahnón et al., in preparation
[8] K. Sánchez et al. Phys. Rev. B 79 (2009) 165203
[9] G. González-Díaz et al., Solar En. Mater. Solar Cells 93 (2009) 1668
[10] K. Sánchez et al. Phys. Rev. B 82 (2010) 165201
[11] P. Wahnón et al., in preparation

Figures:

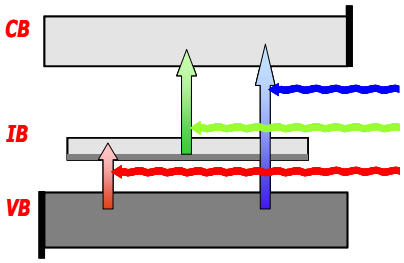

Figure 1: *TFB Scheme of operation of an intermediate band photovoltaic cell*

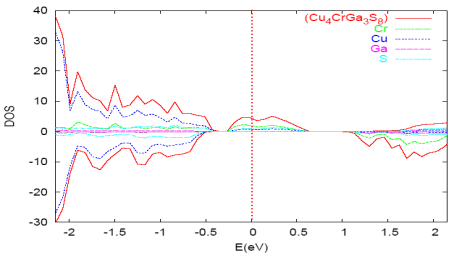

Figure 2: *Density of states (computed with DFT) of $CuGaS_2$ with Ga partially substituted by Cr*

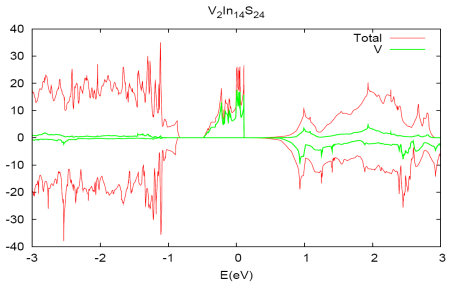

Figure 3: *Density of states (computed with DFT) of In_2S_3 with octahedral In partially substituted by V*

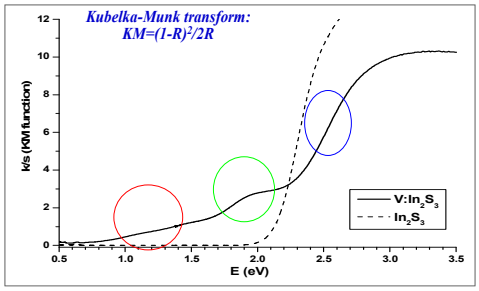

Figure 4: *Experimental diffuse reflectance spectrum of pure and V-doped nanocrystalline In_2S_3*

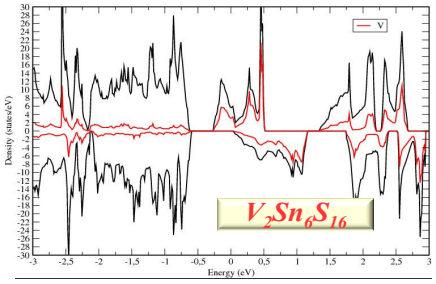

Figure 5: *Density of states (computed with DFT) of SnS_2 with Sn partially substituted by V*

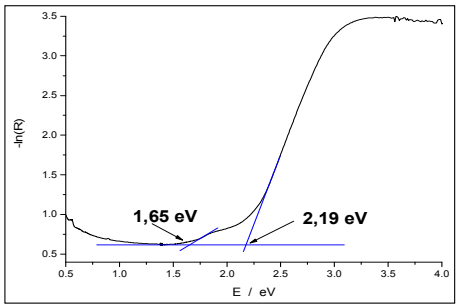

Figure 6: *Experimental diffuse reflectance spectrum of V-doped nanocrystalline SnS_2*

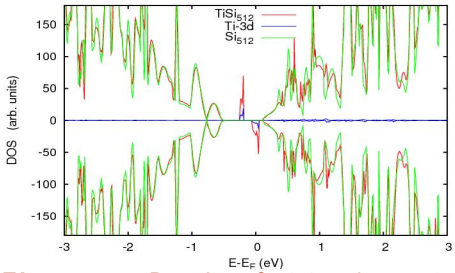

Figure 7: *Density of states (computed with DFT) of Si with Ti located in an interstitial site*

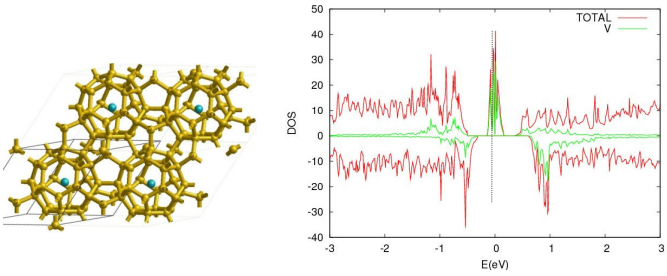

Figure 8: *Estructure of Si clathrate, and density of states computed for it when V substitutes for Si atoms in the lattice*

MICROWAVE SYNTHESIS AND RAMAN SCATTERING OF NANOSTRUCTURED LANTHANIDE-DOPED NATAO3 THERMOELECTRIC MATERIALS

Anderson Dias

Universidade Federal de Ouro Preto, Department of Chemistry, ICEB II, Sala 67, Ouro Preto-MG, Campus Morro do Cruzeiro, 35400-000, Brazil
anderson_dias@iceb.ufop.brl

In the near future, the increasing energy demand will require the energy harvesting of any dispersed energy in industrial processes such as combustion machines, nuclear, geothermal, photovoltaic or solar-thermal devices. For this application, thermoelectric ceramic materials with adequate efficiency appear as the most promising because to their high thermal and chemical stabilities. The production of nanomaterials for energy generation with optimized properties is a challenge in the 21st century. In this respect, environmentally-friendly processes are being currently largely applied to the production of these technological materials. Among the methods nowadays employed to synthesize nanostructured materials, the hydrothermal process is well established for the production of a huge number of important electroceramics. More recently, the use of microwave energy associated with hydrothermal vessels has become a promising route to the production of nanosized materials, offering advantages in comparison with conventional methods, such as low-energy consumption associated with faster precipitation kinetics [1]. Thus, these so-called environmentally-friendly methods are being extensively studied for the production of a wide range of materials. The literature shows some examples of thermoelectric materials designed for energy saving, particularly, Nb-doped $SrTiO_3$ [2], $KTaO_3$, Fe-doped and Ag-doped $NaTaO_3$ [3], and Mn,Cr,Fe,Ti-doped $NaTaO_3$ [4]. $NaTaO_3$ belongs to the family of orthorhombically distorted perovskites with $GdFeO_3$-type structure, which has been determined as *Pbnm* (Z=4) [5]. This structure rules out the possibility of ferroelectricity for this compound, claimed previously by some authors [6], and showed by similar materials like $NaNbO_3$ [7] and $BiInO_3$ [8]. Also, $NaTaO_3$ attracts our attention because it attains the highest photocatalytic quantum yield for water splitting into H_2 and O_2 under UV irradiation among all known materials, exceeding 50%, when doped with La [9]. For these materials, there are no reports on microwave synthesis of lanthanide-doped sodium tantalate. Also, aiming to thermoelectric applications, spectroscopic data could be useful for photodynamic investigations, as well as for structural studies. In this work, lanthanide-doped $NaTaO_3$ nanostructured ceramics were synthesized under microwaves. Raman scattering was used in order to determine the number of vibrational bands and the selection rules based on group-theory calculations. Raman spectroscopy was also employed to investigate the phonon evolution as a function of temperature in order to determine the three high temperature phases. Finally, thermoelectric properties were evaluated as a function of temperature and the results were discussed in terms of structural properties as observed by Raman spectroscopy.

$NaTaO_3$ was obtained from stoichiometric amounts of analytical grade reagents NaOH and $TaCl_5$. After dissolution of each reagent in deionised water (18.2M.cm), they were mixed under stirring and pH=13. A Milestone BatchSYNTH equipment (2.45 GHz) was employed in the microwave syntheses. Double-walled digestion vessels (100 mL of capacity) with an inner line and cover made of Teflon Tetrafluormethaxil (TFM) and an outer high strength vessel shell made of Polyether ether keton (PEEK) were used. The EasyControl Software was employed to draw a temperature-pressure-time profile, which include a heating time of 2 min up to the processing temperature (110°C and 150°C), for times of 10 and 20 min, for the production of the desired materials (the final conditions were 110±1°C, 150±1°C and 1.2±0.2 bar). The magnetic stirring module was used to produce consistent stirring of solutions in all vessels, independent of their position within the cavity. After microwave syntheses, the products were rinsed with deionized water several times and dried at 70°C. The powders were uniaxially pressed at 110 MPa into cylindrical discs of 5mm height and 15mm diameter. The sintering occurred in a covered alumina crucible at 1400°C, for 4h. The obtained ceramics were dense, showing experimental densities above 93% of their theoretical densities. X-ray diffraction technique was employed to study the structural properties using Fe$K\alpha$ radiation, while transmission electron microscopy and high-resolution TEM were carried out to investigate the morphology and crystalline aspects of the nanopowders. Micro-Raman spectra were collected in back-scattering configuration by using an Olympus confocal microscope attached to a Horiba/Jobin-Yvon LABRAM-HR spectrometer, and equipped with 600 and 1800 grooves/mm diffraction gratings. The 632.8 nm line of a He-Ne laser

was used as exciting line and a Peltier-cooled charge coupled device (CCD) detected the scattered light. An edge filter was employed to stray light rejection (Rayleigh).

The TEM (HRTEM) and selected area electron diffraction images for the Er-doped $NaTaO_3$ are showed in Figure 1, where it can be seen crystalline, nanostructured materials, as evidenced by X-ray diffraction after microwave synthesis. The Raman spectrum of Nd-doped $NaTaO_3$ at room temperature is presented in Figure 2. It was possible to discern 21 bands (although some of them, which are very weak and broad, could be combination modes), in good agreement between the predicted and observed number of fundamentals, considering that modes belonging to different i.r. cannot be resolved by unpolarised spectroscopy of unoriented ceramics. It is also worthy noticing the peak splitting of the TaO_6 octahedra mode above $550cm^{-1}$ into several bands (the five or six higher frequency bands), due to the multiple numbers of ions into the unit cell. The same feature occurs relatively to the other regions of the spectra, i.e., we can clearly identify groups of bands in the regions $60\text{-}240cm^{-1}$ (six Na translations), $240\text{-}400cm^{-1}$ (three TaO_6 bending modes) and $400\text{-}520cm^{-1}$ (six TaO_6 rotations or tilting modes). All these features were directly related to the thermoelectric characteristics, as will shown later.

References:

[1] A. Dias et al. Chem. Mater. 15 (2003) 1344-1352.
[2] S. Ohta et al. Appl. Phys. Lett. 87 (2005) 092108.
[3] W. Wunderlich. J. Nuclear Mater. 389 (2009) 57-61.
[4] W. Wunderlich and S Soga. J. Ceram. Proc. Res. 11 (2010) 233-236.
[5] M. Marezio et al. Acta Cryst. B, 26 (1970), 2008–2022.
[6] H.F. Kay and J.L. Miles. Acta Cryst. 10 (1957) 213–218.
[7] S. Lanfredi et al. Appl. Phys. Lett. 80 (2002) 2731–2733.
[8] A.A. Belik et al. Chem. Mater. 18 (2006) 1964–1968.
[9] A. Kudo and H. Kato. Chem Phys. Lett. 331 (2000) 373-377.

Figures:

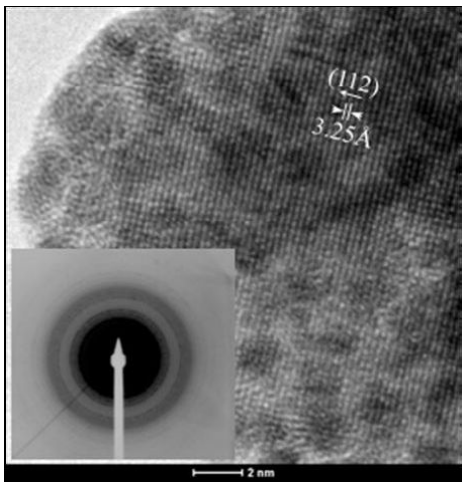

Figure 1: *HRTEM and SAED images for the Er-doped $NaTaO_3$ obtained under microwaves at 110ºC*

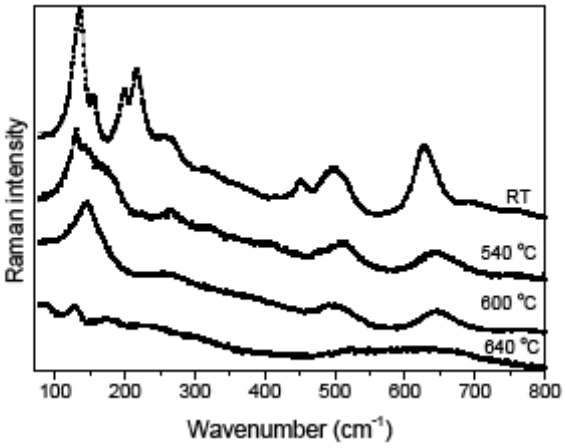

Figure 2: *Raman spectra of Er-doped $NaTaO_3$ at different temperatures.*

CHALCOPYRITE-BASED NANOSTRUCTURES: NEW PROSPECTS FOR HIGHLY EFFICIENT PHOTOVOLTAIC DEVICES

David Fuertes Marrón

Instituto de Energía Solar - ETSIT, Universidad Politécnica de Madrid,
Ciudad Universitaria s.n.,28040 Madrid, Spain
dfuertes@ies-def.upm.es

Cu-containing, chalcopyrite-based solar cells currently lead the energy conversion efficiency ranking of photovoltaic devices based on thin-film technology. With record figures above 20% for 0.5 cm^2 smallarea devices [1] and 15.7% for commercial 1 m^2 modules [2], thin-film photovoltaics is approaching the typical performing ratios of polycrystalline silicon. Not only in terms of efficiency, but also industrial production capacity, thin film photovoltaics is becoming a key player in the development of solar electricity generation [3].

The progress achieved in the performance of chalcopyrite-based photovoltaic devices, by far the most promising approach among all thin-film technologies, has largely been a consequence of phenomenological rather than a fundamental understanding of some of their physical properties. Although a number of important questions remain unanswered, it is already clear that Cu-containing chalcopyrites have unique properties not observed in other semiconducting materials. Such properties are often counterintuitive and challenge our common understanding of semiconductor physics, raising, amongst others, the following questions: how can grain boundaries, ubiquitous in thin films of microcrystalline material, be harmless (if not beneficial) to the electronic transport? Why is it that we can build an efficient electronic device out of a piece of semiconductor even when we are unable to extrinsically control its doping level? Why, ultimately, are the highest efficiencies systematically recorded in devices made from microcrystalline-based material, and not mono-crystalline counterparts? And finally, how can we explain why good solar cells have absorbers with off-stoichiometric compositions?

In this presentation, we will first briefly address some of these intriguing questions and discuss some recent results of research on such topics, highlighting the key role played by material characterization at the nanoscopic level in the search of convincing answers. We will then discuss growth, characterization and design of nanostructures based on Cu-containing chalcopyrites, not only as a means to implement large-scale, thin-film production, but additionally to open new possibilities for the realization of advanced photovoltaic devices beyond conventional architectures. Finally, the current status of research on nanocrystalline chalcopyrites will be reviewed, addressing the fundamental points for their utilization in highly efficient devices.

References:

[1] M.A. Green, K. Emery, Y. Hishikawa, W. Warta, Progress Photovol. Res. & Appl., 19 (2011) 84.
[2] http://www.miasole.com/sites/default/files/MiaSole_release_Dec_02_2010.pdf, press release.
[3] http://investor.firstsolar.com/phoenix.zhtml?c=201491&p=irol-newsArticle&ID=1482647&highlight=, press release.

A Novel Ultra Thin Film Photovoltaic Technology with Alkali Metal Active Region

Arnaldo Galbiati

Solaris Photonics, London, United Kingdom
admin@solaris-photonics.com

The aim of this paper is to discuss the development of a novel ultra thin film photovoltaic technology which employs alkali metals [1] as key photoactive material to directly convert photons of light into electricity. Alkali metals possess the unique property among all the other elements in the periodic table of being able to be ionized by photons of visible light, which is the reason why they are the key component in vacuum photocathode-photomultiplier technology for high efficiency light detection. The proposed photovoltaic devices make use of an ultra thin photoactive alkali layer (<20nm) coupled with a tunnelling junction (<5 nm) of insulating material (i.e.: Si_2O) on top of which a high work function (~5eV) transparent electrode (e.g.: graphene, carbon, gold) is deposited, while on the alkali photoactive side an electron injecting transparent electrode (<20nm) is fabricated using a material with a work function lower than 5 eV (e.g.: Aluminium ~4.2 eV). The transparent electrodes allow visible light to reach the alkali photoactive layer and thus induce the emission of electrons, those emitted electrons are then able to pass through the tunnelling junction to reach the anode (whereas holes are blocked) and induce an electric current in the device due to the internal electric field created by the difference in the work functions of the different layers (Figure 1).

These novel photovoltaic devices have a theoretical quantum efficiency > 30%, and can be readily fabricated using standard physical vapour deposition techniques already employed in industry.

References:

[1] Galbiati, “A thin film photovoltaic device with alkali metal active region”, patent GB2468526A, (2010)
[2] Elster and Geitel, “On the discharge of negative electric bodies by sun and daylight”, Ann. Physik, Vol. 38, (1889) pp. 497-514
[3] Albert Einstein, "On a Heuristic Viewpoint Concerning the Production and Transformation of Light", Annalen der Physik 17, (1905) pp. 132–148

Figures:

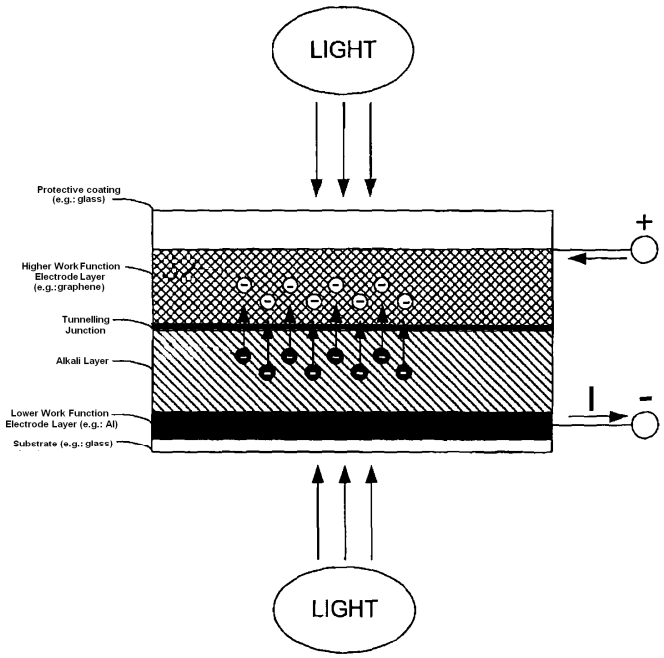

Figure 1: *Sectional view of the structure of an ultra thin film photovoltaic device with alkali metal active region.*

SYNTHESIS OF HIGH-SURFACE-AREA PLATINUM NANOTUBES USING A VIRAL TEMPLATE

Marcin Ł. Górzny[1,2], Alex S. Walton[2], Stephen D. Evans[2], Alexander Bittner[1]

[1]CIC nanoGUNE Consolider, Tolosa Hiribidea, 76, E-20018 Donostia – San Sebastian, Spain,
[2]School of Physics and Astronomy, University of Leeds, Woodhouse Lane, LS2 9JT, Leeds, UK
m.gorzny@nanogune.eu

The demand for green, efficient, low-cost, portable energy supplies has never been greater. One promising approach is the use of fuel cells such as the direct methanol fuel cell (DMFC). These promise significant increase (×10) energy density storage over conventional lithium-ion batteries, with potential to reach levels of 4.8 $kWhL^{-1}$ (or 6.1 Whg^{-1}). A key component in such DMFCs is the anode, at which methanol is oxidized, to produce carbon dioxide, hydrogen ions and electrons. Platinum (and its alloys) has proven to be a material with strong potential for use as an anode, due to its ability to adsorb hydrogen.

A novel method for the synthesis of high surface area, Platinum - Tobacco mosaic virus (Pt-TMV) nanotubes is presented. Platinum salt is reduced to metallic form on the external surface of a rodshaped TMV by methanol, which serves as a solvent and reductant simultaneously. The method provides enhanced control of surface roughness and Pt thickness than under strongly reducing conditions (eg DMAB or $NaBH_4$). It was found that for the same Pt loading, Pt-TMV nanotubes had electrochemically active surface area (ECSA) 3.7 times larger than Pt nanoparticles. The Pt-TMV system, used as a catalyst for methanol oxidation, shows 65% higher catalytic mass activity than catalyst based on Pt nanoparticles [1]. Whilst we present results for coating of TMV, the route is more general and should work on any charged protein/surfactant system.

References:

[1] Marcin Ł. Górzny, Alex S. Walton, and Stephen D. Evans, Adv. Funct. Mater., 2010, 20, 1295-1300

Figures:

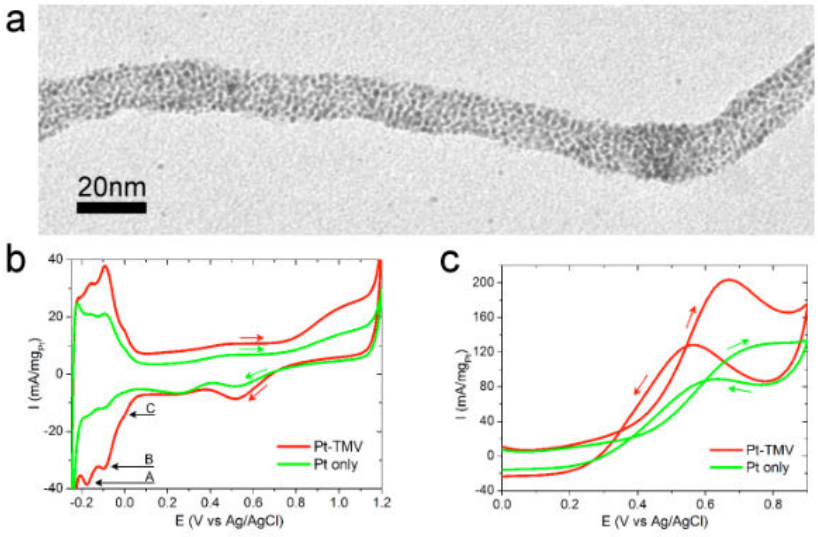

Figure 1: *TEM image of Pt-TMV nanotube (a). Panel b, shows two cyclic voltammogram curves corre sponding to Pt-TMV (red trace) and PtNPs (green trace) in 0.5 M H_2SO_4. Peaks A, B and C correspond to hydrogen adsorption on Pt(110), Pt(100) and Pt(111) crystal planes respectively. These characteristics were used to evaluate the surface area. Panel b shows a cyclic voltammogram curves for the oxidation of methanol. Two CV curves corresponding to Pt-TMV (red trace) and PtNPs (green trace) in mixture of 0.5 M H_2SO_4 and 2 M CH_3OH, nitrogen purged, sweep rate 100 mVs^{-1}.*

THE ADVENT OF MESOSOCOPIC SOLAR CELLS

Michael Graetzel

Laboratory of Photonics and Interfaces, Ecole Polytechnique Fédérale de Lausanne,
Station 6,LPI EPFL, CH-1015, Lausanne, Switzerland
michael.graetzel@epfl.ch

The field of photovoltaic cells has been dominated so far by solid state p-n junction devices made e.g. of crystalline or amorphous silicon or other chalcogenide semiconductors, profiting from the experience and material availability of the semiconductor industry. However, there is an increasing awareness of the possible advantages of devices referred to as “bulk“ junctions due to their interconnected three-dimensional structure. Their embodiment departs completely from the conventional flat p-n junction solid-state cells, replacing them by interpenetrating networks. This lecture focuses on dye sensitized and quantum dot sensitized mesoscopic solar cells (DSCs), which are leading this new generation of photovoltaic devices [1-4]. Imitating the light reaction of natural photo-synthesis, this cell is the only photovoltaic system that uses molecules to generate charges from sunlight accomplishing the separation of the optical absorption from the charge separation and carrier transport processes. It does so by associating a molecular dye with a mesoscopic film of a large band gap semiconductor oxide. The DSC has made phenomenal progress, present conversion efficiencies being over 12 percent for single junction and 17 percent for tandem cells. The validated module efficiency has reached 10 percent, rendering the DSC a credible alternative to conventional thin film p-n junction devices. Commercial large-scale production of flexible DSC modules has started in 2009. These solar cells have become viable contenders for large-scale future solar energy conversion systems on the bases of cost, efficiency, stability and availability as well as environmental compatibility.

References:

[1] B. O’Regan and M. Grätzel , Nature, London 353 (1991).
[2] U.Bach, D.Lupo, P.Comte, J.E.Moser, F.Weissörtel, J.Salbeck, H.Spreitzert and M.Grätzel, Nature, 395, 550 (1998).
[3] M Grätzel , Nature 414, 338344 (2001).
[4] M.Grätzel, Acc. Chem. Res. 42, 1781-1798 (2009).

OPTICALLY TRANSPARENT CATHODE FOR DYE SENSITIZED SOLAR CELLS BASED ON GRAPHENE NANOPLATELETS

Ladislav Kavan[1,2*], Jun Ho Yum[2] and Michael Grätzel

[1]J. Heyrovský Institute of Physical Chemistry, v.v.i., Academy of Sciences of the Czech Republic, Dolejškova 3, CZ-18223 Prague 8, Czech Republic
[2]Laboratory of Photonics and Interfaces, Institute of Chemical Sciences and Engineering, Swiss Federal Institute of Technology, CH-1015 Lausanne, Switzerland
kavan@jh-inst.cas.cz

Commercial graphene nanoplatelets exhibit promising electrocatalytic activity towards I_3^-/I^- redox couple in thin films which are optically semitransparent. Electrochemical impedance spectra confirm that the charge-transfer resistance, R_{CT} is smaller by a factor of 5-6 in ionic liquid electrolyte (Z952) compared to that in traditional electrolyte in methoxypropionitrile solution (Z946). The difference was attributed to solvation-related events, rather than viscosity-control of the charge transfer mechanism. In both electrolytes tested (Z946, Z952) the R_{CT} scaled linearly with the graphene film's absorbance, confirming a simple proportionality between the concentration of active sites (edge defects and oxidic groups) and electrocatalytic properties of the electrode for I_3^-/I^- redox reaction (Figure 1).

Solar efficiency tests confirmed that semitransparent film of graphene nanoplatelets presented no barrier to drain photocurrents at 1 Sun illumination and potentials between 0 to *ca*. 0.3 V. Consistent with the impedance data on symmetrical dummy cells, the graphene cathode exhibited better performance in DSC with ionic liquid electrolyte (Z952). Nevertheless, the RCT of graphene nanoplatelets still needs to be decreased ca. 10 times to improve the behavior of DSC near the open circuit potential and, consequently, the fill factor. Our study points at an optimistic prediction that all-carbon cathode (FTO and Pt-free) is eventually accessible from graphene composites.

Acknowledgment. This work was supported by the Czech Ministry of Education, Youth and Sports (contract No. LC-510), by the Academy of Sciences of the Czech Republic (contracts IAA 400400804 and KAN 200100801), by the EC 7th FP project Orion (contract No. NMP-229036) and by the FP7-Energy-2010-FET project Molesol (contract No. 256617). MG is very grateful to the European Research Council (ERC) for supporting of his research under the ERC-2009-AdG Grant no 247404 MESOLIGHT. JHY acknowledges the support from the Korea Foundation for International Cooperation of Science & Technology through the Global Research Lab. We thank Dr. Shaik M. Zakeeruddin and Mr. Pascal Comte for their kind assistance.

Figures:

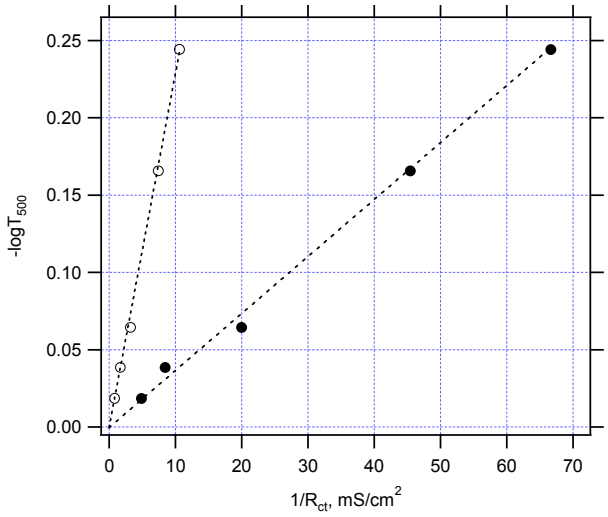

Figure 1: *Optical absorbance of graphene at a wavelength of 500 nm plotted as a function of inverse charge transfer resistance determined from electrochemical impedance spectra in volatile electrolyte, Z946 (open points) and in ionic liquid electrolyte, Z952 (full points).*

INDIRECT NANOPLASMONIC SENSING IN CATALYSIS: SINTERING, REACTANT SURFACE COVERAGE CHANGES AND OPTICAL NANOCALORIMETRY

Elin M. Larsson[1,2,3], Christoph Langhammer[1,2], Julien Millet[1], Stefan Gustafsson[1], Eva Olsson[1], Igor Zoric[1], Magnus Skoglundh[3], Bengt Kasemo[1]

[1]Applied Physics, Chalmers University of Technology, Fysikgränd 3, Gothenburg, Sweden
[2] Insplorion AB, Ekmansgatan 3, Gothenburg, Sweden
[3] Competence Center for Catalysis, Chalmers Univ of Technology, Kemigården, Gothenburg, Sweden
elin.larsson@insplorion.com

We report four different application areas, within catalysis, of a new "nanoplasmonic" (localized surface plasmon resonance, LSPR) method, Indirect Nanoplasmonic Sensing (INPS), which uses a remarkably simple optical transmission (or reflection) measurement. The method can with high sensitivity follow catalytic reactions in real time in-situ and can be applied to both model catalysts and real supported catalysts at realistic catalyst working conditions (i.e. high pressures and temperatures).

A catalyst is a substance that increases the rate of a reaction without itself being destroyed or consumed. Many industrial processes as well as the environmental and energy sectors depend on catalysis. Some of the most important uses for catalysts are to decrease the need for energy and raw materials and to clean industrial and automotive exhausts. To understand and improve heterogeneous catalyst systems it is important to be able to monitor the catalyst's state and to follow the reaction in real time. However, there is still a need for new experimental probes that allow such investigations to be made on the often complex catalyst structures and under realistic catalyst working conditions. Here we present a technique that has the potential to partly fill this need. We show that INPS can be used to monitor changes in adsorbed species on nanoparticle catalysts or chemical changes in a thin film [1], for optical nanocalorimetry [2] and to monitor sintering [3]. Sintering is the deactivation of a catalyst by the coalescence of catalytically active nanoparticles to form larger less active particles. Catalyst sintering causes large economic and environmental costs associated with catalyst regeneration/renewal.

The principle is "nanoplasmonic" sensing, which has been intensely investigated for biosensing. A LSPR is a coherent resonance oscillation of the conduction electrons, a plasmon resonance, in a metal nanoparticle, which can be excited by near-visible light with an appropriate color/wavelength. The wavelength at which the resonance occurs depends e.g. on the dielectric properties of the particle's nanoenvironment and can, therefore, be use for sensing where dielectric changes are to be detected [4]. INPS applies a patent searched [5] sensor chip design (see figure 1A) which allows events such as sintering, surface coverage changes[1], and hydrogen storage [2, 6] in/on nanoparticles/clusters/thin films to be monitored using the plasmon resonance of other nanoparticles in their close vicinity. The INPS technology is being commercialized by Insplorion AB that markets and sells research instruments.

Figure 1B shows real-time data from the storage (8 to 38 minutes) and release (from 38 minutes, induced by adding hydrogen) of nitrogen oxides (NOx) in/from a barium compound [1]. The data shows that the reaction can be monitored with high sensitivity and time resolution and that the obtained signal is concentration dependent. The reaction studied here is relevant in NOx storage and release catalysts extensively researched for lean burn automotive engines and shows that INPS can be used to study such reactions or as a nitrogen oxide sensor. We also show that a change in surface adsorbate from oxygen to hydrogen/carbon monoxide can be monitored with sub-monolayer sensitivity using INPS[1].

For optical nanocalorimetry it is utilized that the plasmon resonance is sensitive to temperature changes. Figure 1C shows light off traces obtained for Pd nanoparticles (average diameter 18.6 nm) deposited on an INPS sensor chip. The Pd particles were exposed to mixtures of hydrogen and oxygen (α= relative hydrogen concentration, total reactant concentration was kept constant) and the external temperature was increased linearly. Figure 1C shows the data after correction for the external temperature change. The data shows a rapid increase in the catalyst temperature at catalytic light off. The peak shift obtained at high temperatures depends on the α-value as expected (different α values

give different maximum reaction rates). We also demonstrate that INPS can be used to study particle size dependent reactivity [2].

In the last application, it is demonstrated that INPS can be used for real-time and intermittent monitoring of catalytic cluster sintering. Sintering of Pt clusters, similar to those in the car exhaust catalyst, was monitored in different gas environments at atmospheric pressure on SiO_2 surfaces. Substantially increased sintering rate were observed in 4% O_2 (in Ar) as compared to in pure Ar. As expected, the sintering rate was also found to increase with increasing temperature (see figure 1D). The optical signal obtained during sintering was calibrated using post-mortem TEM imaging of TEM-window samples, identical to the optical/glass samples, which were run in parallel with the optical measurements.

The obtained data show that INPS is a promising novel technique for real-time measurements of the catalyst state and nanocalorimetry using a low cost, optical transmission/reflection measurement.

References:

[1] E.M. Larsson, C. Langhammer, I. Zoric, B. Kasemo , *Science,* 326 (2009) 1091
[2] C. Langhammer, E.M. Larsson, B.Kasemo, I. Zorić, *Nano Letters* 10 (2010) 3529
[3] E. M. Larsson, C. Langhammer, J. Millet1, S. Gustafsson, E. Olsson, I. Zoric, M. Skoglundh, B. Kasemo, In preparation
[4] E.M. Larsson, J. Alegret, M. Käll, D.S. Sutherland, *Nano Letters* 7 (2007) 1256
[5] C. Langhammer, E.M. Larsson, I. Zorić, B. Kasemo, *Swedish patent application number 0950368-1*. Filed May 2009
[6] C. Langhammer, V. Zdanov, B. Kasemo, I. Zorić, *Review Letters*, 104 (2010) 135502

Figures:

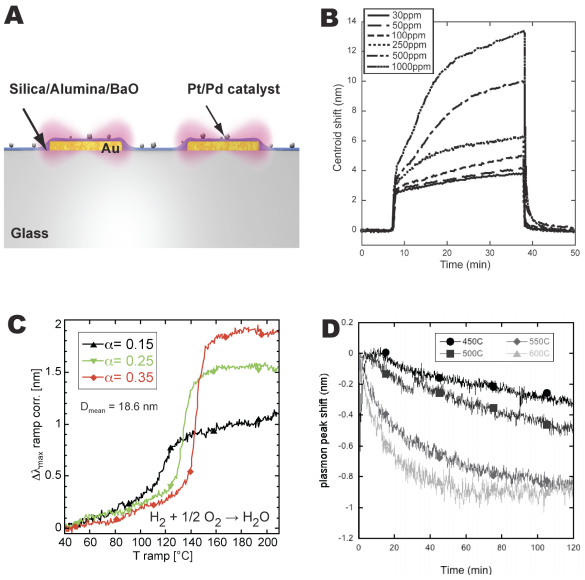

SILICON NANOWIRES AND NANOPILLARS ARRAYS FOR LITHIUM-ION BATTERY AND MICRO-BATTERY: OVERVIEW, CHALLENGES AND PERSPECTIVES

C. Lethien, M. Zegaoui, N. Rolland and P.A Rolland

IEMN CNRS UMR 8520 and IRCICA CNRS USR 3380
Avenue Poincaré, BP 60069, 59652 Villeneuve d'Ascq cedex, France
Université Lille Nord de France

Nowadays, energy autonomy appears to be the main challenge for hybrid/electrical vehicles as well as nomadic electronic devices. Coin and rechargeable batteries remain the only available sources to supply such devices. The energy autonomy is a societal and critical issue and the nanotechnology could help the research community to improve the devices performances in particular in the field of lithium ion battery/micro-battery. A classical lithium ion storage device is composed of a positive electrode (mainly $LiCoO_2$), a lithium ion electrolyte (liquid or solid) and a negative electrode (graphite). The capacity of the graphite electrode is unfortunately limited to 372 mAh/g.

The silicon material appears to be a promising candidate for the negative electrode as it has the potential to be a host material for the lithium ion Li+ with the highest reported specific capacity close to 4200 mAh/g. Unfortunately, the lithiation process (insertion of the lithium ion into the silicon crystal) occurring during the battery charging leads to a silicon's volume variation of 300 %. The high volume expansion of the silicon crystal remains the main cause of both the capacity fading and the pulverization of the fabricated battery. The lifetime of the lithium ion battery based on silicon material is then considerably reduced. Several research groups have developed novel negative electrode topologies using nanostructured silicon material in order to overcome the problem of the volume variation [1-6]. A negative electrode based on silicon material with an empty rate close to 50 % and allowing a volumetric expansion of the silicon crystal owing to the lithiation process is generally proposed. To obtain such empty electrodes, the nanotechnology seems to be a useful tool. Two different approaches could be investigated to produce silicon nanowires or nanopillars array. The bottom up way consists in the growth of silicon nanowires by Chemical Vapor Deposition (CVD) on stainless steel substrate according to the well known Vapor-Liquid-Solid (VLS) or Vapor-Solid (VS) processes. The 2nd path way (top down development) is based on the micromachining of the silicon material either by wet or dry etching [7-8].

This paper reports an overview of the silicon nanowires or nanopillars acting as a negative electrode of a lithium-ion battery or micro-battery. The bottom up (CVD synthesis) and top down (wet or dry etching) approaches will be compared. The potentialities of the silicon nanowires/nanopillars and their integration in a lithium-ion battery or micro-battery will be discussed. An original SiNPL micromachining processes using Deep Reactive Ion Etching and photolithography technologies will be presented. In the depicted process, the SiNPL array is obtained without electron beam nanolithography.

References:

[1] B. Laïk, L. Eude, J.-P. Pereira-Ramos, C. S. Cojocaru, D. Pribat and E. Rouvière 2008 Electrochimica Acta 53 5528-5532
[2] CK. Chan, H. Peng, G. Liu, K. McIlwrath, X. F. Zhang, R. A. Huggins, Y. Cui 2008 Nature Nanotech. 3 31-35
[3] CK. Chan, R. Ruffo, SS. Hong, RA. Huggins and Yi Cui 2009 Journal of Power Sources 189 34–39
[4] Liangbing Hu, Hui Wu, Seung Sae Hong, Lifeng Cui, James R. McDonough, SY Bohy and Yi Cui 2010 Chem Commun 47 367-369
[5] Barbara Laïk, Diane Ung, Amaël Caillard, Costel Sorin Cojocaru, Didier Pribat, Jean-Pierre Pereira-Ramos 2010 J Solid State Electrochem 14 1835–1839
[6] Jang Wook Choi, James McDonough, Sangmoo Jeong, Jee Soo Yoo, Candace K. Chan and Yi Cui 2010 Nano Letters 10 1409–1413
[7] K. Peng et al 2008 Applied Physics Letters 93, 033105-1 033105-3
[8] C. Lethien et al 2011 submitted to Microelectronic Engineering

Figures:

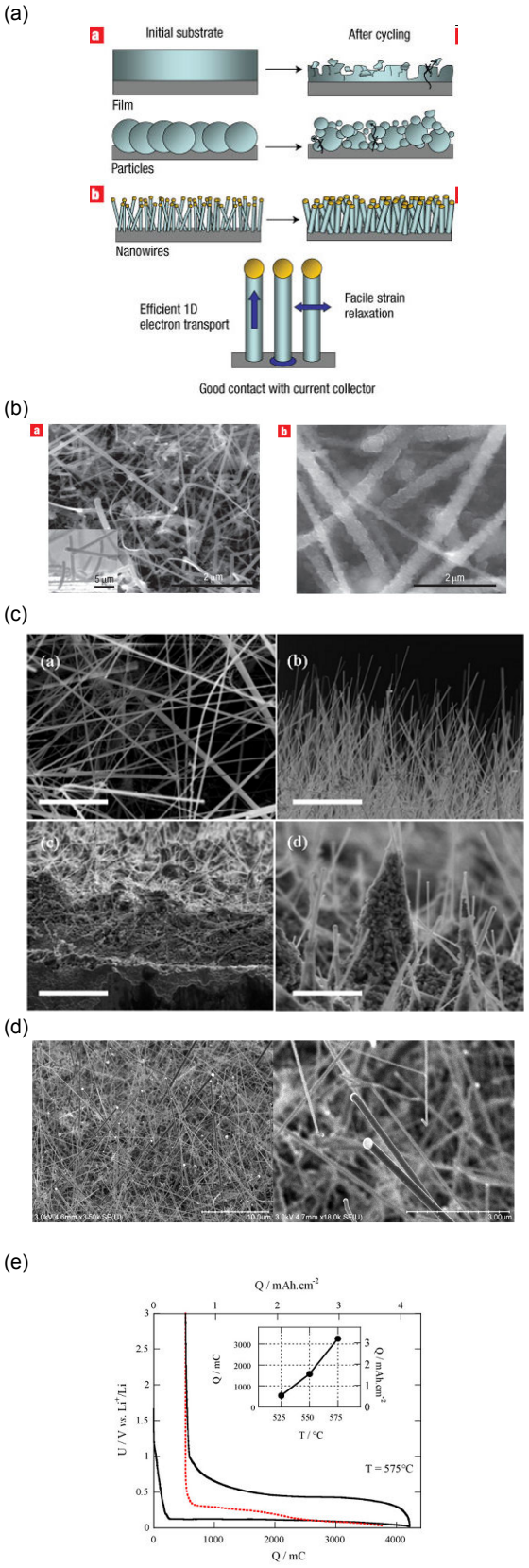

Figure 1: *Bottom up synthesis (Chemical Vapor Deposition) of silicon nanowires acting as a negative electrode of a lithium ion battery ((a), (b) et (c) Y. Cui et al [2, 3, 4, 6]) and (d), (e) Pereira et al [1, 5]*

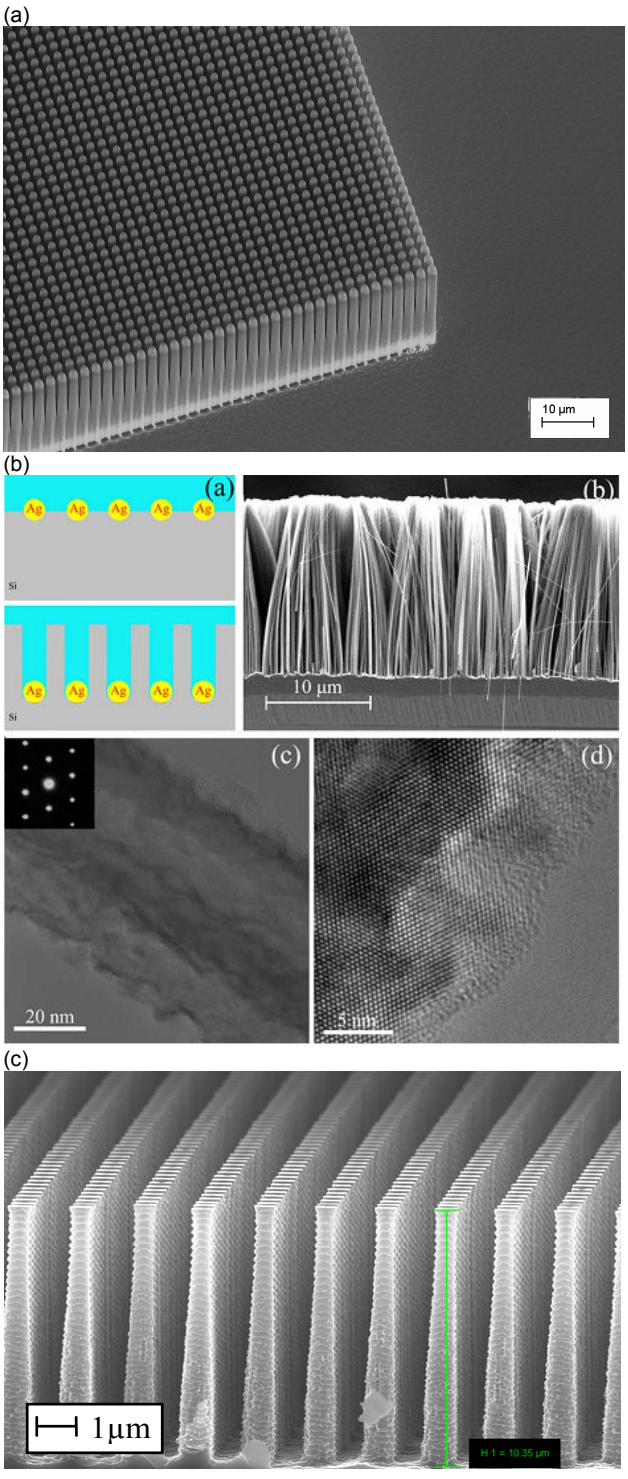

Figure 2*: Silicon nanopillar (SiNPL) array obtained by a top down approach [6-7]. This SiNPL array acts as the negative electrode of a lithium ion micro-battery [7] and is realized by Deep Reactive Ion Etching ((a) and (c)). The silicon nanowires reported in (b) are obtained by chemical wet etching [6].*

NANOTECHNOLOGY FOR MORE EFFICIENT PHOTOVOLTAICS: THE QUANTUM DOT INTERMEDIATE BAND SOLAR CELL

Antonio Luque

Instituto de Energía Solar, Universidad Politécnica de Madrid, 28040 Madrid, Spain
a.luque@upm.es

The intermediate band solar cell [1] has been proposed as a concept able to substantially enhance the efficiency limit of an ordinary single junction solar cell. If a band permitted for electrons is inserted within the forbidden band of a semiconductor then a novel path for photo generation is open: electron hole pairs may be formed by the successive absorption of two sub bandgap photons using the intermediate band (IB) as a stepping stone. While the increase of the photovoltaic (PV) current is not a big achievement —it suffices to reduce the bandgap— the achievement of this extra current at high voltage is the key of the IB concept. In ordinary cells the voltage is limited by the bandgap so that reducing it would also reduce the bandgap. In the intermediate band solar cell the high voltage is produced when the IB is permitted to have a Quasi Fermi Level (QFL) different from those of the Conduction Band (CB) and the Valence Band (VB). For it the cell must be properly isolated from the external contacts, which is achieved by putting the IB material between two n- and p-type ordinary semiconductors [2]. Efficiency thermodynamic limit of 63% is obtained for the IB solar cell1 vs. the 40% obtained [3] for ordinary single junction solar cells. Detailed information about the IB solar cells can be found elsewhere [4].

IB solar cells may be implemented by nanotechnology [5]. In particular the IB can be formed by the bound states of quantum dots of a lower gap semiconductor located inside a wider bandgap host semiconductor. The first practical realization was made with InAs QDs in a GaAs matrix [6]. Other groups have prepared similar devices [7-11]. Highest efficiency so far has been 18% [10]. In reality present QD IB solar cells present a negligible increase of the photocurrent and a substantial reduction of the voltage so that they always present less efficiency than test structures of the same host semiconductor without QDs.

As matter of fact one of the reasons of this reduced efficiency is that the InAs/GaAs system is very inappropriate. The increased thermodynamic efficiency limit is achieved for a bandgap of about 2 eV and a position of the IB band at 0.7 e.V from the CB whereas in the InAs/GaAs system has a total bandgap of 1.42 eV at room temperature and the position of the IB is at about 0.25-0.30 eV form the GaAs CB. Calculations [12] show that for these bandgaps the one-sun efficiency (the one referred to in all the cited publications) cannot exceed that of the cell without IB although the case might be different under concentrated sunlight. However, this materials system has permitted to experimentally prove the operational principles of this concept, namely the two photon mechanism [13] and the three QFL splitting [14] and its direct consequence, the achievement of voltage very close to the GaAs badgap [15]. Unfortunately this has only been possible to detect [13] or achieve [15] at very low temperature when the thermal escape has been suppressed.

The reduction of voltage of present QD IB solar cells is partly due to the reduction of minority carrier lifetime introduced through the dislocations created by the stresses. This has been amended by stress reduction of spacer increase and is not a major problem today. In part it is also due to the reduction of the bandgap due to the invasion of the bandgap by the heavy hole states [12,16] that form a quasi continuous, and by the formation of a wetting later that acts as a quantum well [12]. According to this, it is unfair use single gap cell without QDs with the cell with QDs in the same host material. Changing the bandgap of the host material this problem is solved. Yet the increase of current is very small and this is due by an inherent low absorption of the QDs for interband transitions. We think that the CB wavefunctions have an envelope with S symmetry [16] while this symmetry is absent in the VB wavefunctions. The consequence is that the relevant envelope wavefunctions overlap poorly. We don't know yet the solution to this issue, besides, of course, a photon management strategy to enhance the absorption.

Finally another issue is the thermal escape. It prevents form an easy splitting of the CB and IB QFLs. Best solutions are the reduction of the QD size to prevent QD excited states that may provide a ladder

for the escape of electrons [17] and, of course, to change the material system to better exploit the potentialities of the concept [18].

References:

[1] A. Luque and A. Martí, Physical Review Letters 78, 5014–5017 (1997).
[2] A. Luque and A. Martí, Progress in Photovoltaics: Res. Appl. 9, 73–86 (2001).
[3] W. Shockley and H. J. Queisser, Journal of Applied Physics 32, 510-519 (1961).
[4] A. Luque and A. Marti, Advanced Materials 22, 160-174 (2009).
[5] A. Martí, L. Cuadra, and A. Luque, in Proc. 28th IEEE Photovoltaics Specialists Conference (IEEE, New York, 2000), p. 940-943.
[6] A. Luque, A. Martí, C. Stanley, N. López, L. Cuadra, D. Zhou, and A. Mc-Kee, Journal of Applied Physics 96, 903–909 (2004).
[7] S. M. Hubbard, C. D. Cress, C. G. Bailey, R. P. Raffaelle, S. G. Bailey, and D. M. Wilt, Applied Physics Letters 92, 123512 (2008).
[8] V. Popescu, G. Bester, M. C. Hanna, A. G. Norman, and A. Zunger, Physical Review B 78, 205321 (2008).
[9] R. Oshima, A. Takata, and Y. Okada, Applied Physics Letters 93, 083111 (2008).
[10] S. A. Blokhin, A. V. Sakharov, A. M. Nadtochy, A. S. Pauysov, M. V. Maximov, N. N. Ledentsov, A. R. Kovsh, S. S. Mikhrin, V. M. Lantratov, S. A. Mintairov, N. A. Kaluzhniy, and M. Z. Shvarts, Semiconductors 43, 514–518 (2009).
[11] D. Alonso-Alvarez, A. G. Taboada, J. M. Ripalda, B. Alen, Y. Gonzalez, L. Gonzalez, J. M. Garcia, F. Briones, A. Marti, A. Luque, A. M. Sanchez, and S. I. Molina, Applied Physics Letters 93, 123114 (2008).
[12] A. Marti, E. Antolin, E. Canovas, N. Lopez, P. G. Linares, A. Luque, C. R. Stanley, and C. D. Farmer, Thin Solid Films 516, 6716-6722 (2008).
[13] A. Marti, E. Antolin, C. R. Stanley, C. D. Farmer, N. Lopez, P. Diaz, E. Canovas, P. G. Linares, and A. Luque, Physical Review Letters 97, 247701-4 (2006).
[14] A. Luque, A. Marti, N. Lopez, E. Antolin, E. Canovas, C. Stanley, C. Farmer, L. J. Caballero, L. Cuadra, and J. L. Balenzategui, Applied Physics Letters 87, 083505-3 (2005).
[15] E. Antolín, A. Martí, P. G. Linares, I. Ramiro, E. Hernández, C. D. Farmer, C. R. Stanley, and A. Luque, in Proc.25 Photovoltaic Specialists Conference (IEEE, Honolulu, 2010).
[16] A. Luque, A. Marti, E. Antolín, P. G. Linares, I. Tobías, I. Ramiro, and E. Hernandez, Solar Energy Materials & Solar Cells, to be published (2011).
[17] A. Luque, A. Marti, E. Antolín, P. G. Linares, I. Tobias, and I. Ramiro, submitted (2011).
[18] P. G. Linares, A. Marti, E. Antolin, and A. Luque, Journal of Applied Physics 109, 014313 (2011).

OPTIMIZING THE THERMOELECTRIC FIGURE OF MERIT OF APERIODIC SOLIDS

Enrique Maciá

Dpto. Fisica de Materiales, Facultad CC. Físicas, Univ Complutense de Madrid, Madrid (Spain)
emaciaba@fis.ucm.es

During the last few years we have witnessed a growing interest in searching for novel, high performance thermoelectric materials (TEMs) for energy conversion in small scale power generation and refrigeration devices. Some time ago the appealing question regarding the best possible electronic structure of thermoelectric materials (TEMs) was discussed by Mahan and Sofo [1]. It was proposed on sound theoretical basis that the best TEMs are likely to be found among materials exhibiting a sharp singularity in the density of states (DOS) close to the Fermi level, along with a substantial depletion of the DOS at the Fermi level. In this contribution I will describe the thermoelectric properties of two different classes of materials exhibiting these required spectral features in their electronic structures. The first class of materials are representatives of quasicrystalline alloys exhibiting semiconductor-like, rather than metallic electronic transport properties, along with extremely low thermal conductivity values. Accordingly, quasicrystals can be regarded as an unexpected instance of the so-called electron crystal-phonon glass approach introduced by Slack [2]. Thus, quasicrystals occupy a very promising position in the quest for novel TEMs, naturally bridging the gap between semiconducting materials and metallic ones [3].

As an alternative to bulk materials the study of the thermoelectric properties of single molecules may underpin novel thermal devices such as molecular-scale Peltier coolers (figure) and provide new insight into mechanisms for molecular-scale transport. In this way, the thermoelectric potential of some conducting polymers, like polythiophene and polyaminosquarine, has been recently reviewed on the basis of their electronic band structures. I will focus on the electronic structure and transport properties on DNA based devices, with an special attention to the possible use of a thermoelectric signature for different codons of biological interest in order to explore new sequencing techniques based on physical processes instead of the usual chemical ones [4-7]. In fact, the thermoelectric properties of molecular systems have received a lot of attention during the last few years and it is expected that this attention to increase fast as the necessary experimental techniques are progressively refined [8-10].
We report four different application areas, within catalysis, of a new “nanoplasmonic

References:

[1] G. D. Mahan and J. O. Sofo, “The best thermoelectric”, Proc. Natl. Acad. Sci. USA, 93 (1996) 7436.
[2] G. A. Slack, CRC Handbook of Thermoelectrics, edited by D. M. Rowe (CRC Press, Boca Raton, FL, 1995).
[3] E. Maciá, “Aperiodic Structures in Condensed Matter: Fundamentals and Applications” (CRC Press, Boca Raton, FL, 2009).
[4] E. Maciá, “Codon thermoelectric signature in molecular junctions”, Phys. Rev. B 82 (2010) 045431.
[5] E. Maciá “DNA based thermoelectric devices” in Charge Migration in DNA: Physics, Chemistry and Biology Perspectives, Ed. Chakraborty T (Springer, Berlin, 2007).
[6] E. Maciá “DNA-based thermoelectric devices: A theoretical prospective”, Phys. Rev. B 75 (2007) 035130
[7] E. Maciá, “The role of aperiodic order in science and technology”, Rep. Prog. Phys. 69 (2006) 397.
[8] P. Reddy, S. Y. Jang, R. A. Segalman, and A. Majumdar, “Thermoelectricity in molecular junctions”, Science 315 (2007) 1568 .
[9] K. Baheti, J. A. Malen, P. Doak, P. Reddy, S. Y. Jang, T. D. Tilley, A. Majumdar, and R. A. Segalman, “Probing the chemistry of molecular heterojunctions using thermoelectricity”, Nano Lett. 8 (2008) 715.
[10] A. Tan, S. Sadat, and P. Reddy, “Measurement of thermopower and current-voltage characteristics of molecular junctions to identify orbital alignement”, Appl. Phys. Lett. 96 (2010) 013110.

Figures:

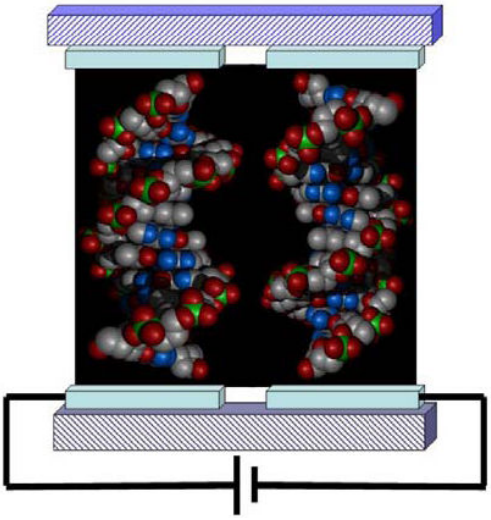

Figure 1: *Sketch illustrating the basic features of a nanoscale DNA based Peltier cell. A polyA-polyT (polyG-polyC) oligonucleotide, playing the role of n-type, left (p-type, right) semiconductor legs, are connected to organic wires (light boxes) deposited onto ceramic heat sinks (dark boxes).*

NANOENGINEERING THERMOELECTRICS FOR ENERGY HARVESTING.

Marisol Martin-Gonzalez

Thermoelectrics Group, Instituto de Microelectrónica de Madrid, IMM-CNM-CSIC.
Tres Cantos Madrid (Spain)
marisol@imm.cnm.csic.es

The growing social alarm over increasing energy cost and global warming related to fossil fuel sources has motivated the search for cleaner, more sustainable energy sources. Among the different feasible technologies, thermoelectric (TE) devices have received attention as these solid-state devices can generate electricity by harvesting waste thermal energy, thereby improving the efficiency of a system. The many advantages of TE devices include solid-state operation, no noise, zero-emissions, vast scalability, no maintenance and a long operating lifetime. The efficiency of TE materials is directly related to a dimensionless figure of merit (ZT). In order to compete with conventional refrigerators, a ZT=3 must be obtained. Although, a device with ZT>2 will be also important in other applications. Due to their limited energy conversion efficiencies (i.e. ZT is ≈1), thermoelectric devices currently are only present in niche applications.

However, there is a renewed interest in the field of thermoelectrics due to quantum size effects, which provide additional ways to enhance energy conversion efficiencies in nanostructured materials. For example, a ZT up to 2.5 was achieved by synthesizing two-dimensional Sb_2Te_3/Bi_2Te_3 superlattice thin films through a chemical vapor deposition (CVD) process, exceeding previous limits of ≈1 for bulk counterparts; theoretical calculations predict that even higher ZTs can be achieved in one-dimensional nanowires.

The successful application of these nanostructures in practical thermoelectric devices must implement a cost-effective and high through-put fabrication process. Among the different techniques electrodeposition has been one of the more successful. For that reason an overview of the state of the art in the electrodeposition, of films and nanowires, of the different thermoelectric: Chalkogenide, Silizide SiGe, TAGS, Skutterudites, Clathrates, etc will be presented here.

Acknowledgments: ERC Starting Grant 2008: 240497

NEW ROUTES FOR THE FABRICATION OF ORGANIC PHOTOVOLTAIC CELLS

Jordi Martorell

ICFO-Institut de Ciencies Fotoniques, 08860 Castelldefels (Barcelona), Spain and
Departament de Fisica i Enginyeria Nuclear, Universitat Politecnica de Catalunya,
08222 Terrassa, Spain

Organic solar cells have been the subject of research for the realization of portable, flexible and transparent modules as renewable energy sources. Here we propose alternative routes to fabricate such type of devices using simple and cost effective fabrication methods based on, the replacement of electron blocking layers by sputtered NiO, the substitution of the ITO electrode by a sputtered thin metal film, and on the fabrication of the organic photovoltaic cells using a dip coating procedure instead of a spin coating one.

Metal electrode relative to ITO		
Electrode type	Cu(9)-Ni(1)	Cu(7)-Ni(1)
Transmission relative to ITO	59%	66%
J_{sc}/J_{sc}(ITO)	73.5%	77.2%
Field Int. in relative to ITO	75%	80%

Table 1: *Performance of Cu-Ni electrode based cells compared to ITO based cells*

We fabricated and tested the performance of P3HT:PCBM bulk hetero-junction solar cells when the PEDOT:PSS, the most commonly used hole transporting layer, is replaced by a thin layer of sputtered NiO, and when the transparent indium tin oxide (ITO) electrode is replaced by a sputtered ultra-thin Cu-Ni bilayer. We show, here, that when NiO is used as the hole transporting layer, the characteristic photovoltaic parameters of such cell are similar or better to those of the device fabricated with PEDOT:PSS. We also studied the lifetime of NiO based cells in comparison to the PEDOT:PSS based ones. We observed that an ambient air processing of the organic materials was not detrimental to the ulterior performance of the NiO based cell, which degraded in ambient air conditions with a time constant larger than 300 hours. On the contrary, the PEDOT:PSS cell degraded very rapidly and the loss in efficiency was shown to be 29 times faster when compared to the NiO cell.

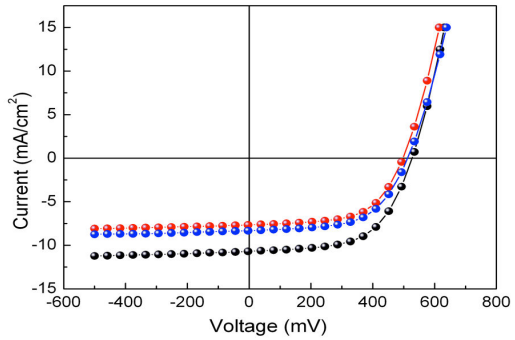

Figure 1: *I-V curves for P3HT/PCBM cells fabricated using ITO (black), Cu(7 nm)-Ni(1 nm) (blue), and Cu(9 nm)-Ni(1 nm) (red).*

In such NiO based cells we also used a Cu-Ni semi-transparent electrode to replace the ITO. Despite the fact that the metal electrode exhibits a transparency that is 65% of the ITO electrode, the short circuit current for the metallic anode based cell is 77% of the ITO based one (see Table 1), which exhibited a power conversion efficiency of 3.3% (see Figure 1). Such discrepancy between the transparency and short circuit current percentage indicates that photon absorption may be enhanced by the optical microcavity formed between the Cu-Ni and Al electrodes.

We also fabricated organic solar cells with a bilayer architecture, in which poly(p-phenylene vinylene) (PPV) was used as the electron donor while Rhodamine 6G as the electron acceptor. We showed that photo-conversion efficiency for such dip coated fabricated cells is 1.4 times higher than that obtained from cells fabricated using the traditional spin coating procedure. Comparing the performance of several cells produced by dip coating on the same substrate we observed a high degree of uniformity, as opposed to the performance of the spin coated cells which exhibited a large dispersion. In addition,

when the dip coating is applied the same coating solutions may be used many times to fabricate cells in a continuous mode. We discuss the use of orthogonal solvents to demonstrate that the technique can also be applied for the fabrication of other polymeric cells such as, for instance, P3HT/PCBM cells. In summary, the proposed method for organic solar cell fabrication is an alternative to obtain photovoltaic devices with a better performance than the spin coated cells. Such technique opens the possibility to implement an alternative route to other procedures that have already been considered for a cost effective large scale production of high efficiency OSCs such as the spray coating or the ink jet printing.

Design of Photoelectrochemical Cells for the Splitting of Water and Production of Fuel

Ana L. Moore, Thomas A. Moore and Devens Gust

Center for Bioenergy and Photosynthesis, Department of Chemistry and Biochemistry,
Arizona State University, Tempe, AZ, 85287-1604, USA
amoore@asu.edu

The design of bioinspired schemes that couple solar energy conversion to the oxidation of water and the subsequent use of the reducing equivalents to synthesize energy-rich compounds, such as hydrogen or fuels based on reduced carbon is the main objective of our present research. [1,2] In order to establish the design principles for a tandem, two junction (or threshold) photochemical cell, we are assembling Grätzel-type photoelectrodes that model photosystems I and II (PSI and PSII) of plants. The photoanode model of PSII will contain a mimic of the donor side (water oxidizing side) of PSII reaction centers. In PSII, tyrosine Z (Tyr_Z) mediates charge transport between the photo-oxidized primary donor ($P680^{\bullet+}$) and the oxygen-evolving complex (OEC). The oxidation of Tyr_Z by $P680^{\bullet+}$ likely occurs with the transfer of the phenolic proton to a hydrogen-bonded histidine residue (His190). This coupling of proton and redox chemistry is thought to poise the Tyr_Z oxidation potential between those of $P680^{\bullet+}$ and the OEC. We have prepared a bioinspired system (BiP-PF_{10}) consisting of a high oxidation potential porphyrin (PF_{10}, 1.59 V vs. NHE, a model of P680) that is covalently attached to a benzimidazole-phenol pair (BiP) that mimics the Tyr_Z-His190 pair in PSII. Electrochemical studies show that the phenoxyl radical/phenol couple of the model system is chemically reversible with a midpoint potential of 1.24 V vs. NHE and is therefore thermodynamically capable of water oxidation. When the BiP-PF_{10} construct is attached to TiO_2 nanoparticles and excited with visible light, it undergoes photoinduced electron transfer. Electrons are injected into the semiconductor and the corresponding holes are localized on either the porphyrin ($BiPPF_{10}^{\bullet+}$-$TiO_2^{\bullet-}$) or the phenol ($BiP^{\bullet+}$-PF_{10}-$TiO_2^{\bullet-}$). EPR provides a clear spectroscopic picture of these processes. [3] The photoelectrode model of PSI will be sensitized by low potential naphthalocyanines or phthalocyanines, which absorb light in the near IR region of the spectrum. Upon photoexcitation, these dyes are designed to inject electrons into semiconductors having sufficiently negative conduction bands to effectively drive the reduction of protons to hydrogen at a cathode. The semiconductor will be electrically wired to a cathode suitable for hydrogen production: either a metal electrode (Pt or Ni) or a hydrogenase-modified carbon electrode. [4]

References:

[1] M. Hambourger, G. F. Moore, D. M. Kramer, D. Gust, A. L. Moore and T. A. Moore, Chemical Society Reviews, 38, (2009) 25–35.
[2] D. Gust, T. A. Moore and A. L. Moore, Acc. Chem. Res., 42, (2009) 1890–1898.
[3] G. F. Moore, M. Hambourger, M. Gervaldo, O. G. Poluektov, T. Rajh, D. Gust, T. A. Moore and A. L. Moore, J. Am. Chem. Soc., 130, (2008) 10466–10467.
[4] M. Hambourger, M. Gervaldo, D. Svedruzic, P. W. King, D. Gust, M. Ghirardi, A. L. Moore and T. A. Moore, J. Am. Chem. Soc., 130, (2008) 2015–2022.

CHEMICAL SOLUTION APPROACHES TO SELF-ASSEMBLED AND NANOCOMPOSITE SUPERCONDUCTING AND FERROMAGNETIC FILMS

Xavier Obradors

Institut de Ciència de Materials de Barcelona, CSIC
Campus de la UAB, 08193 Bellaterra, Spain

Chemical solution deposition (CSD) has emerged in the last years as a very competitive technique to obtain epitaxial films, multilayers, nanocomposite films and interfacial templates of high quality with controlled nanostructures. In particular, the all CSD approach has been shown to be one of the most promising ways for-cost-effective production of second generation superconducting wires with high performances.

The development of nanostructured superconductors with enhanced vortex pinning properties requires the preparation of either nanocomposite epitaxial films or epitaxial films grown on interfacial nanotemplates.

In this presentation we will show different approaches to the preparation of oxide interfacial nanotemplates grown by CSD, either through strain induced self assembling or through the use of nanoporous track-etched polymer templates. Several types of functional oxides have been grown, for instance, CeO_2, $BaZrO_3$ or $(La,Sr)MnO_3$. These oxides have also been used as epitaxial buffer layers for multilayered structures where atomic scale interfacial quality is required.

The Trifluoracetate route (TFA) is the most suitable route to achieve epitaxial $YBa_2Cu_3O_7$ (YBCO) layers with high critical currents and so these precursors have been used to achieve nanocomposites based on interfacial nanotemplates or on randomly distributed nanodots.

Emphasis will be made on understanding the relationship between the different processing parameters, the nanostructure and the physical properties (magnetic and superconducting).

TOWARDS POWER OPTIMIZATION IN NANOSCALE SYSTEMS THROUGH THE USE OF MANY-ELECTRON CORRELATIONS

G. Albareda and **X. Oriols**

Dept. d'Enginyeria Electrònica, Universitat Autònoma de Barcelona, 08193 Bellaterra, Spain
guillem.albareda@uab.cat

Power consumption is one of the main drawbacks that electronics must face up to when scaling down any new technology. Thus, in last few years, the electronic development is being driven not only by the desire of improving circuit density and speed, but also by the aim of reducing power consumption. During last years, the ITRS is being identifying this last constraint as one of the top three overall challenges for the next years [1].

The openness of classical and quantum electron systems has been studied extensively in the literature, but few works are devoted to discuss its effect on the computation of electric power. Here, we provide a novel expression for the accurate estimation of the electric power in nanoscale open systems deduced from a many-particle electron transport formalism that goes beyond the standard mean field approximation [2,3]. Surprisingly, we show that the usual expression of the electric power in the device active region,

$$P_{no-corr} = \langle I(t) \rangle_T \langle V(t) \rangle_T , \qquad (1)$$

written as the product of the (time-averaged) current $\langle I \rangle_T$ through the device and the voltage $\langle V \rangle_T$ drop there, is not fully appropriate when referring to open systems with (time-dependent) correlations beyond the mean field. When such correlations are taken into account, a much more complex recipe is needed for the computation of the electric power of the electrons in the active region. This new receipt opens the path to an original use of the electron correlations to manipulate the way energy is dissipated in different regions of a circuit.

In order to provide a common classical and quantum language for our argumentation, we formulate the problem in terms of the correlation between the (Bohm or classcial) velocity of the *i* electron $\vec{v}_i(t)$ and the electrostatic force $q_i \vec{E}_i(t)$ made by the rest of electrons of the whole (closed) system on it [3]. We use the Bohm approach for extending also our results towards quantum mechanics for a non-relativistic (spinless) Coulomb-interacting electrons system [2-4]. It can be then shown that the mean electric power, P_{corr}, corresponding to the *N(t)* electrons comprised in the open system of figure 1 reads:

$$P_{corr} = \sum_{i=1}^{N(t)} q_i \langle \vec{v}_i(t) \vec{E}_i(t) \rangle_T , \qquad (2)$$

Let us notice that although the electric power defined in (2) refers only to those electrons enclosed in the open system, its value is crucially affected by all the *M* particles composing the whole closed circuit (see Fig. 1a.). Since energy is continuously entering and leaving an open system through the interaction among carriers inside and outside its spatial limits, it is of critical importance to properly model the boundary conditions through which the dynamics of electrons within and outside the open system become correlated [4] (see Fig. 1b.). In addition, it is important to remark that it can be shown that overall energy conservation requirements for the whole (reservoirs plus active region) system states that expression (1) gives the correct value for overall power consumption in the whole circuit. In summary, electron-electron correlations play a crucial role in the conservation of the energy in the whole (reservoirs, active region) system and also on its consumption on each of its parts.
With the aim of highlighting the influence of the electron many-particle correlations in the value of the electrical power, we define the correlation power factor as the following (dimensionless) parameter

$$G = P_{no\_corr} / P_{corr} = \langle I \rangle_T \cdot \langle V \rangle_T / P_{corr} , \quad (3)$$

Expression (3) represents the “unexpected” effects of the many-particle correlations on the electric power in open systems. As it will be shown below, by switching off the Coulomb interaction among electrons we immediately recover the standard expression (1) of the power consumption, i.e. $G = 1$.

In order to numerically demonstrate the above results, we have simulated a nanoscale resistance using, both, a standard single-particle Monte Carlo simulator and a many-particle electron transport approach explained in Refs. [2-4]. In Fig. 2a, we have represented the current-voltage characteristic for a nanoscale resistance using a single-particle (i.e. time-independent electric-field) electron transport approach. As expected, the value of G reduces to unit, indicating that many-particle Coulomb-interaction effects in the power computation are not accessible with single-particle electron transport simulations (Fig.2b). On the contrary, when the many-particle electron transport formalism explained in Refs [2-4] is used, the relevance of correlations in the average power becomes evident (at low bias) in the correlation power factor G depicted in Fig. 3b (see also Fig. 3a). Preliminary results corresponding to double-gate field effect transistors can be also found in Ref. [5].

In this work, we have shown that the expression (1) of electric power consumption is valid when describing the whole (reservoir and active region) circuit consumption. However, the consumption of each (open) part composing it has to be computed according to expression (2). This result opens a new path toward the manipulation of energy consumption in different parts of a circuit by accelerating or slowing down carrier dynamics there through the control of electron-electron correlations.

References:

[1] International Technology Roadmap for Semiconductors (2010 Update) http://www.itrs.net
[1] X. Oriols, Physical Review Letters, 98 (2007) 066803.
[2] G. Albareda, J. Suñé and X. Oriols, Physical Review B, 79 (2009) 075315.
[3] G. Albareda, H. López, X. Cartoixà, J. Suné, and X. Oriols, Time-dependent boundary conditions with lead-sample Coulomb correlations:Application to classical and quantum nanoscale electron device simulators, *Phys. Rev. B, 82, 085301* (2010).
[4] G. Albareda, A. Alarcón, and X. Oriols, Electric power in nanoscale devices with full Coulomb interaction, Int. J. Numer. Model. 23, 354 (2010).

Figures:

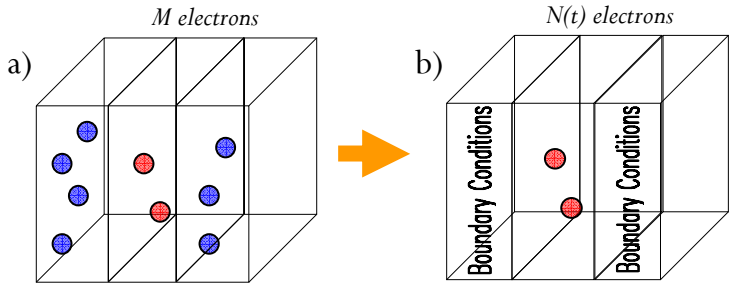

Figure 1: *Schematic representation of the electrons in an electron device. a) A closed (whole) system of M electrons in the active region and the reservoirs and b) the open system of N(t) electrons in the active region.*

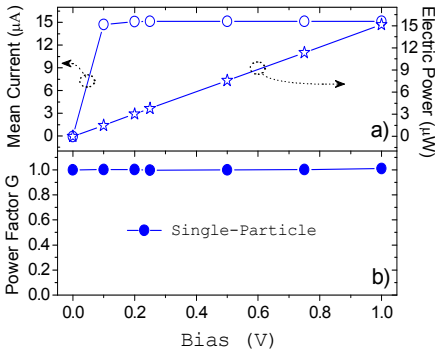

Figure 2: *a) Average current, electric power, and b) correlation power factor, G, defined in the text as a function of bias. Electron transport is computed from a single-particle approach.*

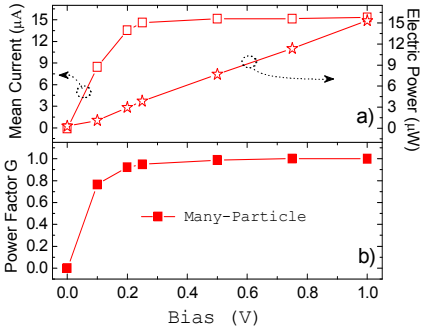

Figure 2: *a) Average current, electric power, and b) correlation power factor, G, defined in the text as a function of bias. Electron transport is computed from the many-particle approach described in [2-4].*

CHARACTERIZATION OF OPTICAL PROPERTIES OF SEMICONDUCTOR QUANTUM DOT-SENSITIZED SOLAR CELLS TOGETHER WITH ULTRAFAST CARRIER DYNAMIC PROPERTIES

T. Toyoda[1] and Q. Shen[1,2]

[1]Department of Engineering Science, Faculty of Informatics and Engineering,
The University of Electro-Communications, 1-5-1 Chfugaoka, Chofu, Tokyo 182-8585, Japan
[2]PREST, Japan Science and Technology Agency, 4-1-8 Honcho,
Kawaguchi, Saitama 332-0012, Japan
toyoda@pc.uec.ac.jp

Semiconductor quantum dots (QDs) could be provided as a sensitizer for the sensitized solar cells [1,2] due to its adjustable energy gaps, large intrinsic dipole moment, and large extinction coefficient. Moreover, QD-sensitzed solar cell has a capability of producing multiple exciton generation (MEG) [3]. We demonstrate CdSe QD-sensitized solar cells based on different kinds of nanostructured TiO_2 electrodes with (1) conventional assembly of nanoparticles, (2) nanotubes [4], and (3) inverse opal structure (photonic crystal) [2,5]. CdSe QDs were adsorbed on the nanostructured TiO_2 electrodes by chemical bath deposition [2,6]. Finally, the surface of electrodes were passivated by ZnS coating [7]. Sandwich structure solar cells were prepared by using the Cu_2S counter electrode [8]. Polysulfide solution was used as a regenerative redox couple. Optical absorption characterization was carried out with photoacoustic (PA) spectroscopy [9]. Incident photon to current conversion efficiency (IPCE) and photovoltaic properties were investigated. Photosensitization by CdSe QDs could be observed in the visible region. The maximum IPCE value of 75% and the maximum photovoltaic conversion efficiency of 3.5% can be obtained. These values are relatively high for semiconductor QD-sensitized solar cells. Photoexcited carrier dynamics is characterized with the improved transient grating (TG) technique [10, 11]. It depends on the refractive index change by photoexcited carrier population. TG measurements show the fast (hole) and slow (electron) relaxation processes with lifetimes of a few picosecond and a few tens to hundred picoseconds, respectively. There are correlations between the lifetimes of photoexcited carrier dynamics and the photovoltaic properties.

References:

[1] Q. Shen, D. Arae, and T. Toyoda, J. Photochem. Photobiol. A: Chem. 164, 75 (2004).
[2] L. J. Diguna, Q. Shen, J. Kobayashi, and T. Toyoda, Appl. Phys. Lett. 91, 023116 (2007).
[3] A. J. Nozik, Physica E 14, 115 (2002).
[4] Q. Shen, A. Yamada, S. Tamura, and T. Toyoda, Appl. Phys. Lett. 97, 123107 (2010).
[5] L. Diguna, M. Murakami, A. Sato, Y. Kumagai, T. Ishihara, N. Kobayashi, Q. Shen, and T. Toyoda, Jpn. J. Appl. Phys. 45, 5563 (2006).
[6] S. Gorer and G. Hodes, J. Phys. Chem. 98, 5338 (1994).
[7] Q. Shen, J. Kobayashi, L. J. Diguna, and T. Toyoda, J. Appl. Phys. 103, 084304 (2008) .
[8] G. Hodes, J. Manassen, and D. Cahen, J. Electrochem. Soc. 127, 544 (1980).
[9] A. Rosencwaig and A. Gersho, J. Appl. Phys. 47, 64 (1977).
[10] Q. Shen, M. Yanai, K. Katayama, T. Sawada, and T. Toyoda, Chem. Phys. Lett. 442, 89 (2007).
[11] Q. Shen, Y. Ayuzawa, K. Katayama, T. Sawada, and T. Toyoda, Appl. Phys. Lett. 97, 263113 (2010)

HPC 2011

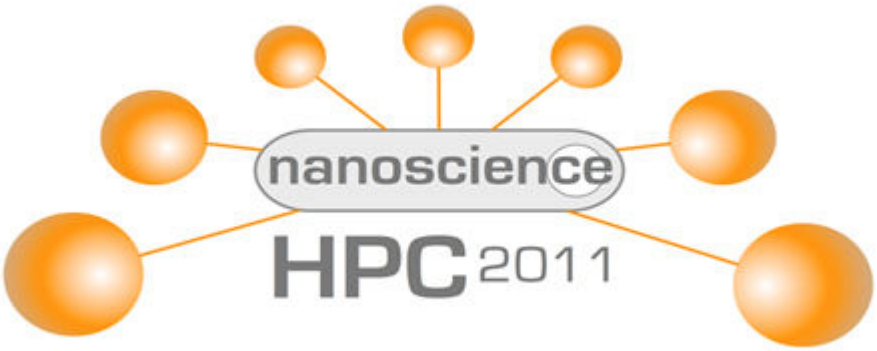

INDEX: INVITED CONTRIBUTIONS

INDEX: ORAL CONTRIBUTIONS

ALPHABETICAL ORDER

I: Invited / O: Oral

HPC 2011

ABSTRACTS
ALPHABETICAL ORDER

TOWARDS REALISTIC ATOMIC-SCALE MODELING OF NANOSCALE DEVICES

Anders Blom, Kurt Stokbro

QuantumWise A/S Lersø Parkalle 107, 2100 Copenhagen, Denmark
Anders.Blom@quantumwise.com

Although electronic device dimensions are rapidly approaching the nanoscale, their dimensions are still large from an atomistic perspective. Certain systems can still be studied with current state-of-the-art technology since the problems are relatively localized, such as interfaces and the effects vacancies or defects in them can have on Schottky barriers and interface resistance. For other properties, such as the influence on the transport and transistor characteristics of the electrostatic environment induced by gate electrodes, the simulation volume and atom count grows rapidly, however.

Therefore, a novel methodology is required in order to scale down current modeling techniques used within TCAD to be able to take into account atomic-scale effects. In this presentation we will present the current state-of-the-art in first-principles device modeling, as implemented in our software Atomistix ToolKit (ATK), and give an outlook to the challenges that lie ahead when scaling up the atomic-scale methods to more realistic dimensions.

We will discuss our recent progress in this area, including efficient Green's function evaluation and parallelization strategies based on block diagonalization techniques and the Krylov subspace method [1,2], the use of scattering states for improved performance of finite bias transport calculations [3], finite-element techniques coupled to first-principles calculations [4], and multi-scale models that take advantage of methods that operate on different complexity levels and length scales [4-6].

References:

[1] D. E. Petersen, H. H. B. Sørensen, P. C. Hansen, S. Skelboe, and K. Stokbro, Journal of Computational Physics 227, 3174-3190 (2008)
[2] S. Skelboe, The Scheduling of a Parallel Tiled Matrix Inversion Algorithm, submitted (2010)
[3] H. H. B. Sørensen, P.C. Hansen, D.E. Petersen, S. Skelboe, and K. Stokbro, Phys. Rev. B 79, 205322 (2009)
[4] J. Avery, Ph.D. Thesis (2011)
[5] K. Stokbro, Journal of Physical Chemistry C, part of the "Mark A. Ratner Festschrift" (2010)
[6] K. Stokbro, D. E. Petersen, S. Smidstrup, M. Ipsen, A. Blom and K. Kaasbjerg, Phys. Rev. B 82, 075420 (2010)

Figures:

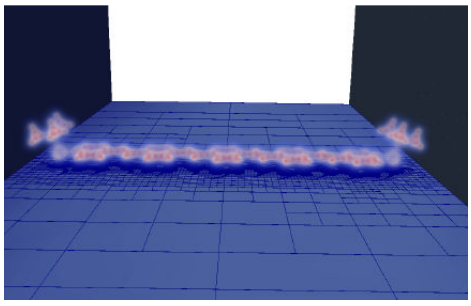

Figure 1: *OPV5-tBu molecule in a single electron transistor environment, colored by the effective potential. This close-up view of the molecule illustrates the extremely high level of detail in the region where the electron density is large. [4]*

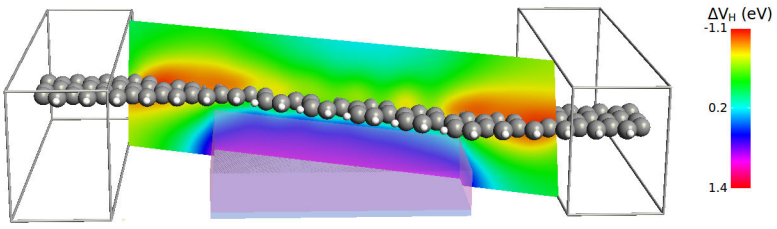

Figure 2: *Graphene nanotransistor consisting of two metallic zigzag nanoribbons connected by a semiconducting armchair ribbon. The nanoribbons are passivated with hydrogen, and the width of the ribbons are is 7 Å. The device is sitting on top of a dielectric and the transport is controlled by an electrostatic backgate. [6]*

BIGDFT: LARGE-SCALE AB INITIO METHODS BASED ON WAVELETS

Thierry Deutsch, Luigi Genovese, Stefan Goedecker, Brice Videau, Ivan Duchemin, Paul Boulanger

CEA, INAC, 17 rue des Martyrs, 38054 Grenoble, France
thierry.deutsch@cea.fr

Daubechies wavelets are a powerful systematic basis set for electronic structure calculations because they are orthogonal and localized both in real and Fourier space. We describe in detail how this basis set can be used to obtain a highly efficient and accurate method for density functional electronic structure calculations. This code, BigDFT, shows high systematic convergence properties, very good performances, and an excellent efficiency for parallel calculations alos in hybrid architectures based on CPU and graphical processing units.

References:

[1] L. Genovese, M. Ospici, T. Deutsch, J.-F. Méhaut, A. Neelov, S. Goedecker, Density functional theory calculation on many-cores hybrid central processing unit-graphic processing unit architectures; Journal of Chemical Physics, Vol. 131, p. 034103 (2009)

[2] L. Genovese, A. Neelov, S. Goedecker, T. Deutsch, S. A. Ghasemi, A. Willand, D. Caliste, O. Zilberberg, M. Rayson, A. Bergman and R. Schneider; Daubechies wavelets as a basis set for density functional pseudopotential calculations; Journal of Chemical Physics, Vol. 129, p. 014109 (2008)

[3] L. Genovese, T. Deutsch, A. Neelov, S. Goedecker and G. Beylkin; Efficient solution of Poisson's equation with free boundary conditions; Journal of Chemical Physics 125, p. 074105 (2006)

[4] L. Genovese, T. Deutsch and S. Goedecker; Efficient and accurate three-dimensional Poisson solver for surface problems; Journal of Chemical Physics 127, p. 054704–6 (2007)

Figures:

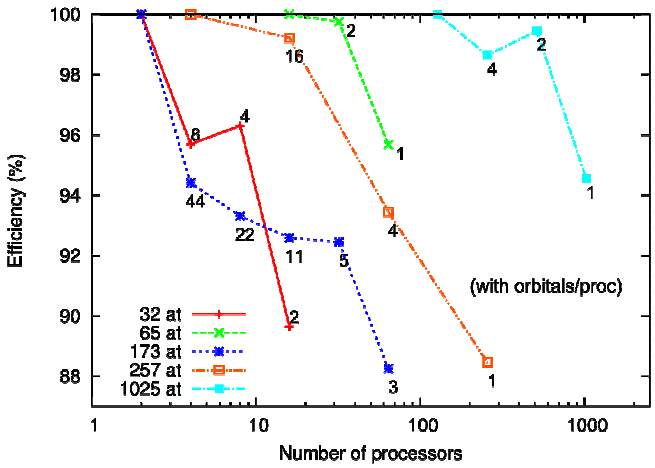

Figure 1: *Efficiency of BigDFT versus the number of cores. The number near the points is the distribution of orbitals per core.*

COMPRESSION OF SETS OF PRODUCTS OF ATOMIC ORBITALS, WITH APPLICATIONS TO TDDFT AND GW

D. Foerster

CPMOH/LOMA, University of Bordeaux I, France
d.foerster@cpmoh.u-bordeaux1.fr

Molecular orbitals in clusters or molecules can be conveniently expressed as linear combinations of localized atomic orbitals. Products of overlapping orbitals occur in electronic densities and these, by contrast, are linearly dependent. An improved solution of this well known technical problem leads to

(i) a new solution of the Petersilka-Gossmann-Gross equation of TDDFT-
(ii) a new $O(N^3)$ implementation, without plasmon parametrization, of Hedin's GW scheme.

Here we describe aspects of the compression algorithms we developed and their effect on the accuracy of spectra and electronic spectral functions in TDDFT and GW, respectively.

References:

[1] D. Foerster J. Chem. Phys. 128, 34108 (2008).
[2] P. Koval, D. Foerster and O. Coulaud, J. Chem. Theory Comput. 6, 2654 (2010).
[3] D. Foerster, P. Koval and D. Sanchez-Portal, arXiv:1101.2065v1, submitted to J.Chem.Phys.

A COMPLETE METHODOLOGY FOR THE SIMULATION OF LARGE NANOSTRUCTURES AND QUANTITATIVE ANALYSIS USING Z-CONTRAST IMAGES

Pedro L. Galindo, Joaquín Pizarro, Elisa Guerrero, Andrés Yáñez,
M. Paz Guerrero, Giovanni Scavello, Sergio I. Molina

Departamento de Lenguajes y Sistemas Informáticos, Universidad de Cádiz,
Campus Río San Pedro, s/n, 11510 Puerto Real, Cádiz, Spain,
pedro.galindo@uca.es

During the last few years, a complete methodology has been developed at the University of Cadiz for the simulation of High Resolution Electron Microscopy images of large nanostructures. Z-contrast imaging in scanning transmission electron microscopy (STEM) constitutes a powerful approach to investigate strained heterostructures on the nanometer scale and it has been proved to be extremely reliable for characterizing nanomaterials[1]. The proposed methodology allows the modeling and simulation of Z-contrast Electron Microscopy images of large nanostructures in reasonable time and it can be used to study materials in the presence of defects, being therefore very useful for a better knowledge of their mechanical properties and therefore of a great technological interest.

Figure 1 depicts the steps for a complete analysis of experimental and simulated HAADF images and quantitative characterization of nanostructures, and it comprises three steps, 3D nanostructure description (geometry, composition, etc.), 3D nanostructure modeling (Finite Element Modeling and/or Molecular Dynamics) and Image simulation.

A) **Geometry Description**: a commercial package (COMSOL™) is used to describe the geometry of the nanostructure (subdomains, boundaries, constraints, symmetries, etc.) and to define the local parameters (composition, initial strains, elastic constants…). The geometry of the nanostructure is usually described based on a-priori knowledge but the compositional distribution is usually extracted from experimental images by electron energy loss spectroscopy and aberration-corrected highresolution Z-contrast imaging.

B) **Nanostructure modeling**: once the geometry is fully described, an atomistic model must be generated. This goal can be accomplished by modeling the nanostructure using finite element analysis (FEA) and solving the equations of the anisotropic elastic theory to obtain the displacement field [2,3]. *SIC_Supercell* software developed at the University of Cadiz provides the corresponding 3D atomistic model from a supercell described as a sequence of (x, y, z) coordinates that have been obtained from FEA model at equilibrium, i.e. atom coordinates according to the local displacement field and occupancy or Debye-Waller factors according to the local composition. A second approach based in Molecular Dynamics is usually applied in our research group in order to obtain the 3D atomistic model [4] Molecular modeling involves theoretical and computational methods needed to model the behavior of a system at atomic scale. The collective behavior of atoms allows the understanding of how the material undergoes deformation, phase changes or other phenomena, providing links between the atomic scale to macro phenomena.

The resulting strain obtained by any of these two techniques may be compared with that obtained directly from experimental images applying a strain mapping technique. Using high-resolution electron microscopy images and under some limitations we may assume there exists a constant spatial relationship between the intensity maxima and the location of atomic columns in the studied material [5]. This relationship appears in the form of a spatial shift of the intensity maxima positions with respect to atomic columns. *Peak Pairs Analysis* is a strain mapping technique developed at the University of Cadiz [6] and implemented in a Digital Micrograph plug-in. It is distributed by HREM Research [7] and improves both, the speed of computation, and memory requirements with respect to other strain mapping approaches.

C) **Image simulation**: STEM image simulation of a few unit cells can take hours and the simulation of medium-size nanostructures, where millions of atoms are involved, is unfeasible in the state of the art personal computers. To overcome this problem, a parallel HAADF-STEM simulation software has been developed [8].The software runs in the University of Cadiz cluster, having 320 nodes and 3.8 Tflops and it is capable to simulate images from nanostructures represented by about 1 million atoms

in a couple of days. The software can generate one dimensional line scans, two dimensional images and focal series and its results has been successfully compared with WinHREM [4,8] software.

References:

[1] S.J. Pennycook and D. E. Jesson. Phys. Rev. Lett. 64, (1990), 938
[2] K. Tillman, M. Lentzen and R. Rosenfeld. Ultramicroscopy 83, (2000), 111
[3] J.L. Taraci, M. Hÿtch, T. Clement, P. Peralta, P. McCartney, J. Drucker and S.T. Picraux. Nanotecnology 16, (2005) 2365
[4] Large-scale Atomic/Molecular Massively Parallel Simulator. - http://lammps.sandia.gov S. Kret, P. Ruterana, A. Rosenauer and D. Gerthsen. Physica Status Solidi (b) 227 (1) 247 (2001)
[5] P Galindo, S. Kret, A. Sanchez, J Laval, A. Yañez, J. Pizarro, E. Guerrero, T. Ben, S. Molina, Ultramicroscopy 107, (2007), 1186-1193
[6] HREM Research – http://www.hremresearch.com/Eng/plugin/PPAEng.html
[7] K. Ishizuka, Ultramicroscopy 90, (2002), 71-83
[8] J. Pizarro, P. L. Galindo, E. Guerrero, A. Yáñez, M. P. Guerrero, A. Rosenauer, D. L. Sales and S. I. Molina. Appl. Phys. Lett. 93, (2008), 153107

Figures:

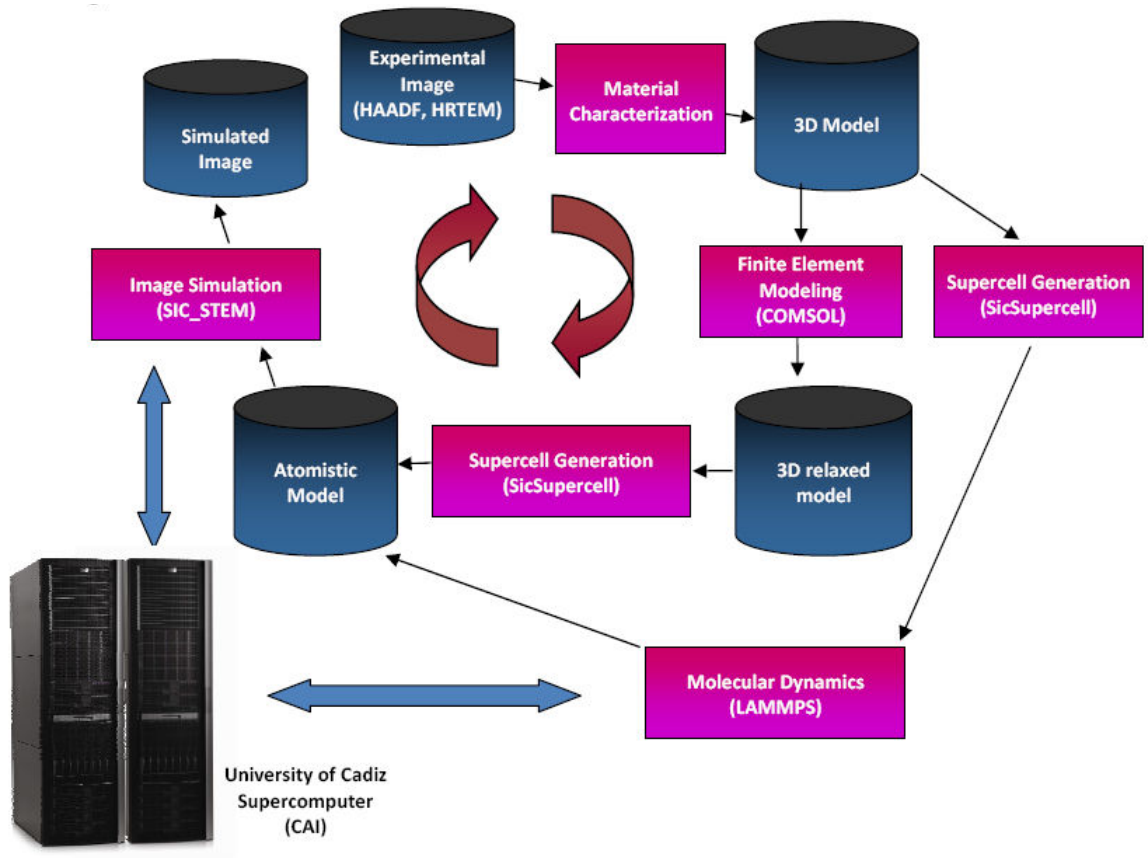

Figure 1: *Schematic diagram of the nanostructure modeling methodology developed at the University of Cadiz*

MONTE CARLO CONFIGURATION INTERACTION FOR MOLECULES AND NANOSTRUCTURES

Jim Greer

Tyndall National Institute, University College Cork, Lee Maltings, Cork, Ireland
jim.greer@tyndall.ie

Wave function methods such as configuration interaction and coupled cluster theory provide systematic treatments of electron correlations in nanoscale systems and provide accurate prediction for photoexcitation spectra in finite quantum systems. Arbitrarily accurate solutions to the many-body Schrödinger equation are possible through a brute force expansion of the wave function in determinants or spin coupled sums of determinants ('configuration state functions'), the so called configuration interaction (CI) or superposition of configurations method. Due to the length required for a complete many-body expansion, the brute force approach becomes computationally intractable except for few-electron problems.

A Monte Carlo technique for sampling configurations and evaluating their contribution to the energy or their weight in the many-electron wave function is designed to find only the most import configurations in many-electron wave functions [1,2] and has been applied to a variety of molecular problems. Recently using this Monte Carlo configuration interaction (MCCI) method, singlet and triplet electronic excitation energies have been calculated for few electron molecules for systems with single and multi-reference 0th order wave functions. We find that vertical photoexcitation energies can be predicted to within a few tens of meV (to within an accuracy of < 1%) of full CI (FCI, or complete many-body basis sets) limits using expansions consisting of only a few thousand configuration state functions as compared to the $O(10^{10})$ to $O(10^{12})$ configurations occurring in the corresponding FCI expansions [3]. The method thus represents the state-of-that art for predicting electronic excitations in few-electron systems with accuracy comparable to the equation-of-motion coupled cluster method with the inclusion of full triple excitations.

Interactions between localized molecular bound states and a continuum of states such as occurring for molecules bonded between electrodes in nanoscale tunnel junctions can be modeled by using an (energy-dependent) self-energy, or approximately through use of a complex potential. We discuss the relation between the two approaches and give a prescription for using the self-energy to construct an energy-independent complex potential [4] that generalizes single-electron electrode self-energies for use with many-electron wave functions. This allows for a treatment of molecular correlations on a nanoscale sub-system while 'opening' the system to allow interaction with larger systems such as electrodes, coupling to bulk bands for localized defect states, or for molecules-surface interactions.

The use of MCCI to the study of the charged nitrogen-vacancy (NV-) center in diamond [5] is presented; interest in the center is motivated by its potential use as a qubit. Within these calculations 116 electrons are correlated using 130 orbitals/260 spin orbitals. Use of the MCCI method allows for a study of the symmetry and spin of the electronic excitations needed to understand the mechanism for spin relaxation and hence lifetimes of the excited states. Our study suggested that the assumed ordering is unlikely to be correct and this theoretical prediction is consistent with recent experimental studies [6].

We will also report on recent results for porting the method to the IBM Blue Gene and discuss scaling of the algorithm in massively parallel environments. Recently several new methods that adaptively construct and refine a many-electron wave function have been reported using quantum Monte Carlo in a determinant space, coupled cluster theory, CI methods and the density matrix renormalization group theory. An overview of the common elements of these recent approaches is highlighted.

References:

[1] J.C. Greer, Journal of Chemical Physics Issue (1995) page
[2] J.C. Greer, Journal of Computational Physics Issue (1995) page
[3] W. Győrffy, R.J. Bartlett, and J.C. Greer, Journal of Chemical Physics 129 (2008) 064103
[4] T.M. Henderson, G. Fagas, E. Hyde and J.C. Greer, Journal of Chemical Physics 125 (2006) 244104
[5] P. Delaney, J.C. Greer and J.A. Larsson, Nano Letters 10 (2010) 610
[6] N.B. Manson, L. Rogers, M.W. Doherty, and L.C.L. Hollenberg, arXiv:1011.2840

Figures:

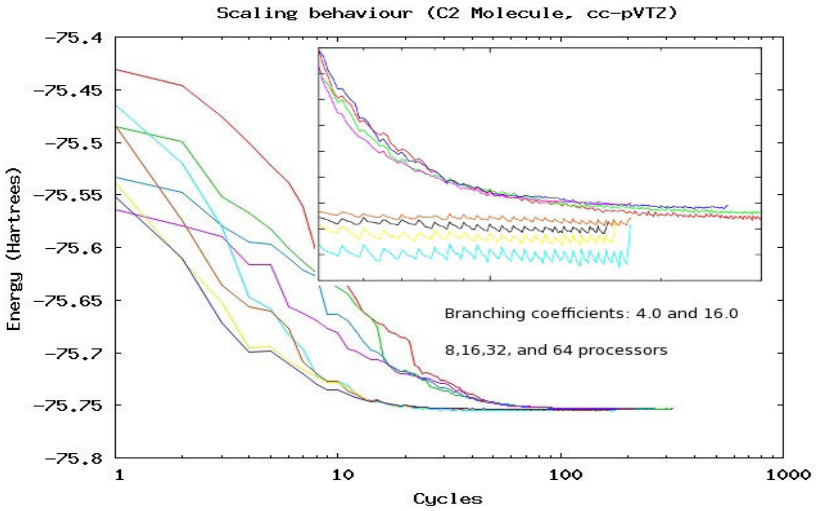

Figure 1: *Convergence behavior for the MCCI algorithm for the C_2 molecule in a correlation consistent polarized valence quadruple-ζ (cc-pVQZ) basis set. The inset reveals that with different sampling conditions, the final total electronic energy agree within a few milli-electron Volt or approximately 1 part in 10^4 In the correlation energy.*

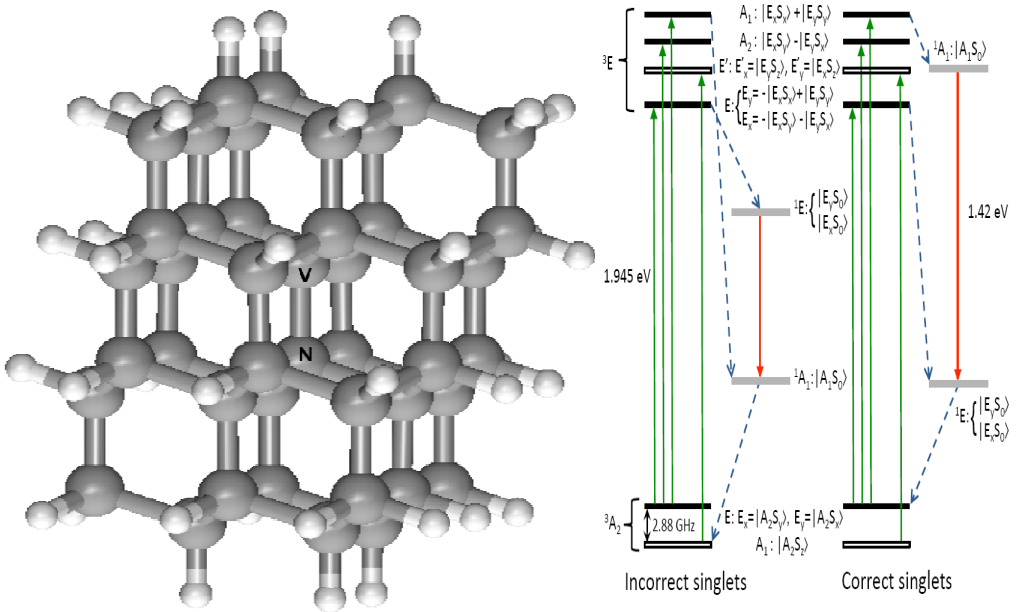

Figure 2: *Convergence Cluster model of the NV- center in diamond. MCCI spectra suggests that the ordering assumed for the singlet A_1 and degenerate E state should be reversed, with the singlet A_1 state lying higher in energy.*

INTEGRATED HPC APPLICATION SERVICES FOR MULTISCALE MATERIALS MODELING

Ivan Kondov[1], Robert Maul[1], Stefan Bozic[1], Wolfgang Wenzel[2]

[1]Steinbuch Centre for Computing, [2]Institute of Nanotechnology
Karlsruhe Institute of Technology, Hermann-von-Helmholtz-Platz 1,
76344 Eggenstein-Leopoldshafen, Germany
ivan.kondov@kit.edu

Computational materials science is essential for development of products with novel properties (examples: catalysis, semiconductors, and alloys). Nevertheless, next generation materials, especially nano-structured materials, exhibit pronounced complexity and multiscale behavior. Also “classical” systems like the biological cell and its building blocks include structures on many length scales. Thus, the physical models and the simulation protocols employ many different well established methods and different codes to treat the steps in these protocols. However, the lack of integration of these individual codes, the increasing complexity of models and the high demand for distributed HPC resources reduces industrial usability of the methods. In addition, joint effort of groups providing expertise for all different methods is needed. These aspects are treated within the project MMM@HPC [1] which brings together scientists from industry and academia into a unified community which is able to use the e-infrastructure to solve modern real-life problems.

We will give an overview of our methodology to provide adequate solutions for the following requirements:

Reusable interfaces and workflows. To this end, we adopted GridBeans [2] which is a modern technology to create application interfaces for use in grid middleware, such as UNICORE 6 [3] or Globus. Every GridBean provides a graphical user interface and can be readily included into different workflows without further modifications. Moreover, the workflows created for one specific task can be reused in other simulations with minor parametric modifications.

Robust tools and standards for data exchange between individual codes. In the field of materials modeling a variety of data formats are used and virtually every individual code has its own non-standard input and output formats. Thus, we aim to enhance data interoperability of individual GridBeans employing the Chemical Markup Language (CML) standard and work together with experienced developers from other projects, currently from UNICORE and OpenMolGrid [4, 5].

Solutions for licensing issues. Unfortunately, many of the codes used in the community are provided under non-free (proprietary) licenses. To treat this aspect we are working on a solution based on the Virtual Organization Membership Service (VOMS) and UNICORE.

Security and reliability. Industrial applications need secure handling (communication, storage) of simulation data. Moreover, the storage, the connection and the processes must be error-tolerant and thus reliable. All these are implemented properties of the underlying generic e-infrastructures and they are reused in our approach.

Capacity (high throughput) and capability (high performance) computing. The applications addressed in the community are particularly demanding with regard to computing and storage resources. This is why the scalable deployment of the application services requires linking to HPC and distributed resources, e.g. such as those provided in the projects EGI and PRACE.

All these user requirements pose a great challenge for both code developers and providers of e-infrastructures. These aspects are addressed in the EU project MMM@HPC. The application protocols are mapped onto scientific workflows and the application interfaces are able to ex-change input/output data using data formats like CML. The platform of our choice is the UNICORE middleware that is broadly and productively deployed in different grid infrastructures such as D-Grid, DEISA and PRACE.

As an example, we present in Figure 1 a model of an Organic Light Emitting Diode (OLED) that requires treatment on different size scales using different code types – quantum mechanics, molecular mechanics, kinetic Monte Carlo (coarse-grained method) and finite element analysis (continuous

method). Two of the interfaces are shown on the figure. We aim genericity of the developed workflow so that we consider several different codes that can perform one specific step in the simulation protocol. For example, an electronics structure calculation can be carried out employing two or more alternative programs. Our code selection criteria are maturity, open accessibility, high parallel performance, and availability of expertise by partners.

To demonstrate the functionalities of the developed tools we consider key applications, including de-novo modeling and simulation of whole devices, such as organic electronics, molecular electronics, carbon nano-device and Li-Ion batteries.

References:

[1] Project MMM@HPC: Multiscale Materials Modelling on High Performance Computer Architectures, Available online under www.multiscale-modelling.eu.

[2] R. Ratering, A. Lukichev, M. Riedel, D. Mallmann, A. Vanni, C. Cacciari, S. Lanzarini, K. Benedyczak, M. Borcz, R. Kluszcynski, P. Bala, G. Ohme, "GridBeans: Support e-Science and Grid Applications," Proceedings of the Second IEEE International Conference on e-Science and Grid Computing (e-Science'06), p. 45, IEEE 2006.

[3] UNICORE 6 - Recent and Future Advancements, A. Streit, P. Bala, A. Beck-Ratzka, K. Benedyczak, S. Bergmann, R. Breu, J. M. Daivandy, B. Demuth, A. Eifer, A. Giesler, B. Hagemeier, S. Holl, V. Huber, N. Lamla, D. Mallmann, A. S. Memon, M. S. Memon, M. Rambadt, M. Riedel, M. Romberg, B. Schuller, T. Schlauch, A. Schreiber, T. Soddemann, W. Ziegler, Report Nr. Jül-4319, ISSN 0944-2952, FZ Jülich 2010.

[4] Sulev Sild, Uko Maran, Mathilde Romberg, Bernd Schuller, Emilio Benfenati, OpenMolGRID: Using Automated Workflows in GRID Computing Environment. In Advances in Grid Computing - EGC 2005, P. M. A. Sloot et al (Eds), Lecture Notes in Computers Sciences, Vol. 3470, pp464-473, Springer 2005.

[5] Sulev Sild, Uko Maran, Andre Lomaka, Mati Karelson, Open Computing Grid for Molecular Science and Engineering, J. Chem. Inf. Model., 46, pp953-959, 2006.

Figures:

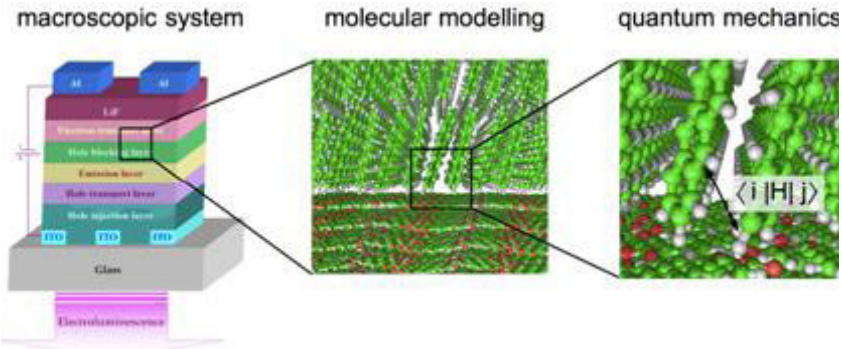

Figure 1: *Multiscale modeling of an Organic Light Emitting Diode (OLED).*

AN O(N^3) IMPLEMENTATION OF HEDIN'S GW APPROXIMATION FOR MOLECULES

Peter Koval[1,2], Daniel Sanchez-Portal[1,2], Dietrich Foerster[3]
[1]Centro de Fisica de Materiales, Paseo Manuel Lardizabal, 5, Donostia-San Sebastian, Spain
[2] Donostia International Physics Center (DIPC), Paseo Manuel de Lardizabal 4, Donostia-San Sebastian, Spain
[3]CPMOH/LOMA, Universite Bordeaux 1, Cours de la Liberation 351, Talence, France
koval.peter@gmail.com

The knowledge of excitation properties of molecules is crucial in developing organic semiconductor devices. Many-body perturbation theory is one of the most promising theories for characterization of excitations in electronic systems. In particular, Hedin's GW approximation for one-electron Green's function is capable of calculating lumo and homo of molecules with O(N^3) computational complexity like TDDFT.

In this work [1], we implement the Hedin's GW approximation on top of DFT calculations performed with SIESTA [2] code. We apply a dominant product technique [3] to span the space of orbital products and to reduce the dimensionality of dielectric matrix. Moreover, to describe the frequency/time dependence of necessary correlators, we use their spectral functions. The spectral function techniques avoids otherwise necessary analytical continuations and allow for Fast Fourier techniques to be applied in our method. As examples of application, we discuss several results for ionization potentials and electron affinities of large molecules, revealing strengths and limitations of our implementation.

References:

[1] D. Foerster, P. Koval, D. Sánchez-Portal, J. Chem. Phys. Submitted. arxiv: http://arxiv.org/abs/1101.2065
[2] J. M. Soler, E. Artacho, J. D. Gale, A. García, J. Junquera, P. Ordejón, D. Sánchez-Portal, J. Phys. C 14, 2745 (2002).
[3] P. Koval, D. Foerster, and O. Coulaud, J. Chem. Theory Comput. 6, 2654 (2010).

Figures:

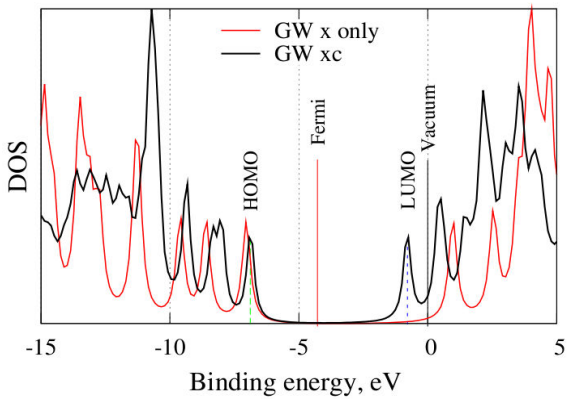

Figure 1: *The density of states of anthracene molecule computed in two approximations: "GW x-only" – only instantaneous part of self-energy is taken into account, while "GW xc" – the correlation effects due to dynamical screening are taken into account. Please, note that it is the correlation effects make our theoretical anthracene an aceptor, while exchange-only self-energy wrongly predicts our anthracene being donor.*

TAILORING THE ATOMIC AND ELECTRONIC STRUCTURE OF TWO-DIMENSIONAL CARBON AND BORON-NITRIDE SYSTEMS WITH ELECTRON AND ION BEAMS

A.V. Krasheninnikov[1,2], J. Kotakoski[1], O. Lehtinen[1], N. Berseneva[2] and R.M. Nieminen[2]

[1]Department of Physics, University of Helsinki, Finland
[2]Department of Applied Physics, Aalto University, Finland
akrashen@acclab.helsinki.fi

Recent experiments (see Refs. [1,2] for an overview) on ion and electron bombardment of nanostructures demonstrate that irradiation can have beneficial effects on such targets and that electron or ion beams can serve as tools to change the morphology and tailor mechanical, electronic and even magnetic properties of various nanostructured materials.

We systematically study irradiation effects in nanomaterilas, including two-dimensional (2D) systems like graphene and hexagonal boron-nitride (h-BN) sheets. By employing various atomistic models ranging from empirical potentials to time-dependent density functional theory we simulate collisions of energetic particles with 2D nanostructures and calculate the properties of the systems with the irradiation-induced defect. In this talk, our latest theoretical results on the response of graphene and h-BN to irradiation will be presented, combined with the experimental results obtained in collaboration with several groups [3,4]. The electronic structure of defected graphene sheets with adsorbed transition metal atoms will be discussed [5], and possible avenues for tailoring the electronic and magnetic structure of graphene by irradiation-induced defects and impurities will be introduced [4,6]. The effects of ion and electron irradiation on boron-nitride sheets and nanotubes will also be touched upon. Finally, we will discuss how electron irradiation and electron beam-assisted deposition can be used for engineering hybrid BN-C nanosystems by substituting B and N atoms with carbon with high spatial resolution.

References:

[1] Krasheninnikov A. V. and Banhart F., Nature Materials, 6, 723 (2007).
[2] Krasheninnikov A. V. and Nordlund K., J. Appl. Phys. (Appl. Phys. Reviews), 107, 071301 (2010).
[3] J. Kotakoski, C. H. Jin, O. Lehtinen, K. Suenaga, and A. V. Krasheninnikov, Phys. Rev. B 82 (2010) 113404.
[4] O. Cretu, A.V. Krasheninnikov, J. A. Rodriguez-Manzo, L.Sun, R.M. Nieminen, and F.Banhart. Phys. Rev. Lett. 105 (2010) 196102.
[5] A. V. Krasheninnikov, P.O. Lehtinen, A.S. Foster, P. Pyykko, and R. M. Nieminen, Phys. Rev. Lett. 102 (2009) 126807.
[6] F. Banhart, J. Kotakoski and A. V. Krasheninnikov, ACS Nano, (2011) in press.

GRAPHENE EDGE MAGNETISM FOR SPINTRONICS APPLICATIONS: DREAM OR REALITY?

Jens Kunstmann[1], Cem Özdo?an[2], Alexander Quandt[3,4], Holger Fehske[3], Hâldun Sevinçli[1], Gianaurelio Cuniberti[1]

[1]Institute for Materials Science, TU Dresden, 01062 Dresden, Germany
[2]Department of Materials Science and Engineering, Cankaya University, Ankara, Turkey
[3]Institut für Physik, Ernst-Moritz-Arndt-Universität Greifswald, Germany
[4]School of Physics and DST/NRF Centre of Excellence In Strong Materials, University of the Witwatersrand, South Africa
jens.kunstmann@tu-dresden.de

We critically discuss the stability of edge states and edge magnetism in zigzag edge graphene nanoribbons (ZGNRs). We point out that magnetic edge states might not exist in real systems, and show that there are at least three very natural mechanisms - edge reconstruction, edge passivation, and edge closure - which dramatically reduce the effect of edge states in ZGNRs or even totally eliminate them. Even if systems with magnetic edge states could be made, the intrinsic magnetism would not be stable at room temperature. Charge doping and the presence of edge defects further destabilize the intrinsic magnetism of such systems. We conclude that edge magnetism within graphenes ZGNRs is much too weak to be of practical significance, in particular for spintronics applications. We further discuss the influence of nonmagnetic edges on the electron transport through ZGNRs.

References:

[1] J. Kunstmann, C. Özdo?an , A. Quandt, H. Fehske, arXiv:1007.2602 (2010).

SIMULATION OF SCANNED PROBE SPECTROSCOPY: A CHALLENGING NUMERICAL PROBLEM

Massimo Macucci, Paolo Marconcini, Demetrio Logoteta

Dipartimento di Ingegneria dell'Informazione Università di Pisa, Via Girolamo Caruso 16, I-56122 Pisa
macucci@mercurio.iet.unipi.it

Scanned probe spectroscopy is an interesting technique developed a few years ago [1,2] for the direct investigation of the flow of electrons and of the position of impurities in nanoscale devices based on a 2- dimensional electron gas. Initial applications [1,2] were to the electron gas obtained by modulation doping in a GaAs/AlGaAs heterostructure and, more recently, to that in a graphene sheet [3]. The basic concept of scanned probe spectroscopy consists in measuring the effect on the device conductance of the potential perturbation due to a negatively biased probe that is scanned over the region of interest of the device. By creating a map of the conductance values in correspondence with the probe positions, interesting information about current paths and impurity scattering can be obtained.

We have been interested in the numerical simulations of these experiments, in order to develop a tool providing a better understanding of what is actually measured in such experiments and a reliable estimate of the achievable resolution. Our initial work was focused on GaAs/AlGaAs heterostructures and, in the last year, we got interested in the simulation of scanned probe spectroscopy experiments performed on graphene flakes [3].

Simulation of this type of experiments requires indeed a significant computational effort, because in principle the conductance across the device has to be re-computed for each probe position. The conductance can be evaluated, via the Landauer-Buettiker formula, from the knowledge of the transmission through the device for a range of energies around the Fermi level. Transmission can be obtained, for example, by means of the recursive Green's function technique or the recursive scattering matrix technique. All of these methods include a first step in which the device is subdivided into slices, within each of which the potential is assumed to be longitudinally constant. Calculation of the transmission is in itself a computationally intensive task, if, at least in some regions, a large number of transverse modes are propagating; then this has to be repeated for a number of times corresponding to the possible positions of the scanning probe. Without some form of optimization, such a calculation would definitely be unfeasible. We have looked into several forms of optimization, starting from preventing the repeated calculation of the transverse wave functions of the sections: the transverse Schroedinger equation is solved again, at each step in the probe position, only for the slices which are directly affected by the probe potential. Furthermore, one could compute the Green's function matrix from each end of the device to any of the intermediate slices (in the absence of the probe), keep this information in memory, and reuse most of it at each scanning step (thereby computing from scratch only the Green's function matrices of the region whose potential is altered by the probe). There is clearly a trade-off in terms of memory occupancy vs. speed, because if we want to keep all of this information, quite significant an amount of memory will be needed. With such an approach we can obtain plots of the results of scanned probe spectroscopy of quantum point contacts (Fig. 1) or of mesoscopic cavities (Fig. 2) with a computational effort of the order of a CPU-day.

Further improvements could be achieved by treating the potential of the probe as a perturbation and recomputing the overall Green's function matrix via the Dyson equation. This has been done with success in Ref. [4], where the effect of the probe was assumed to be localized in a single grid-point. In principle, this approach can be extended to the case of a probe creating a generic perturbation of the potential at the 2DEG level (usually assumed to be a Lorentzian), but the speedup is reduced and, depending on the size of the area affected by the potential perturbation, may not be convenient.

We are currently working on the implementation of scanned probe spectroscopy simulations of grapheme flakes: such simulations pose a very challenging computational problem, since experiments are performed on flakes with a width of the order of 1 micron, which makes approaches based on the atomistic methods usually applied to graphene (such as tight-binding) unfeasible. Therefore we have chosen a continuum approach consisting in the solution of the Dirac equation in each transverse section (which corresponds to the equation for the envelope functions in the vicinity of the band degeneration points). The numerical solution of such an equation is, however, a very challenging

problem in itself, due to the difficulties in finding a proper, consistent discretization. By extending the solution to a domain that is twice the width of the original domain, the boundary conditions become more standard and an efficient algorithm for the numerical solution can be implemented.

References:

[1] M. A. Topinka, B. J. LeRoy, R. M. Westervelt, S. E. J. Shaw, R. Fleischmann, E. J. Heller, K. D. Maranowski, and A. C. Gossard, Nature 410 (2001) 183.

[2] R. Crook, C. G. Smith, M. Y. Simmons, and D. A. Ritchie, J. Phys.: Condens. Matter 12 (2000) L735.

[3] M. R. Connolly, K. L. Chiou, C. G. Smith, D. Anderson, G. A. C. Jones, A. Lombardo, A. Fasoli, A. C. Ferrari, Appl. Phys. Lett. 96 (2010) 113501.

[4] G. Metadilis, P. Bruno, Phys. Rev. B 72 (2005) 235304.

Figures:

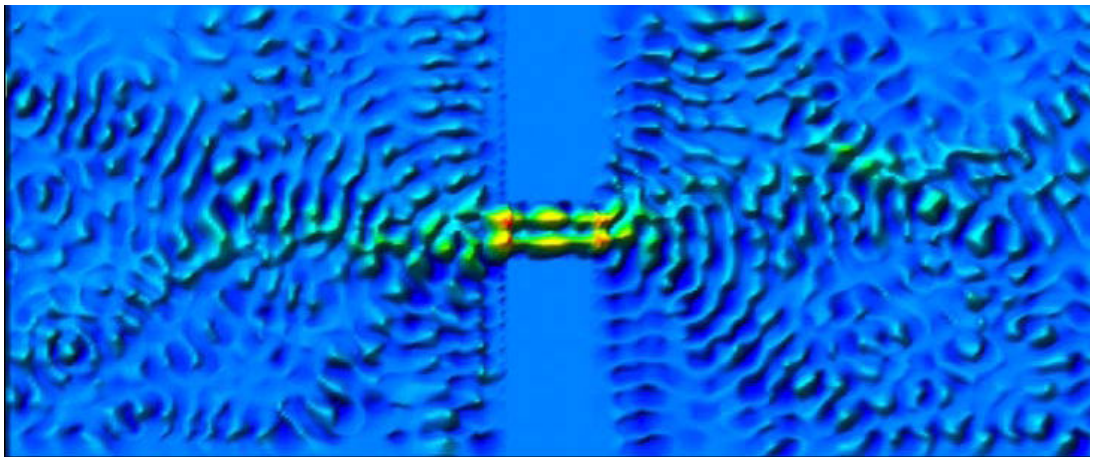

Figure 1: *Results for the scanned probe spectroscopy of a quantum point contact in the presence of a random potential due to dopants.*

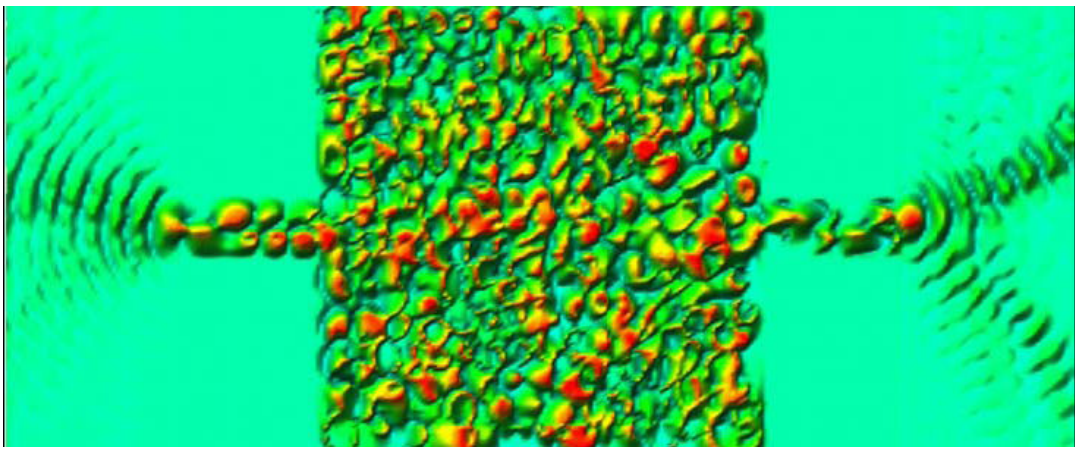

Figure 2: *Results for the scanned probe spectroscopy for a mesoscopic cavity, in the presence of the potential due to randomly located dopants.*

ELECTRONIC AND TRANSPORT PROPERTIES OF CHEMICALLY FUNCTIONALIZED NANOGRAPHENES

Francesco Mercuri, Daniele Selli, Matteo Baldoni, Antonio Sgamellotti

ISTM-CNR, c/o Department of Chemistry – University of Perugia, 06123 Perugia, Italy
francesco.mercuri@cnr.it

Recent advancements in production techniques have allowed the synthesis and characterization of novel nanostructured materials based on graphene.[1] Particularly, recent research efforts have been targeted to the investigations of low-dimensional nanographenes, such as graphene quantum-dots (GQDs) and nanoribbons (GNRs). Here, the dimensional confinement at the nanoscale allows the tuning of the intrinsic electronic properties of graphene, which can potentially be exploited for the production of next-generation nanostructured electronic devices. Nevertheless, limitations in current experimental methodologies hinder both the controlled synthesis of nanographenes, with well-defined electronic properties, and large-scale production. To overcome these issues, the chemical modification of graphenes has been spotted as a viable route to produce materials with controlled and well-defined properties with potential use in applications. However, despite recent theoretical and experimental efforts, [2,3] a comprehensive understanding of the relationships between chemical structure and electronic properties in nanostructured graphenes is still missing. This concern is particularly critical in relation to the electron transport properties of chemically-modified graphenes, in view of their use in nanoelectronics.

In this work, we analyze, by means of density functional theory and non-equilibrium Green's function calculations, the electronic and transport properties of low-dimensional graphene nanostructures subjected to chemical functionalization. Our calculations concern models based on GQDs, GNRs and functionalized nanostructures thereof, targeting systems of interest in recent experiments, focused on oxidization and edge-functionalization of nanographenes.[4] In particular, we demonstrate how the remarkably versatile chemistry of sp^2 carbon and the use of traditional organic chemistry concepts [5,6] provide a reliable guide to rationalize the properties of chemically functionalized graphenes. The application of rigorous concepts in the definition of model systems and the use of high-performance computing platforms constitute crucial prerequisites for realistic simulations of low-dimensional carbon nanostructures aimed at the development of novel materials with potential application in nanoelectronics.

References:

[1] Geim AK, Novoselov KS, Nature Materials, 6 (2007) 183.
[2] Allen MJ, Tung VC, Kaner RB, Chem. Rev., 110 (2010) 132.
[3] Castro Neto AH, Guinea F, Peres, NMR, Novoselov KS, Geim, AK, Rev. Mod. Phys., 81 (2009) 109.
[4] Ruoff R, Nature Nanotechnology, 3 (2008) 10.
[5] Baldoni M, Sgamellotti A, Mercuri F, Org. Lett., 9 (2007) 4267.
[6] Baldoni M, Sgamellotti A, Mercuri F, Chem. Phys. Lett., 464 (2008) 202.

Figures:

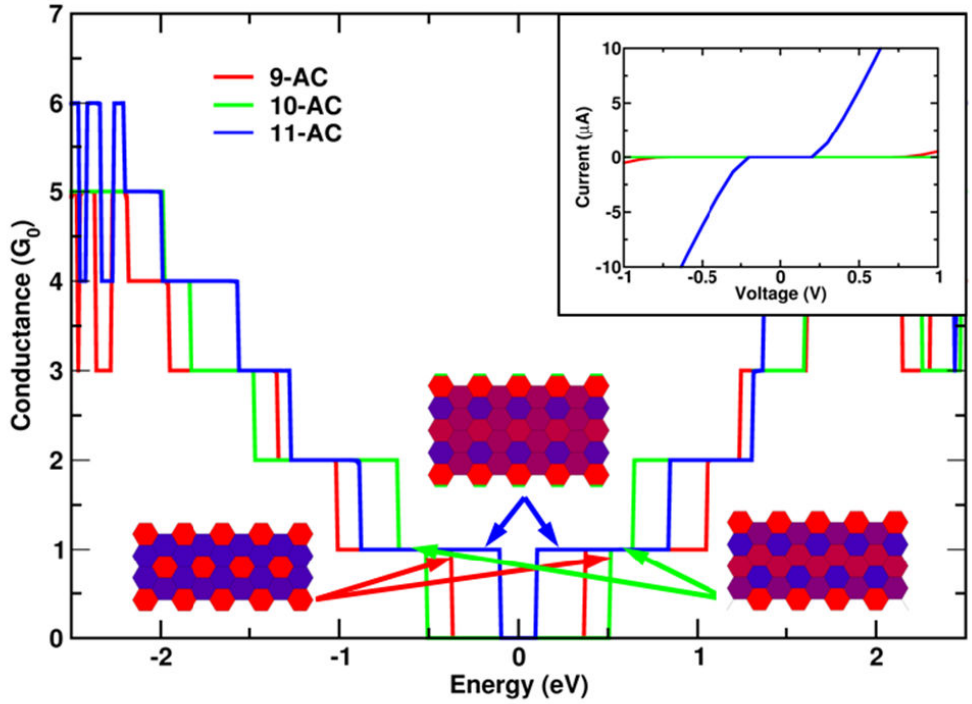

Figure 1: *Transmission spectra and I(V) characteristics (inset) of armchair-edge 9-AC (red lines), 10-AC (green lines) and 11-AC (blue lines) GNRs. Optimized structures, color-coded according to their mean bond length (average of the six C-C bond lengths for each six-term ring), are also depicted above the corresponding transmission plateau.*

MASSIVE COMPUTATION FOR NON-EQUILIBRIUM PHENOMENA IN NANOCARBONS

Yoshiyuki Miyamoto

Nanosystem Research Institute, National Institute of Advanced Industrial Science and Technology (AIST), Japan

In this presentation, I will introduce you computational scheme of extremely strong optical electric field (E-field) generated by compressed laser pulse (femtosecond laser pulse). Since the optical E-field is over 1 V/Å and the pulse has very short time-range (less than 40 fs), the conventional perturbation theory does not work so direct numerical simulation solving electrons' real-time dynamics under time-varying E-field should be solved. For that purpose, we have applied the time-dependent density functional theory combined with molecular dynamics.

As examples of applications we will provide our result for graphene exfoliation from graphite surface [1] and molecular photochemical reaction inside nanotubes [2]. We will also discuss future possible applications of non-equilibrium phenomena on nano-carbons which has high melting temperatures and difficult to deal with conventional thermal processes.

References:

[1] Y. Miyamoto, H. Zhang, and D. Tománek, PRL, 104, 208302 (2010).
[2] Y. Miyamoto, H. Zhang, and A. Rubio, PRL, 105, 248301 (2010).

EXPLORING THE REAL NANO-WORLD USING HPC BEYOND THE AB-INITIO APPROACH

Pablo Ordejón

Centro de Investigación en Nanociencia y Nanotecnología - CIN2 (CSIC-ICN)
Campus de la UAB, 08193 Bellaterra, Barcelona

The advances in the predictive power, speed and reliability of ab-initio methods has occurred in the last few decades at a very fast pace. Simultaneously, the computing power available through HPC facilities has continued growing exponentially. This combination has brought the paradigm of ab-initio simulations as an invaluable tool to understand and predict the behavior of matter at the nanoscale. However, enormous challenges are still ahead of us, to be able to extend the range of practical applicability of these methods to the sizes and time scales which are relevant to most of the practical problems in nanotechnology. In this talk, I will talk about some of these challenges, and discuss strategies to use the information extracted from ab-initio simulations to tackle problems in the length and time scales which are really relevant for practical uses of nanotechnology. In particular, I will describe approaches to study electronic transport properties in nano-to-meso scale devices (see Figure 1) [1], and the interaction of large proteins with inorganic nanostructures. The role of HPC facilities and the interaction between these and the development of simulation tools will also be discussed [2].

Acknowledgements:

Work done in collaboration with Carlos F. Sanz-Navarro (CIN2-ICN), Stephan Roche (CIN2-ICN), Alberto García (ICMAB-CSIC), and Jose M. Cela (BSC). Financial support from Spanish MICINN grants CSD2007-00050 (Supercomputing and e-Science), and FIS2009-12721-C04 are fully acknowledged.

References:

[1] N. Leconte, J. Moser, P. Ordejón, H. Tao, A. Lherbier, A. Bachtold, F. Alsina, C. Sotomayor Torres, J.-C. Charlier and S. Roche, ACS Nano 4 (2010) 4033
[2] C. F. Sanz-Navarro, R. Grima, A. García, Edgar A. Bea, A. Soba, J. M. Cela and P. Ordejón, Theor. Chem. Acc 128 (2011) 825

Figures:

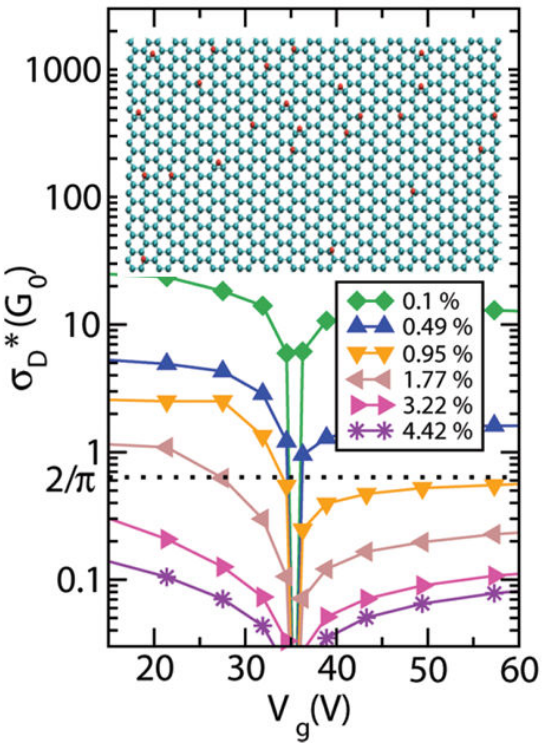

***Figure 1**: Drude conductivity of samples of graphene functionalized with different concentrations of oxygen, in the configuration of epoxide groups, as a function of gate voltage. The inset shows a section of one of the samples. Adapted from Ref. [1]*

BITLLES: A QUANTUM-TRAJECTORY SIMULATION TOOL FOR ELECTRON TRANSPORT IN LARGE ELECTRONIC STRUCTURES

G. Albareda, A. Alarcón, F. L. Traversa, A. Benali, A. Padró, and **X. Oriols**

Dept. d'Enginyeria Electrònica, Universitat Autònoma de Barcelona, 08193 Bellaterra, Spain
guillem.albareda@uab.cat

With the aim of manufacturing smaller and faster devices, the electronic industry is today entering the nano and picosecond scales. In such particular scenarios, electron dynamics becomes affected by strongly correlated quantum dynamics, both in space and time. Thus, in order to provide an enough accurate description of the electron-electron correlations, quantum transport simulators must consider a reasonable approach to the many-particle problem. Anyway the big deal concerns the solution of the many-particle Schrödinger equation nowadays solvable only for very few degrees of freedom.

In this work we present a general purpose time-dependent 3D quantum electron transport simulator based on Bohmian trajectories that we call **BITLLES** [1-3]**.** It is based on a recently published algorithm [1] that, on the grounds of Bohmian Mechanics [2], solves the many-particle Schrödinger equation for hundreds of electrons in terms of multiple single-particle pseudo-Schrödinger equations without losing the explicit Coulomb and exchange correlations among electrons (at a level comparable to the Time Dependent Density Functional Theory) [1-4].

The code of the **BITLLES** simulator is currently made up of more than 15000 FORTRAN lines (see the algorithm in Fig.1). It has also a 3000 C++ lines for a (Windows, MAC and Linux compatible) user friendly environment to design an verify the simulated electronic structures (see Fig. 2). The computational burden associated with the solution of the self-consistent many-particle 3D Poisson-Schrödinger loops involves large simulation times. For example, one week for the complete I-V curve (DC, AC and noise) with a cluster of 24 Intel Xeon CPUs at 2.7GHz.

Same examples of the numerical viability of the **BITLLES** simulations are provided below for a Resonant Tunneling Diode (RTD). Its characteristic I-V curve with Coulomb correlations introduced at different approximation levels is plotted in Fig. 3 [3,5]. Many-particle tunneling phenomena are reveled in the (super-Poissonian) behavior of the Fano factor shown in Fig. 4 [2]. Finally, in Figs. 5 and 6 we show the transient (time-dependent) current response and its Fourier transform respectively, when a voltage step is applied in the negative differential conductance region.

References:

[1] X. Oriols, Quantum trajectory approach to time dependent transport in mesoscopic systems with electron-electron interactions, *Phys. Rev. Let. 98, 066803* (2007).
[2] X. Oriols and J. Mompart, *Applied Bohmian Mechanics: From Nanoscale Systems to Cosmology*, Editorial Pan Stanford.
[3] G. Albareda, H. López, X. Cartoixà, J. Suné, and X. Oriols, Time-dependent boundary conditions with lead-sample Coulomb correlations:Application to classical and quantum nanoscale electron device simulators, *Phys. Rev. B, 82, 085301* (2010).
[4] G. Albareda, F. L. Traversa and X. Oriols, Full counting statistics within bohmian mechanics, *in preparation* (2011).
[5] G. Albareda, J. Suné, and X. Oriols, Many-particle hamiltonian for open systems with full coulomb interaction: Application to classical and quantum time-dependent simulations of nanoscale electron devices, *Phys. Rev. B. 79, 075315* (2009).
[6] A. Alarcón and X. Oriols, Computation of quantum electron transport with local current conservation using quantum trajectories, *J. Stat. Mec. Theor. Exp.. 2009, P01051* (2009).

Figures:

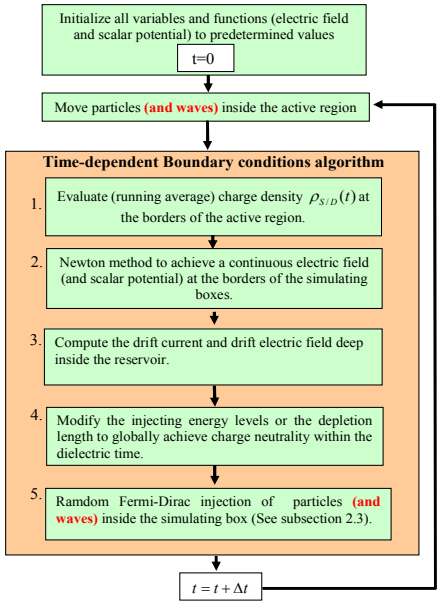

Figure 1: *General algorithm describing the fundamental routines defining the BITLLES simulator.*

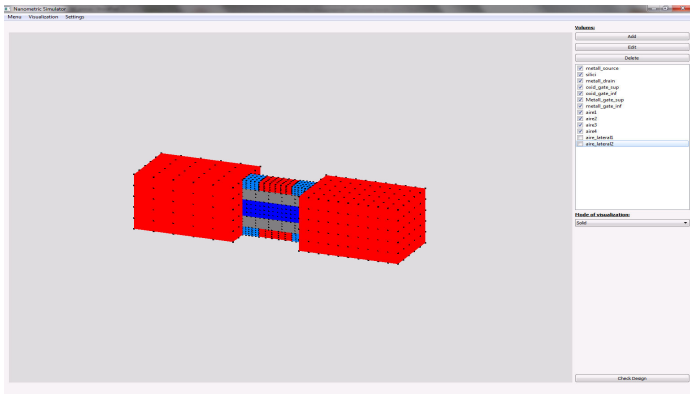

Figure 2: *Very recently BITLLES has been provided with a user friendly interface.*

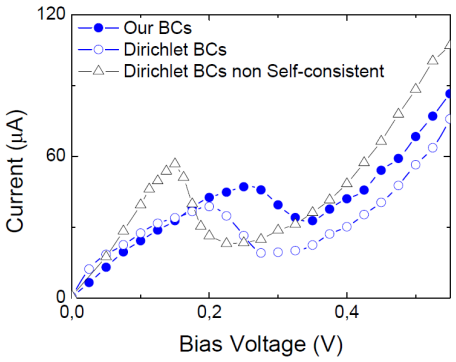

Figure 3: *DC Current for a RTD with Coulomb correlations introduced at different levels of accuracy.*

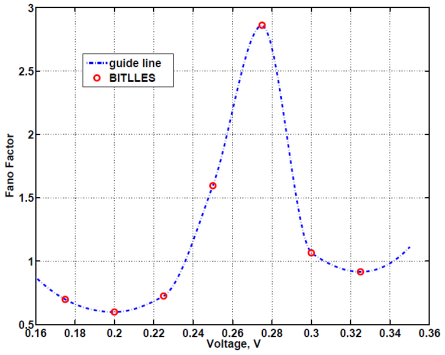

Figure 4: *Fano Factor computed for the RTD of Fig. 1 computed directly from the (time-dependent) current fluctuations.*

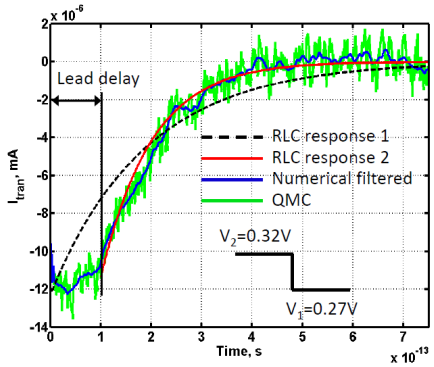

Figure 5: *Current response of the RTD to a step input voltage. Self-consistent boundary conditions including the leads are used*

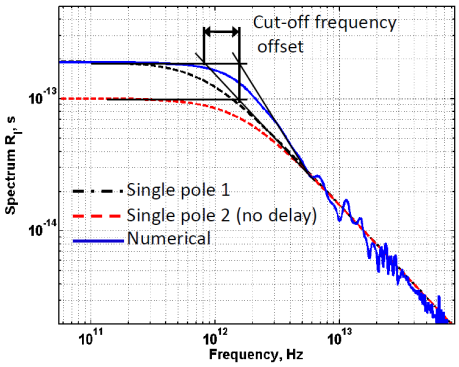

Figure 6: *Spectrum of the current response of Fig. 5. Cut off frequency and its offset due to the lead delay are pointed out.*

MODELING PHOTO-INDUCED DYNAMICAL PROCESSES IN MASSIVE PARALLEL ARCHITECTURES

Angel Rubio

Nano-Bio Spectroscopy Group, Departamento de Física de Materiales, UPV. European Theoretical Spectroscopy Facility (ETSF), Edificio Korta, Avda. Tolosa 72, 20018 San Sebastián, Spain
angel.rubio@ehu.es

There has been much progress in the synthesis and characterization of nanostructures however; there remain immense challenges in understanding their properties and interactions with external probes in order to realize their tremendous potential for applications (molecular electronics, nanoscale opto-electronic devices, light harvesting and emitting nanostructures). In this talk we will review the recent advances within density-functional based schemes to describe spectroscopic properties of those complex systems. Special emphasis will be made in modeling new materials and simulate new time and spatially resolved spectroscopies. We will address both linear and non-linear response regimes to study the optical absorption and luminescence of bio-chromophores, one-dimensional polymers and nanotubes and layered materials. Moreover, we will illustrate how an optimal control theory can be implemented such that we could have control of the quantum state of a molecular structure.

Within the goal of spanning larger time-scales and more complex structures, we will describe a new method to mimic the electron-ion dynamics within the Ehrenfest scheme where no explicit orthogonalization is necessary and we can increase of the time step while keeping the system close to the Born-Oppenheimer surface. The method is easily implemented and scales very well with the system size. Applications to the excited state dynamics in some organic molecules will be used as text cases to illustrate the performance of the approach. We will present the dynamical processes in organic/inorganic charge-transfer systems and biological complexes. In particular we will show the effect of electron-hole attraction in those systems. Pros and cons of present functionals will be highlighted and provide insight in how to overcome those limitations by merging concepts from many-body perturbation theory and time-dependent density functional theory.

All those developments constitute a basic ingredient for the realization of the European Theoretical Spectroscopy Facility (ETSF, http://etsf.eu) as a top-level scientific infrastructure. We implemented all those ideas in the open source computer code OCTOPUS (http://www.tddft.org). This program released in 2002 simulates the dynamics of electrons and nuclei under the influence of arbitrary time-dependent fields. his code is very versatile and can handle diverse physical situations (molecules, solids, 2D quantum dots, etc.) making it an extremely powerful tool for spectroscopy. Thanks to its current parallel capabilities, OCTOPUS was chosen as a benchmark code for the Partnership for Advanced Computing in Europe1 (PRACE) initiative that aims to provide European scientists with world-class leadership supercomputing infrastructures.

References:

[1] http://www.prace-project.eu

TUNABLE BANDGAPS AND EXCITONS IN DOPED SEMICONDUCTING CARBON NANOTUBES MADE POSSIBLE BY ACOUSTIC PLASMONS

Catalin Spataru

Sandia National Labs, USA

Doping of semiconductors is essential in modern electronic and photonic devices. While doping is well understood in bulk semiconductors, the advent of carbon nanotubes and nanowires for nanoelectronic and nanophotonic applications raises some key questions about the role and impact of doping at low dimensionality. Here we show that for semiconducting carbon nanotubes, bandgaps and exciton binding energies can be dramatically reduced upon experimentally relevant doping, and can be tuned gradually over a broad range of energies in contrast to higher dimensional systems. The later feature, made possible by a novel mechanism involving acoustic plasmons, establishes new paradigms for the understanding and design of nanoelectronic and nanophotonic devices.

ELECTRON TRANSPORT OF NANO-CARBON MATERIALS

Syogo Tejima, Satoshi Nakamura,Hisashi Nakamura

Research Organization for Information Science & Technology, Tokyo, Japan

We have investigated electron transport of nano-carbon materials at finite temperatures through the large scale simulation using high-end supercomputers. For our purpose, we have developed an electron transport simulation model, based on a non-equilibrium finite temperature Green's function. The advanced tight-binding, Hamiltonian and molecular dynamical approaches enable us to consider phonon mode effect on electron transport at finite temperatures.

Through oder (N) approach, we are able to simulate meso-scale transport phenomena with several ten thousands of carbon atoms. In addition to calculating fundamental transport coefficient, our method is able to give atomistic electron current for all atomic positions. From the atomistic point of view, we can more clearly understand the interesting behavior of electron transport as nanoscale carbon materials. Our results show that electron current properties of nano-carbon materials strongly depend on a way of attachment of electrodes to such materials. Moreover, a choice of carbon orbital, pi or sigma, which is connected to electrodes, has crucial influence on electron transport behaviors. As for carbon nanotube, grahene, and Macky crystal, we will introduce our progress of researches and our large-scale simulation experiences.

COMPUTATIONAL STUDIES OF DIRAC FERMION MATERIALS AND NANOSTRUCTURES

Oleg V. Yazyev

Department of Physics, University of California, Berkeley, California 94720, USA
Materials Sciences Division, Lawrence Berkeley National Lab, Berkeley, California 94720, USA

Graphene and topological insulators are among the most remarkable scientific discoveries of the past decade. High-performance computing plays important role in exploring various aspects of the physics of these novel materials and derived nanostructures. In my talk, I will cover our recent studies in the field of Dirac fermion materials which involve computational methods of various complexities: model Hamiltonian approaches applied to large nanostructures, density functional theory and many-body perturbation theory techniques. In particular, I will focus on the electronic properties of chiral graphene nanoribbons and on the electronic transport in polycrystalline graphene. Finally, I will discuss our recent investigations of the bismuth-based bulk topological insulators.